

Controls on the stratigraphic architecture of shallow marine systems in syn-rift basins

Bonita Jade Barrett

Submitted in accordance with the requirement for the degree of

Doctor of Philosophy

The University of Leeds

Institute of Applied Geoscience

School of Earth and Environment

August 2019

The research that contributes to this thesis has been targeted towards and published in peer-reviewed journals. It is considered that the alternative thesis format is the most appropriate format for this work. The candidate confirms that the work submitted is his/her own, except where work which has formed part of jointly-authored publications has been included. The contribution of the candidate and the other authors to this work has been explicitly indicated below. The candidate confirms that appropriate credit has been given within the thesis where reference has been made to the work of others. Contributors to jointly-authored publications are outlined below.

Chapter 3 - Published

Barrett, B.J., Hodgson, D.M., Collier, R.E.Ll. & Dorrell, R.M. (2018). Novel 3D sequence stratigraphic numerical model for syn-rift basins: analysing architectural responses to eustasy, sedimentation and tectonics. *Marine and Petroleum Geology*, 92, 270-284.

B. J. Barrett: principal investigator and main author - undertook numerical modelling and data analysis

D.M. Hodgson: discussion and manuscript review

R.E.Ll. Collier: discussion and manuscript review

R.M. Dorrell: assistance with programming for computer modelling and manuscript review

Chapter 4 - Published

Barrett, B.J., Collier, R.E.Ll., Hodgson, D.M., Gawthorpe, R.L., Dorrell, R.M. & Cullen, T.M. (2019). Quantifying faulting and base level controls on syn-rift sedimentation using stratigraphic architectures of coeval, adjacent Early-Middle Pleistocene fan deltas in Lake Corinth, Greece. *Basin Research*, doi: 10.1111/bre.12356.

B. J. Barrett: principal investigator and main author - undertook data collection, analysis and modelling

D.M. Hodgson: discussion and manuscript review

R.E.Ll. Collier: introduced field area (Gulf of Corinth), discussion and manuscript review

R.M. Dorrell: assistance with programming for computer modelling and manuscript review

R.L. Gawthorpe: discussion and manuscript review

T.M. Cullen: field assistance during data collection, discussion and manuscript review

Chapter 5 – Published

Barrett, B.J., Gawthorpe, R.L., Collier, R.E.Ll., Hodgson, D.M. & Cullen, T.M. (2019). Syn-rift delta interfan successions: archives of sedimentation and basin evolution. *The Depositional Record*, doi: 10.1002/dep2.95.

B. J. Barrett: principal investigator and main author - undertook data collection, analysis and modelling

D.M. Hodgson: discussion and manuscript review

R.E.Ll. Collier: introduced field area (Gulf of Corinth), discussion and manuscript review

R.L. Gawthorpe: discussion and manuscript review

T.M. Cullen: field assistance during data collection, discussion and manuscript review

Chapter 6 – Prepared for submission

Barrett, B.J., Hodgson, D.M. & Collier, R.E.Ll. (Prepared for submission). Geometric and volumetric analysis of footwall degradation and hangingwall architecture, northern Carnarvon Basin, NW Shelf, Australia. Prepared for submission.

B. J. Barrett: principal investigator and main author - undertook data collection and analysis

D.M. Hodgson: discussion and manuscript review

R.E.Ll. Collier: discussion and manuscript review

This copy has been supplied on the understanding that it is copyright material and that no quotation from the thesis may be published without proper acknowledgement.

The right of Bonita Barrett to be identified as Author of this work has been asserted by her in accordance with the Copyright, Designs and Patents Act 1988.

© 2019 The University of Leeds and Bonita Jade Barrett

Acknowledgements

There are numerous people to thank individually for their advice, kindness and support throughout my PhD experience, to whom I feel forever indebted. My first thanks go to everyone involved in the project itself. My supervisors, David Hodgson and Richard Collier, originally proposed the PhD project, hired me and have supported me throughout the preparation of papers and the final thesis. I am beyond grateful for their support and belief in my capabilities, especially during the occasions that I was daunted by new concepts and approaches. I also cannot thank Dave enough for his guidance of my personal development; opening my eyes to the options available for my future and truly caring about the career I was carving for myself. Thank you to Rob Dorrell for his supervision and assistance with numerical modelling, and advice from experience as an early career researcher. I am also grateful to Rob Gawthorpe for my 3 month visit to the University of Bergen, where he supervised my project, encouraged additional fieldwork and co-authored two scientific papers.

I am appreciative of those avenues that have facilitated my progress since 2015, including: the project sponsor, Engie who contribute to the research of the Shallow Marine Research Group; the IAS for the Post-Graduate research grant, the BSRG for the Trevor Elliott Memorial grant and VISTA for the scholarship to study in Bergen; all of which have allowed me to travel and extend my research beyond original plans. Thank you to Giannis Xristopolous and other landowners for allowing access to the beautiful Greek outcrops. I also thank all of the reviewers of the manuscripts; the papers benefitted greatly from their constructive and thorough reviews.

I have been fortunate to have Tim Cullen sat by my side for three years in Leeds, Greece and Norway. I appreciate every discussion and could not have asked for a better collaborator. I learned and laughed immensely in the field with Tim, Dan Bell, Hannah Kearns, Luz Gomis-Cartesio and Miquel Poyatos-Moré. Grace Cosgrove has been my PhD partner-in-crime, and every past and present member of the Strat Group and the wider PhD cohort at Leeds has helped me along the path in different ways; to all of whom I am very grateful and hope I have reciprocated their support and friendship.

My family and friends have been an unknowing lifeline throughout my PhD. I am so lucky to have true love and confidence from my Mum, Dad, Nana, Rob, Chaunce, Dean, Serena and Elissa. I also feel very fortunate to have unwavering emotional support from my best friends, Zoe Roseby, Jessica Casey and Emma Bagnall. Thank you to Christopher Lloyd for making me laugh and smile, and providing balance in my life at the most valuable time.

Through my PhD, I have travelled for fieldwork and conferences to South Africa, the USA, Canada, Greece, Spain, Portugal and Norway, attended numerous courses, workshops, and entertaining Strat days. I have made life-long friends and collaborators, and as such could not have asked for a more fulfilling PhD experience. Thank you to everyone responsible.

Abstract

Rift basin-fills preserve complicated stratigraphic architectures due to temporally- and spatially-variable interactions of base level, tectonics and sedimentation. This work aims to reduce uncertainty, and improve interpretations and predictions of shallow marine, syn-rift stratigraphy around normal fault blocks, by: i) accounting for architectural complexities arising from along-strike variability in allogenic controls; ii) deconvolving control signals from the depositional record; iii) using quantitative data, techniques, classification and modelling; and iv) proposing an alternative stratigraphic framework to the ratio of accommodation to supply ($\delta A/\delta S$) for tectonically-active basins. Novel geometric and volumetric, 3D approaches are utilised through numerical modelling (new sequence stratigraphic forward model, 'Syn-Strat'), field and subsurface analysis. Detailed assessment of field data and UAV photogrammetry-based 3D outcrop models is undertaken of coeval and adjacent exposed fan deltas and their interfan area (Gulf of Corinth Greece), and of 3D seismic data imaging footwall-, hangingwall- and axially-derived depositional systems in the subsurface (northern Carnarvon Basin, NW Shelf, Australia).

Tectono-sedimentary models are improved through this work by: better constraints of key surface diachroneity; understanding the relative contribution and interactions of multiple sedimentary systems within a basin; consideration of along-strike depositional system asymmetry and sediment routing; and a 3D approach. Documenting along-strike variability of stratigraphic architecture in rift basin enables control signals to be deconvolved and quantified. The 'non-unique solutions' theory is only arguable in cases with one-dimensional data and limited regional knowledge. By using a multi-system, along-strike distributed approach with interpretation and modelling based on geological rules, it is possible to invert the stratigraphic record. Several flaws in the $\delta A/\delta S$ ratio are highlighted, and a new framework ($\delta AI/\delta AR$) is proposed, which is unbiased, inclusive of all control parameters and possible recorded outcomes. This new approach better allocates time across surfaces and strata in the depositional record, and is applicable to global rift basin analysis.

List of Figures

Chapter 1

Figure 1.1. Block model to demonstrate current gaps and uncertainties in tectono-stratigraphy that will be addressed with this work.

Figure 1.2. Figurative definitions of accommodation between time steps.

Figure 1.3. Representative photographs from fieldwork in northern Peloponnesus, Gulf of Corinth, Greece.

Figure 1.4. Workflow adopted to build 3D outcrop models from UAV-photogrammetry in Agisoft Photoscan software, and quantitative data collection in LIME.

Figure 1.5. Map of the subsurface dataset location, Northern Carnarvon Basin, NW Shelf, Australia.

Figure 1.6. The Gulf of Corinth, Greece study area.

Figure 1.7. Palaeogeographic maps showing the configuration of Australia with respect to the Gondwanaland supercontinent.

Chapter 2

Figure 2.1. Geographical distribution of Earth's rift basins.

Figure 2.2. Idealised schematic diagram to show the mechanism of passive rifting and three models for rifting strain geometries.

Figure 2.3. The main structural elements of a mature rift.

Figure 2.4. Normal fault growth through models, with associated displacement-length profiles.

Figure 2.5. Key elements of a normal fault set.

Figure 2.6. Syn- and post-rift megasequences exposed in Eastern Svalbard.

Figure 2.7. Pre-, syn- and post-rift megasequences in seismic data from NW Shelf, Australia.

Figure 2.8. A range of tectono-sedimentary models for different depositional environments and stages of fault evolution.

Figure 2.9. Sequence stratigraphic schemes in the literature.

Figure 2.10. The geometry and terminology of clinoforms; the building-blocks of fan deltas.

Figure 2.11. Stacking trends within clinoformal parasequence sets in relation to the $\delta A/\delta S$ ratio.

Chapter 3

Figure 3.1. Process of forward stratigraphic modelling of syn-rift basin-fills.

Figure 3.2. Model plot axes options, associated geological setting and example model outputs.

Figure 3.3. Derivation of the 3D eustatic sea level curve.

Figure 3.4. Diagram to illustrate the various relative sea level/accommodation curves at positions along a hangingwall fault block.

Figure 3.5. Derivation of the 3D subsidence curve.

Figure 3.6. Derivation of the 3D sedimentation curve.

Figure 3.7. 3D accommodation plot generated from the convolution of all three major controls.

Figure 3.8. 3D accommodation plot from Figure 3.7 with stacking patterns presented.

Figure 3.9. 3D accommodation plot from Figure 3.7 with systems tracts presented.

Figure 3.10. Diagrams with systems tracts presented to show the difference between two contrasting conceptual scenarios with a high sediment supply: a subsidence-dominated (top) and eustatic sea level-dominated (bottom) system.

Figure 3.11. Diagrams with stacking patterns presented to show the difference between two contrasting conceptual scenarios with a low sediment supply: a subsidence-dominated (top) and eustatic sea level-dominated (bottom) system.

Figure 3.12. Diagrams to show the variation in stacking patterns between three conceptual scenarios with different subsidence rate patterns.

Figure 3.13. Diagrams with systems tracts presented to show differences between three conceptual scenarios with different sedimentation distribution patterns along the fault length.

Chapter 4

Figure 4.1. Map of the study area on the southern side of the Gulf of Corinth, Greece.

Figure 4.2. The stratigraphic architecture of Kerinitis with UAV photogrammetry-based 3D outcrop model.

Figure 4.3. The stratigraphic architecture of Selinous with UAV photogrammetry-based 3D outcrop model.

Figure 4.4. Locations of detailed sedimentological studies at fan delta topset-foreset transitions.

Figure 4.5. Sedimentological details of Facies Associations 1-3.

Figure 4.6. Field photographs of FAs 4a and 4b.

Figure 4.7. Geometric position of shallow water bottomsets (FA4c).

Figure 4.8. Sketch and field photographs to present character of key surfaces at Kerinitis and Selinous.

Figure 4.9. Summary diagram of architectural stacking at both fan deltas in their respective positions along the P-M Fault, with trajectory analyses.

Figure 4.10. Input parameters for numerical model Syn-Strat, derived from field observations, and example outputs.

Figure 4.11. Results from numerical modelling sensitivity tests with Syn-Strat.

Figure 4.12. Along-strike graphical cross-section to show unit thickness decay extrapolation towards the western fault tip.

Chapter 5

Figure 5.1. Source-to-sink block model with interfan areas highlighted in alluvial, deltaic, and deepwater settings.

Figure 5.2. Location map of southern shore of the Gulf of Corinth with the Early-Middle Pleistocene Kerinitis and Selinous fan deltas highlighted.

Figure 5.3. 3D outcrop model showing the study area and data overview.

Figure 5.4. Methodology for stratigraphic architecture interpretation and for obtaining quantitative information from UAV photogrammetry-based 3D digital outcrop models.

Figure 5.5. Shallow water topset – upper shoreface facies association (FA 2b).

Figure 5.6. Representative bottomset logs from Localities L.X and L.VIII in Melissa valley (FA 4a).

Figure 5.7. Section 5 and Unit 8-9 fine-grained interval character at Locality IV.

Figure 5.8. A) Key stratigraphic observations of Section 2.

Figure 5.9. Stratigraphic framework of entire north-facing interfan cliff section (Sections 2-4).

Figure 5.10. Summary diagram of stratigraphic architecture of Kerinitis and Selinous fan deltas.

Figure 5.11. Interfan classification scheme, Types 1-3 in plan view and strike cross-section.

Figure 5.12. Typical evolution of an interfan through Types 1-3 with the progradation of two fan deltas.

Figure 5.13. Strike cross-section schematic diagram of the Early-Middle Pleistocene Kerinitis-Selinous interfan large-scale architecture.

Figure 5.14. The Kerinitis-Selinous interfan evolution.

Chapter 6

Figure 6.1. Study area location, NW Shelf, Australia.

Figure 6.2. Stratigraphy of the northern Carnarvon Basin.

Figure 6.3. Positions on the fault that are used for measuring fault throw, and headward and vertical erosion.

Figure 6.4. 3D capture of the Top Pre-Rift surface across the seismic dataset to reveal a series of normal fault blocks with degraded fault scarps.

Figure 6.5. Seismic cross-section to highlight the degraded fault scarp.

Figure 6.6. Methodology for volume balancing approach (V_{HW}/V_{FW}).

Figure 6.7. Approach for validating cell volume equivalency between the footwall and hangingwall intervals of interest.

Figure 6.8. Six NW-SE trending representative seismic sections along the fault are presented to show the stratigraphic framework.

Figure 6.9. Representative strike section (NE-SW) through the hangingwall stratigraphy with clean and interpreted seismic data.

Figure 6.10. Along-strike variability of footwall-derived fans.

Figure 6.11. Graphs to show results of the footwall analysis.

Figure 6.12. Block models to show the tectono-sedimentary evolution of the basin from Phases 1-4.

Chapter 7

Figure 7.1. Summary block model to present some of the main outcomes of the thesis that represent advances in the field of tectono-stratigraphy.

Figure 7.2. Diachroneity at different positions of a relative base level or accommodation curve.

Figure 7.3. Plot to show the offset in time (diachroneity) between points on an accommodation curve at the fault centre versus the fault tip.

Figure 7.4. Stratigraphic columns and cross-section outputs from Syn-Strat to demonstrate its utility, with stacking patterns presented.

Figure 7.5. Plots to show an example of the accommodation balance approach.

Figure 7.6. Scenario to show the utility of the accommodation balance approach using Syn-Strat.

List of Tables

Table 2.1. Examples of current sequence stratigraphic forward models.

Table 4.1. Summary of facies associations with geometric position and depositional environment interpretations.

Table 4.2. Quantitative field observations and control parameter derivations, with assigned uncertainty values (1-5).

Table 5.1. Facies associations at the Selinous and Kerinitis fan deltas (modified from Chapter 4).

Table 6.1. Seismic facies: example extracts, descriptions and interpretations.

Table 6.2. Stratigraphic framework: seismic unit descriptions.

Table 7.1. Matrix of outcomes for the accommodation balance.

List of Abbreviations

EFT = East fault tip

ELST = Early lowstand systems tract

FA = Facies association

HST = Highstand systems tract

K-S = Kerinitis-Selinous

LST = Lowstand systems tract

LLST = Late lowstand systems tract

MFS = Maximum flooding surface

P-M = Pirgaki-Mamoussia

SB = Sequence boundary

TS = Transgressive surface

TST = Transgressive systems tract

TFBP = Topset-foreset break point

UAV = Unmanned aerial vehicle

WFT = West fault tip

Contents

Chapter 1	1
1.1. Research Questions	2
1.1.1. Research Question 1	2
1.1.2. Research Question 2	7
1.1.3. Research Question 3	9
1.1.4. Research Question 4	10
1.2. Objectives	13
1.3. Approaches adopted in this study	15
1.3.1. Numerical modelling	15
1.3.2. Field data analysis.....	16
1.3.3. Subsurface data analysis	20
1.4. Study areas	21
1.4.1. Gulf of Corinth, Greece	21
1.4.2. Northern Carnarvon Basin, NW Shelf, Australia	25
1.5. Thesis outline	27
1.6. References	28
Chapter 2	39
2.1. Rift basins	40
2.1.1. Rift development	41
2.1.2. Normal faults	44
2.1.3. Tectono-stratigraphy	49
2.1.4. Tectono-sedimentary models	52
2.2. Sequence stratigraphy	58
2.2.1. History of sequence stratigraphy	58
2.2.2. Sequence stratigraphic terminology	59
2.2.3. Application of sequence stratigraphy	62
2.2.4. Sequence stratigraphic numerical modelling	65
2.2.5. Current challenges in sequence stratigraphic analysis	70
2.3. References	72
Chapter 3	89
3.1. Introduction	91
3.2. Model architecture and assumptions	93
3.2.1. Model framework	93
3.2.2. Eustatic sea level.....	96
3.2.3. Subsidence	98

3.2.4. Sedimentation.....	102
3.3. Model output results	106
3.3.1. 3D accommodation surface	106
3.3.2. Stacking patterns	107
3.3.3. Systems tracts.....	108
3.4. Discussion.....	110
3.4.1. Eustatic sea level- vs. subsidence-dominated successions	111
3.4.2. Sensitivity to varying subsidence rates.....	116
3.4.3. Sensitivity to varying sedimentation distribution	118
3.5. Implications and applications for subsurface appraisal.....	121
3.6. Conclusion	122
3.7. Acknowledgements.....	123
3.8. References.....	124
Chapter 4.....	129
4.1. Introduction.....	131
4.2. Tectono-stratigraphic framework.....	134
4.3. The Gilbert-type fan deltas	135
4.3.1. The Kerinitis fan delta.....	135
4.3.2. The Selinous fan delta	139
4.4. Methodology	139
4.4.1. Facies analysis.....	140
4.4.2. Trajectory analysis	140
4.4.3. Numerical modelling with Syn-Strat.....	141
4.5. Results.....	142
4.5.1. Sedimentary facies analysis.....	142
4.5.2. Key surfaces	149
4.5.3. Stratal stacking patterns	153
4.6. Quantification of controls	158
4.7. Reducing uncertainty of control parameters	163
4.7.1. Numerical modelling with Syn-Strat.....	163
4.7.2. Refinement of lake level change using unit thickness extrapolation method	169
4.8. Implications.....	170
4.8.1. Applications to other basins	170
4.8.2. Subsurface appraisal.....	171
4.8.3. Implications of a lake level change amplitude of 10-15 m.....	172
4.9. Conclusions.....	173

4.10. Acknowledgments	174
4.11. References	174
4.12. Appendix	180
Chapter 5	183
5.1. Introduction	185
5.2. Study area	188
5.3. Methodology	193
5.4. Results	194
5.4.1. K-S facies association characterisation.....	194
5.4.2. Stratigraphic architecture.....	203
5.4.3. Interfan end-members	215
5.5. Interpretation of the K-S interfan temporal evolution	219
5.5.1. Phase 1 (Unit set 1).....	220
5.5.2. Phase 2 (Unit set 2).....	221
5.5.3. Phase 3 (Unit set 3).....	222
5.5.4. Phase 4 (Unit set 4).....	223
5.5.5. Phase 5.....	224
5.6. Discussion	226
5.6.1. Style and classification of interfans	226
5.6.2. Asymmetry of fan deltas.....	227
5.6.3. Interfans as stratigraphic archives.....	229
5.7. Conclusions	230
5.8. Acknowledgements	231
5.9. References	231
5.10. Appendix I. Table A. Description of facies (modified from Barrett et al., 2019).....	237
5.11. Appendix II. Measured sections.	240
Chapter 6.....	242
6.1. Introduction	244
6.2. Study area	246
6.3. Geological context.....	248
6.4. Dataset.....	250
6.5. Methodology	251
6.5.1. Stratigraphic analysis (Steps 1-4)	251
6.5.2. Measuring footwall degradation (Steps 5-7).....	252
6.5.3. Volume balancing approach (Step 8).....	253
6.6. Results	259

6.6.1. Stratigraphic framework.....	259
6.6.2. Along-strike variability of hangingwall fans.....	272
6.6.3. Footwall analysis results.....	277
6.6.4. Volume balancing - V_{HW}/V_{FW}	279
6.7. Tectono-stratigraphic evolution.....	279
6.7.1. Phase 1 – Unit set 1.....	279
6.7.2. Phase 2 – Unit set 2.....	280
6.7.3. Phase 3 – Unit set 3.....	281
6.7.4. Phase 4 – Unit set 4.....	283
6.8. Discussion.....	283
6.8.1. Where are the footwall catchments?.....	284
6.8.2. Sediment sources in rift basins.....	287
6.9. Conclusion.....	288
6.10. Acknowledgements.....	289
6.11. References.....	290
Chapter 7.....	295
7.1. Research Question 1.....	296
7.1.1. Diachroneity of key surfaces.....	298
7.1.2. Stacking patterns.....	302
7.2. Research Question 2.....	304
7.3. Research Question 3.....	307
7.3.1. Quantitative data.....	308
7.3.2. Quantitative classification.....	308
7.3.3. Quantitative techniques.....	310
7.3.4. Quantitative modelling.....	310
7.4. Research Question 4.....	314
7.5. References.....	322
Chapter 8.....	329
8.1. Conclusions.....	330
8.2. Future work.....	332
Appendices.....	335
Appendix I – Input table for Syn-Strat. num = the reference value in the Syn-Strat script.....	336
Appendix II – Table of instructions for Syn-Strat.....	337
Appendix III – Syn-Strat script.....	342
Appendix IV - Marine and Petroleum Geology paper (Chapter 3)	
Appendix V - Basin Research paper (Chapter 4)	
Appendix VI - Depositional Record paper proof (Chapter 5)	

Chapter 1

Introduction

This chapter introduces the thesis by outlining the scientific questions addressed with this research and their rationale. It then provides a brief introduction to the approaches adopted in this study: numerical modelling, field and subsurface data analysis; and the two rift basins of focus, the Gulf of Corinth, Greece and northern Carnarvon Basin, NW Shelf, Australia. Detailed description of the methodologies and the geological background of the study areas are presented in each chapter. With a view to avoid repetition, here the contextual information is provided. Finally, an outline of the thesis is presented for guidance.

1.1. Research Questions

Rift basins preserve sedimentary records of climate history, fault evolution, palaeoecology and geological time and inherently, they are archives of continental break-up and Earth history. They store vast resources globally and as such, the ability to make stratigraphic predictions of syn-rift depositional systems are of commercial interest to hydrocarbon, water, and mineral industries. Sequence stratigraphy is a logical framework for the assessment of shallow marine strata through time, but is complicated in rift basins due to the complex and variable interactions between different allogenic controls acting across time and space. The aim of this thesis is to reduce uncertainty, and improve interpretations and predictions of shallow marine, syn-rift stratigraphy around normal fault blocks, by use of quantitative data and numerical techniques, with particular consideration of 3D variability. Novel approaches are introduced to tackle unresolved issues in the science of tectono- and sequence stratigraphy. As a result, the concept of the accommodation and sediment supply ratio as a tool for basin analysis in tectonically-active settings is challenged. Four research questions are posed and justified here, and are addressed across the data chapters to follow (Chapters 3, 4, 5 and 6). Each one is discussed in the discussion, Chapter 7.

1.1.1. Research Question 1

How can the stratigraphic approach be improved to account for architectural complexities arising from along-strike variability in allogenic controls?

Sequence stratigraphy is a chronostratigraphic framework that is used to relate strata, depositional systems and facies in time (Catuneanu, 2006). Commonly, this framework is used to predict strata in the dip direction, for example, a subaerial unconformity on the shelf that could indicate the presence of a lowstand prograding fan on the slope at a given time (Vail et al., 1977; Posamentier et al., 1988; Posamentier & Vail, 1988). However, along-strike variation in allogenic ('external') or autogenic ('internal') processes are less of a focus despite the likely inaccurate lateral prediction and that the framework could be unrepresentative of other positions along the margin (e.g. Madof et al., 2016; Jones et al., 2015; Poyatos-Moré et al., 2019). This is particularly

pertinent in rift basin-fills, where allogenic controls of tectonic movement and sedimentation vary significantly across different length-scales, rendering the ratio of accommodation to supply different at any given time and position (Ravnås & Steel, 1998; Gawthorpe et al., 1994; Gawthorpe & Leeder, 2000). The nature of stratigraphic stacking, and the style and diachroneity of key surfaces vary along-strike as a result of the combined influence of both controls (Gawthorpe et al., 2003; Burgess, 2016; Madof et al., 2016).

Considering a single fault segment, tectonic uplift of the footwall and subsidence of the hangingwall results in substantial across-fault variation in accommodation regime and slope angles (Jackson et al., 1988; Serck & Braathen, 2019), and hence depocentre depth and drainage evolution (Lambiase & Bosworth, 1995; Whittaker et al., 2010; Pechlivanidou et al., 2019). The hangingwall basin itself experiences considerable spatial variation in accommodation away from the fault as subsidence decreases towards the hinge, and along the fault as most strain is accommodated at the fault centre and decreases towards the fault tips (Walsh & Watterson, 1988; Dawers & Anders, 1995; Kim & Sanderson, 2005; Torabi et al., 2019). Further complications arise along-strike with the growth and interaction of fault segments (Cartwright et al., 1995; Cowie et al., 2000; Gawthorpe & Leeder, 2000; Nicol et al., 2016; Jackson et al., 2017; Rotevatn et al., 2018) and relay zones (Larson, 1988; Hemelsdaël & Ford, 2016; Fossen & Rotevatn, 2016; Childs et al., 2019) through time, which change the basin geometry, sediment transport path and position of sediment entry points to the basin.

In addition, sedimentation varies dependently and independently from tectonics across the basin and through time, and as a result, is the most difficult variable to constrain and predict (Burgess, 2016). Erosion rates from scarp degradation along a fault segment have been shown to be dependent on the displacement regime, with most erosion occurring towards the fault centre, and decaying towards the fault tips (Elliott et al., 2012; Bilal et al., 2018). Sediment supply from the hinterland will fluctuate through time with climate and substrate erodibility, and can enter the basin axially from the fault tips, or from the footwall or hangingwall dip slopes (Gawthorpe et al., 2000). This balance of accommodation to sediment supply influences the stacking patterns of

strata, whereby they are characterised by either progradation, retrogradation, aggradation (Van Wagoner et al., 1990) or degradation (Neal & Abreu, 2009; Neal et al., 2016). The relative influence and timing of multiple sedimentary systems across a basin in determining the balance of accommodation to sediment supply and the formation of key surfaces is relatively understudied (Fig. 1.1), with a focus on footwall-derived depositional systems (e.g. Dart et al., 1994; Rohais et al., 2007; Backert et al., 2010; Gobo et al., 2015), likely due to the prolificacy of the rift basins studied that generated these models. In Chapter 6, a well-imaged subsurface example of multiple sedimentary systems entering a hangingwall basin will be used to assess this balance, and how it changes as the basin evolves.

The style of sedimentation is dependent on water depth and process-regime, and will vary across a given marine or lacustrine basin (Leeder & Gawthorpe, 1987). Shoreface systems may arise towards the fault tips, where accommodation is low. Deltas build wherever there is a persistent fluvial sediment supply and space, and submarine fans and slope aprons will arise in areas of deeper water (Gawthorpe & Leeder, 2000). Each depositional system has its own potential record of time, as it is recorded in deposits or as surfaces, and its record can be reworked by dynamic processes and exposure, dependent on basinal position. The presence of sequence boundaries near fault tips and/or absence towards fault centres has been documented in a number of numerical modelling and field studies (Dart et al., 1994; Gawthorpe et al., 1994; 2003; Dorsey & Umhoefer, 2000; Hardy & Gawthorpe, 1998; Jackson et al., 2005; Backert et al., 2010). Key surfaces are often discussed and assumed to be time transgressive (Holbrook & Bhattacharya, 2012; Burgess & Prince, 2015; Hodgson et al., 2016; Madof et al., 2016), but there is yet to be a study that demonstrates the variation of diachroneity in different scenarios within a fault block or through time, or indeed quantification of diachroneity from field data (Fig. 1.1). In Chapter 3, along-strike variation in sedimentary stacking and diachroneity of key surfaces will be investigated through sensitivity tests of control interactions, with a novel, forward sequence stratigraphic model. Chapter 4 will continue this assessment with field data from onshore the Gulf of Corinth. The

model will be reintroduced as real data is input and the diachroneity of maximum flooding surfaces is quantified.

Considering a smaller area than the whole basin, confinement may cause depositional systems to converge and influence each-other in areas known as interfans (Hook et al., 2003; Bhiry & Occhietti, 2004; Leppard & Gawthorpe, 2006; Assine et al., 2015; Turner & Connell, 2018). Deltaic interfans may record a complementary or alternative record of basin history to their axial counterparts. However, their style, character and archive are missing from published conceptual models of tectono-sedimentary evolution (e.g. Gawthorpe & Leeder, 2000; Leeder et al., 2002) (Fig. 1.1). Chapter 5 will address this gap with an investigation of modern interfan geometries and a detailed quantitative analysis of an ancient, outcropping interfan onshore the Gulf of Corinth, Greece.

In summary, along-strike variability of tectonic displacement and sedimentation is inherent for any given rift basin and occurs across different scales, from the whole basin-, to fault segment- and depositional system-scale. How this manifests in terms of stacking patterns and nature of key surfaces has been addressed to some extent along fault segments (references herein), but some gaps persist, including a detailed and quantitative assessment of diachroneity of key surfaces, the along-strike interaction of multiple, spatially-distributed depositional systems and quantitative characterisation of along-strike variation in stratigraphic architecture (Fig. 1.1). These gaps will be addressed across Chapters 3-6.

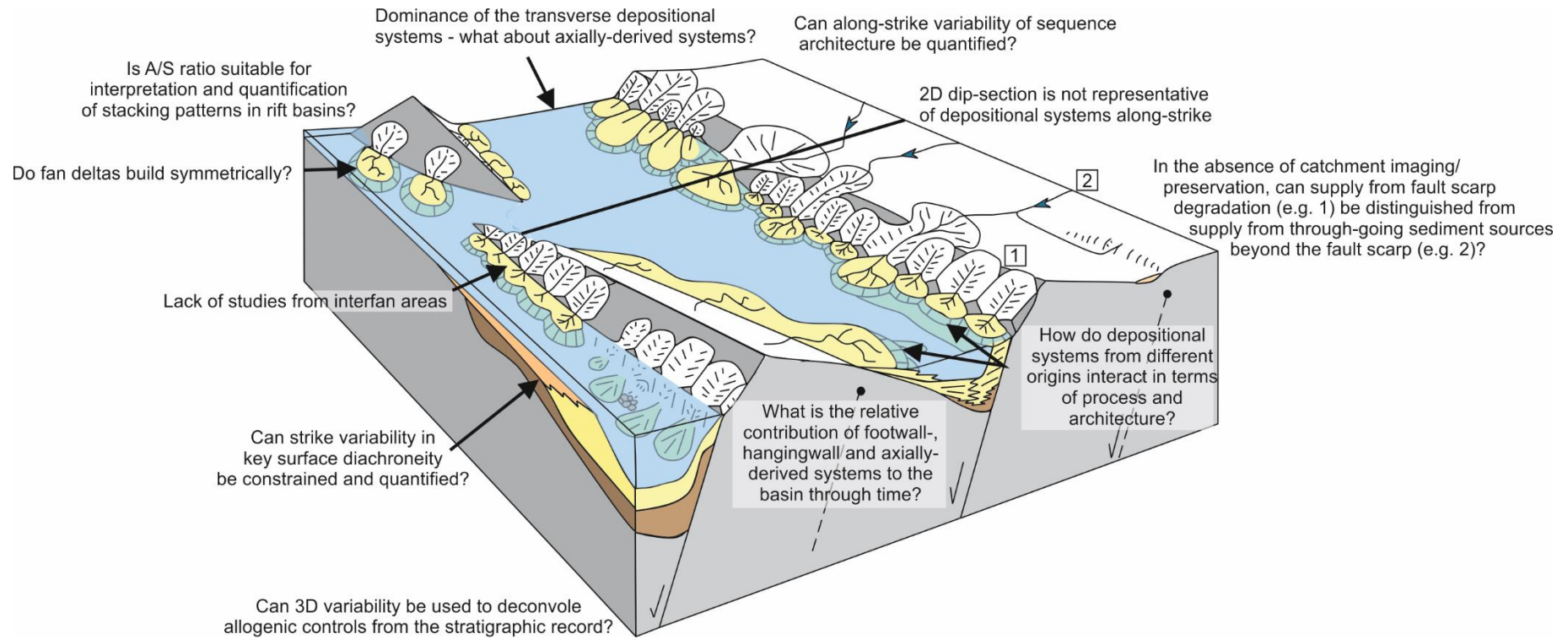


Figure 1.1. Block model to demonstrate current gaps and uncertainties in tectono-stratigraphy that will be addressed with this work. Modified from Gawthorpe & Leeder (2000).

1.1.2 Research Question 2

How can the signal of temporally- and spatially-variable allogenic controls be deconvolved from the depositional record of syn-rift basin-fills?

Original sequence stratigraphic models were founded upon base level forcing coastal migratory trends. The simplified cyclical base level curve was considered responsible for the observed cyclical stacking styles, and its predictability useful for interpretations (Posamentier et al., 1988; Posamentier & Vail, 1988). However, it is the combined influence of base level, tectonic and sedimentation variations that are responsible (Schlager, 1993), rendering prediction, particularly in tectonically-active basins more challenging.

Philip Allen likened a landscape response to “striking a chord”, whereby once perturbed by climatic and tectonic changes, a landscape “resonates with a range of frequencies” (Allen, 2005). In this analogy, each string of a guitar can be considered an individual control on the landscape. When struck together, they sound a response as a chord, which changes according to different fret positions. Just as a musician can listen to a piece of music and establish which chords have played, perhaps less romantically, geologists can look at the stratigraphic record and observe which stacking patterns have accumulated. The tricky part is then to establish which fret positions produced that chord. In the case of stratigraphy, was it high subsidence and low base level, or low subsidence and high base level? Did pulsed sedimentation or cyclic base level cause the vibrato bar? An enduring challenge in sequence stratigraphy is that multiple control combinations can generate similar stratigraphic geometries. Elucidating the individual forcings from the stratigraphic record therefore remains problematic.

Many studies promote accommodation change in their interpretations over sediment supply fluctuations (Van Wagoner et al., 1990; Plint & Nummedal, 2000; Neal & Abreu, 2009), but recent studies have attempted to address this balance by discussing, observing or modelling supply-driven cyclicity (Burgess, 2016; Schwartz et al., 2016; Zhang et al., 2018). Ultimately, an

accommodation curve is the tuned signal of tectonic movement, eustatic base level and sedimentation fluctuations. As such, a maximum flooding surface (on the rising limb of their combined signal) can occur as a result of an increasing base level rate and zero net subsidence, or increasing subsidence and zero net base level change. Similarly in the case of sequence boundaries (on the falling limb), the ‘text-book’ exhumed example for sequence stratigraphy, the Book Cliffs, has recently been re-addressed with an alternative interpretation (Pattison, 2018; 2019a;b). The Panther Tongue Formation, characterised by a distal sand body and absence of coastal plain was previously interpreted to represent a forced regression, and has since been interpreted as a sudden influx of sediment (Howell et al., 2018). ‘Non-unique solutions’ is the term coined for this problem (Heller et al., 1993; Flemings & Grotzinger, 1996; Burgess & Prince, 2015), which invokes the improbability of inverting the stratigraphic record to understand the specific controlling parameters (Burton et al., 1987). Heller et al. (1993) present ‘stratigraphic solution sets’ as a semi-quantitative approach to informing predictions. They explain that a range of values can be placed on the possible controls of a particular shoreline trajectory. The study does not present unique solutions, but provides a reasonable basis for interpretations. Cross & Lessenger (1999) use a combination of stratigraphic inverse and forward modelling to predict stratigraphic and geographic positions of reservoir and seals across a number of basins.

Computer modelling is an efficient way to simulate geological processes and their deposits across different timescales. As such, and with the possibility to test a number of input variables and outcomes, it is the technique that is closest to providing predictive capability. Referring back to the musical analogy, to find the fret combination of a particular chord, a musician will play different combinations to test which is most similar to what they heard. In Chapter 4, sensitivity tests will be undertaken with a numerical model to test which outcome most resembles the observations from the field. In the rationale for the previous research question, it is established that the along-strike influence of spatially-variable controls on stratigraphic architecture is considered in the literature, but is yet to be fully constrained (Fig. 1.1). For this question, a good

and quantitative constraint of along-strike variation will be exploited in Chapter 4 to invert the stratigraphic record, deconvolve and quantify the controlling parameters.

1.1.3. Research Question 3

What is the value of a quantitative approach to stratigraphic analysis?

“...when you can measure what you are speaking about, and express it in numbers, you know something about it; but when you cannot measure it, when you cannot express it in numbers, your knowledge is of a meagre and unsatisfactory kind...” (Kelvin, 1883).

Quantification of a subject or concept allows mathematical theories to be applied and the opportunity for a ‘superior’ analysis. Hubbard (1928) promoted the use of quantitative observations in Geology, which traditionally was not considered to be a numeric science. Today, Earth-system processes continue to be described mathematically across all scales, from the movement of particles along a surface (Le Roux, 2005) to the transfer of heat across the oceans (Rahmstorf, 2003). Stratigraphy seemed to be left behind with its musings of time, but since its fundamental application to mineral and energy exploration, stratigraphic concepts have become quantitative in the drive for successful prediction. Sequence stratigraphy is a logical framework that was built for that very purpose (Posamentier et al., 1988). Its true quantification however, is challenged by the complexity of sedimentary and structural processes that act in the same space across different timescales. Furthermore, different datasets yield information dependent on their resolution and spatial coverage, making a universal approach problematic. In the push for a quantitative approach to stratigraphic analysis (Fig. 1.1). we should consider four aspects: quantitative data, quantitative classification, quantitative techniques and quantitative modelling. Each of these will be utilised across the research presented here and their value will be discussed in Chapter 7.

1.1.4. Research Question 4

How should 'accommodation' be used in interpretations to incorporate the complexity observed in tectonically-active basins, and is the A/S ratio valid?

A well-established concept for understanding depositional system and shoreline migration, and therefore the nature of stratal unit stacking, is the interaction between the rate of accommodation change and the rate of sedimentation change (Sloss, 1962; Curray, 1964; Vail et al., 1977). Accommodation was defined as “the space made available for potential sediment accumulation” and represents relative base level change, incorporating eustatic base level change and tectonic subsidence (Jervey, 1988; Posamentier et al., 1988) and generally equates to depth from the water surface to the top of the depositional surface. The definition of accommodation was revised by Muto & Steel (2000) to “the thickness, measured at a specified site and time, of a space which becomes filled with sediments during a specified time interval”, which is equivalent to “realised accommodation” in Cross (1988) (Fig. 1.2). The original definition includes the clarification that it is “the level above which erosion will occur” (Jervey, 1988). This is important because it implies that further deposition or erosion will elevate or lower the depositional surface and will therefore decrease or increase accommodation. This notion seems to be overlooked in the subsequent literature that utilise the ratio of accommodation (A) to sedimentation (S), A/S (Van Wagoner et al., 1990; Thorne & Swift, 1992; Swift & Thorne, 1992; Neal & Abreu, 2009; Neal et al., 2016) whereby the two terms are considered independent variables, when strictly they are not independent at all (Muto & Steel, 2000). The terms progradation, retrogradation and aggradation were coined to describe the nature of sedimentary stacking in response to the interplay through time of sedimentation rate (δS) and accommodation creation rate (δA) ($\delta S/\delta A$) (Van Wagoner et al., 1990). The ratio was later reversed ($\delta A/\delta S$) (Thorne & Swift, 1992; Swift & Thorne, 1992) and degradation (Bull, 1991) was emphasised by Neal and Abreu (2009) and Neal et al. (2016) to represent scenarios where $\delta A/\delta S$ is <1 and decreasing. In essence, progradation and retrogradation represent a lateral migration of the shoreline and depositional system through time, and aggradation and degradation represent a vertical migration. It should be noted that it is the rate of

change of the parameter, and not the absolute value at a given time that is important for generating stacking patterns. However, a system can maintain a status of stasis (Tipper, 2015) if there is no change in the controlling parameters, or the balance of the controls over time cancels the effect to a state of equilibrium or continuity (Martinius et al., 2014).

Muto and Steel (1992; 1997; 2000) critique the $\delta A/\delta S$ ratio, and highlight the dimensional confusion of comparing units of ‘space’ with that of sediment supply rate. This dimensional confusion in the terminology of A/S can be eliminated if consistent units are utilised in any given system, e.g. volume over time in the same 3D space, or length over time in 1D (Muto & Steel, 2000). This implies that S is actually a ‘sedimentation’ rate (Van Wagoner et al., 1990; Neal & Abreu, 2009) in any given position and not a ‘sediment supply’ rate (Schlager, 1993; Martinius et al., 2014), because a given sediment supply rate at the basin entry point may not accumulate in one position and instead be bypassed downdip (Stevenson et al., 2015) or redistributed along-strike.

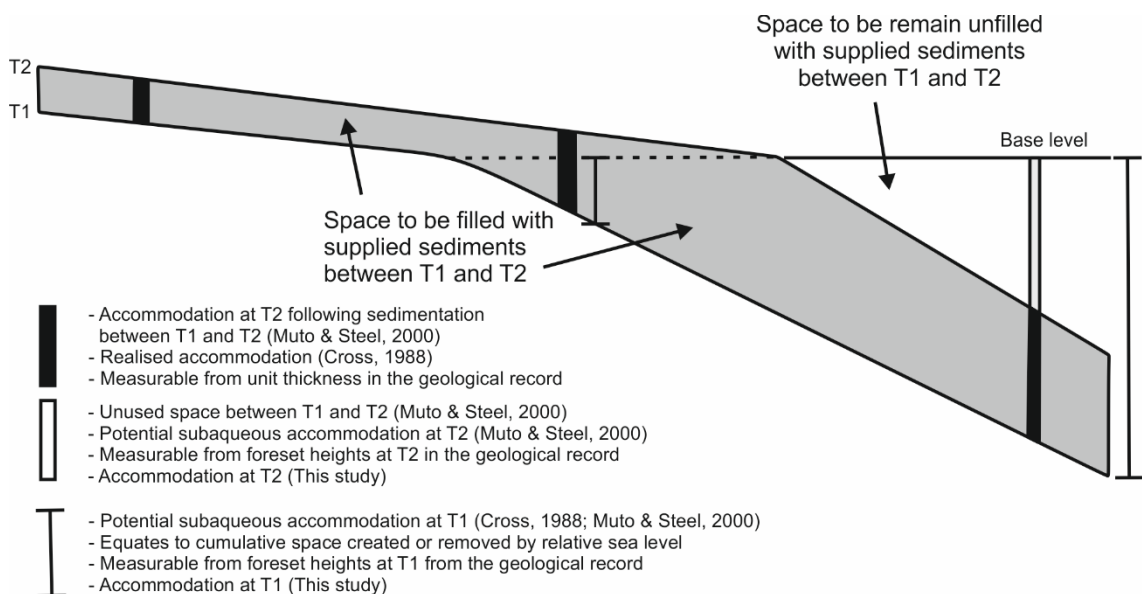


Figure 1.2. Figurative definitions of accommodation between time steps (T1 and T2). Modified from Muto & Steel (2000).

Neal & Abreu (2009) & Neal et al. (2016) advocate the use of A/S as an observation-based approach to building depositional frameworks for prediction. Indeed, stratal terminations, trajectory analysis (Helland-Hansen & Gjelberg, 1994; Helland-Hansen & Martinsen, 1996) and

identification of key stratal surfaces allow depositional sequences (Sloss et al., 1949) and stacking patterns to be identified, which are a useful and pragmatic approach to building a physical framework. However, the assignment of stacking patterns to the A/S ratio for control interpretations and prediction is problematic (Fig. 1.1). Three critical issues with the A/S ratio in its current usage are identified herein:

1. Sedimentation inherently reduces accommodation. If one considers a dynamic system where controls act on a basin over a number of time steps, with all else equal, deposition during one time step reduces the space available for deposition in the next time step. The two variables are therefore not independent, which is problematic if the ratio should incorporate two terms influencing a depositional system equally.
2. Erosion is not considered, yet is an important mechanism for creating space for deposition in a number of settings. The scale of incision can be of magnitudes comparable to other allogenic controls (Backert et al., 2010; Gomis-Cartesio et al., 2017).
3. Geological feedbacks occur between various control mechanisms. For example, sedimentation can vary with climate-induced base level changes (Collier, 1990; Collier et al., 2000), or tectonic displacement (Elliott et al. 2012; Bilal et al., 2018).

Numerical and flume-tank modelling experiments omit the latter problem, as inputs are constrained and controlled. However, it is an unescapable consideration and problem with control interpretations from the geological record. In regard to the first two problems, improvements in this framework are possible and addressed with this work. There is a necessity to establish a framework that incorporates all allogenic controls, including those that reduce space, as well as all of those that create space, and also one that incorporates all stratigraphic outcomes. Such a framework is in mind with the building of the stratigraphic forward model 'Syn-Strat' (Chapters 3 and 4) and this subject is discussed and addressed in Chapter 7.4.

1.2. Objectives

To address the research questions, four data analysis chapters are presented. Each chapter contributes to all of the research questions. The specific objectives of each are outlined below:

Chapter 3

1. Build a 3D sequence stratigraphic geometric forward model that can simulate the interaction of all three allogenic controls in time and space around a fault segment.
2. Test various hypothetical scenarios of allogenic controls in the hangingwall of a normal fault and compare their outcomes of architectural stacking and key surface diachroneity, specifically: i) vary the relative contribution of eustatic base level and tectonic subsidence; ii) vary the subsidence regime through time; and iii) vary the sedimentation distribution along-strike.

Chapter 4

3. Collect field data from two syn-rift fan deltas (Selinous and Kerinitis) onshore, Gulf of Corinth, Greece and build 3D outcrop models for quantitative analysis in Agisoft and LIME software.
4. Use field observations, facies, key surface and trajectory analysis to build a stratigraphic framework.
5. Use the along-strike variation in stratigraphic architecture to quantify allogenic controls acting on delta evolution, where possible. Assign uncertainty values from 1 (low) to 5 (high) to each potential control.
6. Input the interpreted control parameters into Syn-Strat to test the least certain parameter/s (base level change amplitude).
7. Undertake an independent unit thickness extrapolation technique to validate numerical modelling outputs.

Chapter 5

8. Investigate the potential stratigraphic record that interfan areas between fan deltas present.
9. Propose a quantitative classification scheme for deltaic interfans based on modern delta geometries and apply it to the ancient Selinous-Kerinitis fan delta system.
10. Assess the larger-scale tectonic basinal change from net subsidence to net uplift using interfan architectures.
11. Constrain the along-strike variation in the interfan and consider the implications of and controls on asymmetric growth of fan deltas in hangingwall fault blocks.

Chapter 6

12. Identify and map seismic facies and key surfaces in and around a single fault segment in the northern Carnarvon Basin, NW Shelf, Australia.
13. Interpret the stratigraphic framework and assess the relative contribution and timing of various sedimentary inputs.
14. Map and undertake geometrical modelling of footwall-derived fans for volume calculation.
15. Measure displacement, headward and vertical erosion along the footwall of the fault and calculate bulk volume of eroded material.
16. Undertake a novel volume balancing approach using a ratio of hangingwall fill to footwall erosion, to identify the position of fixed, through-going sedimentary inputs from beyond the fault scarp.
17. Revise interpretation of basin evolution based on the subsurface quantitative analysis.

1.3. Approaches adopted in this study

The broad approaches adopted in this study and their rationale are presented in this section. Detailed descriptions of the methodology used for each chapter can be found therein in Chapters 3-6.

1.3.1. Numerical modelling

In this study, a novel 3D sequence stratigraphic model is developed and introduced, called ‘Syn-Strat’. It is a geometric model that produces a 3D graphical surface of accommodation. Although its utility extends to footwall uplift, here we use it to model accommodation in the hangingwall of normal faults. It constructs the 3D surface by combining 1D curves of sedimentation, tectonic subsidence and base level, in time and space (away from and along the fault). Essentially, it produces a 3D construction of multiple relative sea level curves along a fault (Gawthorpe et al., 1994), with the addition of sedimentation curves to represent accommodation that changes through time. Accommodation is defined as the space available for deposition between the water surface and the top depositional surface (*in sensu* Jervey, 1988). The depositional surface changes through time as sediment is deposited, so sedimentation is an important contribution to accommodation. Accommodation can be plotted in two of three dimensions; in time, along the fault and/or away from the fault. For the studies presented here, accommodation is plotted in time, along the fault for a given distance away from the fault. Stacking patterns, or systems tracts, of a given sequence stratigraphic scheme can then be applied to the surface with colour. In the system tracts mode, it presents key stratigraphic surfaces (e.g. sequence boundaries and maximum flooding surfaces) and shows how they vary in time and space. The model is useful because it allows any combination of input parameters (hypothetical or from real data), can compute multiple tests in a short timeframe and produces 3D representation of data. It is therefore ideal for undertaking sensitivity tests of sequence architecture in rift basins, where allogenic controls are highly variable in time and space.

The model input tables can be found in Appendix I and II and the model script can be found in Appendix III. In Chapter 3, the model set-up will be introduced and some of its versatility demonstrated through sensitivity tests, tied to field examples (Alkyonides Gulf, Greece and Loreto Basin, Gulf of California). A number of control scenarios will be tested, including different relative control magnitudes, subsidence rate regimes and sedimentation distribution models. In Chapter 4, real data from outcropping syn-rift fan deltas, onshore the Gulf of Corinth, Greece will be input into the model and used to reduce uncertainty of control parameter estimates.

1.3.2. Field data analysis

A total of six weeks of fieldwork was spent in northern Peloponnesus, Greece (onshore Gulf of Corinth, Greece) for data collection, between 2016 and 2018 (Fig. 1.3). Two field seasons were spent primarily collecting sedimentological and stratigraphic data (e.g. sedimentary logs, palaeocurrents measurements, bedding and structural dip measurements, field sketches, photographs and annotated photo panels) to undertake facies and trajectory analysis of the two fan deltas studied (presented in Chapters 4 and 5). Two field seasons were undertaken with the purpose of collecting UAV photogrammetry data using Mavic Pro and DJI Phantom Pro 3 drones in order to build 3D outcrop models for analysis. A 3D outcrop model is a virtual replica of an outcrop and can be used to provide supplementation to field observations (Xu et al., 2000; Trinks et al., 2005; Hodgetts et al., 2013). It is a useful tool for analysis because the technique increases spatial coverage, geometric and locational accuracy and decreases biasing from ground-based perspective. The photogrammetric method is an alternative to LIDAR (Light Detection and Ranging) techniques, with lower costs, easier transport and better resolution of geological detail on vertical slopes (Nesbit et al., 2018).

3D outcrop models were built by compiling several hundred 2D photographs across a scene and using feature detection and matching algorithms for their relative positioning, in Agisoft Photoscan software (Westoby et al., 2012; Nesbit et al., 2018). A simplified workflow for building the outcrop models with examples from the field area is presented in Figure 1.4. Interpretation of the 3D outcrop models was undertaken using LIME software, which was found to enable more

versatility than Agisoft Photoscan for horizon picking, plane projection and bedding dip measurements. The photogrammetric data was used for assessment of detailed stratal geometries, the nature of major surfaces and for accurate correlation of units and surfaces around topography. This was particularly useful as much of the exposure is inaccessible and hence, it greatly assisted in the development of a stratigraphic framework. Critically, the 3D outcrop models allowed quantitative analysis of the fan deltas to augment the field observations. Dip data from bedding planes, stratigraphic thicknesses, topset-foreset breakpoint trajectories and foreset heights could all be collected from the models. Figurative examples of this approach are presented in Chapter 5. Resolution of the outcrop models varies depending upon the scale and acquisition of the data. Models that focussed on detailed areas could resolve individual beds and cobbles to a lower limit of approximately 10 cm, in agreement with other studies (Nieminski & Graham, 2017; Nesbit et al., 2018). Larger models with greater spatial coverage, aiming to capture larger-scale relationships and landscapes have a lower resolution (~1 m) to optimise processing time. Locational accuracy of the model is dependent upon the accuracy of the in-built GPS on the UAV.



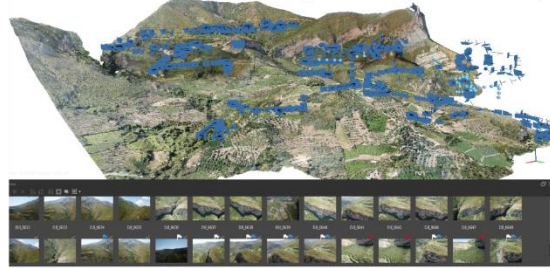
Figure 1.3. Representative photographs from fieldwork in northern Peloponnesus, onshore the Gulf of Corinth, Greece.

3D model building workflow Agisoft Photoscan

1. Import photographs

Sort photos to remove those with poor lighting and those that are repeated to optimise processing time and achieve best quality model.

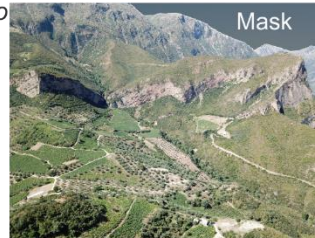
Photo selection and camera positions (blue frames)



2. Mask photographs

Manually select areas of sky or poor quality in each photo to reduce number of tie points in unwanted areas. This improves the quality of the model and speeds up processing time.

Masked photo



3. Align photographs

Use the 'Align' workflow in Agisoft and select 'High accuracy' to generate a sparse tie point cloud.

Sparse point cloud



4. Optimise tie point cloud and re-align photos

Manual and automated removal of erroneous or high uncertainty tie points. After each iteration, optimise the cameras to re-align with the reduced set of tie points.

Dense point cloud



5. Build dense point cloud

Repeat stage 4 for further improvement to the quality of the model.

6. Build mesh

Build mesh from dense point cloud and interpolate - fills holes between tie points.

Textured model

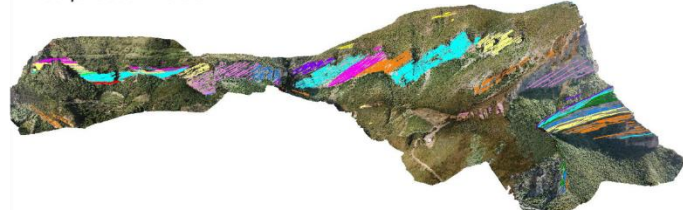


7. Build model texture

Choose best quality images for the texture to create a photorealistic surface.

8. Export model or interpret in Agisoft Photoscan

Interpreted model in LIME



9. Import model into LIME for interpretation

Figure 1.4. Workflow adopted to build 3D outcrop models from UAV-photogrammetry in Agisoft Photoscan software, and quantitative data collection in LIME.

In Chapters 4 and 5, field data and 3D outcrop models will be analysed in order to constrain the along-strike variation in stratigraphic architecture between two fan deltas, Kerinitis and Selinous. In Chapter 4, the along-strike variability will be used to estimate quantitative allogenic control parameters, which will be improved with numerical modelling and validated using a unit thickness extrapolation technique. Chapter 5 presents the quantitative analysis of 3D outcrop models of the interfan area between the fan deltas. Interfan analysis is promoted, with a demonstration of how the architecture of the ancient Selinous-Kerinitis interfan can be used to infer basin evolution.

1.3.3. Subsurface data analysis

A public subsurface dataset from the Australian government agency, Geoscience Australia was used for analysis of tectono-sedimentary interactions (Fig. 1.5). A series of normal fault blocks in the northern Carnarvon Basin, Exmouth Plateau, NW Shelf are imaged in a full angle PSTM (Pre-Stack Time Migrated) processed 3D seismic dataset, HEX07B, originally acquired in 2007 by BHP Billiton. The Thebe-1 exploration well and Thebe-2 appraisal well that sit ~20 km apart and penetrate the footwalls of two adjacent fault segments within the survey area, encountered significant gas discoveries in 2007/2008 (2-3Tcf gas in place; Williams, 2018), within the Mid-Late Triassic fluvio-deltaic Mungaroo Formation. Using a map of the Top Pre-Rift surface (Top Mungaroo Fm.), the most north-western fault in the volume was selected for analysis due to the well data (Thebe-2) available in its footwall for age constraint and correlation, and because almost the entire fault length (~21 km) is seismically-imaged. In addition, the data provides good resolution of a range of reflectivity patterns indicative of different depositional styles and clear degradation of the footwall crest.

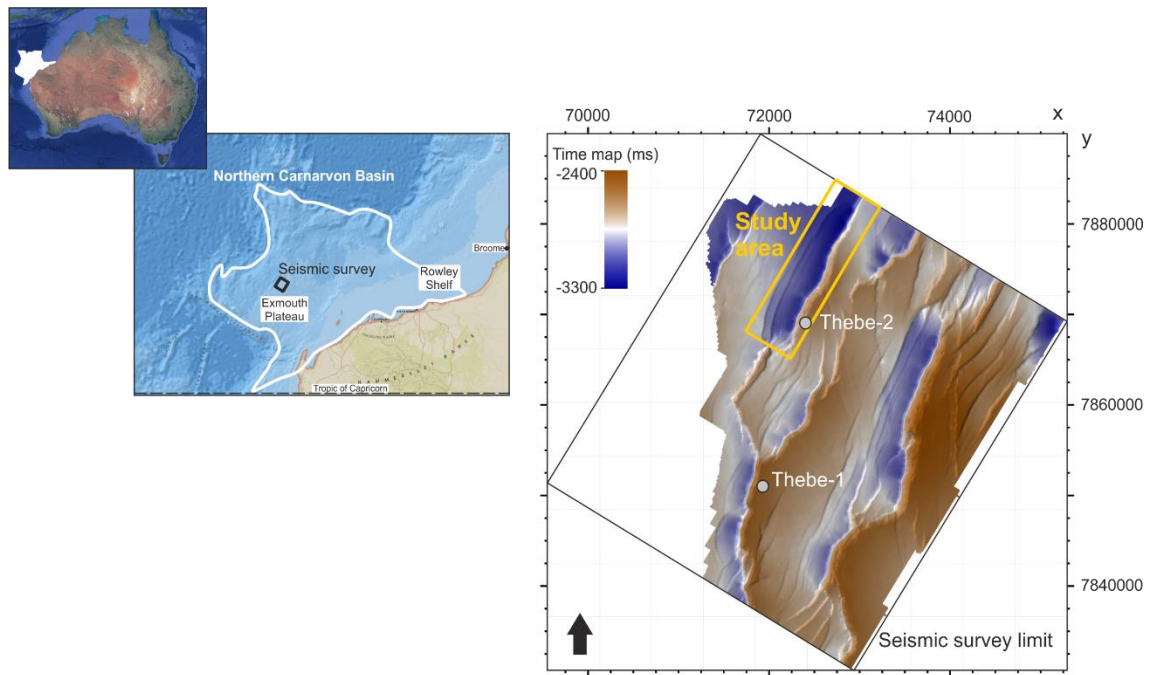


Figure 1.5. Map of the subsurface dataset location, northern Carnarvon Basin, NW Shelf, Australia.

1.4. Study areas

In this study, analysis is focussed upon two rift basins: the modern (Miocene-present), Gulf of Corinth basin, Greece and the subsurface, Early-Middle Jurassic, Northern Carnarvon Basin, NW Shelf, Australia. Further detail can be found in the introductory sections of their associated Chapters 4-6.

1.4.1. Gulf of Corinth, Greece

The Gulf of Corinth, Greece (Fig. 1.6) has attracted a wealth of research as a world-class, modern field example of a lacustrine-marine rift basin. It presents the opportunity to study fault evolution and large-scale rifting mechanics and architecture (Armijo et al., 1996; Avallone et al., 2004; McNeill et al., 2005; Bell et al., 2008; 2009; 2011; Taylor et al., 2011; Vasilakis et al., 2011; Hemelsdaël & Ford, 2016; Nixon et al., 2016; De Gelder et al., 2019), seismicity and geohazard prediction (Doutsos & Poulimenos, 1992; Pantosti et al., 1996; Briole et al., 2000; Stefatos et al., 2002; Bernard et al., 2006; De Barros et al., 2017; Mesimeri & Karakostas, 2018), drainage catchment and source-to-sink evolution (Leeder & Jackson, 1993; Eliet & Gawthorpe, 1995;

Duffy et al., 2014; Watkins et al., 2018; Pechlivanidou et al., 2017; 2019), and the interaction of syn-rift tectonics, climate and sedimentation (Leeder & Gawthorpe, 1987; Collier, 1990; Collier & Dart, 1991; Dart et al., 1994; Gawthorpe et al., 1994; 2003; 2017; 2018; Leeder et al., 1998; 2002; Ford et al., 2007; 2013; 2016; Backert et al., 2010; Gobo et al., 2015). It is a rare example that offers analysis of dip and strike transects from source-to-sink using a swath of geological techniques. Outcrop, geomorphology, bathymetry and seismic data allow the study of the basin evolution from the Miocene to the present-day. The longer term geodynamic and palaeographic context of the rift, and the history of Aegean extension since the Eocene, are reviewed in Van Hinsbergen & Schmid (2012) and papers therein.

The Gulf of Corinth accommodates the ~E-W trending rift axis of the Corinth Rift, which is a rapidly-opening, seismically-active graben, connecting the strike-slip North Anatolian Fault in the north-east to the Kefalonia Fault in the south-west. It forms part of the northern margin of the Aegean microplate that is migrating southwards due to subduction at the Hellenic Trench (Fig. 1.6A; Taylor et al., 2011; Vassilakis et al., 2011). Investigations of the deep structure have shown that with substantial inherited topography from the Parnassos and Pindos nappe stacks and crustal thickness variations along the Corinth Rift, its crustal geometry is more complex than the pure and simple shear end-members for rift development (Zelt et al., 2005; Taylor et al., 2011).

On the southern flank of the rift, there is a 30 km wide early rift zone (Fig. 1.6B), which comprises a series of exhumed, rotated and uplifted fault blocks, exposing up to 2.8 km of syn-rift stratigraphy (Gawthorpe et al., 2018). Active faults define the modern coastline and have uplifted the previous Pleistocene depositional systems in their footwalls, presenting spectacular exposures of syn-rift fan deltas in the incised valleys. The focus of this study is two Early-Middle Pleistocene syn-rift fan deltas in the hangingwall of the Pirgaki-Mamoussia Fault. The Kerinitis fan delta (Ori et al., 1991; Dart et al., 1994; Backert et al., 2010) is positioned near the fault centre, 6 km along-strike from the Selinous fan delta that sits near the western fault tip. The rivers that fed these ancient systems later cut through their own deposits, fed Late Pleistocene fan deltas that are now submerged under the gulf and imaged in bathymetry data (Fig. 1.6C; McNeill et al., 2005), and

continue to feed the modern fan deltas that prograde from the coast. The excellent exposure of dip and strike sections of the two contrasting fan deltas along the same fault segment presents an ideal field laboratory to explore basin controls and attempt quantitative analysis. Furthermore, the Late Pleistocene and modern fan deltas that are fed from the same catchments are highly analogous to their ancient counterparts and allow us to witness first-hand the sedimentary processes in action.

A prolonged attraction of the Gulf of Corinth is its ancient exhumed, tectonically-influenced shallow and deep marine depositional systems that are highly analogous to a number of hydrocarbon plays (Wood et al., 2015), e.g. the Brae Play, including the ‘T-’ and ‘Tree’ Fields (Turner & Cronin, 2018, and papers therein) and the recently discovered Pil and Bue (Fenja) Fields (operated by Neptune Energy) in the Norwegian, northern North Sea. It therefore presents an opportunity to understand sediment routing (for exploration) and reservoir quality (for production) of an appropriate analogue system. A renewed interest in the Gulf of Corinth is being driven by understanding sedimentary responses to climate fluctuations. In 2017, IODP Expedition 381 drilled three sites in the gulf, and four onshore wells were drilled in northern Peloponnesus by the Syn-Rifts Project (lead by the University of Bergen). Publications and data from these projects are becoming available (McNeill et al., 2018; 2019; Shillington et al., 2019).

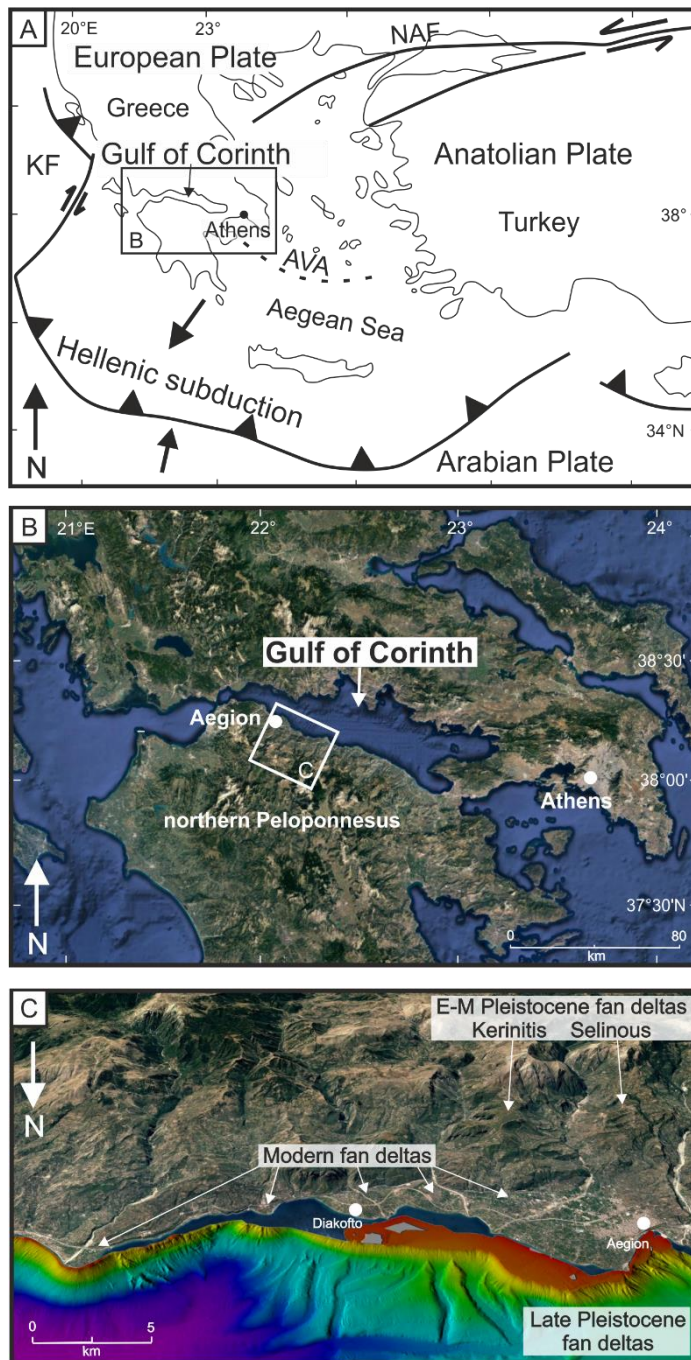


Figure 1.6. The Gulf of Corinth, Greece study area. A) Aegean regional tectonic map showing plates and plate boundaries responsible for the Corinth Rift, Greece. Black box shows position of 'B'. AVA = Aegean Volcanic Arc; NAF = North Anatolian Fault; KF = Kefalonia Fault (modified from Ford et al., 2016). B) Gulf of Corinth regional map from Google Earth. White box shows position of 'C'. C) 3D perspective image of the south-western coast of the Gulf of Corinth, highlighting the juxtaposition of the Early-Middle (E-M) Pleistocene, Late Pleistocene and modern fan deltas. Topography from Google Earth; bathymetry from McNeill et al. (2005).

1.4.2. Northern Carnarvon Basin, NW Shelf, Australia

The northern Carnarvon Basin (Palaeozoic to recent) is a mainly offshore, deep-water basin (800-3000 m) on the NW Shelf of Australia that contains <15 km of sedimentary stratigraphy of Mesozoic-Cenozoic age. The NW Shelf is Australia's principal hydrocarbon province with over 700 exploration wells drilled since 1953. The reservoirs sit in Upper Triassic-Lower Cretaceous formations dominated by siliciclastic fluvial to marine successions and are compartmentalised in NE-trending sub-basins that developed during Late Triassic-Late Jurassic rifting.

The break-up of Gondwanaland resulted in multiple phases of rifting that impacted the development of the NW Shelf, which culminated in Mesozoic rifting that disintegrated Argoland and Greater India and created oceanic abyssal plains (Veevers, 1988; Longley et al., 2002). The northern Carnarvon basin is found on the southern margin of the NW Shelf, and is bounded by the Roebuck and Canning Basins to the north-east, the southern Carnarvon Basin to the south, and the Argo, Gascoyne and Cuvier Abyssal Plains to the north and west. It formed between the Callovian to Oxfordian as continental break-up on the north-eastern margin of Gondwana released the West Burma and Argo microplate from Australia (Fig. 1.7). Seafloor spreading during this time resulted in the final development phase of the ancient Tethys Ocean, of which its last in situ remnants can be found in the Argo Abyssal Plain between the NW Shelf and the Java Trench (Jablonski, 1997; Stagg et al., 1999; Heine & Müller, 2005). Mutter & Larson (1989) propose a hybrid model of pure and simple shear to account for the rift development. Initial deformation was dominated by simple shear, with an eastward dipping detachment (Driscoll & Karner, 1998), and later and wider extension resulted from pure shear (Mutter & Larson, 1989). Various ages from Late Triassic (Bradshaw et al., 1998; Jitmahantakul & McClay, 2013; Gartrell et al., 2016) to Early Jurassic (Etheridge & O'Brien, 1994; Tindale et al., 1988; Longley et al., 2002; Marshall & Lang, 2013) for the onset of Mesozoic rifting have been proposed for the northern Carnarvon Basin, mainly dependent on the study area of focus. Tectonic activity had largely ceased by the Early Cretaceous, and carbonate replaced siliciclastic deposition during the Late Cretaceous as ocean circulation patterns changed following the break-up of Gondwana (Hocking, 1988).

The fault block accommodating the Thebe-2 appraisal well was chosen for analysis in this study (Fig. 1.5). A range of reflectivity patterns indicative of different depositional styles and clear degradation of the footwall crest makes the fault segment an interesting example of competing sedimentary inputs and a good candidate for making footwall-hangingwall stratigraphic associations. Clinoformal geometries dipping away from the fault are resolved in the data and highly resemble field examples studied in the Gulf of Corinth, Greece, making this area an ideal case study for comparison.

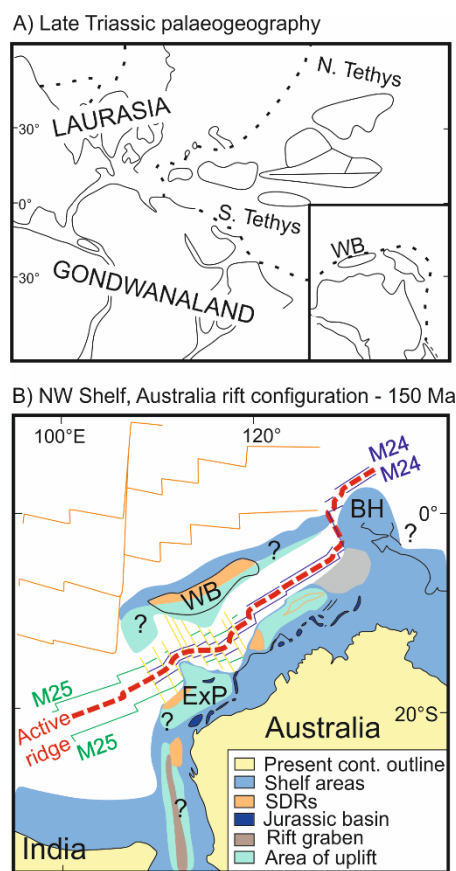


Figure 1.7. A) Palaeogeographic map showing the configuration of Australia with respect to the Gondwanaland supercontinent during the Late Triassic, prior to rifting (modified from Metcalfe, 1991). B) Palaeogeographic reconstruction of the NW Shelf at 150 Ma. Australia is fixed in its present-day coordinates (modified from Heine & Müller, 2005). Abbreviations: WB = West Burma; Exp = Exmouth Plateau; BH = Bird's Head. M25 and M24 indicate magnetic anomaly isochrons (geo-magnetic timeline from Gradstein et al., 1994).

1.5. Thesis outline

This thesis comprises eight chapters. Chapter 1 introduces the thesis by presenting the research questions to be addressed, the objectives, approaches and study areas. Chapter 2 presents the research context in terms of the broader literature, specifically focusing upon rift basins and sequence stratigraphy. Chapters 3, 4, 5 and 6 represent four scientific papers that have been or are intended to be submitted to international journals for publication. At the time of thesis submission, Chapter 3 has been published in *Marine and Petroleum Geology*, Chapter 4 has been published in *Basin Research* and Chapter 5 is published in *The Depositional Record*. Typset versions of the published papers are included in the Appendix IV, V and VI. Chapter 6 is prepared for submission. Chapter 7 is the discussion that draws from results of the preceding chapters to discuss and answer the four research questions posed in Chapter 1. Finally, Chapter 8 includes a concise conclusion and suggestions for future work

Data chapters' status and publication reference:

Chapter 3 - Published

Barrett, B.J., Hodgson, D.M., Collier, R.E.LI. & Dorrell, R.M. (2018). Novel 3D sequence stratigraphic numerical model for syn-rift basins: analysing architectural responses to eustasy, sedimentation and tectonics. *Marine and Petroleum Geology*, 92, 270-284.

Chapter 4 - Published

Barrett, B.J., Collier, R.E.LI., Hodgson, D.M., Gawthorpe, R.L., Dorrell, R.M. & Cullen, T.M. (2019). Quantifying faulting and base level controls on syn-rift sedimentation using stratigraphic architectures of coeval, adjacent Early-Middle Pleistocene fan deltas in Lake Corinth, Greece. *Basin Research*, doi: 10.1111/bre.12356.

Chapter 5 – Published

Barrett, B.J., Gawthorpe, R.L., Collier, R.E.Ll., Hodgson, D.M. & Cullen, T.M. (2019). Syn-rift delta interfan successions: archives of sedimentation and basin evolution. *The Depositional Record*, doi: 10.1002/dep2.95.

Chapter 6 – Prepared for submission

Barrett, B.J., Hodgson, D.M. & Collier, R.E.Ll. (Prepared for submission). Geometric and volumetric analysis of footwall degradation and hangingwall architecture, northern Carnarvon Basin, NW Shelf, Australia.

1.6. References

Allen, P. (2005). Striking a chord. *Nature*, 434, 961.

Armijo, R., Meyer, B., King, G.C.P., Rigo, A. & Papanastassiou, D. (1996). Quaternary evolution of the Corinth Rift and its implications for the Late Cenozoic evolution of the Aegean. *Geophysical Journal International*, 126, 11-53.

Assine, M.L., Renato Merino, E., Do Nascimento Pupin, F., De Azevedo Macedo, H. & Guerreiro Martinho Dos Santos, M. (2015). The Quaternary alluvial systems tract of the Pantanal Basin, Brazil. *Brazilian Journal of Geology*, 45, 475-489.

Avallone, A., Briole, P., Agatza- Balodimou, A.M., Billiris, H., Charade, O., Mitsakaki, C., Nercessian, A., Papazissi, K., Paradissis, D. & Veis, G. (2004). Analysis of eleven years of deformation measured by GPS in the Corinth Rift Laboratory area. *Comptes Rendus Geoscience*, 336, 301-311.

Backert, N., Ford, M. & Malartre, F. (2010). Architecture and sedimentology of the Kerinitis Gilbert-type fan delta, Corinth Rift, Greece. *Sedimentology*, 57, 543-586.

Bell, R.E., Duclaux, G., Nixon, C.W., Gawthorpe, R.L. & McNeill, L.C. (2017). High-angle, not low-angle, normal faults dominate early rift extension in the Corinth Rift, central Greece. *Geology*, 46, 115-118.

Bell, R.E., McNeill, L.C., Bull, J.M. & Henstock, T.J. (2008). Fault architecture, basin evolution and evolution of the Gulf of Corinth Rift, central Greece. *Basin Research*, 21, 824-855.

Bell, R.E., McNeill, L.C., Bull, J.M. & Henstock, T.J. (2009). Evolution of the offshore western Gulf of Corinth. *Geol. Soc. Am. Bull.*, 120, 156-178.

Bell, R.E., McNeill, L.C., Henstock, T.J. & Bull, J.M. (2011). Comparing extension on multiple time and depth scales in the Corinth Rift, Central Greece. *Geophysical Journal International*, 186, 463-470.

Bernard, P., Lyon, H., Briole, P., Deschamps, A., Boudin, F., Makropoulos, K., Papadimitriou, P., Lemeille, F., Patau, G., Billiris, H., Paradissis, P., Papazissi, K., Castarède, H., Charade, O., Nercessian, A., Avallone, A., Pacchiani, F., Zahradnik, J., Sacks, S. & Linde, A. (2006). Seismicity, deformation and seismic hazard

in the western rift of Corinth: New insights from the Corinth Rift Laboratory (CRL). *Tectonophysics*, 426, 7-30.

Bhiry, N. & Occhietti, S. (2004). Fluvial sedimentation in a semi-arid region: the fan and interfan system of the Middle Souss Valley, Morocco. *Proceedings of the Geologists' Association*, 115, 313-324.

Bilal, A., McClay, K. & Scarselli, N. (2018). Fault-scarp degradation in the central Exmouth Plateau North West Shelf, Australia. In: K.R. McClay & J.A. Hammerstein (Eds.), *Passive margins: tectonics, sedimentation and magmatism*. Geological Society, London, Special Publications, 476.

Bradshaw, J., Sayers, J., Bradshaw, M., Kneale, R., Ford, C., Spencer, I. & Lisk, M. (1998). Paleogeography and its impact on the petroleum systems of the North West Shelf, Australia. In: P.G. Purcell & R.R. Purcell (Eds.), *The North West Shelf, Australia: Proceedings of Petroleum Exploration Society of Australia Symposium*. PESA, Perth, 651pp.

Briole, P., Rigo, A., Lyon- Caen, H., Ruegg, J.C., Papazissi, K., Mitsakaki, C., Balodimou, A., Veis, G., Hatzfeld, D. & Deschamps, A. (2000). Active deformation of the Corinth rift, Greece: results from repeated Global Positioning System surveys between 1990 and 1995. *Journal of Geophysical Research*, 105, 25605-25625.

Bull, W.B. (1991). *Geomorphic Responses to Climatic Change*. Oxford University Press, London, 312pp.

Burgess, P.M. (2016). The future of the sequence stratigraphy paradigm: Dealing with a variable third dimension. *Geology*, 44, 335-336.

Burgess, P.M. & Prince, G.D. (2015). Non-unique stratal geometries: Implications for sequence stratigraphic interpretations. *Basin Research*, 27, 351-365.

Burton, R., Kendall, C.G.S.C. & Lerchie, I. (1987). Out of our depth: on the impossibility of fathoming eustasy from the stratigraphic record. *Earth-Science Reviews*, 24, 237-277.

Cartwright, J.A., Trudgill, B.D. & Mansfield, C.S. (1995). Fault growth by segment linkage: an explanation for scatter in maximum displacement and trace length data from the Canyonlands Grabens of SE Utah. *Journal of Structural Geology*, 17, 1319-1326.

Catuneanu, O. (2006). *Principles of sequence stratigraphy*. Elsevier, Amsterdam, The Netherlands. 375pp.

Childs, C., Worthington, R.P., Walsh, J.J. & Roche, V. (2019). Conjugate relay zones: geometry of displacement transfer between opposed-dipping normal faults. *Journal of Structural Geology*, 118, 377-390.

Collier, R.E.LI. (1990). Eustatic and tectonic controls upon Quaternary coastal sedimentation in the Corinth Basin, Greece. *J. Geol. Soc.*, 147, 301-314.

Collier, R.E.LI. & Dart, C.J. (1991). Neogene to Quaternary rifting, sedimentation and uplift in the Corinth Basin, Greece. *J. Geol. Soc. London*, 148, 1049-1065.

Collier, R.E.LI., Leeder, M.R., Trout, M., Ferentinos, G., Lyberis, E. & Papatheodorou, G. (2000). High sediment yields and cool, wet winters: test of last glacial paleoclimates in the northern Mediterranean. *Geology*, 28, 999-1002.

Cowie, P.A., Gupta, S. & Dawers, N.H. (2000). Implications of fault array evolution for synrift depocentre development: insights from a numerical fault growth model. *Basin Research*, 12, 241-261.

Cross, T.A. (1988). Controls on coal distribution in transgressive– regressive cycles, Upper Cretaceous, Western Interior, U.S.A. In: C.K. Wilgus, B.S. Hastings, C.G.St.C. Kendall, H.W. Posamentier, C.A. Ross & J.C. Van Wagoner (Eds.), *Sea-Level Changes: An Integrated Approach*. Soc. Econ. Paleontol. Mineral., Spec. Publ., 42, 371-380.

- Cross, T.A. & Lessenger, M.A. (1999). Construction and application of a stratigraphic inverse model. In: J.W. Harbaugh, W.L. Watney, E.C. Rankey, R. Slingerland, R.H. Goldstein & E.K. Franseen (Eds.), *STRATA: freeware for analysing classic stratigraphic problems*. *GSA Today*, 6, 1-7.
- Curray, J.R. (1964). Transgressions and regressions. In: R.L. Miller (Ed.), *Papers in Marine Geology*. Macmillan, New York, 175-203.
- Dart, C.J., Collier, R.E.L., Gawthorpe, R.L., Keller, J.V.A. & Nichols, G. (1994). Sequence stratigraphy of (?)Pliocene-quaternary synrift, gilbert-type fan deltas, Northern Peloponnesos, Greece. *Mar. Pet. Geol.*, 11, 545-560.
- Dawers, N. H. & Anders, M.H. (1995). Displacement-length scaling and fault linkage. *J. Struct. Geol.*, 17, 607-614.
- De Barros, L., Deschamps, A., Sladen, A., Lyon-Caen, H. & Voulgaris, N. (2017). Investigating Dynamic Triggering of Seismicity by Regional Earthquakes: The Case of the Corinth Rift (Greece). *Geophysical Research Letters*, 44, 10921-10929.
- De Gelder, G., Fernández-Blanco, D., Melnick, D., Duclaux, G., Bell, R.E., Jara-Muñoz, J., Armijo, R. & Lacassin, R. (2019). Lithospheric flexure and rheology determined by climate cycle markers in the Corinth Rift. *Scientific Reports*, 9, doi: 10.1038/s41598-018-36377-1.
- Dorsey, R.J. & Umhoefer, P.J. (2000). Tectonic and eustatic controls on sequence stratigraphy of the Pliocene Loreto Basin, Baja California Sur, Mexico. *GSA Bull.*, 112, 177-199.
- Doutsos, T. & Poulimenos, G. (1992). Geometry and kinematics of active faults and their seismotectonic significance in the western Corinth-Patras rift (Greece). *Journal of Structural Geology*, 14, 689-699.
- Driscoll, N.W. & Karner, G.D. (1998). Lower crustal extension across the Northern Carnarvon basin, Australia: evidence for an eastward dipping detachment. *Journal of Geophysical Research*, 103, 4975-4991.
- Duffy, O.B., Brocklehurst, S.H., Gawthorpe, R.L., Leeder, M.R. & Finch, E. (2014). Controls on landscape and drainage evolution in regions of distributed normal faulting: Perachora Peninsula, Corinth Rift, Central Greece. *Basin Research*, 27, 474-494.
- Eliet, P.P. & Gawthorpe, R.L. (1995). Drainage development and sediment supply within rifts, examples from the Sperchios basin, central Greece. *Journal of the Geological Society*, 152, 883-893.
- Elliott, G.M., Wilson, P., Jackson, C.A.-L., Gawthorpe, R.L., Michelsen, L. & Sharp, I. (2012). The linkage between fault throw and footwall scarp erosion patterns: an example from the Bremstein Fault Complex, offshore Mid-Norway. *Basin Research*, 24, 180-197.
- Etheridge, M.A. & O'Brien, G.W. (1994). Structural and tectonic evolution of the Western Australian margin system. *PESA Journal*, 22, 45-63.
- Flemings, P.B. & Grotzinger, J.P. (1996). STRATA: Freeware for analysing classic stratigraphic problems. *GSA Today*, 6, 1-7.
- Ford, M., Hemelsdaël, R., Mancini, M. & Palyvos, N. (2016). Rift migration and lateral propagation: evolution of normal faults and sediment-routing systems of the western Corinth rift (Greece). In: C. Childs, R.E. Holdsworth, C.A.-L. Jackson, T. Manzocchi, J.J. Walsh & G. Yielding, *The Geometry of Normal Faults*. Geol. Soc. London, Special Publications, 439, doi: 10.1144/SP439.15.
- Ford, M., Rohais, S., Williams, E.A., Bourlange, S., Jousset, D., Backert, N. & Malartre, F. (2013). Tectosedimentary evolution of the western Corinth rift (Central Greece). *Basin Research*, 25, 3-25.
- Ford, M., Williams, E.A., Malartre, F. & Popescu, S.M. (2007). Stratigraphic architecture, sedimentology and structure of the Vouraikos Gilbert-type fan delta, Gulf of Corinth, Greece. In: G. Nichols, E. Williams

& C. Paola (Eds.), *Sedimentary Processes, Environments and Basins. A Tribute to Peter Friend*. Int. Assoc. Sedimentol. Spec. Publ., 38, 49-90.

Fossen, H. & Rotevatn, A. (2016). Fault linkage and relay structures in extensional settings – a review. *Earth-Science Reviews*, 154, 14-28.

Gartrell, A., Torres, J., Dixon, M. & Keep, M. (2016). Mesozoic rift onset and its impact on the sequence stratigraphic architecture of the Northern Carnarvon Basin. *The APPEA Journal*, 56, 143-158.

Gawthorpe, R.L., Andrews, J.E., Collier, R.E.L., Ford, M., Henstra, G.A., Kranis, H., Leeder, M.R., Muravchik, M. & Skourtsos, E. (2017). Building up or out? Disparate sequence architectures along an active rift margin – Corinth rift, Greece. *Geology*, 45, 111-114.

Gawthorpe, R.L., Fraser, A. & Collier, R.E.L. (1994). Sequence stratigraphy in active extensional basins: implications for the interpretation of ancient basin fills. *Marine and Petroleum Geology*, 11, 642-658.

Gawthorpe, R.L., Hardy, S. & Ritchie, B. (2003). Numerical modelling of depositional sequences in half-graben rift basins. *Sedimentology*, 50, 169-185.

Gawthorpe, R.L. & Leeder, M.R. (2000). Tectono-sedimentary evolution of active extensional basins. *Basin Research*, 12, 195-218.

Gawthorpe, R.L., Leeder, M.R., Kranis, H., Skourtsos, E., Andrews, J.E., Henstra, G.A., Muravchik, M., Turner, J.A. & Stamatakis, M. (2018). Tectono-sedimentary evolution of the Plio-Pleistocene Corinth rift, Greece. *Basin Research*, 30, 448-479.

Gobo, K., Ghinassi, M. & Nemec, W. (2015). Gilbert-type deltas recording short-term base-level changes: delta-brink morphodynamics and related foreset facies. *Sedimentology*, 62, 1923-1949.

Gomis-Cartesio, L.E., Poyatos-Moré, M., Hodgson, D.M. & Flint, S.S. (2017). Shelf- margin clinothem progradation, degradation and readjustment: Tanqua depocentre, Karoo Basin (South Africa). *Sedimentology*, 65, 809-841.

Gradstein, F.M., Agterberg, F.P., Ogg, J.G., Hardenbol J., Van Veen, P., Thierry, J. & Huang, Z. (1994). A Mesozoic time scale. *Journal of Geophysical Research*, 99, 24051-24074.

Hardy, S. & Gawthorpe, R.L. (1998). Effects of variations in fault slip rate on sequence stratigraphy in fan deltas: insights from numerical modeling. *Geology*, 26, 911-914.

Heine, C. & Müller, R.D. (2005). Late Jurassic rifting along the Australian North West Shelf: margin geometry and spreading ridge configuration. *Australian Journal of Earth Sciences*, 52, 27-39.

Helland-Hansen, W. & Gjelberg, J. (1994). Conceptual basis and variability in sequence stratigraphy: a different perspective. *Sedimentary Geology*, 92, 31-52.

Helland-Hansen, W. & Martinsen, O. (1996). Shoreline trajectories and sequences: description of variable depositional dip scenarios. *Journal of Sedimentary Research*, 66, 670-688.

Heller, P.L., Burns, B.A. & Marza, M. (1993). Stratigraphic solution sets for determining the roles of sediment supply, subsidence and sea level on transgressions and regressions. *Geology*, 21, 747-750.

Hemelsdaël, R. & Ford, M. (2016). Relay zone evolution: a history of repeated fault propagation and linkage, central Corinth rift, Greece. *Basin Research*, 28, 34-56.

Hocking, R.M. (1988). Regional Geology of the Northern Carnarvon Basin. In: P.G. Purcell and R.R. Purcell (Eds.), *The North West Shelf, Australia. Proceedings of Petroleum Exploration Society of Australia Symposium*. PESA, Perth, 97-114.

- Hodgetts, D. (2013). Laser scanning and digital outcrop geology in the petroleum industry: A review. *Marine and Petroleum Geology*, 46, 335-354.
- Hodgson, D.M., Kane, I.A., Flint, S.S., Brunt, R.L., & Ortiz-Karpf, A. (2016). Time-transgressive confinement on the slope and the progradation of basin-floor fans: implications for the sequence stratigraphy of deep-water deposits. *Journal of Sedimentary Research*, 86, 73-86.
- Holbrook, J.M., Bhattacharya, J.P. (2012). Reappraisal of the sequence boundary in time and space: case and considerations for an SU (subaerial unconformity) that is not a sediment bypass surface, a time barrier, or an unconformity. *Earth-Science Reviews*, 113, 271-302.
- Hook, J., Abhvani, A., Gluyas, J.G. & Lawlor, M. (2003). The Birch Field, Block 16/12a, UK North Sea. In: J.G. Gluyas, & H.M. Hitchens (Eds.), *United Kingdom Oil and Gas Fields', Commemorative Millennium Volume*. Geological Society, London, Memoir, 20, 167-181.
- Howell, J.A., Eide, C.H. & Hartley, A.J. (2018). No evidence for sea level fall in the Cretaceous strata of the Book Cliffs of Eastern Utah. *EarthArXiv Preprints*, doi: 10.31223/osf.io/2ju3d.
- Hubbard, G.D. (1928). Quantitative vs. qualitative studies in Geology. *Science*, 68, 171-174.
- Jablonski, D. (1997). Recent advances in the sequence stratigraphy of the Triassic to Lower Cretaceous succession in the northern Carnarvon Basin, Australia. *The APPEA Journal*, 37, 429-454.
- Jackson, C.A.-L., Bell, R.E., Rotevatn, A., Tvedt, A.B.M. (2017). Techniques to determine the kinematics of syn-sedimentary normal faults and implications for fault growth models. In: C. Childs, R.E. Holdsworth, C.A.-L. Jackson, T. Manzocchi, J.J. Walsh & G. Yielding (Eds.), *The Geometry and Growth of Normal Faults*. Geological Society, London, Special Publications, 439, 187-217.
- Jackson, C.A.L., Gawthorpe, R.L., Carr, I.D. & Sharp, I.R. (2005). Normal faulting as a control on the stratigraphic development of shallow marine syn-rift sequences: the Nukhul and Lower Rudeis Formations, Hammam Faraun fault block, Suez Rift, Egypt. *Sedimentology*, 52, 313-338.
- Jackson, J.A., White, N.J., Garfunkel, Z. & Anderson, H. (1988). Relations between normal-fault geometry, tilting and vertical motions in extensional terrains: an example from the southern Gulf of Suez. *Journal of Structural Geology*, 10, 155-170.
- Jervey, M. (1988). Quantitative geological modeling of siliciclastic rock sequences and their seismic expression, In: C. Wilgus, B.S. Hastings, C.G.S.C. Kendall, H.W. Posamentier, C.A. Ross & J.C. Van Wagoner (Eds.), *Sea level changes: an integrated approach*. SEPM Spec. Pub., 42, 47-69.
- Jitmahantakul, S. & McClay, K. (2013). Late Triassic-Mid-Jurassic to Neogene extensional faults systems in the Exmouth Sub-basin, Northern Carnarvon Basin, North West Shelf, Western Australia. In: M. Keep & S.J. Moss (Eds.), *The Sedimentary Basins of Western Australia 3: Proceedings of the Petroleum Society of Australia Symposium*. PESA, Perth, 966pp.
- Jones G.E.D., Hodgson D.M. & Flint S.S. (2015). Lateral variability in clinoform trajectory, process regime, and sediment dispersal patterns beyond the shelf-edge rollover in exhumed basin margin-scale clinothems. *Basin Research*, 27, 657-680.
- Kelvin, W. (1883). Electrical Units of Measurement. *Popular Lectures*, 1, 73.
- Kim, Y.-S. & Sanderson, D.J. (2005). The relationship between displacement and length of faults: a review. *Earth-Science Reviews*, 68, 317-334.
- Lambiase, J.J. & Bosworth, W. (1995). Structural controls on sedimentation in continental rifts. In: J.J. Lambiase (Ed.), *Hydrocarbon Habitat in Rift Basins*. Geological Society, London, Special Publications, 80, 117-144.

- Larsen, P.H. (1988). Relay structures in a Lower Permian basement-involved extension system, East Greenland. *Journal of Structural Geology*, 10, 3-8.
- Le Roux, J.P. (2005). Grains in motion: a review. *Sedimentary Geology*, 178, 285-313.
- Leeder, M.R. & Gawthorpe R.L. (1987). Sedimentary models for extensional tilt-block/half-graben basins. In: M.P. Coward, J.F. Dewey & P.L. Hancock (Eds.), *Continental Extensional Tectonics*. Geological Society, London, Special Publications, 28, 139-152.
- Leeder, M.R. & Jackson, J.A. (1993). The interaction between normal faulting and drainage in active extensional basins, with examples from the western United States and central Greece. *Basin Research*, 5, 79-102.
- Leeder, M.R., Collier, R.E.LI., Abdul Aziz, L.H., Trout, M., Ferentinos, G., Papatheodorou, G. & Lyberis, E. (2002). Tectono-sedimentary processes along an active marine/lacustrine half-graben margin: Alkyonides Gulf, E. Gulf of Corinth, Greece. *Basin Research*, 14, 25-41.
- Leeder, M.R. & Gawthorpe, R.L. (1987). Sedimentary models for extensional tilt block/half-graben basins. In: M.P. Coward, J.F. Dewey & P.L. Hancock (Eds.), *Continental Extensional Tectonics*. Geological Society, London, Special Publications, 28, 139-152.
- Leeder, M.R., Harris, T. & Kirkby, M.J. (1998). Sediment supply and climate change: implications for basin stratigraphy. *Basin Research*, 10, 7-18.
- Leppard, C.W. & Gawthorpe, R.L. (2006). Sedimentology of rift climax deep water systems; Lower Rudeis Formation, Hammam Faraun Fault Block, Suez Rift, Egypt. *Sedimentary Geology*, 191, 67-87.
- Longley, I.M., Buessenschuett, C., Clydsdale, L., Cubitt, C.J., Davis, R.C., Johnson, M.K., Marshall, N.G., Murray, A.P., Somerville, R., Spry, T.B. & Thompson, N.B. (2002). The North West Shelf of Australia – a Woodside perspective. In: M. Keep & S.J. Moss (Eds.), *The Sedimentary Basins of Western Australia 3: Proceedings of the Petroleum Society of Australia Symposium*. PESA, Perth, 966pp.
- Madof, A.S., Harris, A.D. & Connell, S.D. (2016). Nearshore along-strike variability: is the concept of the systems tracts unhinged? *Geology*, 44, 319-322.
- Marshall, N.G. & Lang, S.C. (2013). A new sequence stratigraphic framework for the North West Shelf, Australia. In: M. Keep & S.J. Moss (Eds.), *The Sedimentary Basins of Western Australia 4: Proceedings of the Petroleum Exploration Society of Australia Symposium*. PESA, Perth.
- Martinius, A.W., Elfenbein, C. & Keogh, K.J. (2014). Applying accommodation versus sediment supply ratio concepts to stratigraphic analysis and zonation of a fluvial reservoir. In: A.W. Martinius, R. Ravnås, J.A. Howell, R.J. Steel & J.P. Wonham, (Eds.), *From Depositional Systems to Sedimentary Successions on the Norwegian Continental Margin, First Edition*. International Association of Sedimentologists, 46, 101-125.
- McNeill, L.C., Cotterill, C.J., Henstock, T.J., Bull, J.M., Stefatos, A., Collier, R.E.LI., Papatheoderou, G., Ferentinos, G. & Hicks, S.E. (2005). Active faulting within the offshore western Gulf of Corinth, Greece: implications for models of continental rift deformation. *Geology*, 33, 241–244.
- McNeill, L.C., Shillington, D.J. & Carter, G.D.O. (2018). Rift history, syn-rift sedimentation and paleoenvironment of the Corinth Rift basin: IODP Expedition 381 preliminary results. AGU Fall Meeting, Washington, DC, USA, 10th-14th December, 2018.
- McNeill, L.C., Shillington, D.J., Carter, G.D.O., Everest, J.D., Gawthorpe, R.L., Miller, C., Phillips, M.P., Collier, R.E.LI., Cvetkoska, A., De Gelder, G., Diz, P., Doan, M.L., Ford, M., Geraga, M., Gillespie, J., Hemelsdaël, R., Herrero-Bervera, E., Ismaiel, M., Janikian, L., Kouli, K., Le Ber, E., Li, S., Maffione, M., Mahoney, C., Machlus, M.L., Michas, G., Nixon, C.W., Oflaz, S.A., Omale, A.P., Panagiotopoulos, K., Pechlivanidou, S., Sauer, S., Seguin, J., Sergiou, S., Zakharova, N.V. & Green, S. (2019). High-resolution record reveals climate-driven environmental and sedimentary changes in an active rift. *Scientific Reports*, 9, doi: 10.1038/s41598-019-40022-w.

- Mesimeri, M. & Karakostas, V. (2018). Repeating earthquakes in western Corinth Gulf (Greece): implications for aseismic slip near locked faults. *Geophysical Journal International*, 215, 659-676.
- Muto, T. & Steel, R.J. (1992). Retreat of the front in a prograding delta. *Geology*, 20, 967-970.
- Muto, T. & Steel, R.J. (1997). The accommodation concept in sequence stratigraphy: some dimensional problems and possible redefinition. *Sedimentary Geology*, 130, 1-10.
- Muto, T. & Steel, R.J. (2000). The accommodation concept in sequence stratigraphy: some dimensional problems and possible redefinition. *Sedimentary Geology*, 130, 1-10.
- Mutter, J.C. & Larson, R.L. (1989). Extension of the Exmouth Plateau, offshore northwestern Australia: deep seismic reflection/refraction evidence for simple and pure shear mechanisms. *Geology*, 17, 15-18.
- Neal, J. & Abreu, V. (2009). Sequence stratigraphy hierarchy and the accommodation succession method. *Geology*, 37, 779-782.
- Neal, J.E., Abreu, V., Bohacs, K.M., Feldman, H.R. & Pederson, K.H. (2016). Accommodation succession sequence stratigraphy: observational method, utility, and insights into sequence boundary formation. *Journal of the Geological Society, London*, 173, 803-816.
- Nesbit, P.R., Durkin, P.R., Hugenholtz, C.H., Hubbard, S.M. & Kucharczyk, M. (2018). 3-D stratigraphic mapping using a digital outcrop model derived from UAV images and structure-from-motion photogrammetry. *Geosphere*, 14, 2469-2486.
- Nicol, A., Childs, C., Walsh, J.J., Manzocchi, T. & Schöpfer, M.P.J. (2016). Interactions and growth of faults in an outcrop-scale system. In: Childs, C., Holdsworth, R.E., Jackson, C.A.-L., Manzocchi, T., Walsh, J.J. & Yielding, G. (Eds.), *The Geometry and Growth of Normal Faults*. Geological Society, London, Special Publications, 439, 23-39.
- Nieminski, N.M. & Graham, S.A. (2017). Modeling stratigraphic architecture using small unmanned aerial vehicles and photogrammetry: Examples from the Miocene East Coast basin, New Zealand. *Journal of Sedimentary Research*, 87, 126-132.
- Nixon, C.W., McNeill, L.C., Bull, J.M., Bell, R.E., Gawthorpe, R.L., Henstock, T.J., Christodoulou, D., Ford, M., Taylor, B., Sakellariou, D., Ferentinos, G., Papatheodorou, G., Leeder, M.R., Collier, R.E.LI., Goodliffe, A.M., Sachpazi, M. & Kranis, H. (2016). Rapid spatiotemporal variations in rift structure during development of the Corinth Rift, central Greece. *Tectonics*, 35, 1225-1248.
- Ori, G.G., Roveri, M. & Nichols, G. (1991). Architectural patterns in large-scale Gilbert-type delta complexes, Pleistocene, Gulf of Corinth, Greece. In: A.D. Miall & N. Tyler (Eds.), *The Three-Dimensional Facies Architecture of Terrigenous Clastic Sediments and Its Implications for Hydrocarbon Discovery and Recovery* Miall. Concepts in Sedimentology and Paleontology, 3, Society for Sedimentary Geology (SEPM), 207-216.
- Pantosti, D., Collier, R.E.LI., D'Addezio, G., Masana, E. & Sakellariou, D. (1996). Direct geological evidence for prior earthquakes on the 1981 Corinth fault (central Greece). *Geophysical Research Letters*, 23, 3795-3798.
- Pattison, S.A.J. (2018). Rethinking the Incised-Valley Fill Paradigm For Campanian Book Cliffs Strata, Utah–Colorado, U.S.A.: Evidence For Discrete Parasequence-Scale, Shoreface-Incised Channel Fills. *Journal of Sedimentary Research*, 88, 1381-1412.
- Pattison, S.A.J. (2019a). No evidence for an unconformity at the base of the lower Castlegate Sandstone in the Campanian Book Cliffs, Utah–Colorado, U.S.A.: Implications for sequence stratigraphic models. *AAPG Bulletin*, doi:10.1306/07151918158.
- Pattison, S.A.J. (2019b). Re-evaluating the sedimentology and sequence stratigraphy of classic Book Cliffs outcrops at Tusher and Thompson canyons, eastern Utah, USA: Applications to correlation, modelling, and

prediction in similar nearshore terrestrial to shallow marine subsurface settings worldwide. *Marine and Petroleum Geology*, 102, 202-230

Pechlivanidou, S., Cowie, P.A., Duclaux, G., Nixon, C.W., Gawthorpe, R.L. & Salles, T. (2019). Tipping the balance: shifts in sediment production in an active rift setting. *Geology*, 47, 259-262.

Pechlivanidou, S., Cowie, P.A., Hannisdal, B., Whittaker, A.C., Gawthorpe, R.L., Pennos, C. & Riiser, O.S. (2017). Source-to-sink analysis in an active extensional setting: Holocene erosion and deposition in the Sperchios rift, central Greece. *Basin Research*, 522-543.

Plint, A.G. & Nummedal, D. (2000). The falling stage systems tract: recognition and importance in sequence stratigraphic analysis. In: D. Hunt & R.L. Gawthorpe (Eds.), *Sedimentary Response to Forced Regression*. Geological Society, London, Special Publications, 172, 1-17.

Posamentier, H. Jervy, M. & Vail, P. (1988). Eustatic controls on clastic deposition I conceptual framework. In: C. Wilgus, B.S. Hastings, C.G.S.C. Kendall, H.W. Posamentier, C.A. Ross & J.C. Van Wagoner (Eds.), *Sea level changes: an integrated approach*. SEPM Spec. Pub., 42, 109-124.

Posamentier, H. & Vail, P. (1988). Eustatic controls on clastic deposition II- sequence and systems tract models. In: C. Wilgus, B.S. Hastings, C.G.S.C. Kendall, H.W. Posamentier, C.A. Ross & J.C. Van Wagoner (Eds.), *Sea level changes: an integrated approach*. SEPM Spec. Pub., 42, 125-154.

Poyatos-Moré, M., Jones, G.D., Brunt, R.L., Tek, D., Hodgson, D.M. & Flint, S.S. (2019). Clinoform architecture and along-strike variability through an exhumed erosional to accretionary basin margin transition. *Basin Research*, doi: 10.1111/12351.

Rahmstorf, S. (2003). Thermohaline circulation: the current climate. *Nature*, 421, 699.

Ravnås, R. & Steel, R.J. (1998). Architecture of Marine Rift-Basin Successions. *AAPG Bulletin*, 82, 110-146.

Rohais, S., Eschard, R., Ford, M., Guillocheau, F. & Moretti, I. (2007). Stratigraphic architecture of the Plio-Pleistocene infill of the Corinth Rift: implications for its structural evolution. *Tectonophysics*, 440, 5-28.

Rotevatn, A., Jackson, C.A.-L, Tvedt, A.B.M., Bell, R.E. & Blækkan, I. (2018). How do normal faults grow? *Journal of Structural Geology*, doi: 10.1016/j.jsg.2018.08.005.

Schlager, W. (1993). Accommodation and supply - A dual control on stratigraphic sequences. *Sedimentary Geology*, 86, 111-136.

Schwarz, E., Veiga, G.D., Álvarez Trentini, G., Spalletti, L.A. (2016). Climatically versus eustatically controlled, sediment-supply-driven cycles: carbonate-siliciclastic, high frequency sequences in the Valanginian of the Neuquén Basin (Argentina). *Journal of Sedimentary Research*, 86, 312-335.

Serck, C.S. & Braathen, A. (2019). Extensional fault and fold growth: impact on accommodation evolution and sedimentary infill. *Basin Research*, doi: 10.1111/br.12353.

Shillington, D.J., McNeill, L.C., Carter, G.D.O. and the Expedition 381 Participants. (2019). Expedition 281 Preliminary Report: Corinth Active Rift Development. International Ocean Discovery Program, ISSN 2371-9562.

Sloss, L.L. (1962). Stratigraphic models in exploration. *AAPG Bulletin*, 46, 1050-1057.

Sloss, L.L. Krumbein, W. & Dapples, E. (1949). Integrated facies analysis, In: C. Longwell (Ed.), *Sedimentary facies in geologic history: Geological Society America, Memoir*, 39, 91-124.

- Stagg, H. M. J., Wilcox, J. B., Symonds, P. A., O'Brien, G. W., Colwell, J. B., Hill, P. J. A., Lee, C.-S., Moore, A.M.G. & Struckmeyer, H.I. M. (1999). Architecture and evolution of the Australian continental margin. *AGSO Journal of Australian Geology & Geophysics*, 17, 17-33.
- Stefatos, A., Papatheodorou, G., Ferentinos, G., Leeder, M.R. & Collier, R.E.LI. (2002). Seismic reflection imaging of active offshore faults in the Gulf of Corinth: their seismotectonic significance. *Basin Research*, 14, 487-502.
- Stevenson, C.J., Jackson, C.A.-L., Hodgson, D.M., Hubbard, S.M. & Eggenhuisen, J.T. (2015). Deep-water sediment bypass. *Journal of Sedimentary Research*, 85, 1058-1081.
- Swift, D.J.P. & Thorne, J. A. (1992). Sedimentation on continental margins, I: a general model for shelf sedimentation. In: D.J.P. Swift, G.F. Oertel, R.W. Tillman & J.A. Thorne (Eds.), *Shelf Sand and Sandstone Bodies: Geometry, Facies and Sequence Stratigraphy*. Special Publications of International Association of Sedimentologists, 14, Blackwell Publishing Ltd., Oxford, UK, 3-31.
- Taylor, B., Weiss, J.R., Goodliffe, A.M., Sachpazi, M., Laigle, M. & Hirn, A. (2011). The structures, stratigraphy and evolution of the Gulf of Corinth rift, Greece. *Geophysical Journal International*, 185, 1189-1219.
- Thorne, J. A. & Swift, D.J.P. (1992). Sedimentation on continental margins, II: application of the regime concept. In: D.J.P. Swift, G.F. Oertel, R.W. Tillman & J.A. Thorne (Eds.), *Shelf Sand and Sandstone Bodies: Geometry, Facies and Sequence Stratigraphy*. Special Publications of International Association of Sedimentologists, 14, Blackwell Publishing Ltd., Oxford, UK, 33-58.
- Tindale, K., Newell, N., Keall, J. & Smith, N. (1998). Structural evolution and charge history of the Exmouth Sub-basin, northern Carnarvon Basin, Western Australia. In: P.G. Purcell & R.R. Purcell (Eds.), *The Sedimentary Basins of Western Australia 2: Proceedings of Petroleum Exploration Society of Australia Symposium*. PESA, Perth, 742pp.
- Tipper, J.C. (2015). The importance of doing nothing: stasis in sedimentation systems and its stratigraphic effect. In: D.G. Smith, R.J. Bailey, P.M. Burgess & Fraser, A.J. (Eds.), *Strata and Time: Probing the Gaps in Our Understanding*. Geological Society, London, Special Publications, 404, 105-122.
- Torabi, A., Alaei, B. & Libak, A. (2019). Normal fault 3D geometry and displacement revisited: insights from faults in the Norwegian Barents Sea. *Marine and Petroleum Geology*, 99, 135-155.
- Trinks, I., Clegg, P., McCaffrey, K.J.W., Jones, R.R., Hobbs, R., Holdsworth, B., Holliman, N.S., Imber, J., Waggott, S. & Wilson, R.W. (2005). Mapping and analysing virtual outcrops. *Visual Geosciences*, 10, 13-19.
- Turner, C.C. & Connell, E.R. (2018). Mid to Late Jurassic graben margin development and evolution of shallow marine to submarine fan systems in the Brae area of the South Viking Graben, U.K. North Sea. In: C. C. Turner & B. T. Cronin (Eds.), *Rift-related coarse-grained submarine fan reservoirs; the Brae Play, South Viking Graben, North Sea*. AAPG Memoir, 115, 163-212.
- Turner, C.C. & Cronin, B.T (2018). *Rift-related coarse-grained submarine fan reservoirs; the Brae Play, South Viking Graben, North Sea: Memoir*. AAPG Memoirs, 115, doi: DOI:10.1306/13652176M1153311.
- Vail, P., Mitchum, R.M. & Thompson, S. (1977). Seismic stratigraphy and global changes in sea level, In: C. Payton (Ed.), *Seismic stratigraphy: applications to hydrocarbon exploration*. AAPG Memoir, 26, 49-212.
- Van Hinsbergen, D.J.J. & Schmid, S.M. (2012). Map view restoration of Aegean-West Anatolian accretion and extension since the Eocene. *Tectonics*, 31, TC5005, doi: 10.1029/2012TC003132.
- Van Wagoner, J.C., Mitchum, R.M.Jr., Campion, K.M. & Rahmanian, V.D. (1990). Siliciclastic sequence stratigraphy in well logs, core and outcrops: concepts for high-resolution correlation of time and facies. *AAPG Methods in Exploration Series*, 7, 55.

- Vassilakis, E., Papanikolaou, D. & Royden, L. (2011). Kinematic links between subduction along the Hellenic trench and extension in the Gulf of Corinth, Greece: a multidisciplinary analysis. *Earth and Planetary Letters*, 303, 108-120.
- Veevers, J.J. (1988). Morphotectonics of Australia's northwestern margin – a review. In: P.G. Purcell & R.R. Purcell (Eds.), *The North West Shelf, Australia: Proceedings of Petroleum Exploration Society of Australia Symposium*. PESA, Perth, 651pp.
- Walsh, J.J. & Watterson, J. (1988). Analysis of the relationship between displacements and dimensions of faults. *J. Struct. Geol.*, 10, 239-247.
- Watkins, S.E., Whittaker, A.C., Bell, R.E., McNeill, L.C., Gawthorpe, R.L., Brooke, S.A.S., Nixon, C.W. (2018). Are landscapes buffered to high-frequency climate change? A comparison of sediment fluxes and depositional volumes in the Corinth Rift, central Greece, over the past 130kyr. *GSA Bulletin*, 131, 371-388.
- Westoby, M.J., Brasington, J., Glasser, N.F., Hambrey, M.J. & Reynolds, J.M. (2012). “Structure-from-motion” photogrammetry: A low-cost, effective tool for geoscience applications. *Geomorphology*, 179, 300-314.
- Whittaker, A.C., Attal, M. & Allen, P.A. (2010). Characterising the origin, nature and fate of sediment exported from catchments perturbed by active tectonics. *Basin Research*, 22, 809-828.
- Williams, R.M. (2018). Derisking the Thebe Discovery through cognitive interpretation. *First Break*, 36, 71-78.
- Wood, A.M., Paton, D.A., Collier, R.E.L. & O'Connor, V. (2015). Understanding regional scale structural uncertainty: The onshore Gulf of Corinth Rift as a hydrocarbon exploration analogue. *Interpretation*, 3, SAC35-SAC53.
- Xu, X., Aiken, C.L.V., Bhattacharya, J.P., Corbeanu, M., Nielsen, K.C., McMechan, G.A. & Abdelsalam, M.G. (2000). Creating virtual 3-D outcrop. *The Leading Edge*, 19, 2, 197-202.
- Zelt, B.C., Taylor, B., Sachpazi, M. & Hirn, A. (2005). Crustal velocity and Moho structure beneath the Gulf of Corinth, Greece, *Geophys. J. Int.*, 162, 257-268.
- Zhang, J., Burgess, P., Granjeon, D. & Steel, R.J. (2018). Can sediment supply variations create sequences? Insights from stratigraphic forward modelling. *Basin Research*, 31, 274-289.

Chapter 2

Research Context

This chapter provides a fundamental overview of the literature covering the research areas addressed in this thesis and is designed to give context to the research that follows. Two broad fields of research are introduced and reviewed: rift basins and sequence stratigraphy. The importance of rift basin research and how rift basins, and specifically normal faults develop provides a broad mechanical background to the basins that are studied herein. An introduction to tectono-stratigraphy is provided to understand the time setting of the stratigraphy in relation to structural development, as well as current tectono-sedimentary models. Later in the thesis, these are compared to models established within the study areas and challenged or refined. Sequence stratigraphy is a fundamental approach used for basin analysis and is utilised here as it allows time relationships to be established between strata, stratal surfaces, facies and depositional systems. A brief history of sequence stratigraphy, its applied process explanation and previous stratigraphic numerical modelling techniques are detailed. The overall application of sequence stratigraphy to rift basins is critically assessed throughout this research and discussed in Chapter 7. The introductory sections of each chapter provide more detailed literature reviews that are specific to the research within.

2.1. Rift basins

Rift basins are sedimentary basins that have formed globally as a result of lithospheric extension and are distributed across a range of environments on Earth's surface (Fig. 2.1). They have been the subject of physical and intellectual exploration as hosts of some of the most prolific hydrocarbon reserves in the world, responsible for 30% of the world's largest accumulations greater than 500×10^6 BBL (Mann et al., 2001). Geological research has focussed on the geometry, mechanics, evolution and architecture of rift basins, from crustal to fault-block scale (e.g. McKenzie, 1978; Dewey, 1982; Coward, 1986; Kusznir & Ziegler, 1992; Morley, 1995; Gupta et al., 1998; Gawthorpe & Leeder, 2000; Jackson et al., 2017), due to their commercial interest from hydrocarbon, water, and mineral industries, and the quest for knowledge in continental break-up and Earth history. Moreover, their sedimentary records can preserve important information concerning fault evolution and the history of climate, palaeoecology and geological time. Despite the wealth of literature, the variable impact of rift-related movement on sedimentary architecture in three dimensions is difficult to distinguish from the influence of other allogenic controls, such as eustasy and sediment supply. Quantification of the controls on rift basin evolution remains a problem in basin analysis.

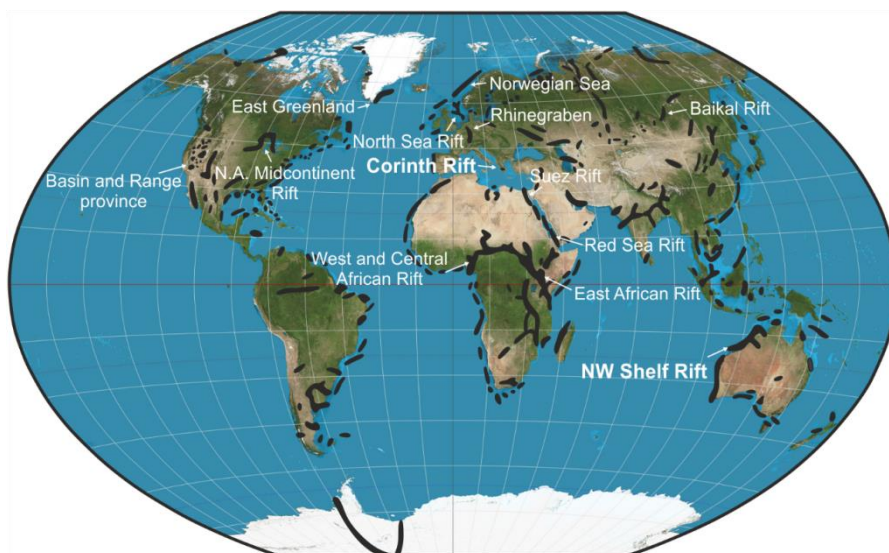


Figure 2.1. Geographical distribution of Earth's rift basins. A number of basins cited in the text are annotated. Positions and geometries are approximate (redrawn from Fraser et al., 2007; map from Strebe, 2011).

2.1.1. Rift development

Rift basins can develop over tens of millions of year timescales, but the duration can be highly variable, with a number of rifts presenting polyphase histories, including the East Greenland-Norwegian Sea (Parsons et al., 2017; Rotevatn et al., 2018a) and West and Central African rift systems (Fairhead et al., 2013; Fig. 2.1). Rifting occurs either through active rifting or passive rifting (Keen, 1985). In active rifting, a thermal plume in the mantle uplifts and heats the lithosphere, resulting in lithospheric thinning and sometimes isostatic uplift (Allen & Allen, 2013). This study focuses on passive rifts, where distant forces act to mechanically extend the lithosphere (Fig. 2.2). Stretching and thinning of the crust and sub-crustal lithosphere ensues and the asthenosphere passively upwells and produces a thermal anomaly (Falvey, 1974; McKenzie, 1978). Brittle deformation of the crust results in faulting (generally in dip-slip style) and subsidence from the isostatic response to stretching, which is dependent on the thickness of the crust relative to the initial thickness of the lithosphere, and the amount of stretching (β). This is followed by a longer phase of passive subsidence from thermal relaxation during cooling of the asthenosphere and stretched lithosphere, which decays exponentially through time (Fig. 2.2A) (McKenzie, 1978).

Rifts are characterised by extensional faulting, elevated rift shoulder topography, negative gravity and high thermal anomalies (Allen & Allen, 2013). Typical heat flows in rifts are up to a factor of two higher than in unstretched areas, and are on average 90-110 mWm⁻² (Morgan, 1982). The value is typically higher in rifts with volcanic activity and is largely dependent on the radiogenic properties of the crust.

Pure shear (Fig. 2.2 B1) (McKenzie, 1978), simple shear (Fig. 2.2 B2) (Wernicke, 1985) and hybrid models of pure and simple shear (Fig. 2.2 B3) (Kusznir et al., 1991) are used to explain the style of deformation and degree of symmetry across a rift axis, in order to account for the range of rift geometries that are observed globally. The pure shear model arises from uniform, symmetrical stretching between the crust and sub-crustal lithosphere (McKenzie, 1978). Simple

shear invokes that the sub-crustal lithosphere deforms laterally relative to the crust by a large-scale, low-angle detachment (shear zone) and produces an asymmetric lithospheric geometry (Wernicke, 1985). The hybrid model treats the crust with simple shear and the more ductile sub-crustal lithosphere with pure shear, such that detachment occurs at the boundary between the two (Kusznir et al., 1991).

The geometry of a rift can be highly influenced by structural inheritance from pre-existing weaknesses, which localises deformation and influences the nucleation and growth of faults (e.g. Daly et al., 1989; Bladon et al., 2015; Phillips et al., 2016; 2018). Ultimately, a rift basin geometry is dependent on its rheological properties and thus forms as a result of the thermal and elastic response of the lithosphere to extension (Van der Beek et al., 1994; Huisman & Beaumont, 2002; 2008). By way of example, the width of the rift zone can be highly variable depending on the lithospheric strength (Buck, 1991), with hot and weak lithospheres producing wide rifts of the order of several hundred kilometres (e.g. Basin and Range, North America; Hamilton, 1987), and cool and rigid lithospheres producing narrow rifts of less than 100 kilometres (e.g. Rhinegraben, Illies & Greiner, 1978; East African Rift, Chorowicz, 2005; and the Baikal Rift, Mats & Perepelova, 2011; Fig. 2.1). The eventual consequence of rifting is full continental break-up with a seafloor spreading centre that generates large oceans, such as the Atlantic and Pacific. However, insufficient stretching can render a rift 'failed', whereby the early stage of rifting is fossilised and the margin becomes passive, for example, the Gulf of Suez, North Sea and North America's Midcontinent Rifts (Ziegler, 1990; Khalil & McClay, 2002; Stein et al., 2018; Fig. 2.1).

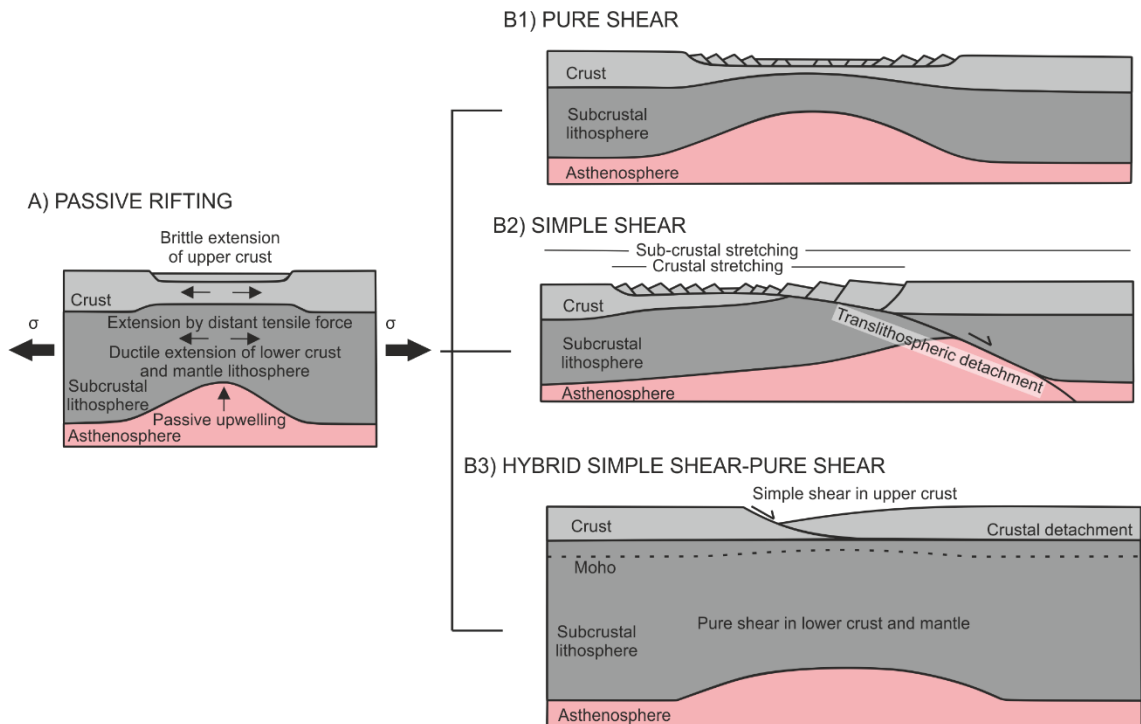


Figure 2.2. A) Idealised schematic diagram to show the mechanism of passive rifting from external, tensile forces, σ_{xx} , resulting in extension, thinning of the crust and sub-crustal lithosphere and passive upwelling of the asthenosphere. B) Three models for rifting strain geometries. B1) Pure shear model from uniform stretching between the crust and sub-crustal lithosphere (McKenzie, 1978), resulting in a symmetrical geometry. B2) Simple shear model with a low angle detachment through the lithosphere producing an asymmetric geometry (Wernicke, 1985). B3) Hybrid shear model invoking simple shear in the crust and pure shear in the sub-crustal lithosphere (Kusznir et al., 1991). Modified from Allen & Allen (2013).

Current structural research themes in rift basins, but beyond the scope of this study include:

- the mechanical behaviour of rifts that interact with and are modified by salt, and its influence on sedimentation (Kane et al., 2010; Wonham et al., 2014; Jackson et al., 2018);
- the influence of structural inheritance on rift basin geometry (Mortimer et al., 2016; Phillips et al., 2016; 2018; Gouiza & Paton, 2019; Henstra et al., 2019; Heilman et al., 2019);
- magmatic variability along rifted margins and its influence on rift dynamics and architecture (Buck, 2017; Paton et al., 2017; McDermott et al., 2018; Norcliffe et al., 2018);

- strain distribution across rifts and its influence on seismicity patterns and geohazard assessment (Roure et al., 2009; Cloetingh et al., 2012);

Recent studies have shown that the extension measured from tilted fault block geometries is insufficient to explain the magnitude of thinning and subsidence observed in rift basins (e.g. Doré & Lundin, 2015). McDermott & Reston (2015) attribute this to the limited ability of seismic data to image polyphase faulting. As with all structural models, we are at the mercy of subsurface dataset resolution. Opportunities to improve structural models in rift basins continue to arise as our ability to image the subsurface advances.

2.1.2. Normal faults

Generally, mature rifts exhibit a number of common structural features (Gabrielsen, 1986; Nøttvedt et al., 1995; Withjack et al., 2002) that influence topography, drainage and accommodation development when they interact with, and breach, the free surface (Leeder & Jackson, 1993). Planar and low-angle listric faults develop with stretching, and in their rotation can produce up-thrown and down-thrown blocks with a horst-graben morphology. Strike-slip faults also arise depending on the orientation of the rift axis relative to the main direction of extension, with more oblique relationships producing a greater number of strike-slip faults (e.g. Burchfiel & Stewart, 1966). A typical dip-oriented cross-section showing major structural elements of a mature rift is presented in Figure 2.3. However, not all elements may be present in a given dip section due to the along-strike interaction of faults and transfer zones (Bosworth, 1985).

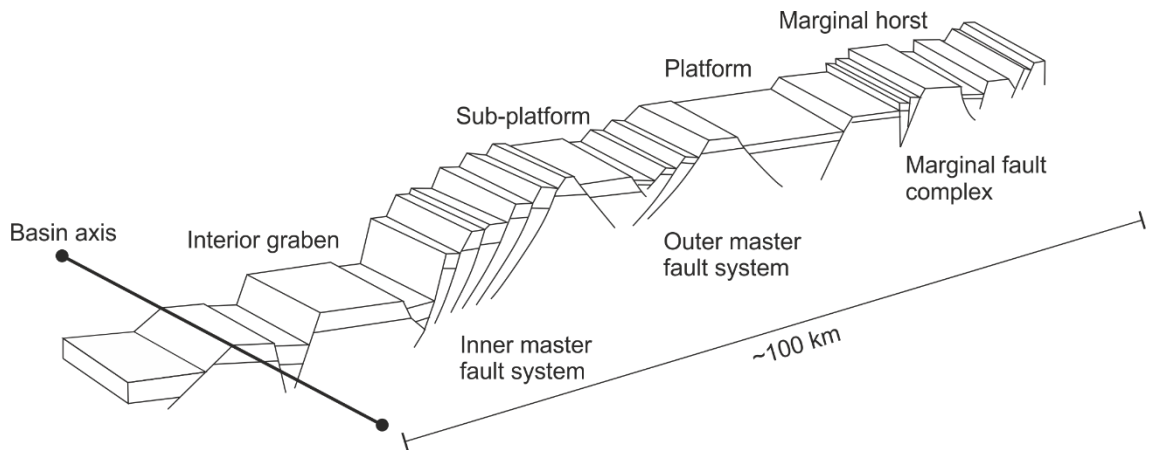


Figure 2.3. The main structural elements of a mature rift (modified from Nøttvedt et al., 1995).

Normal faults that move during sedimentation and influence stratigraphic architecture are known as ‘growth faults’ (e.g. Childs et al., 2003). These are the focal mechanism of tectonically-induced accommodation (Serck & Braathen, 2019) in this study. During faulting, in their respective positions, hangingwall subsidence increases accommodation and footwall uplift reduces accommodation, as the hangingwall is downthrown relative to the footwall (Jackson et al., 1988; King et al., 1988). Hangingwall subsidence is typically 6 to 10 times greater than footwall uplift (Stein & Barrientos, 1985). This relationship is often expressed as a ratio and is a function of the elastic response of the rocks to faulting and lithospheric loading (deposition and erosion) (McNeill & Collier, 2004). Accommodation development is not uniform along the fault due to along-strike displacement variation. It has been shown through numerous datasets that a typical displacement-length (D-L) profile exhibits maximum displacement at the fault centre, which diminishes to zero at the fault tips (*in sensu* of works on cracks by Dugdale, 1960; and Walsh & Watterson, 1988; Dawers & Anders, 1995), but how this geometry (D/L) varies over different length- and time-scales is more contentious (Kim & Sanderson, 2005; Torabi et al., 2019).

Generally, it is accepted that faults grow by coalescence from initiation of smaller fault segments through interaction and linkage until a through-going fault zone is established (Fig. 2.4; Peacock & Sanderson, 1991; Cartwright et al., 1995; Cowie et al., 2000; Gawthorpe & Leeder, 2000). This evolution influences depocentre geometry and accommodation distribution, which varies through

time according to whether linkage and accumulation of fault length is established early or late in the development of the fault. In this regard, two fault growth models are presented in the literature: the propagating (or ‘isolated’) model (Watterson, 1986; Walsh & Watterson, 1988; Cartwright et al., 1995; Dawers & Anders, 1995) and the constant length model (Morley, 2002; Walsh et al., 2003; Schlagenhauf et al., 2008; Nicol et al., 2016; Jackson et al., 2017). The propagating model is based on a linear relationship between displacement and fault length (e.g. Cowie & Scholz, 1992) and exhibits progressive movement of the fault tips through time. The constant-length model has recently been shown to be more common than previously assumed (Jackson & Rotevatn, 2013; Jackson et al., 2017; Rotevatn et al., 2018b). It suggests that a fault grows rapidly to its final length in the earliest growth stage prior to its main accumulation of displacement and therefore the fault tips remain ‘pinned’ throughout most of the fault growth.

The fault growth model is important to consider for not only the accommodation distribution through time, but also for sediment dispersal. Sediments are commonly sourced from relay zones, which are areas of rotation between pairs of overlapping, sub-parallel fault segments (Larson, 1988; Peacock & Sanderson, 1991; Hemelsdaël & Ford, 2016; Fossen & Rotevatn, 2016; Childs et al., 2019; Fig. 2.5). The degree of propagation of the fault tip will determine the time period through which the sediment source is pervasive during the lifetime of the fault. For example, pinned fault tips (constant length model) allow a relay drainage system to develop early in the fault development, whereas propagated fault tips (isolated model) restrict the drainage system to develop in the fault tips’ final position at the latest stage of fault development (Jackson et al., 2017). Figure 2.5 shows the key elements of a normal fault set in 3D, with data from the NW Shelf, Australia (Fig. 2.5A), schematically (Fig. 2.5B), and with the two fault growth models (Fig. 2.5C).

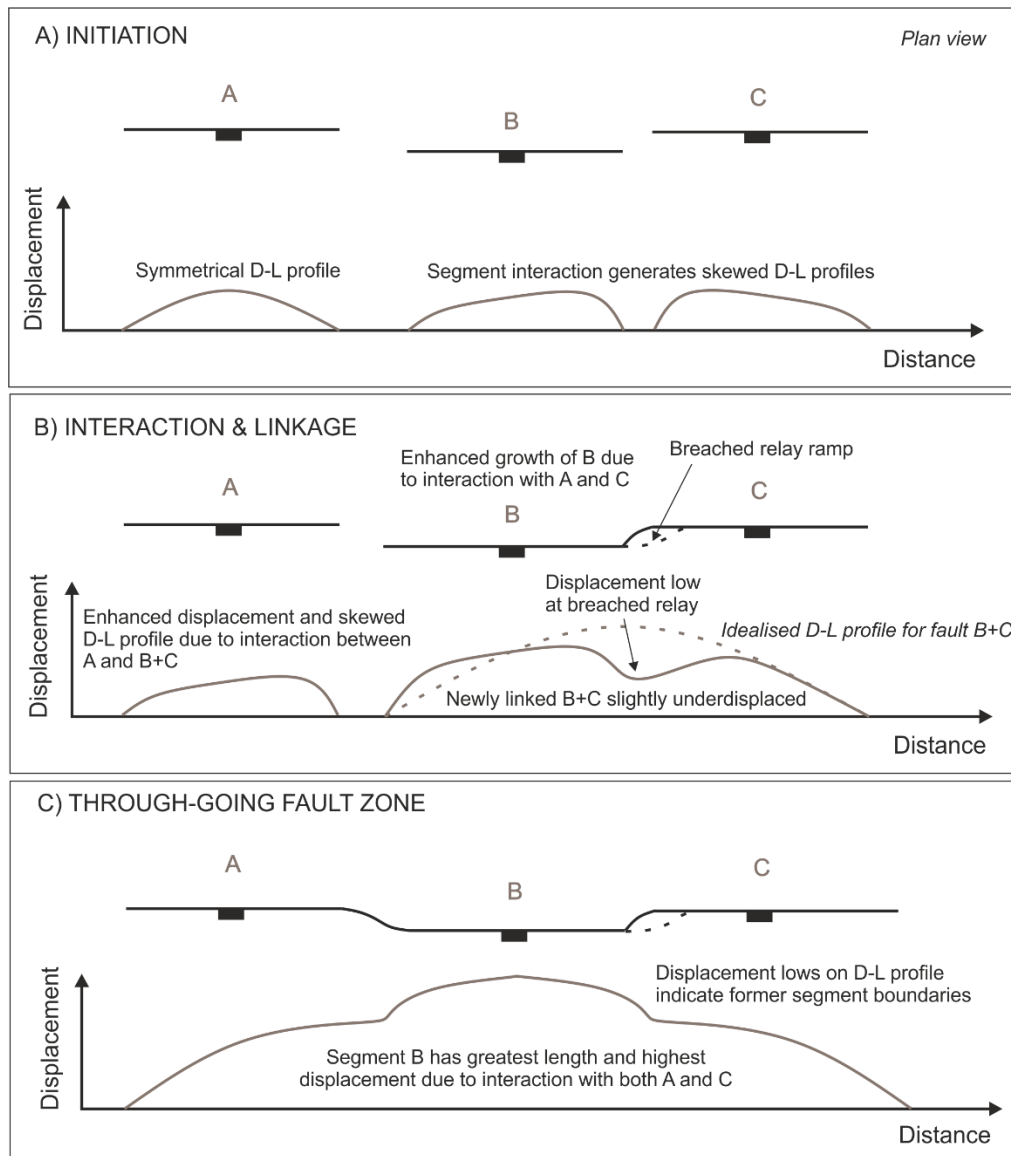


Figure 2.4. Normal fault growth through A) initiation, B) interaction and linkage to C) a through-going fault zone, with associated displacement-length (D-L) profiles. Modified from Gawthorpe & Leeder (2000).

As well as recent fault shape (e.g. Torabi et al., 2019) and growth (e.g. Jackson et al., 2017; Rotevatn et al., 2018b) model reviews and advances, normal faults are attracting research in areas of:

- spatial distribution of strain across relay zones (Childs et al., 2019; Nixon et al., 2019) and its impact on fluid flow (Fossen & Rotevatn, 2016; Botter et al., 2017; Dimmen et al., 2017);

- fault-propagation folding and its influence on accommodation distribution (Lewis et al., 2015; Khalil & McClay, 2016; 2018; Smart & Ferrill, 2018; Serck & Braathen, 2019); and
- predictive model improvement of hydrocarbon migration across faults (Wood et al., 2015a,b; Pei et al., 2015; Fisher et al., 2018)

Numerical models have proven to be instrumental in understanding fault evolution mechanics and accommodation development (Cowie & Scholz, 1992; Cowie et al., 2000; Finch et al., 2004; Hardy & Finch, 2005; 2006; Carmona et al., 2010; Botter et al., 2014; 2016; Smart & Ferrill, 2018). The improved capability of numerical models, particularly from advanced computing power, will continue to contribute to solving future fault-related challenges.

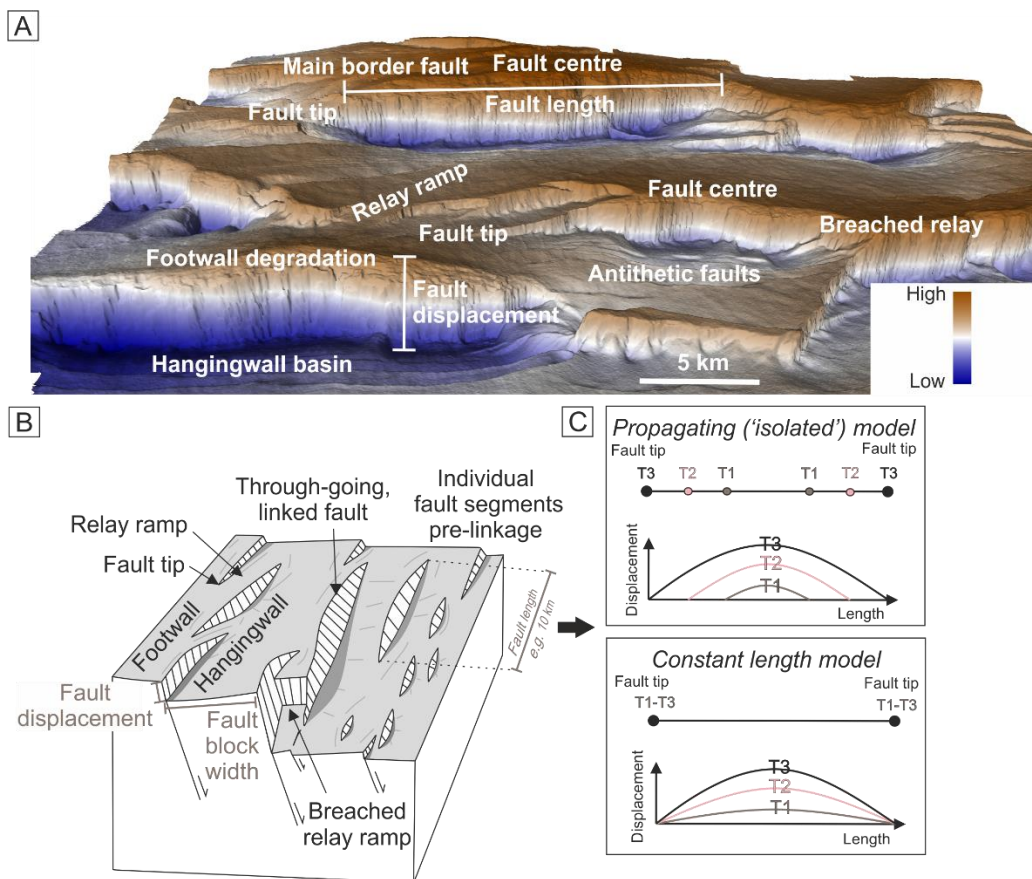


Figure 2.5. Key elements of a normal fault set. A) Time map from NW Shelf, Australia with a strike view and key features labelled. B) Key features labelled on a schematic diagram with cross-

sectional and 3D view (modified from Schultz et al., 2009). C) The two fault growth models describing the displacement-length relationship over time (modified from Jackson et al., 2017).

2.1.3. Tectono-stratigraphy

Tectono-stratigraphy is the discipline that focuses upon the analysis of depositional systems that are influenced by tectonics (Prosser, 1993). One major control on the sedimentary infill of a half-graben basin (Bosworth, 1985; Rosendahl et al., 1986) is the fault-related displacement rate. When a fault is active, subsidence increases incrementally over time as a result of a series of earthquakes and in each event, the hangingwall subsides, and accommodation is created for sediments to fill (Jervey, 1988; King et al., 1988; Stein et al., 1988). Subsidence increases to its maximum rate during the rift climax and decreases thereafter until fault activity ceases (Hooke, 1972; Scholz et al., 1986). The greater creation of accommodation in the hangingwall allows a thicker accumulation of sediments than on the footwall (Prosser, 1993). Accommodation creation is greatest in the immediate hangingwall of the fault and decreases away from the fault to the axis of fault block rotation ('hinge' or 'fulcrum') (Ravnås & Steel, 1998). As a result, across-fault thickening, a hangingwall growth wedge and gradual tilting of hangingwall strata are typical features of sedimentary sequences that are influenced by movement on the fault (Jackson et al., 1988; Prosser, 1993; Nøttvedt et al., 1995). The resulting succession is known as the 'syn-kinematic' or 'syn-rift' megasequence and can be identified based on these criteria in field or seismic data (e.g. Figs. 2.6 and 2.7). Pre-rift strata underlie the syn-rift megasequence. The pre-rift megasequence has a conformable thickness across and away from the fault and no rotation in the hangingwall, but is rotated in the uplifting and tilting footwall block. Post-rift strata are deposited when fault activity has ceased. If accommodation remains in the basin, it is possible for across-fault thickening and a wedge-shaped geometry to persist until sediments fill the basin (Ravnås & Steel, 1998). It can therefore be cryptic to interpret the syn- to post-rift transition. However, the strata will no longer be rotated towards the fault when faulting ceases and thus the change from tilted to sub-horizontal strata defines the cessation of fault activity.

Stratigraphy was first divided into pre-, syn- and post-rift megasequences related to distinct phases of tectonic plate motion by Hubbard et al. (1985). Prosser (1993) proposed a four-part framework that subdivides the sedimentary succession in rift basins into the rift initiation, rift climax, early post-rift and late post-rift phases. Modern studies hardly deviate from this framework, with the exception of fault-segment scale studies that tend to alternatively refer to the stratigraphy associated with individual growth stages of faults (e.g. ‘fault initiation’, ‘fault linkage’, ‘through-going fault’, ‘fault death’, in sensu Cowie et al., 2000; Gawthorpe & Leeder, 2000), rather than the rift development stage. Characterising stratigraphy in relation to the onset, cessation and duration of faulting is a valuable approach for analysis of basin control. It is important to consider that a megasequence may represent the syn-kinematic sequence to a particular fault, but could represent the post-kinematic sequence to an adjacent fault if fault activity was diachronous. Similarly, activity on a particular fault may have ceased, but if overall stretching persists, the post-rift megasequence to that fault represents the syn-rift megasequence on the scale of the whole rift basin. An understanding of diachroneity within and across different length scales is therefore an important consideration in basin-scale studies and has important implications for the development of key surfaces in the stratigraphic record. This is discussed further in section 2.2.

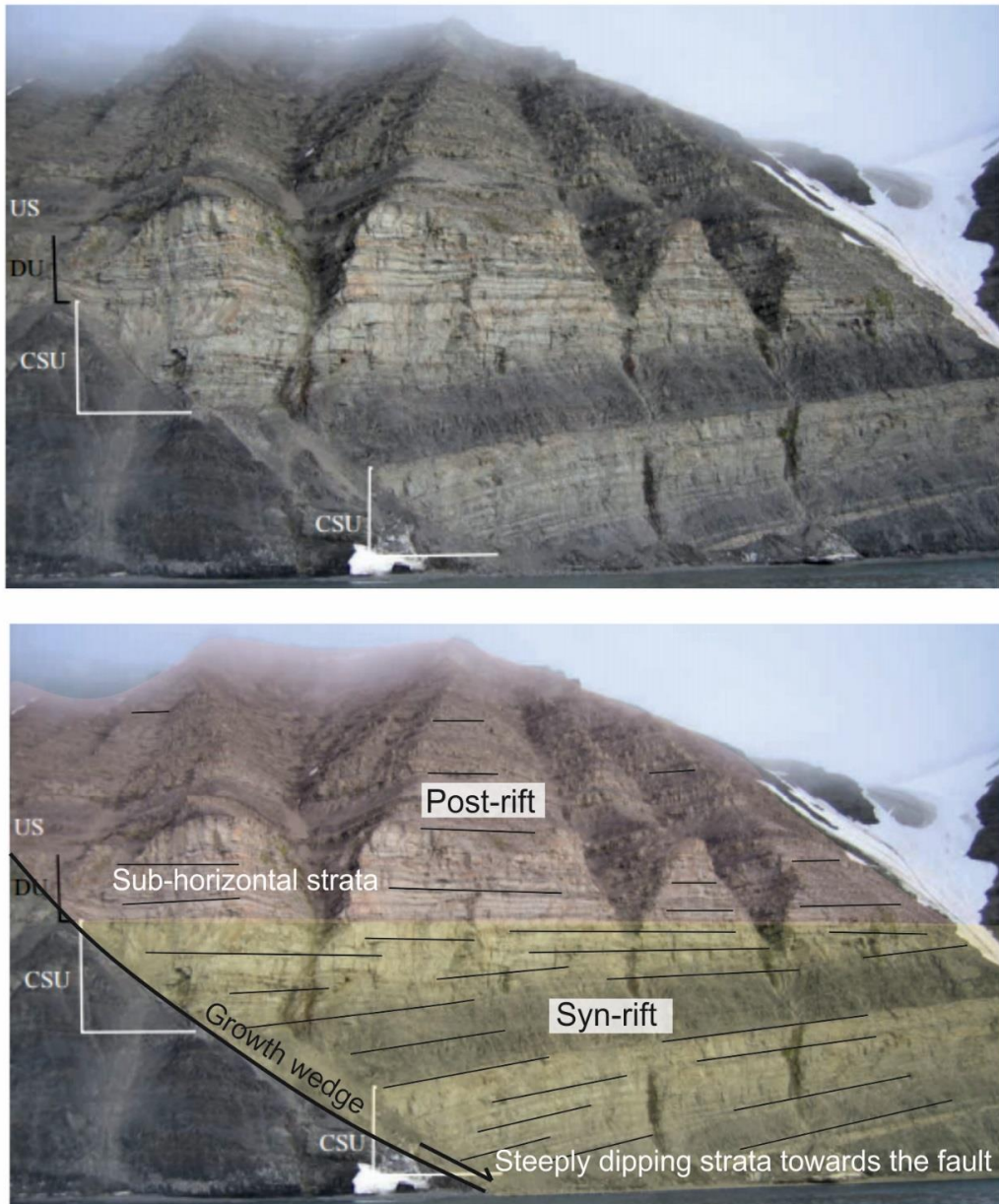


Figure 2.6. Syn- and post-rift megasequences exposed in Eastern Svalbard (Osmundsen et al., 2014). Note the syn-rift growth wedge (yellow) that thickens towards the fault. Therein strata dip steeply towards the fault at the base and shallow towards the top. There is no thickening towards the fault and strata dip sub-horizontally in the post-rift megasequence (pink). CSU = composite sandstone unit; DU = draping unit; US = upper shale from Osmundsen et al. (2014).

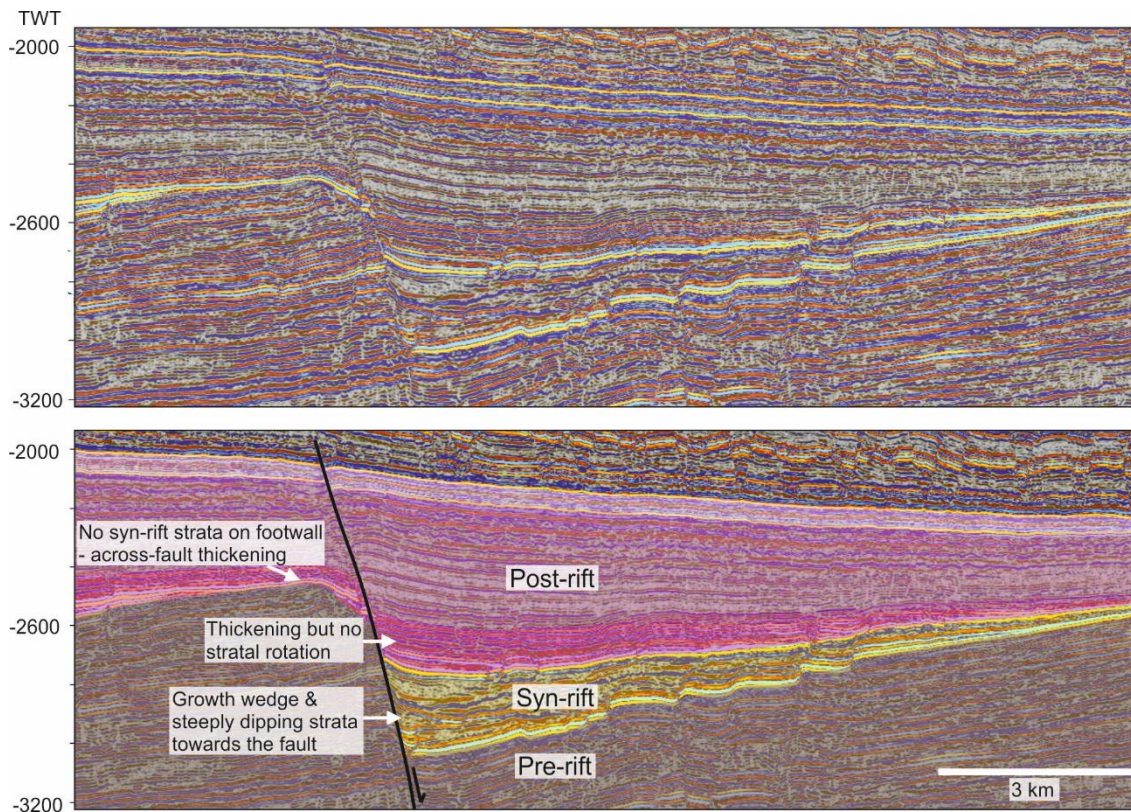


Figure 2.7. Pre-, syn- and post-rift megasequences in seismic data from NW Shelf, Australia. Note the syn-rift growth wedge (yellow) that thickens towards the fault. Therein strata dip steeply towards the fault at the base and shallow towards the top. Across-fault thickening is apparent with no syn-rift strata on the footwall. Early post-rift strata (dark pink) present thickening towards the fault due to prior underfilling, but no stratal rotation. Later post-rift strata (light pink) heal the topography. The fault is later reactivated producing stratal offsets in the younger sequences.

2.1.4. Tectono-sedimentary models

In rift basins, allogenic controls of tectonics and sedimentation vary significantly across different length-scales, rendering the ratio of accommodation to supply different at any given time and position. Accordingly, the nature of stratigraphic stacking, and the style and diachroneity of key surfaces vary along-strike as a result of the combined influence of both controls. Tectono-sedimentary evolution on the rift margin varies substantially from that towards the rift axis. Elevated rift shoulder topography at the margin promotes continental basins with a dominance of aeolian and fluvial processes, whereas marine basins characterised by shelf to slope processes may develop towards the axis (Gawthorpe & Leeder, 2000). On a fault-block scale, the growth

and evolution of normal faults has a profound impact on the depositional environment, facies distribution, stacking patterns and ultimately the stratigraphic architecture preserved within a rift basin. A range of tectono-sedimentary models for continental to marine environments at various stages of fault evolution are presented in Figure 2.8. The most recent comprehensive summary of environmental development around evolving normal faults in rift basins is provided by Gawthorpe & Leeder (2000) and the full suite of tectono-sedimentary evolutionary block models can be found therein. Structure influences the key elements responsible for deposition and preservation of sediment: the sediment source, transport pathway, sediment entry point and sink. The sediment is sourced from subaerial or submarine highground, is transported largely following the structural gradient and is deposited where streampower is diminished and accommodation persists.

2.1.4.1. Sediment source and transport pathway

The sediment source arises at the distal hinterland or from the rift interior. Its sediment yield is influenced by the substrate; from the rock type, its erodibility and its transport capacity, which vary spatially and temporally as successive layers become unroofed (Evans, 1990; Mortimer & Carrapa, 2007; Bilal et al., 2018). As footwall uplift rate increases, the relief of the sediment source follows suit, until it reaches equilibrium with the denudation rate (Gawthorpe & Leeder, 2000). The ability of a drainage network to supply the sediment from the source relies on topographic gradients generated by the pre-rift topography (Seeger & Alexander, 1993; Ravnås & Steel, 1998) and the syn-rift structural evolution and its interaction with climate (Milliman & Syvitski, 1992; Jackson & Leeder, 1993; Lambiase & Bosworth, 1995; Allen, 2008; Whittaker et al., 2010). The half-graben morphology generates steep slopes at fault scarps, moderate slopes along relay zones and gentle slopes down and along the hangingwall towards the deepest part of the basin. The slopes promote sediment flux via rivers and landslides in the subaerially exposed areas (Whittaker et al., 2010) and sediment gravity flows in their submarine counterparts. Slopes can vary over time as tilting occurs in response to active faulting and causes sediment transport pathways to adjust accordingly in a dynamic landscape (Cowie et al., 2006; Attal et al., 2008).

The drainage can be transverse (perpendicular to the fault trend) or axial (parallel to the fault trend) (Leeder et al., 1996). Its area (A) relates to the principal stream length (L) and therefore length of the tectonic slope, through Hack's Law (Hack, 1957), $L = 1.4A^{-0.6}$ (Leeder et al., 1991). Catchments derived on footwalls are therefore generally smaller than those on hangingwall dip slopes. Moreover, it has been shown that drainage catchments are generally larger towards the centre of faults, where displacement is greatest, than towards the fault tips (Elliott et al., 2012; Bilal et al., 2018). In order for rivers to maintain their course during active rifting, their downcutting erosion rate must exceed or equal uplift rates (Ravnås & Steel, 1998; Gawthorpe & Leeder, 2000), otherwise they become diverted and even reversed. Drainage reversal is documented in a number of rift basins including, but not limited to: the Plio-Pleistocene Palomas Basin, southern Rio Grande Rift, New Mexico, USA (Leeder et al., 1996); the Middle Jurassic-Palaeocene, North Træna Basin, Lofoten Margin, Norway (Henstra et al., 2017); the Miocene, El Qaa Fault Block, Suez Rift, Egypt (Muravchik et al., 2018) and the Lower Cretaceous Tanan sub-basin of the Tamtsag Basin in Mongolia (Zhou et al., 2014).

2.1.4.2. Sediment entry points

Sediment entry points to the basin arise downdip of erodible substrate from major footwall crests and islands (Surlyk, 1978; Leeder et al., 1991; Roberts et al., 1993), at transfer zones (Leeder & Gawthorpe, 1987; Gawthorpe & Hurst, 1993) and at antecedent drainage system outlets (Leeder et al., 1988). As a result, there are complex process and architectural interactions between depositional systems within the same basin, but with different origins. The Upper Jurassic fill within the Snorre Fault Block, Norwegian northern North Sea presents a good example of multiple syn-rift hydrocarbon reservoirs forming from various sedimentary inputs within a single fault block (Nøttvedt et al., 2000).

The resultant depositional system type depends upon the water depth (amount of accommodation) and in shallow water environments, the dominant river, wave or tidal process regime. Hangingwall and footwall-derived shorefaces, fan deltas, talus cones, submarine fans and slope

aprons are some of the depositional systems that can be observed across a given rift basin, as well as axially-derived systems (Leeder & Gawthorpe, 1987; Ravnås & Steel, 1998; Gawthorpe & Leeder, 2000). It has been suggested that the size of a fan is related to the hangingwall subsidence rate (Allen & Densmore, 2000; Allen & Hovius, 1998), which is temporally variable.

2.1.4.3. Sediment sinks

The coarsest sediment becomes trapped in the closest sub-basins to the hinterland (e.g. Balázs et al., 2017) and the more distal areas receive most of their coarsest sediment from rift interior sources. In a simple case of rift interior sources, the difference in volume between a pre-rift subaerial footwall and its post-rift degraded subaerial footwall is equal to the volume of sediment in the adjacent, submerged sink, assuming no along-strike resedimentation, hangingwall-derived additions or submarine degradation of the fault scarp (Ravnås & Steel, 1998). As a result, source terrain that is close to base level prior to rifting produces small depositional systems relative to the size of the sink and accordingly, underfilled basins arise. This contrasts with high relief source terrain, for a given substrate type, which has a greater erosion potential, can produce larger depositional systems, and thus filled basinal sinks; as demonstrated by Geurts et al. (2018) from numerical modelling of the central Italian Apennines. As well as the assumptions outlined above, this does not account for the effect of backtilting on footwall sediment flux. Pechlivanidou et al. (2019) recently countered previous models that show enhanced sediment flux with higher fault-related catchment relief (cf. Syvitski & Milliman, 2007), by presenting reduced erosion rates as a result of backtilting.

The overall infill type of a basin can be overfilled, balanced, underfilled or sediment starved (Ravnås et al., 2000), which is a function of the amount of sedimentation relative to the amount of accommodation. The structural role on this balance is dependent on the spatial and temporal variation in hangingwall subsidence and footwall uplift rates, and therefore: 1) the location and size of the drainage catchment, 2) the distance from source to sink, 3) the structural gradients of the sediment transport path, 4) the potential for sediment to reach the basin, 5) overall

accommodation of the sink, and 6) the depositional style. Of course, structure also plays a fundamental role in the ultimate preservation of the stratigraphy, with rapid uplift and exhumation resulting in denudation of archival landscapes (DiPietro, 2018).

The accommodation and process regime can vary significantly through time in rift basins as a result of variable fault displacement rates, its interplay with other major controls and control system feedbacks. As such, depositional systems can advance basinwards, retreat landwards, be switched off, diverted or degraded, resulting in complex stacking patterns. Better constraint of this variation in three dimensions would facilitate inversion of the stratigraphic record to deconvolve and quantify the relative importance of allogenic controls.

Furthermore, there is a dominance of footwall-derived depositional systems presented in the literature that may be unrepresentative of the distribution and relative importance of sediment input points within rift basins in general. In part, this is due to the proliferacy of the rift basins studied that generated these models. The Gulf of Corinth has been particularly influential in this regard, as it is characterised by a number of large, antecedent, transverse drainage systems that are excellently exposed (Dart et al., 1994; Gawthorpe et al., 1994; Ford et al., 2007; Rohais et al., 2007; Backert et al., 2010; Gobo et al., 2015). We later contrast the relative importance of various sediment input points within this basin to those within the northern Carnarvon Basin, NW Shelf, Australia.

This section focusses on the tectonic control on stratigraphy, but other allogenic controls (climate, base level) and their influence on sediment supply, also play major roles. These have been considered extensively in the literature and have resulted in the development of sequence stratigraphy as a framework in basin analysis. Sequence stratigraphy will hence be the focus of the following section. Ultimately, tectonic influences must be incorporated into sequence stratigraphy for a comprehensive understanding and in order to make predictions in rift basins.

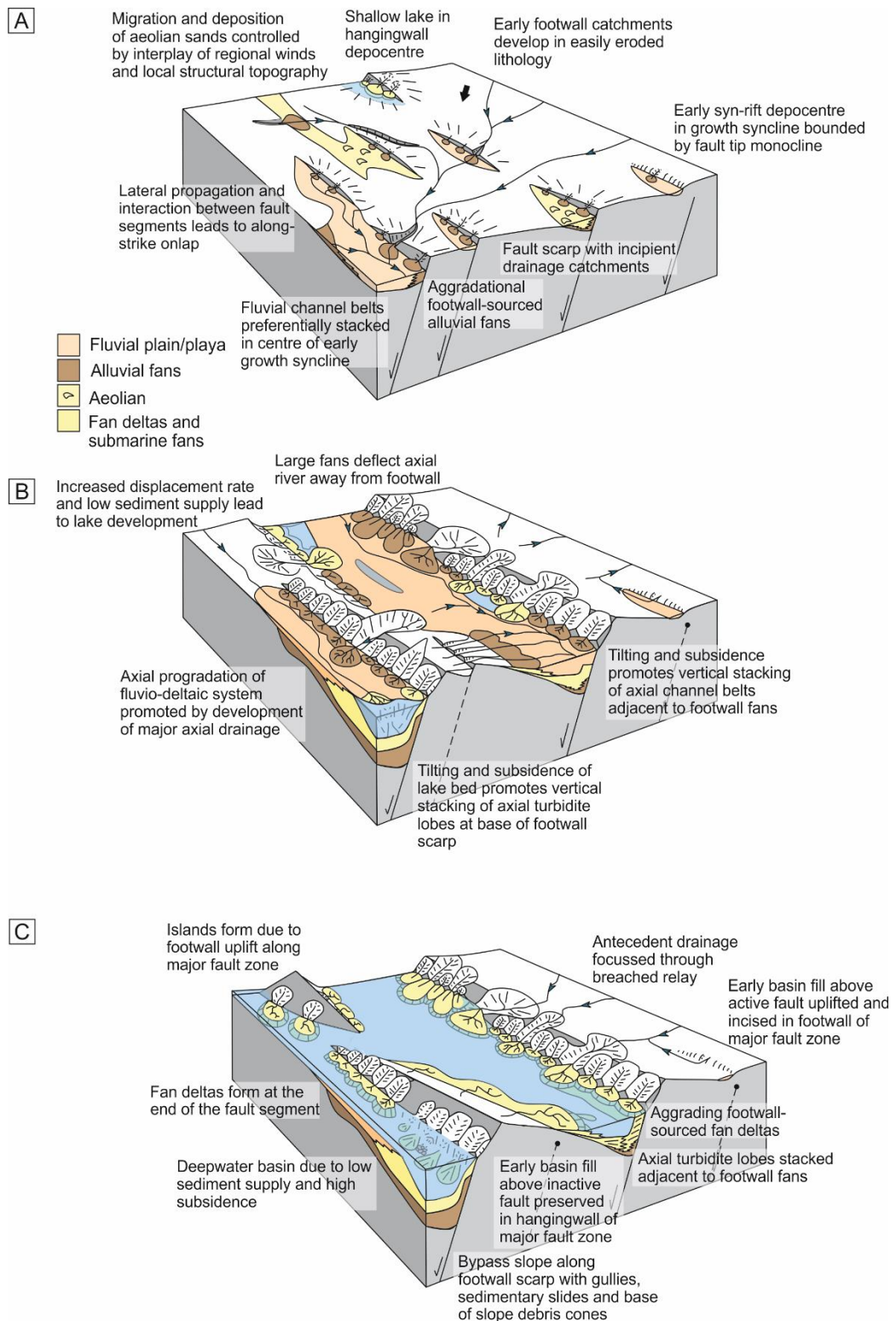


Figure 2.8. A range of tectono-sedimentary models for different depositional environments and stages of fault evolution. A) Evolution of a continental environment during fault initiation stage. B) Evolution of a continental environment from the fault interaction and linkage to the through-going fault stage. C) Evolution of a coastal/marine environment at the fault through-going fault stage. Modified from Gawthorpe & Leeder (2000).

2.2. Sequence stratigraphy

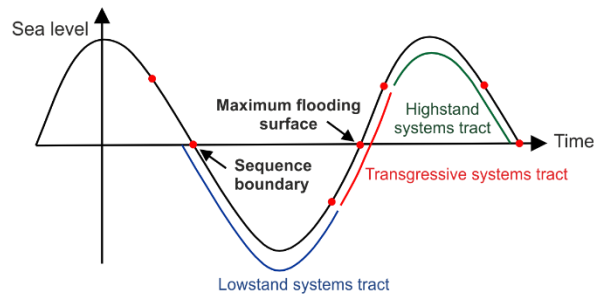
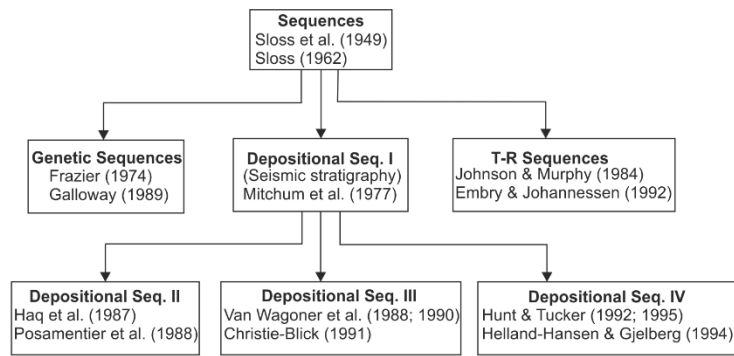
2.2.1. History of sequence stratigraphy

Sequence stratigraphy is both a method and model that is used for description, interpretation and prediction of strata, with a number of important applications in basin analysis across different scales. It is defined as “the study of rocks within a framework wherein the vertical succession of rocks is subdivided into genetically related units bounded by surfaces, including unconformities and their correlative conformities” (Mitchum et al., 1977). As a chronostratigraphic framework, it fundamentally relates stratigraphic units, facies and depositional elements within sedimentary basins in time (Catuneanu, 2006), and to some extent, space. The wave of sequence stratigraphy theory started with the defining of a ‘sequence’ as a stratigraphic unit bounded by regional unconformities (Sloss et al., 1949). Following this, a series of papers by Harry Wheeler documented the development of unconformities and sequences, using a model based on sediment supply imprinted on a cyclic base level (Wheeler & Murray, 1957; Wheeler, 1958; 1959; 1964a,b). It was not until 1977 that sequence stratigraphy became a mainstream practice, when the Exxon Production Research Company used seismic data to demonstrate its value for stratigraphic subdivision, correlation and interpretation of depositional history (Payton, 1977 and papers therein; e.g. Vail et al., 1977; Mitchum et al., 1977). Eustatic sea level was used as a framework for stratal stacking, whereby its forcing on coastal migratory trends was considered responsible for the observed cyclical stacking styles, and its predictability useful for interpretations (Posamentier et al., 1988; Posamentier & Vail, 1988). Later, tectonic influences were incorporated, particularly as it was acknowledged that deposition could occur during eustatic sea level fall, and net ‘relative’ sea level (base level) rise was required for preservation (Hunt & Tucker, 1992; Posamentier & James, 1993; Christie-Blick & Driscoll, 1995; Posamentier & Allen, 1999). A plethora of sequence stratigraphy terminology ensued in the literature as the model was applied to different datasets in different basins (section 2.2.2) and later work suggested a return to observation-based stratigraphy, rather than the assignment of model-driven interpretations (Neal & Abreu, 2009; Neal et al., 2016) (section 2.2.3). Most recently, it has been

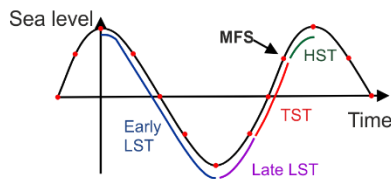
acknowledged that fluctuations in tectonic subsidence (Dorsey et al., 1995; Mortimer et al., 2005) and sediment supply can produce equivalent cyclical stacking patterns to those from eustatic base level cycles (Burgess, 2016; Schwarz et al., 2016; Zhang et al., 2018), but whether the stratigraphic outcomes are truly non-unique (Burgess & Prince, 2015), is yet to be found.

2.2.2. Sequence stratigraphic terminology

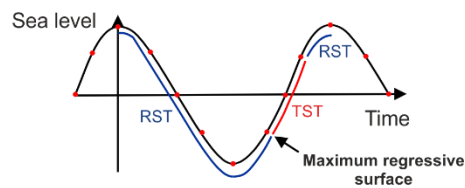
Key surfaces observed in the rock record are associated to positions on a cyclical base level curve (Fig. 2.9); notably, the maximum flooding surface and the sequence boundary. The sequence boundary (or subaerial unconformity as originally recognised) corresponds to the point with the maximum falling gradient on a relative sea level curve, i.e. when relative sea level falls at the greatest rate (e.g. Sloss, 1949; Vail et al., 1977; Posamentier et al., 1988; Van Wagoner et al., 1988). Conversely, the maximum flooding surface generally corresponds to the point with the maximum rising gradient on a relative sea level curve, i.e. when relative sea level increases at the greatest rate (Galloway, 1989; Posamentier et al., 1988; Van Wagoner et al., 1988). Systems tracts are assigned to the rocks deposited during the phases of the relative sea level curve between key surfaces (Fig. 2.9). In Posamentier & Vail (1988), the lowstand systems tract occurs on the falling limb of the relative sea level curve, between the sequence boundary and a position near the start of relative sea level rise; the point often referred to as the transgressive surface (Van Wagoner, 1995) or maximum regressive surface (Helland-Hansen & Martinsen, 1996). The transgressive systems tract occupies the rising limb of the relative sea level curve. The highstand systems tract corresponds to the period between the end of relative sea level rise to the subsequent sequence boundary (Posamentier & Vail, 1988). The definition of a sequence, the precise positions of key surfaces and systems tracts with reference to a relative sea level curve and overall nomenclature have been debated in the literature and applied differently according to the limitations of individual datasets (Fig. 2.9). A summary and review of the various schemes is provided in Catuneanu (2006) and Catuneanu et al. (2009).



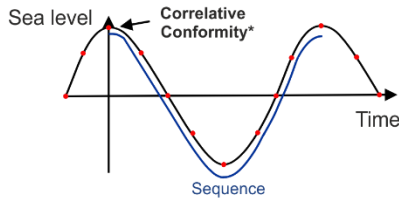
Genetic Sequence



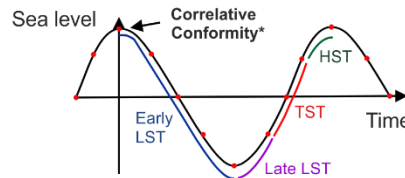
T-R Sequence



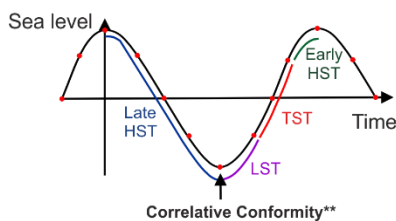
Depositional Sequence I



Depositional Sequence II



Depositional Sequence III



Depositional Sequence IV

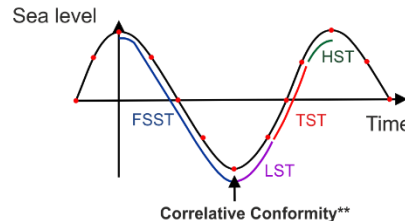


Figure 2.9. Sequence stratigraphic schemes in the literature. HST = Highstand Systems Tract; TST = Transgressive Systems Tract; LST = Lowstand Systems Tract; FSST = Falling Stage Systems Tract; RST = Regressive Systems Tract; T-R = Transgressive-Regressive; MFS = Maximum Flooding Surface; Correlative Conformity* = according to Posamentier & Allen (1999); Correlative Conformity** = according to Hunt and Tucker (1992). Modified from Catuneanu (2006) and Catuneanu et al. (2009).

The definition of a sequence became contentious with the introduction of correlative conformities as sequence bounding surfaces. Unlike the subaerial unconformity that is more straightforward to identify, the correlative conformity is its subsurface counterpart and more cryptic to map and correlate, particularly in outcrop, core or wireline data. Early work with seismic data ('Depositional Sequence I; Fig. 2.9) uses the subaerial unconformity and its correlative conformity as the sequence bounding surface (Mitchum et al., 1977). In relation to timing, the refined placement of the correlative conformity, either at the onset or end of base level fall, separates the later sequence stratigraphic schemes 'Depositional Sequence II' (Haq et al., 1988; Posamentier et al., 1988; Posamentier & Allen, 1999; Catuneanu, 2006) and 'Depositional Sequence III and IV' (Van Wagoner et al., 1988; 1990; Christie-Blick, 1991; Hunt & Tucker, 1992; 1995; Plint & Nummedal, 2000; Catuneanu, 2006; Fig. 2.9). This separation is important because they are defined as either the base (oldest clinoform associated with offlap) or top (youngest clinoform associated with offlap) of the regressive, prograding sedimentary package. Arguably, the latter is the more preservable choice, as it is deposited immediately before a base level rise and importantly separates a prograding trend during regression from an onlapping, potentially retrograding trend during transgression (Catuneanu, 2006), although this assumes an unchanging sediment supply, which is contended throughout this work and elsewhere (Schlager, 1993; Muto & Steel, 1997; Neal & Abreu, 2009; Burgess, 2016; Zhang et al., 2018; Toby et al., 2019). Associating the base of the prograding package with the onset of base level fall is also problematic in deep water environments, because the initiation of sediment gravity flows to the basin floor can occur much later than the onset of base level fall, with an arguably higher dependence on sediment supply and autogenic factors.

An alternative sequence bounding surface was presented with the 'Genetic sequence' scheme (Frazier, 1974; Galloway, 1989; Catuneanu, 2006), as the maximum flooding surface. The maximum flooding surface has lesser diachroneity downdip (Catuneanu, 2002) than surfaces dependent on erosional processes, but as with all sequence stratigraphic surfaces, can present substantial diachroneity along-strike, particularly in tectonically-active settings (Gawthorpe et al., 2003; Jackson et al., 2005). Most importantly, maximum flooding surfaces are the easiest to

identify on a basin-scale within extensive condensed sections that have numerous identifiable criteria, including: low acoustic impedance contrasts in seismic data due to the homogeneous lithology; high gamma-ray responses in well data due to high organic matter content; the top of the fining-upward sequence in core and outcrop (textural analysis in thin section may be required) (Catuneanu, 2006); highest bioturbation index or landward shift in ichnofacies, with perhaps ichnofacies that are resilient to low oxygen conditions, such as *Zoophycos*; and/or the presence of firmgrounds or hardgrounds (high cementation) due to diminished sediment supply (Pemberton & MacEachern, 1995; Ghibaudo et al., 1996).

2.2.3. Application of sequence stratigraphy

Successful application of sequence stratigraphy to sedimentary basin analysis firstly requires a thorough, observation-based description of the rock succession. Cross-sections are required to identify key stratigraphic surfaces and units. These may or may not coincide with lithostratigraphic contacts and units, which are highly diachronous and can develop within sequence stratigraphic units (Catuneanu, 2006). In order to identify sequence stratigraphic surfaces, the contact type must be identified (conformable, unconformable) with the use of stratal terminations, and the change of depositional system across the surface must be interpreted based on sedimentary facies changes. The identification of the changes are at the mercy of the dataset; facies changes and sequences that are observed in outcrop (e.g. m-scale) would be encompassed within a single wavelet in seismic data (e.g. 10 m-scale). In this respect, higher resolution datasets often yield a higher frequency cyclicity in the observations. The pre-requisite of a robust palaeo-environmental interpretation is a unique aspect of sequence stratigraphy and therefore requires prior detailed sedimentological analysis to characterise rock bodies. To this avail, detailed facies analysis is undertaken in each data chapter herein. Fluvial, marginal and to some extent, deep marine depositional systems migrate predictably with base level changes, whereby with a base level rise the depositional systems (and shoreline) retreat landwards (transgress), and with a base level fall the depositional systems advance basinwards (regress). According to Walther's Law, a vertical succession of juxtaposed shallower-deeper depositional environments is therefore

diagnostic of lateral facies shifts and the controlling base level changes (Middleton, 1973; Bates & Jackson, 1987; Miall, 1990; 1997; Posamentier & Allen, 1999). The notion of shoreline migration was used as the foundation of sequence stratigraphy as the shallow marine environment acts as the transition zone between non-marine and marine environments and is most sensitive to base level changes. Sequence stratigraphy has been applied to systems farther afield, but here the focus is within the marginal realm.

Depositional trends are clearly presented in clinoforms. A clinoform is a sigmoidal geometric form that comprises of flat-lying topsets, basinward-dipping foresets and flat-lying bottomsets that can arise across a number of scales from coast to shelf in different settings (Gilbert, 1885; Rich, 1951; Pirmez et al., 1998; Steel & Olsen, 2002; Patruno et al., 2015; Patruno & Helland-Hansen, 2018; Cosgrove, 2019). Fan deltas produce typical clinoformal geometries in cross-section and are a focus of investigation here (Fig. 2.10). The break in slope between topsets and foresets is known as the topset-foreset breakpoint (Fig. 2.10) and similarly to the shoreline, its trajectory through time can be used in the analysis of depositional trends and thus, base level changes ('trajectory analysis': Helland-Hansen & Hampson, 2009).

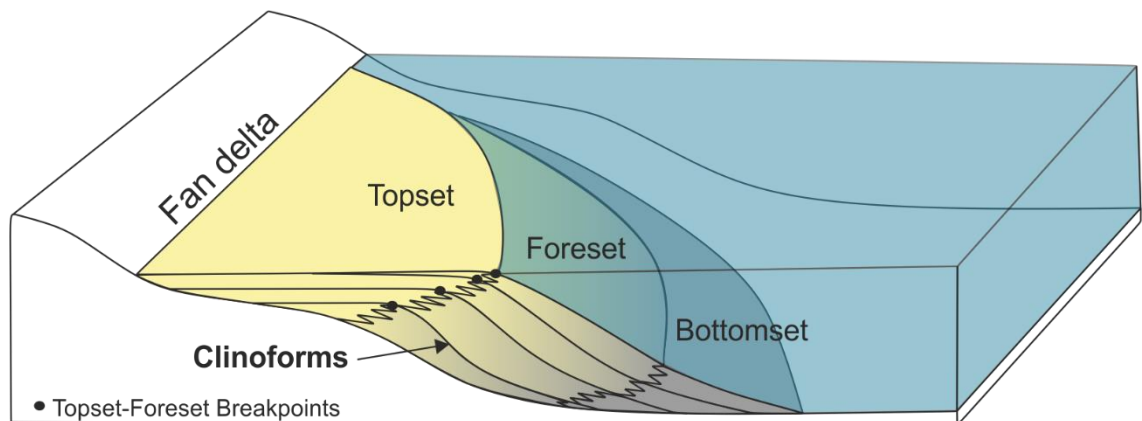


Figure 2.10. The geometry and terminology of clinoforms; the building-blocks of fan deltas (after Gilbert 1885; Steel & Olsen, 2002).

A well-established concept for understanding depositional system and shoreline migration, and therefore the nature of stratal unit stacking, is the ratio of rate of accommodation change to rate of sediment supply change ($\delta A/\delta S$) (Sloss, 1962; Curray, 1964; Vail et al., 1977).

Accommodation is defined as “the space made available for potential sediment accumulation” and represents relative base level change, incorporating eustatic base level change, tectonic subsidence and uplift (Jervey, 1988; Posamentier et al., 1988), and generally equates to depth from the water surface to the top of the depositional surface. As presented in Figure 2.11, the following concepts in regard to shoreline migration are generally accepted: 1) when a depositional system regresses and the stacking is progradational, that $A < S$ and A/S is < 1 ; 2) when a depositional system transgresses and the stacking is retrogradational, that $A > S$ and A/S is > 1 ; 3) when a depositional system neither advances nor retreats, it aggrades such that $A = S$ and A/S is equal to 1. The terms progradation, retrogradation and aggradation (Fig. 2.11) were coined to describe the nature of sedimentary stacking in response to this interplay through time (Van Wagoner et al., 1990). Degradation was emphasised by Neal and Abreu (2009) and Neal et al. (2016) to represent scenarios where A/S is < 1 and decreasing. In essence, progradation and retrogradation represent a lateral migration in the shoreline and depositional system through time, and aggradation and degradation represent a vertical migration.

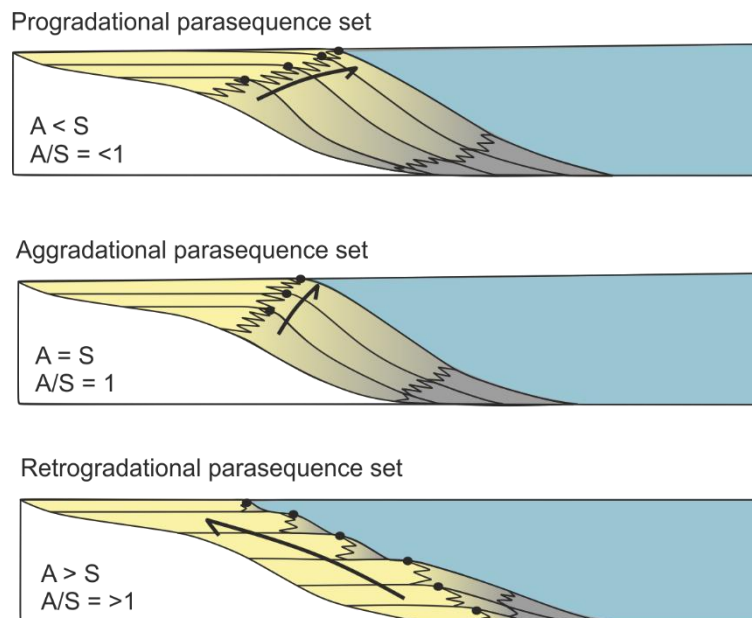


Figure 2.11. Stacking trends within clinoformal parasequence sets in relation to the $\delta A/\delta S$ ratio (after Galloway, 1989; Van Wagoner et al., 1990).

The $\delta A/\delta S$ ratio is as an observation-based approach to building predictive frameworks (Neal & Abreu 2009; Neal et al., 2016), by using stratal terminations, trajectory analysis (Helland-Hansen & Gjelberg, 1994; Helland-Hansen & Martinsen, 1996) and key stratal surfaces to identify depositional sequences (Sloss et al., 1949) and stacking patterns. The $\delta A/\delta S$ ratio has been criticised due to the dimensional confusion of comparing units of 'space' with that of sediment supply (Muto and Steel, 1992; 1997). The assignment of stacking patterns to the $\delta A/\delta S$ ratio for control interpretations and prediction is also problematic, because sedimentation reduces accommodation. The two terms of the ratio are not independent. Other problems include the absence of erosion as a mechanism for creating space on a large-scale (e.g. Backert et al., 2010; Gomis-Cartesio et al., 2017) and the feedbacks that occur between processes, for example, sedimentation can vary with climate-induced base level changes (Collier et al., 1990; 2000), or tectonic displacement (Elliott et al. 2012; Bilal et al., 2018). Ultimately, a framework should be established that incorporates all potential inputs and outcomes.

Once facies, key surfaces and stratal stacking within the succession are identified, described and interpreted, sequences can be assigned to their respective systems tracts of the relative sea level curve. The sequence stratigraphic framework is then established and can be used to make predictions beyond the immediate dataset. Numerical modelling is particularly useful for making predictions due its ability to simulate multiple scenarios and outcomes.

2.2.4. Sequence stratigraphic numerical modelling

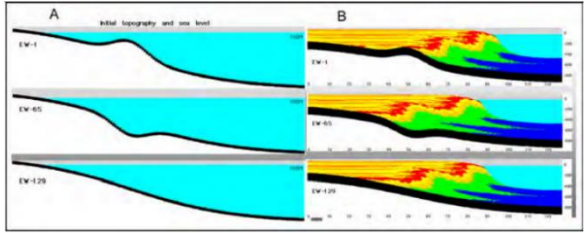
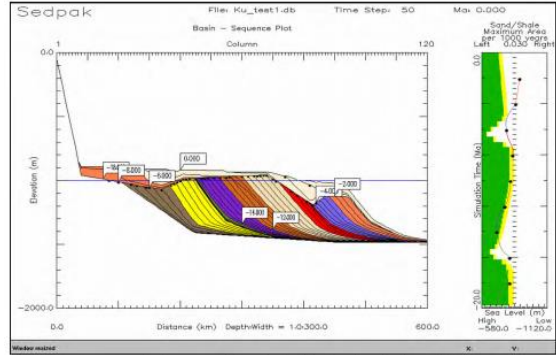
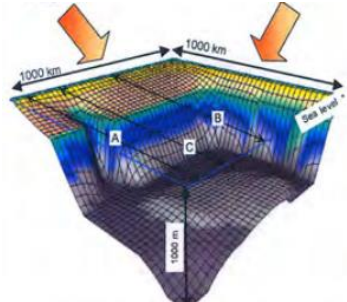
Computer modelling is an efficient way to simulate geological processes and their deposits across different timescales. As such, and with the possibility to test a number of possible input variables and outcomes, it is the technique that enables us to become closest to predictive capability. Forward models use a known process response to a given set of numerical input parameters to simulate a product (Cross & Lessenger, 1999; Watney et al., 1999; Burgess, 2012). The first pivotal forward sequence stratigraphic model was developed and published by Mac Jervy of Exxon in 1988 (Jervy, 1988). The model incorporated sinusoidal sea-level change and hinged

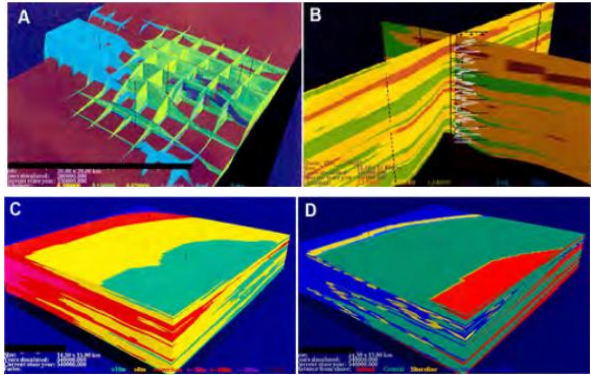
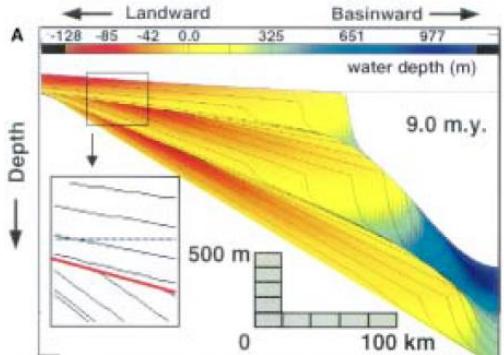
subsidence to simulate accommodation generation and assumed a constant sediment supply. Three examples of subsidence rate were adopted (low, intermediate and high), which are regarded to represent three locations, near, intermediate, and far from the basin margin, if subsidence rate is assumed to increase toward the basin centre. The model successfully predicted the two significant surfaces that had been observed in seismic data (unconformities and downlap surfaces) and inferred their location to be at the inflection points of a eustatic sea-level cycle, where the rate of sea-level change is fastest. Alongside low resolution seismic data, the model was used by Exxon to provide the theoretical underpinning of sequence stratigraphy (Van Wagoner et al., 1988; Posamentier et al., 1988; Posamentier & Vail, 1988).

Today, computing power has significantly advanced and has facilitated the generation of multiple stratigraphic numerical models. Paola (2000) categorises models into a number of types, from deductive to rule-based, coupled and uncoupled, and analytical to simulation models. Huang et al. (2015) also review several specific models in terms of their geological function, advantages and disadvantages. For simplicity here, geometric models are distinguished from process-based models (Table 2.1). Geometric models are generally based on simple mathematical rules and generate stacking patterns in response to accommodation and supply variations, for example SEDPAK (Strobel et al., 1989; Kendall et al., 1991a,b). They do not model processes themselves, rather the consequence of processes, and as a result avoid many of the underlying assumptions of process-based models. To date, geometric models only simulate 2D cross-sections, although there have been attempts to combine multiple 2D cross-sections along-strike to make pseudo-3D plots (Thorne & Swift, 1992; Steckler et al., 1993; Wehr, 1993; Ross et al., 1995). Process-based models utilise various algorithms to simulate process regimes across different settings and include diffusion, fuzzy logic and hydraulic operating models. DIONISOS (Granjeon, 1997; 2014; Granjeon & Joseph, 1999); STRATA and SEDSIM (Tetzlaff & Harbaugh, 1989; Flemings & Grotzinger, 1996) are particularly prevalent in the literature (Table 2.1). These models may resemble the geological process regime more accurately than geometric models, but are beholden to the appropriateness of the specific algorithm to the particular depositional system and can be computationally intensive (Huang et al., 2015).

Recently, numerical modelling studies have been undertaken in the challenge to better understand sequence stratigraphic stacking and drainage dynamics. Burgess & Prince (2015) utilise a 3D stratigraphic forward model, 'Dionisos' to model stratal geometries in cross-section. They conclude that stratigraphic surfaces can be diachronous due to variable sediment supply, and emphasise the non-uniqueness of stratal geometries, i.e. a number of controlling parameters can produce the same geometry (Burgess & Prince, 2015). Madof et al. (2016) draws similar conclusion using a near-shore model that focuses upon along-strike variability in stratal geometries as a result of variable deposition. They explain the variations in terms of changing the orientation of a shoreline trend, resembling rotation around a hinge (Madof et al., 2016). Previous stratigraphic modelling of fan deltas using stratigraphic timelines and sedimentary volumes has recently been expanded to include sediment properties and internal deformation processes (Hardy, 2019). Early studies (Waltham, 1992; Hardy et al., 1992; 1994; Hardy & Gawthorpe, 1998; 2002; Ritchie et al., 1999; 2004a,b) made important progress in 3D modelling of fan deltas and analysis of their along-strike variability in sequence architecture, including the along-strike extent of key stratigraphic surfaces. Geurts et al. (2018) undertake drainage system modelling with CASCADE (Braun & Sambridge, 1997) to demonstrate drainage integration and discuss its possible occurrence in the absence of tectonic forcing. Pechlivanidou et al. (2019) use 'pyBadlands' (Salles et al., 2018) to show how Corinth Rift landscape evolution in response to active tectonic forcing impacts sediment flux to the basin. Numerical modelling studies are making rapid headway in improving our understanding of earth system processes, particularly those studies that are integrated with authentic data from the field or subsurface. However, there is yet to be a geometric model introduced that takes an unbiased approach to testing multiple allogenic controls and focuses on 3D variability of sequence architecture and key surfaces in the area around a single fault segment. Its integration with real data to deconvolve and quantify controls and outcomes would be a significant step forward.

Table 2.1. Examples of current sequence stratigraphic forward models.

Model	Type	2D/ 3D	Application	Advantages	Limitations	Example	References
CSM Suite	Process-based	2D	Clastic non-marine to shelf, carbonates and deep water packages	<ul style="list-style-type: none"> - The shelf model incorporates all allogenic controls, faulting, isostasy and subdivision of block 	<ul style="list-style-type: none"> - Does not include grain size considerations - No tides, only wave processes - 2D 		<p>Cross & Lessenger (1999); Paola (2000); Shafie & Madon (2008); Huang et al. (2015)</p>
SEDPAC	Geometric	2D	Clastic and carbonate shelf	<ul style="list-style-type: none"> - Includes allogenic controls plus water depth, erosion, faulting, compaction and isostasy - Defines a chronostratigraphic framework 	<ul style="list-style-type: none"> - Tectonic movement only varies vertically - Parameters are uncoupled - Models consequences of processes, not processes themselves 		<p>Strobel et al. (1989); Kendall et al. (1991a,b); Paola (2000); Shafie & Madon (2008); Huang et al. (2015)</p>
DIONISOS	Process-based; diffusion	3D	Clastic and carbonate shelf	<ul style="list-style-type: none"> - Includes simple tectonic constraints - Considers long- and short-term evolution/events 	<ul style="list-style-type: none"> - Uses diffusion approach to simulate sediment transport – appropriateness must be considered per scenario 		<p>Granjeon (1997; 2014); Granjeon & Joseph, (1999); Paola (2000); Shafie & Madon (2008); Huang et al. (2015)</p>

Model	Type	2D/ 3D	Application	Advantages	Limitations	Example	References
SEDSIM	Process-based; hydraulics	3D	Clastic and carbonate shelf	<ul style="list-style-type: none"> - Variable grid size - Petroleum systems focus - Outputs palaeoenv. map - Incorporates tectonics, loading, currents, storms - Fluid flow follows topography - Hydraulics approach more accurately represents sediment transport 	<ul style="list-style-type: none"> - Computationally intensive - Numerous assumptions that must be considered per scenario 		<p>Tetzlaff & Harbaugh (1989); Paola (2000); Shafie & Madon (2008); Huang et al. (2015)</p>
STRATA	Process-based; diffusion	3D	Clastic and carbonate shelf	<ul style="list-style-type: none"> - Incorporates all allogenic controls - Produces chronostratigraphic diagrams 	<ul style="list-style-type: none"> - Basic constraints - Diffusion approach not always appropriate 		<p>Flemings & Grotzinger (1996); Paola (2000); Shafie & Madon (2008); Huang et al. (2015)</p>

2.2.5. Current challenges in sequence stratigraphic analysis

Despite refinement of the sequence stratigraphic method to account for new data and different scales of investigation, sequence stratigraphic concepts themselves have scarcely evolved since their development in the 1970s and it has recently been acknowledged that they do not account for the many heterogeneities and complexities that practitioners regularly encounter. Inherent in the framework is its simplicity. For example, a symmetrical sinusoidal base level curve is typically employed to convey sequence stratigraphic concepts (e.g. Fig. 2.9). In reality, the symmetry is seldom valid or representative when considering glacio-eustatic fluctuations. Shorter stages of base level rise than fall have been shown to be prevalent throughout the Pleistocene as ice cap melting (base level rise) is a faster process than ice cap building (base level fall) (Shackleton, 1987; Blum & Price, 1998; Hay et al., 2014; Rovere et al., 2016), which has implications for the duration of sedimentation during each relative sea level phase. Arguably, the most significant simplification is the dip-directed relationship of strata with time. Indeed, depositional systems follow structural gradients, but this assumption ignores any along-strike variation in allogenic or autogenic processes that could lead to variability in stratigraphic architecture along-strike. As such, sequence stratigraphic interpretations undertaken on a given dip section may be unrepresentative of other positions along the margin (Jones et al., 2015; Poyatos-Moré et al., 2019). This is particularly pertinent in rift basins, where allogenic controls of tectonics and sedimentation vary significantly across different length-scales, rendering the ratio of accommodation to supply different at any given time and position (Hardy & Gawthorpe, 1998; Ravnås & Steel, 1998; Gawthorpe et al., 1994; Gawthorpe & Leeder, 2000). The impact that this has on the formation and diachroneity of key stratigraphic surfaces is particularly important, as correlations rely on them being spatially-continuous time-lines, which is seldom true (Holbrook & Bhattacharya, 2012; Burgess & Prince, 2015; Hodgson et al., 2016; Madof et al., 2016). In fact, a number of studies demonstrate the lateral discontinuity or absence of sequence boundaries as a result of fault displacement gradients along-strike (Dart et al., 1994; Gawthorpe et al., 1994; 2003; Dorsey & Umhoefer, 2000; Hardy & Gawthorpe, 1998; Jackson et al., 2005; Backert et al., 2010).

The Geological Society William Smith meeting in 2014, and related papers published in 2016, focussed upon the current and future state of sequence stratigraphy. The key subject in question was that as a paradigm, encompassing both a method and a model, whether sequence stratigraphy requires an ‘evolution or revolution’ in its future development (Burgess et al., 2016). Neal et al. (2016) argue that recent progress in distinguishing the sequence stratigraphic method from the model, and focussing on a common observation-based approach (Neal & Abreu, 2009), has already allowed sequence stratigraphy to be a tool that is both useful and predictive. Burgess (2016) points out that standardisation of the method is valuable, but should not be extended to interpretations. An ‘evolution’ is favoured over a ‘revolution’ in the respect of introducing the method to new datasets and data types (Turner et al., 2016) and approaching data with a broad mindset considering multiple interpretations (Hampson, 2016). The inclusion of autostratigraphic (local) controls, e.g. channel avulsion, lobe-switching, hydrodynamic forces, into sequence stratigraphy is a challenge yet to be fulfilled or widely accepted, although Muto et al. (2016) argue that it should be the forthcoming ‘revolution’. Although autostratigraphy should be fully considered in interpretations (e.g. Hampson, 2016), it could be argued that the incorporation of autostratigraphic notions for prediction is unlikely to become universal, due to the complexity of processes, their high spatial variability, system sensitivity and data resolution-dependency. However, potential lies in advancing numerical models, where outcomes of multiple scenarios of allogenic or autogenic controls can be tested (Burgess, 2016; Burgess et al., 2016; Muto et al., 2016; Balázs et al., 2017; Toby et al., 2019).

In summary, current challenges facing sequence stratigraphy are:

- 3D, particularly along-strike variability and diachroneity of sequence architecture and key surfaces
- application of the sequence stratigraphic method to tectonically-active basins
- expression of supply-driven sequences
- non-unique outcomes of multiple system controls
- application of the method to new data types

- incorporation of autostratigraphy

Indeed, numerical modelling and consideration of multiple scales and datasets is likely to be the way forward in addressing a number of these challenges. The research presented in this thesis addresses a number of the described challenges, particularly probing issues 1, 2 and 4 outlined above, but a single thesis cannot solve every issue facing the science of sequence stratigraphy. As such, the next decade of research will be an interesting time for scientific development and involvement in the sequence stratigraphic field.

2.3. References

- Allen, P.A. (2008). From landscapes into geological history. *Nature*, 451, 274-276.
- Allen, P.A. & Allen, J.R. (2013). *Basin Analysis: Principles and application to petroleum play assessment, Third edition*. John Wiley & Sons, Ltd., 619pp.
- Allen, P.A. & Densmore, A.L. (2000). Sediment flux from an uplifting fault block. *Basin Research*, 12, 367-380.
- Allen, P.A. & Hovius, N. (1998). Sediment supply from landslide-dominated catchments: implications for basin-margin fans. *Basin Research*, 10, 19-36.
- Attal, M., Tucker, G.E., Whittaker, A.C., Cowie, P.A. & Roberts, G.P. (2008). Modeling fluvial incision and transient landscape evolution: influence of dynamic channel adjustment. *Journal of Geophysical Research*, 113, F03013, doi:10.1029/2007JF000893.
- Backert, N., Ford, M. & Malartre, F. (2010). Architecture and sedimentology of the Kerinitis Gilbert-type fan delta, Corinth Rift, Greece. *Sedimentology*, 57, 543-586.
- Balázs, A., Granjeon, D., Matenco, L., Sztanó, O. & Cloetingh, S. (2017). Tectonic and climatic controls on asymmetric half-graben sedimentation: inferences from 3-D numerical modelling. *Tectonics*, 36, 2123-2141.
- Bates, R.L. & Jackson, J.A. (1987). *Glossary of Geology 3rd edition*. American Geological Institute, Alexandria, Virginia, 788pp.
- Bilal, A., McClay, K. & Scarselli, N. (2018). Fault-scarp degradation in the central Exmouth Plateau North West Shelf, Australia. In: K.R. McClay & J.A. Hammerstein (Eds.), *Passive margins: tectonics, sedimentation and magmatism*. Geological Society, London, Special Publications, 476, doi: 10.1144/SP476.11.
- Bladon, A. J., Clarke, S. M. & Burley, S. D. (2015). Complex rift geometries resulting from inheritance of pre-existing structures: Insights and regional implications from the Barmer Basin rift. *J. Struct. Geol.*, 71, 136-154.
- Blum, M.D. & Price, D.M. (1998). Quaternary alluvial plain construction in response to glacio-eustatic and climatic controls, Texas Gulf coastal plain. In: K.W. Shanley & P.J. McCabe (Eds.), *Relative Role of Eustasy, Climate and Tectonism in Continental Rocks*. SEPM Special Publication, 59, 31-48.

Braun, J. & Sambridge, M. (1997). Modelling landscape evolution on geological timescales: A new method based on irregular spatial discretization. *Basin Research*, 9, 27-52.

Bosworth, W. (1985). Geometry of propagating continental rifts. *Nature*, 316, 625-627.

Botter, C., Cardozo, N., Hardy, S., Lecomte, I., Paton, G. & Escalona, A. (2016). Seismic characterisation of fault damage in 3D using mechanical and seismic modelling. *Marine and Petroleum Geology*, 77, 973-990.

Botter, C., Cardozo, N., Hardy, S., Lecomte, I., Escalona, A. (2014). From mechanical modeling to seismic imaging of faults: A synthetic workflow to study the impact of faults on seismic. *Marine and Petroleum Geology*. 57, 187-207.

Botter, C., Cardozo, N., Lecomte, I., Rotevatn, A. & Paton, G. (2017). The impact of faults and fluid flow on seismic images of a relay ramp over production time. *Petroleum Geoscience*, 23, 17-28.

Buck, W.R. (1991). Modes of continental lithospheric extension. *Journal of Geophysical Research*, 96, 20161-20178.

Buck, W.R. (2017). The role of magmatic loads and rift jumps in generating seaward dipping reflectors on volcanic rifted margins. *Earth Planet. Sci. Lett.*, 466, 62-69.

Burchfiel, B.C. & Stewart, J.H. (1966). "Pull-apart" origin of the central segment of Death Valley, California. *GSA Bulletin*, 77, 439-442.

Burgess, P.M. (2012). A brief review of developments in stratigraphic forward modelling, 2000-2009. In: D.G Roberts & A.W. Bally (Eds.), *Regional Geology and Tectonics: Principles of Geologic Analysis*. Elsevier, Amsterdam, The Netherlands, 900pp.

Burgess, P.M. (2016). The future of the sequence stratigraphy paradigm: Dealing with a variable third dimension. *Geology*, 44, 335-336.

Burgess, P.M., Allen, P.A. & Steel, R.J. (2016). Introduction to the future of sequence stratigraphy: evolution or revolution? *Journal of the Geological Society*, 173, 801-802.

Burgess, P.M. & Prince, G.D. (2015). Non-unique stratal geometries: Implications for sequence stratigraphic interpretations. *Basin Research*, 27, 351-365.

Carmona, A., Clavera-Gispert, R. & Gratacós, O. & Hardy, S. (2010). Modelling syntectonic sedimentation: combining a discrete element model of tectonic deformation and a process-based sedimentary model in 3D. *Math Geosci.*, 42, 519-534.

Cartwright, J.A., Trudgill, B.D. & Mansfield, C.S. (1995). Fault growth by segment linkage: an explanation for scatter in maximum displacement and trace length data from the Canyonlands Grabens of SE Utah. *Journal of Structural Geology*, 17, 1319-1326.

Catuneanu, O. (2002). Sequence stratigraphy of clastic systems: concepts, merits and pitfalls. *Journal of African Earth Sciences*, 35, 1-43.

Catuneanu, O. (2006). *Principles of sequence stratigraphy*. Elsevier, Amsterdam, The Netherlands. 375pp.

Catuneanu, O., Abreu, V., Bhattacharya, J.P., Blum, M.D., Dalrymple, R.W., Eriksson, P.G., Fielding, C.R., Fisher, W.L., Galloway, W.E., Gibling, M.R., Giles, K.A., Holbrook, J.M., Jordan, R., Kendall, C.G. S.C., Macurda, B., Martinsen, O.J., Miall, A.D., Neal, J.E., Nummedal, D., Pomar, L., Posamentier, H.W., Pratt, B.R., Sarg, J.F., Shanley, K.W., Steel, R.J., Strasser, A., Tucker, M.E. & Winker, C. (2009). "Towards the Standardization of Sequence Stratigraphy". *Earth Science Reviews*, 92, 1-33.

Childs, C., Nicol, A., Walsh, J.J. & Watterson, J. (2003). The growth and propagation of synsedimentary faults. *Journal of Structural Geology*, 25, 633-648.

- Childs, C., Worthington, R.P., Walsh, J.J. & Roche, V. (2019). Conjugate relay zones: geometry of displacement transfer between opposed-dipping normal faults. *Journal of Structural Geology*, 118, 377-390.
- Chorowicz, J. (2005). The East African rift system. *Journal of African Earth Sciences*, 43, 379-410.
- Christie-Blick, N. (1991). Onlap, offlap, and the origin of unconformity-bounded depositional sequences. *Marine Geology*, 97, 35-56.
- Christie-Blick, N. & Driscoll, N.W. (1995). Sequence stratigraphy. *Annual Review of Earth and Planetary Sciences*, 23, 451-478.
- Cloetingh, S., Tibaldi, A. & Burov, E. (2012). Coupled deep Earth and surface processes and their impacts on geohazards. *Global and Planetary Change*, 90, 1-19.
- Collier, R.E.LI. (1990). Eustatic and tectonic controls upon Quaternary coastal sedimentation in the Corinth Basin, Greece. *J. Geol. Soc.*, 147, 301-314.
- Collier, R.E.LI., Leeder, M.R., Trout, M., Ferentinos, G., Lyberis, E. & Papatheodorou, G. (2000). High sediment yields and cool, wet winters: test of last glacial paleoclimates in the northern Mediterranean. *Geology*, 28, 999-1002.
- Cosgrove, G.I.E. (2019). The Continental Shelf: a Conveyor and/or Filter of Sediment to Deep-Water? PhD Thesis, University of Leeds, Leeds.
- Coward, M.P. (1986). Heterogeneous stretching, simple shear and basin development. *Earth and Planetary Science Letters*, 80, 325-336.
- Cowie, P.A., Attal, M., Tucker, G.E., Whittaker, A.C., Naylor, M., Ganas, A. & Roberts, G.P. (2006). Investigating the surface process response to fault interaction and linkage using a numerical modelling approach. *Basin Research*, 18, 231-266.
- Cowie, P.A., Gupta, S. & Dawers, N.H. (2000). Implications of fault array evolution for synrift depocentre development: insights from a numerical fault growth model. *Basin Research*, 12, 241-261.
- Cowie, P.A. & Scholz, C.H. (1992). Physical explanation for displacement-length relationship for faults using a post-yield fracture mechanics model. *J. Struct. Geol.*, 14, 1133-1148.
- Cross, T.A. & Lessenger, M.A. (1999). Construction and application of a stratigraphic inverse model. In: J.W. Harbaugh, W. L. Watney, E.C. Rankey, R. Slingerland, R.H. Goldstein, E.K. Franseen (Eds.), *Numerical Experiments in Stratigraphy Recent Advances in Stratigraphic and Sedimentologic Computer Simulations*. SEPM Special Publications, 62, doi: 10.2110/pec.99.62.0069.
- Curry, J.R. (1964). Transgressions and regressions. In: R.L. Miller (Ed.), *Papers in Marine Geology*. Macmillan, New York, 175-203.
- Daly, M. C., Chorowicz, J., & Fairhead, J. D. (1989). Rift basin evolution in Africa: the influence of reactivated steep basement shear zones. *Geological Society, London, Special Publication*, 44, 309-334.
- Dart, C.J., Collier, R.E.LI., Gawthorpe, R.L., Keller, J.V.A. & Nichols, G. (1994). Sequence stratigraphy of (?)Pliocene-quaternary synrift, gilbert-type fan deltas, Northern Peloponnesos, Greece. *Marine and Petroleum Geology*, 11, 545-560.
- Dawers, N. H. & Anders, M.H. (1995). Displacement-length scaling and fault linkage. *J. Struct. Geol.*, 17, 607-614.
- Dewey, J.F. (1982). Plate tectonics and the evolution of the British Isles. *Geological Society of London Journal*, 139, 371-412.

- Dimmen, V., Rotevatn, A., Peacock, D.C.P., Nixon, C.W. & Nærland, K. (2017). Quantifying structural controls on fluid flow: insights from carbonate-hosted fault damage zones on the Maltese Islands. *Journal of Structural Geology*, 101, 43-57.
- DiPietro, J.A. (2018). Normal fault systems. In: J.A. DiPietro (Ed.), *Geology and Landscape Evolution (2nd edition)*. Elsevier, 429-471.
- Doré, T. & Lundin E. (2015). Hyperextended continental margins: Knowns and unknowns. *Geology*, 43, 95-96.
- Dorsey, R.J. & Umhoefer, P.J. (2000). Tectonic and eustatic controls on sequence stratigraphy of the Pliocene Loreto Basin, Baja California Sur, Mexico. *GSA Bull.*, 112, 177-199.
- Dorsey, R.J., Umhoefer, P.J. & Renne, P.R. (1995). Rapid subsidence and stacked Gilbert-type fan deltas, Pliocene Loreto basin, Baja California Sur, Mexico. *Sedimentary Geology*, 98, 181-204.
- Dugdale, D. S. (1960). Yielding of steel sheets containing slits. *J. Mech. Phys. Solids*, 8, 100-104.
- Elliott, G.M., Wilson, P., Jackson, C.A.-L., Gawthorpe, R.L., Michelsen, L. & Sharp, I. (2012). The linkage between fault throw and footwall scarp erosion patterns: an example from the Bremstein Fault Complex, offshore Mid-Norway. *Basin Research*, 24, 180-197.
- Embry, A.F. & Johannessen, E.P. (1992). T-R sequence stratigraphy, facies analysis and reservoir distribution in the uppermost Triassic–Lower Jurassic succession, Western Sverdrup Basin, Arctic Canada. In: T. O. Vorren, E. Bergsager, O. A. Dahl-Stammes, E. Holter, B. Johansen, E. Lie & T. B. Lund, (Eds.), *Arctic Geology and Petroleum Potential*. Norwegian Petroleum Society, Special Publication, 2, 2121-146.
- Evans, A.L. (1990). Miocene sandstone provenance relations in the Gulf of Suez: insights into synrift unroofing and uplift history. *AAPG Bulletin*, 9, 1386-1400.
- Fairhead, J.D., Green, C.M., Masterton, S.M. & Guiraud, R. (2013). The role that plate tectonics, inferred stress changes and stratigraphic unconformities have on the evolution of the West and Central African Rift System and the Atlantic continental margins. *Tectonophysics*, **594**, 118-127.
- Falvey, D.A. (1974). The development of continental margins in plate tectonic theory. *Australian Petroleum Production and Exploration Association Journal*, 14, 95-106.
- Finch, E., Hardy, S. & Gawthorpe, R.L. (2004). Discrete-element modelling of extensional fault-propagation folding above rigid basement fault blocks. *Basin Research*, 16, 489-506.
- Fisher, Q.J., Haneef, J., Grattoni, C.A., Allshorn, S. & Lorinczi, P. (2018). Permeability of fault rocks in siliciclastic reservoirs: Recent advances. *Marine and Petroleum Geology*, 91, 29-42.
- Flemings, P.B. & Grotzinger, J.P. (1996). STRATA: Freeware for analysing classic stratigraphic problems. *GSA Today*, 6, 1-7.
- Ford, M., Hemelsdael, R., Mancini, M. & Palyvos, N. (2016). Rift migration and lateral propagation: evolution of normal faults and sediment-routing systems of the western Corinth rift (Greece). In: C. Childs C., R.E. Holdsworth, C.A.-L. Jackson, T. Manzocchi, J.J. Walsh, G. Yielding (Eds.), *The Geometry of Normal Faults*. Geol. Soc. London, Special. Publication, 439, 131-168.
- Ford, M., Williams, E.A., Malartre, F. & Popescu, S.M. (2007). Stratigraphic architecture, sedimentology and structure of the Vouraikos Gilbert-type fan delta, Gulf of Corinth, Greece. In: G. Nichols, E. Williams & C. Paola (Eds.), *Sedimentary Processes, Environments and Basins. A Tribute to Peter Friend*. Int. Assoc. Sedimentol. Spec. Publ., 38, 49-90.
- Fossen, H. & Rotevatn, A. (2016). Fault linkage and relay structures in extensional settings – a review. *Earth-Science Reviews*, 154, 14-28.

- Fraser, S.I., Fraser, A.J., Lentini, M.R. & Gawthorpe, R.L. (2007). Return to rifts – the next wave: fresh insights into the petroleum geology of global rift basins. *Petroleum Geoscience*, 13, 99-104.
- Frazier, D. E. (1974). Depositional episodes: their relationship to the Quaternary stratigraphic framework in the northwestern portion of the Gulf Basin. *University of Texas at Austin, Bureau of Economic Geology, Geological Circular*, 4, 28 pp.
- Gabrielsen, R. H. (1986). Structural elements in graben systems and their influence on hydrocarbon trap types. In: A.M. Spencer (Ed.), *Habitat of Hydrocarbons on the Norwegian Continental Shelf*. Norwegian Petroleum Society, Graham and Trotman, London, 55-60.
- Galloway, W. (1989). Genetic stratigraphic sequences in basin analysis I: architecture and genesis of flooding surface bounded depositional units. *AAPG Bull*, 73, 125-142.
- Gawthorpe, R. L., Fraser, A.J. & Collier, R.E.LI. (1994). Sequence stratigraphy in active extensional basins: implications for the interpretation of ancient basin-fills. *Marine and Petroleum Geology*, 11, 642-658.
- Gawthorpe, R.L., Hardy, S. & Ritchie, B. (2003). Numerical modelling of depositional sequences in half-graben rift basins. *Sedimentology*, 50, 169-185.
- Gawthorpe, R. L. & Hurst, J.M. (1993). Transfer zones in extensional basins: their structural style and influence on drainage development and stratigraphy. *Journal of the Geological Society, London*, 150, 1137-1152.
- Gawthorpe, R.L. & Leeder, M.R. (2000). Tectono-sedimentary evolution of active extensional basins. *Basin Research*, 12, 195-218.
- Geurts, A.H., Cowie, P.A., Duclaux, G., Gawthorpe, R.L., Huismans, R.S., Pedersen, V.K. & Wedmore, L.N.J. (2018). Drainage integration and sediment dispersal in active continental rifts: a numerical modelling study of the central Italian Apennines. *Basin Research*, doi: 10.1111/bre.12289.
- Ghibaudo, G., Grandesso, P., Massari, F. & Uchman, A. (1996). Use of trace fossils in delineating sequence stratigraphic surfaces (Tertiary Venetian Basin, northeastern Italy). *Palaeogeography, Palaeoclimatology, Palaeoecology*, 120, 261-279.
- Gilbert, G.K. (1885). The topographic features of lake shores. *US Geol. Surv. Ann. Rep.*, 5, 69-123.
- Gobo, K., Ghinassi, M. & Nemeč, W. (2015). Gilbert-type deltas recording short-term base-level changes: delta-brink morphodynamics and related foreset facies. *Sedimentology*, 62, 1923-1949.
- Gomis-Cartesio, L.E., Poyatos-Moré, M., Hodgson, D.M. & Flint, S.S. (2017). Shelf- margin clinothem progradation, degradation and readjustment: Tanqua depocentre, Karoo Basin (South Africa). *Sedimentology*, 65, 809-841.
- Gouiza, M. & Paton, D.A. (2019). The role of inherited lithospheric heterogeneities in defining the crustal architecture of rifted margins and the magmatic budget during continental breakup. *Geochemistry, Geophysics, Geosystems*, doi: 10.1029/2018GC007808.
- Gradstein, F.M., Agterberg, F.P., Ogg, J.G., Hardenbol J., Van Veen, P., Thierry, J. & Huang, Z. (1994). A Mesozoic time scale. *Journal of Geophysical Research*, 99, 24051-24074.
- Granjeon, D. (1997). Modelisation stratigraphique deterministe: conception et applications d'un modele diffusif 3D multilithologique. These Doct. University of Rennes, France.
- Granjeon, D. (2014). 3D forward modelling of the impact of sediment transport and base level cycles on continental margins and incised valleys. In: A.W. Martinius, R. Ravnås, J.A. Howell, R.J. Steel & J.P. Wonham, (Eds.), *From Depositional Systems to Sedimentary Successions on the Norwegian Continental Margin, First Edition*. International Association of Sedimentologists, 46, 453-472.

- Granjeon, D. & Joseph, P. (1999). Concepts and applications of a 3D multiple lithology, diffusive model in stratigraphic modeling. In: J.W. Harbaugh, W.L. Watney, E.C. Rankey, R. Slingerland, R.H. Goldstein & E.K. Franseen (Eds.), *Numerical Experiments in Stratigraphy: Recent Advances in Stratigraphic and Sedimentological Computer Simulations*. SEPM Special Publication, 62, 197-210.
- Gupta, S., Cowie, P.A., Dawers, N.H. & Underhill, J.R. (1998). A mechanism to explain rift-basin subsidence and stratigraphic patterns through fault-array evolution. *Geology*, 26, 595-598.
- Hack, J. T. (1957). Studies of longitudinal stream profiles in Virginia and Maryland. U.S. Geological Survey Professional Paper 294B, 1-97.
- Hamilton, W. (1987). Crustal extension in the Basin and Range Province, southwestern United States. In: M.P. Coward, J.F. Dewey & P.L. Hancock (Eds.), *Continental Extensional Tectonics*, Geological Society, London, 28, 155-176.
- Hampson, G.J. (2016). Towards a sequence stratigraphic solution set for autogenic processes and allogenic controls: Upper Cretaceous strata, Book Cliffs, Utah, USA. *Journal of the Geological Society, London*, 173, 817-836.
- Haq, B.U., Hardenbol, J. & Vail, P.R. (1987). Chronology of fluctuating sea levels since the Triassic (250 million years ago to present). *Science*, 235, 1156-1166.
- Hardy, S. (2019). Novel discrete element modelling of Gilbert-type delta formation in an active tectonic setting- first results. *Basin Research*, 31, 77-91.
- Hardy, S., Dart, C.J. & Waltham, D. (1994). Computer modelling of the influence of tectonics on sequence architecture of coarse-grained fan deltas. *Marine and Petroleum Geology*, 11, 561-574.
- Hardy, S. & Finch, E. (2005). Discrete-element modelling of detachment folding. *Basin Research*, 17, 507-520.
- Hardy, S. & Finch, E. (2006). Discrete-element modelling of the influence of cover strength on basement-involved fault-propagation folding. *Tectonophysics*, 415, 225-238.
- Hardy, S. & Gawthorpe, R.L. (1998). Effects of variations in fault slip rate on sequence stratigraphy in fan deltas: insights from numerical modeling. *Geology*, 26, 911-914.
- Hardy, S. & Gawthorpe, R.L. (2002). Normal fault control on bedrock channel incision and sediment supply: insights from numerical modeling. *J. Geophys. Res.*, 107, 2246.
- Hardy, S. & Waltham, D. (1992). CLASTIC 2.0: a Clastic modelling program for the Macintosh (User Manual). Department of Geology, Royal Holloway & Bedford New College, University of London, London, UK, 17p.
- Hay, C., Mitrovica, J.X., Gomez, N., Creveling, J.R., Auermann, J. & Kopp, R.R. (2014). The sea-level fingerprints of ice-sheet collapse during interglacial periods. *Quat Sci Rev.*, 80, 60-67.
- Heilman, E., Kolawole, F., Atekwana, E.A. & Mayle, M. (2019). Controls of basement fabric on the linkage of rift segments. *Tectonics*, 38, 1337-1366.
- Helland-Hansen, W. & Gjelberg, J. (1994). Conceptual basis and variability in sequence stratigraphy: a different perspective. *Sedimentary Geology*, 92, 31-52.
- Helland-Hansen, W. & Hampson, G.J. (2009). Trajectory analysis: concepts and applications. *Basin Research*, 21, 454-483.
- Helland-Hansen, W. & Martinsen, O. (1996). Shoreline trajectories and sequences: description of variable depositional dip scenarios. *Journal of Sedimentary Research*, 66, 670-688.

- Hemelsdaël, R. & Ford, M. (2016). Relay zone evolution: a history of repeated fault propagation and linkage, central Corinth rift, Greece. *Basin Research*, 28, 34-56.
- Henstra, G.A., Gawthorpe, R.L., Helland-Hansen, W., Ravnås, R. & Rotevatn, A. (2017). Depositional systems in multiphase rifts: seismic case study from the Lofoten margin, Norway. *Basin Research*, 29, 447-469.
- Henstra, G.A., Kristensen, T.B., Rotevatn, A. & Gawthorpe, R.L. (2019). How do pre-existing normal faults influence rift geometry? A comparison of adjacent basins with contrasting underlying structure on the Lofoten Margin, Norway. *Basin Research*, doi: 10.1111/bre.12358.
- Hodgson, D.M., Kane, I.A., Flint, S.S., Brunt, R.L., & Ortiz-Karpf, A. (2016). Time-transgressive confinement on the slope and the progradation of basin-floor fans: implications for the sequence stratigraphy of deep-water deposits. *Journal of Sedimentary Research*, 86, 73-86.
- Holbrook, J.M., Bhattacharya, J.P. (2012). Reappraisal of the sequence boundary in time and space: case and considerations for an SU (subaerial unconformity) that is not a sediment bypass surface, a time barrier, or an unconformity. *Earth-Science Reviews*, 113, 271-302.
- Hooke, R.L.E.B. (1972). Geomorphic evidence for Late Winsconsin and Holocene tectonic deformation, Death Valley, California. *Geological Society of America Bulletin*, 83, 2073-2098.
- Huang, X., Griffiths, C.M. & Liu, J. (2015). Recent development in stratigraphic forward modelling and its application in petroleum exploration. *Aust. J. Earth Sci.*, 62, 903-919.
- Hubbard, R.J., Pape, J. & Roberts, D. G. (1985). Depositional sequence mapping as a technique to establish tectonic and stratigraphic framework and evaluate hydrocarbon potential on a passive continental margin. In: O.R. Berg. & D.G. Woolverton (Eds.), *Seismic Stratigraphy II*. American Association of Petroleum Geologists Memoir, 39, 79-92.
- Huisman, R.S. & Beaumont, C. (2002). Asymmetric lithospheric extension: The role of frictional plastic strain softening inferred from numerical experiments. *Geology*, 30, 211-214.
- Huisman, R.S. & Beaumont, C. (2008). Complex rifted continental margins explained by dynamical models of depth-dependent lithospheric experiments. *Geology*, 36, 163-166.
- Hunt, D. & Tucker, M.E. (1992). Stranded parasequences and the forced regressive wedge systems tract: deposition during base level fall. *Sedimentary Geology*, 81, 1-9.
- Hunt, D. & Tucker, M.E. (1995). Stranded parasequences and the forced regressive wedge systems tract: deposition during base-level fall – reply. *Sedimentary Geology*, 95, 47-160.
- Illies, J. H. & Greiner, G. (1978). Rhinegraben and the Alpine system. *Geol. Soc. Am. Bull.*, 89, 770-782.
- Jackson, C.A.-L., Bell, R.E., Rotevatn, A., Tvedt, A.B.M. (2017). Techniques to determine the kinematics of syn-sedimentary normal faults and implications for fault growth models. In: Childs, C., Goldsworth, R.E., Jackson, C.A.-L., Manzocchi, T., Walsh, J.J., Yielding, G. (Eds.), *The Geometry and Growth of Normal Faults*. Geological Society, London, Special Publications, 439, 187-217.
- Jackson, C.A.L., Gawthorpe, R.L., Carr, I.D. & Sharp, I.R. (2005). Normal faulting as a control on the stratigraphic development of shallow marine syn-rift sequences: the Nukhul and Lower Rudeis Formations, Hammam Faraun fault block, Suez Rift, Egypt. *Sedimentology*, 52, 313-338.
- Jackson C.A.-L., Royce-Rogers E., Elliott G.M., Gawthorpe R.L., Aas, T.E. (2018). Salt thickness and composition influence rift structural style, northern North Sea, offshore Norway. *Basin Research*, doi: 10.1111/bre.12332.

- Jackson, C.A.-L. & Rotevatn, A. (2013). 3D seismic analysis of the structure and evolution of a salt-influenced normal fault zone: a test of competing fault growth models. *Journal of Structural Geology*, 54, 215-234.
- Jackson, J. A. & Leeder, M.R. (1993). Drainage systems and the evolution of normal faults: an example from Pleasant Valley, Nevada. *Journal of Structural Geology*, 16, 1041-1059.
- Jackson, J.A., White, N.J., Garfunkel, Z. & Anderson, H. (1988). Relations between normal-fault geometry, tilting and vertical motions in extensional terrains: an example from the southern Gulf of Suez. *Journal of Structural Geology*, 10, 155-170.
- Jervey, M. (1988). Quantitative geological modeling of siliciclastic rock sequences and their seismic expression, In: C. Wilgus, B.S. Hastings, C.G.S.C. Kendall, H.W. Posamentier, C.A. Ross & J.C. Van Wagoner (Eds.), *Sea level changes: an integrated approach*. SEPM Spec. Pub., 42, 47-69.
- Johnson, J.G. & Murphy, M.A. (1984). Time-rock model for Siluro-Devonian continental shelf, western United States. *Geological Society of America Bulletin*, 95, 1349-1359.
- Jones G.E.D., Hodgson D.M. & Flint S.S. (2015). Lateral variability in clinoform trajectory, process regime, and sediment dispersal patterns beyond the shelf-edge rollover in exhumed basin margin-scale clinothems. *Basin Research*, 27, 657-680.
- Kane, K.E., Jackson, C.A.- L., Larsen, E. (2010). Normal fault growth and fault-related folding in a salt-influenced rift basin: South Viking Graben, offshore Norway. *Journal of Structural Geology*, 32, 490-506.
- Keen, C.E. (1985). The dynamics of rifting: deformation of the lithosphere by active and passive driving forces. *Geophysical Journal of the Royal Astronomical Society*, 80, 95-120.
- Kendall, C. G. S. C., Moore, P., Strobel, J., Cannon, R., Perlmutter, M., Bezdek, J. & Biswas, G. (1991a). Simulation of the sedimentary fill of basins. In: E.K. Franseen, W.L. Watney, C.G.S.C. Kendall & W. Ross (Eds.), *Sedimentary Modeling: Computer Simulations and Methods for Improved Parameter Definition*. Kansas Geological Survey Bulletin, Lawrence, Kansas, USA, 233, 9-30.
- Kendall, C.G.S.C., Strobel J., Cannon, R., Bezdek, J. & Biswas, G. (1991b). The simulation of the sedimentary fill of basins. *Journal of Geophysical Research*, 96, 6911-6929.
- Khalil, S.M. & McClay, K.R. (2002). Tectonic evolution of the NW Red Sea – Gulf of Suez rift system. In: Wilson, R.C.L., Whitmarsh, R.B., Taylor, B. & Frotzheim, N. (Eds.), *Non-Volcanic Rifting of Continental Margins: A Comparison of Evidence from Land and Sea*. Geological Society, London, Special Publications, 187, 453-473.
- Khalil, S.M. & McClay, K.R. (2018). Extensional fault-related folding in the northwestern Red Sea, Egypt: segmented fault growth, fault linkages, corner folds and basin evolution. In: K.R. McClay & J.A. Hammerstein (Eds.), *Passive Margins: Tectonics, Sedimentation and Magmatism*. Geological Society, London, Special Publications, 476, doi: 10.1144/SP476.12.
- Khalil, S.M. & McClay, K.R. (2016). 3D Geometry and kinematic evolution of extensional fault-related folds, northwestern Red Sea, Egypt. In: C. Childs, R.E. Holdsworth, C.A.-L. Jackson, T. Manocchi, J.J. Walsh. & G. Yielding (Eds.), *The Geometry and Growth of Normal Faults*. Geological Society, London, Special Publications, 439, 109-130.
- Kim, Y.-S. & Sanderson, D.J. (2005). The relationship between displacement and length of faults: a review. *Earth-Science Reviews*, 68, 317-334.
- King, G.C.P., Stein, R.S. & Rundle, J.B. (1988). The growth of geological structures by repeated earthquakes 1. Conceptual framework. *Journal of Geophysical Research*, 93, 13307-13318.
- Kuszniir, N.J., Marsden, G. & Egan, S.S. (1991). A flexural-cantilever simple-shear/pure-shear model of continental lithosphere extension: applications to the Jeanne d'Arc Basin, Grand Banks and Viking Graben,

- North Sea. In: A.M. Roberts, G. Yielding & B. Freeman (Eds.), *The Geometry of Normal Faults*, Geological Society, London, Special Publications, 56, 41-60.
- Kusznir, N. J. & Ziegler, P. A. (1992). The mechanics of continental extension and sedimentary basin formation: a simpleshear/pure-shear flexural cantilever model. *Tectonophysics*, 215, 117-131.
- Lambiase, J.J. & Bosworth, W. (1995). Structural controls on sedimentation in continental rifts. In: J.J. Lambiase (Ed.), *Hydrocarbon Habitat in Rift Basins*. Geological Society, London, Special Publications, 80, 117-144.
- Larsen, P.H. (1988). Relay structures in a Lower Permian basement-involved extension system, East Greenland. *Journal of Structural Geology*, 10, 3-8.
- Leeder, M.R. & Gawthorpe R.L. (1987). Sedimentary models for extensional tilt-block/half-graben basins. In: M.P. Coward, J.F. Dewey & P.L. Hancock (Eds.), *Continental Extensional Tectonics*. Geological Society, London, Special Publications, 28, 139-152.
- Leeder, M. R. & Jackson, J. A. (1993). The interaction between normal faulting and drainage in active extensional basins, with examples from the western United States and central Greece. *Basin Research*, 5, 79-102.
- Leeder, M.R., Mack, G.H. & Salyards, S.L. (1996). Axial-transverse fluvial interactions in half graben: Plio-Pleistocene Palomas Basin, southern Rio Grande Rift, New Mexico, USA. *Basin Research*, 8, 225-241.
- Leeder, M. R., Ord, D.M. & Collier, R.E.LI. (1988). Development of alluvial fans and fan-deltas in neotectonic extensional settings: implications for the interpretation of basin-fills. In: W. Nemeč & R. J. Steel (Eds.), *Fan deltas: sedimentology and tectonic settings*. Blackie and Son Ltd, Glasgow, 173-185.
- Leeder, M.R., Seger, M. & Stark, C.P. (1991). Sedimentology and tectonic geomorphology adjacent to active and inactive normal faults in the Megara Basin and Alkyonides Gulf, Central Greece. *J. Geol. Soc. London*, 148, 331-343.
- Lewis, M.M., Jackson, C.A.-L., Gawthorpe, R.L. & Whipp, P.S. (2015). Early synrift reservoir development on the flanks of extensional forced folds: a seismic-scale outcrop analog from the Hadahid fault system, Suez rift, Egypt. *AAPG Bulletin*, 99, 985-1012.
- Madof, A.S., Harris, A.D. & Connell, S.D. (2016). Nearshore along-strike variability: is the concept of the systems tracts unhinged? *Geology*, 44, 319-322.
- Mann, P., Gahagan, L. & Gordon, M. (2001). Tectonic setting of the world's giant oil fields. *World Oil*, 42-50.
- Mats, V.D. & Perepelova, T.I. (2011). A new perspective on evolution of the Baikal Rift. *Geoscience Frontiers*, 2, 349-365.
- McDermott, C., Lonergan, L., Collier, J.S., McDermott, K.G. & Bellingham, P. (2018). Characterization of seaward-dipping reflectors along the S. American Atlantic margin and implications for continental breakup. *Tectonics*, 37, 3303-3327.
- McDermott, K. & Reston, T. (2015). To see, or not to see? Rifted margin extension. *Geology*, 43, 967-970.
- McKenzie, D.P. (1978). Some remarks on the development of sedimentary basins. *Earth and Planetary Science Letters*, 40, 25-32.
- McNeill, L. & Collier, R.E.LI. (2004). Uplift and slip rates of the eastern Eliki fault segment, Gulf of Corinth, Greece, inferred from Holocene and Pleistocene terraces. *Journal of the Geological Society*, 161, 91-92.

- Miall, A.D. (1990). *Principles of Sedimentary Basin Analysis, 2nd edition*. Springer. 668pp.
- Miall, A.D. (1997). *The Geology of Stratigraphic Sequences*. Springer-Berlag, 433pp.
- Middleton, G.V. (1973). Johannes Walther's Law of the Correlation of Facies. *Geological Society of America Bulletin*, 84, 979-988.
- Milliman, J.D. & Syvitski, J.P. (1992). Geomorphic control of sediment discharge to the ocean: the importance of small mountain rivers. *Journal of Geology*, 100, 525-544.
- Mitchum, R, Vail, P. & Thompson, S. (1977). Seismic stratigraphy and global changes in sea level, part 2: the depositional sequence as the basic unit for stratigraphic analysis, In: C. Payton, C.(Ed.), *Seismic stratigraphy: application to hydrocarbon exploration*. AAPG Memoir, 26, 53-62.
- Morgan, P. (1982). Heat flow in rift zones. In: *Continental and Oceanic Rifts* (ed. by G. Pálmason), Geodynamics Series, 8, 107-122.
- Morley, C.K. (1995). Developments in the structural geology of rifts over the last decade and their impact on hydrocarbon exploration. In: Lambiase, J.J. (Eds.) *Hydrocarbon Habitat in Rift Basins*. Geological Society, London, Special Publications, 80, 1-32.
- Morley, C.K. (2002). Evolution of large normal faults: evidence from seismic reflection data. *American Association of Petroleum Geologists Bulletin*, 86, 961-978.
- Mortimer, E.J. & Carrapa, B. (2007). Footwall drainage evolution and scarp retreat in response to increasing fault displacement: Loreto fault, Baja California Sur, Mexico. *Geology*, 35, 651-654.
- Mortimer, E., Gupta, S. & Cowie, P. (2005). Clinoform nucleation and growth in coarse-grained deltas, Loreto basin, Baja California Sur, Mexico: a response to episodic accelerations in fault displacement. *Basin Research*, 17, 337-359.
- Mortimer, E.J., Paton, D.A., Scholz, C.A. & Strecker, M.R. (2016). Implications of structural inheritance in oblique rift zones for basin compartmentalization: Nkhata Basin, Malawi Rift (EARS). *Marine and Petroleum Geology*, 72, 110-121.
- Muravchik, M., Gawthorpe, R.L., Sharp, I.R., Rarity, F. & Hodgetts, D. (2018). Sedimentary environment evolution in a marine hangingwall dip slope setting. El Qaa Fault Block, Suez Rift, Egypt. *Basin Research*, 30, 452-478.
- Muto, T. & Steel, R.J. (1992). Retreat of the front in a prograding delta. *Geology*, 20, 967-970.
- Muto, T. & Steel, R.J. (1997). The accommodation concept in sequence stratigraphy: some dimensional problems and possible redefinition. *Sedimentary Geology*, 130, 1-10.
- Muto, T., Steel, R.J. & Burgess, P. (2016). Contributions to sequence stratigraphy from analogue and numerical experiments. *Journal of the Geological Society*, 173, 2015-2127.
- Neal, J. & Abreu, V. (2009). Sequence stratigraphy hierarchy and the accommodation succession method. *Geology*, 37, 779-782.
- Neal, J.E., Abreu, V., Bohacs, K.M., Feldman, H.R. & Pederson, K.H. (2016). Accommodation succession sequence stratigraphy: observational method, utility, and insights into sequence boundary formation. *Journal of the Geological Society, London*, 173, 803-816.
- Nicol, A., Childs, C., Walsh, J.J., Manzocchi, T. & Schöpfer, M.P.J. (2016). Interactions and growth of faults in an outcrop-scale system. In: Childs, C., Holdsworth, R.E., Jackson, C.A.-L., Manzocchi, T., Walsh, J.J. & Yielding, G. (Eds.), *The Geometry and Growth of Normal Faults*. Geological Society, London, Special Publications, 439, 23-39.

- Nixon, C.W., Vaagan, S., Sanderson, D.J. & Gawthorpe, R.L. (2019). Spatial distribution of damage and strain within a normal fault relay at Kilve, UK. *Journal of Structural Geology*, 118, 194-209.
- Norcliffe, J.R., Paton, D.A., Mortimer, E.J., McCaig, A.M., Nicholls, H., Rodriguez, K., Hodgson, N. & van der Spuy, D. (2018). Laterally confined volcanic successions (LCVS); recording rift-jumps during the formation of magma-rich margins. *Earth and Planetary Science Letters*, 504, 53-63.
- Nøttvedt, A., Berge, A.M., Dawers, N.H., Færseth, R.B., Häger, K.O., Mangerud, G. & Puigdefabregas, C. (2000). Syn-rift evolution and resulting play models in the Snorre-H area, northern North Sea. In: A. Nøttvedt (Ed.), *Dynamics of the Norwegian Margin*. Geological Society, London, Special Publications, 167, 179-218.
- Nøttvedt, A., Gabrielsen, R.H. & Steel, R.J. (1995). Tectonostratigraphy and sedimentary architecture of rift basins, with reference to the northern North Sea. *Marine and Petroleum Geology*, 12, 881-901.
- Osmundsen, P.T., Braathen, A., Rød & Hynne, I.B. (2014). Styles of normal faulting and fault-controlled sedimentation in the Triassic deposits of Eastern Svalbard. *Norwegian Petroleum Directorate Bulletin*, 11, 61-79.
- Paola, C. (2000). Quantitative models of sedimentary basin filling. *Sedimentology*, 47, 121-178.
- Parsons, A.J., Whitham, A.G., Kelly, S.R.A., Vautravers, B.P.H., Dalton, T.J.S., Andrews, S.D., Pickles, C.S., Strogen, D.P., Braham, W., Jolley, D.W. & Gregory, F.J. (2017). Structural evolution and basin architecture of the Traill Ø region, NE Greenland: a record of polyphaser rifting of the East Greenland continental margin. *Geosphere*, 13, 733-770.
- Paton, D.A., Pindell, J., McDermott, K., Bellingham, P. & Horn, B. (2017). Evolution of seaward-dipping reflectors at the onset of oceanic crust formation at volcanic passive margins: insights from the South Atlantic. *Geology*, 45, 439-442.
- Patruno, S., Hampson, G.J. & Jackson, C.A.-L. (2015). Quantitative characterisation of deltaic and subaqueous clinofolds. *Earth Science Reviews*, 142, 79-119.
- Patruno, S. & Helland-Hansen, W. (2018). Clinofold systems: Review and dynamic classification scheme for shorelines, subaqueous deltas, shelf edges and continental margins. *Earth Science Reviews*, 185, 202-233.
- Payton, C.E. (1977). *Seismic Stratigraphy – Applications to Hydrocarbon Exploration*. AAPG Memoir, 26, 516pp.
- Peacock, D.C.P. & Sanderson, D.J. (1991). Displacement and segment linkage and relay ramps in normal fault zones. *Journal of Structural Geology*, 13, 721-733.
- Pechlivanidou, S., Cowie, P.A., Duclaux, G., Nixon, C.W., Gawthorpe, R.L. & Salles, T. (2019). Tipping the balance: shifts in sediment production in an active rift setting. *Geology*, 47, 259-262.
- Pei, Y., Paton, D.A., Knipe, R.J. & Wu, K. (2015). A review of fault sealing behaviour and its evaluation in siliciclastic rocks. *Earth-Science Reviews*, 150, 121-138.
- Pemberton, S.G. & MacEachern, J.A. (1995). The sequence stratigraphic significance of trace fossils: examples from the Cretaceous foreland basin of Alberta, Canada. In: J.C. Van Wagoner & G. Bertrum (Eds.), *Sequence stratigraphy of foreland basin deposits – outcrop and subsurface examples from the Cretaceous of North America*. AAPG Memoir, 64, 429-475.
- Phillips, T.B., Jackson, C. A. L., Bell, R. E. & Duffy, O. B. (2018). Oblique reactivation of lithosphere-scale lineaments controls rift physiography – the upper-crustal expression of the Sorgenfre-Tornquist Zone, offshore southern Norway. *Solid Earth*, 9, 403-429.

- Phillips, T. B., Jackson, C. A. L., Bell, R. E., Duffy, O. B., & Fossen, H. (2016). Reactivation of intrabasement structures during rifting: A case study from offshore southern Norway. *Journal of Structural Geology*, 91, 54-73.
- Pirmez, C., Pratson, L.F. & Steckler, M.S. (1998). Clinof orm development by advection– diffusion of suspended sediment: modelling and comparison to natural systems. *Journal of Geophysical Research*, 103, 141-157.
- Plint, A.G. & Nummedal, D. (2000). The falling stage systems tract: recognition and importance in sequence stratigraphic analysis. In: D. Hunt & R.L. Gawthorpe (Eds.), *Sedimentary Response to Forced Regression*. Geological Society, London, Special Publications, 172, 1-17.
- Posamentier, H.W. & Allen, G.P. (1999). Siliciclastic sequence stratigraphy: concepts and applications. *SEPM Concepts in Sedimentology and Paleontology*, 7, 210.
- Posamentier, H.W. & James, D.P. (1993). Sequence stratigraphy – uses and abuses. In: H.W. Posamentier, C.P. Summerhayes, B.U. Haq & G.P. Allen (Eds.), *Sequence stratigraphy and facies associations*. International Association of Sedimentologists Special Publication, 18, 3-18.
- Posamentier, H. Jervy, M. & Vail, P. (1988). Eustatic controls on clastic deposition I conceptual framework. In: C. Wilgus, B.S. Hastings, C.G.S.C. Kendall, H.W. Posamentier, C.A. Ross & J.C. Van Wagoner (Eds.), *Sea level changes: an integrated approach*. SEPM Spec. Pub., 42, 109-124.
- Posamentier, H. & Vail, P. (1988). Eustatic controls on clastic deposition II- sequence and systems tract models. In: C. Wilgus, B.S. Hastings, C.G.S.C. Kendall, H.W. Posamentier, C.A. Ross & J.C. Van Wagoner (Eds.), *Sea level changes: an integrated approach*. SEPM Spec. Pub., 42, 125-154.
- Poyatos-Moré, M., Jones, G.D., Brunt, R.L., Tek, D., Hodgson, D.M. & Flint, S.S. (2019). Clinof orm architecture and along-strike variability through an exhumed erosional to accretionary basin margin transition. *Basin Research*, doi: 10.1111/12351.
- Prosser, S. (1993). Rift-related linked depositional systems and their seismic expression. *Geological Society, London, Special Publications*, 71, 35-66.
- Ravnås, R., Nøttvedt, A., Steel, R.J. & Windelstad, J. (2000). Syn-rift sedimentary architectures in the northern North Sea. In: A. Nøttvedt (Ed.), *Dynamics of the Norwegian Margin*. Geological Society, London, Special Publication, 167, 133-177.
- Ravnås, R. & Steel, R.J. (1998). Architecture of Marine Rift-Basin Successions. *AAPG Bulletin*, 82, 110-146.
- Rich, J.L. (1951). Three critical environments of deposition and criteria for recognition of rocks deposited in each of them. *GSA Bulletin*, 62, 1-20.
- Ritchie, B. D., Gawthorpe, R. L. & Hardy, S. (2004a). Three- dimensional numerical modeling of deltaic depositional sequence 1: Influence of the rate and magnitude of sea- level change. *Journal of Sedimentary Research*, 74, 203-220.
- Ritchie, B. D., Gawthorpe, R. L. & Hardy, S. (2004b). Three- dimensional numerical modeling of deltaic depositional sequences 2: Influence of local controls. *Journal of Sedimentary Research*, 74, 221-238.
- Ritchie, B.D., Hardy, S. & Gawthorpe, R.L. (1999). Three dimensional numerical modeling of coarse-grained clastic deposition in sedimentary basins. *Journal of Geophysical Research*, 104, 17759-17780.
- Roberts, A. M., Yielding, G. & Badley, M.E. (1993). Tectonic and bathymetric controls on stratigraphic sequences within evolving half-graben. In: G. D. Woudiamis & A. Dobb (Eds.), *Tectonics and seismic sequence stratigraphy*. Geological Society Special Publication, 71, 87-121.

- Rohais, S., Eschard, R., Ford, M., Guillocheau, F. & Moretti, I. (2007). Stratigraphic architecture of the Plio-Pleistocene infill of the Corinth Rift: implications for its structural evolution. *Tectonophysics*, 440, 5-28.
- Rosendahl, B.R., Reynolds, D.J., Lorber, P.M., Burgess, C.F., McGill, J., Scott, D., Lambiase, J.J. & Derksen, S.J. (1986). Structural expressions of rifting: lessons from Lake Tanganyika, Africa. In: L. E. Frostick, R. W. Renaut, I. Reid, and J.-J. Tiercelin (Eds.), *Sedimentation in the east-African rifts*. Geological Society, London, Special Publication 25, 29-43.
- Ross, W. C., Watts, D. E. & May, T. A. (1995). Insights from stratigraphic modeling: mud-limited versus sand-limited depositional systems. *American Association of Petroleum Geologists Bulletin*, 79, 231-258.
- Rotevatn, A., Jackson, C.A.-L, Tvedt, A.B.M., Bell, R.E. & Blækkan, I. (2018b). How do normal faults grow? *Journal of Structural Geology*, doi: 10.1016/j.jsg.2018.08.005.
- Rotevatn, A., Kristensen, T.B., Ksienzyk, A.K., Wemmer, K., Henstra, G.A., Midtkandal, I., Grundvåg, S.-A. & Andresen, A. (2018a). Structural inheritance and rapid rift-length establishment in a multiphase rift: the East Greenland rift system and its Caledonian orogenic ancestry. *Tectonics*, 37, 1858-1875.
- Roure, F., Cloetingh, S., Scheck-Wenderoth, M. & Ziegler, P.A. (2009). Achievements and challenges in sedimentary basin dynamics: a review. In: S. Cloetingh & J. Negendank (Eds.), *New Frontiers in Integrated Solid Earth Sciences*, Springer-Verlag, 145-233.
- Rovere, A., Stocchi, P. & Vacchi, M. (2016). Eustatic and relative sea level changes. *Current Climate Change Reports*, 2, 221-231.
- Salles, T., Ding, X. & Brocard, G. (2018). pyBadlands: A framework to simulate sediment transport, landscape dynamics and basin stratigraphic evolution through space and time. *PLoS One*, 13, e0195557, doi: 10.1371/journal.pone.0195557.
- Schlagenhauf, A., Manighetti, I., Malavieille, J. & Dominguez, S. (2008). Incremental growth of normal faults: Insights from a laser-equipped analog experiment. *Earth and Planetary Science Letters*, 273, 299-311.
- Schlager, W. (1993). Accommodation and supply - A dual control on stratigraphic sequences. *Sedimentary Geology*, 86, 111-136.
- Scholz, C. H., Aviles, C. A. & Wesnousky, S. G. (1986). Scaling differences between large interplate and intraplate earthquakes. *Bulletin of the Seismological Society of America*, 76, 65-70.
- Schwarz, E., Veiga, G.D., Álvarez Trentini, G., Spalletti, L.A. (2016). Climatically versus eustatically controlled, sediment-supply-driven cycles: carbonate-siliciclastic, high frequency sequences in the Valanginian of the Neuquén Basin (Argentina). *Journal of Sedimentary Research*, 86, 312-335.
- Seger, M. & Alexander, J. (1993). Distribution of Plio-Pleistocene and modern coarse-grained deltas south of the Gulf of Corinth, Greece. In: L. E. Frostick & R. J. Steel (Eds.), *Tectonic controls and signatures in sedimentary successions*. International Association of Sedimentologists Special Publication, 20, 37-48.
- Serck, C.S. & Braathen, A. (2019). Extensional fault and fold growth: impact on accommodation evolution and sedimentary infill. *Basin Research*, doi: 10.1111/bre.12353.
- Shackleton, N.J. (1987). Oxygen isotopes, ice volume and sea level. *Quaternary Science Reviews*, 6, 183-190.
- Shafie, K. & Madon, M. (2008). A review of stratigraphic simulation techniques and their applications in sequence stratigraphy and basin analysis. *Bulletin of the Geological Society of Malaysia*, 54, 81-89.
- Sloss, L.L. (1962). Stratigraphic models in exploration. *AAPG Bulletin*, 46, 1050-1057.

- Sloss, L.L. Krumbein, W. & Dapples, E. (1949). Integrated facies analysis, In: C. Longwell (Ed.), *Sedimentary facies in geologic history: Geological Society America, Memoir*, 39, 91-124.
- Smart, K.J. & Ferrill, D.A. (2018). Discrete element modeling of extensional fault-related monocline formation. *Journal of Structural Geology*, 115, 82-90.
- Steckler M. S., Reynolds, D. J., Coakley, B. J., Swift, B. A. & Jarrard, R. (1993). Modelling passive margin sequence stratigraphy. In: H.W. Posamentier, C.P. Summerhayes, B.U. Haq & G.P. Allen (Eds.), *Sequence Stratigraphy and Facies Associations*. International Association of Sedimentologists Special Publication, 18, Blackwell Scientific Publications, Oxford UK, 19-41.
- Steel, R.J. & Olsen, T. (2002). Clinoforms, clinoform trajectory and deepwater sands. In: J.M. Armentrout & N.C. Rosen (Eds.), *Sequence Stratigraphic Models for Exploration and Production: Evolving Methodology, Emerging Models and Application Histories*. GCS-SEPM Special Publication, 367-381.
- Stein, R.S. & Barrientos, S.E. (1985). Planar High-Angle Faulting in the Basin and Range' Geodetic Analysis of the 1983 Borah Peak, Idaho, Earthquake. *Journal of Geophysical Research*, 90, 11355-11366.
- Stein, R.S., King, G.C.P. & Rundle, J.B. (1988). The growth of geological structures by repeated earthquakes 2. Field examples of continental dip-slip. *Journal of Geophysical Research*, 93, 13319-13331.
- Stein, S., Stein, C.A., Elling, R., Kley, J., Keller, G.R., Wyession, M., Rooney, T., Frederiksen, A. & Moucha, R. (2018). Insights from North America's failed Midcontinent Rift into the evolution of continental rifts and passive continental margins. *Tectonophysics*, 744, 403-421.
- Strebe, D.R. (2011). A world map on the Winkel triple projection. Imagery from NASA's Blue Marble summer month composite. Image created with Geocart map projection software. Wikipedia. File downloaded 26th April, 2019.
- Strobel, J., Cannon, R., Kendall, C.G.S.C., Biswas, G. & Bezdek, J. (1989). Interactive (SEDPACK) simulation of clastic and carbonate sediments in shelf to basin settings. *Computers & Geosciences*, 15, 1279-1290.
- Surlyk, F. (1978). Submarine fan sedimentation along fault scarps on tilted fault blocks (Jurassic–Cretaceous boundary, East Greenland). *Bulletin Grønlands Geologiske Undersøgelse*, 128, 1-108.
- Syvitski, J.P.M. & Milliman, J.D. (2007). Geology, geography, and humans battle for dominance over the delivery of fluvial sediment to the coastal ocean. *Journal of Geology*, 115, 1-19.
- Tetzlaff, D.M. & Harbaugh, J.W. (Eds.) (1989). *Simulating Elastic Sedimentation*. Van Nostrand Reinhold, New York.
- Thorne, J. A. & Swift, D.J.P. (1992). Sedimentation on continental margins, II: application of the regime concept. In: D.J.P. Swift, G.F. Oertel, R.W. Tillman & J.A. Thorne (Eds.), *Shelf Sand and Sandstone Bodies: Geometry, Facies and Sequence Stratigraphy*. Special Publications of International Association of Sedimentologists, 14, Blackwell Publishing Ltd., Oxford, UK, 33-58.
- Toby, S.C., Duller, R.A., De Angelis, S. & Straub, K.M. (2019). A stratigraphic framework for the preservation and shredding of environmental signals. *Geophysical Research Letters*, doi: 10.1029/2019GL082555.
- Torabi, A., Alaei, B. & Libak, A. (2019). Normal fault 3D geometry and displacement revisited: insights from faults in the Norwegian Barents Sea. *Marine and Petroleum Geology*, 99, 135-155.
- Turner, B.W., Tréanton, J.A. & Slatt, R. (2016). The use of chemostratigraphy to refine ambiguous sequence stratigraphic correlations in marine mudrocks. An example from the Woodford Shale, Oklahoma, USA. *Journal of the Geological Society, London*, 173, 854–868.

- Vail, P., Mitchum, R.M. & Thompson, S. (1977). Seismic stratigraphy and global changes in sea level, In: C. Payton (Ed.), *Seismic stratigraphy: applications to hydrocarbon exploration*. AAPG Memoir, 26, 49-212.
- Van der Beek, P.A., Cloetingh, S. & Andriessen, P.A.M. (1994). Extensional basin formation mechanisms and vertical motions at rift flanks: constraints from tectonic modelling and fission-track thermochronology. *Earth Planet. Sc. Lett.*, 121, 417-433.
- Van Wagoner, J.C. (1995). Sequence stratigraphy of foreland basin deposits: terminology, summary of papers, and glossary of sequence stratigraphy. In: J.C. Van Wagoner & G.T. Bertrum (Eds.), *Sequence stratigraphy of foreland basin deposits*. American Association of Petroleum Geologists Memoir, 64, 137-225.
- Van Wagoner, J.C., Mitchum, R.M.Jr., Campion, K.M. & Rahmanian, V.D. (1990). Siliciclastic sequence stratigraphy in well logs, core and outcrops: concepts for high-resolution correlation of time and facies. *AAPG Methods in Exploration Series*, 7, 55.
- Van Wagoner, J.C., Posamentier, H.W., Mitchum, R.M.Jr., Vail, P.R., Sarg, J.F., Loutit, T.S. & Hardenbol, J. (1988). An overview of the fundamentals of sequence stratigraphy and key definitions. In: C.K. Wilgus, B.S. Hastings, C.G.St.C. Kendall., H.W. Posamentier, C.A. Ross & J.C. Van Wagoner (Eds.), *Sea Level Changes- An Integrated Approach*. SEPM Special Publication, 42, 39-45.
- Walsh, J.J., Bailey, W.R., Childs, C., Nicol, A. & Bonson, C.G. (2003). Formation of segmented normal faults: a 3-D perspective. *Journal of Structural Geology*, 25, 1251-1262.
- Walsh, J.J. & Watterson, J. (1988). Analysis of the relationship between displacements and dimensions of faults. *J. Struct. Geol.*, 10, 239-247.
- Watney, W.L., Rankey, E.C. & Harbaugh, J. (1999). Perspectives on Stratigraphic Simulation Models: Current Approaches and Future Opportunities. In: J.W. Harbaugh, E.C. Rankey, R. Slingerland, R.H. Goldstein & E.K. Franseen (Eds.), *Numerical Experiments in Stratigraphy: Recent Advances in Stratigraphic and Sedimentologic Computer Simulations*. SEPM Special Publication, 62, 3-19.
- Watterson, J. (1986). Fault dimensions, displacement and growth. *Pure and Applied Geophysics*, 124, 365-373.
- Wehr F. L. (1993). Effects of variations in subsidence and sediment supply on parasequence stacking patterns. In: P. Weimer P. & H.W. Posamantier (Eds.), *Siliciclastic Sequence Stratigraphy: Recent Developments and Applications*. American Association of Petroleum Geologists Memoir, 58, 369-379.
- Wernicke, B. (1985). Uniform-sense normal simple shear of the continental lithosphere. *Canadian Journal of Earth Science*, 22, 108-125.
- Wheeler, H.E. (1958). Time stratigraphy. *AAPG Bulletin*, 42, 1208-1218.
- Wheeler, H.E. (1959). Stratigraphic units in time and space. *American Journal Science*, 257, 692-706.
- Wheeler, H.E. (1964a). Base level, lithosphere surface and time stratigraphy. *Geological Society America Bulletin*, 75, 599-610.
- Wheeler, H.E. (1964b). Base level transit cycle. In: D.F. Merriam (Ed.), *Symposium on cyclic sedimentation*. Kansas Geological Survey, 169, 623-629.
- Wheeler, H.E. & Murray, H. (1957). Base level control patterns in cyclothem sedimentation. *AAPG Bulletin*, 41, 1985-2011.
- Whittaker, A.C., Attal, M. & Allen, P.A. (2010). Charaterising the origin, nature and fate of sediment exported from catchments perturbed by active tectonics. *Basin Research*, 22, 809-828.

Withjack, M.O., Schlische, R., & Olsen, P.E. (2002). Rift-basin structure and its influence on sedimentary systems. In: R.W. Renaut & G.M. Ashley (Eds.), *Sedimentation in Continental Rifts*. SEPM Special Publication, 73, 57-81.

Wonham, J.P., Rodwell, I., Lein-Mathisen, T. & Thomas, M. (2014). Tectonic control on sedimentation, erosion and redeposition of Upper Jurassic sandstones, Central Graben, North Sea. In: A.W. Martinus, R. Ravnås, J.A. Howell, R.J. Steel & J.P. Wonham, (Eds.), *From Depositional Systems to Sedimentary Successions on the Norwegian Continental Margin, First Edition*. International Association of Sedimentologists, 46, 473-512.

Wood, A.M., Paton, D.A. & Collier, R.E.Ll. (2015a). The missing complexity in seismically imaged normal faults: what are the implications for the geometry and production response? *Geological Society, London, Special Publications*, 421, 213-230.

Wood, A.M., Paton, D.A., Collier, R.E.Ll. & O'Connor, V. (2015b). Understanding regional scale structural uncertainty: The onshore Gulf of Corinth Rift as a hydrocarbon exploration analogue. *Interpretation*, 3, SAC35-SAC53.

Zhang, J., Burgess, P., Granjeon, D. & Steel, R.J. (2018). Can sediment supply variations create sequences? Insights from stratigraphic forward modelling. *Basin Research*, 31, 274-289.

Zhou, Y., Ji, Y., Piggott, J., Meng, Q. & Wan, L. (2014). Tectono-stratigraphy of Lower Cretaceous Tanan sub-basin, Tamtsag Basin, Mongolia: sequence architecture, depositional systems and controls on sediment infill. *Marine and Petroleum Geology*, 49, 176-202.

Ziegler, P.A. (1990). Tectonic and palaeogeographic development of the North Sea rift system. In: Blundell, D.J. & Gibbs, A.D. (Eds.), *Tectonic Evolution of the North Sea Rifts*. International Lithosphere Programme, 81, 1-36.

Chapter 3

Novel 3D sequence stratigraphic numerical model for syn-rift basins: analysing architectural responses to eustasy, sedimentation and tectonics

Publication

Barrett, B.J., Hodgson, D.M., Collier, R.E.Ll. & Dorrell, R.M. (2018). Novel 3D sequence stratigraphic numerical model for syn-rift basins: analysing architectural responses to eustasy, sedimentation and tectonics. *Marine and Petroleum Geology*, 92, 270-284.

Abstract

Syn-rift clastic sedimentary systems preserve a complicated stratigraphic architecture that records the interplay of tectonics, eustatic sea level and storage and routing of sediments. Previous conceptual models describe and explain changes in depositional stacking patterns along a fault segment. However, stacking patterns, and the nature of key stratigraphic surfaces, is challenging to predict accurately with conventional sequence stratigraphic models that do not consider the three-dimensional interplay of subsidence, sedimentation, and eustasy. We present a novel, geometric, 3D sequence stratigraphic model ('Syn-Strat'), which applies temporally- and spatially-variable, fault-scale tectonic constraints to stratigraphic forward modelling, as well as allowing flexibility in the other controls in time and space.

Syn-Strat generates a 3D graphical surface that represents accommodation. Although the model has the capacity to model footwall variation, here we present model results from the hangingwall of a normal fault, with temporal and spatial (dip and strike) predictions made of stacking patterns and systems tracts for a given set of controls. Sensitivity tests are tied to the depositional architecture of field-based examples from the Loreto Basin, Gulf of California and Alkyonides Basin, Gulf of Corinth. Here, the relative influence of major sedimentary controls, different subsidence histories, varying sedimentation distribution, including along-strike variation in stacking patterns, are assessed and demonstrate the potential of Syn-Strat for reducing subsurface uncertainties by resolving multiple scenarios. In addition, the model demonstrates the nature of diachroneity of key stratigraphic surfaces that can arise in syn-rift settings, which could be represented by a bypass surface (sequence boundary) or reservoir seal (maximum flooding surface) in the rock record. Enabling a quantitative assessment of these surfaces is critical for prospect analysis in hangingwall half-graben-fills, where these surfaces are heavily relied upon for well correlations that are used for hydrocarbon volume and production rate predictions.

3.1. Introduction

Syn-rift depositional sequences preserve a complicated architecture, due to the spatially- and temporally-variable interplay of major sedimentary controls (eustatic sea level, subsidence and sedimentation). Conventional sequence stratigraphic models (Wheeler, 1958, 1959, 1964; Sloss, 1962, 1991; Mitchum et al., 1977; Vail et al., 1977; Leeder & Gawthorpe, 1987; Jervey, 1988; Posamentier et al., 1988; Posamentier & Vail, 1988; Van Wagoner et al., 1988; Posamentier & Weimer, 1993; Ravnås & Steel, 1998) struggle to predict the depositional architecture of syn-rift successions and the 3D distribution of reservoirs and seals. Various studies have attempted to address this issue by integrating sub-seismic, structural and sedimentological data in order to build tectono-stratigraphic frameworks in various rift settings, including: the Gulf of Suez (e.g. Gawthorpe et al., 1997; Gupta et al., 1999; Young et al., 2002; Jackson et al., 2005), the Gulf of Corinth (e.g. Poulimenos et al., 1993; Gawthorpe et al., 1994; Collier & Gawthorpe, 1995; Leeder et al., 2002), the Gulf of California (e.g. Dorsey et al., 1995; Dorsey & Umhoefer, 2000; Mortimer et al., 2005), and the Crati Basin (Italy) (e.g. Colella et al. 1987; Colella, 1988a,b,c). Burgess (2016) highlights four key uncertainties in general sequence stratigraphic theory: i) rare quantitative analysis, ii) limited consideration for along-strike variability in sequence architecture (also pointed out by Martinsen & Helland-Hansen, 1995), iii) limited constraint for sediment supply rates, and iv) few studies that demonstrate the interplay of accommodation and supply in three dimensions. These uncertainties are exacerbated in active rift basins, and constraining the interaction of allogenic controls in three dimensions remains challenging.

Sequence stratigraphic forward modelling can support interpretation and prediction of depositional sequences and key stratigraphic surfaces (Fig. 3.1). Early numerical sequence stratigraphic models, which incorporated sinusoidal sea level change and hinged subsidence to simulate accommodation generation and assumed a constant sediment supply, predicted key surfaces in seismic (Jervey, 1988). Burgess and Allen (1996) extended this approach to include temporal variability in sediment supply rate. Subsequently, various stratigraphic forward models have been developed in order to better understand and predict dynamic depositional systems.

DIONISOS (Granjeon & Joseph, 1999) and STRATA (Flemings & Grotzinger, 1996) represent significant advances in the power of three-dimensional stratigraphic forward models, and various other geometric, diffusion, fuzzy logic and hydraulic models have emerged, reviewed by Huang et al. (2015). Diffusion-based models are regularly utilised for sediment supply, and have successfully applied hypothesis-testing approaches to some systems (e.g. Burgess & Prince, 2015). However, they are unable to accurately predict mixed process regime systems, gravity-flow dominated systems, and tectonically active systems. Various studies have demonstrated diachronous stratigraphic surfaces due to variable sediment supply and basin margin physiography (Burgess & Prince, 2015; Madof et al., 2016). Hardy et al. (1994), Hardy & Gawthorpe (1998; 2002) and Gawthorpe et al. (2003) (following the methods of Ritchie et al., 1999) introduced simplified tectonic constraints into 2D numerical modelling to assess stratal geometries and suggested that major stratigraphic surfaces may be limited in spatial extent (Gawthorpe et al., 2003). However, there has been little assessment of the full impact of along-strike variations in fault-related subsidence, and especially, differential tectonic constraints in both time and space and the combined influence of all three variable allogenic controls.

Here, we present a novel, flexible and more comprehensive sequence stratigraphic forward model that applies fault-scale tectonic constraints to 3D sequence stratigraphy. The model demonstrates the sensitivity of sequence architecture (stacking patterns and key stratigraphic surfaces) to the three-dimensional interplay of major sedimentary controls in a hangingwall half-graben by use of experiments, validated by field-based examples from the literature. Within the framework of the model, limitless parameter combinations for testing in any rift setting is permitted. Here, the objectives are: i) to assess the stratigraphic response to various temporal and spatial interactions of eustasy, tectonics and sedimentation patterns, ii) to explore the diachroneity of key stratigraphic surfaces, and the conditions under which the nature of those might vary, and iii) to apply temporally- and spatially-variable tectonic constraints to stratigraphic forward modelling for the first time. Syn-Strat demonstrates and illustrates important stratigraphic concepts in a unique

manner, which allows syn-rift systems to be explored in 3D and allows scope for testing of all possible outcomes, and assessing the stratigraphic response.

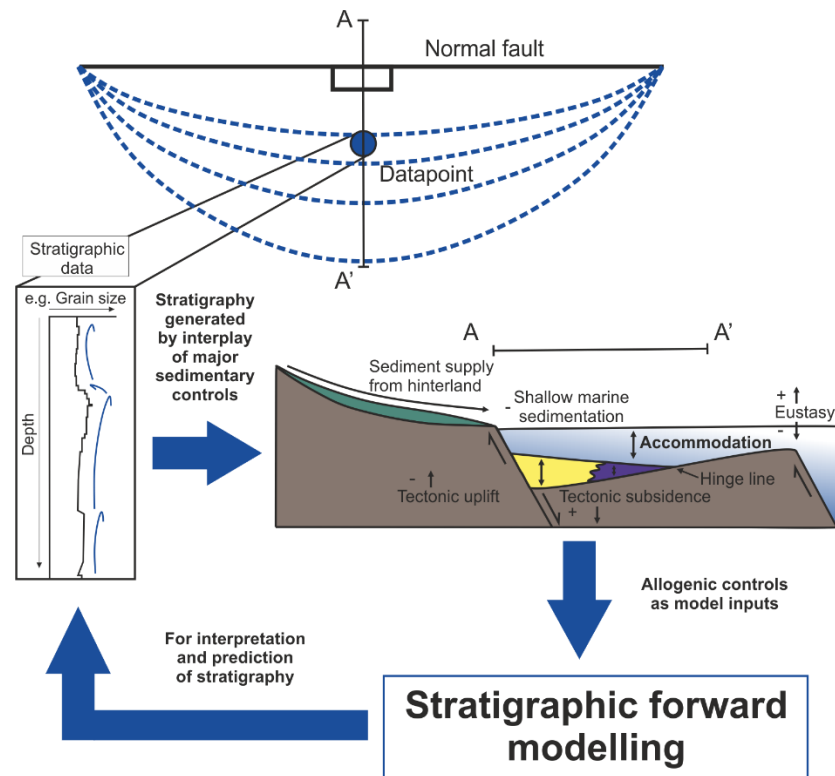


Figure 3.1. Process of forward stratigraphic modelling of syn-rift basin-fills. Stratigraphy at a position within the hangingwall of a normal fault is the result of the interplay of the three major sedimentary controls: eustatic sea level, fault-related subsidence and sedimentation. These controls can be modelled to provide insight for interpretation and prediction of syn-rift strata.

3.2. Model architecture and assumptions

3.2.1. Model framework

‘Syn-Strat’ is a geometric model that allows investigation of the interplay of eustasy, sediment supply, and tectonic subsidence in rift basins. The model sums changing i) eustatic sea level, ii) fault-related subsidence, and iii) sedimentation curves, to generate a 3D ‘accommodation’ curve, which is used to predict the stratigraphic infill of a half-graben basin adjacent to an individual normal fault segment. Syn-Strat also allows the opportunity to explore a number of other variables that contribute towards these major controls, such as accounting for crustal strength, isostasy and

erosion in subsidence. This is because each major control curve can be constructed from composite curves that contribute towards defining that variable and can be varied in time and space. For example, the eustatic sea level variable can be composed of a glacio-eustatic curve and a thermal expansion curve. However, for simplicity, here we use the resultant control curves to show the responses to the sensitivity tests.

We specifically define accommodation as the measurable space (thickness or volume) available at any given time for subsequent deposition that results from the combined influence of the preceding eustatic sea level, tectonic displacement and sedimentation. Eustatic sea level rise, tectonic subsidence and large-scale erosion from mass wasting are mechanisms that increase accommodation at any specific location, and eustatic sea level fall, uplift and sedimentation are mechanisms that reduce (or fill) accommodation. Our definition of accommodation follows original work by Jervey (1988) as the ‘space available for deposition’, which was also used by Catuneanu et al. (2009), and closely corresponds to definitions by Cross (1988), whereby ‘potential accommodation’ is the cumulative space created or removed by relative sea level changes and ‘realised accommodation’ is the volume of sediment that is actually accumulated. In this terminology, our model plots the sum of ‘potential’ and ‘realised’ accommodation, which in a shallow marine setting can be equated to water depth, but need not in other settings. It is ‘real-time’ accommodation, as opposed to interpreted accommodation from the stratigraphic record that other studies focus upon (Muto and Steel, 2000). To this avail, an assessment can be made of dynamic changes in accommodation as a result of variable controls.

The 3D accommodation function that is visualised as a graphical surface has dynamic along-strike, ‘x’, down-dip, ‘y’, and temporal, ‘t’, controls, to which stacking patterns (progradation, aggradation and retrogradation) or systems tracts, following any convention, can be ascribed. This forms a valuable, large-scale stratigraphic framework for a given set of controls, to which a process model could then be applied to predict the nature of a deposit.

The accommodation surface is defined on a three-dimensional mesh and stored in matrix form. At any point of ‘x’, ‘y’ and ‘t’, the accommodation surface, $A_s(x,y,t)$, is equal to the sum of

eustatic sea level, $E(x,y,t)$, and the total amount of tectonic subsidence until time t , $T(x,y,t)$, minus the total amount of sediment accumulated until time t , $S(x,y,t)$ (after Jervey, 1988; Posamentier & Allen, 1999; Catuneanu, 2002),

$$1) A_s(x,y,t) = -S(x,y,t) + E(x,y,t) + T(x,y,t).$$

A heuristic model is employed to specify the variables that sum to yield A_s . Variables (V) are separated into three normalised functions describing relative spatial and temporal variation, V_x , V_y and V_t that represent the given control i) along the fault length, ii) away from the fault and iii) in time, respectively. For example, sedimentation, S is defined in x (V_x), in y (V_y) and in t (V_t). The product of the three functions and the maximum scalar value of the variable, V_{sc} , yields the variable in each case,

$$2) V = V_{sc} V_x(x) V_y(y) V_t(t).$$

The dimensionless 3D accommodation surface that 'Syn-Strat' outputs, A_s' , is provided to enable comparison between different fault settings. For example, if two fault settings are compared with different subsidence, eustasy and sedimentation histories, the accommodation surface from each is normalised using the maximum amount of cumulative tectonic subsidence for each, to allow comparison between the two, $\max(T)$,

$$3) A_s' = A_s / \max(T).$$

The accommodation surface is plotted in terms of two of the three variables in dimensionless form: distance along fault divided by total fault length, x' , which is any line parallel to the fault segment; distance away from fault divided by distance from fault to the hinge line, y' , which is any line orthogonal to the fault segment; and time divided by the fault evolution timescale, t' . Therefore, three different visualisations are possible from the model (Fig. 3.2):

- A. Plot of accommodation (A') on any line parallel to the fault in the hangingwall in time, for any given distance away from the fault (x' , t')
- B. Plot of accommodation (A') on any line orthogonal to the fault in the hangingwall in time, for any given position along the fault (y' , t')

C. Plot of accommodation (A') in space (parallel to and orthogonal to the fault), for any given time (x', y')

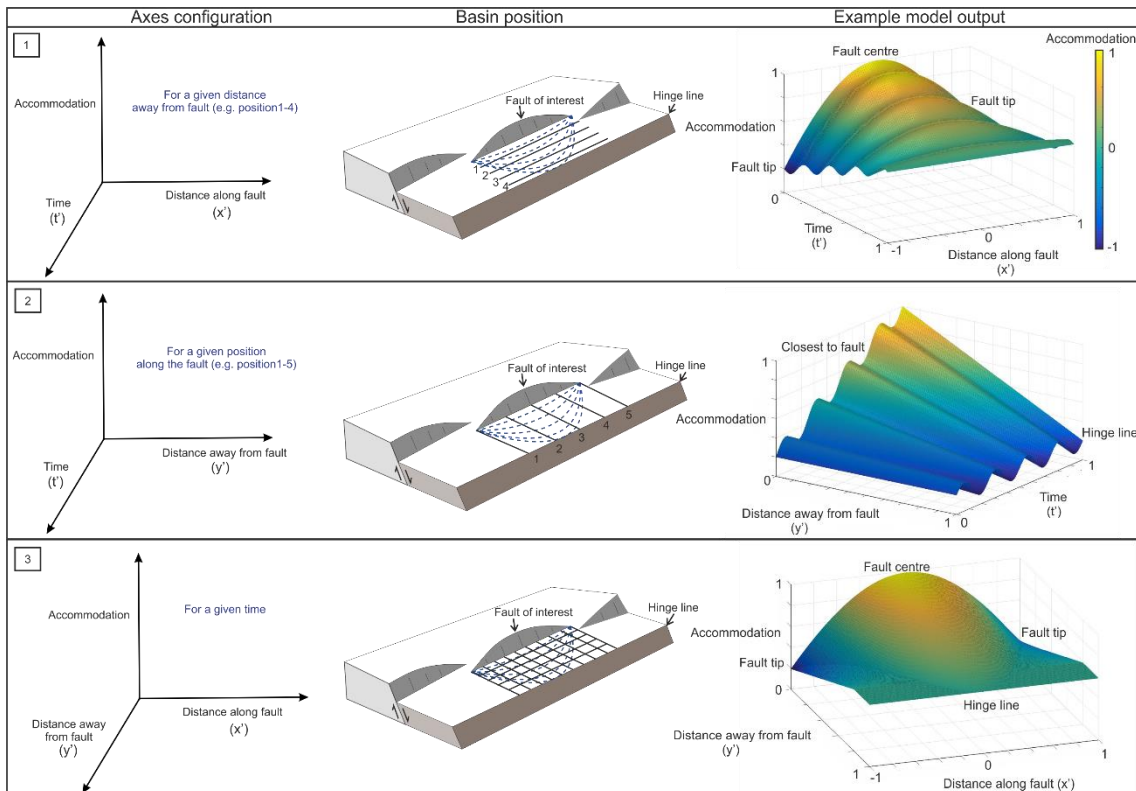


Figure 3.2. Model plot axes options, associated geological setting and example model outputs. 1) Plot of accommodation on any line parallel to the fault in the hangingwall in time, for any given distance away from the fault (x', t'). 2) Plot of accommodation on any line orthogonal to the fault in the hangingwall in time, for any given position along the fault (y', t'). 3) Plot of accommodation in space (parallel to and orthogonal to the fault), for any given time (x', y'). Structural contours shown by blue dashed lines. All figures hereafter utilise the axes shown in '1'.

3.2.2. Eustatic sea level

Eustatic sea level is a major control on accommodation, whereby a rising eustatic sea level increases accommodation and a falling eustatic sea level decreases accommodation (Wheeler & Murray, 1957; Wheeler, 1964; Mitchum et al., 1977; Vail et al., 1977; Jervey 1988). In Syn-Strat, eustatic sea level is defined in time, and is constant along the length of the fault and away from the fault. Figure 3.3 uses a simple sine wave for variation in time, although complex, real curves can be applied. Once defined, the time curve is multiplied by the two constant spatial curves to

produce a 3D graphical surface. Figure 3.3 illustrates this information by plotting eustatic sea level along the fault and in time, for a position in the immediate hangingwall of the fault.

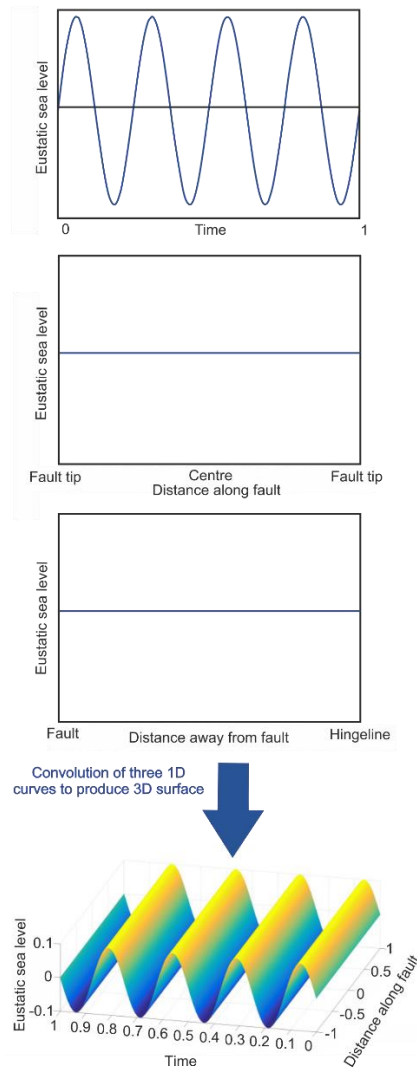


Figure 3.3. Derivation of the 3D eustatic sea level curve. Eustasy defined geometrically in time (top), along the fault length (upper middle) and away from the fault (lower middle). The three curves are convolved to give the 3D plot (bottom) in a given configuration (1 of Figure 3.2). Axes are dimensionless. ‘Time’ varies between 0 and 1. ‘Distance along fault’ varies between -1 and 1, where these are the fault tips and 0 represents the fault centre. ‘Distance away from fault’ varies between 0 and 1, where 0 is closest to the fault and 1 is the hinge-line.

3.2.3. Subsidence

3.2.3.1. Subsidence along the fault length

Tectonic displacement is defined in three dimensions: in time, and along and away from the fault. In the model, we are interested in tectonic displacement on the hangingwall of a single fault segment, which is subsidence. Cumulatively, hangingwall subsidence is zero at the two fault tips and maximum at the fault centre. When these three data points for subsidence are available, a parabola is calculated that describes the displacement change along the fault length. This distribution of subsidence along-strike of a fault has been extensively documented in the literature (e.g. Stein & Barrientos, 1985; Cowie & Scholz, 1992; Cowie et al., 2000) and is primarily used in our modelling. An observed temporally-variable subsidence distribution along the fault length could be applied instead.

Gawthorpe et al. (1994) and Collier & Gawthorpe (1995) highlight that the curve derived from the sum of the eustatic sea-level and tectonic subsidence curves will be steeper at the centre of a fault in a phase of relative sea level rise, where subsidence is greatest (position 1 in Fig. 3.4), than on either side (position 2 in Fig. 3.4). At the fault tips subsidence is zero, so accommodation varies due to eustasy alone (position 3 in Fig. 3.4).

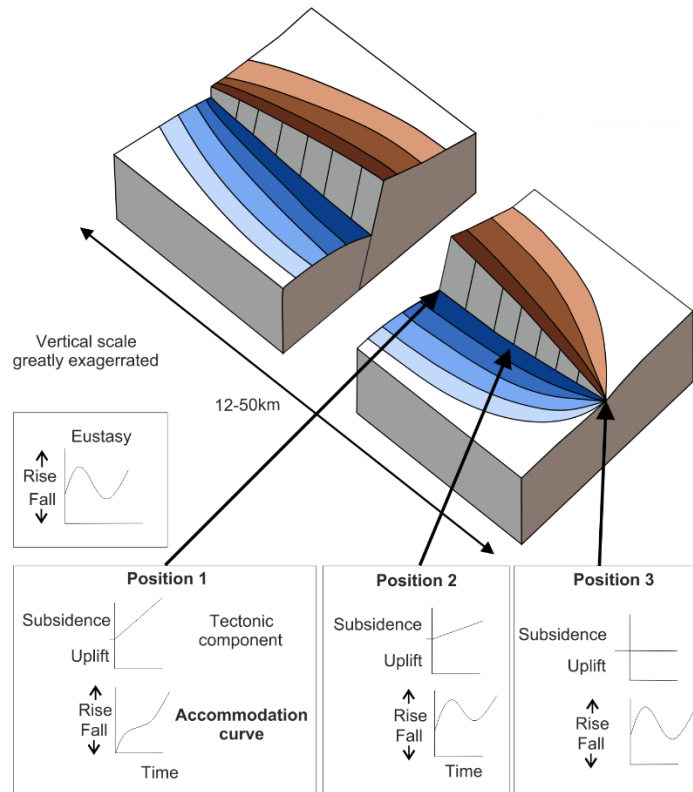


Figure 3.4. Diagram to illustrate the various relative sea level/accommodation curves that can be derived from the convolution of eustatic sea level and subsidence at three positions along a hangingwall fault block. The eustatic sea level curve that is used for all three positions is displayed on the left hand side. Modified from Collier & Gawthorpe (1995).

For the parabolic displacement distribution along the length of the fault, the model utilises a normal distribution curve. This permits alteration of the distribution curve shape depending on the system by varying the standard deviation, skewness and kurtosis. Assigning these variables with a value of one produces a parabola (Fig. 3.5). The model assumes that during growth, the fault is fixed in length, i.e. it is pinned at the fault tips. This growth model is supported by other studies that document examples of faults demonstrating constant-length growth (Walsh et al., 2002, 2003; Childs et al., 2003; Schlagenhauf et al., 2008; Jackson & Rotevatn, 2013; Nicol et al., 2016; Jackson et al., 2017). In cases when fault tips propagate, stacking will vary from that anticipated by the model, or it can be used to represent the central growth phase of the fault, when it is no longer undergoing linkage (in the terminology of Cowie et al., 2000).

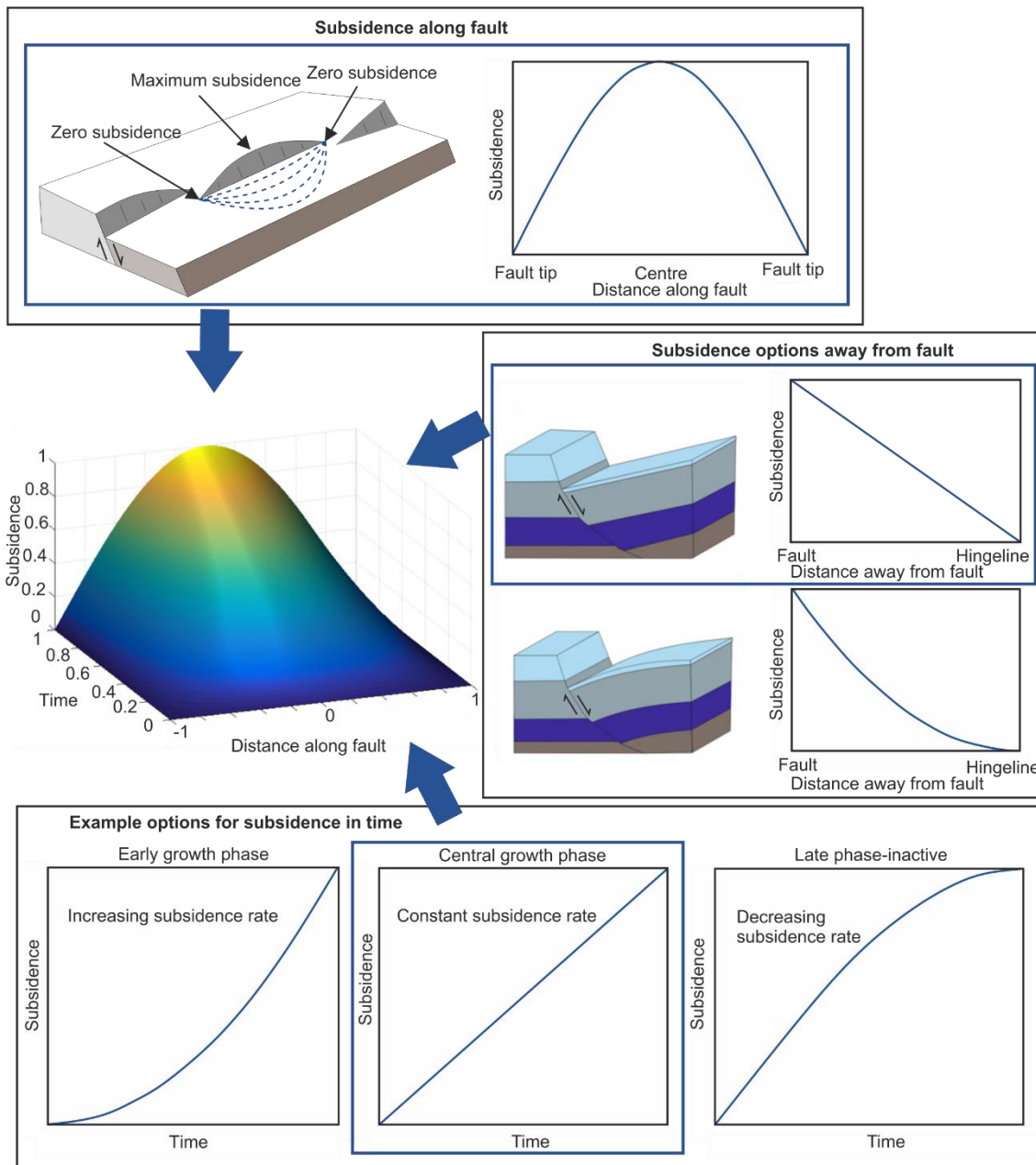


Figure 3.5. Derivation of the 3D subsidence curve. Subsidence is defined geometrically in time (lower box), with in-built options of either an increasing, constant, or decreasing subsidence rate. Subsidence is defined along the fault length (upper box), where a parabola describes the distribution of subsidence, and away from the fault (middle-right box), where two configurations are presented as options: either a linear or parabolic regression away from the fault. The highlighted blue boxes denote the chosen input in each case for the example 3D convolution. The resultant 3D subsidence plot, in a given configuration (1 of Fig. 3.2), is shown to the middle-left. It shows the variation of subsidence with the chosen parameters along the length of the fault, in time, in the immediate hangingwall of the fault.

3.2.3.2. Subsidence away from the fault

In a half graben, rotation is focussed at the hinge line, and beyond this point the net movement is uplift. The model considers subsidence from the immediate hangingwall where it is maximum, up to the hinge line of the block where it is zero. As subsidence is zero at the fault tips and maximum at the fault centre, the displacement from a slip event is distributed radially away from the fault. The structure contours resemble the parabolic shape of the displacement curve along the fault length and a 'zero contour line', the line of zero subsidence, is defined. The model generates the parabolic subsidence curve along the length of the fault, the equivalent zero contour line away from the fault, and the user defines the style of interpolation between them, which can be either linear or parabolic (Fig. 3.5). The interpolation (decay curve) style is determined by the manner in which the hangingwall deforms. If the hangingwall subsides without changing geometry, i.e. the hangingwall does not deform in dip-section as it rotates, a linear decay curve should be assigned. If the surface of the hangingwall adopts a convex geometry in dip-section during subsidence, a parabolic decay curve can be assigned.

3.2.3.3. Subsidence in time

During the syn-rift phase of fault growth, cumulative subsidence increases incrementally over time as a result of a series of earthquakes, and the hangingwall will subside in each event. As a result, the hangingwall deepens through time and accommodation is created. The subsidence rate is considered as the subsidence per earthquake over a given recurrence period. For example, the subsidence rate for earthquakes with a subsidence of 5m per event and a recurrence period of 500 years would be 10 mm/yr.

Syn-Strat allows a choice of in-built conceptual subsidence curves with time or the input of an observed subsidence curve. Figure 3.5 illustrates three examples of conceptual subsidence curves: a constant, an increasing, and a decreasing subsidence rate. A linear increase in subsidence through time represents a constant subsidence rate. In this scenario, the hangingwall cut-off deepens by the same increment with each earthquake. For the central growth phase of a fault, it

is perhaps most appropriate to choose a linear increase, as the fault is no longer linking with other faults and growth is no longer accelerating (as in Gupta et al., 1998; Cowie et al., 2000). An exponential increase of subsidence in time would represent an increasing strain rate and subsidence rate. In this scenario, each subsequent earthquake must produce a greater amount of subsidence, or there must be an increasing frequency of earthquakes. This could represent the early syn-rift phase of fault evolution, during fault linkage and strain localisation. Conversely, for a decreasing subsidence rate, there must be a reducing amount of subsidence for each subsequent earthquake, or a reduced frequency of earthquakes, which could represent the late syn-rift phase of fault evolution. Composite subsidence curves can be constructed. For example, a curve that represents the evolution of the fault from early- to late-syn rift phases, or a curve that defines the transition from active fault subsidence to either fault inactivity, as strain is partitioned to an adjacent fault, or to a post-rift basinal phase. Similarly, the subsidence rate can be varied through time to show a higher resolution of fault activity, e.g. earthquake clustering on one of a number of faults.

The subsidence curves in each dimension are multiplied to produce a 3D graphical surface. Figure 3.5 represents subsidence along the length of the fault, through time in the immediate hangingwall of the fault (configuration 1 of Fig. 3.2). It is composed of a parabolic displacement curve along the length of the fault, a linear increase in subsidence over time, and a linear decrease in subsidence away from the fault. Without consideration of eustatic sea level and sediment supply, this represents fault-related, temporal and spatial variations in accommodation.

3.2.4. Sedimentation

Sedimentation reduces the available space for subsequent deposition. Therefore, sedimentation is subtracted from combined eustatic sea level and subsidence to give the resultant graphical accommodation surface.

Spatial and temporal variations in sediment supply and the number and location of drainage input points arise as a result of climate variability (wind, temperature, rainfall, vegetation and their

seasonal fluctuations), size and physiography of each drainage basin (gradient, relief and orientation) and hinterland geology (e.g. Hack, 1957, Leeder & Gawthorpe, 1987, Ravnås & Steel, 1998). Spatial and temporal changes in sediment supply is a complicated variable that is difficult to constrain even in recent systems (Mullenbach & Nittrouer, 2006; Romans et al., 2009; Allen et al., 2013; Warrick, 2014; Romans et al., 2016). Syn-Strat utilises sediment accumulation (or sedimentation), rather than sediment flux. Sedimentation is defined geometrically, in contrast to some other models that utilise a process-based, commonly diffusion-type, approach (e.g. Rivænes, 1992; Flemings & Grotzinger, 1996; Granjeon & Joseph, 1999; Burgess & Prince, 2015). Although the geometric approach has its own inherent assumptions (discussed in Section 3.2), it avoids some of the limitations of process-based models in relation to the interaction of different process-regimes and dispersal mechanisms. The initial and final sedimentation accumulations are assigned, as well as the shape of the input curve in time and in space. A sedimentation rate is not assigned unless a linear curve in time is utilised, as in all other cases, it varies.

3.2.4.1. Sedimentation along the fault length

Here we model examples of shoreline-attached systems. In some scenarios, these prograde from the relay zones of a fault with, if accommodation allows, maximum deposition occurring at the fault tips and reducing towards the centre of the fault. In a scenario with equal sedimentation from both fault tips, an inverse parabola is used to model the sediment distribution along the length of the fault (Fig. 3.6). For this distribution, the percentage of total sedimentation that reaches the centre of the fault is defined. Any geometric curve that describes the distribution of sedimentation along the length of the fault can be utilised. For this study, we utilise curves with maximum deposition at a given location along the fault (the source point), which decreases away from that point radially to represent a prograding, shallow marine system, such as a delta. In a scenario of multiple footwall point sources (Fig. 3.6), Syn-Strat allows the user to alter the number, location, magnitude, shape and range of sediment input points. For the sediments (and predicted stacking) to be preserved, accommodation values must exceed zero; any ‘negative’ accommodation values

generated from the model represent sediments that would be bypassed to deeper water and/or redistributed along strike. However, an exception is with the presence of pre-existing accommodation, such as antecedent bathymetry, or regional tectonic subsidence that are not included in the model results presented here, and would allow preservation in modelled areas of ‘negative’ accommodation.

3.2.4.2. Sedimentation away from the fault

Sedimentation with distance away from the fault is not limited to a zero contour line (as with subsidence), and is defined as a linear, parabolic or exponential decrease towards zero at a chosen distance away from the fault. Figure 3.6 provides two examples of such options: a linear decrease and a parabolic decrease to zero at the hinge line.

3.2.4.3. Sedimentation in time

There are a number of controls that cause temporal variations in sedimentation, including changes in climate, source geology and drainage basin physiography on a range of timescales. In Syn-Strat, the user can define sedimentation over time from observed data or from a number of in-built options in the model, e.g. a linear or exponential increase, or decrease, a constant rate or a sinusoidal variation (Fig. 3.6). The product of sedimentation in each dimension is a 3D graphical surface. For example, Figure 3.6 uses an inverse parabola to describe sedimentation along the length of the fault, a linear increase in sedimentation over time and a linear decrease in sedimentation away from the fault to the hinge line. The 3D graphical plot presents sediment accumulation, along the length of the fault, through time in the immediate hangingwall of the fault (configuration 1 of Fig. 3.2).

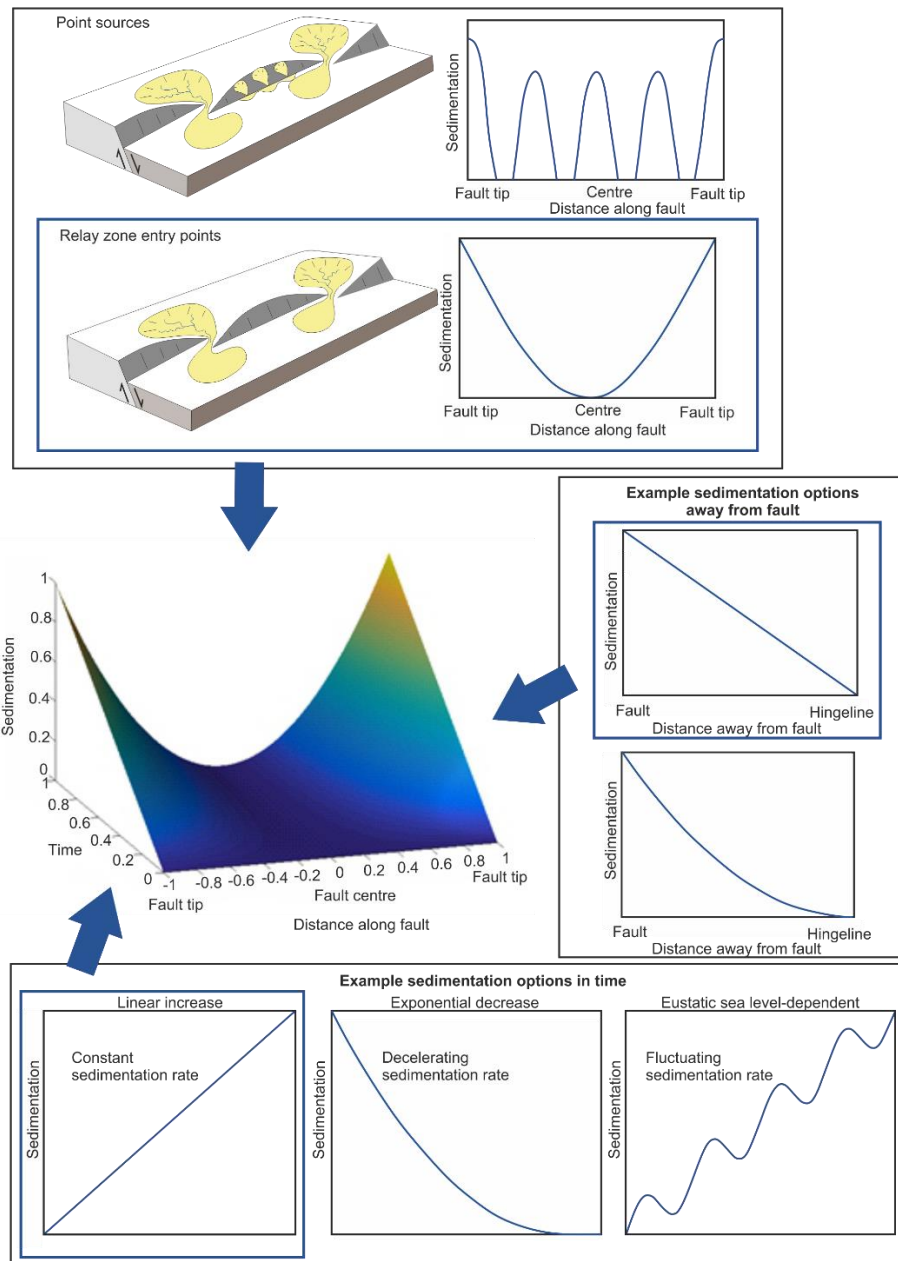


Figure 3.6. Derivation of the 3D sedimentation curve. Sedimentation is defined geometrically in time (lower box), where three examples of sedimentation curves that could be chosen are presented: a constant, decreasing, or fluctuating sedimentation rate. Sedimentation is defined along the fault length (upper box), where two examples of sediment distribution curves that could be chosen are presented: relay zone entry points and footwall point sources. Sedimentation is defined away from the fault (middle-right box), where two configurations are presented as options: either a linear or parabolic regression away from the fault up to the hinge line. The highlighted blue boxes denote the chosen input in each case for the 3D convolution. The resultant 3D sedimentation plot, in a given configuration (1 of Fig. 3.2), is shown to the middle-left. It shows the variation of sedimentation with the chosen parameters along the length of the fault, in time, in the immediate hangingwall of the fault.

3.3. Model output results

3.3.1. 3D accommodation surface

A 3D graphical surface that represents accommodation is produced by summing eustasy and tectonics and subtracting sedimentation. This is presented in Figure 3.7, with accommodation along the length of the fault, through time in the immediate hangingwall of the fault (configuration 1 of Fig. 3.2). In the example shown, subsidence is maximum and sedimentation is minimum at the centre of the fault. In this case, accommodation generally rises over time and is modified by a lower amplitude sinusoidal sea level. At the fault tip, subsidence is zero and sedimentation is maximum, and accommodation decreases over time into negative values as the basin fills to an overfilled state. This plot describes the interaction of the major controls, from which systems tracts can be identified and stacking patterns can be predicted.

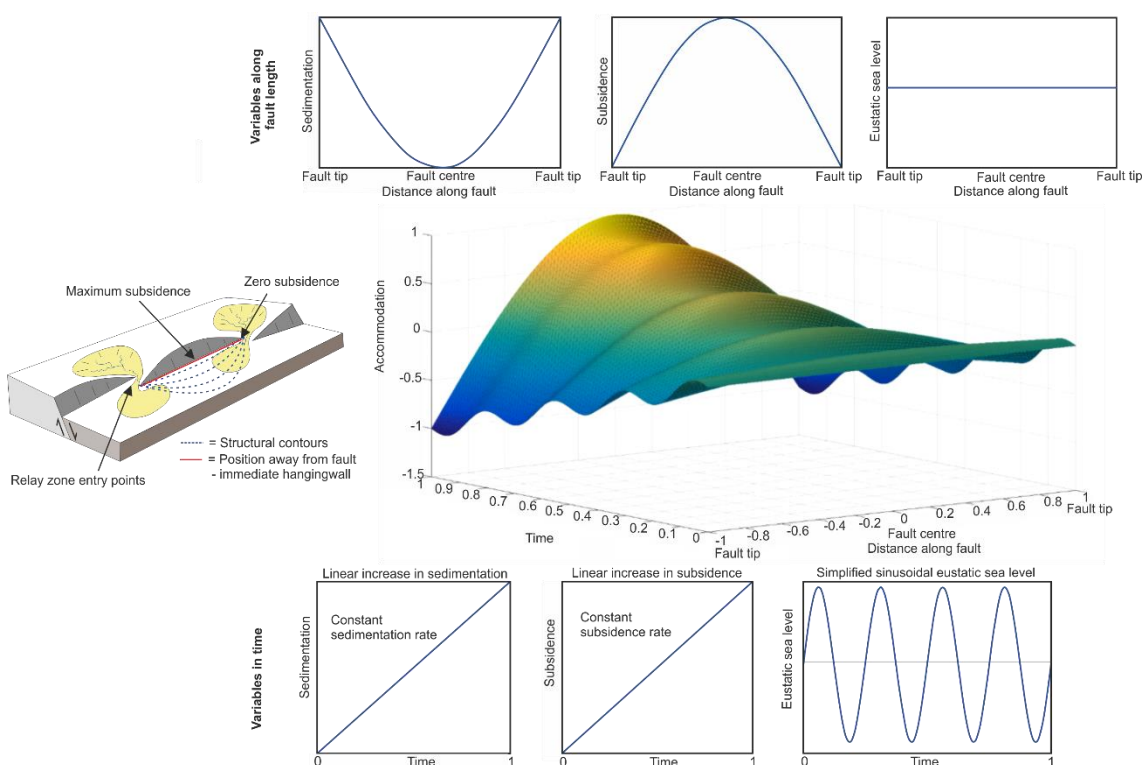


Figure 3.7. 3D accommodation plot (configuration 1 of Fig. 3.2A), generated from the convolution of all three major controls: eustatic sea level, subsidence and sedimentation. The input curves for each control along the fault length and in time are presented above and below the plot, respectively. A block diagram to show the setting of the plot is provided to the left, where the red line shows the position of the plot, in the immediate hangingwall of the fault.

3.3.2. Stacking patterns

For descriptions of stratal stacking patterns, Neal & Abreu (2009) and Neal et al. (2016) propose mainly observation-based, physical stratigraphy that describes the coastal response to accommodation creation and sedimentary fill. The terms progradation, aggradation, retrogradation and degradation are used to describe the way in which a depositional environment moves in space and thus, and how sediments are stacked through time. During progradation, the depositional system advances basinward as deposition exceeds available accommodation. In this case, marginal facies overlie basinal facies, characterised by a coarsening-upwards siliciclastic succession in core and outcrop and a decreasing gamma ray response in well-logs. During retrogradation, the system retreats (landwards) as accommodation exceeds deposition. Here, basinal facies overlie marginal facies and there is a fining-upwards succession in core and outcrop and an increasing gamma ray response in well-logs. During aggradation, deposition is equal to accommodation and the system neither advances nor retreats.

Syn-Strat colours the 3D surface according to these terms and utilises 5 classifications: strong retrogradation, weak retrogradation, aggradation, weak progradation and strong progradation (Fig. 3.8). The plot shows an overlay of Figure 3.7, with progradation (in warm colours) during relative sea level fall and retrogradation (in cold colours) during relative sea level rise. The model output also illustrates enhanced periods of retrogradation near the fault centre, where space is greater than deposition, and enhanced periods of progradation near the fault tips, where deposition is greater than available space. The plot provides the user with visualisation of how the sediments stack in time and space. Such information is useful to improve prediction of stacking patterns in areas with poor data constraint.

As shown, the model can generate the system response to major sedimentary controls in the form of stacking patterns, but does not predict the nature of the deposit. For this, various autogenic controls and the process regimes (transport mechanisms and directions) responsible for transport and deposition, and remobilisation, need to be considered, which challenge all existing numerical models of stratigraphic architecture. For example, where Syn-Strat anticipates areas of system

retrogradation, the deposit may exhibit a fining-upwards profile or there may be a condensed section in the rock record. Similarly, where Syn-Strat shows areas of system progradation, the deposit may exhibit a coarsening-upwards profile or there may be a regressive surface indicating basinward sediment bypass (*sensu* Stevenson et al., 2015). In regard to preservation, areas of the plot with accommodation values less than zero will have low preservation potential. For a more accurate restoration of preservation, the antecedent topography and the broader scale effect of thermal subsidence at the scale of the basin would need to be considered. Therefore, the model is best utilised to provide the stratigraphic framework to which a process-regime(s) can be applied to predict sediment dispersal patterns.

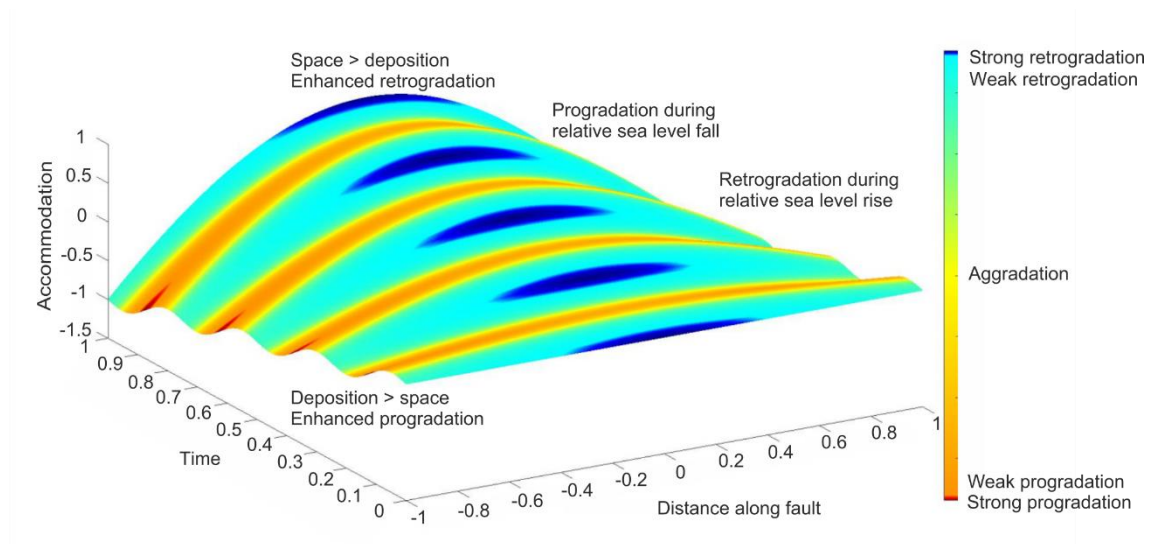


Figure 3.8. 3D accommodation plot from Figure 3.7 with stacking patterns presented. Plot shows the along-strike variation in stacking patterns as a result of laterally variable allogenic controls. Surface is coloured by 5 classifications: strong retrogradation (dark blue) and weak retrogradation (light blue), occurring during the relative sea level rises; aggradation (yellow); weak progradation (orange) and strong progradation (red), occurring during the relative sea level falls. A block diagram to show the setting of the plot is provided in Figure 3.7.

3.3.3. Systems tracts

Systems tracts are used to subdivide a depositional sequence based upon its position on a relative sea level curve (or accommodation curve). As sequence stratigraphy theory has evolved, so

complicated and non-universal systems tract schemes have developed (see Catuneanu, 2006, 2009 for summary). For plotting systems tracts, Syn-Strat allows any one of these sequence stratigraphic approaches to be assigned and colours the accommodation surface accordingly (Fig. 3.9). The example 3D curve presented is an overlay of Figure 3.7 and adopts the ‘genetic sequence’ approach (e.g. Frazier, 1974 and Galloway, 1989), whereby the Highstand Systems Tracts (HST), the Early Lowstand Systems Tracts (ELST), the Late Lowstand Systems Tracts (LLST) and the Transgressive Systems Tracts (TST) are represented by the yellow, purple, blue and green segments, respectively (Fig. 3.8). Application of the systems tracts to the 3D surface helps visualisation of the temporal variation in the development of key sequence stratigraphic surfaces along the fault, e.g. maximum flooding surfaces (MFS) and sequence boundaries (SB). The sequence boundary (or ‘correlative conformity’) between the HST in yellow and the ELST in purple is diachronous, and occurs at a later time at the centre of the fault than at the fault tips. In the ‘genetic sequence’ scheme, the MFS is taken to be the position between TST and HST and it also occurs at a later time towards the centre of the fault than at the fault tips (Fig. 3.8). We later discuss the implications of selecting an alternative MFS position on a relative sea level curve, because this choice will determine the nature of the diachroneity of the MFS along the fault.

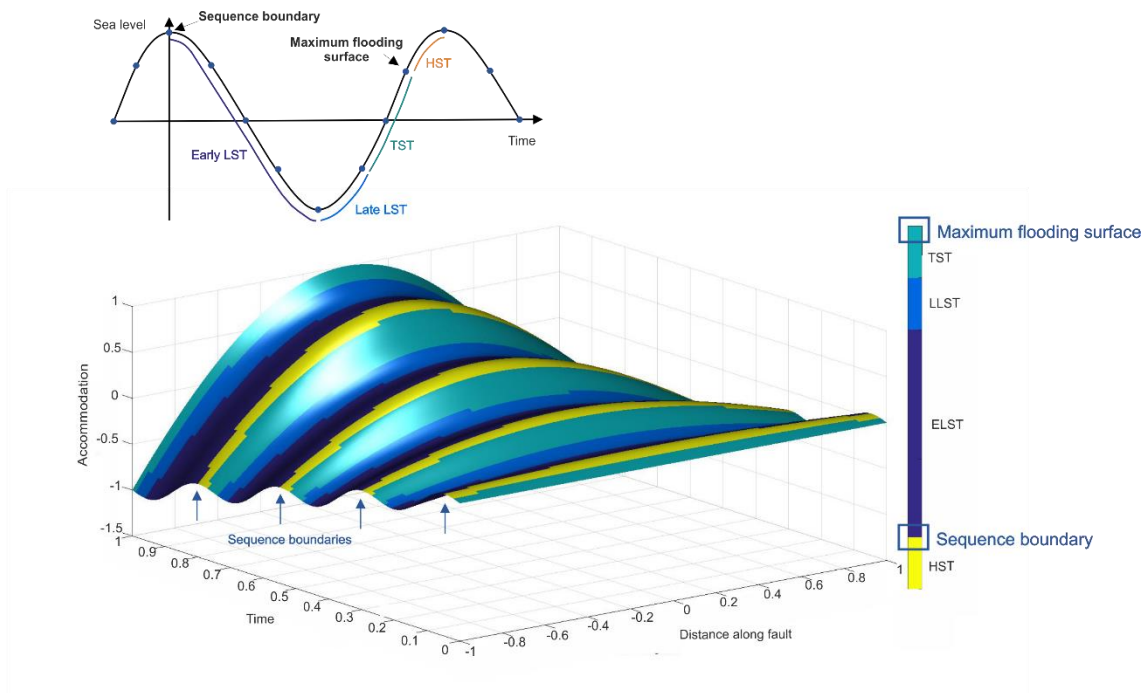


Figure 3.9. 3D accommodation plot from Figure 3.7 with systems tracts presented. Colours represent systems tracts as per the scheme named 'Genetic sequence' in Catuneanu et al. (2009), where: TST = Transgressive Systems Tract, LLST = Late Lowstand Systems Tract, ELST = Early Lowstand Systems Tract and HST = Highstand Systems Tract. Sequence boundaries are indicated by the blue arrows between the HST and ELST and can be seen to be diachronous along the fault, i.e. occurring at a later time towards the centre of the fault than towards the fault tips. The sections of the relative sea level curve that each stage refers to is illustrated on the relative sea level curve at the top-left. A block diagram to show the setting of the plot is provided in Figure 3.7.

3.4. Discussion

The sensitivity of sequence architecture to major sedimentary controls and the utility of this model are discussed using a number of conceptual tests. In these tests, the major controls in terms of relative magnitude, rates through time and spatial distribution have been varied, with reference to documented examples from exhumed and modern systems.

3.4.1. Eustatic sea level- vs. subsidence-dominated successions

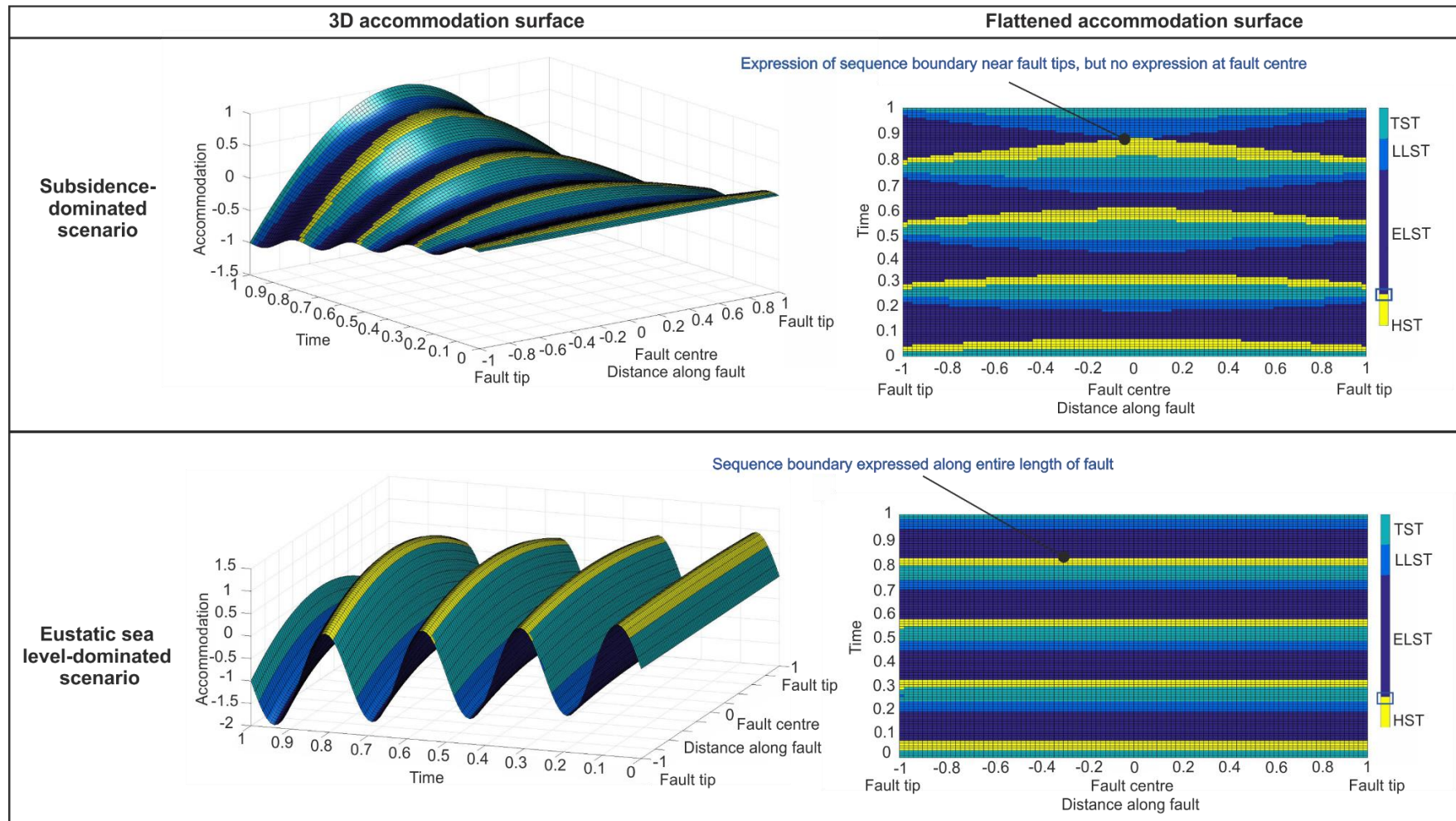
Two conceptual scenarios that demonstrate the differences between subsidence-dominated and eustatic sea level-dominated systems have been modelled (Fig. 3.10). In both cases, the rate of change of the dominant control is an order of magnitude higher than the subordinate control. Sedimentation from both fault tips is high and of the same magnitude as the dominant control, resulting in a balanced state in both scenarios. A sinusoidal eustatic sea level and exponential increase in subsidence from zero, through time are applied. Figure 3.10 shows the 3D graphical accommodation surface along the length of the fault, in time, in the immediate hangingwall of the fault and is coloured by systems tracts. The sequence boundaries between the HST and ELST are identified in a flattened version. In the subsidence-dominated scenario, the sequence boundaries are diachronous and the expression is lost in the model output at the fault centre towards the end of the time-frame. Here, the rate of subsidence outpaces the maximum rate of eustatic sea level fall with a resultant relative sea level rise. In the rock record, an unconformity that represents the sequence boundary would be expressed in this area as a correlative conformity. In the eustatic sea level-dominated scenario, the sequence boundaries are expressed and are isochronous along the length of the fault.

3.4.1.1. Field-based example: Loreto Basin

These scenarios strongly resemble the partially-constrained, sediment-rich depositional system of the Piedras Rodadas Formation, Loreto Basin, Gulf of California, which is sub-divided into two sub-basins: the Central sub-basin and the SE sub-basin. Subsidence rates of the Loreto Fault in both sub-basins from 2.6 to 2.4 Ma were derived by Umhoefer et al. (1994) and refined by Dorsey & Umhoefer (2000). The Central sub-basin experienced subsidence rates of 8 mm/yr and the SE sub-basin experienced lower subsidence rates of 1.5 mm/yr over the 200 kyr period. With an estimated eustatic sea level change rate of 4-5 mm/yr (supported by Raymo et al., 1992; Blanchon & Shaw, 1995), Dorsey & Umhoefer (2000) present the contrast between the subsidence-dominated Central sub-basin to the eustatic sea level-dominated SE sub-basin. The authors

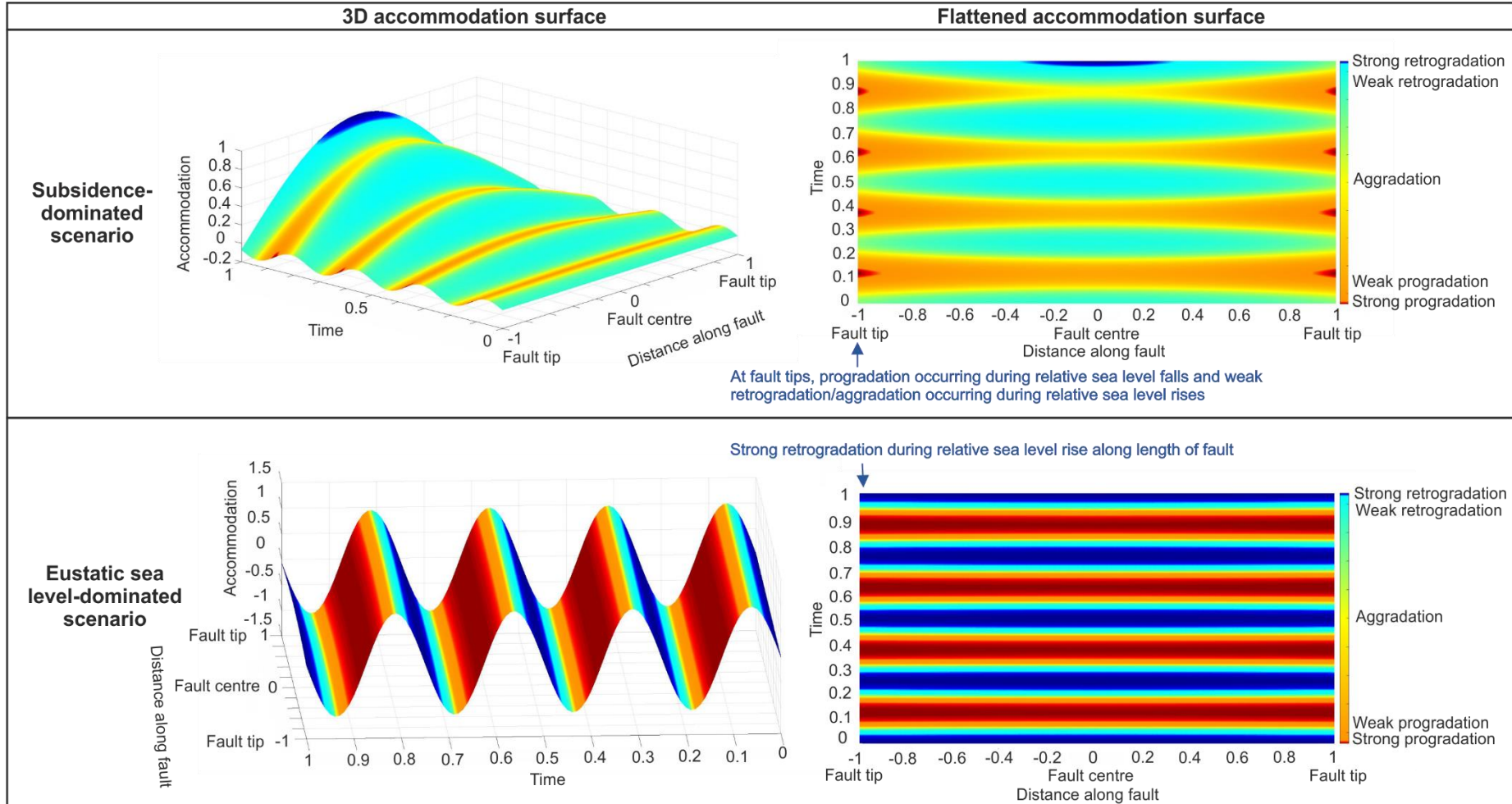
observe the presence of sequence boundaries in the SE sub-basin and a distinct lack of sequence boundary expression in the central sub-basin, which is consistent with our model results.

Figure 3.10. Diagrams with systems tracts presented to show the difference between two contrasting conceptual scenarios with a high sediment supply: a subsidence-dominated (top) and eustatic sea level-dominated (bottom) system; analogous to the two sub-basins of the Piedras Rodadas Formation, Loreto Basin, Gulf of California. A 3D accommodation surface is shown for both cases with a flattened version adjacent. Both scenarios incorporate high sedimentation from the fault tips, simplified, sinusoidal eustatic sea level and an increasing subsidence rate through time. The rate of change of the dominating control is an order of magnitude higher than that of the subordinate control, in both cases. In the subsidence-dominated scenario, it is clear that each sequence boundary is diachronous and its expression is lost at the fault centre towards the end of the time-frame. In the eustatic sea level-dominated scenario, the sequence boundaries are expressed and are isochronous along the length of the fault.



A second test (Fig. 3.11) shows two contrasting model outputs using the same input parameters and configuration (1 of Fig. 3.2A) as in Figure 3.10, except with a low sediment input from the fault tips. Hence, the basin is in a sediment-starved state, as opposed to a balanced state. Here, stacking patterns are presented, rather than systems tracts. In this test, the stacking patterns show more along-strike variation in the subsidence-dominated scenario than the eustatic sea level-dominated scenario due to the influence of subsidence distribution on the accommodation curve. Strong progradation only occurs from the fault tips over short periods during the maximum rate of relative sea level fall. The period of each progradational phase shortens towards the centre of the fault, and the period of each retrogradational phase shortens towards the fault tips. Weak retrogradation/aggradation occurs at the fault tips during relative sea level rise. In contrast, the eustatic sea level-dominated plot reveals laterally continuous patterns of alternating strong retrogradation and progradation as eustatic sea level varies through time. In comparison to the previous example (Fig. 3.10), the accommodation curve shows less along-strike variation due to the lesser influence of sedimentation in this underfilled scenario.

Figure 3.11. Diagrams with stacking patterns presented to show the difference between two contrasting conceptual scenarios with a low sediment supply: a subsidence-dominated (top) and eustatic sea level-dominated (bottom) system; analogous to the Holocene-active system surrounding the Psatha-Skinos-Alepori fault system, Alkyonides Gulf, Greece. A 3D accommodation surface is shown for both cases with a flattened version adjacent. Both scenarios incorporate low sedimentation from the fault tips, simplified, sinusoidal eustatic sea level and an increasing subsidence rate through time. The rate of change of the dominating control is an order of magnitude higher than that of the subordinate control in both cases. There is more along-strike variation in the subsidence-dominated scenario than the eustatic sea level-dominated scenario.



3.4.1.2. Field-based example: Alkyonides Basin

A modern analogue for this example is the partially-constrained, Holocene-active system surrounding the Psatha-Skinos-Aleporochori fault system in the Alkyonides Gulf, Greece. Here, sediment inputs have arisen from the relay zones of the fault system. An average sedimentation rate of 1.1 mm/yr (Collier et al., 2000; Bell et al., 2009), an average eustatic sea level rise rate of 5.8 mm/yr (70 m rise in 12 kyr; Collier et al., 2000), and an average hangingwall subsidence rate of 0.5-0.6 mm/yr established near the fault tips (Leeder et al., 2002) over the last 12 kyr have been constrained. This suggests that over the last 12 kyr, the system has been eustatic sea level-dominated, and relatively sediment starved, with low subsidence approaching zero towards the fault tips, and as a result, the beach barriers extending from both fault tips are retrograding (Collier & Gawthorpe, 1995). This pattern is anticipated in the model results during the relative sea level rises of the eustatic sea level-dominated model (Fig. 3.11). With the exception of the possibility of fault tip propagation during this time, it is only this interplay of controls that allow significant retrogradation at the fault tips, in such a eustatically-dominated period such as the Late Quaternary. The sedimentary successions may exhibit greater retrogradation in areas with higher subsidence, such as the centre of the fault. This has been observed in a shallow piston core study from the hangingwall of the West Channel fault, at the western end of the Gulf of Corinth (Bell et al., 2009).

3.4.2. Sensitivity to varying subsidence rates

Depositional sequences are defined by the relative influence of the major sedimentary controls, and are influenced by the nature of that control through time. Three modelled examples with different subsidence histories demonstrate this (Fig. 3.12): an increasing subsidence rate (A), an episodic subsidence rate (B), and a decreasing subsidence rate (C). In each example, the same eustatic sea level and sedimentation models are used, hence any variations in the stacking patterns may be attributed solely to variations in subsidence. There is no pre-inherited accommodation. The plot in Figure 3.12 is presented in configuration 1 of Figure 3.2.

The scenario with an increasing subsidence rate (Fig. 3.12A) reveals progressively longer periods of retrogradation and shorter progradational periods, particularly towards the centre of the fault where subsidence is maximal. Because subsidence rate increases through time, the system reveals more along-strike variation in stacking patterns. A scenario with six phases of subsidence (Fig. 3.12B) reveals a cyclic pattern with periods of progradation separated by periods of strong retrogradation, particularly near the fault centre. Each subsidence event is the same magnitude and duration. The effects of each subsidence event would be more strongly expressed in a scenario with a lower amplitude eustatic sea level signal, as here they are superimposed onto higher amplitude eustatic sea level variations through time. Dorsey & Umhoefer (2000) and Mortimer et al. (2005) attribute episodic, fault-controlled subsidence along the Loreto Fault as the principal control on the accumulation and timing of several fluvio-deltaic progradational units in the Central sub-basin of Loreto, Gulf of California. Each progradational unit is capped by a MFS, expressed as a shell bed. A MFS is predicted during the strong retrogradational periods in the model (Fig. 3.12B). In the third scenario (Fig. 3.12C), subsidence rate decreases to zero after 80% of the time has lapsed. This pattern of subsidence may represent a syn- to post-faulting transition, whereby a fault switches off as strain is taken up on an adjacent fault. The output largely shows the inverse of the first scenario, whereby longer periods of strong retrogradation near the fault centre are expressed initially when subsidence rates are highest, and these are suppressed through time with decreasing subsidence rate. Initially, there are marked along-strike variations in stacking patterns, but as subsidence decreases through time, eustatic sea level becomes increasingly dominant and the stacking patterns become more laterally continuous.

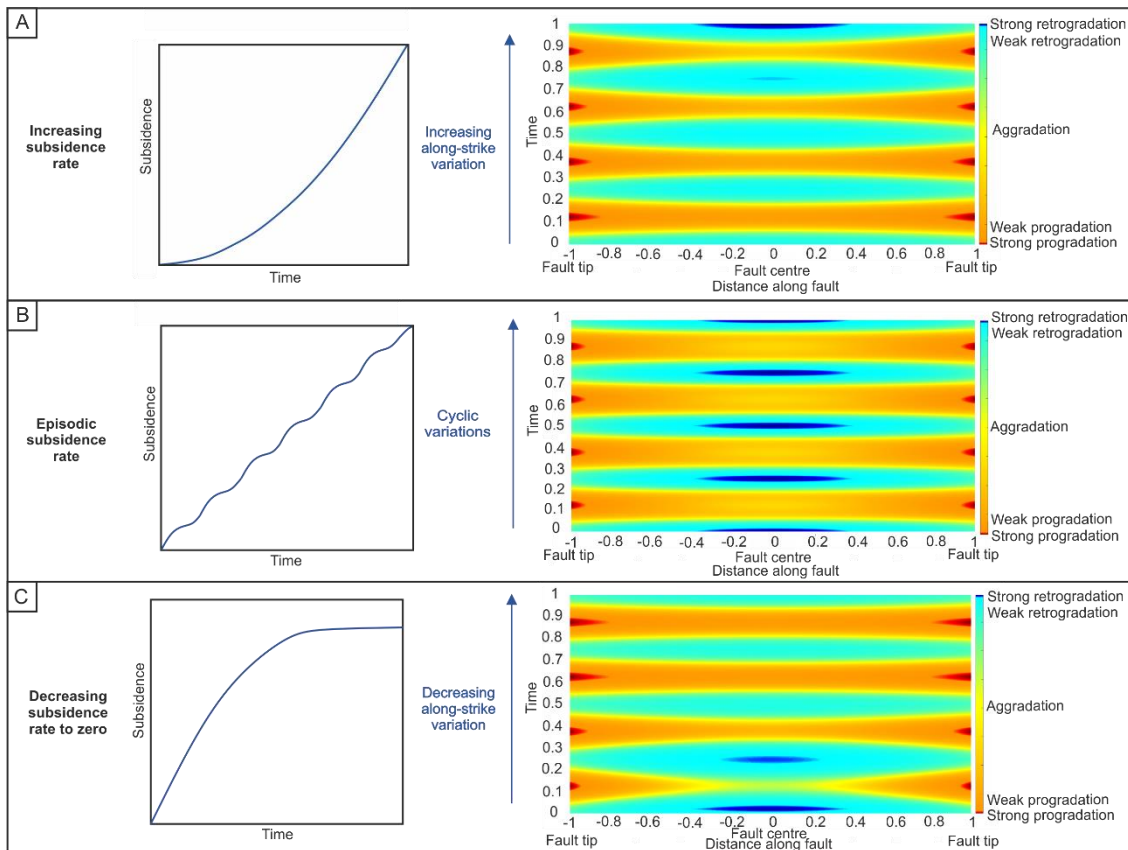


Figure 3.12. Diagrams to show the variation in stacking patterns between three conceptual scenarios with different subsidence rate patterns: an increasing (A), episodic (B) and decelerating (C) subsidence rate. Graphs to show the subsidence input through time are presented on the left and flattened accommodation surfaces are presented on the right. The plots exhibit increasing along-strike variation through time, cyclic variations and decreasing along-strike variation through time, respectively.

3.4.3. Sensitivity to varying sedimentation distribution

Spatial and temporal variations in sediment flux from drainage basins to sedimentary basins are hard to quantify, and have been less emphasised in sequence stratigraphic interpretations than accommodation-driven changes (Burgess, 2016). To assess the sensitivity of stacking to sedimentation patterns, three different sedimentation models are superimposed upon the same subsidence and eustatic sea level models in each case (Fig. 3.13 – in configuration 1 of Fig. 3.2), in which subsidence is high and the amplitude of eustatic sea level change is an order of magnitude lower. The distribution of sedimentation along the fault is varied but the magnitude of maximum sedimentation (and rate) is the same in each scenario. With all other controls uniform between the

tests, any changes observed in the nature of the SBs and MFSs may only be attributed to the sedimentation model. The three scenarios tested are: a system with equal sediment input from the fault tips (A), a system with sediment input from one fault tip (B) and a system with sediment input from point sources that could represent fan deltas (C).

Figure 3.13A utilises the sedimentation model with equal input from both fault tips. The sequence boundaries are highlighted and it can be seen that they are diachronous due to the combined influence of laterally variable subsidence and sedimentation. As a result of sedimentation being equal from both fault tips, the diachroneity of the sequence boundaries is symmetrical over the centre of the fault. Conversely, where sedimentation occurs from one fault tip (Fig. 3.13B), the nature of the sequence boundaries is not symmetrical over the centre of the fault. The side that experiences the most sedimentation expresses more prominent diachroneity of sequence boundaries than the sediment-starved side, where they are isochronous. At the fault tip with sediment input, the sediment supply counteracts the effects of relative sea level rise because the space that is being created is being filled. It promotes the relative sea level fall and progradation. This effect decreases towards the centre of the fault, away from the sediment source, enhancing the along-strike diachroneity. On the side of the fault where there is no sediment source, the sequence boundaries are influenced only by eustasy and decreasing subsidence towards the fault tip. The 3D accommodation surface illustrates the decreasing accommodation on the sediment-rich side through time, whereas accommodation on the sediment-starved side varies only with eustatic sea level.

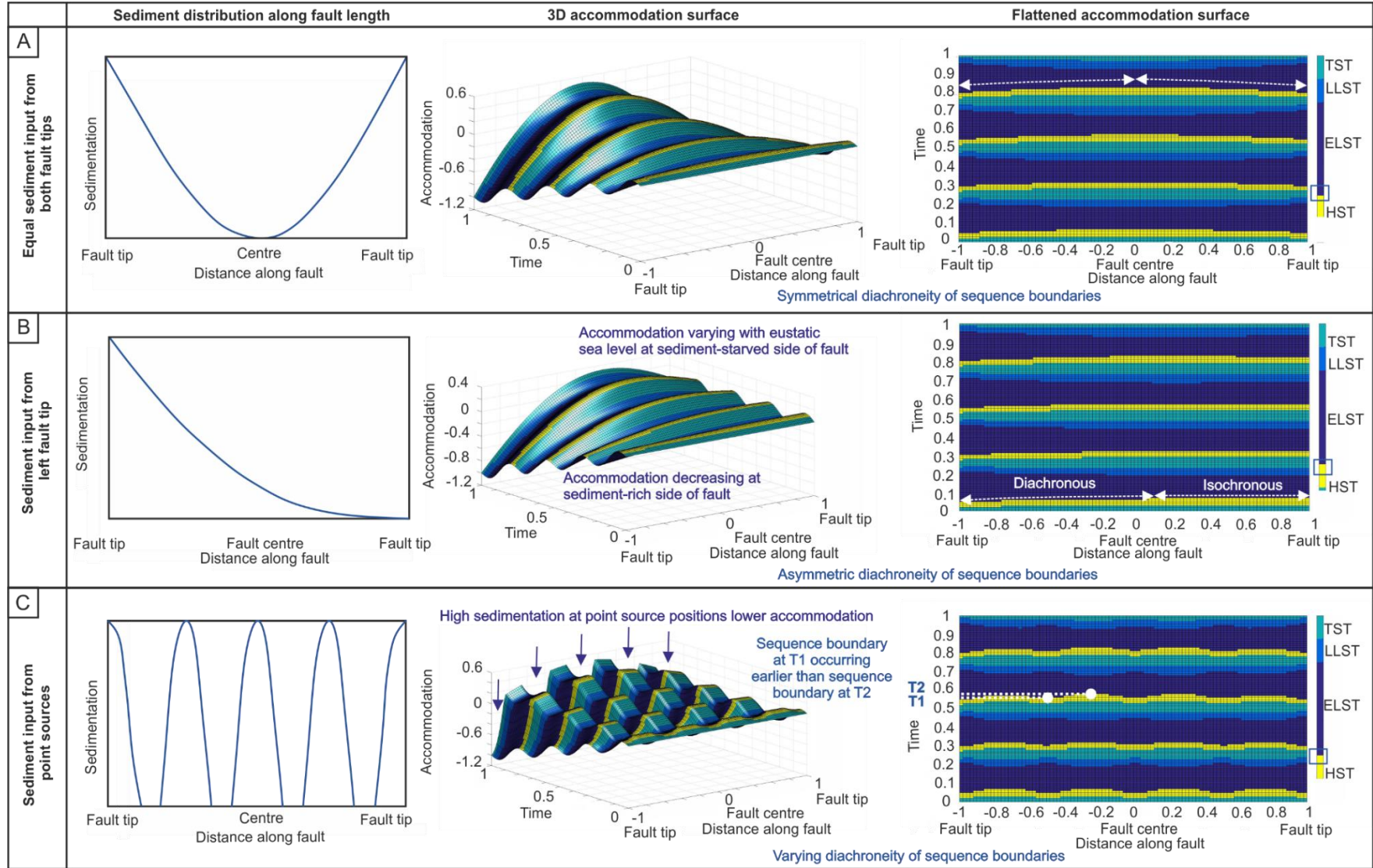


Figure 3.13. Diagrams with systems tracts presented to show differences between three conceptual scenarios with different sedimentation distribution patterns along the fault length: equal input from both fault tips (A), input from left fault tip (B) and point sources (C). Graphs to show the sedimentation input along the fault length (left), output 3D accommodation surfaces (middle) and flattened accommodation surfaces (right) are presented. The nature of diachroneity of sequence boundaries varies in each scenario, as labelled in white.

In the scenario with sedimentation from five point sources (Fig. 3.13C), the amount of sedimentation and degree of dispersal is equal from each source. The plot shows a reduction in accommodation where the point sources are located, hence the irregular shape of the surface. The sequence boundaries are highlighted in the flattened plot and their degree of diachroneity varies along the fault length. For example, the sequence boundary occurs earlier where the point sources (T1 in Fig. 3.13) are located than it does in the areas between them (T2 in Fig. 3.13). These scenarios support the inference that temporal and spatial changes in sediment supply need to be considered when making sequence stratigraphic interpretations, as well as accommodation changes from eustasy and tectonics that are usually emphasised.

3.5. Implications and applications for subsurface appraisal

During hydrocarbon prospect appraisal and static model generation, key stratigraphic surfaces, such as the MFS and SB, are used to correlate between wells, with the assumption that they are isochronous surfaces. However, recent studies have shown that such surfaces are time transgressive in a range of environments (e.g. Holbrook & Bhattacharya, 2012; Burgess & Prince, 2015; Hodgson et al., 2016; Madof et al., 2016). Here, we not only demonstrate that such surfaces are diachronous along the length of syn-rift faults due to along-strike variation in both sedimentation and subsidence, but also demonstrate the nature of that diachroneity. In the case of the MFS, which likely forms part of the seal to a hydrocarbon reservoir, understanding the temporal relationships along-strike of a fault are of critical importance for hydrocarbon volume calculations and production rate predictions. When the MFS is used for correlation, care should be taken when choosing the representative position on the relative sea level curve, or which sequence stratigraphic scheme to adopt because the nature of diachroneity varies between the

different positions. Consider a comparison between two options for MFS position choice: 1) the position between TST and HST, following the ‘genetic sequence’ scheme, 2) the position between LLST and TST (the initial transgressive surface). Both surfaces are diachronous along the fault, but the nature of that diachroneity is different between them, with the former occurring later at the centre of the fault than at the fault tips (Fig. 3.8), and the latter occurring earlier towards the centre of the fault than at the fault tips. This difference could be important for trap-seal analysis, where understanding the variability of the shale intervals caused by flooding in time and space is fundamental. Syn-Strat allows the user to visualise such variations qualitatively and to quantify the variations for a given magnitude of each control. The model also permits flexibility on timing and duration of dominance of one control to the other and thus allows an iterative approach to sequence stratigraphic tests when constraining controlling parameters. Producing a solid foundation to which process-based models can be applied is crucial for prediction of large-scale stacking in complex settings. The Syn-Strat model approach is particularly useful for low-resolution datasets, such as seismic, where small-scale deposition characteristics are not readily apparent. It allows insight into the way a system responds to particular controls and shows the differences by making spatial and temporal adjustments to those controls. An assessment of all the possible outcomes from a particular setting allows the stratigrapher to obtain the best understanding of the controls in play. If a good correspondence is made between the data and the model in one area, the model may then be used to anticipate the potential stacking further along-strike or down-dip, in the absence of good quality data.

3.6. Conclusion

Syn-Strat, a novel 3D sequence stratigraphic forward model is presented, which introduces both temporally- and spatially-variable tectonic components to sequence stratigraphic modelling. The model provides a framework to which process-based models could be applied and provides the scope to test multiple scenarios where the controlling parameters are poorly constrained, and

outcomes with a unique, useful and universal presentation style. Syn-Strat considers along-strike, down-dip and time variability in sequence architecture on a fault segment-scale and can be used to improve interpretation and prediction of syn-rift depositional architectures, which are the focus of exploration in a number of hydrocarbon basins, by constraining system response to any combination of allogenic controls.

By calculating accommodation in three dimensions, Syn-Strat is able to demonstrate the sensitivity of sequence architecture to laterally variable tectonic constraints and different relative magnitudes of allogenic controls. A basin largely modified by faulting will exhibit different depositional architecture to one dominated by eustasy, and the model outputs demonstrate how this difference is expressed in terms of stacking patterns and stratigraphic surfaces. The model has demonstrated the potential for analysis of along-strike variations in stacking patterns due to different subsidence rate characteristics, and the nature of diachroneity of key stratigraphic surfaces as a result of different sedimentation distribution models. Stratigraphic surfaces are known to be diachronous in these settings. However, understanding how the diachroneity of these surfaces changes spatially represents a significant step forward for petroleum system interpretations, where such surfaces may represent bypass zones or stratigraphic traps seals and are heavily relied upon for well correlations, and hence reservoir connectivity and production rate predictions. Additionally, the ability to understand how stacking patterns vary spatially and temporally is highly valuable in areas with little data constraint. Such variation is visualised in the sensitivity tests presented in this paper that are tied to field analogues, but in the future may be constrained with quantitative data from real input parameters.

3.7. Acknowledgements

We thank the project sponsor, Engie that support the SMRG (Shallow Marine Research Group). We also thank the two reviewers and the editor, Professor Massimo Zecchin for their contribution; the manuscript has benefited from their insights and comments.

3.8. References

- Allen, P.A., Armitage, J.J., Carter, A., Duller, R.A., Michael, N.A., Sinclair, H.D., Whitchurch, A.L. & Whittaker, A.C. (2013). The Q_s problem: sediment volumetric balance of proximal foreland basin systems. *Sedimentology*, 60, 102-130.
- Bell, R.E., McNeill, L.C., Bull, J.M., Henstock, T.J., Collier, R.E.Ll. & Leeder, M.R. (2009). Fault architecture, basin structure and evolution of the Gulf of Corinth Rift, central Greece. *Basin Research*, 21, 824-855.
- Blanchon, P. & Shaw, J. (1995). Reef drowning during the last deglaciation: Evidence for catastrophic sea-level rise and ice-sheet collapse. *Geology*, 23, 4-8.
- Burgess, P.M. (2016). The future of the sequence stratigraphy paradigm: Dealing with a variable third dimension. *Geology*, 44, 335-336.
- Burgess, P.M. & Allen, P.A. (1996). A forward-modelling analysis of the controls on sequence stratigraphical geometries. *Geological Society, London, Special Publications*, 103, 9-24.
- Burgess, P.M. & Prince, G.D. (2015). Non-unique stratal geometries: Implications for sequence stratigraphic interpretations. *Basin Research*, 27, 351-365.
- Catuneanu, O. (2002). Sequence stratigraphy of clastic systems: concepts, merits and pitfalls. *Journal of African Earth Sciences*, 35, 1-43.
- Catuneanu, O. (2006). *Principles of Sequence Stratigraphy*, 1st edn. Elsevier, Amsterdam, The Netherlands, 375pp.
- Catuneanu, O., Abreu, V., Bhattacharya, J.P., Blum, M.D., Dalrymple, R.W., Eriksson, P.G., Fielding, C.R., Fisher, W.L., Galloway, W.E., Gibling, M.R., Giles, K.A., Holbrook, J.M., Jordan, R., Kendall, C.G.St.C., Macurda, B., Martinsen, O.J., Miall, A.D., Neal, J.E., Nummedal, D., Pomar, L., Posamentier, H.W., Pratt, B.R., Sarg, J.F., Shanley, K.W., Steel, R.J., Strasser, A., Tucker, M.E. & Winker, C. (2009). Towards the standardization of sequence stratigraphy. *Earth-Science Reviews*, 92, 1-33.
- Childs, C., Nicol, A., Walsh, J.J. & Watterson, J. (2003). The growth and propagation of synsedimentary faults. *Journal of Structural Geology*, 25, 633-648.
- Colella, A. (1988a). Fault-controlled marine Gilbert-type fan deltas. *Geology*, 16, 1031-1034.
- Colella, A. (1988b). Pliocene-Holocene fan deltas and braid deltas in the Crati Basin, southern Italy: a consequence of varying tectonic. In: W. Nemeč & R. Steel (Eds.), *Fan Deltas: Sedimentology and Tectonic Settings*. Blackie and Son, Glasgow and London, 50-74.
- Colella, A. (1988c). Gilbert-type fan deltas in the Crati Basin (Pliocene-Holocene, southern Italy). In: A. Colella (Ed.), *Excursion Guidebook*. International Workshop on Fan Deltas, Calabria, Italy, 19-77.
- Colella, A., De Boer, P.L. & Nio, S.D. (1987). Sedimentology of a marine intermontane Pleistocene Gilbert-type fan delta complex in the Crati Basin, Calabria, southern Italy. *Sedimentology*, 34, 721-736.
- Collier, R.E.Ll. & Gawthorpe, R.L. (1995). Neotectonics, drainage and sedimentation in central Greece: insights into coastal reservoir geometries in syn-rift sequences. In: J.J. Lambiase (Ed.), *Hydrocarbon Habitat in Rift Basins*. Geological Society Special Publications, 80, 165-181.

- Collier, R.E.LI., Leeder, M.R., Trout, M., Ferentinos, G., Lyberis, E. & Papatheodorou, G. (2000). High sediment yields and cool, wet winters: Test of last glacial palaeoclimates in the northern Mediterranean. *Geology*, 28, 999-1002.
- Cowie, P.A. & Scholz, C.H. (1992). Physical explanation for displacement-length relationship for faults using a post-yield fracture mechanics model. *J. Struct. Geol.*, 14, 1133-1148.
- Cowie, P.A., Gupta, S. & Dawers, N.H. (2000). Implications of fault array evolution for synrift depocentre development: insights from a numerical fault growth model. *Basin Research*, 12, 241-261.
- Cross, T.A. (1988). Controls on coal distribution in transgressive-regressive cycles, Upper Cretaceous, Western Interior, U.S.A. In: C.K. Wilgus, B.S. Hastings, C.G.St.C. Kendall, H.W. Posamentier, C.A. Ross & J.C. Van Wagoner (Eds.), *Sea Level Changes: An Integrated Approach*. Soc. Econ. Palaeontol. Mineral., Special Publication, 42, 371-380.
- Dorsey, R.J. & Umhoefer, P.J. (2000). Tectonic and eustatic controls on sequence stratigraphy of the Pliocene Loreto basin, Baja California Sur, Mexico. *GSA Bulletin*, 112, 177-199.
- Dorsey, R.J., Umhoefer, P.J. & Renne, P.R. (1995). Rapid subsidence and stacked Gilbert-type fan deltas, Pliocene Loreto basin, Baja California Sur, Mexico. *Sedimentary Geology*, 98, 181-204.
- Flemings, P.B. & Grotzinger, J.P. (1996). STRATA: Freeware for analysing classic stratigraphic problems. *GSA Today*, 6, 1-7.
- Frazier, D. (1974). Depositional episodes: their relationship to the Quaternary stratigraphic framework in the northwestern portion of the Gulf Basin. *Bureau of Economic Geology, University of Texas, Geological Circular*, 74-1, 26p.
- Galloway, W.L. (1989). Genetic stratigraphic sequences in basin analysis I: architecture and genesis of flooding surface bounded depositional units. *AAPG Bulletin*, 73, 125-142.
- Gawthorpe, R.L., Fraser, A. & Collier, R.E.LI. (1994). Sequence stratigraphy in active extensional basins: implications for the interpretation of ancient basin fills. *Marine and Petroleum Geology*, 11, 642-658.
- Gawthorpe, R.L., Sharp, I., Underhill, J.R. & Gupta, S. (1997). Linked sequence stratigraphic and structural evolution of propagating normal faults. *Geology*, 25, 795-798.
- Gawthorpe, R.L., Hardy, S. & Ritchie, B. (2003). Numerical modelling of depositional sequences in half-graben rift basins. *Sedimentology*, 50, 169-185.
- Granjeon, D. & Joseph P. (1999). Concepts and applications of a 3D multiple lithology, diffusive model in stratigraphic modeling. In: J.W. Harbaugh, W.L. Watney, E.C. Rankey, R. Slingerland, R.H. Goldstein & E.K. Franseen (Eds.), *Numerical Experiments in stratigraphy: Recent Advances in Stratigraphic and Sedimentological Computer Simulations*. SEPM Special Publication, 62, 197-210.
- Gupta, S., Cowie, P.A., Dawers, N.H. & Underhill, J.R. (1998). A mechanism to explain rift-basin subsidence and stratigraphic patterns through fault-array evolution. *Geology*, 26, 595-598.
- Gupta, S., Underhill, J.R., Sharp, I.R. & Gawthorpe, R.L. (1999). Role of fault interactions in controlling synrift sediment dispersal patterns: Miocene, Abu Alaq Group, Suez Rift, Sinai, Egypt. *Basin Research*, 11, 167-189.
- Hack, J.T. (1957). Studies of longitudinal stream profiles in Virginia and Maryland. *US Geological Survey Prof. Pape.*, 294.
- Hardy, S. & Gawthorpe, R.L. (1998). Effects of variations in fault slip rate on sequence stratigraphy in fan deltas: insights from numerical modeling. *Geology*, 26, 911-914.

- Hardy, S. & Gawthorpe, R.L. (2002). Normal fault control on bedrock channel incision and sediment supply: insights from numerical modeling. *Journal of Geophysical Research*, 107, 2246.
- Hardy, S., Dart, C.J. & Waltham, D. (1994). Computer modelling of the influence of tectonics on sequence architecture of coarse-grained fan deltas. *Marine and Petroleum Geology*, 11, 561-574.
- Hodgson, D.M., Kane, I.A., Flint, S.S., Brunt, R.L. & Ortiz-Karpf, A. (2016). Time-transgressive confinement on the slope and the progradation of basin-floor fans: implications for the sequence stratigraphy of deep-water deposits. *Journal of Sedimentary Research*, 86, 73-86.
- Holbrook J.M. & Bhattacharya J.P. (2012). Reappraisal of the sequence boundary in time and space: case and considerations for an SU (subaerial unconformity) that is not a sediment bypass surface, a time barrier, or an unconformity. *Earth Science Reviews*, 113, 271-302.
- Huang, X., Griffiths C.M. & Liu, J. (2015). Recent development in stratigraphic forward modelling and its application in petroleum exploration. *Australian Journal of Earth Sciences*, 62, 903-919.
- Jackson, C.A.-L., Gawthorpe, R.L., Carr, I.D. & Sharp, I.R. (2005). Normal faulting as a control on the stratigraphic development of shallow marine syn-rift sequences: the Nukhul and Lower Rudeis Formations, Hammam Faraun fault block, Suez Rift, Egypt. *Sedimentology*, 52, 313-338.
- Jackson, C.A.-L. & Rotevatn, A. (2013). 3D seismic analysis of the structure and evolution of a salt-influenced normal fault zone: a test of competing fault growth models. *Journal of Structural Geology*, 54, 215-234.
- Jackson, C.A.-L., Bell, R.E., Rotevatn, A. & Tvedt, A.B.M. (2017). Techniques to determine the kinematics of syn-sedimentary normal faults and implications for fault growth models. In: C. Childs, R.E. Holdsworth, C.A.-L. Jackson, T. Manzocchi, J.J. Walsh & G. Yielding (Eds.), *The Geometry and Growth of Normal Faults*. Geological Society, London, Special Publications, 439, 187-217.
- Jervey, M.T. (1988). Quantitative geological modeling of siliciclastic rock sequences and their seismic expression. In: C.K. Wilgus, B.S. Hastings, C.G.St.C. Kendall, H.W. Posamentier, C.A. Ross. & J.C. Van Wagoner (Eds.), *Sea-Level Changes: An Integrated Approach*. SEPM Special Publications, 42, 47-69.
- Leeder, M.R. & Gawthorpe, R.L. (1987). Sedimentary models for extensional tilt-block/half-graben basins. In: M.P. Coward, J.F. Dewey & P.L. Hancock (Eds.) *Continental Extensional Tectonics*. Geological Society, London, Special Publications, 28, 139-152.
- Leeder, M.R., Collier, R.E.Ll., Abdul Aziz, L.H., Trout, M., Ferentinos, G., Papatheodorou, G. & Lyberis, E. (2002). Tectono-sedimentary processes along an active marine/lacustrine half-graben margin: Alkyonides Gulf, E. Gulf of Corinth, Greece. *Basin Research*, 14, 25-41.
- Madof, A.S., Harris, A.D. & Connell, S.D. (2016). Nearshore along-strike variability: is the concept of the systems tracts unhinged? *Geology*, 44, 319-322.
- Martinsen, O.J. & Helland-Hansen, W. (1995). Strike variability of clastic depositional systems: Does it matter for sequence stratigraphic analysis? *Geology*, 23, 439-442.
- Mitchum, R.M., Jr., Vail, P.R. & Thompson, S., III. (1977). Seismic stratigraphy and global changes of sea-level, Part 2: The depositional sequence as a basic unit for stratigraphic analysis. In: C.E. Payton (Ed.), *Seismic Stratigraphy—Applications to Hydrocarbon Exploration*. American Association of Petroleum Geologists Memoir, 26, 53-62.
- Mortimer, E., Gupta, S. & Cowie, P. (2005). Clinof orm nucleation and growth in coarse-grained deltas, Loreto basin, Baja California Sur, Mexico: a response to episodic accelerations in fault displacement. *Basin Research*, 17, 337-359.
- Mullenbach, B.L. & Nittrouer, C.A. (2006). Decadal record of sediment export to the deep sea via Eel Canyon. *Continental Shelf Research*, 26, 2157-2177.

- Muto, T. & Steel, R.J. (2000). The accommodation concept in sequence stratigraphy: some dimensional problems and possible redefinition. *Sedimentary Geology*, 130, 1-10.
- Neal, J. & Abreu, V. (2009). Sequence stratigraphy hierarchy and the accommodation succession method. *Geology*, 37, 779-782.
- Neal, J.E., Abreu, V., Bohacs, K.M., Feldman, H.R. & Pederson, K.H. (2016). Accommodation succession sequence stratigraphy: observational method, utility, and insights into sequence boundary formation. *Journal of the Geological Society, London*, 173, 803-816.
- Nicol, A., Childs, C., Walsh, J.J., Manzocchi, T. & Schöpfer, M.P.J. (2016). Interactions and growth of faults in an outcrop-scale system. In: C. Childs, R.E. Holdsworth, C.A.-L. Jackson, T. Manzocchi, J.J. Walsh & G. Yielding (Eds.), *The Geometry and Growth of Normal Faults*. Geological Society, London, Special Publications, 439, 187-217.
- Posamentier, H.W. & Vail, P.R. (1988). Eustatic controls on clastic deposition II—sequence and systems tracts models. In: C.K. Wilgus, B.S. Hastings, C.G.St.C. Kendall, H.W. Posamentier, C.A. Ross & J.C. Van Wagoner (Eds.), *Sea-Level Changes: An Integrated Approach*. SEPM Special Publications, 42, 125-154.
- Posamentier, H.W., Jervey, M.T. & Vail, P.R. (1988). Eustatic controls on clastic deposition I—conceptual framework. In: C.K. Wilgus, B.S. Hastings, C.G.St.C. Kendall, H.W. Posamentier, C.A. Ross. & J.C. Van Wagoner (Eds.), *Sea-Level Changes: An Integrated Approach*. SEPM Special Publications, 42, 109-124.
- Posamentier, H.W. & Allen, G.P. (1999). *Siliciclastic sequence stratigraphy; sequence stratigraphy: concepts and applications*. SEPM Concepts in Sedimentology and Paleontology, 7, 210pp.
- Posamentier, H.W. & Weimer, P. (1993). Siliciclastic sequence stratigraphy and petroleum geology--where to from here? *AAPG Bulletin*, 77, 731-742.
- Poulimenos, G., Zelilidis, A., Kontopoulos, N. & Doutsos, T. (1993). Geometry of trapezoidal fan deltas and their relationship to extensional faulting along the south-western active margins of the Corinth rift. *Basin Research*, 5, 179-192.
- Ravnås, R. & Steel, R.J. (1998). Architecture of marine rift-basin successions. *AAPG Bulletin*, 82, 110-146.
- Raymo, M.E., Hodell, D. & Jansen, E. (1992). Response of deep ocean circulation to initiation of Northern Hemisphere glaciation (3–2 Ma). *Paleoceanography*, 7, 645-672.
- Ritchie, B.D., Hardy, S. & Gawthorpe, R.L. (1999). Three dimensional numerical modeling of coarse-grained clastic deposition in sedimentary basins. *Journal of Geophysical Research*, 104, 17759-17780.
- Rivænes J.C. (1992). Application of a dual-lithology, depth-dependent diffusion equation in stratigraphic simulation. *Basin Research*, 4, 133-146.
- Romans, B.W., Castellort, S., Covault, J.A., Fildani, A. & Walsh, J.P. (2016). Environmental signal propagation in sedimentary systems. *Earth-Science Reviews*, 153, 7-29.
- Romans, B.W., Normark, W.R., McGann, M.M., Covault, J.A. & Graham, S.A. (2009). Coarse-grained sediment delivery and distribution in the Holocene Santa Monica Basin, California: implications for evaluating source-to-sink flux at millennial time scales. *Geol. Soc. Am. Bull.*, 121, 1394-1408.
- Schlagenhauf, A., Manighetti, I., Malavieille, J. & Dominguez, S. (2008). Incremental growth of normal faults: Insights from a laser-equipped analog experiment. *Earth and Planetary Science Letters*, 273, 299-311.
- Sloss, L.L. (1962). Stratigraphic models in exploration. *Journal of Sedimentary Research*, 32, 415-422.
- Sloss, L.L. (1991). The tectonic factor in sea-level change: a countervailing view. *Journal of Sedimentary Research*, 96, 6609-6617.

- Stein, R.S. & Barrientos, S.E. (1985). Planar High-Angle Faulting in the Basin and Range' Geodetic Analysis of the 1983 Borah Peak, Idaho, Earthquake. *Journal of Geophysical Research*, 90, 11355-11366.
- Stevenson, C.J., Jackson, C.A.L., Hodgson, D.M., Hubbard, S.M. & Eggenhuisen, J.T. (2015). Deep-water sediment bypass. *Journal of Sedimentary Research*, **85**, 1058-1081.
- Umhoefer, P.J., Dorsey, R.J. & Renne, P. (1994). Tectonics of the Pliocene Loreto basin, Baja California Sur, Mexico, and evolution of the Gulf of California. *Geology*, 22, 649-652.
- Vail, P.R., Mitchum, R.M., Jr. & Thompson, S., III. (1977). Seismic stratigraphy and global changes of sea level, part 3: relative changes of sea level from coastal onlap. In: C.E. Payton (Ed.), *Seismic Stratigraphy-Applications to Hydrocarbon Exploration*. AAPG, Memoirs, 26, 63-81.
- Van Wagoner, J.C., Posamentier, H.W., Mitchum, R.M., Vail, P.R., Sarg, J.F., Loutit, T.S. & Hardenbol, J. (1988). An overview of the fundamentals of sequence stratigraphy and key definitions. In: C.K. Wilgus, B.S. Hastings, C.G.St.C. Kendall, H.W. Posamentier, C.A. Ross. & J.C. Van Wagoner (Eds.), *Sea-Level Changes: An Integrated Approach*. SEPM Special Publications, 42, 39-45.
- Walsh, J.J., Nicol, A. & Childs, C. (2002). An alternative model for the growth of faults. *Journal of Structural Geology*, 24, 1669-1675.
- Walsh, J.J., Bailey, W.R., Childs, C., Nicol, A. & Bonson, C.G. (2003). Formation of segmented normal faults: a 3-D perspective. *Journal of Structural Geology*, 25, 1251-1262.
- Warrick, J.A. (2014). Eel River margin source-to-sink sediment budgets: revisited. *Marine Geology*, 351, 25-37.
- Wheeler, H.E. & Murray, H.H. (1957). Base level control patterns in cyclothem sedimentation. *AAPG Bulletin*, 41, 1985-2011.
- Wheeler, H.E. (1958). Time stratigraphy. *AAPG Bulletin*, 42, 1047-1063.
- Wheeler, H.E. (1959). Unconformity bounded units in stratigraphy. *AAPG Bulletin*, 43, 1975-1977.
- Wheeler, H.E. (1964). Base level, lithosphere surface, and time stratigraphy. *Geological Society of America Bulletin*, 75, 599-610.
- Young, M.J., Gawthorpe, R.L. & Sharp, I.R. (2002). Architecture and evolution of the syn-rift clastic depositional systems towards the tip of major fault segment, Suez Rift, Egypt. *Basin Research*, 14, 1-23.

Chapter 4

Quantifying faulting and base level controls on syn-rift sedimentation using stratigraphic architectures of coeval, adjacent Early-Middle Pleistocene fan deltas in Lake Corinth, Greece

Publication

Barrett, B.J., Collier, R.E.L., Hodgson, D.M., Gawthorpe, R.L., Dorrell, R.M. & Cullen, T.M. (2019). Quantifying faulting and base level controls on syn-rift sedimentation using stratigraphic architectures of coeval, adjacent Early-Middle Pleistocene fan deltas in Lake Corinth, Greece. *Basin Research*, doi: 10.1111/bre.12356.

Abstract

Quantification of allogenic controls in rift basin-fills requires analysis of multiple depositional systems because of marked along-strike changes in depositional architecture. Here, we compare two coeval Early-Middle Pleistocene syn-rift fan deltas that sit 6 km apart in the hangingwall of the Pirgaki-Mamoussia Fault, along the southern margin of the Gulf of Corinth, Greece. The Selinous fan delta is located near the fault tip, and the Kerinitis fan delta towards the fault centre. Selinous and Kerinitis have comparable overall aggradational stacking patterns. Selinous comprises fifteen cyclic stratal units (~25 m thick), whereas at Kerinitis eleven (~60 m thick) are present. Eight facies associations are identified. Fluvial and shallow water, conglomeratic facies dominate the major stratal units in the topset region, with shelfal fine-grained facies constituting ~2 m thick intervals between major topset units, and thick conglomeratic foresets building down-dip. It is possible to quantify delta build times (Selinous: 615 kyrs; Kerinitis: >450 kyrs), and average subsidence and equivalent sedimentation rates (Selinous: 0.65 m/kyrs; Kerinitis: >1.77 m/kyrs). The presence of sequence boundaries at Selinous, but their absence at Kerinitis, enables sensitivity analysis of the most uncertain variables using a numerical model, 'Syn-Strat', supported by an independent unit thickness extrapolation method. Our study has three broad outcomes: 1) the first estimate of lake level change amplitude in Lake Corinth for the Early-Middle Pleistocene (10-15 m), which can aid regional palaeoclimate studies and inform broader climate-system models; 2) demonstration of two complementary methods to quantify faulting and base level signals in the stratigraphic record – forward modelling with Syn-Strat and a unit thickness extrapolation - which can be applied to other rift basin-fills; and 3) a quantitative approach to the analysis of stacking patterns and key surfaces that could be applied to stratigraphic pinch-out assessment and cross-hole correlations in reservoir analysis.

4.1. Introduction

Distinguishing faulting, sediment supply and base level signals and quantifying these basin controls in an active rift setting remains problematic, particularly due to along-strike variability in depositional architecture. Characterisation of multiple coeval depositional systems within the same rift basin is required to resolve the record of each control. Syn-rift, Gilbert-type fan deltas (Gilbert, 1885; 1890) provide an ideal record of stratigraphic evolution to achieve this due to their position adjacent to normal growth faults, with high and variable sediment supply rates derived from independent drainage catchments. However, most previous studies focus on single systems, rather than multiple, along-strike spatially distributed deltas (e.g. Garcia-Mondéjar, 1990; Dart et al., 1994; Dorsey et al., 1995; Mortimer et al., 2005; Garcia-Garcia et al., 2006; Ford et al., 2007; Backert et al., 2010).

Previous work on the stratigraphic record around normal faults at rifted margins has focussed on the theoretical aspects of sequence development from the interplay of controls in these areas. Leeder & Gawthorpe (1987) assessed the influence of tectonically-induced slopes on facies models. Variation in stacking patterns and sequence stratigraphic surfaces across rift settings (Gawthorpe et al., 1994), and as a result of propagating normal faults (Gawthorpe et al., 1997) became the later focus. An influential series of conceptual models for tectono-sedimentary evolution in extensional basins was presented by Gawthorpe & Leeder (2000). Eustasy/base level, tectonics and sedimentation influence the nature of sedimentary stacking through the accommodation/sediment supply ratio (Jervey, 1988; Neal & Abreu, 2009) as eustasy and tectonic subsidence act to control space available for deposition (A) and sedimentation fills that space (S). Numerical modelling has supported understanding of rift basin sequence stratigraphy, particularly as simplified tectonic constraints were introduced into forward models (Jervey et al., 1988; Hardy et al., 1994; Hardy & Gawthorpe, 1998; 2002; Ritchie et al., 1999) and stratigraphic surfaces were shown to be limited in spatial extent (Gawthorpe et al., 2003; Jackson et al., 2005). Barrett et al. (2018) demonstrate and quantify the three-dimensional and along-strike variability in sequence architecture, and diachroneity of stratigraphic surfaces in hangingwall fault blocks, using

sensitivity tests with a 3D sequence stratigraphic forward model, ‘Syn-Strat’. Complementary field studies have shown that sequence boundary development is best expressed at fault tip regions (Dorsey & Umhoefer, 2000 – Loreto Basin), and observed stratigraphic cyclicity has been attributed to fault-related subsidence events (Dorsey et al., 1995 – Loreto Basin) and climatic forcing (Dart et al., 1994; Backert et al., 2010 – Gulf of Corinth). Marked differences occur in the sequence stratigraphy of two coeval fan deltas 50 km apart, due to contrasting tectonic controls between footwall (Kryoneri) and hangingwall (Kerinitis) sites (Gawthorpe et al., 2017a). However, along-strike and down-dip variation on smaller length-scales (<10 km) within the same hangingwall basin has not yet been attempted. Furthermore, quantification of tectonism, base level and sedimentation signals is also lacking. This is because isolating these controls is difficult, yet is critical to improving our understanding of palaeoenvironmental evolution and for making predictions beyond data limits.

Here, we present an integrated field and numerical modelling investigation of two adjacent and contemporaneous syn-rift fan deltas, six km along-strike from one another in the hangingwall of the same normal fault; the Pyrgaki-Mamoussia Fault. The fan deltas are referred to as the Selinous near the fault tip, and the Kerinitis near the fault centre (Fig. 4.1). This is the first detailed sedimentological and stratigraphic study of the Selinous fan delta, and with comparison to the Kerinitis fan delta, allows a unique insight into the controlling parameters during rift basin evolution. The aim of the study is to resolve and quantify the contribution of tectonics and base level change to sequence architecture in Lake Corinth through the Early-Middle Pleistocene. In doing so, methodologies that are applicable to any basin with given data constraints are demonstrated. To satisfy the aim, the objectives are: 1) to derive quantified estimates of the controlling parameters based on comparisons of facies, stacking patterns and the nature of key stratigraphic surfaces between the deltas, 2) to reduce uncertainty of the quantified allogenic control estimates by use of sensitivity tests with the 3D sequence stratigraphic forward model ‘Syn-Strat’ (Barrett et al., 2018) and to elucidate the amplitude of lake level change for Early-Middle Pleistocene Lake Corinth, 3) to validate derivations using an independent unit thickness extrapolation method; and 4) to make quantitative predictions of unit thickness along-strike

variation and diachroneity of key stratigraphic surfaces. This work can be applied to other basin-fills by demonstrating two complementary methodologies for discerning and quantifying faulting and base level signals in the stratigraphic record. We undertake a quantitative analysis of unit thicknesses and surfaces that could be used in stratigraphic pinchout assessment and cross-hole correlations in syn-rift reservoirs. Finally, the palaeoclimatic data on lake level changes derived from the geological record can be used to inform climate-system models for the Pleistocene.

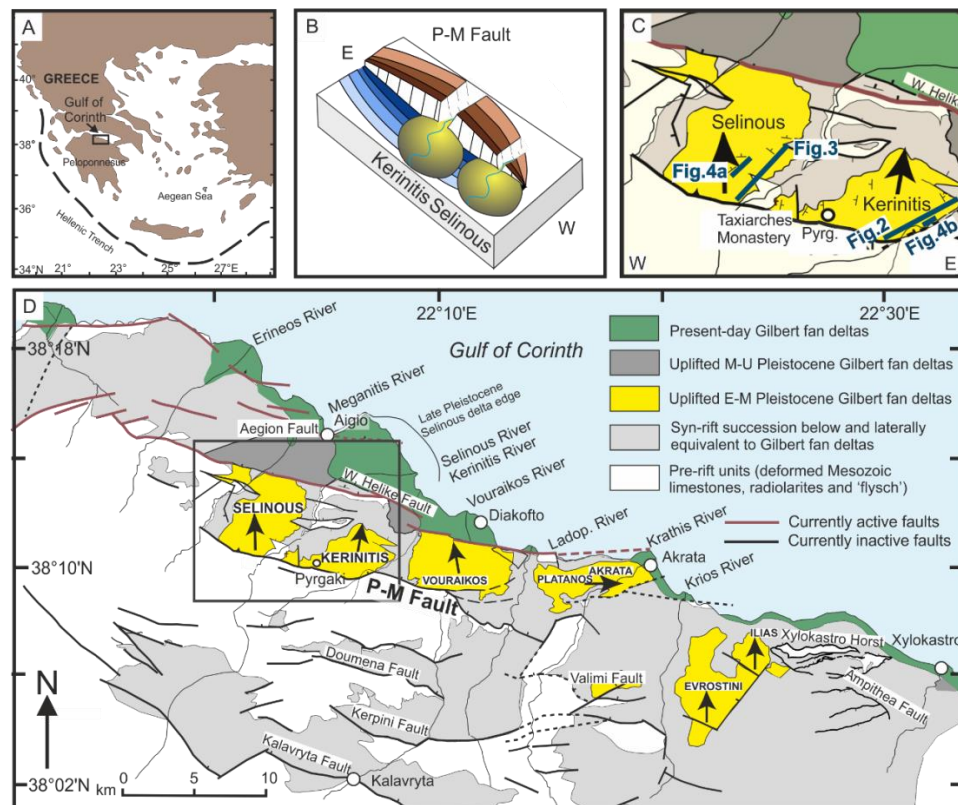


Figure 4.1. Map of the study area on the southern side of the Gulf of Corinth, Greece. A) Map of Greece. B) Schematic diagram of the Selinous and Kerinitis syn-rift fan deltas. C) The highlighted position of the two fan deltas along the P-M Fault with the locations of Figures (4.)2, 3 and 4. Early-Middle Pleistocene fan deltas that are of interest are shaded in yellow and differentiated from present-day fan deltas (green), Middle-Upper Pleistocene fan deltas (grey pattern), other contemporaneous syn-rift stratigraphy (grey) and pre-rift strata (white). The main fan delta progradation directions are indicated by black arrows. Small ticks on faults indicate throw and dip-direction. Currently active faults are in purple and inactive faults are in black. Map is modified from Ford et al. (2007; 2013; 2016) after Ghisetti & Vezzani (2004). Active faults and mapping of eastern area around the Xylokastro Horst and Ampithea Fault from Gawthorpe et al. (2017b).

4.2. Tectono-stratigraphic framework

The Gulf of Corinth marks the axis of the ~100 km long, 60-80 km wide Corinth Rift that was activated during the Late Miocene/Early Pliocene (~5 Ma; Collier & Dart, 1991; Leeder et al., 2008; Ford et al., 2016; Gawthorpe et al., 2017b). Present-day N-S geodetic extension rates are up to 15 mm/yr (Clarke et al., 1997; Briole et al., 2000; Avallone et al., 2004; Floyd et al., 2010), which are accommodated on N- and S-dipping normal faults (McNeill et al., 2005; Bernard et al., 2006; Bell et al., 2008). The oldest part of the rift (Rift 1, ~5-3.6 to 2.2-1.8 Ma; Ford et al., 2013; 2016; Nixon et al., 2016; Gawthorpe et al., 2017b) lies furthest south in northern Peloponnesos, where faulting was focussed at that time on the Kalavryta, Doumena, Valimi Faults (Fig. 4.1) and other southern border faults. At this time the Kalavryta alluvial system fed sediment northwards, and fluvial and marginal lacustrine environments prevailed (Lower Group; Ford et al., 2016). In the eastern part of the rift (Fig. 4.1), the Kyllini, Mavro, Kefalari and Nemea fan deltas built out into the basin (as described by Gawthorpe et al., 2017b). There was an upward deepening through the 'Rift 1' sequence at ~3.6 Ma (Gawthorpe et al., 2017b) from deposition of the fluvial-marginal Korfiotissa and Ano Pitsa Formations, to the deep lacustrine Pellini and Rethi-Dendro Formations, referred to as the 'Great Deepening' (Leeder et al., 2012).

Northward migration of faulting (Goldsworthy & Jackson, 2001; Ford et al., 2013; 2016; Nixon et al., 2016) onto the Pyrgaki-Mamoussia (P-M) Fault in the west and faults to the east occurred at ~1.8 Ma (Ford et al., 2016; Gawthorpe et al., 2017b). In the immediate hangingwall of the faults, thick syn-rift fan deltas built northwards. Four syn-rift fan deltas that sit along-strike from one another in the hangingwall of the P-M Fault developed in the west: the Selinous, Kerinitis, Vouraikos and Platanos fan deltas (from W-to-E, Fig. 4.1). The early development of syn-rift fan deltas along the whole length of the P-M Fault suggests that it grew rapidly in length. The contemporaneous P-M Fault hangingwall fan deltas sit within the Middle Group (Ford et al., 2007; Rohais et al., 2007; Backert et al., 2010). Pollen analysis at Vouraikos was used to date the Middle Group, which constrained the development of the P-M fan deltas to the Early-Middle Pleistocene (~1.8-0.7 Ma) but within a period of 500-800 kyr (Ford et al., 2007). Subsequent

northward fault migration onto the Helike fault system at ~800 ka (Ford et al., 2016) resulted in the uplift of western Plio-Pleistocene syn-rift stratigraphy in the footwall of the modern, parallel West Helike Fault, exposing a ~6 km wide fault block terrace. During uplift, the fan deltas were subject to erosion from their own feeder rivers that now supply the modern fan delta systems on the coast. Predominant lacustrine conditions with discrete periods of marine incursion lasted until ~600 ka, before marine conditions prevailed due to opening at the western end of the gulf to the Ionian Sea (Rion Straits) and/or at the eastern end to the Aegean Sea (Corinth Isthmus) (Collier & Thompson, 1991; Ford et al., 2016; Nixon et al., 2016; Gawthorpe et al., 2017b).

Here, we focus on the system in the hangingwall of the P-M Fault (Fig. 4.1), which dips 50-55° towards the north, and has a maximum throw of >1200 m. The P-M Fault strikes WNW-ESE and is traced ~24 km from SW of Aigio to SW of Akrata. The fault juxtaposes pre-rift Mesozoic limestones in the footwall against Plio-Pleistocene hangingwall syn-rift fan delta deposits. We study two syn-rift fan deltas, the Selinous that sits towards the western fault tip, and the adjacent Kerinitis that sits nearer the fault centre. The fan deltas were influenced by: a) high slip rates on the P-M Fault as a result of rapid extension across the rift; and b) cyclic lake level and sedimentation changes from climatic variations.

4.3. The Gilbert-type fan deltas

4.3.1. The Kerinitis fan delta

The Kerinitis Gilbert-type fan delta is presented in Figure 4.2 in the form of a 3D outcrop model. Kerinitis, studied since the 1990s (Ori et al., 1991; Dart et al., 1994; Gawthorpe et al., 1994; Backert et al., 2010), is exposed on the western side of the modern Kerinitis river valley (~200 m above sea level) along a 3.8 km SW-NE dip section from the P-M Fault towards the West Helike Fault. Topsets are back-tilted by ~18° and thicken towards the P-M Fault (Fig. 4.2). The exposed section cuts the fan delta's eastern side, where foresets dip ~25° towards N040°. The fan delta extends laterally ~6 km along the P-M Fault, west of the Kerinitis River where it interfingers with

the Selinous fan delta between the village of Pyrgaki and the Taxiarches Monastery (Fig. 4.1). In total, Kerinitis covers an area of 15 km² and is ~800 m thick; the base of the fan delta is not exposed in the Kerinitis valley, but is exposed in the footwall of the West Helike Fault. The point source of the Kerinitis fan delta incised the P-M footwall at a topographic low on an early relay zone (Backert et al., 2010), shown as a hard link on the fault (Fig. 4.1). Its position was locked into the landscape as fault linkage occurred. We interpret the lack of deformation penetrating the Kerinitis delta from the western end of the Mamoussia Fault to indicate early fault linkage with the Pyrgaki Fault with respect to the exposed fan delta strata.

Backert et al. (2010) undertook the most recent and comprehensive study of the Kerinitis fan delta, whereby they characterised its architecture and facies, presented a trajectory analysis, and interpreted three stages of fan delta growth linked to initiation, growth and death of the controlling P-M Fault. The fan delta is divided into three zones from south to north, comprising fan delta topsets, a transition zone, and fan delta foresets, respectively (Fig. 4.2). They identify four facies associations (topset, foreset, bottomset and prodelta) and 11 key surfaces. Trajectory analysis reveals abrupt landward shifts in the topset-foreset breakpoint at each key surface, followed by gradual basinward progradation through each stratal unit. The cyclic stratal units within the fan delta are interpreted to record eustatic variations upon a background subsidence-dominated regime, in which high rates of fault subsidence overcame base level falls, in agreement with earlier studies (Dart et al., 1994; Gawthorpe et al., 1994).

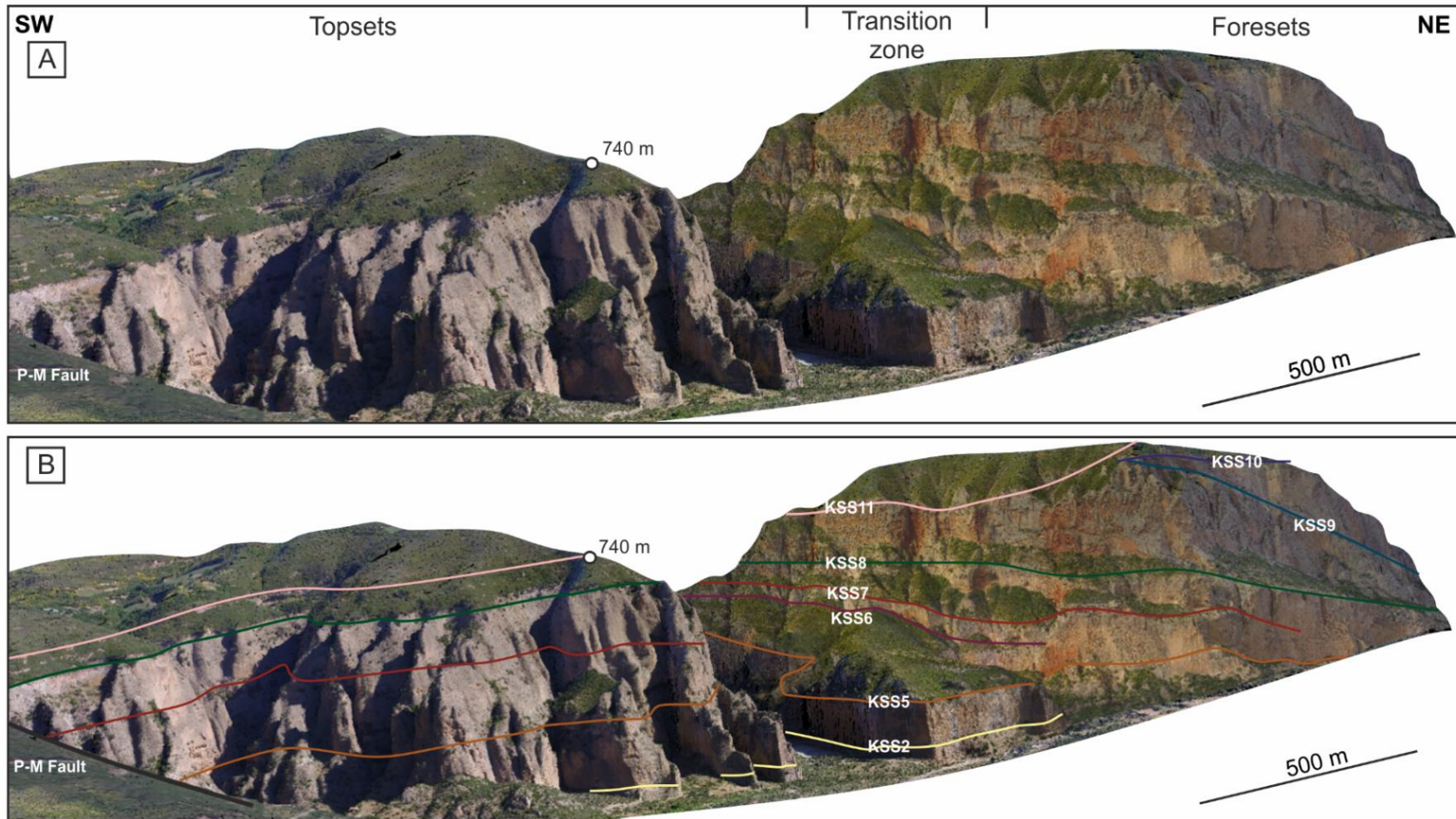


Figure 4.2. The stratigraphic architecture of Kerinitis. A) UAV photogrammetry-based 3D outcrop model. B) Key stratigraphic surfaces interpretation by Backert et al. (2010) overlain onto 3D outcrop model. Note overall aggradational stacking trend between units and on the scale of the whole delta, with topsets generally overlying topsets and foresets generally overlying foresets.

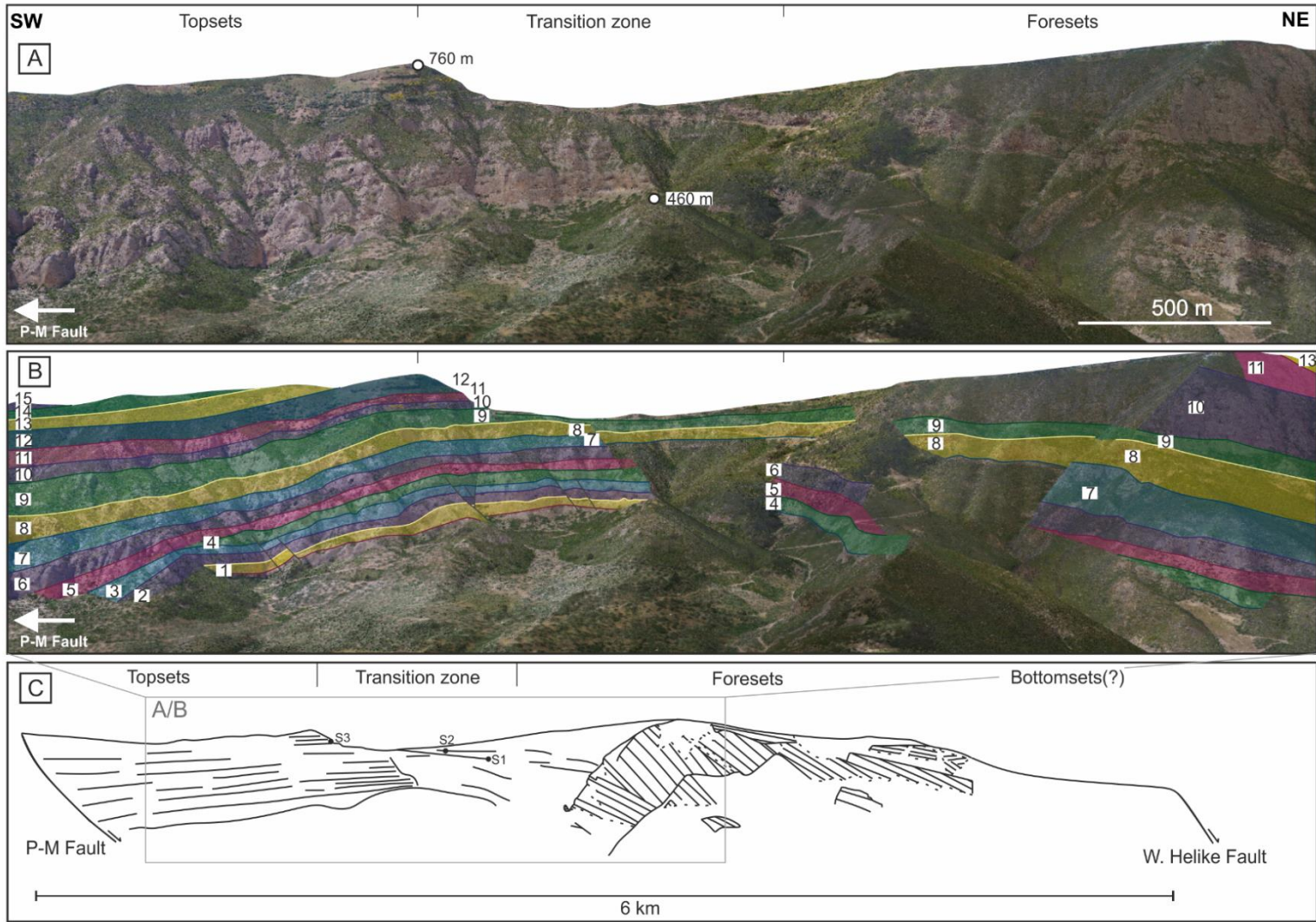


Figure 4.3. The stratigraphic architecture of Selinous. A) UAV photogrammetry-based 3D outcrop model. B) Interpretation of major stratigraphic units and surfaces overlain onto 3D outcrop model – colours are arbitrarily assigned to highlight the individual units. C) Cross-sectional sketch of the Selinous fan delta with grey box to indicate area of outcrop model images in A and B. Note the aggradational stacking trend on the scale of the whole fan delta, with topsets generally overlying topsets and foresets generally overlying foresets.

4.3.2. The Selinous fan delta

The Selinous Gilbert-type fan delta is presented in Figure 4.3 using a 3D outcrop model and schematic dip section. It is referred to as Selinous in Ford et al. (2007; 2013) and Backert et al. (2010), and as Palaeo-Meganitis in Ford et al. (2016). The Selinous fan delta has a width of ~6 km and its centre sits ~4 km from the western tip of the P-M Fault. It is exposed on the western side of the modern Selinous river valley (~150 m above sea level in the valley floor) along a 6 km long SSW-NNE dip section from the P-M Fault towards the West Helike Fault. Topsets thicken and are back-tilted by ~12° towards the P-M Fault (Fig. 4.3). The main section is along the west side of the Selinous river valley, where foresets dip ~21° towards N310°. On the eastern side of the valley, foresets dip ~23° towards 097° (Fig. 4.1). The fan delta's eastern limit interfingers with foresets of Kerinitis. The base of the fan delta is exposed in the valley in the footwall of a secondary normal fault that trends parallel to the P-M Fault. The maximum thickness of Selinous is ~400 m. The point source of the Selinous fan delta incises the P-M Fault and continues to feed the Late Pleistocene and modern fan deltas. As with Kerinitis, the Selinous fan delta can also be divided into three broad zones from south to north, with the most southerly ~2 km zone comprising delta topsets, a ~1 km transition zone in the central part and a ~3 km zone of foresets and bottomsets to the north (Fig. 4.3).

4.4. Methodology

In this study we integrate field data with numerical techniques through the five stages of analysis listed below.

- 1) Facies and stratigraphic architecture are analysed in the field and augmented with Unmanned Aerial Vehicle (UAV) photogrammetry-based 3D outcrop models.
- 2) Field observations and trajectory analysis of the middle-upper units of the two fan deltas are used to resolve and quantify each allogenic control acting on the delta evolution.
- 3) Each control parameter (e.g. subsidence rate, sedimentation rate etc.) is assigned a qualitative uncertainty value from 1-5, whereby 1 represents a very low uncertainty estimate and 5 represents a very high uncertainty estimate. This is undertaken in order to ascertain which variable is most uncertain and in need of refinement with numerical model testing.
- 4) The interpreted control parameters are input into 3D sequence stratigraphic forward model, Syn-Strat (Barrett et al., 2018), to test the least certain parameter(s).
- 5) Finally, an independent unit thickness extrapolation technique is adopted to validate the outputs of the numerical modelling.

4.4.1. Facies analysis

The facies analysis of major stratal units and key stratigraphic surfaces was undertaken by sedimentary logging at cm-scale, documenting lithology, grain size, sedimentary structures and the nature of contacts. For characterising the thicker conglomeratic units, sections were logged at a dm-scale with support of sketches to capture the geometry of larger-scale features. Palaeocurrent data were collected from ripple cross laminations, clast imbrication, and cross-bed and foreset plane measurements. Facies associations for both fan deltas are constructed from combinations of identified facies, which are presented in correspondence with those of Backert et al. (2010) for Kerinitis in Table A in the Appendix. Correlation of key stratigraphic surfaces was carried out by walking out beds and surfaces, by annotations of photopanel in the field, and by using UAV photogrammetry-based 3D outcrop models in Agisoft Photoscan software.

4.4.2. Trajectory analysis

Trajectory analysis of the topset-foreset breakpoint (TFBP) was undertaken at both fan deltas for the accessible middle units: 4-8 at Kerinitis and 7-11 at Selinous. The position of the TFBP is identified from the transition from flat-lying topsets to steeply-dipping foresets. In inaccessible

locations, 3D outcrop models are used to identify the TFBP and assess the spatial continuity of stratal surfaces across which the breakpoint moves. If the TFBP is not observed directly, it is inferred from environmental transitions between down-dip outcrops at the same stratigraphic level. It should be noted that the units at Kerinitis are not correlatable to those analysed at Selinous.

4.4.3. Numerical modelling with Syn-Strat

In order to refine the quantification of controlling parameters in the basin, we use a 3D sequence stratigraphic forward model, Syn-Strat (Barrett et al., 2018). Syn-Strat produces a 3D graphical surface representing accommodation in the hangingwall of a normal fault, resulting from spatially- and temporally-variable, tectonic subsidence, sedimentation and base level inputs. Syn-Strat constructs this surface by combining one-dimensional graphical curves that represent each control in time and space. Each parameter is defined along the fault, away from the fault and in time. In this study, we plot accommodation along the fault (x) and in time (y), for a given distance away from the fault. Stacking patterns or systems tracts are then applied to the surface with colours. In this study, we subdivide the relative base level curve with a falling limb and shorter periods of lowstand, transgression and highstand on the rising limb. This resembles the sequence stratigraphic scheme used by Frazier (1974) and Galloway (1989), and termed ‘genetic sequence’ by Catuneanu et al. (2009).

Previously, the model was used to demonstrate the sensitivity of sequence architecture to multiple hypothetical control scenarios, including different relative control magnitudes, subsidence rate regimes and sedimentation distribution models. Key outcomes were the quantitative constraint of along-strike variation in stacking pattern, and of the nature of diachroneity of sequence boundaries and maximum flooding surfaces (Barrett et al., 2018). Here, we input real control parameters derived from field observations and trajectory analyses. We refine the least certain control parameter (amplitude of base level change) with a number of discrete tests, whilst keeping all other control parameters constant, by comparing the modelled output with field observations. The test set-up and results are presented in section 4.7.1.

4.5. Results

4.5.1. Sedimentary facies analysis

The central parts of the fan deltas are the focus of sedimentological descriptions and interpretations, where the topset-foreset transition records base level change and the relative influence of accommodation and sediment supply. At Selinous, three down-dip locations over ~800 m distance, covering the middle-to-upper units of the fan delta were studied: S1 - Units 7 and 8, S2 - Units 8 and 9, and S3 - Units 10 and 11. At Kerinitis, our study also focuses on three down-dip locations over ~700 m, covering the lower-middle units of the delta: K1a, b, c - Units 4 and 7, K2 - Units 5 and 6, and K3 - Units 2 and 3. These are presented on the 3D outcrop models in Figure 4.4, but are not constrained as time-equivalent units.

Sedimentary facies characteristics are similar between the Selinous and Kerinitis fan deltas. Eighteen sedimentary facies have been identified: six conglomeratic facies (abbreviated as 'Co'), six sandy facies (abbreviated as 'Sa') and six finer facies comprising mudstones and siltstones (abbreviated as 'Fi'). Detailed facies descriptions are provided in Table A in the Appendix and further facies information on the Kerinitis fan delta can be found in Backert et al. (2010). The facies have been organised into four facies associations (FA) (Figs. 4.5 and 4.6, and Table 4.1) that are differentiated based on geometric position (denoted by number) and eight sub-associations that are differentiated based on depositional environment (denoted by letter). The fluvial and shallow water topset FAs (1a-b and 2a-b) and the foreset FA (3) construct the main stratal units of the deltas. The bottomset FAs (4a-c) form the thinner, finer-grained intervals between the units.

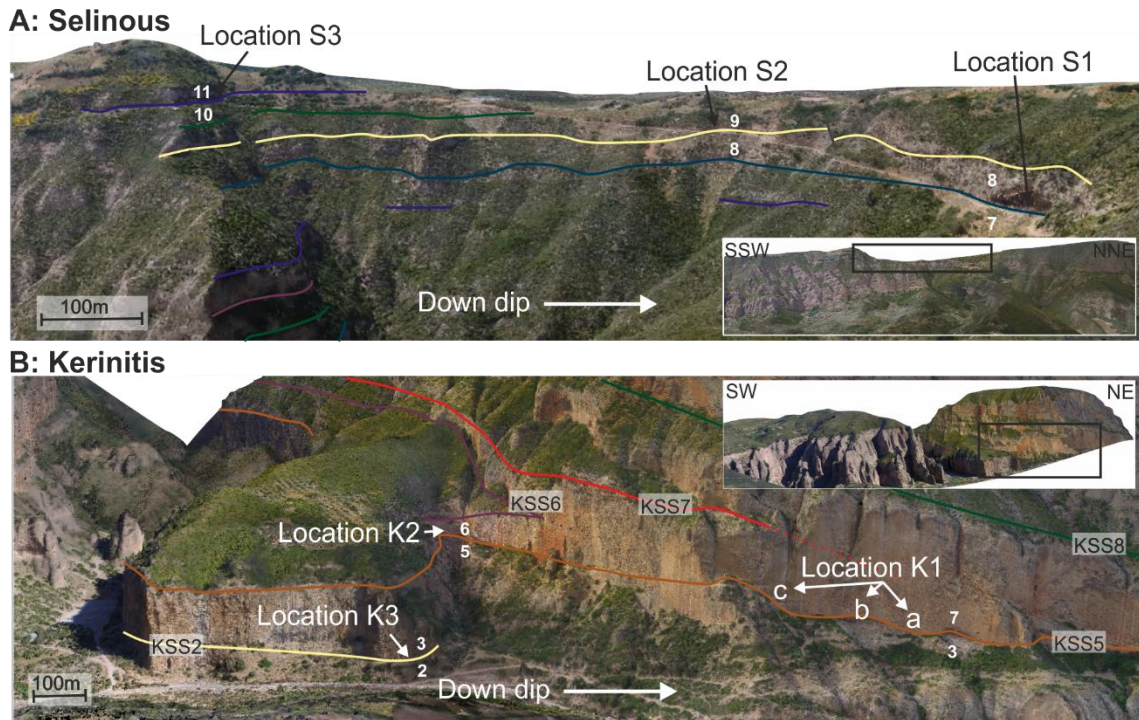


Figure 4.4. Locations of detailed sedimentological studies at fan delta topset-foreset transitions: A) at Selinous and B) at Kerinitis. Unit interpretations are overlain onto the 3D outcrop models. Unit numbers are shown in white. Key stratigraphic surfaces (KSS) are differentiated by colour arbitrarily and at Kerinitis, assigned according to the interpretation by Backert et al. (2010). Middle-upper units, Units 7-11 are the focus at Selinous and lower-middle units, Units 2-7 are the focus at Kerinitis. Insets show position (black box) in the context of each fan delta on wider 3D outcrop models. Locations of sections are shown in Figure 4.1.

Table 4.1. Summary of facies associations with geometric position and depositional environment interpretations.

FA code	Constituent facies	FA interpretation	Sub-association
1a	Co1, Co2	Fluvial topset	Channel fill
1b	Co1, Sa2, Sa6, Fi3		Delta plain
2a	Co4, Co5	Shallow	Beach barrier
2b	Co5	marine topset	Lower shoreface
3	Co3, Co4, Sa4	Foreset	
4a	Sa1, Sa3, Fi1, Fi2, Fi4	Bottomset	Distal
4b	Sa1, Sa2, Sa4, Sa5, Fi1-3, Fi5, Fi6		Intermediate
4c	Co6, Sa1-6, Fi1, Fi2		Proximal

4.5.1.1. FA1 - Fluvial topsets

We identify two fluvial topset FAs with 1a) channel-fill and 1b) delta plain interpretations (Fig. 4.5). The channel-fill FA constructs the largest proportion of the fan delta topset deposits (~95%). FA 1a is characterised in Unit 7 at Location S1 (Selinous) and in Unit 3 at Location K3 (Kerinitis) as a poorly-sorted, sandy gravel-cobble conglomerate with crude laminations and clast imbrication. The clasts are sub-angular to sub-rounded and the bed bases are highly erosional (facies Co1 and Co2 in Table A, Appendix). We interpret this deposit to be the product of bedload transport in a high-energy fluvial flow regime.

The fan delta plain FA (1b) is characterised in Unit 8 at Location S2 (Selinous) (Figs. 4.4 and 4.5) and at the top of Unit 2 at Location K3 (Kerinitis) as a poorly-sorted, sandy gravel-cobble conglomerate (facies Co1, Sa2, Sa6 and Fi3 in Table A, Appendix). The cobbles are <10 cm diameter and sub-angular, implying limited transport time from source to deposition. The gravelly coarse sand beds present normal grading and contain cm-thick, red palaeosols, indicating subaerial exposure.

4.5.1.2. FA2 - Shallow water topsets

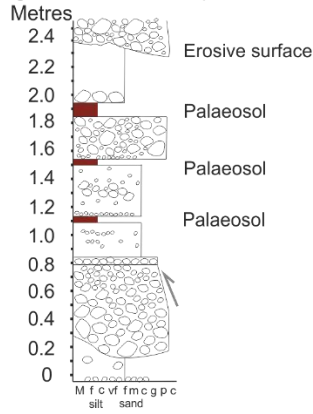
Two shallow-water topset FAs have been identified: 2a) beach barrier and 2b) lower shoreface (Fig. 4.5). The beach barrier FA (2a) is characterised at Location S3 (Selinous) by bi-directional metre-scale cross-beds with well-sorted, open-framework, rounded and discoidal pebbles (facies Co4 and Co5 in Table A, Appendix). This indicates textural maturity and character typical of beach reworking (Fig. 4.5). FA 2a is present at the top of Unit 10 at Selinous Location S3 and is overlain by a finer-grained interval and subsequently by the 10 m-scale foresets of Unit 11 (Fig. 4.4). We have not observed FA 2a at Kerinitis, but Backert et al. (2010) report a foreshore FA at the top of Unit 7. The lower shoreface FA is present in the lower part of Unit 8 at Location S2 (Selinous) and comprises m-scale bi-directional, asymptotic cross-beds resembling hummocky-cross stratification (facies Co5 in Table A, Appendix), typical of storm reworking below fair weather wave base.

4.5.1.3. FA3 - Foresets

The foreset FA represents most of the down-dip parts of the exposed fan delta successions (Figs. 4.1, 4.2 and 4.5). At Selinous, the foreset FA is apparent in Unit 8 at Location S1, Unit 9 at Location S2, and Unit 11 at Location S3 (Fig. 4.4). At the Kerinitis study locations, the foreset FA is apparent in Unit 7 at Location K1a, b and c and Unit 6 at K2. The foreset FA is represented by steep, basinward-dipping (between 22° and 25°), 10-350 m high cross-beds. The cross-beds comprise well-sorted, clast-supported (and sometimes open-framework), sub-rounded cobble conglomerate with some inverse grading and many scours (facies Co3, Co4 and Sa4 in Table A, Appendix). In some places, the conglomeratic foreset units are separated by preserved, gently-dipping finer-grained intervals (e.g. Fig. 4.5), but in most cases these are eroded. The foreset facies association was emplaced in a high energy environment occupied by avalanching sediment gravity flows, characteristic of the upper foreset slope. The height of the foresets indicates the palaeo-water depth and ranges from a few metres when the foresets built over a previous delta topset (e.g. S1-3; Fig. 4.4), to a few hundred metres, when they built beyond the previous fan delta TFBP and into the deep water basin (e.g. Figs. 4.5 and 4.7).

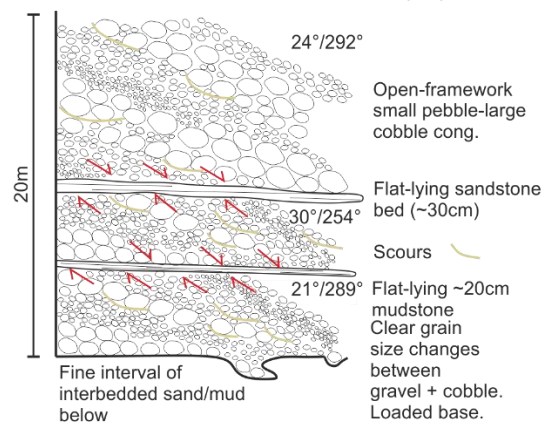
A Facies Association: 1 - Fluvial topsets

Log of FA 1b - Delta plain fluvial topset - Unit 9 (S2)



C Facies Association: 3 - Foresets

Sketch of FA 3 - Foresets - Unit 11 (S3)



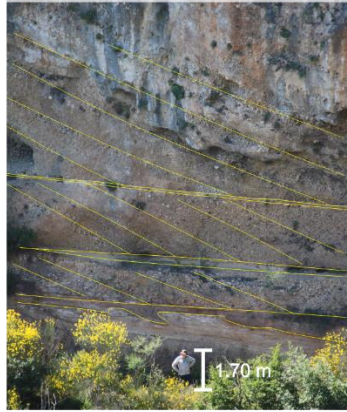
FA 1b - Delta plain - Unit 9 (S2)



FA 1a - Fluvial channel fill - Unit 2 (K3)



FA 3 - Foresets - Unit 11 (S3)



FA 3 - Foresets - Unit 11 (S3)

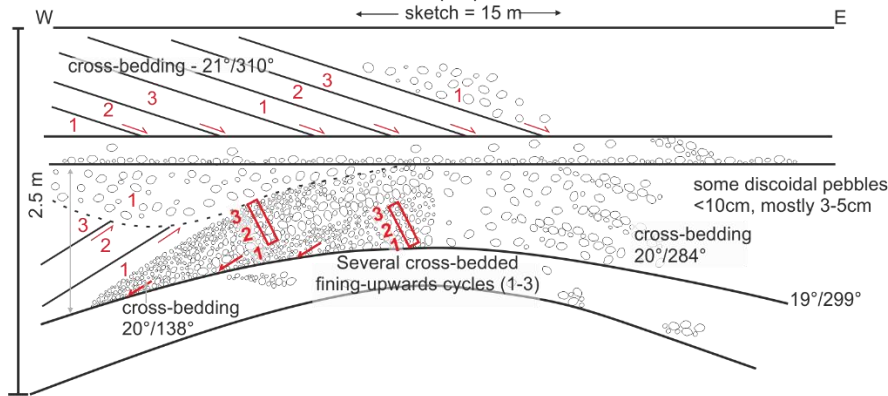


FA 3 - Foresets - Unit 7 (K1)



B Facies Association: 2 - Shallow water topsets

Sketch of FA 2a - Beach barrier - Unit 10 (S3)



FA 2a - Beach barrier - Unit 10 (S3)



FA 2b - Lower shoreface - Units 8 (S2)



Figure 4.5. Sedimentological details of Facies Associations 1-3 – fluvial topsets, shallow water topsets and foresets. A) FA 1: log and field photograph of FA 1b (delta plain fluvial topset) highlighting presence of palaeosol horizons, and field photograph of FA 1a (fluvial channel fill). B) FA 2: sketch and field photograph of FA 2a (beach barrier) and field photograph of FA 2b (lower shoreface). Note m-scale asymptotic hummocky cross-stratification in FA 2b. Sketch of the outcrop section revealing FA 2a is provided to highlight key features – m-scale, bi-directional cross-beds, texturally mature clasts and normally graded cycles (facies Co5). Facies Co5 is subdivided here to show fining upwards cycles (1-3); 1 = poorly-sorted, matrix-supported, rounded gravel-pebble conglomerate; 2 = open-framework rounded pebbles; 3 = poorly-sorted gravel. 3) FA 3: field photographs of 10 m-scale and 100 m-scale foresets at Selinous and Kerinitis, and sketch log of foresets at Unit 11, Selinous Location S3.

4.5.1.4. FA4 - Bottomsets

Three bottomset FAs have been identified across the fan deltas and are interpreted to represent distal (4a), intermediate (4b) and proximal (4c) positions with respect to the sediment input point (Fig. 4.6 and Table 4.1). These deposits form the fine-grained intervals between the major stratigraphic units.

The distal bottomset FA (4a) is mainly represented by calcareous mudstone-siltstone (marl) beds, and is apparent in the interval between Units 7 and 8 at Location S1 (Selinous; Figs. 4.4 and 4.6). There is evidence of soft-sediment deformation and cm-wide, 10 cm-length, sand- and mud-filled burrows (facies Sa1, Sa3, Fi1, Fi2 and Fi4, in Table A, Appendix). A 0.8 m thick, laterally discontinuous, poorly-sorted, clast-supported sandstone-cobble-grade conglomerate (facies Co4 in Table A, Appendix) cuts into the finer sediments. We interpret the fine sediments to be deposited from dilute turbidity currents and suspension fall-out in a low energy environment, and the conglomerate as a debrite sourced from the delta front.

The intermediate bottomset FA (4b) is evident between Units 10 and 11 at Location S3 (Figs. 4.4 and 4.6). It is characterised by interbedded sandstone and mudstone beds with some wavy laminations. The sandstones are inversely graded with slightly erosive bases and gravel lags (facies Sa1, Sa2, Sa4, Sa5, Fi1, Fi2, Fi3, Fi5 and Fi6 in Table A, Appendix), and are interpreted as turbidites. Muddy intervals represent periods of quiescence between events, or dilute turbidity current deposits. The proximal bottomset FA (4c) is observed between Units 8 and 9 at Location

S2, between Units 5 and 6 at Location K2, and between Units 4 and 7 at Location K1a (Figs. 4.4 and 4.6). It is characterised by coarser, mainly well-sorted sand-gravel-grade sediments (facies Co6, Sa1-6, Fi1 and Fi2 in Table A, Appendix), with symmetrical and asymmetrical ripple laminations, gravel dune-scale cross-beds, wavy and planar laminations, soft sediment deformation (convolute laminations, folds and dewatering structures) and bioturbation. The range of structures is interpreted to be due to a more proximal position with respect to the river outlet, where hyperpycnal flows and wave processes may have operated near the base of small foreset slopes in shallow water.

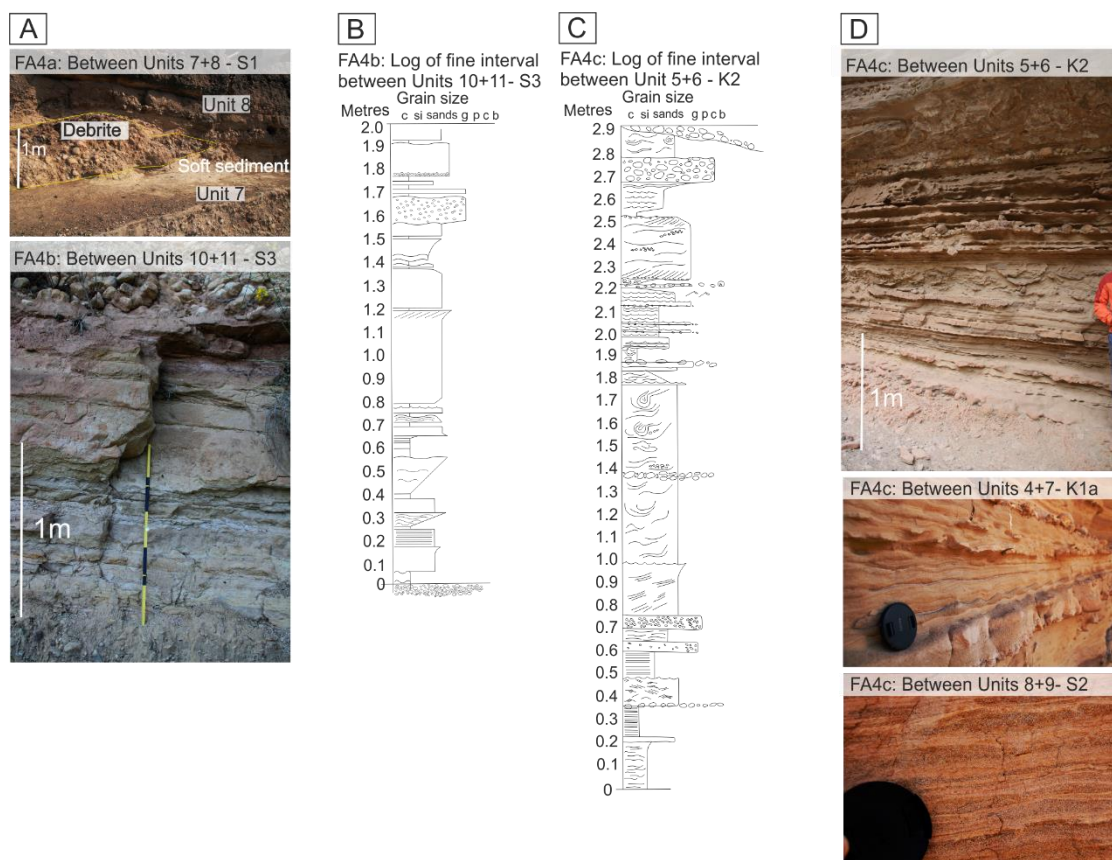


Figure 4.6. A) Field photographs of FAs 4a and 4b. B) Log of FA4b from the fine interval between Units 10 and 11 at Selinous Location S3. C) Log of FA4c from the fine interval between Units 5 and 6 at Kerinitis Location K2. D) Field photographs of FA4c – note symmetrical ripples, indicating shallow water depth.

4.5.2. Key surfaces

4.5.2.1. Flooding surfaces

Fan delta successions can be subdivided into major stratal units based on stratal terminations (e.g. downlaps, onlaps, and truncations) and major facies changes (Mitchum et al., 1977). Fine-grained intervals are present between conglomeratic units in the topset regions and transition zones. Basinward, fine-grained units are poorly preserved, with one exception at Location K1b (Kerinitis). However, their correlative expression can be traced down-dip into the foreset region using onlap and downlap patterns, and dip changes between foresets. In both fan deltas, the fine-grained intervals are similar in their position (generally preserved in the topset regions and transition zones) and thickness (~2 m). Locally, the bases of the fine-grained intervals are slightly erosional. The facies of the fine-grained intervals range from laminated mudstones and deformed siltstones (FA 4a), interbedded siltstones-sandstones (FA 4b), to rippled sandstones and gravels (FA 4c).

The base of the fine-grained intervals are interpreted to represent transgressive surfaces. The maximum flooding surfaces are speculated to be within the fine-grained units in the topset region of the deltas above each transgressive surface. The upper part of the fine-grained intervals may be contemporaneous with the foreset progradation and therefore represent the subsequent regressive trend. In the analogous modern conglomeratic deltas along the southern shore of the Gulf of Corinth, fine-grained deposits are restricted to: 1) inter-distributary bays, 2) lagoons, 3) fluvial overbanks, and 4) shelfal, shallow water bottomsets, away from the dynamic, coarse-grained, gravity-driven processes in the foreset region, and where dilute turbidity currents and suspension fall-out processes dominate. The two former interpretations are omitted based on the absence of rootlets, palaeosols, intact fauna or overall palaeocurrent changes that would indicate delta lobe avulsion and thus a migration to an inter-distributary bay setting. In addition, the fine-grained intervals are too widespread to represent a single lagoon in this setting. In the more proximal parts of the fan delta, it is not possible to characterise the fine-grained intervals, so it is

possible that they could comprise of fluvial overbank deposits (Backert et al., 2010). However, an interpretation of transgressive reworking of the topset region and deposition of shelfal fines is favoured.

We do not infer a great water depth for the deposition of the bottomset facies, and interpret the fine-grained deposits to represent shelfal fines as opposed to slope/abyssal plain fines when positioned landward of the large, basinward-dipping foresets. Where small foresets prograde in shallow water in the proximal topset region, widespread bottomset deposition over the previous fan delta topset occurs (Fig. 4.7). If the previous delta topset, and thus the subsequent overlying bottomset, lies at a water depth above storm wave base, upper and lower shoreface environmental facies are possible, even though geometrically they were deposited in the bottomsets (FA4b and FA4c). Bathymetry data of the Late Pleistocene and modern Selinous deltas (Cotterill, 2002; McNeill et al., 2005; Fig. 4.7) support the intercalation of bottomset and topset deposits. The topset of the Late Pleistocene delta (Y in Fig. 4.7) is overlain by the fine sediment of the modern system's bottomset (X in Fig. 4.7). Debris from the modern system are identified in the bottomset of X that are placed on the topset of Y.

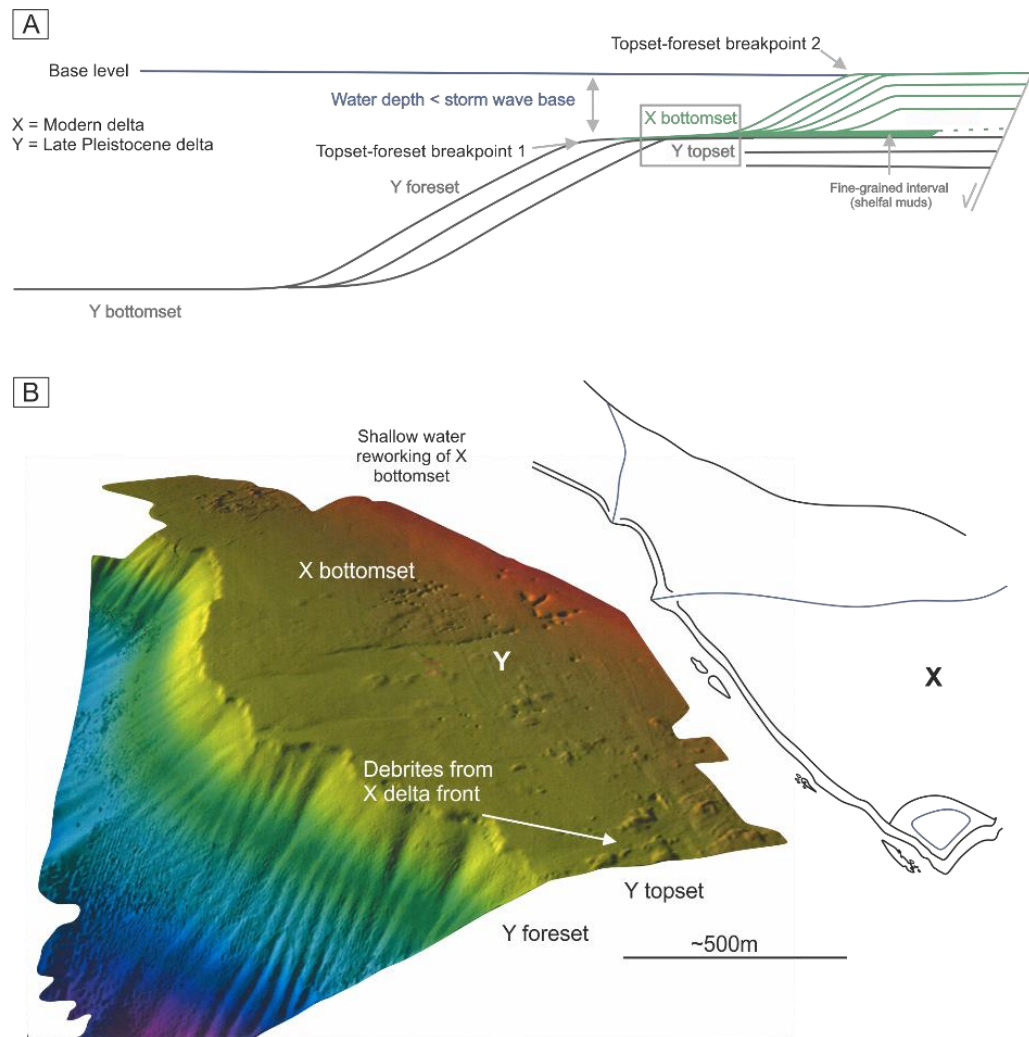


Figure 4.7. Geometric position of shallow water bottomsets (FA4c). A) Diagram shows the position of two hypothetical delta units X and Y to show the juxtaposition of underlying topsets of Y and overlying bottomsets of X in shallow water. The bottomsets of X are in a water depth above storm wave base and therefore present shallow water facies even though they are geometric bottomsets. B) Sketch of the modern Selinous fan delta (X), prograding over the Late Pleistocene Selinous fan delta (Y) as an example of the juxtaposition shown in A (position shown in Fig. 4.1). Bathymetry data from Cotterill et al. (2002) and McNeill et al. (2005).

4.5.2.2. Sequence boundaries

In most cases, there is evidence for minor erosion of the fine-grained intervals by overlying topset units during progradation. However, deeper erosion (at the scale of several metres depth) that is subaerial in nature is only expressed at Selinous. At Selinous Location S2, the progradational

foresets of Unit 9 infill a ~4 m deep erosional surface that incises into the underlying fine-grained interval. Where the fine-grained interval is missing, foresets are seen to directly overlay Unit 8, which comprises fluvial delta plain facies (FA1b) with several palaeosols (Fig. 4.8). The large lateral extent of the surface, traceable across the length of the whole fan delta, and the basinward shift of depositional environments, supports an interpretation of the erosive surface as a sequence boundary formed by a relative base level fall. Between Units 7 and 8 at S1, another surface with erosion of several metres depth is apparent and could be a sequence boundary. The bottomset deposit at this location is finer, and therefore interpreted to be more distal, than those at S2.

At Kerinitis, there is a ~100 m deep erosional cut at Key Stratal Surface 5 (KSS5) between the foresets of Units 3 and 7. Backert et al. (2010) attribute this to a large-scale submarine mass failure unrelated to relative base level change. Otherwise, major surfaces at Kerinitis appear to be either: 1) associated with major facies changes with limited erosion, or 2) erosive with a lack of subaerial indicators and occurring at the base of foresets ('cusate erosion surfaces' in Backert et al., 2010). These erosion surfaces are not interpreted to represent sequence boundaries due to the lack of evidence of subaerial exposure. We interpret that the erosion surfaces form by autocyclic processes, in agreement with the interpretation from Backert et al. (2010). Figure 4.8 shows the difference in the nature of key stratigraphic surfaces between Selinous (erosive sequence boundary) and Kerinitis (non-erosive surface) with examples from S2 and K3.

In summary, sequence boundaries are interpreted near the fault tip at Selinous, but not near the fault centre at Kerinitis. One explanation is that Kerinitis is positioned near the fault centre where greater subsidence could counteract basinwide relative base level falls (cf. Gawthorpe et al., 1994).

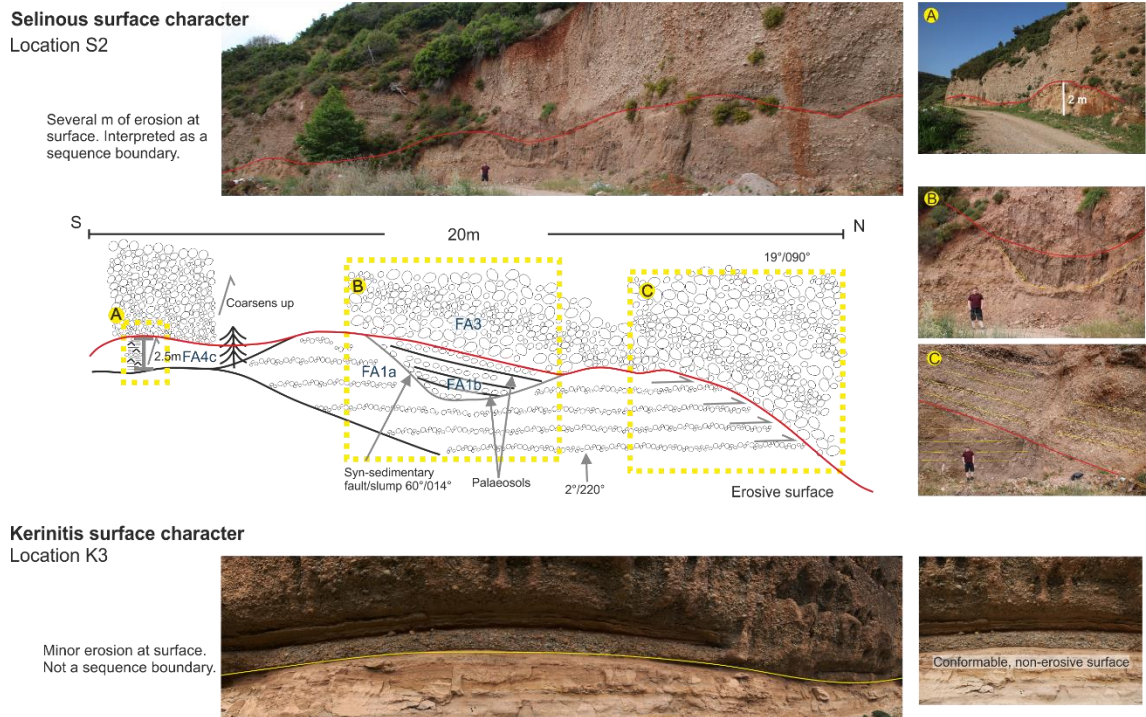


Figure 4.8. Sketch and field photographs to present an erosional surface apparent at Selinous Location S2 between Units 8 and 9, interpreted to be a sequence boundary. Photographs shown from KSS2 between Units 1 and 2 of a non-erosive surface at Kerinitis as comparison. Geologist for scale is 1.75 m. Numbers indicated in blue represent Facies Association codes.

4.5.3. Stratal stacking patterns

4.5.3.1. Description of stratal stacking patterns

At both fan deltas, the major stratal units are dominated by conglomerates, comprising FA 1 and 2 in the topsets and FA 3 in the foresets. The topsets extend for up to 2 km away from the fault to the TFBP, where restored stratigraphic dips increase from sub-horizontal to 20-25°. Average unit thickness is thinner at Selinous (~25 m) at Selinous compared to Kerinitis (~60 m). At both fan deltas, the units thicken towards the fault by ca. 10 m. The thicknesses of the units are generally uniform through time at Selinous. At Kerinitis, unit thickness generally increases towards the middle part of the fan delta and thins towards the top (Backert et al., 2010). The units also thicken into the foreset regions down-dip with foreset heights reaching >350 m, as the fan deltas prograded into deeper water depths towards the basin centre. At Selinous, we observe fifteen

stratal units. At Kerinitis, we observe eleven stratal units, but the base of the Kerinitis succession is not observed. Previously, Kerinitis has been subdivided into twelve (Dart et al., 1994) or eleven stratigraphic units, with the uppermost unit designated as the Kolokotronis fan delta of the Upper Group (Backert et al., 2010). A ‘proto-delta’ (Stratal Unit 0 in Backert et al., 2010) recording initiation of subsidence is also identified towards the base of Kerinitis and is differentiated based on the interpretation of a sequence boundary at the top, drainage realignment and basinward shift of the subsequent units (Backert et al., 2010).

Trajectory analysis of the TFBP (Figs. 4.7 and 4.9) was undertaken at both fan deltas for the middle units: Units 4-8 at Kerinitis and Units 7-11 at Selinous. It should be noted that these units were chosen for analysis based on accessibility alone and there is no evidence for correlation between the units. Trajectory analysis for the whole of the Kerinitis fan delta is presented by Backert et al. (2010). Figure 4.9 shows schematic dip sections of the two fan deltas juxtaposed along the P-M Fault, with the trajectory analysis of each for comparison. The unit thicknesses are normalised to emphasise the relative patterns in the trajectory styles. From the trajectory analysis, it appears that the stacking patterns are similar at both fan deltas across three scales, from stacking within units (10 m-scale), stacking between units (100 m-scale), to stacking of the whole fan delta succession (several 100 m-scale).

At Selinous, there is a progradational-to-aggradational style within Units 7-10, as shown by the climbing basinward trajectory of the TFBP. Unit 11 has a different trajectory, as small-scale (10 m) foresets are apparent closer to the fault. This is shown by the proximal climbing basinward trajectory of the TFBP (aggrading), followed by the horizontal basinward trajectory (prograding). Between Units 7 and 11 at Selinous there is generally retrogradation, i.e. the final TFBP of each unit is landward of that of the previous unit (Fig. 4.9). However, the Selinous fan delta is aggradational given the overall limited horizontal migration of the TFBP. Within Units 4-8 at Kerinitis, there appears to be a progradational-aggradational stacking pattern that resembles the style of Units 7-11 at Selinous. The final TFBP of Unit 5 is landward of that of Unit 4, indicating a phase of retrogradation. The final TFBP of Units 6 and 7 are basinward of their underlying units,

indicating a phase of retrogradation. Finally, Unit 8 is landward of that of Unit 7, and indicates retrogradation. Backert et al. (2010) compile the fan delta units into three packages and interpret the lower package (Units 1-3) as progradational, the middle package as progradation-aggradational (Units 4-9) and the upper package as progradational (Units 10-11). Although there are variations in stacking pattern, the overall position of the TFBP between Units 4 and 8, and indeed of the whole fan delta, migrated a limited distance (~1.5 km; Fig. 4.9). Therefore, Kerinitis also exhibits an overall aggradational stacking pattern. It is not possible to access and characterise the fine-grained intervals across much of the topset part of the fan deltas with some exceptions, so it is not possible to define the landward extent of flooding.

4.5.3.2. Interpretation of stratal stacking patterns

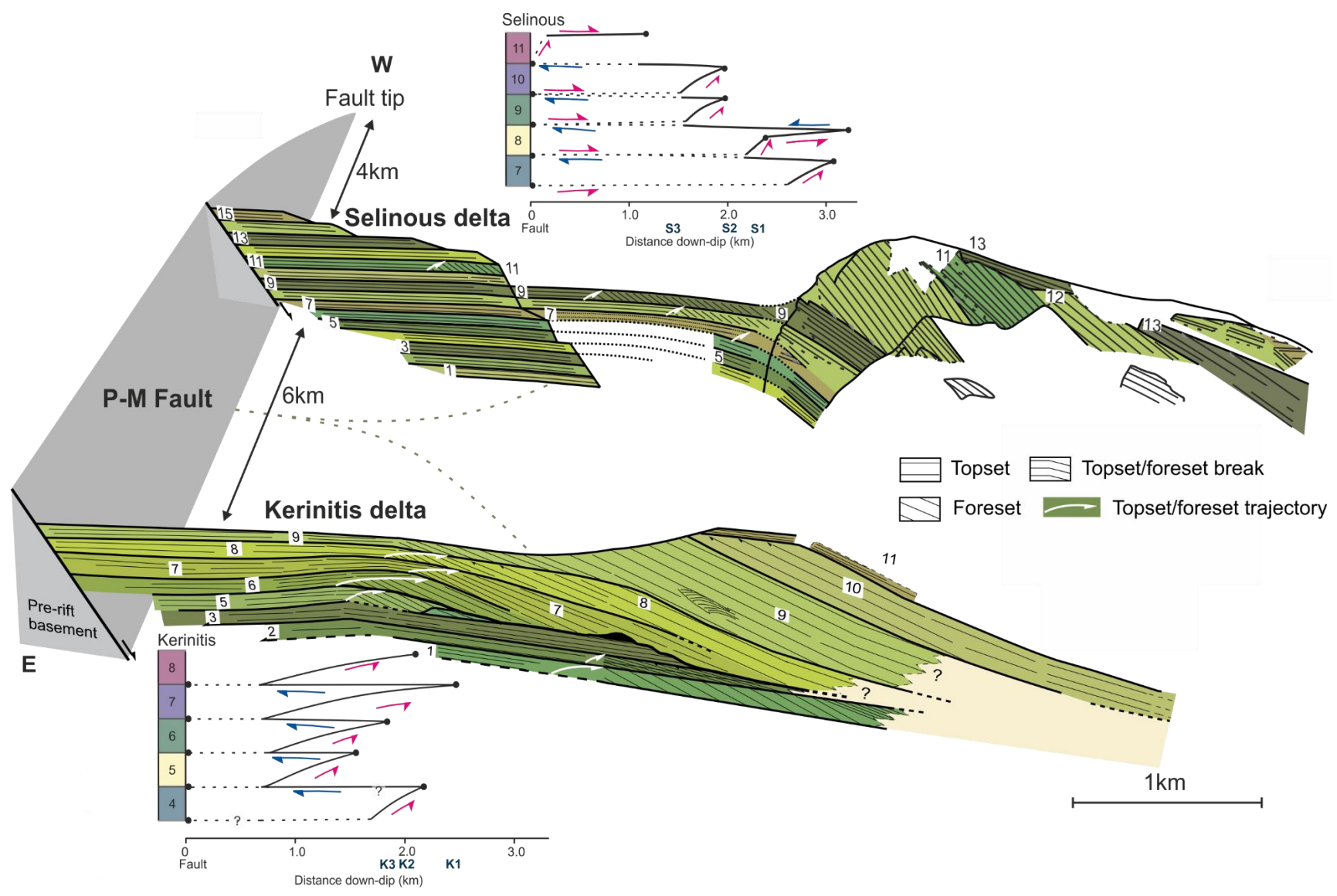
The progradation-aggradation within the units at both fan deltas was a response to building out into space created by base level rise and subsidence, with sedimentation initially exceeding and then keeping pace with space creation. The retrogradational phase at Selinous, between Units 7-11, represents a time when the relative base level rise outpaced the sedimentation rate. The aggradational phase at Kerinitis between Units 4-8 represents a time when sedimentation was equal to the space available. The overall aggradational trend observed in both fan deltas is a response to overall sedimentation having kept pace with accommodation generation. The greater unit thickness in the topset region at Kerinitis than Selinous may be attributed to the greater space made available from a higher subsidence rate near the fault centre than near the fault tip.

At both fan deltas there is clear cyclicity, with several major conglomeratic stratal units separated by fine-grained intervals, both with relatively constant thickness within each fan delta. Autocyclic switching of channel position is intrinsic to the architecture of fan delta tops. However, based on previous studies and repeated airborne photography of the Gulf of Corinth over the last 75 years, it is apparent that the rivers on the delta tops avulse on a decadal-centennial timescales (Soter & Katsonopoulou, 1998; McNeill & Collier, 2004). Here we are characterising an assumed larger scale cyclical behaviour. Such organised cyclicity is unlikely to develop from clustering of seismic activity (Scholz, 2010) as the long term velocity field over this timescale of 10-100 kyr

is constant, due to the viscous flow of the lower crust (Wdowinski et al., 1989). Given this, and the fact that low-mid latitude Pleistocene lakes are characterised by high amplitude base level fluctuations (Gasse et al., 1989; Benson et al., 1998; Marshall et al., 2011; Lyons et al., 2015; Marchegiano et al., 2017), the cyclicity is attributed to periodicity in lake level change associated with climate. Previous authors also advocate this interpretation (Dart et al., 1994; Backert et al., 2010). Sediment supply is also likely to fluctuate with climate (Collier et al., 1990; 2000). Therefore, during the existence of the lake, climatic changes associated with orbital forcing influenced the evolution of the coast through fluctuations in both base level and sediment supply (Collier, 1990; Leeder et al., 1998; Moretti et al., 2004; Gawthorpe et al., 2017b). Lake level is interpreted to have risen and fallen multiple times throughout the Early-Middle Pleistocene with close to zero net change over the build times of the fan deltas. Without the addition of fault-related subsidence, there would be no space for the sediments to accumulate on the topsets, as each base level fall would remove the space created by each base level rise. Instead, distinctly progradational stacking pattern would be apparent with a consistent sediment supply, which is not apparent. Sedimentation must therefore have kept pace with the space creation from subsidence.

Figure 4.9. Summary diagram of architectural stacking at both fan deltas in their respective positions along the P-M Fault. Trajectory analyses of topset-foreset breakpoint of both fan deltas are shown alongside the cross-sections. Topset-foreset breakpoints are shown by black filled circles and trajectory paths are shown by black lines. Study Locations S1-3 and K1-3 are indicated. Unit thicknesses on trajectory analysis diagrams are normalised to emphasise the relative patterns in the trajectory styles. The trajectory of Unit 4 is less certain (question marks). Solid lines show observable trajectories in the transition zone and dashed lines show our interpretation of retrogradation back to the fault and/or correlative surfaces to downdip maximum flooding surfaces. Kerinitis cross-section from Gawthorpe et al. (2017a) after Backert et al. (2010).

157



4.6. Quantification of controls

Here, we attempt to use the field data to discern and quantify the architectural controls on fan delta evolution. Subsidence rates can be estimated using the thickness of the syn-rift successions over the time through which the fan deltas built (fan delta build time), sedimentation rates from the combination of thickness accumulated and stacking pattern over time, and base level change from extrapolation of unit thickness to the fault tip where subsidence is zero. We assign qualitative uncertainty values (1-5) to each control parameter, where 1 represents a very low uncertainty estimate and 5 represents a very high uncertainty estimate. This approach identified which variable is most uncertain and would be a focus for numerical model testing. Table 4.2 presents each control parameter and uncertainty estimate.

Local climate varied in response to orbital forcing during the Early-Middle Pleistocene with the ~41 kyr dominant cyclicity (Capraro et al., 2005; Dodonov, 2005; Suc & Popescu, 2005) that is recorded worldwide (Emiliani, 1978; Head & Gibbard, 2005; Lisiecki & Raymo, 2007). This is assigned a low uncertainty value of 1. The Gulf of Corinth was mainly lacustrine (Lake Corinth) between ~3.6 Ma and ~600 ka (Freyberg, 1973; Collier, 1990; Moretti et al., 2004; Gawthorpe et al., 2017b). It is likely that lake levels fluctuated as a result of the well-constrained cyclical climatic changes, but it is not known how the lake level changed and whether it mimicked global sea level fluctuations. Various studies from the Late Pleistocene show low-mid latitude lakes fluctuating with the same periodicity as global sea level, e.g. Lake Lisan, Dead Sea (Torfstein et al., 2013), Lakes Tana and Tanganyika, East Africa (Gasse et al., 1989; Marshall et al., 2011), Mono and Owens Lakes, California (Benson et al., 1998), Lake Trasimeno, Italy (Marchegiano et al., 2017), with low lake levels corresponding to events during glacial periods (low global sea level). However, the climate response (precipitation-evaporation balance) to such events is spatially variable and it is also unknown whether this Late Pleistocene trend is representative of climate changes during the Early-Middle Pleistocene. The cyclical stratigraphy and facies of the deltas indicate that lake level changes did occur, and a frequency of ~41 kyr in line with climate during the Early-Middle Pleistocene is consistent with the age of the fan deltas.

Palynological data from the adjacent and contemporaneous Vouraikos delta indicate that the fan deltas started to build at ~1.8 Ma (Ford et al., 2007), and stopped developing when they began to be uplifted in the footwall of the West Helike Fault. Using uplift rates on the contiguous East Helike Fault of 1-1.5 mm/yr (De Martini et al., 2004) and present-day final topset elevation (~800 m) of the fan delta, an age for their demise is estimated as 530-800 ka (Ford et al., 2007). The age constraint from palynology and uplift rates of ~1.8-~700 ka supports the use of ~41 kyr as the dominant cyclicity.

Assuming the cyclicity is not autogenic, and each fine-grained interval contains a maximum flooding surface on the rising limb of a relative base level curve, the deposition of each unit represents one climatic cycle. At Selinous, there are fifteen stratal units, each representing ~41 kyr of deposition, from which we infer that the fan delta built over a total of 615 kyr. At Kerinitis, the base is not exposed, but there are at least eleven stratal units and so the minimum delta build time is 450 kyr. If the 'proto-delta' at the base was to be included in our framework or the lower units were exposed, this estimated build time would be longer. These approximations are consistent with previous estimates of fan delta build time based on palynological analysis of the concurrent and adjacent Vouraikos fan delta of 500-800 kyr (Malarte et al., 2004; Ford et al., 2007), and therefore we assign these build time estimates with a low uncertainty value of 2.

There is far greater uncertainty on the amplitude of lake level change. The unit thicknesses at Kerinitis are ~60 m and at Selinous are ~25 m. As both fan deltas developed only 6 km apart, in the hangingwall of the same fault, the lake level fluctuations affecting both systems were the same, and the difference in unit thicknesses is mainly due to variation in local subsidence rate. Subsidence was greater at Kerinitis than at Selinous; at least 35 m of unit thickness accounts for the contribution from additional subsidence at Kerinitis. Therefore, the maximum base level rise during one cycle is 25 m. As Selinous sits close to the fault tip but still underwent subsidence, lake level change would have been less than 25 m. The amplitude of lake level rise is assigned a high uncertainty value of 4.

Neither succession has undergone significant burial or compaction. The thickness of syn-rift sediments against the fault, and therefore maximum total subsidence at Selinous is ~400 m. The

sediment is inferred to have accumulated over 615 kyr, which gives an average subsidence rate of 0.65 m/kyr. At Kerinitis, there is an estimated thickness, and therefore estimated total subsidence of ~800 m, which is calculated based on average topset unit thickness of 65 m, average topset thickening into the fault of ~10 m and 11 observable units. We infer that the sediment accumulated during 11 cycles over at least 450 kyr, which gives a minimum average subsidence rate of 1.77 m/kyr. The axes of the two fan deltas are positioned 6 km apart along-strike of the fault, and therefore using the two estimated average subsidence rates, subsidence decay per kilometre is approximately 0.19 m/kyr towards the fault tip. As Kerinitis is positioned 10 km from the western fault tip and the fault is ~24 km in length, it sits ~2 km to the east of the fault centre, and therefore the average subsidence rate there is slightly lower than the maximum on the fault. The Vouraikos fan delta sits ~3-4 km to the west of the fault centre and has a thickness of >800m (Ford et al., 2007). Extrapolating the subsidence decay rate derived between Selinous and Kerinitis towards the fault centre gives an estimated average minimum subsidence rate at the centre of the fault of 2.15 m/kyr. This estimate is highly comparable to Holocene fault-related subsidence rates from the Gulf of Corinth (2.2-3.5 mm/yr, McNeill & Collier, 2004), the Gulf of Patras, central Greece (average of 2-5 mm/yr, and 1-2 mm/yr away from the main border faults, Chronis et al., 1991) and the Wasatch Fault Zone, Basin and Range Province, USA (<2 mm/yr, Schwartz & Coppersmith, 1984; Machette et al., 1991; Gawthorpe et al., 1994). The syn-rift sediment thicknesses (total subsidence) is well-constrained and we consider the fan delta build time has relatively low uncertainty, hence the subsidence rates are assigned an equivalent low uncertainty value of 2. If each cycle had a ~20 kyr or ~100 kyr period, then the calculated subsidence rate would change, but this is neither consistent with the current understanding of climate in Greece in the Early-Middle Pleistocene, nor typical fault displacement rates in the region (McNeill & Collier, 2004; Capraro et al., 2005; Dodonov, 2005; Suc & Popescu, 2005). The aggradational stacking trend at both fan deltas reveals that overall sedimentation rate kept pace with subsidence rate over the fan delta build times. Accordingly, as aggradation is present at both fan deltas and there is greater subsidence at Kerinitis, the sedimentation rate must be higher at Kerinitis. By dividing the total thickness of syn-rift sediment by the time taken for the sediment

to accumulate, the average sedimentation rate at Selinous must be ~ 0.65 m/kyr, and at Kerinitis the average sedimentation rate is higher at ~ 1.77 m/kyr. This is similar to estimates for the Vouraikos fan delta that sits along-strike from Kerinitis (Fig. 4.1), where sedimentation rates are estimated to be 1.3-2 mm/yr (Ford et al., 2007). We refer to a sedimentation rate, and not a sediment supply rate, as some of the sediment may have been bypassed to the deep basin (e.g. Stevenson et al., 2015), or redistributed along-strike. Although justified as an estimate, an average sedimentation rate does not reflect any probable variation over the fan delta build time, for example from climate or slip rate related changes in erosion rate, we therefore assign these a high uncertainty value of 4.

Table 4.2. Quantitative field observations and control parameter derivations, with assigned uncertainty values (1-5). 1 = low uncertainty; 5 = high uncertainty.

Parameter	Selinous	Kerinitis	Uncertainty value (1-5)	
Observations	Number of units	15	11	1
	Total thickness of fan deltas	ca. 400 m	> 800 m	1
	Thickness of units	25 m	60 m	1
	Distance between the two fan deltas	6 km		1
	Unit thickness decay rate along fault	5.8 m/km		1
Interpretations	Total subsidence	ca. 400 m	>800 m	1
	Climate change periodicity	ca. 41 kyrs		1
	Lake level change periodicity	ca. 41 kyrs		2
	Delta build time	615 kyrs	>451 kyrs	2
	Subsidence rate	0.65 m/kyrs	>1.77 m/kyrs	2
	Magnitude of lake level rise through each climatic cycle	<25 m		4
		10-15 m ^a		2 ^a
		12 m ^b		2 ^b
Average sedimentation rate	0.65 m/kyrs	>1.77 m/kyrs	2	
Sedimentation model through time	Variable		4	

^aValues refined from numerical modelling exercise with Syn-Strat

^bValues refined using independent thickness extrapolation method

4.7. Reducing uncertainty of control parameters

4.7.1. Numerical modelling with Syn-Strat

To reduce the uncertainty and more accurately quantify the major controls, we undertake a numerical modelling exercise using Syn-Strat (Barrett et al., 2018). Syn-Strat produces a 3D graphical surface representing accommodation in the hangingwall of a normal fault, resulting from tectonic subsidence, sedimentation and sea- or lake-level inputs. Stacking patterns or systems tracts can be applied to the surface. Control parameters that have been derived from the field data are input into the model (Fig. 4.10). Various sensitivity tests are performed, whereby one of the controls with the least uncertainty is varied to assess the closest match to the field observations. Magnitude of base level change and sedimentation rate have the greatest uncertainty (Table 4.2). Although the variation in sedimentation rate through time is unknown, we have some constraint on average sedimentation rate from the aggradational stacking patterns at both fan deltas. Lake level change amplitude was tested, and is varied at 5 m intervals from 5 m to 30 m (Fig. 4.11). The field observations that we compare are the presence of sequence boundaries at Selinous and absence at Kerinitis, and are taken from sections cutting the eastern margins of the fan deltas (positions are indicated on the flattened plots, CI-CVI in Fig. 4.11 by the dashed lines). Figure 4.10 explains the set-up of the numerical modelling tests. The size of the basin is defined first in the model and represented by the size of the matrix. In this case, we define the fault block width (6 km) and length (24 km), and the distance between the axis of each fan delta (6 km). The sediment input points are placed at the respective positions of the fan deltas along the fault; 4 km (Selinous) and 10 km (Kerinitis) from the western fault tip. For the timescale, we take the maximum fan delta build time, which is derived from Selinous as 615 kyr. Each parameter is defined with one dimensional graphical curves plotted along the fault (x), away from the fault (y), and in time (t) (Fig. 4.10A1).

We present the subsidence and lake level controls alone (Fig. 4.10A), in order to show the resultant relative base level curve without sedimentation inputs. All parameters are kept constant, other than the parameter in question (lake level amplitude). The 3D output shows relative base

level change at every point along the length of the fault for a position in the immediate hangingwall of the fault (red line on the schematic diagram in B2 of Fig. 4.10). This position is chosen as it is where the maximum topset unit thickness is observed and has been used to calculate the subsidence and sedimentation rates. Systems tracts (or stages of a base level curve) can be applied to a 3D relative base level (A2 and A3 of Fig. 4.10), just as they can to a traditional 1D relative base level curve. With the given parameters, it is apparent that the key stratigraphic surfaces are diachronous along the fault due to the subsidence variation. The falling limb of the relative base level curve (purple segment on Fig. 4.10A) and therefore sequence boundary is defined as the onset of the fall (between yellow and purple segments). It is not expressed at the fault centre, because subsidence outpaces the maximum rate of lake level fall. Sedimentation fills the space made available through time (Fig. 4.10B), so that at each time step, the space for subsequent deposition is a result of the preceding base level change, subsidence and sedimentation (Barrett et al., 2018). The addition of the sedimentation curves in time and space (Fig. 4.10B1) produces an accommodation curve that is reduced from sediment-filling at the positions of the fan deltas (Fig. 4.10B3).

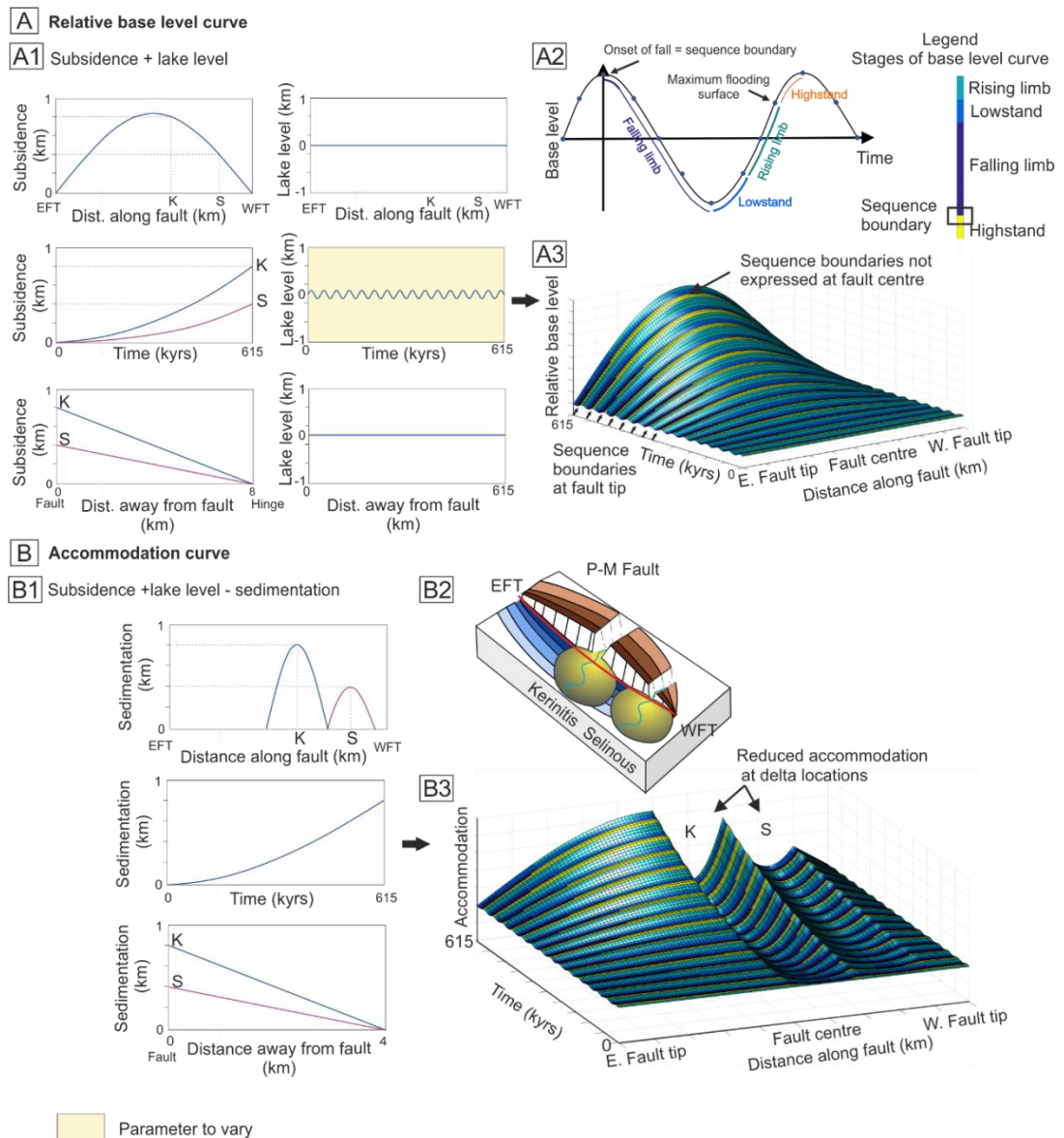


Figure 4.10. Input parameters for numerical model Syn-Strat, derived from field observations, and example outputs. A) Relative base level curve inputs and output: A1) 1D input curves representing subsidence and lake level in time and space; A2) the subdivision of a relative base level curve that is applied to the 3D surfaces; A3) resultant surface showing 3D relative base level through time, along the length of the fault. B) Sedimentation inputs incorporated to produce an accommodation surface: B1) 1D inputs of sedimentation in time and space B2) schematic diagram with red line to indicate position of the plots relative to the fault, i.e. a position in the immediate hangingwall of the fault; B3) resultant 3D accommodation surface. Positions of Kerinitis and Selinous are shown by K and S labels, respectively. Sequence boundaries are positioned between yellow and purple sections and are apparent at the fault tips, but absent towards the fault centre in both A3 and B3. Note reduced accommodation at fan delta locations in B3 due to sediment-filling. Amplitude of lake level change is varied in the sensitivity tests (pale yellow). EFT = East Fault Tip; WFT = West Fault Tip.

The suite of sensitivity tests show that the diachroneity of stratigraphic surfaces decreases with increasing amplitude of base level, as the subsidence control becomes less dominant (Fig. 4.11). In the test with the lowest base level change (5 m; CI), the onset of relative base level fall occurs ~6-12 kyr earlier at the centre of the fan deltas than at the margins, whereas in the highest amplitude base level change test (30 m; CVI), it appears to occur at the same time along the fault, and any diachroneity is below the resolution of the model. There is a clear difference in the nature of sequence boundaries diachroneity between the tests. There are also changes within each test through time. It appears that the diachroneity generally increases through time and in doing so, progressively limits the sequence boundaries to positions closer towards the centre of the fan deltas. This is likely to be in response to the subsidence and sedimentation rates increasing through time in the model (Fig. 4.10). Our analysis was undertaken in the middle to upper units of the fan deltas and so it is here in the model outputs that we assess the presence or absence of sequence boundaries.

When the amplitude of base level change is >20 m (Fig. 4.11, CIV, CV and CVI), sequence boundaries are expressed across both Kerinitis and Selinous. In the field, however, we observe sequence boundaries at Selinous, but not at Kerinitis. In the 5 m amplitude test (Fig. 4.11, CI), sequence boundaries are present at the centre of both fan deltas as here there is maximum sedimentation; the sediments fill and exceed the available accommodation and this causes the system to prograde basinwards. However, at the margins of the fan deltas, where sedimentation is lower, the sequence boundaries are not expressed. As we observe sequence boundaries at the margin of Selinous, this test is also not comparable to our observations. For base level change amplitudes of 10 m and 15 m (Fig. 4.11, CII and CIII), sequence boundaries are expressed in the model results in the middle-upper units at the margin of Selinous, but not at Kerinitis, which match our field observations. These tests are performed with average sedimentation rate equivalent to subsidence. Sedimentation rate is unlikely to be higher than our estimates, but could be lower. In this case, the effect of a relative base level rise would be amplified, so a lower lake level amplitude would be required to give the same response to match our field observations. The lake level change amplitude estimate is therefore a maximum value. In the 15 m amplitude change

test (Fig. 4.11, CIII), sequence boundaries are absent at Kerinitis in the upper units, but present in the middle units. In the field, the middle units (Units 4-8) do not reveal sequence boundaries, hence the 10 m amplitude lake level change amplitude is more consistent with field observations than the 15 m. However, we recognise that uncertainties in the inputs do not allow us to constrain the magnitude of lake level amplitude change to less than 5 m, henceforth we utilise a unit thickness extrapolation approach to validate the numerical modelling output.

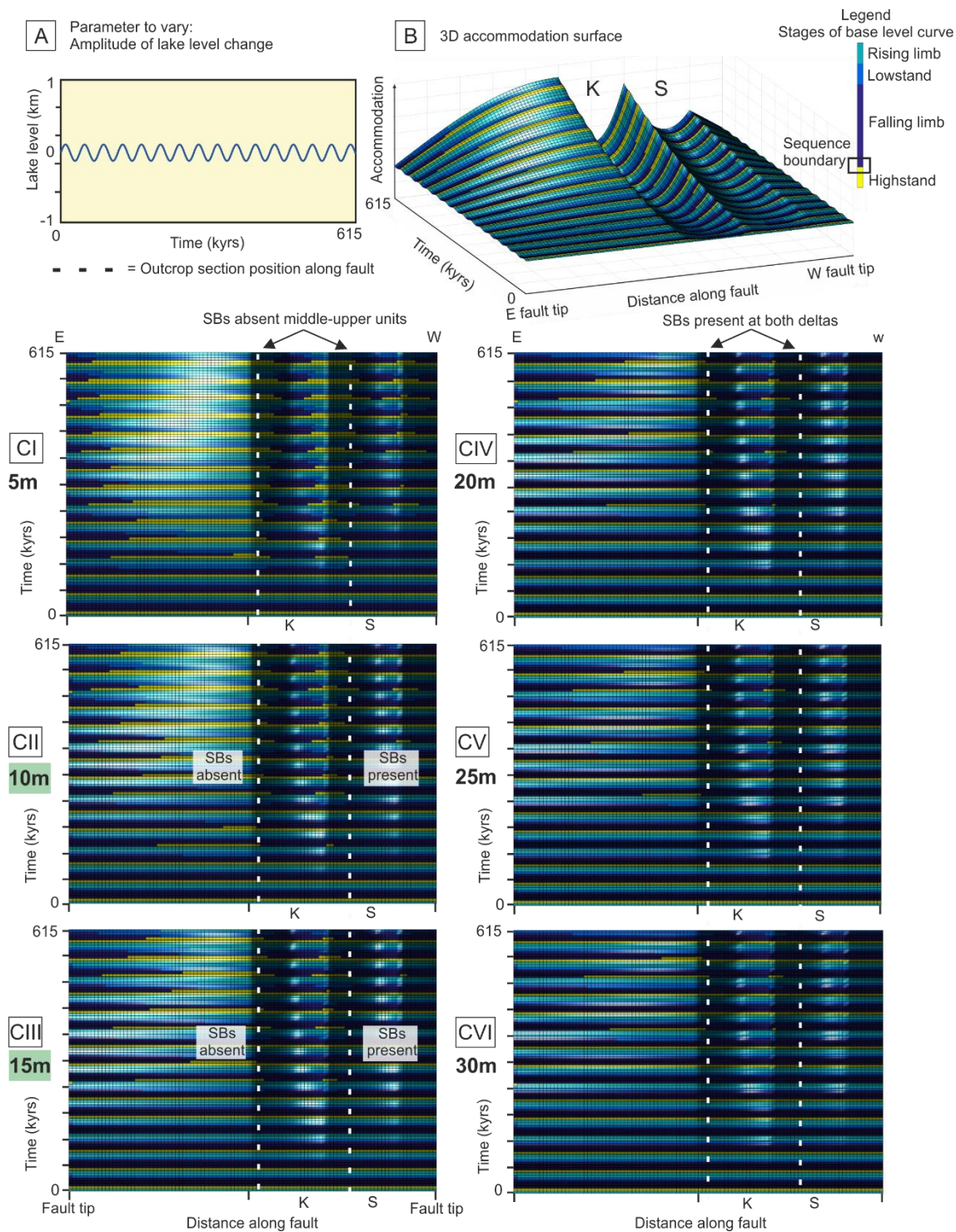


Figure 4.11. Results from numerical modelling sensitivity tests with Syn-Strat. The amplitude of lake level (A) is varied from 5 m to 30 m at 5 m intervals. 3D accommodation surface is shown as example (B). Flattened accommodation surfaces are presented for each test with stages of base level curve presented to allow visualisation of stratigraphic surface extent (CI-CVI). Sequence boundaries (SBs) are between yellow and purple sections. Positions of Kerinitis and Selinous are shown by K and S labels, respectively. Approximate outcrop section positions are indicated by

dashed lines. The 5 m amplitude test (CI) reveals sequence boundary absence at both outcrop section positions, and the 20-30 m (CIV-CVI) amplitude tests reveal the presence of sequence boundaries at both outcrop section positions – not comparable to field observations. The 10 m and 15 m amplitude tests (CII and CIII, highlighted in green) reveal absence of sequence boundaries at the outcrop section position at Kerinitis and presence of sequence boundaries at the outcrop section position at Selinous – most comparable to field observations – refining the amplitude of lake level fluctuations during the Early-Middle Pleistocene to 10-15 m.

4.7.2. Refinement of lake level change using unit thickness extrapolation method

Lake level changes of 10-15 m amplitude are supported by the extrapolation of unit thicknesses towards the fault tip (Fig. 4.12). Average unit thickness of the Kerinitis topsets is ~60 m and at Selinous is ~25 m. The thickness contribution from subsidence is at least 35 m at Kerinitis and reduces towards the fault tip (in blue on Fig. 4.12). The unit thickness decay between Kerinitis and Selinous occurs over 6 km, with a decay rate of 5.8 m/km. If the same assumed linear unit decay trend is extrapolated a further 4 km to the fault tip, where fault-controlled subsidence is theoretically zero, the units would hypothetically lose a further 23 m thickness, leaving 12 m of possible unit thickness at the fault tip. There must be a space created for this thickness of sediment to accumulate at the fault tip as subsidence is zero, and fluctuation of lake level associated with climate change is the most likely mechanism. There is no actual stratigraphy preserved at the fault tip because there is no net accommodation gain in the immediate hangingwall of the P-M Fault. This analysis assumes that there is no additional space creation from other nearby faults, background subsidence or underlying topography for the sediments to fill. The calculated 12 m base level change is comparable with the model estimate of 10-15 m.

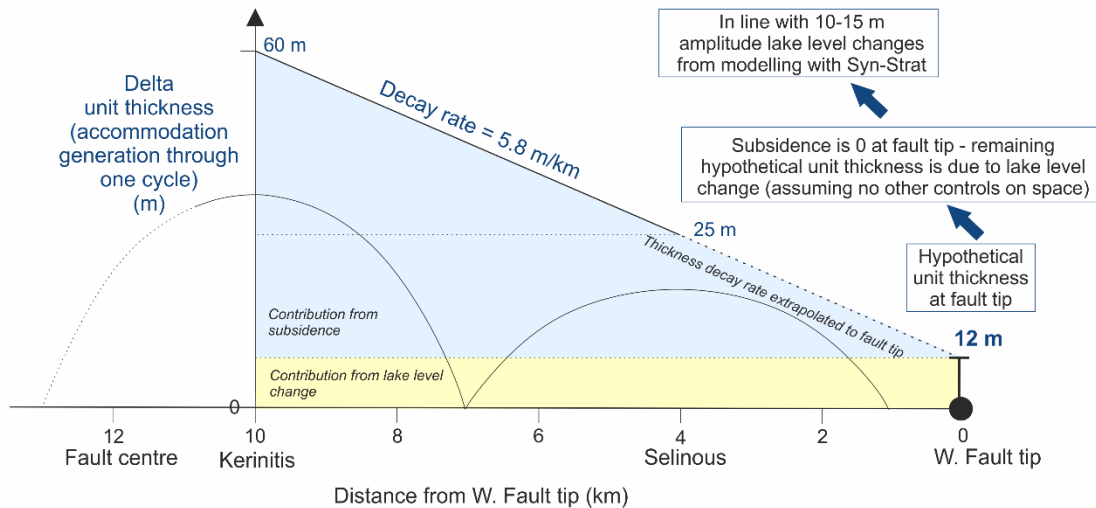


Figure 4.12. Along-strike graphical cross-section to show unit thickness decay extrapolation towards the western fault tip. This is to derive a hypothetical unit thickness at the fault tip, where subsidence is zero and any remaining thickness may have accumulated in space derived from base level change, thus providing an independent derivation of the amplitude of base level change through the Early-Middle Pleistocene in Lake Corinth (12 m), in support of our modelling results (10-15 m). The semi-circular lines are presented to show the extent of the deltas along the fault and to highlight the greater thickness of Kerinitis than Selinous.

4.8. Implications

The implications for this work are threefold: 1) we demonstrate a method for dissociating base level from faulting, which could be applied to a number of other rift basin-fills; 2) we present a quantitative modelling approach to the analysis of stacking and surfaces, constrained by field data, that could be applied to stratigraphic pinchout assessment and cross-hole correlations in reservoir analysis; and 3) we derive a lake level change amplitude for the region, which could aid regional palaeoclimate studies and inform broader climate-system models.

4.8.1. Applications to other basins

Two independent methods – forward modelling with Syn-Strat and unit thickness extrapolation – provided comparable results for lake level change amplitude in Lake Corinth through the Early to Middle Pleistocene (10-15 m). Other studies have presented the problem of dissociating base

level from faulting in rift basins. Dorsey & Umhoefer (2000) attribute the accommodation creation for the Pliocene vertically stacked deltas in the Loreto Basin, Gulf of California to episodic fault-controlled subsidence near the fault centre, and to eustasy near the fault tip, by correlation of parasequences to a marine oxygen isotope curve. It is likely that subsidence rate outpaced eustasy near the fault centre to restrict the development of sequence boundaries to the fault tips. By utilising our methods, it would be possible to affirm whether the stacking cyclicity observed is attributable to faulting or base level change. The numerical modelling approach with Syn-Strat is not limited to rift basins. Any mechanism that creates or reduces accommodation (e.g. salt diapirism or thrust folding) could replace the normal fault in the model and sequence stratigraphic evolution in these settings could be assessed. In areas with good age/eustatic sea level constraints, and for given sedimentation rates, different structural styles could be tested to find the best fit to the observed stratigraphy.

4.8.2. Subsurface appraisal

By comparing two fan deltas we have been able to constrain the interplay of allogenic controls responsible for their depositional architectures. The study of a single fan delta would not have been sufficient to do this, hence we highlight the importance of studying multiple systems within a single basin-fill. With subsidence rates of 0.65 m/kyr at Selinous at ~4 km from the western fault tip, 1.77 m/kyr at Kerinitis at ~10 km from the tip, there should be a maximum subsidence rate of 2.14 m/kyr at the fault centre (~2 km further along-strike). Unit thickness could, for instance, be extrapolated along-strike to provide a hypothetical estimate of 72 m at the fault centre, assuming predominantly aggradational stacking geometries. We cannot test this in the area as no fan delta is located exactly at the fault centre and there is no point source at the fault tip. However, in other settings the ability to predict the variation of stratigraphic thickness along-strike is important for assessment of stratigraphic pinchout in hydrocarbon reservoirs. The modelling work also demonstrates the extent and nature of diachroneity of sequence boundaries along-strike. Such spatiotemporal variability in erosion can have implications for reservoir unit correlation and connectivity. Barrett et al. (2018) demonstrate that the surfaces are not only diachronous, but how

that diachroneity may change along the fault and through time for given scenarios. Here, we go one step further and quantify that variation. For example, in the 10 m lake level amplitude test, the sequence boundary occurs ~6 kyr earlier at the centre of the fan deltas than at the margins (Fig. 4.11). In a subsurface setting, this method could improve confidence in cross-hole correlations of these surfaces.

4.8.3. Implications of a lake level change amplitude of 10-15 m

Early-Middle Pleistocene climate for the Mediterranean region has been studied using palynology (e.g. Capraro et al., 2005; Suc & Popescu, 2005; Joannin et al., 2007) and speleothem analysis as a proxy for local rainfall and air temperature (e.g. Dotsika et al., 2010). Climate fluctuated between cold and dry, and warm and wet periods in association with global climatic records during this time (Head & Gibbard, 2005, and references therein). We interpret that these climate changes resulted in changes in the level of Lake Corinth, which have been estimated to have an amplitude of 10-15 m. The geological record of amplitude is a valuable resource and our estimated value could inform hydrological budget calculations in both regional palaeoclimate studies of the Gulf of Corinth or Mediterranean, and broader climate-system numerical models that require lake level data as an input. Numerical models used to predict how future climate may impact a region require quantitative palaeoclimatic data from multiple proxies from the land and ocean to understand the forcing mechanisms behind observed climatic patterns, and also to validate and improve the models themselves (Abrantes et al., 2012, Luterbacher et al., 2012).

The volume of water that a 10-15 m change in lake level represents is crudely calculated for the Middle Pleistocene Lake Corinth. The lake boundaries are taken from Nixon et al. (2016) and do not include the Alkyonides Basin that may have been disconnected at that time (Nixon et al., 2016). A ~240 km perimeter is estimated and a volume change of ~17-26 km³ (order of 10¹⁰ m³). How a 10-15 m rise would have impacted the coastline is dependent on the coastal gradient and local sediment supply. With an average gradient of the shelf slope in the Gulf of Corinth of 2.8° (from the Alkyonides Basin, Leeder et al., 2002), a 10-15 m change in lake level would cause the

coastline to shift by 250-310 m. However, considering parts of the coastline positioned on a fan delta, with topset gradients of $<0.1^\circ$ and foreset gradients of $\sim 22^\circ$, this shift would be highly variable, depending on whether there is a lake level rise or fall. Starting at the topset-foreset breakpoint, a fall of 10-15 m, would cause the shoreline to advance only 25-40 m due to the steep foreset slope (not including effects on sediment supply). On the other hand, a rise of 10-15 m from the breakpoint would cause a potential shoreline shift of 5-10 km, due to the near-horizontal (0.1°) topset. In reality, coastal topography and the border faults would prevent such a dramatic shift, but this could explain the ~ 2.5 -3 km extent from the P-M Fault of the fine-grained intervals that contain the maximum flooding surfaces between each major unit observed at both Selinous and Kerinitis.

4.9. Conclusions

We have undertaken the first sedimentological and stratigraphic study of the Selinous syn-rift fan delta in the Gulf of Corinth, Greece, and made comparisons with the adjacent and contemporaneous Kerinitis syn-rift fan delta. In doing so, we demonstrate that a multi-system-study approach is an effective way of understanding and quantifying allogenic basin controls. This is the first detailed comparison of stratigraphic architectures between along-strike systems in the hangingwall of a normal fault, positioned near the fault centre and near the fault tip. Eighteen facies and eight facies associations were identified between the deltas, and distinguished in terms of their topset to bottomset geometric position and depositional environments. Maximum flooding surfaces are apparent at both fan deltas between the major stratal units, but sequence boundaries are only observed at Selinous, near the fault tip. In spite of this, stacking patterns are similar between the fan deltas, as shown by trajectory analyses of both, with evidence of: 1) progradation within the units (10 m-scale), 2) retrogradation at Selinous and aggradation at Kerinitis between middle-upper units (100 m-scale), 3) aggradation at the fan delta scale (400-800 m). This implies that overall sedimentation kept pace with accommodation in both cases. As subsidence rate is lower at Selinous near the fault tip, average sedimentation rate must also be

lower there than at Kerinitis. The duration for the whole of each fan delta to build were estimated - 615 kyr for Selinous and at least 450 kyr for Kerinitis. Controlling parameters were quantified from field observations, including subsidence and average sedimentation rates of 0.65 m/kyr at Selinous and >1.77 m/kyr at Kerinitis, and assigned uncertainty values from 1-5. The amplitude of lake level change through time was deemed the most uncertain parameter. Numerical modelling with Syn-Strat was undertaken using the presence of sequence boundaries at both localities in various scenarios, to reduce the uncertainty and better constrain the amplitude of lake level change. Lake level changes of 10-15 m were estimated from the model and supported by an independent calculation of 12 m from unit thickness extrapolation towards the fault tip. The study has three broad outcomes: 1) demonstration of two complementary methods to identify and quantify faulting and base level signals in the stratigraphic record, which could be applied to other rift basin-fills, 2) a quantitative approach to the analysis of stacking and surfaces, constrained by field data, that can be applied to stratigraphic pinchout assessment and cross-hole correlations in reservoir analysis; and 3) an estimate of lake level change amplitude in Lake Corinth for the Early-Middle Pleistocene, which could aid regional palaeoclimate studies and inform broader climate-system models.

4.10. Acknowledgments

We thank the project sponsor, Neptune Energy, who support the SMRG (Shallow Marine Research Group). Barrett was partially sponsored by a VISTA Visiting Scholarship at the University of Bergen. Gawthorpe acknowledges support from the VISTA Professorship.

4.11. References

- Abrantes, F., Voelker, A.H.L., Sierro, F.J., Naughton, F., Rodrigues, T., Cacho, I., Ariztegui, D., Brayshaw, D., Sicre, M-A. & Batista, L. (2012). 1 – Paleoclimate variability on the Mediterranean region. *The Climate of the Mediterranean Region, from the past to the future*, Elsevier, London. 1-86pp.
- Avallone, A., Briole, P., Agatza-Balodimou, A.M., Billiris, H., Charade, O., Mitsakaki, C., Nercessian, A., Papazissi, K., Paradissis, D. & Veis, G. (2004). Analysis of eleven years of deformation measured by GPS in the Corinth Rift Laboratory area. *Comptes Rendus Geoscience*, 336, 301-311.

- Backert, N., Ford, M. & Malartre, F. (2010). Architecture and sedimentology of the Kerinitis Gilbert-type fan delta, Corinth Rift, Greece. *Sedimentology*, 57, 543-586.
- Barrett, B., Hodgson, D.M., Collier, R.E.Ll. & Dorrell, R.M. (2018). Novel 3D sequence stratigraphic numerical model for syn-rift basins: analysing architectural responses to eustasy, sedimentation and tectonics. *Marine and Petroleum Geology*, 92, 270-284. doi: 10.1016/j.marpetgeo.2017.10.026.
- Bell, R.E., McNeill, L.C., Bull, J.M. & Henstock, T.J. (2008). Evolution of the offshore western Gulf of Corinth. *Geol. Soc. Am. Bull.*, 120, 156-178.
- Benson, L.V., Lund, S.P., Burdett, J.W., Kashgarian, M., Rose, T.P., Smoot, J.P. & Schwartz, M. (1998). Correlation of Late-Pleistocene Lake-Level Oscillations in Mono Lake, California, with North Atlantic Climate Events. *Quaternary Research*, 49, 1-10.
- Bernard, P., Lyon-Caen, H., Briole, P., Deschamps, A., Boudin, F., Makropoulos, K., Papadimitriou, P., Lemeille, F., Patau, G., Billiris, H., Paradissis, D., Papazissi, K., Castarede, H., Charade, O., Nercessian, A., Avallone, A., Pacchiani, F., Zahradnik, J., Sacks, S. & Linde, A. (2006). Seismicity, deformation and seismic hazard in the western rift of Corinth: new insights from the Corinth Rift Laboratory (CRL). *Tectonophysics*, 426, 7-30.
- Briole, P., Rigo, A., Lyon-Caen, H., Ruegg, J.C., Papazissi, K., Mitsakaki, C., Balodimou, A., Veis, G., *et al.* (2000). Active deformation of the Corinth rift, Greece: Results from repeated Global Positioning System surveys between 1990 and 1995. *Journal of Geophysical Research-Solid Earth*, 105, 25605-25625.
- Capraro, L., Asioli, A., Backman, J., Bertoldi, R., Channell, J.E.T., Massari, F. & Rio, D. (2005). Climatic patterns revealed by pollen and oxygen isotope records across the Matuyama-Brunhes Boundary in the central Mediterranean (southern Italy). *Geological Society, London, Special Publications*, 247, 159-182.
- Catuneanu, O., Abreu, V., Bhattacharya, J.P., Blum, M.D., Dalrymple, R.W., Eriksson, P.G., Fielding, C.R., Fisher, W.L., Galloway, W.E., Gibling, M.R., Giles, K.A., Holbrook, J.M., Jordan, R., Kendall, C.G.S.T.C., Macurda, B., Martinsen, O.J., Miall, A.D., Neal, J.E., Nummedal, D., Pomar, L., Posamentier, H.W., Pratt, B.R., Sarg, J.F., Shanley, K.W., Steel, R.J., Strasser, A., Tucker, M.E., Winker, C. (2009). Towards the standardization of sequence stratigraphy. *Earth Sci. Rev.*, 92, 1-33.
- Clarke, P.J., Davies, R.R., England, P.C., Parsons, B.E., Billiris, H., Paradissis, D., Veis, G., Denys, P.H., Cross, P.A., Ashkenazi, V. & Bingley, R. (1997). Geodetic estimate of seismic hazard in the Gulf of Korinthos. *Geophysical Research Letters*, 24, 1303-1306.
- Chronis, G., Piper, D. J. W. & Anagnostou, C. (1991). Late Quaternary evolution of the Gulf of Patras, Greece: tectonism, deltaic sedimentation and sea-level change. *Marine Geology*, 97, 191-209.
- Collier, R.E.Ll. (1990). Eustatic and tectonic controls upon Quaternary coastal sedimentation in the Corinth Basin, Greece. *J. Geol. Soc.*, 147, 301-314.
- Collier, R.E.Ll. & Dart, C.J. (1991). Neogene to Quaternary rifting, sedimentation and uplift in the Corinth Basin, Greece. *J. Geol. Soc. London*, 148, 1049-1065.
- Collier, R.E.Ll., Leeder, M.R. & Maynard, J.R. (1990). Transgressions and regressions: a model for the influence of tectonic subsidence, deposition and eustasy, with application to Quaternary and Carboniferous examples. *Geol. Mag.*, 127, 117-128.
- Collier, R.E.Ll., Leeder, M.R., Trout, M., Ferentinos, G., Lyberis, E. & Papatheodorou, G. (2000). High sediment yields and cool, wet winters: test of last glacial paleoclimates in the northern Mediterranean. *Geology*, 28, 999-1002.
- Collier, R.E.Ll. & Thompson, J. (1991). Transverse and linear dunes in an Upper Pleistocene marine sequence, Corinth Basin, Greece. *Sedimentology*, 38, 1021-1040.
- Cotterill, C.J. (2002). A high resolution Holocene fault activity history of the Aigion shelf, Gulf of Corinth, Greece. PhD Thesis, School of Ocean and Earth Sciences, University of Southampton, UK.

- Dart, C.J., Collier, R.E.L., Gawthorpe, R.L., Keller, J.V.A. & Nichols, G. (1994). Sequence stratigraphy of (?)Pliocene-Quaternary synrift, Gilbert-type fan deltas, Northern Peloponnesos, Greece. *Mar. Pet. Geol.*, 11, 545-560.
- De Martini, P., Pantosti, D., Palyvos, N., Lemeille, F., McNeill, L. & Collier, R.E.L. (2004). Slip rates of the Aigion and Eliki faults from uplifted marine terraces, Corinth Gulf, Greece. *C. R. Geosci.*, 336, 325-334.
- Dodenov, A.E. (2005). The stratigraphic transition and suggested boundary between the Early and Middle Pleistocene in the loess record of northern Eurasia. *Geological Society, London, Special Publications*, 247, 209-219.
- Dorsey, R.J. & Umhoefer, P.J. (2000). Tectonic and eustatic controls on sequence stratigraphy of the Pliocene Loreto Basin, Baja California Sur, Mexico. *GSA Bull.*, 112, 177-199.
- Dorsey, R.J., Umhoefer, P.J. & Renne, P.R. (1995). Rapid subsidence and stacked Gilbert-type fan deltas, Pliocene Loreto Basin, Baja California Sur, Mexico. *Sediment. Geol.*, 98, 181-204.
- Dotsika E., Psomiadis D., Zanchetta G., Spyropoulos N., Leone G., Tzavidopoulos I. & Poutoukis D. (2010). Pleistocene palaeoclimatic evolution from Agios Georgios Cave speleothem (Kilkis, N. Greece). *Bulletin of the Geological Society of Greece, Proceedings of the 12th International Congress, Patras*, 2, 886-895.
- Emiliani, C. (1978). The cause of the ice ages. *Earth & Planetary Science Letters*, 37, 349-352.
- Floyd, M.A., Billiris, H., Paradissis, D., Veis, G., Avallone, A., Briole, P., McClusky, S., Nocquet, J.-M., Palamartchouk, K., Parsons, B. & England, P.C. (2010). A new velocity field for Greece: implications for the kinematics and dynamics of the Aegean. *Journal of Geophysical Research*, 115, B10403.
- Ford, M., Hemelsdael, R., Mancini, M. & Palyvos, N. (2016). Rift migration and lateral propagation: evolution of normal faults and sediment-routing systems of the western Corinth rift (Greece). In: C. Childs, R.E. Holdsworth, C.A.-L. Jackson, T. Manzocchi, J.J. Walsh & G. Yielding (Eds.), *The Geometry and Growth of Normal Faults*. Geological Society, London, Special Publications, 439, 131-168.
- Ford, M., Rohais, S., Williams, E.A., Bourlange, S., Jouselin, D., Backert, N. & Malartre, F. (2013). Tectosedimentary evolution of the western Corinth rift (Central Greece). *Basin Research*, 25, 3-25.
- Ford, M., Williams, E.A., Malartre, F. & Popescu, S.M. (2007). Stratigraphic architecture, sedimentology and structure of the Vouraikos Gilbert-type fan delta, Gulf of Corinth, Greece. In: G. Nichols, E. Williams and C. Paola (Eds.), *Sedimentary Processes, Environments and Basins. A Tribute to Peter Friend*. Int. Assoc. Sedimentol. Spec. Publ., 38, 49-90.
- Frazier, D. (1974). Depositional Episodes: Their Relationship to the Quaternary Stratigraphic Framework in the Northwestern Portion of the Gulf Basin. *Bureau of Economic Geology, University of Texas, Geological Circular 74-1*, pp. 26.
- Freyberg, B. Von (1973). Geologie des Isthmus von Korinth. *Erlanger Geologische Abhandlungen*, 95. Junge und Sohn, Universitäts-Buchdruckerei, Erlangen.
- Galloway, W.L. (1989). Genetic stratigraphic sequences in basin analysis I: architecture and genesis of flooding surface bounded depositional units. *AAPG Bull.*, 73, 125-142.
- Garcia-Garcia, F., Fernandez, J., Viseras, C. & Soria, J.H. (2006). Architecture and sedimentary facies evolution in a delta stack controlled by fault growth (Betic Cordillera, southern Spain, late Tortonian). *Sed. Geol.*, 185, 79-92.
- Garcia-Mondéjar, J. (1990). Sequence analysis of a marine Gilbert-type delta, La Miel, Albian Lunada Formation of northern Spain. In: Coarse-Grained Deltas (Ed. by A. Colella and D.B. Prior), *Int. Assoc. Sedimentol. Spec. Publ.*, 10, 255-269.

- Gasse, F., Lédée, V., Massault, M. & Fontes, J.-C. (1989). Water-level fluctuations of Lake Tanganyika in phase with oceanic changes during the last glaciation and deglaciation. *Nature*, 342, 57-59.
- Gawthorpe, R.L., Andrews, J.E., Collier, R.E.L., Ford, M., Henstra, G.A., Kranis, H., Leeder, M.R., Muravchik, M. & Skourtsos, E. (2017a). Building up or out? Disparate sequence architectures along an active rift margin – Corinth rift, Greece. *Geology*, 45, 111-114.
- Gawthorpe, R.L., Fraser, A. & Collier, R.E.L. (1994). Sequence stratigraphy in active extensional basins: implications for the interpretation of ancient basin fills. *Marine and Petroleum Geology*, 11, 642-658.
- Gawthorpe, R.L., Hardy, S. & Ritchie, B. (2003). Numerical modelling of depositional sequences in half-graben rift basins. *Sedimentology*, 50, 169-185.
- Gawthorpe, R.L., Leeder, M.R., Kranis, H., Skourtsos, E., Andrews, J.E., Henstra, G.A., Muravchik, M., Turner, J.A. & Stamatakis, M. (2017b). Tectono-sedimentary evolution of the Plio-Pleistocene Corinth rift, Greece. *Basin Res.*, 1-32, doi: 10.1111/bre.12260.
- Gawthorpe, R.L. & Leeder, M.R. (2000). Tectono-sedimentary evolution of active extensional basins. *Basin Research*, 12, 195-218.
- Gawthorpe, R.L., Sharp, I., Underhill, J.R. & Gupta, S. (1997). Linked sequence stratigraphic and structural evolution of propagating normal faults. *Geology*, 25, 795-798.
- Ghisetti, F. & Vezzani, L. (2004). Plio-Pleistocene sedimentation and fault segmentation in the Gulf of Corinth (Greece) controlled by inherited structural fabric. *Comptes Rendus Geosciences*, 336, 243-249.
- Gilbert, G.K. (1885). The topographic features of lake shores. *US Geol. Surv. Ann. Rep.*, 5, 69-123.
- Gilbert, G.K. (1890). Lake Bonneville. *US Geol. Surv. Monogr.*, 1, 1-438.
- Goldsworthy, M. & Jackson, J. (2001). Migration of activity within normal fault systems: examples from the Quaternary of mainland Greece. *Journal of Structural Geology*, 23, 489-506.
- Hardy, S., Dart, C.J. & Waltham, D. (1994). Computer modelling of the influence of tectonics on sequence architecture of coarse-grained fan deltas. *Marine and Petroleum Geology*, 11, 561-574.
- Hardy, S. & Gawthorpe, R.L. (1998). Effects of variations in fault slip rate on sequence stratigraphy in fan deltas: insights from numerical modeling. *Geology*, 26, 911-914.
- Hardy, S. & Gawthorpe, R.L. (2002). Normal fault control on bedrock channel incision and sediment supply: insights from numerical modeling. *Journal of Geophysical Research*, 107, 2246.
- Head, M.J. & Gibbard, E.L. (2005). Early-Middle Pleistocene Transitions: The Land-Ocean Evidence. *Geological Society, London, Special Publications*, 247, 1-18.
- Jackson, C.A.-L., Gawthorpe, R.L., Carr, I.D. & Sharp, I.R. (2005). Normal faulting as a control on the stratigraphic development of shallow marine syn-rift sequences: the Nukhul and Lower Rudeis Formations, Hammam Faraun fault block, Suez Rift, Egypt. *Sedimentology*, 52, 313-338.
- Jervey, M.T. (1988). Quantitative geological modeling of siliciclastic rock sequences and their seismic expression. In: C.K. Wilgus, B.S. Hastings, C.G. Kendall, H.W. Posamentier, C.A. Ross. & J.C. Van Wagoner (Eds.), *Sea-Level Changes: An Integrated Approach*. SEPM Special Publications, 42, 47-69.
- Joannin, S., Quillévéré, F., Suc, J.-P., Lécuyer, C. & Martineau, F. (2007). Early Pleistocene climate changes in the central Mediterranean region as inferred from integrated pollen and planktonic foraminiferal stable isotope analyses. *Quaternary Research*, 67, 264-274.

- Leeder, M.R., Mark, D.F., Gawthorpe, R.L., Kranis, H., Loveless, S., Pedentchouk, N., Skourtsos, E., Turner, J., Andrews, J.E. & Stamatakis, M. (2012). A “Great Deepening”: Chronology of rift climax, Corinth rift, Greece. *Geology*, 40, 999-1002.
- Leeder, M.R., Collier, R.E.LI., Abdul Aziz, L.H., Trout, M., Ferentinos, G., Papatheodorou, G. & Lyberis, E. (2002). Tectono-sedimentary processes along an active marine/lacustrine half-graben margin: Alkyonides Gulf, E. Gulf of Corinth, Greece. *Basin Research*, 14, 25-41.
- Leeder, M.R. & Gawthorpe, R.L. (1987). Sedimentary models for extensional tilt block/half-graben basins. In: M.P. Coward, J.F. Dewey & P.L. Hancock (Eds.), *Continental Extensional Tectonics*. Geological Society, London, Special Publications, 28, 139-152.
- Leeder, M.R., Harris, T. & Kirkby, M.J. (1998). Sediment supply and climate change: implications for basin stratigraphy. *Basin Research*, 10, 7-18.
- Leeder, M.R., Mack, G.H., Brasier, A.T., Parrish, R.R., Mintosh, W.C., Andrews, J.E. & Duremeijer, C.E. (2008). Late-Pliocene timing of Corinth (Greece) rift-margin fault migration. *Earth and Planetary Science Letters*, 274, 132-141.
- Lisiecki, L.E. & Raymo, M.E. (2007). Plio–Pleistocene climate evolution: trends and transitions in glacial cycle dynamics. *Quaternary Science Reviews*, 26, 56-69.
- Luterbacher, J., García-Herrera, R., Akcer-On, S., Allan, R., Alvarez-Castro, M-C., Benito, G., Booth, J., Büntgen, U., Cagatay, N., Colombaroli, D., Davis, B., Esper, J., et al. (2012). 2 – A review of 2000 years of paleoclimatic evidence in the Mediterranean. *The Climate of the Mediterranean Region, from the past to the future*. Elsevier, London. 87-185pp.
- Lyons, R.P., Scholtz, C.A., Cohen, A.S., King, J.W., Brown, E.T., Ivory, S.J., Johnson, T.C., Deino, A.L., Reinthal, P.N., Mcglue, M.M. & Blome, M.W. (2015). Continuous 1.3-million-year record of East African hydroclimate, and implications for patterns of evolution and biodiversity. *Proceedings of the National Academy of Sciences of the United States of America*, 112, 15568-15573.
- Machette, M. N., Persounius, S. F. & Nelson, A. R. (1991). The Wasatch fault zone, Utah -- segmentation and history of Holocene earthquakes. *J. Struct. Geol.*, 13, 137-149.
- Malatre F., Ford M. & Williams E.A. (2004). Preliminary biostratigraphy and 3D lithostratigraphy of the Vouraikos Gilbert-type fan delta. Implications for the evolution of the Gulf of Corinth, Greece. *C.R. Geoscience*, 336, 269-280.
- Marchegiano, M., Francke, A., Gliozzi, E., Ariztegui, D. (2017). Arid and humid phases in central Italy during the Late Pleistocene revealed by the Lake Trasimeno ostracod record. *Palaeogeography, Palaeoclimatology, Palaeoecology*, 490, 55-69.
- Marshall, M.H., Lamb, H.F., Huws, D., Davies, S.J., Bates, R., Bloemendal, J., Boyle, J., Leng, M.J., Umer, M., Bryant, C. (2011). Late Pleistocene and Holocene drought events at Lake Tana, the source of the Blue Nile. *Global and Planetary Change*, 78, 147-161.
- McNeill, L.C & Collier, R.E.LI. (2004). Uplift and slip rates of the eastern Eliki fault segment, Gulf of Corinth, Greece, inferred from Holocene and Pleistocene terraces. *Journal of the Geological Society, London*, 161, 81-92.
- McNeill, L.C., Cotterill, C.J., Henstock, T.J., Bull, J.M., Stefatos, A., Collier, R., Papatheoderou, G., Ferentinos, G. & Hicks, S.E. (2005). Active faulting within the offshore western Gulf of Corinth, Greece: implications for models of continental rift deformation. *Geology*, 33, 241–244.
- Mitchum, R.M., Vail, P.R. & Thompson, S. (1977). Seismic stratigraphy and global changes of sea level, Part 2: The depositional sequence as a basic unit for stratigraphic analysis. In: C.E. Payton (Ed.), *Seismic Stratigraphy – Applications to Hydrocarbon Exploration*. AAPG Mem., 26, 53-62.

- Moretti, I., Lykousis, V., Sakellariou, D., Reynaud, J.Y., Benziene, B. & Prinzoffer, A. (2004). Sedimentation and subsidence rate in the Gulf of Corinth: what we learn from the Marion Dufresne's long-piston coring. *C.R. Geosci.*, 336, 291-299.
- Mortimer, E., Gupta, S. & Cowie, P. (2005). Cliniform nucleation and growth in coarse-grained deltas, Loreto basin, Baja California Sur, Mexico: a response to episodic accelerations in fault displacement. *Basin Research*, 17, 337-359.
- Neal, J. & Abreu, V. (2009). Sequence stratigraphy hierarchy and the accommodation succession method. *Geology*, 37, 779-782.
- Nixon, C.W., McNeill, L.C., Bull, J.M., Bell, R.E., Gawthorpe, R.L., Henstock, T.J., Christodoulou, D., Ford, M., Taylor, B., Sakellariou, D., Ferentinos, G., Papatheodorou, G., Leeder, M.R., Collier, R.E.L., Goodliffe, A.M., Sachpazi, M. & Kranis, H. (2016). Rapid spatiotemporal variations in rift structure during development of the Corinth Rift, central Greece. *Tectonics*, 35, 1225-1248.
- Ori, G.G., Roveri, M. & Nichols, G. (1991). Architectural patterns in large-scale Gilbert-type delta complexes, Pleistocene, Gulf of Corinth, Greece. In: A.D. Miall & N. Tyler (eds.), *The Three-Dimensional Facies Architecture of Terrigenous Clastic Sediments and Its Implications for Hydrocarbon Discovery and Recovery. Concepts in Sedimentology and Paleontology*, 3. Society for Sedimentary Geology (SEPM), 207-216.
- Ritchie, B.D., Hardy, S. & Gawthorpe, R.L. (1999). Three dimensional numerical modeling of coarse-grained clastic deposition in sedimentary basins. *Journal of Geophysical Research*, 104, 17759-17780.
- Rohais, S., Eschard, R., Ford, M., Guillocheau, F. And Moretti, I. (2007). Stratigraphic architecture of the Plio-Pleistocene infill of the Corinth Rift: implications for its structural evolution. *Tectonophysics*, 440, 5-28.
- Scholz, C. (2010). Large earthquake triggering, clustering, and the synchronization of faults. *Bull. Seismol. Soc. Am.*, 100, 901-909.
- Schwartz, D. P. & Coppersmith, K. J. (1984). Fault behaviour and characteristic earthquakes - examples from the Wasatch and San Andreas fault zones. *J. Geophys. Res.*, 89, 5681-5698.
- Soter, S. & Katsonopoulou, D. (1998). The search for ancient Helike, 1988-1995: geological, sonar and bore hole studies. In: D. Katsonopoulou, D., S. Soter & D. Scilardi, (Eds.), *Ancient Helike and Aigalieia*. The Helike Society, Aigion, 67-116.
- Stevenson, C.J., Jackson, C.A.L., Hodgson, D.M., Hubbard, S.M., Eggenhuisen, J.T. (2015). Deep-water sediment bypass. *Journal of Sedimentary Research*, 85, 1058-1081.
- Suc, J-P. & Popescu, S-M. (2005). Pollen records and climatic cycles in the North Mediterranean region since 2.7 Ma. *Geological Society, London, Special Publications*, 247, 147-158.
- Torfstein, A., Goldstein, S.L., Stein, M. & Enzel, Y. (2013). Impacts of abrupt climate changes in the Levant from Last Glacial Dead Sea levels. *Quaternary Science Reviews*, 69, 1-7.
- Wdowinski, S., O'connell, R.J. & England, P. (1989). A continuum model of continental deformation above subduction zones' application to the Andes and the Aegean. *Journal of Geophysical Research*, 94, 10331-10346.

4.12. Appendix

Table A. Summary of sedimentary facies identified across Selinous and Kerinitis deltas with code, description and indication of corresponding facies codes from Backert et al. (2010) from Kerinitis. Facies abbreviations: Co, conglomerates; Sa, sandstones, Fi, siltstones and mudstones.

Facies code	Facies description	Process interpretation	Backert et al. (2010) scheme code
Co1: Matrix-supported conglomerate	Poorly-sorted, matrix-supported (sand-gravel), gravel-cobble grade conglomerate. Sub-rounded to sub-angular clasts <15 cm. Some cases of normal grading to fine sand. Cm- to dm-thick beds.	High energy bedload transport	G2: Matrix-supported conglomerate
Co2: Stratified conglomerate	Poorly-sorted, variable matrix- and clast-support (sand-gravel), pebble-cobble grade conglomerate, sub-horizontal bedding. Cm- to dm-thick beds.	Bedload transport/longitudinal bedforms	G1c: Crudely stratified conglomerate
Co3: Dipping conglomerate	Steeply dipping (~25°), poorly-sorted, clast-supported gravel-boulder conglomerate. Mostly sub-rounded, large pebble and cobble clasts (<15 cm diameter), occasional small boulders (<25 cm). Matrix of coarse sand-gravel. In some cases locally imbricated. <1m thick open framework lenses. Cuts and scours. >10 m-thick beds.	Gilbert-type delta foresets, characterised by erosive sediment gravity flows on steep slopes	G1b: Steeply dipping conglomerate
Co4: Clast-supported conglomerate	Well to poorly-sorted, clast-supported, pebbly conglomerate with occasional cobbles. Mainly sub-rounded to sub-angular clasts (<10 cm). Inverse grading. Some beds pinch out laterally. Cm-dm thick beds.	Granular flow	G1a: Well-to poorly-sorted structureless conglomerate
Co5: Cross-bedded conglomerate	Well-sorted, matrix- and clast-supported parts (some open-framework), gravel-cobble conglomerates. Clasts are mainly rounded-discoidal (<16 cm). Dm- to m-scale cross-beds with 21-24° dip, locally with an asymptotic geometry. Some beds pinch out laterally. Inverse and normal grading within beds and gradational contacts.	Dune migration by bedload transport and wave and storm reworking	G1e: Cross-stratified conglomerate
Co6: Interbedded conglomerate-gravelly sand	Mostly poorly-sorted, matrix-supported interbedded pebble-cobble grade conglomerate and gravelly coarse sand. Sand is generally laminated with gravel and with dispersed pebbles. Some cobble beds are open-framework and well-sorted or poorly-sorted and clast-supported. Beds <20 cm thick.	Variable energy regime sediment gravity flows - avalanche grain flows and high density turbidity currents	
Sa1: Graded sandstone	Well-sorted, inverse or normal grading, very fine-very coarse sandstone. Mainly massive, but in some cases with some parallel laminations at the base or faint cross-beds near the top. Cm- to dm-thick beds.	Turbidity current – Bouma TA-C	S4: Inversely or normal graded sandstone
Sa2: Massive sandstone	Poorly-sorted, massive fine-medium sandstone with cm-scale gravel lag at bases. Some cases evidence of weak normal grading. Dm-thick beds.	Medium energy flow regime, bedload transport	S1: Structureless sandstone

Sa3: Interbedded sand and gravel lenses with shell clusters	Interbedded fine sand and gravel lenses (<5 cm thick and <50 cm length), pinching out over 15-150cm. Occasional sub-rounded pebble clasts. Some gravel lenses fine laterally into fine-medium sand. Broken shell fragments, often in clusters within red-coloured gravelly-coarse sand matrix. Dm-thick beds.	Storm current reworking shallow marine sediment and transporting downdip	
Sa4: Planar- and wavy-laminated sandstone	Flat-lying, planar- or wavy-laminated very fine-fine sandstone. Sometimes inversely graded. Cm- to dm-thick beds.	Upper stage plane beds with variable flow conditions	S2: Laminated sandstone
Sa5: Cross-bedded sandstone	Low-angle cross-bedded very fine-medium sand. Medium sand grade lenses (<2 cm long and ~0.5 cm thick). Symmetrical and/or asymmetrical ripples with silt drapes (<0.5 cm). Cm- to dm-thick beds.	Wave or current ripple and dune migration with periods of intermittent quiescence	S3: Cross-bedded sandstone
Sa6: Gravelly sandstone	Poorly-sorted, gravelly coarse sand, some gravelly laminations and small floating pebbles. Sometimes with erosive base. Cm- to dm-thick beds.	Medium energy bedload transport or high density turbidity current	S1: Structureless sandstone
Fi1: Wavy-laminated siltstone	Wavy-laminated, ripple cross-bedded, fine calcareous siltstone with scours and soft sediment deformation. Normal or inverse grading. Cm-width, 10cm-length sand- and mud-filled <i>Planolites</i> burrows. Cm-thick beds.	Occasional turbidity current events – Bouma TD-E – with periods of quiescence for colonisation. Loading from dense conglomerate above	F2: Laminated siltstone
Fi2: Planar-laminated siltstone	Planar-laminated siltstone (cm- to dm-thick beds). Some variations in colour from red - cream – orange.	Suspension fall-out and intermittent dilute turbidity current	F2: Laminated siltstone
Fi3: Red-coloured sandy siltstone	Varying thickness (cm-scale) red-coloured sandy silt.	Palaeosol	F3b: Variegated siltstone
Fi4: Organic-rich, structureless mudstone	Structureless claystone, dark colour - organic rich. Cm-thick beds.	Suspension fall-out with anoxic conditions	
Fi5: Structureless mudstone	Structureless calcareous mudstone. Cream or red coloured. Cm- to dm-thick beds.	Suspension fall-out	F4a: Claystone
Fi6: Interbedded sandstone-mudstone	Interbedded wavy very fine sandstone and white or pink coloured mudstone. Cm-thick beds.	Suspension fall-out and intermittent dilute turbidity current	F3a: Interbedded siltstone

Chapter 5

Syn-rift delta interfan successions: archives of sedimentation and basin evolution

Publication

Barrett, B.J., Gawthorpe, R.L., Collier, R.E.Ll., Hodgson, D.M. & Cullen, T.M. (2019). Syn-rift delta interfan successions: archives of sedimentation and basin evolution. *The Depositional Record*, doi: 10.1002/dep2.95.

Abstract

Models that aim to capture the interactions between sediment supply, base level and tectonism recorded in fan delta successions in rift basins have not considered the stratigraphic archive preserved in interfan areas; yet interfan stratigraphy can provide a complementary record to the fan delta axes. The exhumed Early-Middle Pleistocene Kerinitis and Selinous fan deltas, in the hangingwall of the Pyrgaki-Mamoussia Fault, Corinth Rift, Greece, offer an ideal laboratory for the assessment of interfan architecture. Furthermore, using the geometry of adjacent present-day fan deltas, interfans are classified into three end-members. The classification is based on their lateral separation, which determines the degree of interfingering of topset, foreset and bottomset deposits. Qualitative (facies, stratal geometries, nature of key surfaces) and quantitative (stratigraphic thickness, bedding dip, palaeocurrents, breakpoint trajectories) data were collected in the field and from unmanned aerial vehicle photogrammetry-based 3D outcrop models of the exhumed fan delta successions. The ancient Kerinitis-Selinous interfan architectures record: i) initial westward progradation of the Kerinitis fan delta into the interfan area (Phase 1), ii) subsequent progradation of the Selinous fan delta into the interfan area and asymmetric growth of both fan deltas eastward (Phase 2), iii) stratal interfingering of foresets from both systems (Phase 3), and iv) relative base level fall, erosion and reworking of sediments into the interfan area (Phases 4-5). The K-S interfan evolution is linked to initial net subsidence of the P-M Fault (Phases 1-3) and subsequent net uplift (Phases 4-5) resulting from a northward shift in fault activity. The interfan area provides a more complete stratigraphic record than the proximal axial areas of the fan deltas of the early stages of basin uplift, through higher preservation potential and protracted submergence. Therefore, for the most comprehensive insight into basin evolution, interfan analysis should be undertaken in concert with analysis of the fan delta axes.

5.1. Introduction

The sedimentary successions preserved between adjacent, contemporaneous fluvial, deltaic or deep water fan systems (Fig. 5.1) preserve an alternative stratigraphic archive to the fan axes (Higgs, 1990; Hook et al., 2003; Bhiry & Occhietti, 2004; Leppard & Gawthorpe, 2006; Assine et al., 2015; Turner & Connell, 2018). The interfan area is defined here as the area between two lines that project from the apices of two fan deltas to their intersection at the most distal point of bottomset interfingering (Fig. 5.1). In this area, the fans coalesce from the proximal to distal parts. Identification of the most distal point of bottomset interfingering in modern and ancient systems is challenging, and as such the definition can be considered a theoretical, rather than a measurable limit.

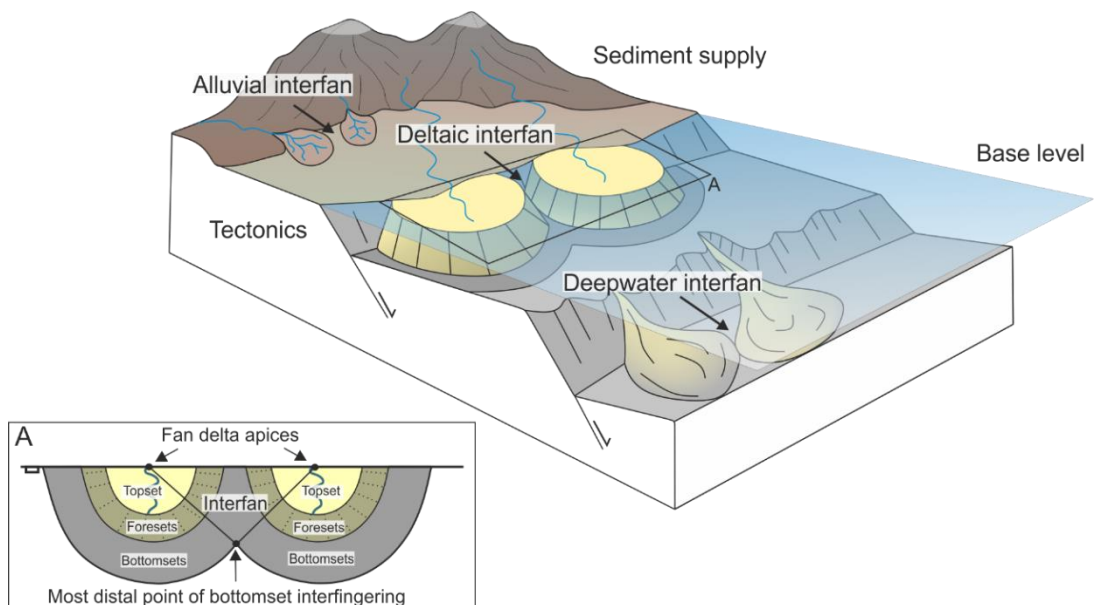


Figure 5.1. Source-to-sink block model with interfan areas highlighted in alluvial, deltaic, and deepwater settings. A: shows deltaic interfans more specifically defined as the area between two lines that project from the two fan delta apices to their intersection at the most distal point of bottomset interfingering.

The interfan areas between fan deltas may record the sedimentary response to relative base level changes, yet are unstudied and therefore remain a missing piece in the published conceptual models that aim to capture the interactions of sediment supply, base level and tectonism in rift basins (Leeder & Gawthorpe, 1987; Gawthorpe et al., 1994, 1997; Gawthorpe & Leeder, 2000,

Leeder et al., 2002; Young et al., 2002). The interfan offers a complementary stratigraphic record to the fan delta axes of relative base level change and tectono-sedimentary evolution. For example, during a relative base level fall, the fan delta axis may become exposed and degraded, but the deeper and more sediment-starved interfan will remain submerged and thus preserve a more complete record of sedimentation and basin evolution. The frontal deepwater setting along the fan delta axis may also record this transition in deepwater sediments, but the interfan area captures the interaction of two adjacent fan deltas through basinal change, as well as offering a more proximal record. The key regressive and transgressive surfaces that mark the pivotal moments in relative base level change can also be expressed differently (e.g. suppressed erosion or thicker condensed intervals) and may be diachronous (Barrett et al., 2018). Thus, a better grasp of interfan sedimentary facies, architecture and stratal surfaces would allow a more complete understanding of along-strike interactions between adjacent fan deltas during basin evolution.

The southern shore of the Gulf of Corinth (Fig. 5.2) offers an ideal field laboratory for exploring interfan architectures, as there are a series of modern fan deltas along the coast, Late Pleistocene lowstand fan deltas that are submerged and imaged in bathymetry data, and a number of exhumed syn-rift fan deltas that formed along normal faults since ~1.8 Ma (Ford et al., 2016; Gawthorpe et al., 2017a). A number of studies focus upon the stratigraphic architecture of the Early-Middle Pleistocene Gilbert-type fan deltas in the Gulf of Corinth: Evrostini/Ilias (Zelilidis & Kontopoulos, 1996; Zelilidis, 2003; Rohais et al., 2007a; 2008; Gobo et al., 2014; 2015), Kryoneri (Gawthorpe et al., 2017b), Vouraikos (Ford et al., 2007), Kerinitis (Ori et al., 1991; Poulimenos et al., 1993; Dart et al., 1994; Gawthorpe et al., 1994; Backert et al., 2010; Gawthorpe et al., 2017b) and Selinous fan deltas (Poulimenos et al., 1993; Barrett et al., 2019). These studies highlight the sedimentary facies distribution and sequence stratigraphic relationships within these deposits, and the role of tectonics, lake level and sediment supply on fan delta development. However, none of these studies address the interfan areas between the fan deltas.

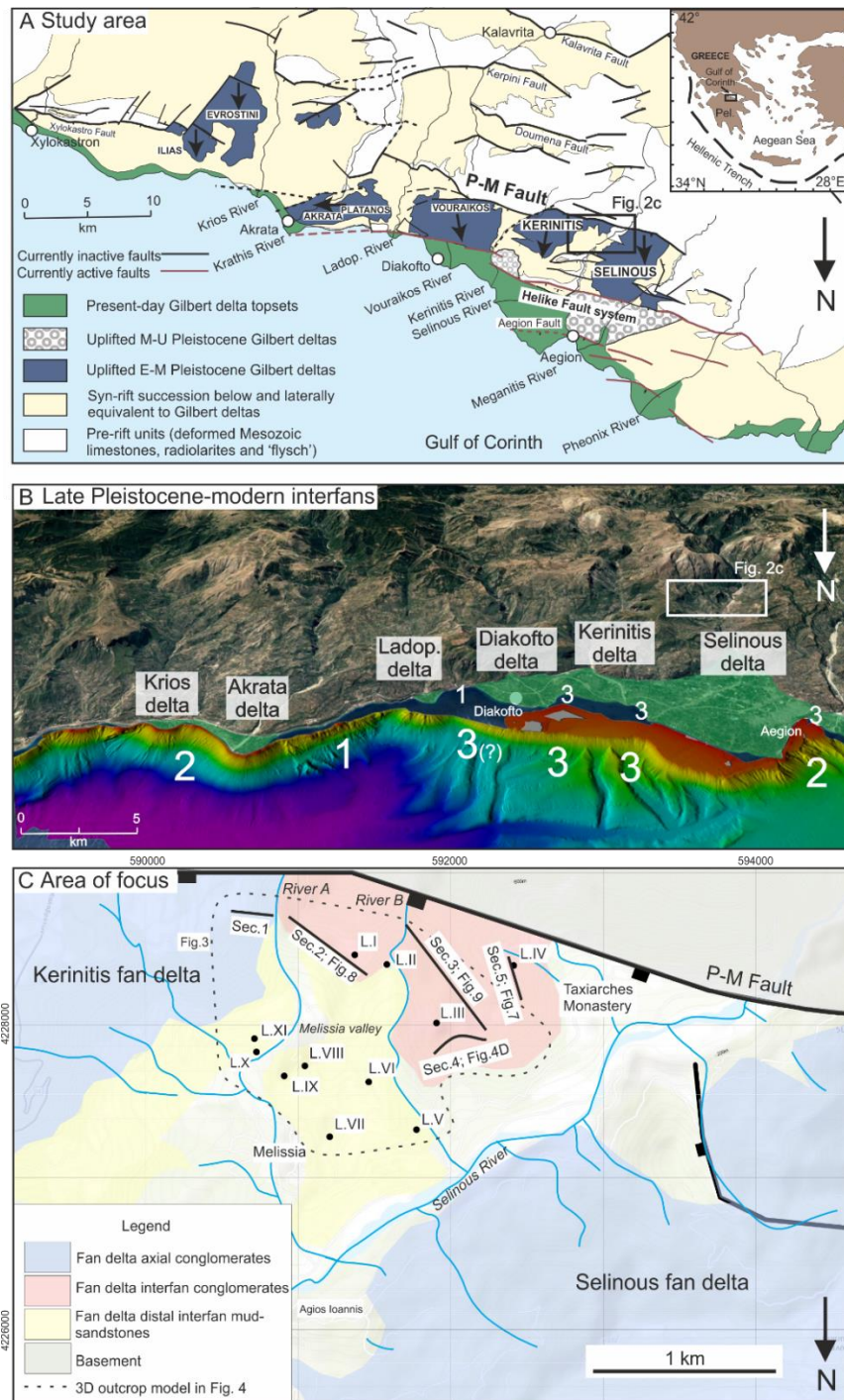


Figure 5.2. A) Location map of southern shore of the Gulf of Corinth with the Early-Middle Pleistocene Kerinitis and Selinous fan deltas highlighted. Modified from Barrett et al. (2019) after Ford et al. (2007; 2013; 2016), Ghisetti & Vezzani (2004) and Gawthorpe et al. (2017a). B) Modern fan deltas on topographic map (Google Earth) and Late Pleistocene examples imaged in bathymetry data. Numbers denote interfan classification according to scheme in Fig. 5.11. Bathymetry data from McNeill et al. (2005) and Cotterill et al. (2002). C) Area of focus with key sections and localities indicated. Position of C is indicated in A and B. Pel. = Peloponnesus. Locations of Figs. (5.) 3, 4, 7, 8 and 9 are indicated.

Here, the focus is placed upon the interfan area between the Early-Middle Pleistocene, Selinous and Kerinitis syn-rift fan deltas located in the immediate hangingwall of the Pyrgaki-Mamoussia Fault. Geometric observations from the associated modern and Late Pleistocene submerged fan deltas are used to inform the analysis. The aim of this paper is to advance our understanding of along-strike interactions in syn-rift settings through analysis of interfan stratigraphy. Using field data and UAV photogrammetry-based 3D outcrop models, the objectives of the study are to: 1) describe and interpret the Kerinitis-Selinous (K-S) interfan evolution from the stratigraphic architecture and sedimentology; 2) propose a classification scheme for ancient interfans based on modern delta geometries; 3) discuss the mechanisms for the observed asymmetry in the ancient and modern fan deltas, and the value of including interfan analysis in sedimentary basin analysis.

5.2. Study area

The Corinth Rift was activated at ~5 Ma (Collier & Dart, 1991; Leeder et al., 2008) and currently accommodates extension rates of up to 5-10 mm/yr across the Gulf of Corinth (Clarke et al., 1997; Briole et al., 2000; Avallone et al., 2004; Floyd et al., 2010). The locus of faulting on the southern coast of the present gulf has migrated northwards over time (Goldsworthy & Jackson, 2001; Leeder et al., 2008; Ford et al., 2013; 2016; Nixon et al., 2016), recording two major rifting phases (Gawthorpe et al., 2017a; Rohais & Moretti, 2017). Rift 1 occurred from 5-3.6 Ma to 2.2-1.8 Ma, and strain was accommodated on the present-day onshore faults. In the west, activity was focussed upon the Kalavrita Fault in Northern Peloponnesos, before activity migrated basinwards onto the Pyrgaki-Mamoussia (P-M) Fault (study area, Fig. 5.2) at ~1.8 Ma (Ford et al., 2016; Gawthorpe et al., 2017a). Rift Phase 2 commenced, and the Kerinitis and Selinous fan deltas formed, before activity migrated from the P-M Fault onto the Helike Fault system around ~0.8 Ma (Ford et al., 2013). Today, strain is primarily accommodated on faults offshore in the Gulf of Corinth (Nixon et al., 2016). Lacustrine conditions prevailed during Rift 1, with a transition from episodic marine incursions to periodically fully-marine conditions during Rift 2 (~0.6 Ma). This occurred as the

Gulf of Corinth opened during interglacial highstands to the Ionian and Aegean seas and into its modern configuration (Freyberg, 1973; Collier, 1990; Collier & Thompson, 1991; Moretti et al., 2004; Rohais et al., 2007b; Ford et al., 2016; Nixon et al., 2016; Gawthorpe et al., 2017a; Rohais & Moretti, 2017).

Siliciclastic sediments sourced from the Hellenide fold and thrust belt (eroded Mesozoic carbonates, radiolarites and Cenozoic turbidites) were transported northwards and deposited syn-kinematically during Rift phases 1 and 2 (Degnan & Robertson, 1998; Ford et al., 2013; Gawthorpe et al., 2017a). The related stratigraphy is split into three groups in the study area; the Lower, Middle and Upper Groups (Rohais et al., 2007a; Ford et al., 2007; 2013; 2016). The Lower Group was deposited during Rift 1, and the Middle and Upper groups during Rift 2. The earliest fluvial and marginal lacustrine deposition occurred from the widespread Kalavrita River system, now preserved in the Lower Group. Subsequently, giant syn-rift fan deltas prograded into the hangingwalls of the major faults: Platanos, Vouraikos, Kerinitis and Selinous (from east to west) in the hangingwall of the P-M Fault, and Evrostini/Ilias to the east of the study area (Fig. 5.2).

The P-M Fault hangingwall deltas constitute the Middle Group, deposited during early Rift 2 (Gawthorpe et al., 2017a). The age of these deltas is constrained to ~1.8-0.7 Ma based on pollen analysis at the Vouraikos fan delta (Ford et al., 2007). These syn-rift sediments on the P-M Fault terrace are the target of this study. Previous studies interpret the mudstone-sandstone deposits in Melissia Valley (Figs. 5.2 and 5.3) as the fluvio-lacustrine Melissia Formation (Backert et al., 2010), constituting part of the older Lower Group (Ford et al., 2007; 2013). These authors describe this succession as being unconformable with overlying fine-grained deposits of the Zoodhochos Formation within the Middle Group, which are interpreted to represent distal turbidites in a bottomset setting (Backert et al., 2010). However, the present study did not observe substantial facies variations between the deposits of the Zoodhochos and Melissia formations, nor was the erosive contact reported by Backert et al. (2010) identified. An alternative interpretation is that all of the fine-grained deposits in Melissia Valley represent fan delta bottomsets to the Selinous and Kerinitis foresets updip (Middle Group), and are equivalent to the Zoodhochos Formation of

Backert et al. (2010). Projection of key surfaces within the Selinous foresets into the bottomsets using 3D outcrop models has allowed their correlative foreset packages to be approximately constrained. In addition, the base of the Selinous fan delta axis directly overlies basement rocks; fine-grained fluvio-lacustrine deposits are absent. The Upper Group consists of younger marine terraces and smaller Gilbert-type fan deltas with erosive bases, primarily deposited in the hangingwall of the Helike Fault system (Rohais et al., 2007a; Ford et al., 2007; 2013; 2016).

The focus of this study is the eastern part of the Selinous fan delta and the western part of the Kerinitis fan delta, in the hangingwall of the P-M Fault (Middle Group) (Figs. 5.2C and 5.3). The Kerinitis fan delta is positioned slightly to the west of the P-M fault centre and the Selinous fan delta is positioned ~4 km from the western fault tip. Barrett et al. (2019) quantify the minimum period of deposition, average subsidence and sedimentation rates at the Kerinitis and Selinous fan deltas as >451 kyrs and 615 kyrs, and 0.65 m/kyrs and >1.77 m/kyrs, respectively, based upon stratigraphic observations. Numerical modelling was used to quantify the amplitude of climate-induced lake level changes in Lake Corinth during the Early-Middle Pleistocene at 10-15 m (Barrett et al., 2019). Previous studies focus on the facies and stratigraphic architecture of the axial sections of the Kerinitis and Selinous fan deltas (Dart et al., 1994; Gawthorpe et al., 1994; Backert et al., 2010; Gawthorpe et al., 2017b; Barrett et al., 2019).

The study area consists of a ~300 m high conglomeratic cliff with a ~2 km wide, main north-facing exposure (Sections 1-3; Figs. 5.2C and 5.3), and additional west- (Section 4; Figs. 5.2C and 5.3) and south-facing (Section 5; Figs. 5.2C and 5.3) exposures that provide 3D constraints. Section 1 exhibits thick, west-dipping ('W-dipping') units from the Kerinitis fan delta. While these are considered in the interpretation, they are not characterised within the stratigraphic framework due to limited access and difficulty in obtaining reliable UAV-photogrammetric data in that region. The units within Section 2 are generally thinner and stratigraphically higher than the units in Sections 3-5, and both east-dipping ('E-dipping') and 'W-dipping' units are present with interfingering geometries. This is considered to be the centre of the interfan area. Section 3 consists of several thick 'E-dipping' foreset units from the Selinous fan delta. Section 4 is a

curved, generally west-facing section and Section 5 faces SW. Both Sections 4 and 5 consist of 'E-dipping' units. The Old Taxiarches Monastery is built into the Selinous foresets in Section 5. Here, part of the conglomeratic section and a thin, fine-grained interval is accessible (Locality IV; Figs. 5.2C and 5.3). Otherwise, access to the interfan sections is limited. Associated fine-grained exposures can be found in the valley to the north of the cliff, near Melissa (Localities V-XI; Figs. 5.2C and 5.3) and represent the fan delta bottomsets.

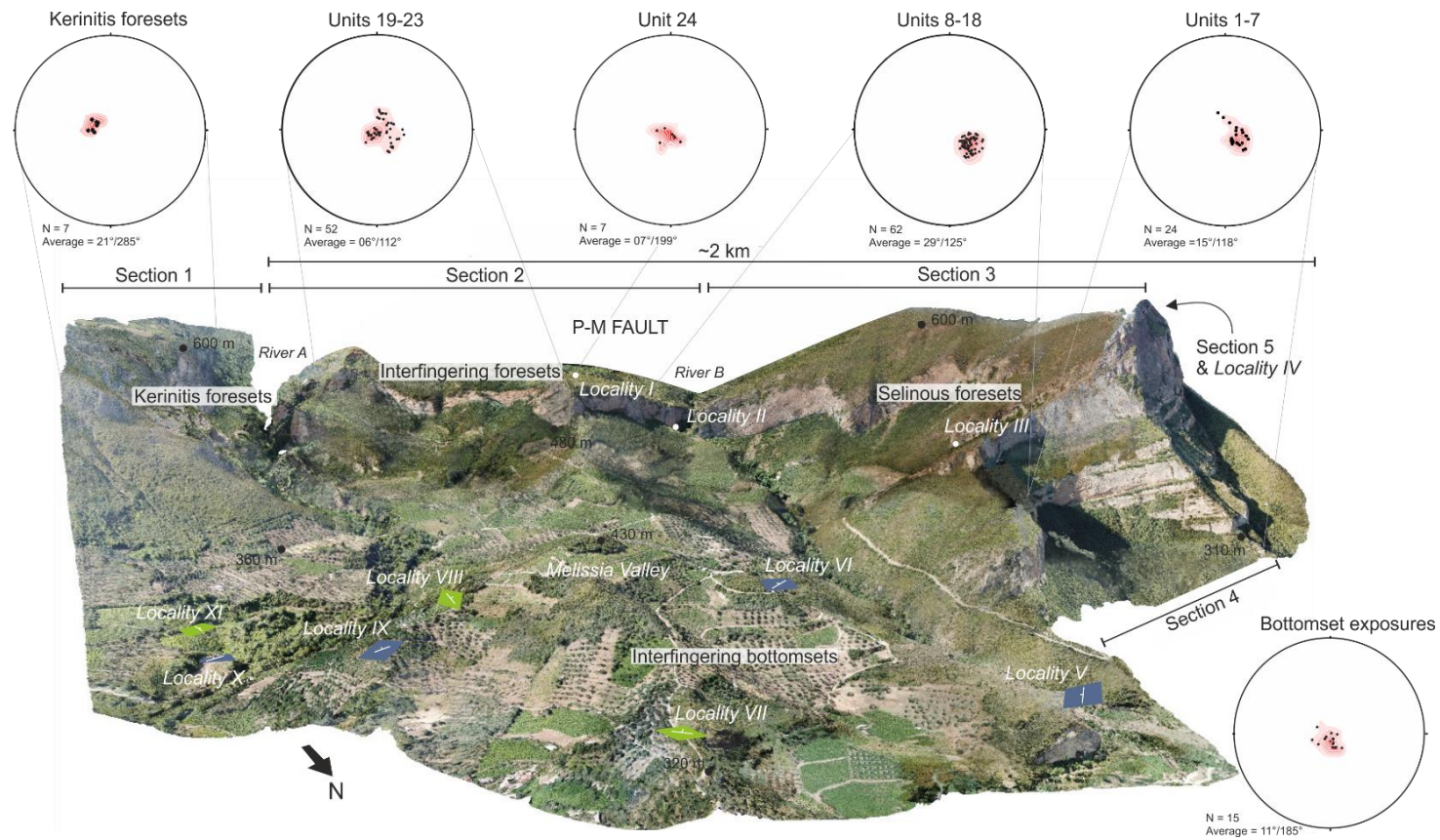


Figure 5.3. Study area and data overview. 3D outcrop model of the interfan study area was created using UAV-photogrammetry data and Agisoft Photoscan software. Stereonets, Sections 1-5, Localities I-XI (bottomset outcrops with coloured planes – created using LIME software) are presented. Green planes represent W-dipping (Kerinitis-derived) outcrops. Blue planes represent E-dipping (Selinous-derived) outcrops. Dip data is taken from the field and from 3D outcrop model structural planes in LIME software and presented with southern hemisphere-projected stereonet plots using Stereonet software. N = number of data points.

5.3. Methodology

A DJI Mavic Pro drone was used to collect the photogrammetric data that was augmented by annotated photograph panels and field sketches. Agisoft Photoscan/Metashape and LIME software were used to build and interpret the 3D outcrop models (e.g. Fig. 5.3). Sedimentological and structural data were collected directly in the field where access allowed and complemented by outcrop model measurements where the exposures were inaccessible. Measured sections of sandstone successions were collected at millimetre to centimetre-scale to document lithology, grain size, sedimentary structures and the nature of bedding contacts. Conglomeratic units were logged at decimetre-scale, with the support of sketches to capture the geometry of large-scale features, such as the continuity of surfaces. Palaeocurrent data were collected from ripple cross laminations, clast imbrication, cross-bed plane measurements and dips of foresets generated from sediment gravity flows. Presented data are uncorrected due to the lack of a reliable palaeo-horizontal datum, but the steepest tectonic tilt is $\sim 12^\circ$ (S).

Figure 5.4 outlines the methodology for extracting data from 3D outcrop models, which are able to represent measurable objects with a lower limit of ~ 10 cm. The stratigraphic framework was established from interpretation of the interfan cliff section using LIME software to map stratal surfaces. The 3D outcrop models allowed qualitative (detailed stratal geometries, nature of major surfaces and accurate correlation of surfaces around topography) and quantitative (dip data from bedding planes, stratigraphic thickness, topset-foreset breakpoint trajectories and height of foresets) data collection (Fig. 5.4). In total, 167 bedding dip measurements were collected in the field and using LIME software-based mapping of the 3D outcrop models (Fig. 5.3). Multiple measurements within each unit were taken for averages to be calculated. The data have not been re-orientated in the absence of a reliable palaeo-horizontal datum. Bedding data collected from the outcrop models were validated against field measurements at the Old Taxiarches Monastery (Fig. 5.2). The east and west components of dip are used to differentiate between beds or units from the Selinous and Kerinitis fan delta systems, respectively. Bedding measurements often have north or south dip components as well, but as both fan deltas prograde northward and both are

back-tilted to the south towards the P-M fault, the east and west components are the most useful diagnostic criteria.

Correlation of surfaces around topography and constraining the stratigraphic position of associated bottomset outcrops in the valley were refined with the use of 3D outcrop models. By projecting planes following the dip of the foresets in Sections 3 and 4 into Melissia Valley, the E-dipping (Selinous) fine-grained, bottomset outcrops could be correlated to their updip foreset counterparts in the interfan area. A typical clinof orm profile shallows in dip at the foreset-bottomset transition. Therefore, the constant dip of the projected foreset planes mean that the units assigned to bottomset deposits are approximate, but are more likely to be associated with lower units than higher units. Where the bottomset outcrops are W-dipping, they are derived from the Kerinitis fan delta and cannot be tied updip, but instead their relative position to Selinous units is recorded.

5.4. Results

5.4.1. K-S facies association characterisation

Eight facies associations (FAs) characterise the Selinous and Kerinitis fan deltas, based on geometric position (topset-bottomset) and depositional environment (Table 5.1; Figs. 5.5-7). The main fan delta units are constructed from conglomeratic, fluvial and shallow water topset and foreset facies associations (FA 1a-b; 2a-b; 3). The facies associations observed in the interfan area are the focus: the foreset facies association that occupies the majority of the interfan cliff sections (FA 3), and the bottomset facies associations that are found in Melissia Valley, and in the Unit 8-9 fine-grained interval/flooding surface (FA 4a). An additional facies association to the scheme of Barrett et al. (2019) is FA 2c (upper shoreface, which occurs in the shallow water topset; Locality I; Fig. 5.2; Table 5.1). Four facies (Table A in Appendix) have been added to the bottomset facies association of Barrett et al. (2019).

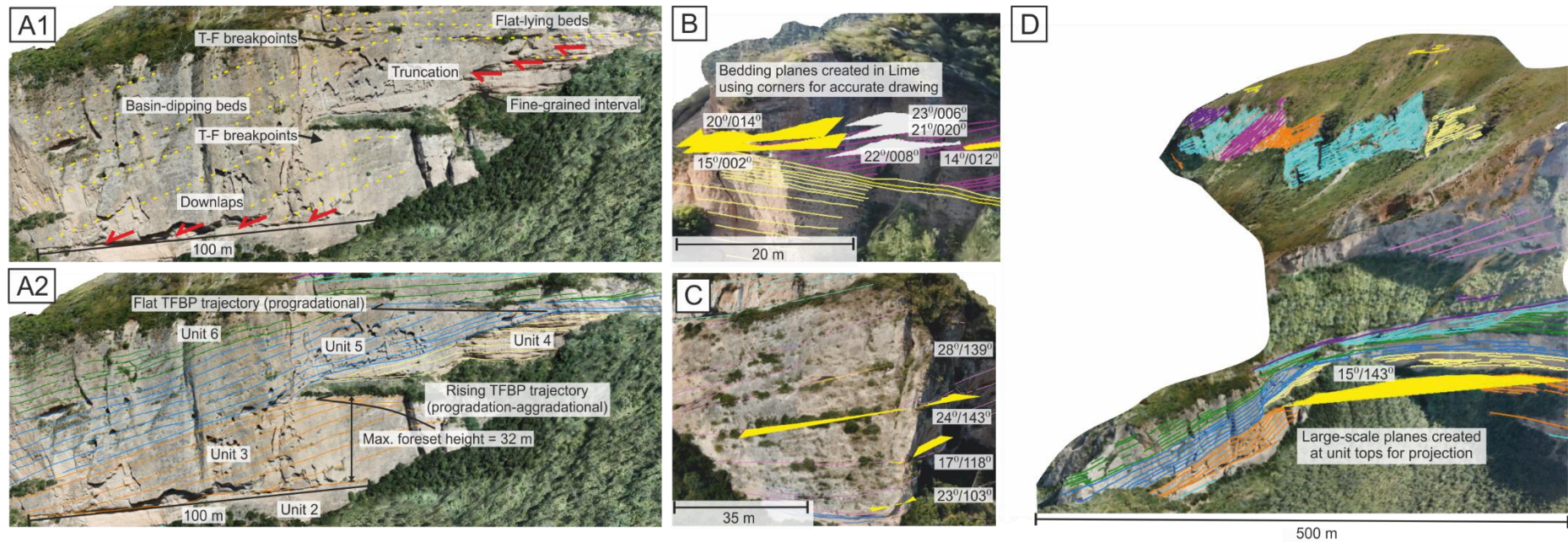


Figure 5.4. Methodology for stratigraphic architecture interpretation and for obtaining quantitative information from UAV photogrammetry-based 3D digital outcrop models. A1: observations from part of Section 4, where remnants of fine-grained intervals, truncation, and clear stratal termination geometries allow units to be divided and contacts to be classified. Topset-foreset breakpoints (TFBPs) can be identified. A2: interpretation of section shown in A1 with TFBP trajectories and foreset heights indicated. B and C: demonstrations of obtaining accurate dip data (convention: dip/dip direction) from small-scale bedding planes (assured using field data) in parts of Section 2. D: large-scale planes from unit tops are created and used for projecting across valleys to assist correlations and constraining the stratigraphic position of bottomset outcrops (Sections 3 and 4). 3D outcrop models created in Agisoft Photoscan and interpreted in LIME software.

Table 5.1. Facies associations at the Selinous and Kerinitis fan deltas (modified from Barrett et al., 2019). See Table A in the Appendix for facies information.

FA code	Constituent facies	FA interpretation	Sub-association
1a	Co1, Co2	Fluvial topset	Channel-fill
1b	Co1, Sa2, Sa6, Fi3		Delta plain
2a	Co4, Co5	Shallow water topset	Beach barrier
2b	Co1, Co4, Co5, Co7, Sa1, Sa2 and Sa4		Upper shoreface
2c	Co5		Lower shoreface
3	Co3, Co4, Sa4	Foreset	
4a	Sa1-6, Fi1-2, Fi4-8	Bottomset	Deep-water
4b	Co6, Sa1-6, Fi1, Fi2		Shallow-water

5.4.1.1. FA 1: Fluvial topsets

Two fluvial topset facies associations are identified from the fan delta axes: FA 1a) channel-fill, and FA 1b) delta plain depositional environments. Channel-fill (FA 1a) is the most common and comprises poorly-sorted, sub-angular to sub-rounded, sandy gravel-cobble conglomerate with clast imbrication and erosive bed bases. These deposits are interpreted to represent bedload deposits during high energy fluvial flow regime. The delta plain FA 1b comprises poorly-sorted, sub-angular, sandy gravel-cobble conglomerates interbedded with normally graded, gravelly-coarse sand beds. Red palaeosols (centimetre-thick) are found between gravelly coarse sandstone beds (Barrett et al., 2019). A variable, periodic flow regime is envisaged, with periods of subaerial exposure indicative of overbank deposits in a delta plain environment.

5.4.1.2. FA 2: Shallow water topsets

The shallow water topset (FA 2) is divided into three sub-associations: 2a) beach barrier, 2b) upper shoreface, and 2c) lower shoreface. Only the upper shoreface (FA 2b) is observed in the interfan area, during the latest stage. The beach barrier (FA 2a) consists of a mounded body and internal bi-directional metre-scale cross-beds, with well-sorted, open-framework and mainly rounded pebbles. This indicates textural maturity and character typical of beach reworking. The lower shoreface FA 2c comprises metre-scale bi-directional, asymptotic cross-beds resembling

hummocky-cross stratification (Barrett et al., 2019). These deposits are characteristic of storm reworking below fair weather wave base.

The upper shoreface (FA 2b) is identified in the interfan area (Locality I, Section 2, Fig. 5.2; logs and photographs in Fig. 5.5). Locality I is situated 650-800 m from the fault and the FA 2b are the highest and youngest rocks encountered. Figure 5.5 presents representative logs and photographs of two of the exposures; one where cross-beds dip eastward and are part of the Selinous fan delta, and one where cross-beds dip westward and are part of the Kerinitis fan delta. Despite opposing bedding dips between the various outcrops at Locality I, the facies are similar, comprising interbedded fine sand to pebble conglomerate (decimetre-scale) beds, between thicker (metre-scale) and coarser grained conglomerates at the bases and tops. Several pebbly gravel beds pinch out laterally over 1-2 m with slight convex-up geometries. These bedforms generally have erosive bases and are matrix- and clast-supported, with sub-angular to rounded clasts. Beds are well-sorted, either normally or inversely graded and sands contain gravel and pebble clasts. The thicker conglomeratic beds generally coarsen upwards (sometimes normally-graded) and are poorly-sorted, mostly clast-supported, pebble-cobble grade with sub-rounded to rounded clasts (<18 cm). Clasts are imbricated following the bedding dip (e.g. Log 2; Fig. 5.5).

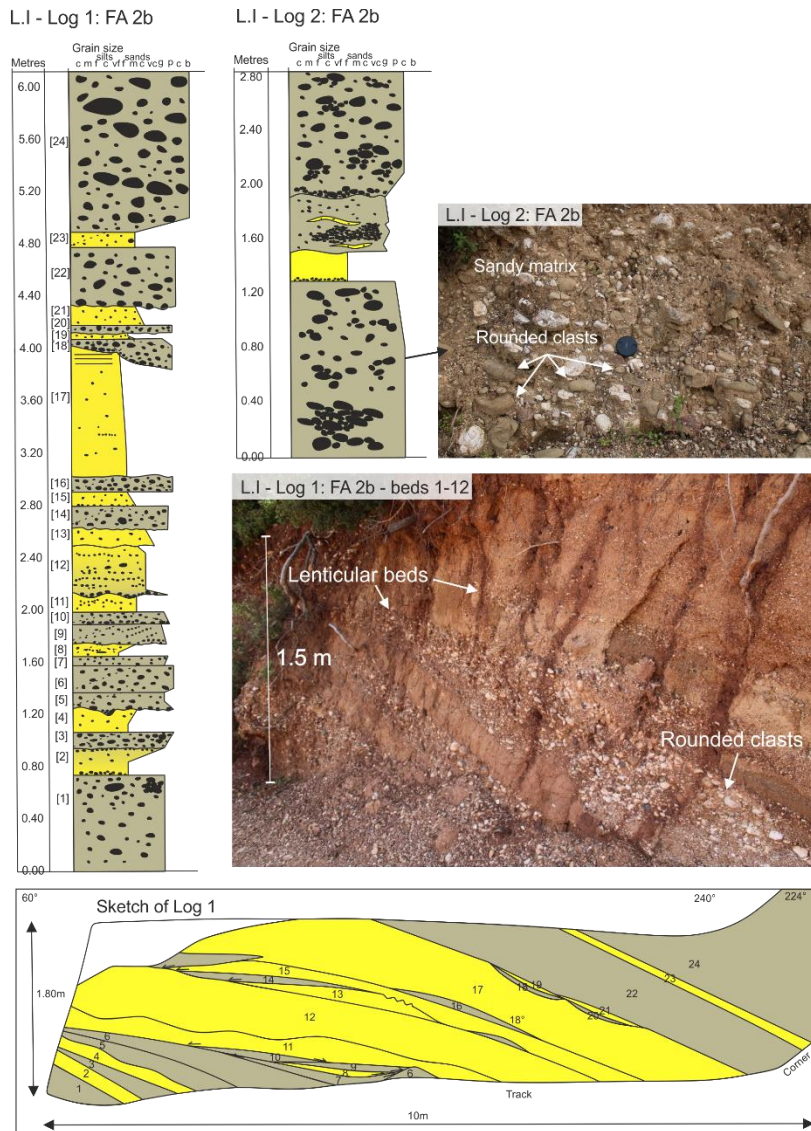


Figure 5.5. Shallow water topset – upper shoreface facies association (FA 2b). Logs 1 and 2 and associated photographs show two representative outcrops from Locality I. The bracketed numbers on Log 1 correspond to the numbered beds on the outcrop sketch. Yellow = sandstone; grey = conglomerate. Log 1 and Log 2 outcrops have an average bed dip/dip direction of $17^{\circ}/270^{\circ}$ (Kerinitis-derived) and $05^{\circ}/160^{\circ}$ (Selinous-derived), respectively.

These deposits are interpreted to represent a variable, but generally high energy regime. The lack of fine-grained sediment, and the observed lenticular geometry of the beds, maturity of the clasts and spatial context within a flat-lying unit, suggests reworking of material in the interfan topset area and bedform migration by wave-related currents. The sediments are interpreted to have been deposited in an upper shoreface environment with longshore transport as the main depositional process. Similar processes are observed at the modern Selinous and Meganitis fan deltas in the

Gulf of Corinth, as sediments are reworked with the prevailing westerly wind/wave direction into interfan embayments (Fig. 5.2A).

5.4.1.3. FA 3: Foresets

The foreset facies association was described previously by Backert et al. (2010) and Barrett et al. (2019) and occupies most of the interfan cliff section. It comprises well- to poorly-sorted, clast-supported and open-framework, sub-rounded, mainly pebble-cobble conglomerates. Scours and inverse grading are common. Any matrix is sand-gravel grade, and locally clasts are imbricated. Foresets comprise steep, basinward-dipping (22° - 25°) beds with heights ranging from ten to a few hundred metres, dependent on palaeo-water depth (and subsequent erosion). The processes responsible are interpreted to be dominated by sediment gravity flows (conglomerate-rich inertial grain flows to non-cohesive debris flows) on the delta foresets (Postma, 1984; Nemeč, 1990; Orton & Reading, 1993; Sohn et al., 1997; Sohn, 2000; Rohais et al., 2008; Gobo et al., 2015). In the interfan, the foresets are accessible and described at Localities II and III on Section 3 and Locality IV on Section 5 (Figs. 5.2C and 5.3).

5.4.1.4. FA 4: Bottomsets

Bottomset deposits occur in relatively shallow water when delta clinothems build out over a previous fan delta topset following a transgression (shallow water bottomsets) and in deeper water, basinward of the foreset slope, when it builds past the topset-foreset breakpoint (deep water bottomsets). The interfan bottomset deposits here are characterised within this scheme and provide further insight into the processes at the toe of the foreset slope in interfan areas.

Within both shallow and deep bottomset facies associations, pebble-cobble horizons are present within fine-grained sections, representing sediment gravity flows or rock falls. In other cases, thicker beds are present that comprise poorly-sorted, matrix-supported (fine-coarse sand), graded, gravel-boulder conglomerates with erosive and/or loaded bases and occasional injectites in the underlying beds (Fig. 5.6). These deposits are interpreted as debrites sourced from the delta foresets.

5.4.1.4.1. FA 4a: Deep water bottomsets

Deep water bottomsets (FA 4a) comprise interbedded sandstones and calcareous mudstones (FA 4a and 4b in Barrett et al., 2019). Soft sediment deformation features, such as convolute laminations at the upper contact with overlying conglomerates are common. At the fan delta axes, the sandstones contain wavy laminations, inverse grading, slightly erosive bases and localised gravel lags (Backert et al., 2010; Barrett et al., 2019). In the interfan area, the more extensive and thicker exposures allow this FA to be characterised further. Representative logs and photos are presented in Figure 5.6. Locally, thin, current-ripple laminated sandstones are draped by black organic material (e.g. Locality X; Fig. 5.6), or intercalated with decimetre-scale, organic-rich mudstone-siltstone beds (e.g. Locality VIII; Fig. 5.6). Thicker normally graded sandstone beds (~5-10 cm) with planar and wavy-laminations, gravel and mudstone clasts, and broken and whole brachiopod shells (<2 cm diameter) are common.

Much like the fan delta axes, the conglomeratic interfan succession is punctuated by thin (<2 m) fine-grained intervals. The only fine-grained interval that is accessible in the interfan area is exposed in Section 5 (Locality IV), within the Old Taxiarches Monastery (Fig. 5.7). The section comprises a coarsening-upwards succession of mudstone to gravel, overlain by an erosional ~1 m thick, poorly sorted, clast-supported gravel-cobble conglomerate (mainly large pebble) with sub-rounded to sub-angular clasts. The mudstone-siltstones at the base of the section are planar and wavy laminated. There are two thin, normally graded sandstones before a dark, organic-rich silty mudstone. The mudstone is overlain by lower medium sandstone (0.8-0.9 m) containing gravel and broken shell lenses (gravelly-coarse sand matrix) with evidence for soft sediment deformation (Fig. 5.7). The interval is positioned basinward of the topset-foreset breakpoint and between two units of high (>100 m), steeply-dipping foresets, suggesting a relatively deep water position that is below wave base, even allowing for changes in base level.

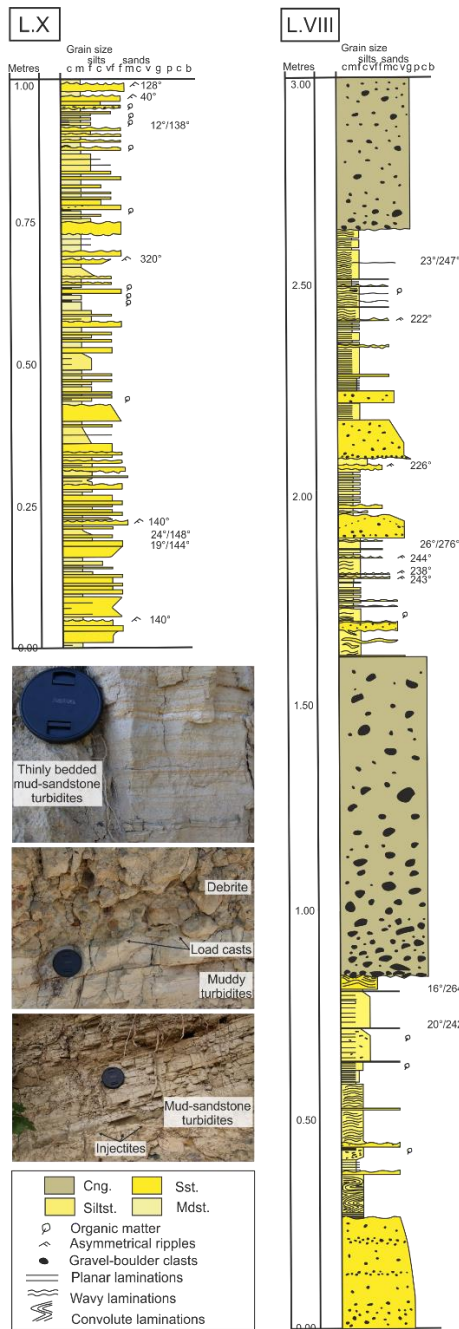


Figure 5.6. Representative bottomset logs from Localities L.X and L.VIII (Figs. 5.2C and 5.4) in Melissia valley (FA 4a). Mudstone-sandstone turbiditic successions with occasional debrites are shown. The sandstone-mudstone content is variable between them. Palaeocurrent directions suggest input from both Kerinitis and Selinous systems and in some cases with a southerly component, suggesting redirection from local topography. Photographs illustrate some of the features in the logs. Cng = conglomerate, Sst = sandstone, Siltst. = siltstone, Mdst = mudstone.

L.IV - FA 4a - Deep water bottomsets
 Fine-grained interval (between Units 8-9)



Figure 5.7. Section 5 and Unit 8-9 fine-grained interval character at Locality IV. Photographs of foreset facies association (FA 3). Log and photographs of distal bottomset facies association (FA 4a) and facies Sa3 (Table A, Appendix) therein.

The sandstones are interpreted to be turbidites, with finer-grained beds representing quiet periods between events, or dilute turbidity currents. Some outcrops have a narrow palaeocurrent dispersal pattern (e.g. Locality VIII, Fig. 5.6), which implies the deposits are inherited from a single system. Others have multiple palaeocurrent directions between beds (e.g. Locality X, Fig. 5.6) implying both Kerinitis and Selinous fan delta sources (Fig. 5.6). In addition, a number of palaeocurrent measurements have a southerly component, opposite to the regional trend, which could indicate flow reflection and deflection from local topography (e.g. Potter & Pettijohn, 1977; Kneller et al., 1991; Lomas & Joseph, 2004; Bell et al., 2018).

5.4.1.4.2. FA 4b: Shallow water bottomsets

Barrett et al. (2019) previously classified the shallow water bottomset (FA 4b) as coarse (sand to gravel-grade) sediments with multiple and diverse sedimentary structures, such as symmetrical and asymmetrical ripple laminations, wavy and planar laminations, dune-scale gravel cross-beds and soft-sediment deformation, indicating sediment gravity flows and wave reworking operating at the base of slope in shallow water. This facies association is identified at the fan delta axis (Barrett et al., 2019), but not in the interfan area. Some bottomset deposits are observed in Section 2 of the interfan area (Fig. 5.8) at the downdip termination of relatively short foresets that could exhibit FA 4b, but it is not possible to access them to constrain the facies.

5.4.2. Stratigraphic architecture

5.4.2.1. Key stratal surfaces

Key surfaces were identified in the field and 3D outcrop models, and are used to subdivide the interfan succession into stratal units associated with both the Selinous and Kerinitis fan deltas. Key surfaces are recognised based on the presence of fine-grained deposits, deeply erosional surfaces and/or evidence of onlap, downlap, offlap or truncated stratal relationships. Fine-grained intervals (<2 m thick) are apparent between the delta topsets, with some remnants between foreset units, both in the fan axes and in the interfan area. The interpretation of each surface is described as either confident or uncertain.

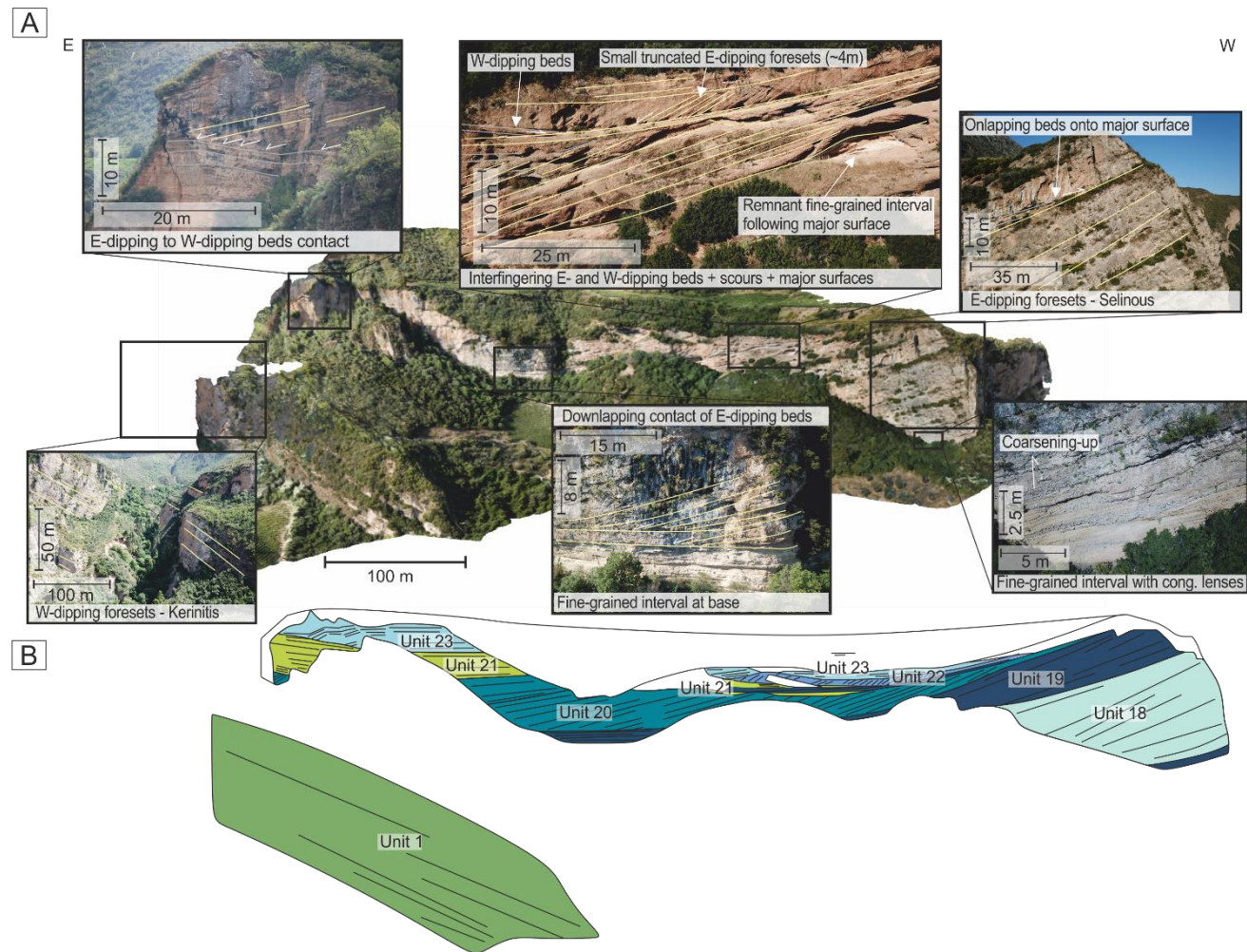


Figure 5.8. A) Key stratigraphic observations of Section 2. E-dipping beds are Selinous-derived and W-dipping beds are Kerinitis-derived. B) Stratigraphic framework of the central interfan face – Units 18-23 (Section 2). 3D outcrop model created in Agisoft Photoscan.

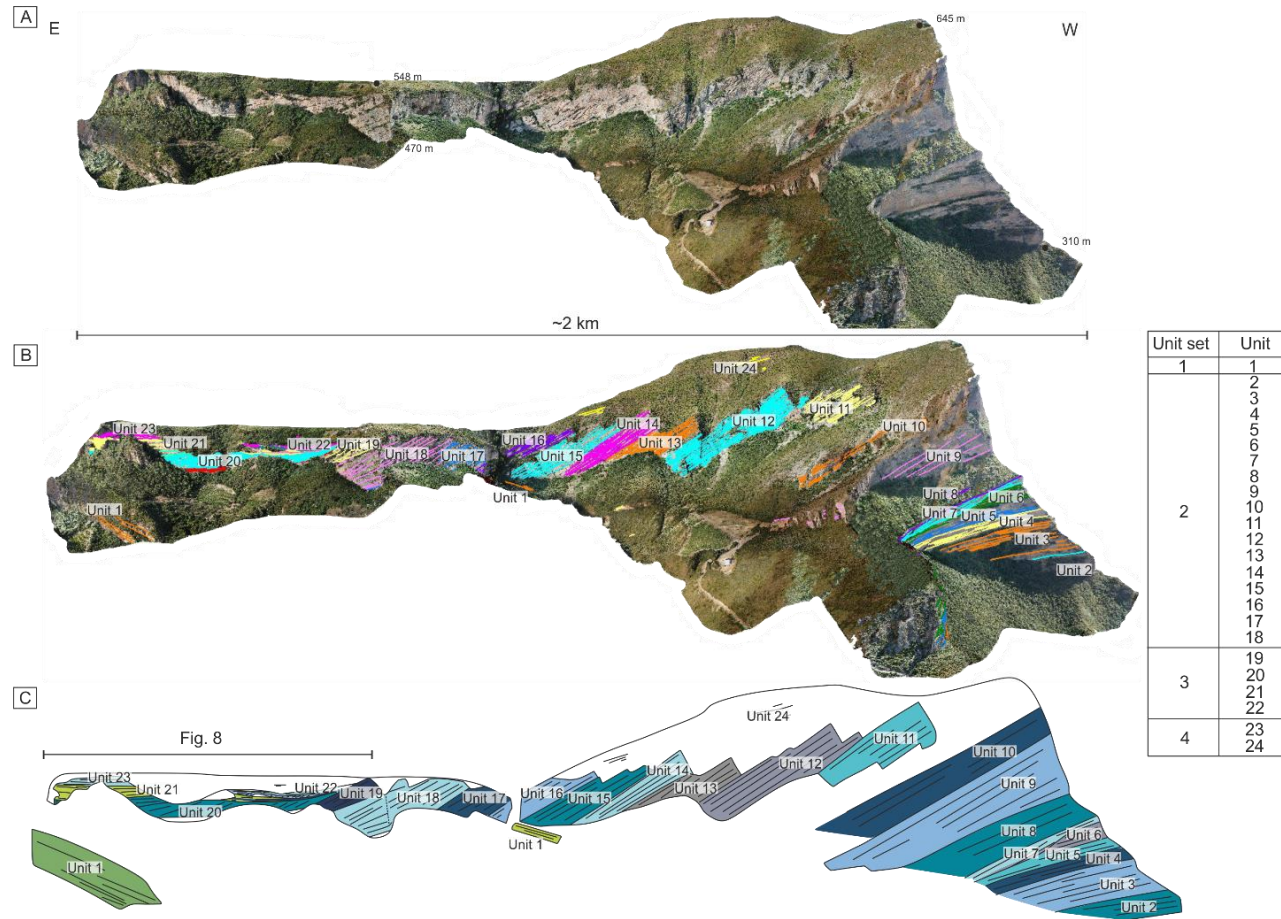


Figure 5.9. Stratigraphic framework of entire north-facing interfan cliff section (Sections 2-4). A: clean 3D outcrop model. B: interpreted 3D outcrop model with stratigraphic framework - Units 1-24. C: schematic cross-section of stratigraphic framework. Blues indicate units from Selinous; green indicates unit from Kerinitis. 3D outcrop models are UAV-photogrammetry based, built in Agisoft Photoscan and interpreted with LIME software. Inset table shows the corresponding units within the four unit sets.

Table 5.2. Stratigraphic information of the units in the K-S interfan area.

Unit	Observed position of unit	Average dip/dip dir.	Nature of basal contact	Top contact interp.	Fine-grained interval at top? (Y/N)	Nature of top contact	Observation type for contacts	Stratigraphic thickness	Foreset height	T-F breakpoint apparent? (Y/N)	T-F breakpoint trajectory
1	Section 2 and 3	20°/345°	Not exposed	Confident	N	Downlapped by overlying, E-dipping beds	Multiple 2D	> 60 m	> 100 m	N	
2	Section 4	12°/140°	Not exposed	Confident	Y	Conformable contact with thin (<2m) fine-grained interval at top	2D	> 18 m; Max. preserved 35 m		N	
3	Section 4	14°/074° 15°/143°	Slightly erosive contact with downlapping beds onto the fine-grained interval between Units 2 and 3	Confident	Y	Conformable contact with thin (<2m) fine-grained interval at top	2D	33 m	32 m	Y	Progradation-aggradation
4	Section 4	15°/075° 15°/150°	Erosive contact with fine-grained interval	Confident	N	Erosive	2D	16 m	> 8 m	Y	Aggradation
5	Section 4	17°/088° 17°/146°	Erosive contact in NE-dipping region and conformable in SE-dipping region	Confident	N	Conformable contact with Unit 6	2D	8-22 m	> 45 m	Y	Progradation
6	Section 4	25°/104°	Conformable	Confident	Y	Erosive	2D	Max. preserved 25 m	> 45 m	N	
7	Section 4	26°/133°	Erosive	Confident	N	Slightly erosive		< 23 m		N	
8	Section 4 and 5	22°/136°	Erosive	Confident	Y	Conformable contact with thin (<2m) fine-grained interval at top	Multiple 2D	~35 m		N	
9	Section 4 and 5	27°/117°	Slightly erosive contact with fine-grained interval	Confident	N	Poorly imaged at top of outcrop model	Multiple 2D	90 m	> 50 m	N	

Unit	Observed position of unit	Average dip/dip dir.	Nature of basal contact	Top contact interp.	Fine-grained interval at top? (Y/N)	Nature of top contact	Observation type for contacts	Stratigraphic thickness	Foreset height	T-F breakpoint apparent? (Y/N)	T-F breakpoint trajectory
10	Section 3	29°/111°	Appears conformable in western section	Uncertain	N	Poorly exposed	2D	< 80 m	> 100 m	N	
11	Section 3	34°/140°	Poorly exposed	Uncertain	N	Dip and geomorphological change	2D	~60 m	> 100 m	N	
12	Section 3	36°/111°	Dip and geomorphological change	Uncertain	N	Geomorphological surface - cut back into cliff	2D	~65 m	> 90 m	N	
13	Section 3	38°/135°	Geomorphological surface - cut back into cliff	Confident	Y	Conformable contact with fine-grained interval	2D	~43 m	> 90 m	N	
14	Section 3	37°/125°	Erosive	Confident	Y	Conformable contact with fine-grained interval	2D	~30 m	> 80 m	N	
15	Section 3	31°/111°	Slightly erosive	Confident	Y	Conformable contact with fine-grained interval	2D	~40 m	> 50 m	N	
16	Section 2 and 3	27°/123°	Conformable	Uncertain	N	Conformable	Multiple 2D	~30 m	> 50 m	N	
17	Section 2	26°/134°	Conformable	Confident	Y	Erosive and fine-grained interval present	2D	~65 m	> 50 m	N	
18	Section 2	24°/125°	Erosive in places and coarsens up from underlying fine-grained interval	Confident	Y	Slightly erosive and remnants of fine-grained interval	2D	~58 m	> 50 m	N	
19	Section 2	26°/127°	Slightly erosive and remnants of a fine-grained interval	Confident	Y	Erosive and fine-grained interval present	2D	~27 m	> 40 m	N	
20	Section 2	16°/073°	Downlaps underlying erosive surface and fine-grained interval	Confident	N	Erosive	2D	16-26 m	> 25 m	N	

21	Section 2	12°/247° 09°/196° 08°/231° 14°/133° 14°/236°	Erosive	Confident	N	Conformable	2D	7-16 m		N
22	Section 2	28°/148°	Downlapping Unit 21	Confident	N	Erosive	2D	< 4-5 m	> 4 m	N
23	Section 2	19°/015°	Truncates Unit 22 in central part and downlaps Unit 21 in eastern part	Uncertain	Not exposed	Not exposed	2D	> 18 m		N
24	Section 3	15°/113°	Not exposed	Not exposed	Not exposed	Not exposed	2D	> 20 m		N

The nature of each surface is described in Table 5.2 and examples from Section 2 are presented in Figure 5.8. Units 1-9 (Section 4; Fig. 5.2C and Fig. 5.9) and 13-15 (Section 3; Fig. 5.2C and Fig. 5.9) have top contacts that have been identified confidently as key surfaces. The top of Unit 1 is a major downlap surface (Unit 15). Fine-grained intervals are preserved in places at the tops of Units 2, 3, 8 and 13-15, despite their position in the dynamic foreset region where fine-grained material has a low preservation potential. Units 3-5 have topset-foreset breakpoint trajectories exposed, suggesting a transitional position between delta topsets and foresets, but generally the interfan is characterised by steeply-dipping, foreset units. Erosive surfaces that clearly truncate underlying foresets are present at the tops of Units 4, 6 and 7. The interpretation of the top contacts of Units 10-12 and 16 are uncertain. Units 17-22 have confident key surfaces identified at their tops. Surfaces at the tops of Units 17-19 are erosive and fine-grained intervals are preserved. Erosional surfaces are more pervasive towards the top of the section and fine-grained intervals are not present between the upper units (20-22). The tops of Units 23 and 24 are not exposed.

5.4.2.2. Key stratal surface interpretation

The base of each fine-grained interval is interpreted to represent a transgressive surface, although the lateral extent of the surfaces are unknown. Fine-grained intervals are present between units in all of the fan deltas in the hangingwall of the P-M Fault, but due to lack of age constraint it is not possible to correlate the surfaces. Between Units 8-9, an organic-rich silty mudstone bed separates graded sandstones in a generally coarsening-upward, mudstone to gravel sequence. This could be interpreted to contain a maximum flooding surface, but the regional continuity of the surface is unknown. The surface is overlain by storm reworked shallow marine deposits (overlying broken shell fragments in gravelly sand lenses) and turbidites, likely associated with the progradation of the subsequent foreset unit.

In the topsets, abrupt shifts in depositional environment are apparent from facies changes and evidence of subaerial exposure. Deep erosion surfaces overlain by palaeosols are interpreted to occur as a result of relative base level fall, but cannot be correlated across adjacent fan deltas. In the foreset to bottomset regions, as with the interfan, base level changes and stratigraphic surfaces

can be expressed differently to topset axial regions. Lack of subaerial exposure and significant environmental shift during relative base level fall mean that major sediment bypass zones (Stevenson et al., 2015) are candidate sequence boundaries. However, erosive events are not only triggered by relative base level fall, particularly in seismically-active regions. As such, sequence boundaries can either be masked or simply misinterpreted – a common problem in deep water successions (Covault & Graham, 2010; Hodgson et al., 2016). Where foresets overlie fine-grained prodelta deposits, there are often erosive contacts (‘cuspaté’ erosion surfaces at the Kerinitis fan delta axis; Backert et al., 2010), which could be slide scars or scour surfaces. Unlike the Selinous fan delta, subaerial unconformities are absent at Kerinitis, because the rate of accommodation increase exceeded the rate of base level fall at the fault centre (Gawthorpe et al., 1994; Hardy and Gawthorpe, 1998; Backert et al., 2010; Barrett et al., 2019).

The base level changes are attributed to changes in lake level (~10-15 m; Barrett et al., 2019) in response to climate variations that followed 41 kyr orbital cycles. This cyclicity is documented in Greece and the Mediterranean (Capraro et al., 2005; Dodonov, 2005; Suc & Popescu, 2005) and globally during the Early-Middle Pleistocene (Emiliani, 1978; Head & Gibbard, 2005; Lisiecki & Raymo, 2007). There is some evidence of episodic marine flooding, as global sea level rise opened Lake Corinth to the Ionian and Aegean seas during interglacial highstands (Freyberg, 1973; Collier, 1990; Moretti et al., 2004; Rohais et al., 2007b; 2008). Overall, relative base level changes were superimposed onto a lower frequency, background tectonic regime, initially dominated by high subsidence rates on the P-M Fault, and later by uplift from the West Helike Fault. A variable sedimentation rate is also likely influenced by climate-driven fluctuations in sediment supply (Collier et al., 1990; 2000).

5.4.2.3. Major unit sets

The fan delta stratigraphy is generally made up of topset or foreset conglomerate beds (10s m thick), separated by thinner (<2 m) finer-grained mudstone-sandstone intervals. Twenty four stratal units are identified in the interfan area, comprising both E-dipping (Selinous-derived) and W-dipping (Kerinitis-derived) beds. These units are separated by the key stratal surfaces

described above. Considering only the key surfaces interpreted confidently, there are a minimum of 20 units. At the fan delta axes, 15 units are identified at the Selinous fan delta (Barrett et al., 2019), and 11 are identified at Kerinitis fan delta, although the base of the Kerinitis fan delta is not exposed (Backert et al., 2010). Successive units that share characteristics are compiled into unit sets. The common characteristics are progradation direction and/or relative geometrical position. Units and unit sets are defined based on observations and may or may not have sequence stratigraphic significance; they do not imply a particular position within a depositional sequence. Observations and the stratigraphic framework of Section 2 are presented in Figure 5.8. The stratigraphic framework for the whole interfan (Sections 2-4) is presented in Figure 5.9. Table 5.2 summarises data derived from each unit. Bedding data is presented with dip and dip direction (Fig. 5.3).

The surfaces from the interfan cannot be accurately correlated to those at the Selinous and Kerinitis axes due to accessibility, outcrop continuity across river valleys and the absence of chronostratigraphic data. However, it is assumed that all units expressed at the Selinous fan delta axis (15 units) are observed in the interfan area (20 Selinous-derived units). Unit 1 in the interfan is part of the Kerinitis fan delta and can be traced updip to sit within the middle of the Kerinitis axial stratigraphy. The foresets markedly thicken and become higher in Units 9 and 10 at both the axis of Selinous (Barrett et al., 2019) and in the interfan stratigraphy, so the lower stratigraphy in the interfan (Units 2-16) is tentatively correlated to the axial Selinous units (Fig. 5.10). Correlations of the bottomset deposits in Melissia Valley were attempted using the 3D outcrop models, but these remain uncertain given the limited continuity of the outcrop.

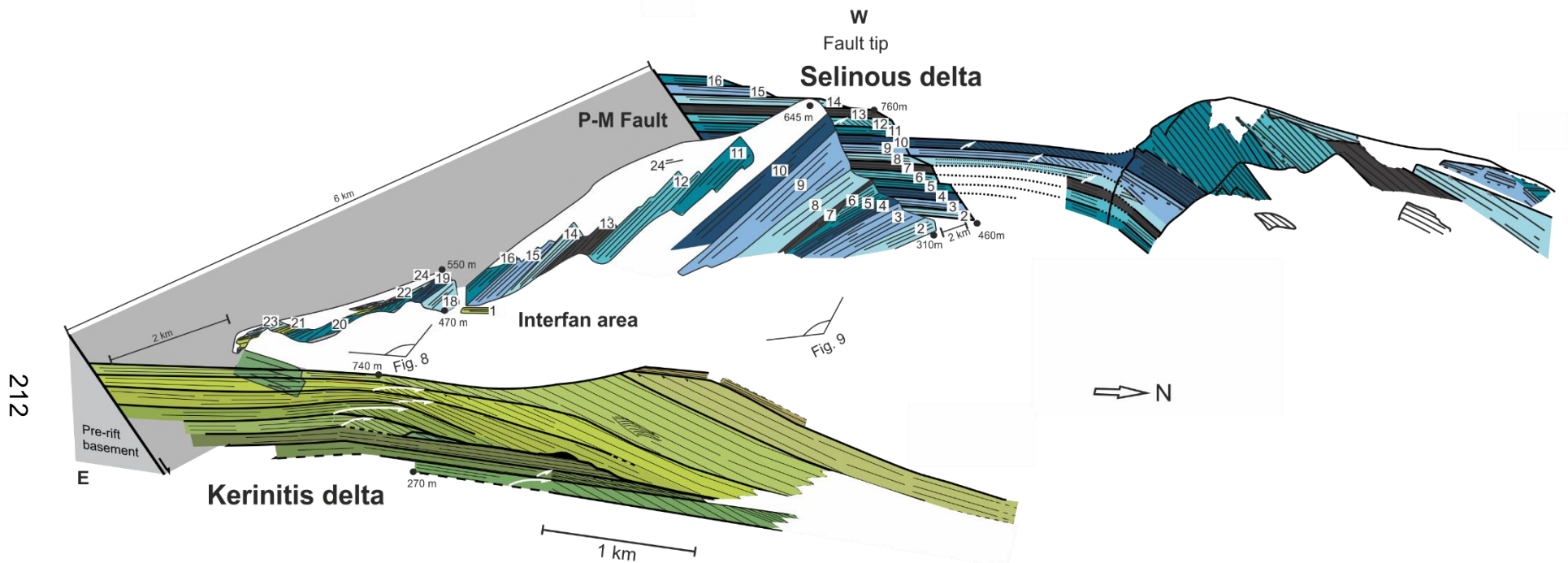


Figure 5.10. Summary diagram of stratigraphic architecture of Kerinitis (green units) and Selinous (blue units) fan deltas. Two dip sections are presented (modified from Barrett et al., 2019). An along-strike section from this study showing interfingering of the two systems in the interfan area is added to show both down-dip and along-strike stratigraphic architecture. White arrows indicate topset-foreset breakpoint trajectories. Numbers correspond to unit numbers from this study. Correlative topset units are numbered at the Selinous fan delta axis, but do not correspond to unit numbers in Barrett et al. (2019). Positions of Figs. (5.) 8 and 9 are indicated.

5.4.2.3.1. Unit set 1

Unit set 1 only comprises Unit 1, a foreset unit (FA 3) with average foreset dips of 20° towards 345° , which suggests it is part of the Kerinitis fan delta. The unit is at least 60 m thick, although the base is not observed. In Section 3, the top is downlapped by E-dipping beds of Unit 15 (Fig. 5.9). It is not possible to tie this unit directly to the stratigraphic framework of the Kerinitis axis, but it sits somewhere within the middle units of Kerinitis. Bottomsets at Locality VII (FA 4b; Fig. 5.3) also dip westward, supporting a Kerinitis fan delta origin. The outcrop is positioned between planes projected from the top of Unit 2 and top of Unit 3 Selinous foresets. However, these planes have a constant dip and likely overestimate bedding dip. This, combined with the absence of W-dipping foresets associated with Unit set 2, indicates that these bottomsets are likely to be associated with Unit 1.

5.4.2.3.2. Unit set 2

Units 2 to 18 comprise Unit set 2, and all have eastward bedding dips (average 27° towards 122°) indicating they are part of the Selinous fan delta (Figs. 5.3 and 5.9). According to projected planes in the 3D outcrop model, the bottomset outcrop at Locality V in Melissia Valley (FA 4b; position in Fig. 5.3) is E-dipping and positioned between the top of Unit 1 and the top of Unit 2, and is therefore assigned to Unit 2.

Topset-foreset breakpoints are apparent in the lower Units 3 to 5 (Fig. 5.4). Within Unit 3, the topset-foreset breakpoint presents a progradational-aggradational trajectory. Beds are observed that dip to the NE (14° towards 074°) and SE (15° towards 143°) revealing the radial pattern of the fan delta. The NE-dipping beds downlap the fine-grained interval below, and the SE-dipping beds project into the outcrop face. The maximum height of the NE-dipping foresets from topset-foreset breakpoint to the downlap position is 32 m (Fig. 5.4). A thin, fine-grained interval overlies Unit 3, which is eroded by Unit 4. The topset-foreset breakpoint of Unit 4 is observed above that of Unit 3 and has an aggradational (near vertical) trajectory. Beds dip to the NE (15° towards 075°) and SE (15° towards 150°). The height of the youngest foreset before Unit 5 is 8 m. The

upper part of Unit 4, with NE-dipping beds, is eroded by Unit 5. The topset-foreset breakpoint of Unit 5 reveals a near-horizontal, i.e. progradational, trajectory (Fig. 5.4). The beds dip eastward (15° towards 088°) and SE (17° towards 146°). The thickness in the SE-dipping region is 8 m and thickness in the ENE-dipping region is 22 m. At the top, there is a conformable contact with Unit 6. The upper part of Unit 6 comprises a fine-grained interval which is widely removed by an ~17 m deep erosion surface.

Units 10 to 18 are thicker (average 52 m), and comprise steeply-dipping (towards SE) foreset packages (Fig. 5.9). Foresets are taller than those in the lower units (>100 m) (Fig. 5.4). Bottomset outcrops at Locality VI (FA 4b; Fig. 5.3) are positioned just above the projected plane from the top of Unit 12, and are therefore assigned to Unit 13. Outcrops at Localities VIII and IX (FA 4b; Figs. 5.3 and 5.6) are positioned between the top of Unit 12 and the top of Unit 16. The Locality IX outcrop is E-dipping and is associated with Units 13-16. The Locality VIII outcrop is W-dipping (Kerinitis-derived) and stratigraphically higher, so deposited at the same time as Units 13-16, but after that at Locality IX. Outcrops at Localities X and XI (FA 4b; Fig. 5.3) are positioned just below the projected plane for the top of Unit 16. The Locality X outcrop is E-dipping and assigned to Unit 16. The Locality XI outcrop is W-dipping and deposited at a similar time to the Locality X outcrop (Fig. 5.3).

5.4.2.3.3. Unit set 3

Unit set 3 comprises Units 19-22 and is differentiated from Unit set 2 by the presence of shallower foreset dips, smaller preserved foreset heights (4-40 m), overall thinner units (average 16 m) and the interfingering of E- and W-dipping beds (Fig. 5.8). The dominant facies association is FA 3 (foresets). Unit 19 bedding (26° towards 127° ; i.e. Selinous) shallows eastward, and is ~27 m thick. In the western part, it is eroded at the top. A ~7 m thick flat-lying fine-grained interval (3° towards 154°) in the centre of Section 2 is interpreted to represent the correlative bottomsets (Fig. 5.8). Unit 20 is also part of the Selinous fan delta, and its foresets downlap the erosion surface and the fine-grained interval at the centre of the outcrop. Unit 20 comprises thinner-bedded, smaller foresets than those in Unit set 2, although it is truncated at the top by an erosion surface

(7° towards 154°). Within the unit, the bedding dip shallows eastward (from 16° towards 073°, to 7° towards 138°), but correlative bottomsets are not identified. Unit 21 is part of the Kerinitis fan delta and thins and shallows westward. In the area that it is thinnest, E-dipping, Selinous-derived beds (14° to 133°) interfinger and downlap W-dipping beds (10° to 233°). The E-dipping beds cannot be traced updip as they are eroded by the base Unit 22 surface. Unit 22 downlaps that surface and is distinct with thinly-bedded, small (4-5 m high) foresets dipping eastward (28° toward 148° - from Selinous). It is top truncated by a flat-lying erosion surface (Fig. 5.8).

5.4.2.3.4. Unit set 4

Unit set 4 comprises Units 23 and 24, which are distinct from lower units as they have northward dip components (19° towards 015°), and in the west are flat-lying relative to the underlying Unit set 2. Eastward, there is a sharp, angular lower contact with Unit 21, marked by downlap of Unit set 4 foresets. The top is not exposed, but the unit has a minimum thickness of 18 m. Limited exposures of Unit 24 are apparent in Section 3 (min. 20 m thick) (Fig. 5.9), but outcrops are accessible at Locality I (FA 2c) (Figs. 5.3 and 5.5).

5.4.3. Interfan end-members

To augment the interpretation of the K-S interfan, a classification scheme is proposed for interfans using modern fan delta morphologies (Fig. 5.2B). Interfans can be classified as one of three end-members according to their separation relative to fan delta topset and foreset radius, which determines the degree of interfingering of fan delta topset, foreset and bottomset deposits. The three types are presented in planform view and in strike cross-section in Figure 5.11, and with modern examples in Figure 5.2B. In Type 1, fan deltas are separated by a distance greater than the foreset radius and the interfan area is occupied by interfingering bottomset deposits. In Type 2, fan deltas are separated by a distance greater than the topset radius and less than the foreset radius, and both foresets and bottomsets interfinger in the interfan area. In Type 3, topsets, foresets and bottomsets interfinger as the fan delta systems are closely abutted at a distance less than the

topset radius. The equivalent of a Type 3 interfan in an alluvial setting is a bajada (Blackwelder, 1931; Hooke, 1972; Bull, 1977; Miliareisis, 2001).

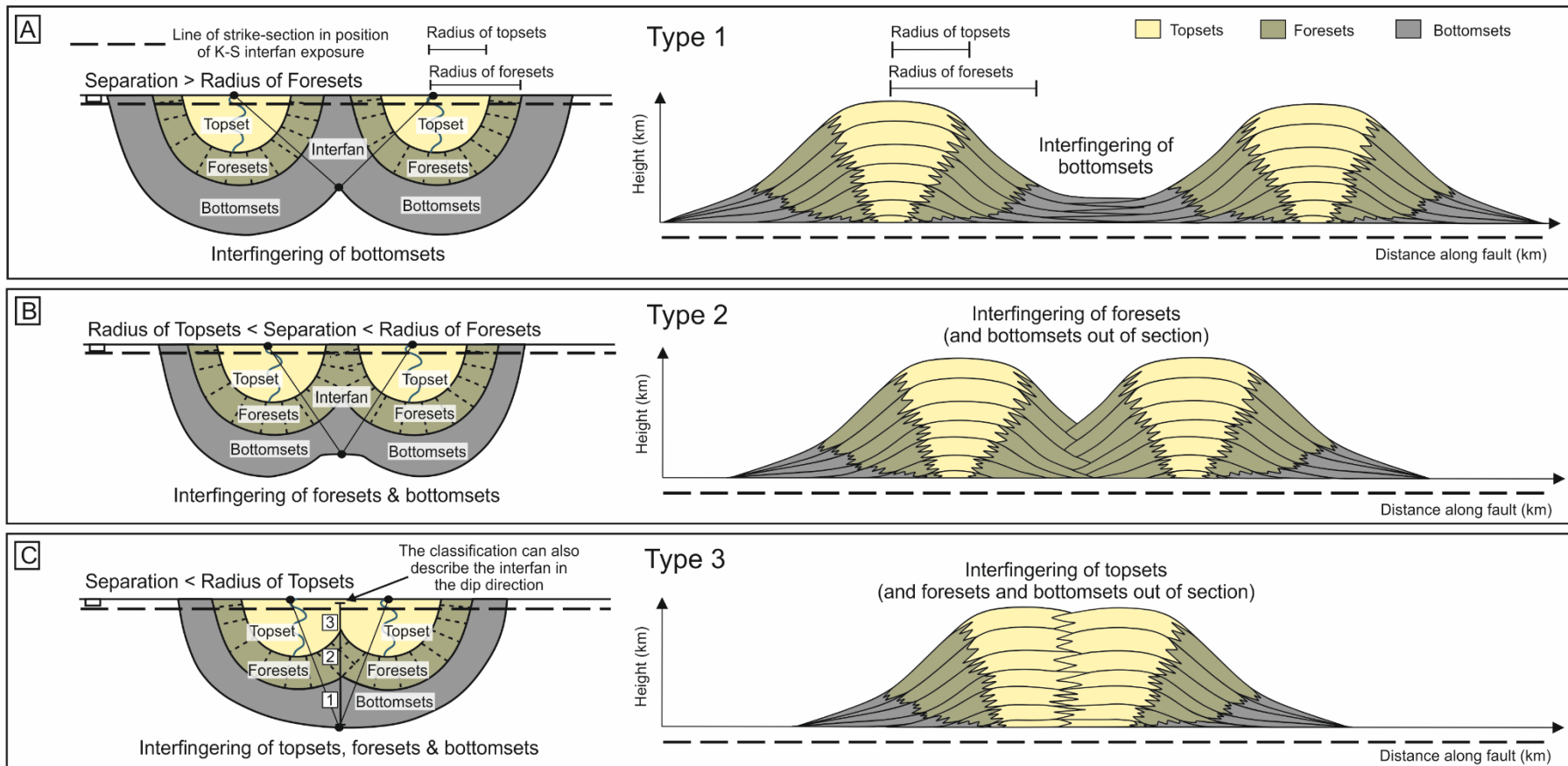


Figure 5.11. Interfan classification scheme, Types 1-3 in plan view and strike cross-section. A: Type 1- two adjacent fan deltas are separated by a distance > foreset radius and only the bottomsets interfingering in the interfan. B: Type 2 - two adjacent fan deltas are separated by a distance > topset radius and < foreset radius, and foresets and bottomsets interfingering in the interfan. C: Type 3 - two adjacent fan deltas are separated by a distance < topset radius, and topsets, foresets and bottomsets interfingering in the interfan.

In each type, the interacting process regime and deposits will differ. When considering the evolution of an interfan, the geometry may evolve between these types and will depend largely on the allogenic forcing responsible for the building of the fan deltas and the basin evolution. Figure 5.12 shows a model for the evolution of an interfan area as two fan deltas prograde and coalesce. Three synthetic logs are presented to show the differences in the stratigraphic record through this process at different positions: the proximal axis, the distal axis and the interfan area. In this respect, each type can be considered as a single stage of evolution. This classification also represents the degree of coalescence in the dip direction. For example, an interfan could present Type 3 geometry in the proximal region and Types 2 and 1 with distance away from the sediment source (Fig. 5.11C).

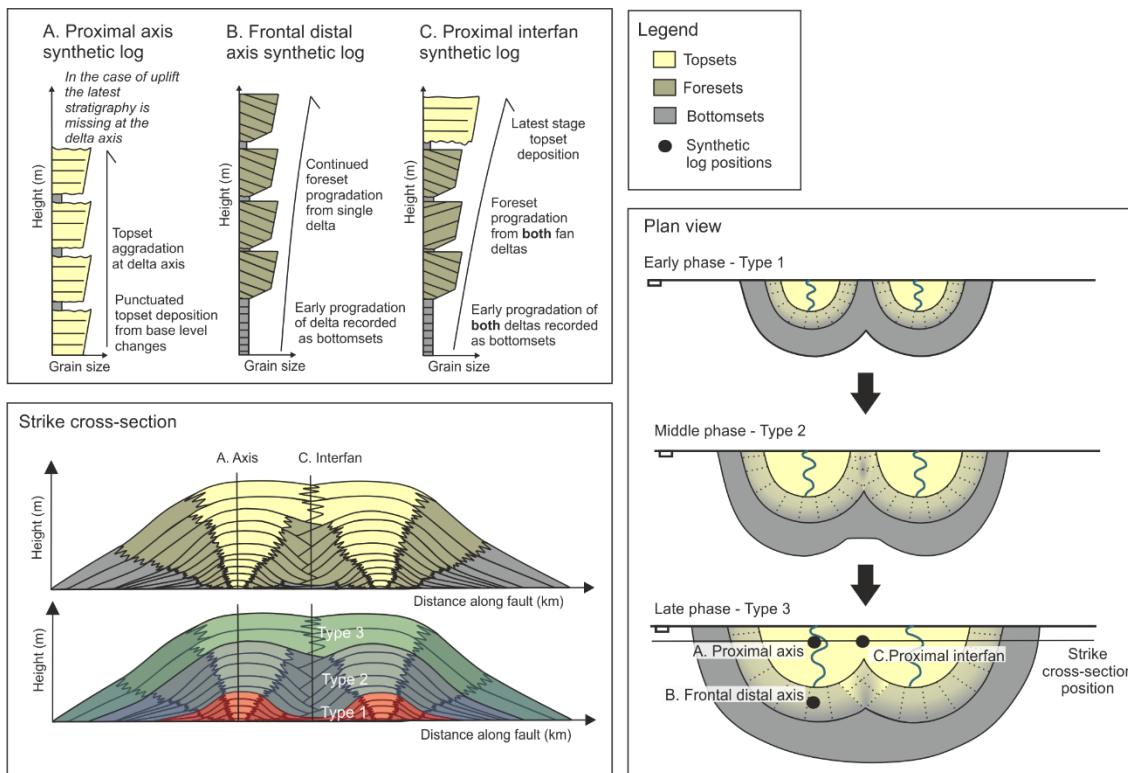


Figure 5.12. Typical evolution of an interfan through Types 1-3 with the progradation of two fan deltas. A) Synthetic logs to show the differences in stratigraphic evolution between the delta axes and the interfan area. Synthetic logs are shown from the proximal axis (A), frontal distal axis (B) and the interfan (C). B) Plan view evolution of the fan deltas, coalescing further as they grow and transitioning through interfan Types 1-3. C) Strike cross-section through the proximal part of the deltas (position shown in B).

5.5. Interpretation of the K-S interfan temporal evolution

The stratigraphic framework at Selinous and Kerinitis is presented as a fence diagram to illustrate an along-strike section across the interfan (Fig. 5.9) and dip sections through the deltas axes (Fig. 5.10; after Backert et al., 2010; Gawthorpe et al., 2017b; Barrett et al., 2019). The interfan evolved through five distinct phases of progradation:

- 1) Initial progradation of the fan deltas into the interfan area, starting with Kerinitis,
- 2) Progradation of the Selinous fan delta into the interfan area and asymmetric eastward delta growth,
- 3) Aggradation and interfingering of the two systems, and shallowing of the interfan area,
- 4) Relative base level fall, erosion and reworking of eroded sediments into the interfan area,
- 5) Continued uplift of the W. Helike footwall and exposure of the Early-Middle Pleistocene deltas and growth of Late Pleistocene deltas in the W. Helike hangingwall basin.

These phases are further described in the following sections and are presented in Figures 5.13 and 5.14.

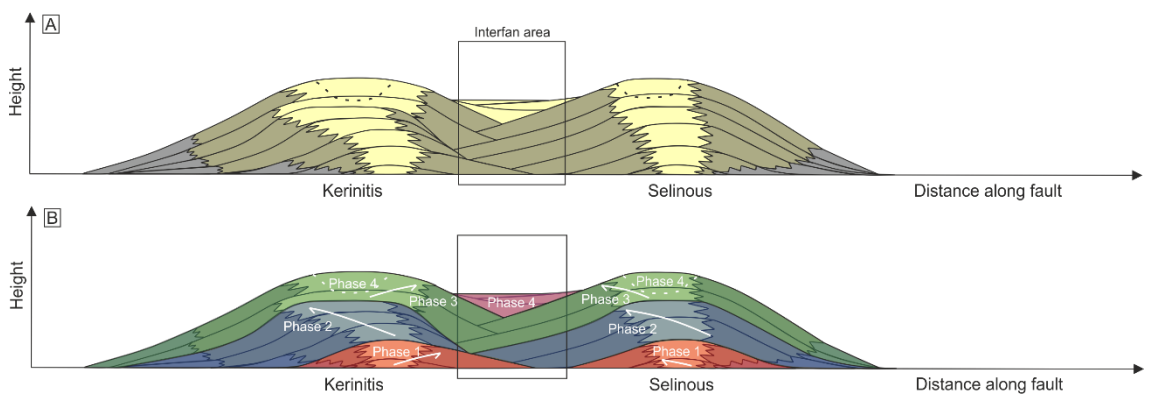


Figure 5.13. A) Strike cross-section schematic diagram of the Early-Middle Pleistocene Kerinitis-Selinous interfan (grey box) large-scale architecture. B) Diagram overlain with colours indicating Phases 1-4 of interfan evolution. Dashed lines indicate erosion during Phase 4. White arrows indicate progradation direction of each fan delta during each phase.

5.5.1. Phase 1 (Unit set 1)

Activity on the P-M Fault began ~1.8 Ma (Ford et al., 2016) and hangingwall subsidence created space for sediments to accumulate. The Kerinitis and Selinous Rivers cut through the uplifting footwall and fed sediment to the new hangingwall basin. The development of Gilbert-type fan deltas along the fault suggests that the fault line defined the coastline at this time. Displacement is greatest at fault centres (e.g. Walsh & Watterson, 1988; Dawers & Anders, 1995), resulting in the greatest accommodation at this position. The first unit apparent in the interfan area (Unit 1 within Unit set 1) is W-dipping and part of the Kerinitis fan delta, which sits closest to the fault centre. Unit 1 is not tied directly to the Kerinitis axial stratigraphy, but can be traced up-dip approximately to the middle units. This suggests that earlier progradation of Kerinitis did not extend as far as the interfan study area, and that the interfan is younger than early units deposited at the Kerinitis delta axis. It is unclear whether the progradation of the Kerinitis fan delta into the interfan area represents directional westward progradation, or overall expansion of the fan during this phase. There is no evidence that Selinous foresets prograded as far as the interfan area during deposition of Unit set 1, as downlap at this location is only observed in later units. A plane projection of the top Unit 1 surface using the 3D outcrop model indicates that in the west, it sits below the earliest E-dipping units from Selinous. Hence, Kerinitis prograded into the interfan area before Selinous (Figs. 5.13 and 5.14).

During Phase 1, the interfan can be classified as Interfan Type 1, separated by a distance greater than the radius of the foresets (Fig. 5.11), as only Kerinitis foresets are evident in the interfan at this stage. It is not Type 2 because Selinous foresets are absent and thus the foresets of the two systems are not interfingering. Bottomset exposures in the interfan area linked to early Selinous progradation are not observed, but it is likely that fine-grained bottomset deposits were interfingering in the interfan area at this time.

5.5.2. Phase 2 (Unit set 2)

During Phase 2, the Selinous fan delta began to prograde eastward into the interfan area, as indicated by E-dipping Unit set 2 (Units 2-18). Units 3-5 reveal topset-foreset breakpoint trajectories (Helland-Hansen & Hampson, 2009) at a distance of ~1 km from the fault (Section 4), suggesting the shoreline was proximal to the fault in the interfan area. The progradation-aggradational trajectory of Unit 3, suggests that sedimentation rate was high, and kept pace and exceeded the rate of accommodation creation. The progradational trajectory of Unit 4 suggests sedimentation rate exceeded the rate of accommodation creation, whereas the aggradational trajectory of Unit 5 suggests sedimentation rate kept pace with the rate of accommodation creation. The middle units at the Selinous delta axis present similar progradational-aggradational trajectories (Barrett et al., 2019). Through the development of these three units the breakpoint remains in a similar position, suggesting overall aggradation (i.e. sedimentation kept pace with the rate of accommodation creation). In Unit 3, a full clinof orm is preserved with a foreset height of 32 m, suggesting a ~30 m palaeo-water depth in the interfan area at this time. Foreset height increases to <200 m in Units 9-18. Foreset height increases as a result of the greater space available in the deeper water into which the foresets prograded. The fact that the foresets aggraded as well as prograded, suggests relative base level rise outpaced sediment supply, most likely because of high subsidence rates of the P-M Fault hangingwall.

The E-dipping Unit 15 (Selinous-derived) downlaps onto the W-dipping Unit 1 (Kerinitis-derived; Unit set 1) (Figs. 5.13 and 5.14). This is the first evidence of foresets interfingering between the two fan deltas. Units 16-19 continue to build up the flanks of these older Kerinitis foresets. They decreased in height as they built out into shallower water. At this stage, there is no evidence of Kerinitis building into the interfan area. Thus, Kerinitis was likely prograding to the north and east at this time. It is clear that there is an asymmetric architecture in the interfan during Phase 2, with significant progradation from Selinous to the east, and inferred progradation from Kerinitis in the same direction. Presumably, therefore, both Selinous and Kerinitis exhibited

asymmetric planform geometries, comparable to that of the modern Meganitis, Selinous, Kerinitis and Ladopotamos fan deltas (Fig. 5.2).

During Phase 2, the interfan evolves from a Type 1 to Type 2 interfan (Fig. 5.11) as foresets from both fan deltas are now apparent and interfingering in the interfan area. However, this interfingering occurred in two discrete phases, firstly from Kerinitis and then from Selinous (Fig. 5.13), as opposed to continuous abutting (Fig. 5.11).

5.5.3. Phase 3 (Unit set 3)

Phase 3 is differentiated from Phase 2 by shallower dips, thinner units and continuous interfingering of E- (Selinous) and W- dipping (Kerinitis) beds, which suggest a different depositional setting to Phase 2. During Phase 3, Selinous prograded eastward and Kerinitis prograded westward, into the interfan area (Unit set 3; Figs. 5.13 and 5.14). Bedding dips within Unit 19 decrease laterally and have correlative bottomsets apparent in Section 2 (Fig. 5.8). Unit 20 bed dips shallow upwards, and Units 20-22 are thinner than the preceding units (5-25 m thick), suggesting less available accommodation. Therefore, Selinous built into gradually shallower water as it encroached onto the Kerinitis margin. Sharp contacts formed as progradation from both systems caused foresets to downlap onto each other. Unit 22 comprises thinly-bedded, small (4-5 m high) foresets that are top truncated. Despite the truncation meaning that the true height of the foresets cannot be determined, water depth clearly shallowed significantly. Progradation occurred within the units, but generally the units aggraded, rather than prograded. This is likely to be a result of restricted lateral space as Selinous built up the flanks of Kerinitis, but with sufficient water depth for aggradation. The units thin towards the top of the section as they aggraded, which is likely to be due to decreasing activity on the P-M Fault causing reduced subsidence rates. Units 20 and 22 are truncated by major erosion surfaces. The top erosional contact of Unit 22 reveals a transition from small foresets to flat-lying beds that could be topsets. There is also a lack of fine-grained intervals towards the top of Unit set 3. This may be due to erosion, with the higher energy conditions limiting fine-grained sediment preservation. Alternatively, their formation was restricted by either: slowing subsidence rates reducing the rate

of base level rise such that climate-induced lake level falls could overcome it, or new activity on the parallel, basinward W. Helike Fault causing uplift of the footwall, and the associated overall relative base level fall exceeding any climate-induced lake level rises.

During Phase 3, the interfan continues to present the Type 2 interfan geometry, whereby foresets interfinger in the interfan area. However, the foreset interfingering is expressed differently to that of Phase 2, with consistent abuttal, rather than discrete phases of progradation.

5.5.4. Phase 4 (Unit set 4)

Unit set 4 (Units 23-24) developed during Phase 4. Unit set 4 is more flat lying than the steeply-dipping underlying units, has a northern component of dip and consists of metre-scale, well-sorted lenses of sand and conglomerate (FA 2b) that dip eastward and westward (Figs. 5.5, 5.13 and 5.14). These are interpreted to represent subaqueous migrating bedforms that are made up of reworked material transported into the interfan area by wave-related longshore currents, e.g. longshore bars (Orme, 1985; Ashley, 1990; Larson, & Kraus, 1992; Drønen & Deigaard, 2007). Some accommodation (shallow water) therefore existed in the interfan at this time. Activity on the P-M Fault ceased at ~0.7 Ma, at which time the W. Helike Fault became active and dominant (Ford et al., 2007). Uplift of the W. Helike footwall caused the delta axes to become exposed above base level (relative base level fall). The uplift rate of the contiguous E. Helike Fault is 1-1.5 mm/yr (De Martini et al., 2004), and the Kerinitis and Selinous rivers incised their own topsets. The modern geomorphology of the valleys shows that the main river direction and sediment pathway was, and continues to be, northwards. Unit set 4 deposits are interpreted to mark the erosion and reworking of topset material into the shallow interfan in response to basinward migration of strain and net basin uplift. The shallow water topsets from Selinous and Kerinitis were abutting at this time (Fig. 5.13). The interfan therefore finally evolved to Type 3 during this phase.

5.5.5. Phase 5

Phase 5 is not recorded in the interfan stratigraphy, but soil development and surficial erosion has occurred during and since Phase 5. Late Pleistocene fan deltas formed in the hangingwall of the W. Helike Fault. By this time, the shoreline had therefore migrated to the W. Helike Fault scarp. The Early-Middle Pleistocene fan deltas continued to be eroded by their feeder rivers (Fig. 5.14).

In summary, the Kerinitis and Selinous interfan evolution can be divided into two parts according to the basin evolution (Fig. 5.14). In the first part, growth of the P-M Fault caused net subsidence of the hangingwall basin and resulted in Phases 1 to 3 of interfan evolution: initial progradation of the fan deltas into the interfan area, starting with Kerinitis (Phase 1), asymmetric Selinous fan delta growth eastward (Phase 2), and interfingering of the two systems and shallowing of the interfan (Phase 3). In the second part, the P-M Fault ceased to be active and strain was accommodated on the W. Helike Fault (basinward fault set switch), causing uplift of the W. Helike Fault footwall and thus net uplift of the P-M Fault hangingwall basin through its transition from a marginal fault block to fault terrace. This resulted in relative base level fall, erosion and reworking of sediments into the interfan area (Phase 4), and continued uplift until base level fell below the W. Helike fault scarp, which cut off the Early-Middle Pleistocene deltas and accommodated growth of Late Pleistocene fan deltas in the W. Helike hangingwall basin (Phase 5).

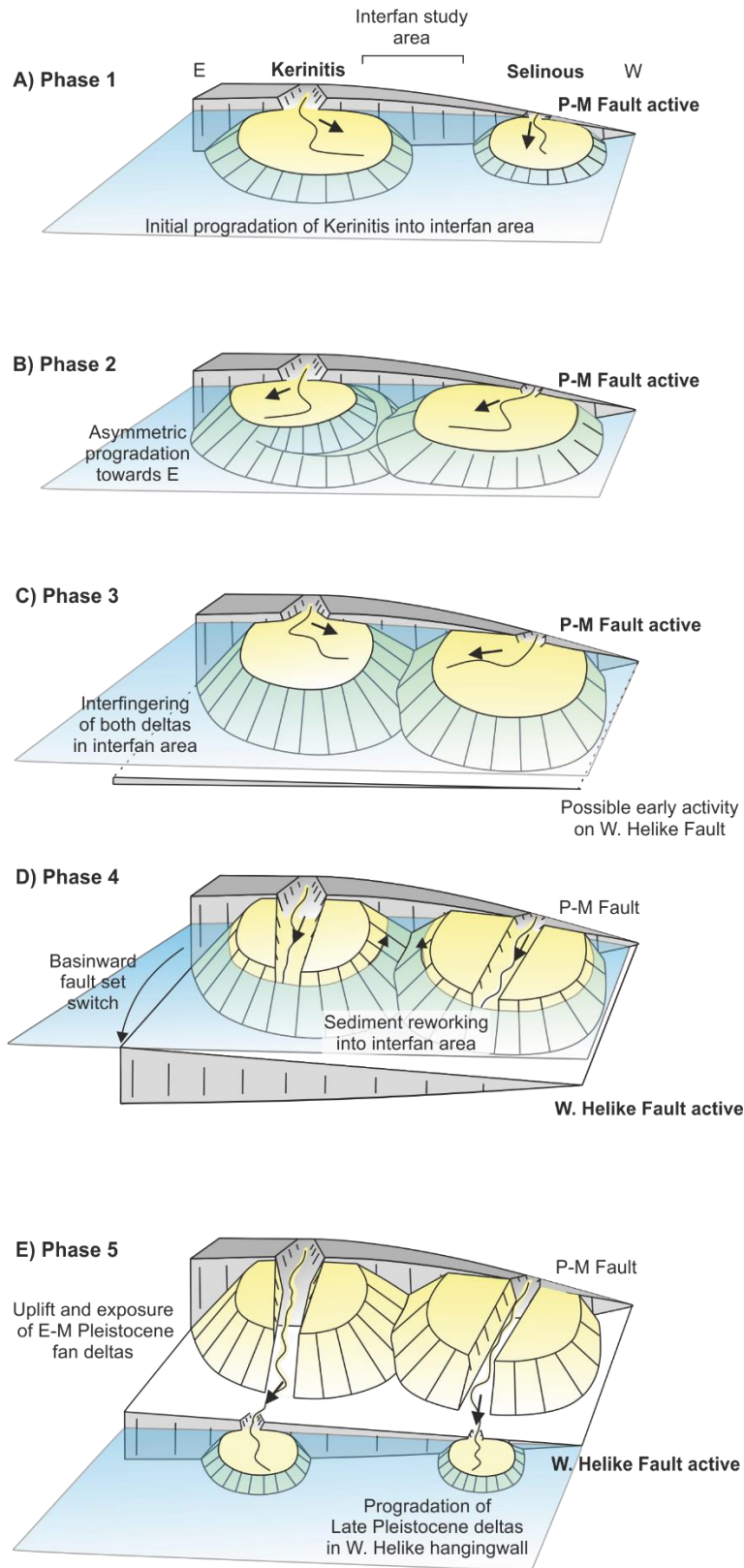


Figure 5.14. The Kerinitis-Selinous interfan evolution records: progradation of deltas into the interfan area (Phase 1), asymmetry of growth towards the east (Phase 2), stratal interfingering during net subsidence (Phase 3) and relative base level fall, erosion and reworking during net uplift, as a result of a basinward fault set switch (Phases 4-5).

5.6. Discussion

Based on observations of modern fan deltas and detailed analysis of the exhumed Early-Middle Pleistocene interfan between the Kerinitis and Selinous fan deltas, there emerges a more complete understanding of the stratal architecture resulting from along-strike interfingering of fan deltas during basin evolution. The following section discusses the classification scheme for interfans in terms of its applicability to other ancient systems, the mechanisms for the observed asymmetry in the ancient and modern systems, and the value of including interfan analysis in basin research.

5.6.1. Style and classification of interfans

Proposed here is the first classification scheme for deltaic interfans based on modern fan delta geometries, which has been used to describe the evolution of the ancient system studied. Interfan styles are differentiated based on their separation relative to the radius of the delta topsets and foresets; this determines the interfingering of topsets, foresets and bottomsets in the interfan area (Fig. 5.11). The interfan between the Kerinitis and Selinous fan deltas evolved from Type 1 (Phase 1) to Type 2 (Phases 2 and 3), and finally reached Type 3 (Phase 4). The interfan evolved through all three end-members (Fig. 5.11). Although these types were characterised from, and represent end-members of modern systems (Fig. 5.2B), they also represent an evolutionary continuum of an interfan, assuming a sufficient sediment supply and progradation that eventually occupies the distance between the fan deltas (Fig. 5.12). It is also possible to use the classification scheme to subdivide an interfan in the dip direction (Fig. 5.11C). In the exhumed system studied, it is the geometries proximal to the fault/sediment source that are considered for the classification (strike line presented in Fig. 5.11). However, in a case with topsets adjoined in the proximal area (Type 3), the interfan will also exhibit Type 2 and Type 1 in a proximal to distal trend (Fig. 5.11C).

The scheme is presented with adjacent fan deltas in the hangingwall of a fault, but it is worth noting that the scheme also applies to adjacent systems in the footwall, and also fans that are obliquely prograding. For example, one fan prograding down a relay ramp may coalesce with one in the immediate hangingwall and the classification scheme is still applicable (Fig. 5.2B).

5.6.2. Asymmetry of fan deltas

In previously published models of fan deltas in rift settings (e.g. Gawthorpe & Leeder, 2000), and in the interfan models presented here (Fig. 5.11), a symmetrical planform geometry and architecture of fan deltas is assumed. This follows the originally described Gilbert-type fan delta descriptions from the tectonically quiescent Lake Bonneville (e.g. American Fork delta; Gilbert, 1890; Milligan & McDonald, 2016) that were principally controlled by lacustrine base level change in a glacial climate and which exhibit a symmetrical delta architecture (Gilbert, 1890; Lemons et al., 1996; Godsey et al., 2005). However, it is clear that during Phase 2 the Selinous fan delta, and most likely the Kerinitis fan delta, were asymmetric, and skewed eastward (Figs. 5.13 and 5.14). Many of the modern fan deltas along the southern shore of the Gulf of Corinth also have an asymmetric delta plain geometry, representing a snap-shot of their tectono-stratigraphic evolution (e.g. the Meganitis, Selinous, Kerinitis and Akrata fan deltas; Fig. 5.2A and 5.2B). The definition of the interfan is proposed here as ‘the area between two lines that project from the apices of two fan deltas to their intersection at the most distal point of bottomset interfingering’ is applicable to asymmetric fans, but the limit of distal interfingering is more challenging to pinpoint in these cases.

There are two potential mechanisms for this asymmetry: 1) preferential reworking of sediments from the dominant wind and wave direction and/or, 2) principal sediment supply towards structural lows. In the modern Gulf of Corinth, a westerly wind and wave direction prevails, conditions that are expected to have been similar in the Early-Middle Pleistocene. The carrying energy of the longshore current would have been dependent on the weather conditions, with local storms producing currents with a higher energy that allow greater loads to be transported along-shore (Bagnold, 1966). A number of formulas have been derived to predict longshore sediment transport in swell and storm conditions (Bijker, 1967; Engelund & Hansen, 1967; Ackers & White, 1973; Van de Graaff & Van Overeem, 1979; Bailard & Inman, 1981; Van Rijn, 1984; Watanabe et al., 1991); and these are compared in Bayram et al. (2001). As a result, sediments above wave base have been pervasively reworked eastward. This is a likely mechanism for the

skewing of planform topset geometry in the modern fan deltas (Fig. 5.2A and 5.2B) and may have driven migration of the barforms present in Unit 24 of the K-S interfan (Fig. 5.5). In cases where shallow water foresets have prograded over a previously flooded delta topset there is also the potential for longshore current reworking. For example, the foresets of the modern Selinous delta that overlie the submerged Late Pleistocene Selinous fan delta (Fig. 5.2B).

For the overall fan delta architecture to be asymmetrical, there must be a driver to deflect the rivers. Differential subsidence along the border faults results in structural gradients, where the lowest point typically lies at the fault centre (Walsh & Watterson, 1988; Dawers & Anders, 1995). Over time, the rivers and resultant fan deltas preferentially follow the structural contours. A structural influence on river course has been documented for the modern Selinous and Kerinitis Rivers. The modern Kerinitis River has migrated towards the north-west since AD 450-1400 (Schmidt, 1879; Soter & Katsonopoulou, 1998; McNeill & Collier, 2004) as a result of differential displacement in the relay zone between the E. and W. Heliki Faults (Fig. 5.2). The modern Selinous River has gradually migrated towards the south-east in response to growth of the Aigion Fault (Soter & Katsonopoulou, 1998, McNeill & Collier, 2004; Fig. 5.2). Asymmetry of fan delta architecture should be expected in tectonically-active settings subjected to differential subsidence. Interfans in these settings are therefore likely to exhibit a dominant influence from one fan delta, as can be seen in the K-S interfan, where the Selinous fan delta dominates during Phase 2. The highest rates of hangingwall subsidence are interpreted during Phase 2, which coincides with the most pronounced asymmetry. Ultimately, the degree of asymmetry through time is controlled by the interplay of external controls. In rift basins, this can be complicated by fault segment linkage that influences along-strike subsidence patterns. If the fan deltas prograde towards the area with more subsidence, which may change its position through time, the rivers will respond to change the dominant system in the interfan area.

In summary, the observed asymmetry in the ancient succession is architectural, with large foresets from the Selinous fan delta dominating the interfan succession (Figs. 5.9 and 5.13), and thus reflecting a response to the structural gradient towards the fault centre. The asymmetry observed

in the planform geometry of the modern fan deltas (Fig. 5.2), and in the higher units of the interfan (Fig. 5.8), are more likely to be a result of the prevailing wind and wave direction.

5.6.3. Interfans as stratigraphic archives

Interactions of tectonics, base level and sediment supply are spatially and temporally complex. Interfan stratigraphy can record the complexity of the temporal evolution in rift settings, and the transition from net subsidence to net uplift, which is not recorded stratigraphically at the fan delta axes. Here, this regime shift was the result of a 6 km northward (basinward) transfer of fault activity from the P-M Fault to the W. Helike Fault, and is recorded by i) an overall shallowing upwards facies trend from Unit set 2-4, ii) reduced foreset heights, iii) a vertical stacking pattern suggesting a restriction of lateral space, iv) a greater number of units in the interfan than at the delta axes, and v) subsequent erosion and progradation of younger fan deltas in the hangingwall of the W. Helike Fault. During basin uplift, due to its deeper water position, the K-S interfan retained accommodation for longer than the delta axes, which became exposed first. Although, the axial parts of fan deltas record the earliest phases of delta evolution, prior to progradation into the interfan area, the K-S interfan provides a more complete stratigraphic record of the final stages of delta evolution (Figs. 5.13 and 5.14). In Figure 5.12, synthetic logs are presented to show the differences in the stratigraphic record at three positions through the progradation of two fan deltas: the proximal axis, the frontal distal axis and the interfan area. The proximal axis records the aggradation of topset units from the earliest growth phase, but in the case of uplift, is missing the latest stage of evolution. At the frontal distal axis, the earliest progradation of a single fan delta is recorded with bottomset deposits, and becomes overlain by foresets from that fan delta. As it is in a deeper water position, the frontal distal axis continues to preserve stratigraphy during the latest stage, but only from one fan delta. On the other hand, the proximal interfan records the early progradation of both fan deltas as interfingering bottomset deposits. The middle phase is represented by the progradation of foresets from both fan deltas and the latest stage is occupied by topset deposition. Thus, the interfan area not only provides a more complete record through uplift, but also records the history of both fan deltas, their architectural interactions through time,

and potentially reveals their asymmetry more readily than in axial dip sections. Both the axial and interfan areas are complementary and together yield the most complete record of basin evolution (Fig. 5.12), which has high utility. For example, if more complete biostratigraphic and palaeomagnetic records were available from fine-grained intervals and with more accurate correlation of stable, cosmogenic and radiogenic isotope curves to the fan delta succession, greater confidence in dating and tying of the eustatic sea level curve to the stratigraphy could be achieved (Emiliani, 1955; Imbrie et al., 1984; Lisiecki & Raymo, 2005). Interfan areas could therefore represent valuable but underutilised stratigraphic archives, which merit further investigation.

5.7. Conclusions

This is the first detailed study of syn-rift stratigraphic architectures in the interfan area of coeval fan deltas. Field data and UAV photogrammetry-based 3D outcrop models are used to extract qualitative and quantitative data from the Early-Middle K-S interfan. Modern planform geometries of interfan areas allow the classification of interfans into three end-members based on their separation according to delta topset and foreset radius, which can be applied to ancient systems. The Early-Middle Pleistocene K-S interfan evolved from Type 1 to Type 3 through five evolutionary phases from net subsidence to net uplift, due to a northward migration of fault activity from the P-M Fault to the W. Helike Fault. The interfan architectures record: early progradation of the Kerinitis delta into the interfan area (Phase 1), subsequent progradation of the Selinous delta into the interfan area and asymmetry of growth of both fan deltas eastward (Phase 2), stratal interfingering of foresets from both fan deltas during net subsidence (Phase 3), and relative base level fall, erosion and reworking during net uplift, as a result of a basinward fault set switch (Phases 4-5). Planform asymmetry in the modern fan deltas is interpreted to be a result of wind and wave directional reworking. Architectural asymmetry is interpreted to be due to preferential river avulsion towards structural lows driven by subsidence patterns along active faults. Thus, architectural asymmetry may be a common feature in rift basins, and as such

interfans in these settings are likely to preserve evidence of a dominant depositional system. Interfan areas provide a condensed, and potentially more complete, stratigraphic record than the axial areas of the fan deltas through high preservation potential and longer submergence during the early stages of basin uplift, and therefore allow further insight into basin evolution. Interfan areas are underrepresented in terms of their importance in the literature, yet could be exploited as important stratigraphic archives that complement fan delta axial records.

5.8. Acknowledgements

Hannah Kearns is thanked for her assistance on fieldwork. The authors are grateful to Casey Nixon for the loan of a Mavic Pro drone and to Simon Buckley for access and assistance with LIME software. The authors thank the project sponsor, Neptune Energy, who support the SMRG (Shallow Marine Research Group). Barrett is also grateful for fieldwork support from the BSRG Trevor Elliott fund and an IAS Post-Graduate Research grant. Stereonets were generated using Rick Allmendinger's Stereonet 10 software. Gawthorpe acknowledges support from VISTA and the Syn-Rift Systems Project, the Research Council of Norway (project number 255229). The manuscript has benefited from constructive reviews by Sébastien Rohais and Christopher Jackson.

5.9. References

- Ackers, P. & White, W.R. (1973). Sediment transport: new approach and analysis. *Journal of Hydraulics Division*, 99, 2041-2060.
- Ashley, G.M. (1990). Classification of large-scale subaqueous bedforms; a new look at an old problem. *Journal of Sedimentary Research*, 60, 160-172.
- Assine, M.L., Renato Merino, E., Do Nascimento Pupin, F., De Azevedo Macedo, H. & Guerreiro Martinho Dos Santos, M. (2015). The Quaternary alluvial systems tract of the Pantanal Basin, Brazil. *Brazilian Journal of Geology*, 45, 475-489.
- Avallone, A., Briole, P., Agatza-Balodimou, A.M., Billiris, H., Charade, O., Mitsakaki, C., Nercessian, A., Papazissi, K., Paradissis, D. & Veis, G. (2004). Analysis of eleven years of deformation measured by GPS in the Corinth Rift Laboratory area. *Comptes Rendus Geoscience*, 336, 301-311.

- Backert, N., Ford, M. & Malartre, F. (2010). Architecture and sedimentology of the Kerinitis Gilbert-type fan delta, Corinth Rift, Greece. *Sedimentology*, 57, 543-586.
- Bailard, J.A. & Inman, D.L. (1981). An energetics bedload model for plane sloping beach: local transport. *Journal of Geophysical Research*, 86, 2035-2043.
- Barrett, B., Hodgson, D.M., Collier, R.E.LI. & Dorrell, R.M. (2018). Novel 3D sequence stratigraphic numerical model for syn-rift basins: analysing architectural responses to eustasy, sedimentation and tectonics. *Marine and Petroleum Geology*, 92, 270-284. doi: 10.1016/j.marpetgeo.2017.10.026.
- Barrett, B., Collier, R.E.LI, Hodgson, D.M., Gawthorpe, R.L., Dorrell, R.M. & Cullen, T.M. (2019). Quantifying faulting and base level controls on syn-rift sedimentation using stratigraphic architectures of coeval fan deltas: constraining Early-Middle Pleistocene base-level amplitude change in Lake Corinth. *Basin Research*, doi: 10.1111/bre.12356.
- Bayram, A., Larson, M., Miller, H.C. & Kraus, N.C. (2001). Cross-shore distribution of longshore sediment transport: comparison between predictive formulas and field measurements. *Coastal Engineering*, 44, 79-99.
- Bell, D., Stevenson, C.J., Kane, I.A., Hodgson, D.M., Poyatos-Moré, M. (2018). Topographic Controls on the Development of Contemporaneous but Contrasting Basin-Floor Depositional Architectures. *Journal of Sedimentary Research*, 88, 1166-1189.
- Bhiry, N. & Occhietti, S. (2004). Fluvial sedimentation in a semi-arid region: the fan and interfan system of the Middle Souss Valley, Morocco. *Proceedings of the Geologists' Association*, 115, 313-324.
- Bijker, E.W. (1967). Some considerations about scales for coastal models with movable bed. Delft Hydraulics Laboratory, Publication 50, Delft, the Netherlands. *Journal of the Waterways, Harbors and Coastal Engineering Division*, 97, 687.
- Blackwelder, E. (1931). Desert plains. *Journal of Geology*, 39, 133-140.
- Briole, P., Rigo, A., Lyon-Caen, H., Ruegg, J.C., Papazissi, K., Mitsakaki, C., Balodimou, A., Veis, G., et al. (2000). Active deformation of the Corinth rift, Greece: Results from repeated Global Positioning System surveys between 1990 and 1995. *Journal of Geophysical Research-Solid Earth*, 105, 25605-25625.
- Bull, W. (1977). The alluvial fan environment. *Progress in Physical Geography*, 1, 222-270.
- Capraro, L., Asioli, A., Backman, J., Bertoldi, R., Channell, J.E.T., Massari, F. & Rio, D. (2005). Climatic patterns revealed by pollen and oxygen isotope records across the Matuyama-Brunhes Boundary in the central Mediterranean (southern Italy). *Geological Society, London, Special Publications*, 247, 159-182.
- Clarke, P.J., Davies, R.R., England, P.C., Parsons, B.E., Billiris, H., Paradissis, D., Veis, G., Denys, P.H., Cross, P.A., Ashkenazi, V. & Bingley, R. (1997). Geodetic estimate of seismic hazard in the Gulf of Korinthos. *Geophysical Research Letters*, 24, 1303-1306.
- Collier, R.E.LI. (1990). Eustatic and tectonic controls upon Quaternary coastal sedimentation in the Corinth Basin, Greece. *J. Geol. Soc. London*, 147, 301-314.
- Collier, R.E.LI. & Dart, C.J. (1991). Neogene to Quaternary rifting, sedimentation and uplift in the Corinth Basin, Greece. *J. Geol. Soc. London*, 148, 1049-1065.
- Collier, R.E.LI., Leeder, M.R., Trout, M., Ferentinos, G., Lyberis, E. & Papatheodorou, G. (2000). High sediment yields and cool, wet winters: test of last glacial paleoclimates in the northern Mediterranean. *Geology*, 28, 999-1002.
- Collier, R.E.LI. & Thompson, J. (1991). Transverse and linear dunes in an Upper Pleistocene marine sequence, Corinth Basin, Greece. *Sedimentology*, 38, 1021-1040.
- Cotterill, C.J. (2002). A high resolution Holocene fault activity history of the Aigion shelf, Gulf of Corinth, Greece. PhD Thesis, School of Ocean and Earth Sciences, University of Southampton, UK.
- Covault, J.A. & Graham, S.A. (2010). Submarine fans at all sea-level stands: tectonomorphologic and climatic controls on terrigenous sediment delivery to the deep sea. *Geology*, 38, 939-942.

- Dart, C.J., Collier, R.E.L., Gawthorpe, R.L., Keller, J.V.A. & Nichols, G. (1994). Sequence stratigraphy of (?)Pliocene-Quaternary synrift, Gilbert-type fan deltas, Northern Peloponnese, Greece. *Mar. Pet. Geol.*, 11, 545-560.
- Dawers, N. H. & Anders, M.H. (1995). Displacement-length scaling and fault linkage. *J. Struct. Geol.*, 17, 607-614.
- Degnan, P.J. & Robertson, A.H.F. (1998). Mesozoic-early Tertiary passive margin of the Pindos ocean (NW Peloponnese, Greece). *Sediment. Geol.*, 117, 33-70.
- De Martini, P., Pantosti, D., Palyvos, N., Lemeille, F., McNeill, L. & Collier, R.E.L. (2004). Slip rates of the Aigion and Eliki faults from uplifted marine terraces, Corinth Gulf, Greece. *C. R. Geosci.*, 336, 325-334.
- Dodenov, A.E. (2005). The stratigraphic transition and suggested boundary between the Early and Middle Pleistocene in the loess record of northern Eurasia. *Geological Society, London, Special Publications*, 247, 209-219.
- Drønen, N. & Deigaard, R. (2007). Quasi-three-dimensional modelling of the morphology of longshore bars. *Coastal Engineering*, 54, 197-21.
- Emiliani, C. (1955). Pleistocene temperatures. *Journal of Geology*, 63, 538-578.
- Emiliani, C. (1978). The cause of the ice ages. *Earth & Planetary Science Letters*, 37, 349-352.
- Engelund, F. & Hansen, E. (1967). A Monograph On Sediment Transport in Alluvial Streams. Teknisk Forlag, Copenhagen, Denmark.
- Floyd, M.A., Billiris, H., Paradissis, D., Veis, G., Avallone, A., Briole, P., McClusky, S., Nocquet, J.-M., Palamartchouk, K., Parsons, B. & England, P.C. (2010). A new velocity field for Greece: implications for the kinematics and dynamics of the Aegean. *Journal of Geophysical Research*, 115, B10403.
- Ford, M., Hemelsdael, R., Mancini, M. & Palyvos, N. (2016). Rift migration and lateral propagation: evolution of normal faults and sediment-routing systems of the western Corinth rift (Greece). In: C. Childs, R.E. Holdsworth, C.A.-L. Jackson, T. Manzocchi, J.J. Walsh & G. Yielding (Eds.), *The Geometry of Normal Faults*. Geol. Soc. London, Spec. Publ., 439, 131-168.
- Ford, M., Rohais, S., Williams, E.A., Bourlange, S., Jousset, D., Backert, N. & Malartre, F. (2013). Tectonosedimentary evolution of the western Corinth rift (Central Greece). *Basin Research*, 25, 3-25.
- Ford, M., Williams, E.A., Malartre, F. & Popescu, S.M. (2007). Stratigraphic architecture, sedimentology and structure of the Vouraikos Gilbert-type fan delta, Gulf of Corinth, Greece. In: G. Nichols, E. Williams & C. Paola (Eds.), *Sedimentary Processes, Environments and Basins. A Tribute to Peter Friend*. Int. Assoc. Sedimentol. Spec. Publ., 38, 49-90.
- Freyberg, B. Von (1973). Geologie des Isthmus von Korinth. Erlanger Geologische Abhandlungen, 95. Junge und Sohn, Universitäts-Buchdruckerei, Erlangen.
- Gawthorpe, R.L., Andrews, J.E., Collier, R.E.L., Ford, M., Henstra, G.A., Kranis, H., Leeder, M.R., Muravchik, M. & Skourtsos, E. (2017b). Building up or out? Disparate sequence architectures along an active rift margin – Corinth rift, Greece. *Geology*, 45, 111-114.
- Gawthorpe, R.L., Fraser, A. & Collier, R.E.L. (1994). Sequence stratigraphy in active extensional basins: implications for the interpretation of ancient basin fills. *Marine and Petroleum Geology*, 11, 642-658.
- Gawthorpe, R.L. & Leeder, M.R. (2000). Tectono-sedimentary evolution of active extensional basins. *Basin Research*, 12, 195-218.
- Gawthorpe, R.L., Leeder, M.R., Kranis, H., Skourtsos, E., Andrews, J.E., Henstra, G.A., Muravchik, M., Turner, J.A. & Stamatakis, M. (2017a). Tectono-sedimentary evolution of the Plio-Pleistocene Corinth rift, Greece. *Basin Res.*, 30, 1-32, doi: 10.1111/bre.12260.
- Gawthorpe, R.L., Sharp, I., Underhill, J.R. & Gupta, S. (1997). Linked sequence stratigraphic and structural evolution of propagating normal faults. *Geology*, 25, 795-798.

- Ghisetti, F. & Vezzani, L. (2004). Plio-Pleistocene sedimentation and fault segmentation in the Gulf of Corinth (Greece) controlled by inherited structural fabric. *Comptes Rendus Geosciences*, 336, 243-249.
- Gilbert, G.K. (1890). Lake Bonneville. U.S. *Geological Survey Monograph*, 1, 438 p.
- Gobo, K., Ghinassi, M. & Nemeč, W. (2015). Gilbert-type deltas recording short-term base-level changes: Delta-brink morphodynamics and related foreset facies. *Sedimentology*, 62, 1923-1949.
- Gobo, K., Ghinassi, M. & Nemeč, W. (2014). Reciprocal Changes in Foreset to Bottomset Facies in a Gilbert-Type Delta: Response to Short-Term Changes in Base Level. *Journal of Sedimentary Research*, 84, 1079-1095.
- Godsey, H.S., Currey, D.R. & Chan, M.A. (2005). New evidence for an extended occupation of the Provo shoreline and implications for regional climate change, Pleistocene Lake Bonneville, Utah, USA. *Quaternary Research*, 63, 212-223.
- Goldsworthy, M. & Jackson, J. (2001). Migration of activity within normal fault systems: examples from the Quaternary of mainland Greece. *Journal of Structural Geology*, 23, 489-506.
- Hardy, S. & Gawthorpe, R.L. (1998). Effects of variations in fault slip rate on sequence stratigraphy in fan deltas: insights from numerical modeling. *Geology*, 26, 911-914.
- Head, M.J. & Gibbard, E.L. (2005). Early-Middle Pleistocene transitions: an overview and recommendation for defining the boundary. In: M.J. Head & P.L. Gibbard (Eds.), *Early-Middle Pleistocene Transitions: The Land-Ocean Evidence*. Geological Society, London, Special Publications, 247, 1-18.
- Helland-Hansen, W. & Hampson, G.J. (2009). Trajectory analysis: concepts and applications. *Basin Research*, 21, 454-483.
- Higgs, R. (1990). Sedimentology and tectonic implications of Cretaceous fan-delta conglomerates, Queen Charlotte Islands, Canada. *Sedimentology*, 37, 83-103.
- Hodgson, D.M., Kane, I.A., Flint, S.S., Brunt, R.L. & Ortiz-Karpf, A. (2016). Time-transgressive confinement on the slope and the progradation of basin-floor fans: implications for the sequence stratigraphy of deep-water deposits. *J. Sediment. Res.*, 86, 73-86.
- Hook, J., Abhvari, A., Gluyas, J.G. & Lawlor, M. (2003). The Birch Field, Block 16/12a, UK North Sea. In: J.G. Gluyas & H.M. Hitchens (Eds.), *United Kingdom Oil and Gas Fields', Commemorative Millennium Volume*. Geological Society, London, Memoir, 20, 167-181.
- Hooke, R. (1972). Geomorphic evidence for late-Wisconsin and Holocene tectonic deformation, Death Valley, California. *Geological Society of America Bulletin*, 83, 2073-2098.
- Imbrie, J., Hays, J. D., Martinson, D. G., McIntyre, A. , Mix, A. C. , Morley, J. J. , Pisias, N. G., Prell, W. L. & Shackleton, N. J. (1984). The orbital theory of Pleistocene climate: Support from a revised chronology of the marine delta 18O record. In: A. Berger et al. (Eds.), *Milankovitch and Climate*. Plenum Reidel, Dordrecht, 269-305pp.
- Larson, M. & Kraus, N.C. (1992). Dynamics of longshore bars. In: B.L. Edge (Ed.), *Proceedings of 23rd Conference on Coastal Engineering, Venice, Italy*, 23, 2219-2232.
- Leeder, M.R., Collier, R.E.Ll., Abdul Aziz, L.H., Trout, M., Ferentinos, G., Papatheodorou, G. & Lyberis, E. (2002). Tectono-sedimentary processes along an active marine/lacustrine half-graben margin: Alkyonides Gulf, E. Gulf of Corinth, Greece. *Basin Research*, 14, 25-41.
- Leeder, M.R. & Gawthorpe, R.L. (1987). Sedimentary models for extensional tilt block/half-graben basins. In: M.P. Coward, J.F. Dewey & P.L. Hancock (Eds.), *Continental Extensional Tectonics*. Geological Society, London, Special Publications, 28, 139-152.
- Leeder, M.R., Mack, G.H., Brasier, A.T., Parrish, R.R., Mintosh, W.C., Andrews, J.E. & Duremeijer, C.E. (2008). Late-Pliocene timing of Corinth (Greece) rift-margin fault migration. *Earth and Planetary Science Letters*, 274, 132-141.

- Lemons, D.R., Milligan, M.R. & Chan, M.A. (1996). Paleoclimatic implications of late Pleistocene sediment yield rates for the Bonneville Basin, northern Utah. *Palaeogeography, Palaeoclimatology, Palaeoecology*, 123, 147-159.
- Leppard, C.W. & Gawthorpe, R.L. (2006). Sedimentology of rift climax deep water systems; Lower Rudeis Formation, Hammam Faraun Fault Block, Suez Rift, Egypt. *Sedimentary Geology*, 191, 67-87.
- Lisiecki, L.E. & Raymo, M.E. (2005). A Pliocene-Pleistocene stack of 57 globally distributed benthic delta 18O records. *Paleoceanography*, 20, PA1003, doi: 10.1029/2004PA001071.
- Lisiecki, L.E. & Raymo, M.E. (2007). Plio–Pleistocene climate evolution: trends and transitions in glacial cycle dynamics. *Quaternary Science Reviews*, 26, 56-69.
- Lomas, S.A. & Joseph, P. (2004). Confined turbidite systems. In: S.A. Lomas & P. Joseph (Eds.), *Confined Turbidite Systems*. Geological Society, London, Special Publications, 222, 1-7.
- Kneller, B., Edwards, D., Mccaffery, W. & Moore, R. (1991). Oblique reflection of turbidity currents. *Geology*, 19, 250-252.
- McNeill, L.C. & Collier, R. (2004). Uplift and slip rates of the eastern Eliki fault segment, Gulf of Corinth, Greece, inferred from Holocene and Pleistocene terraces. *J. Geol. Soc. Lond.*, 161, 81-92.
- McNeill, L.C., Collier, R.E.L., De Martini, P.M., Pantosti, D. & D'addezio, G. (2005). Recent history of the Eastern Eliki Fault, Gulf of Corinth: geomorphology, palaeoseismology and impact on palaeoenvironments. *Geophysical Journal International*, 16, 154-166.
- Miliaresis, G., Ch. (2001). Extraction of bajadas from digital elevation models and satellite imagery. *Computers & Geosciences*, 27, 1157-1167.
- Milligan, M. & McDonald, G. (2016). Shorelines and vertebrate fauna of Pleistocene Lake Bonneville, Utah, Idaho and Nevada. Geology of the Intermountain West, 4. A Field Guide Prepared For Society of Vertebrate Paleontology Annual Meeting, October 26-29, 2016, Grand America Hotel, Salt Lake City, Utah, USA.
- Moretti, I., Lykousis, V., Sakellariou, D., Reynaud, J.Y., Benziane, B. & Prinzhofer, A. (2004). Sedimentation and subsidence rate in the Gulf of Corinth: what we learn from the Marion Dufresne's long-piston coring. *C.R. Geosci.*, 336, 291-299.
- Nemec, W. (1990). Aspects of sediment movement on steep delta slopes. In: A. Collela & D.B. Prior (Eds.), *Coarse-Grained Deltas*. Special Publications of International Association of Sedimentology, 10, 29-73.
- Nixon, C.W., McNeill, L.C., Bull, J.M., Bell, R.E., Gawthorpe, R.L., Henstock, T.J., Christodoulou, D., Ford, M., Taylor, B., Sakellariou, D., Ferentinos, G., Papatheodorou, G., Leeder, M.R., Collier, R.E.L., Goodliffe, A.M., Sachpazi, M. & Kranis, H. (2016). Rapid spatiotemporal variations in rift structure during development of the Corinth Rift, central Greece. *Tectonics*, 35, 1225-1248.
- Ori, G.G., Roveri, M. & Nichols, G. (1991). Architectural patterns in large-scale Gilbert-type delta complexes, Pleistocene, Gulf of Corinth, Greece. In: A.D. Miall & N. Tyler (Eds.), *The three dimensional facies architecture of terrigenous clastic sediments and its implications for hydrocarbon discovery and recovery*. SEPM, Concept in Sedimentology and Paleontology, 207-216.
- Orme, A.R. (1985). The behaviour and migration of longshore bars. *Physical Geography*, 6, 142-164.
- Orton, G.J. & Reading, H.G. (1993). Variability of deltaic processes in terms of sediment supply, with particular emphasis on grain size. *Sedimentology*, 40, 475-512.
- Postma, G. (1984). Slumps and their deposits in fan delta front and slope. *Geology*, 12, 27-30.
- Potter, P.E. & Pettijohn, F.J. (1977). *Paleocurrents and Basin Analysis*. 2nd Edition, Springer-Verlag, New York, 425p.
- Poulimenos, G., Zelilidis, A., Kontopoulos, N. & Doutsos, T. (1993). Geometry of trapezoidal fan deltas and their relationship to extensional faulting along the south-western active margins of the Corinth rift, Greece. *Basin Research*, 5, 179-192.

- Rohais, S., Eschard, R. & Guillocheau, F. (2008). Depositional model and stratigraphic architecture of rift climax Gilbert-type fan deltas (Gulf of Corinth, Greece). *Sedimentary Geology*, 210, 132-145, doi:10.1016/j.sedgeo.2008.08.001.
- Rohais, S., Eschard, R., Ford, M., Guillocheau, F. & Moretti, I. (2007a). Stratigraphic architecture of the Plio-Pleistocene infill of the Corinth Rift: Implications for its structural evolution. *Tectonophysics*, 440, 5-28.
- Rohais, S., Joannin, S., Colin, J.P., Suc, J.P., Guillocheau, F. & Eschard, R. (2007b). Age and environmental evolution of the syn-rift fill of the southern coast of the gulf of Corinth (Akrata-Derveni region, Greece). *Bull. Soc. Géol. France*, 178, 231-243.
- Rohais, S. & Moretti, I. (2017). Structural and stratigraphic architecture of the Corinth rift (Greece): an integrated onshore to offshore basin-scale synthesis. In: F. Roure et al. (Eds), *Lithosphere Dynamics and Sedimentary Basins of the Arabian Plate and Surrounding Areas*. Frontiers in Earth Sciences, 89-120, doi: 10.1007/978-3-319-44726-1_5.
- Schmidt, J. (1879). Studien uber Erdbeben, Leipzig. 68-83pp.
- Sohn, Y.K. (2000). Coarse-grained debris-flow deposits in the Miocene fan deltas, SE Korea: a scaling analysis. *Sedimentary Geology*, 130, 45-64.
- Sohn, Y.K., Kim, S.B., Hwang, I.G., Bahk, J.J., Choe, M.Y. & Chough, S.K. (1997). Characteristics and depositional processes of large-scale gravelly Gilbert-type foresets in the Miocene Doumsan fan delta, Pohang Basin, SE Korea. *Journal of Sedimentary Research*, 67, 130-141.
- Soter, S. & Katsonopoulou, D. (1998). The search for ancient Helike, 1988–1995: geological, sonar and bore hole studies. In: D. Katsonopoulou, S. Soter & D. Scilardi (Eds.), *Ancient Helike and Aigalieia*. The Helike Society, Aigion, 67-116.
- Stevenson, C.J., Jackson, C.A.-L., Hodgson, D.M., Hubbard, S.M. & Eggenhuisen, J.T. (2015). Deep-water sediment bypass. *Journal of Sedimentary Research*, 85, 1058-1081.
- Suc, J-P. & Popescu, S-M. (2005). Pollen records and climatic cycles in the North Mediterranean region since 2.7 Ma. In: M.J. Head & P.L. Gibbard (Eds.), *Early-Middle Pleistocene Transitions: The Land-Ocean Evidence*. Geological Society, London, Special Publications, 247, 147-158.
- Turner, C.C. & Connell, E.R. (2018). Mid to Late Jurassic graben margin development and evolution of shallow marine to submarine fan systems in the Brae area of the South Viking Graben, U.K. North Sea. In: C.C. Turner & B.T. Cronin (Eds.), *Rift-related coarse-grained submarine fan reservoirs; the Brae Play, South Viking Graben, North Sea*. AAPG Memoir, 115, 163-212.
- Van De Graaff & Van Overeem, J. (1979). Evaluation of sediment transport formulae in coastal engineering practice. *Coastal Engineering*, 3, 1-32.
- Van Rijn, L.C. (1984). Sediment transport: Part I: Bed load transport; Part II: Suspended load transport; Part III: Bed forms and alluvial roughness. *Journal of Hydraulic Division*, 110, 1431-1754.
- Walsh, J. J. & Watterson, J. (1988). Analysis of the relationship between displacements and dimensions of faults. *J. Struct. Geol.*, 10, 239-247.
- Watanabe, A., Shimizu, T. & Kondo, K. (1991). Field application of a numerical model for beach topography change. *Proceedings of Coastal Sediments*, 91, 1814-1829.
- Young, M.J., Gawthorpe, R.L. & Sharp, I.R. (2002). Architecture and evolution of the syn-rift clastic depositional systems towards the tip of major fault segment, Suez Rift, Egypt. *Basin Research*, 14, 1-23.
- Zelilidis, A. (2003). The geometry of fan-deltas and related turbidites in narrow linear basin. *Geological Journal*, 37, 1-16.
- Zelilidis, A. & Kontopoulos, N. (1996). Significance of fan deltas without toe-sets within rift and piggyback basins: examples from the Corinth graben and the Meso-hellenic trough, Central Greece. *Sedimentology*, 43, 253-262.

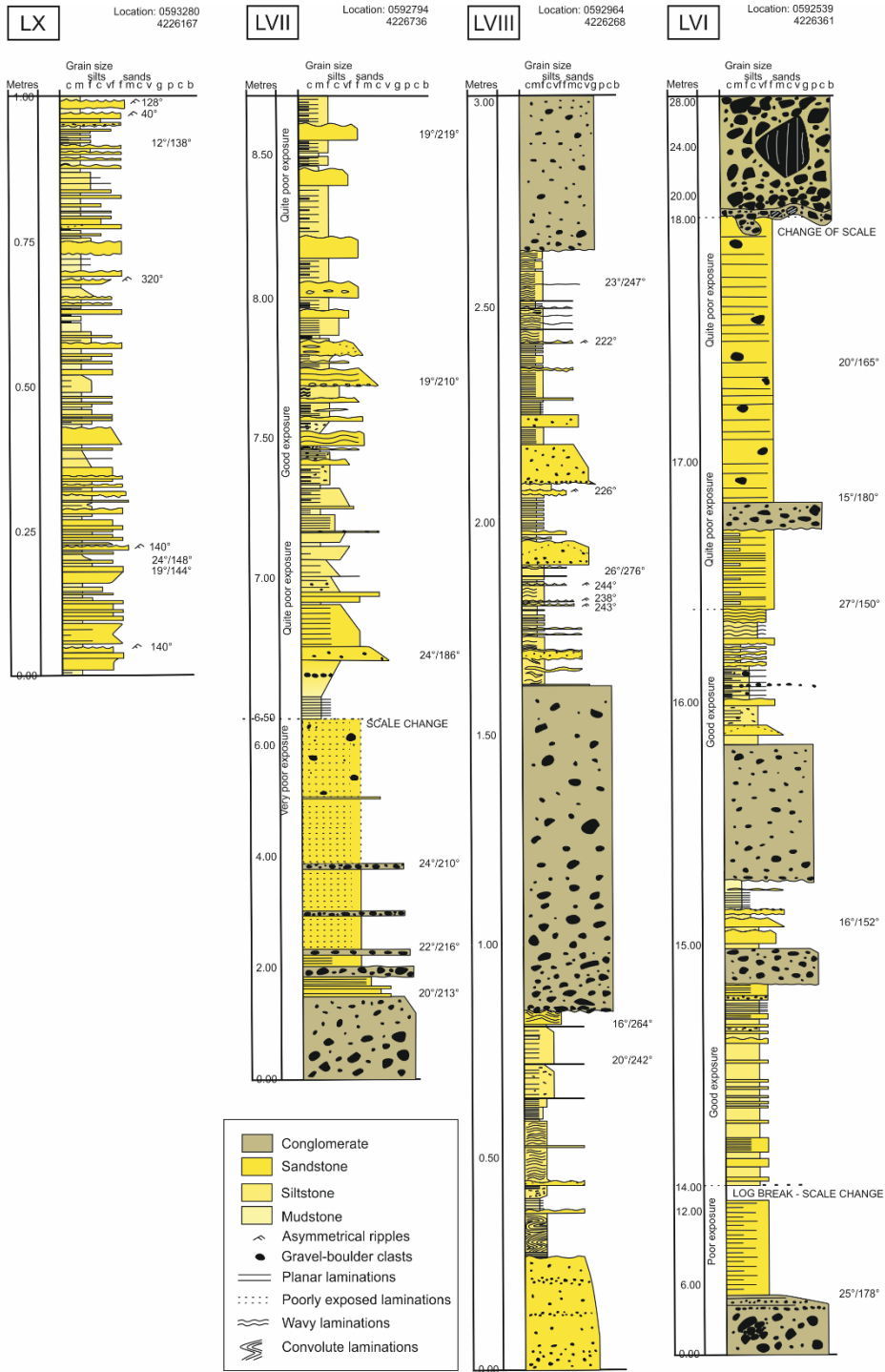
5.10. Appendix I. Table A. Description of facies (modified from Barrett et al., 2019).

Facies code	Facies description	Process interpretation	Backert et al. (2010) scheme code
Co1: Matrix-supported conglomerate	Poorly-sorted, matrix-supported (sand-gravel), gravel-cobble grade conglomerate. Sub-rounded to sub-angular clasts <15 cm. Some cases of normal grading to fine sand. Cm- to dm-thick beds.	High energy bedload transport	G2: Matrix-supported conglomerate
Co2: Stratified conglomerate	Poorly-sorted, variable matrix- and clast-support (sand-gravel), pebble-cobble grade conglomerate, sub-horizontal bedding. Cm- to dm-thick beds.	Bedload transport/longitudinal bedforms	G1c: Crudely stratified conglomerate
Co3: Dipping conglomerate	Steeply dipping (~25°), poorly-sorted, clast-supported gravel-boulder conglomerate. Mostly sub-rounded, large pebble and cobble clasts (<15 cm diameter), occasional small boulders (<25 cm). Matrix of coarse sand-gravel. In some cases locally imbricated. <1m thick open framework lenses. Cuts and scours. >10 m-thick beds.	Gilbert-type delta foresets, characterised by erosive sediment gravity flows on steep slopes	G1b: Steeply dipping conglomerate
Co4: Clast-supported conglomerate	Well to poorly-sorted, clast-supported, pebbly conglomerate with occasional cobbles. Mainly sub-rounded to sub-angular clasts (<10 cm). Inverse grading. Some beds pinch out laterally. Cm-dm thick beds.	Granular flow	G1a: Well-to poorly-sorted structureless conglomerate
Co5: Cross-bedded conglomerate	Well-sorted, matrix- and clast-supported parts (some open-framework), gravel-cobble conglomerates. Clasts are mainly rounded-discoidal (<16 cm). Dm- to m-scale cross-beds with 21-24° dip, locally with an asymptotic geometry. Some beds pinch out laterally. Inverse and normal grading within beds and gradational contacts.	Dune migration by bedload transport and wave and storm reworking	G1e: Cross-stratified conglomerate
Co6: Interbedded conglomerate-gravelly sand	Mostly poorly-sorted, matrix-supported interbedded pebble-cobble grade conglomerate and gravelly coarse sand. Sand is generally laminated with gravel and with dispersed pebbles. Some cobble beds are open-framework and well-sorted or poorly-sorted and clast-supported. Beds <20 cm thick.	Variable energy regime sediment gravity flows - avalanche grain flows and high density turbidity currents	
Co7: Densely-packed gravel conglomerate	Open framework, densely-packed, well-sorted gravel. Beds pinch and swell with some minor grain size changes within gravel. Clasts are sub-angular and imbricated. Contains fine-medium sand lense.	Dune migration by bedload transport and wave and storm reworking	

Facies code	Facies description	Process interpretation	Backert et al. (2010) scheme code
Co8: Very angular, poorly-sorted conglomerate	Very poorly-sorted, mostly matrix-supported, some parts clast-supported, very angular, gravel to boulder conglomerate. Some sheared clasts and some rounded clasts. Striations on very large boulder - also sheared (1m x1m) Several large boulders near the top. Medium sand matrix. Highly erosive and loaded base. Large ball and flame structures.	Fault scarp degradation	
Sa1: Graded sandstone	Well-sorted, inverse or normal grading, very fine-very coarse sandstone. Mainly massive, but in some cases with some parallel laminations at the base or faint cross-beds near the top. Cm- to dm-thick beds.	Turbidity current – Bouma TA-C	S4: Inversely or normal graded sandstone
Sa2: Massive sandstone	Poorly-sorted, massive fine-medium sandstone with cm-scale gravel lag at bases. Some cases evidence of weak normal grading. Dm-thick beds.	Medium energy flow regime, bedload transport	S1: Structureless sandstone
Sa3: Interbedded sand and gravel lenses with shell clusters	Interbedded fine sand and gravel lenses (<5 cm thick and <50 cm length), pinching out over 15-150cm. Occasional sub-rounded pebble clasts. Some gravel lenses fine laterally into fine-medium sand. Broken shell fragments, often in clusters within red-coloured gravelly-coarse sand matrix. Dm-thick beds.	Storm current reworking shallow marine sediment and transporting downdip	
Sa4: Planar- and wavy-laminated sandstone	Flat-lying, planar- or wavy-laminated very fine-fine sandstone. Sometimes inversely graded. Cm- to dm-thick beds.	Upper stage plane beds with variable flow conditions	S2: Laminated sandstone
Sa5: Cross-bedded sandstone	Low-angle cross-bedded very fine-medium sand. Medium sand grade lenses (<2 cm long and ~0.5 cm thick). Symmetrical and/or asymmetrical ripples with silt drapes (<0.5 cm). Cm- to dm-thick beds.	Wave or current ripple and dune migration with periods of intermittent quiescence	S3: Cross-bedded sandstone
Sa6: Gravelly sandstone	Poorly-sorted, gravelly coarse sand, some gravelly laminations and small floating pebbles. Sometimes with erosive base. Cm- to dm-thick beds.	Medium energy bedload transport or high density turbidity current	S1: Structureless sandstone
Fi1: Wavy-laminated siltstone	Wavy-laminated, ripple cross-bedded, fine calcareous siltstone with scours and soft sediment deformation. Normal or inverse grading. Cm-width, 10cm-length sand- and mud-filled <i>Planolites</i> burrows. Cm-thick beds.	Occasional turbidity current events – Bouma TD-E – with periods of quiescence for colonisation. Loading from dense conglomerate above	F2: Laminated siltstone

Fi2: Planar-laminated siltstone	Planar-laminated siltstone (cm- to dm-thick beds). Some variations in colour from red - cream – orange.	Suspension fall-out and intermittent dilute turbidity current	F2: Laminated siltstone
Fi3: Red-coloured sandy siltstone	Varying thickness (cm-scale) red-coloured sandy silt.	Palaeosol	F3b: Variegated siltstone
Fi4: Organic-rich, structureless mudstone	Structureless claystone, dark colour - organic rich. Cm-thick beds.	Suspension fall-out with anoxic conditions	
Fi5: Structureless mudstone	Structureless calcareous mudstone. Cream or red coloured. Cm- to dm-thick beds.	Suspension fall-out	F4a: Claystone
Fi6: Interbedded sandstone-mudstone	Interbedded wavy very fine sandstone and white or pink coloured mudstone. Cm-thick beds.	Suspension fall-out and intermittent dilute turbidity current	F3a: Interbedded siltstone

5.11. Appendix II. Measured sections.



L.I

Location: 0592632
4225454
UTM 34 S

L.I.I

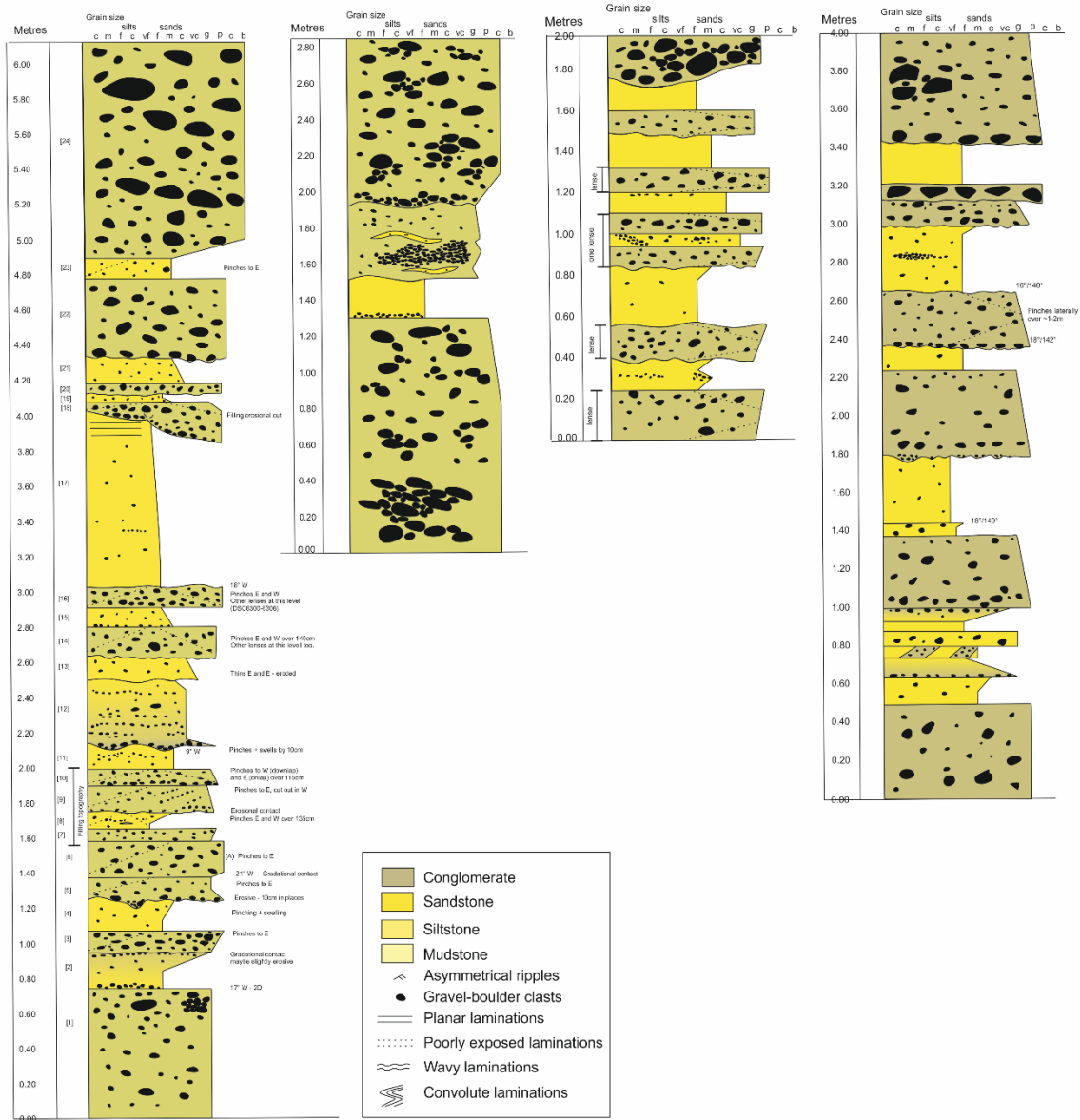
Location: 0592562
4225457

L.I.III

Location: 0592562
4225457

L.I.V

Location: 0592507
4225459



Chapter 6

Geometric and volumetric analysis of footwall degradation and hangingwall architecture, northern Carnarvon Basin, NW Shelf, Australia

Prepared in the format for submission

Barrett, B.J., Hodgson, D.M. & Collier, R.E.Ll. (Prepared for submission). Geometric and volumetric analysis of footwall degradation and hangingwall architecture, northern Carnarvon Basin, NW Shelf, Australia.

Abstract

In rift basin-fills, the interaction of footwall-, hangingwall- and axially-derived depositional systems results in a complex stratigraphic architecture. Moreover, it can be challenging to distinguish deposits derived from fault crest erosion from those derived from established catchments beyond the fault crest. Here, a detailed geometric and volumetric analysis of the footwall degradation and hangingwall fill of an individual fault block in the northern Carnarvon Basin, NW Shelf, Australia is undertaken. Fault throw, vertical and headward erosion are measured and twelve stratal units are defined within the hangingwall seismic stratigraphic framework. Seismic facies and stratal geometries allow the along-strike architectural variability of the footwall-derived fans to be constrained. Depositional systems from different origins interfinger, abruptly downlap, build up the flanks of others and route around each other. The volume balance between footwall erosion to associated hangingwall-fill across ten quadrants along the fault highlights areas of sediment bypass and the positions of through-going sediment input points. A quantitatively-informed interpretation of the tectono-sedimentary evolution of the basin suggests that it evolved through four phases linked to the evolution of the main border fault and a number of parallel, antithetic faults. Exposure of the border fault footwall and adjacent fault terraces produced small catchments from beyond the fault crest that fed the hangingwall basin. One source persisted throughout hangingwall infill and its position coincides with a topographic high in the basin, a fault throw minimum, peaks in vertical and headward erosion, and sustained clinof orm development in the immediate hangingwall. During the earliest stage of fault activity, two fault segments are interpreted, with a relay focussing sediment transport to the basin. Typically, preservation and/or subsurface imaging of erosional landscapes is limited, therefore, the quantitative approach for identifying through-going sediment input points could be applied to other basin-fills and also to identify areas dominated by sediment bypass.

6.1. Introduction

Fault crest degradation is a common feature along footwall highs in rift basins (Morley et al., 2007; Mortimer & Carrapa, 2007; Elliott et al., 2012; Henstra et al., 2016; Bilal et al., 2018). Degradation during faulting results in the eroded sediment being fed directly into the hangingwall basin and associated syn-rift subaerial and subaqueous fans to form (McLeod & Underhill, 1999; Sharp et al., 2000; Fraser et al., 2002; Stewart & Reeds, 2003). Fault crest degradation (Bilal et al., 2018), catchment size (Elliott et al., 2012) and the stratigraphic architecture of hangingwall fans (Gawthorpe et al., 1994; 2017; Dorsey et al., 1995; Barrett et al., 2019) are reported to follow fault throw distribution, which is broadly parabolic along a given fault (Walsh & Watterson, 1988; Dawers & Anderson, 1995). As such, the greatest throw, largest catchments, greatest fault scarp degradation and aggradational-retrogradational stacking in the hangingwall typically occur at the fault centre, and decrease with sedimentary stacking becoming more progradational towards the fault tips. The balance between accommodation generation and sediment supply is paramount in determining the nature of these erosional and depositional responses.

Climate and base level are consistent across small (10s kms) basins, but structural elements can influence topography and gradients over short length scales, which cause the balance of accommodation and sediment supply to become highly variable. Footwall-derived depositional systems are most commonly reported (Gawthorpe et al., 1994; Leppard & Gawthorpe, 2006; Ford et al., 2007; Backert et al., 2010; Turner & Cronin, 2018) and record along-strike variability in stratigraphic architecture (Dorsey & Umhoefer, 2000; Ghinassi, 2007; Gawthorpe et al., 2017; Barrett et al., 2018). Their controls can be quantified (Barrett et al., 2019) and recent studies have demonstrated associated along-strike variability in footwall catchment size and scarp degradation (Elliott et al., 2012; Bilal et al., 2018). However, in basins where pre-rift topography, syn-rift antithetic faults, folds and interacting fault arrays are prevalent features, in addition to footwall-derived sources, hangingwall- and axial-derived systems can equally contribute to basin infill (Leeder et al., 1996; Jackson et al., 2011; McArthur et al., 2016a). How multiple depositional systems interact within a fault-confined basin and how those interactions evolve with the growth

of structural elements across a basin is relatively understudied, and there are few studies that undertake an integrated assessment of footwall degradation and hangingwall architecture (Collier & Gawthorpe, 1995; Pechlivanidou et al., 2018), particularly in three dimensions.

Considering the footwall-derived component of deposition, two sources supply the basin: 1) degradation of the fault crest and, 2) through-going sediment inputs from established catchments beyond the immediate fault crest (Gawthorpe & Leeder, 2000). Differentiating the two supply signals in the rock record is difficult without well constraint, and imaging of drainage catchments is rare because of the limited preservation of erosional landscapes. The ability to resolve the two inputs is important for understanding sediment transport to and around the basin; the position of supplying rivers and areas of likely sediment bypass are common enigmas. Differentiation is also important for reservoir quality assessment. Mature, reworked sediments from long-lived, through-going catchments are likely to provide a better hydrocarbon host than more poorly-sorted slumps from the fault crest (Reading & Richards, 1994; Richards et al., 1998; Leppard & Gawthorpe, 2006). Thus, there is a requirement for an alternative method for determining the location of through-going sediment input points to seismic mapping alone. Mass balancing is a common approach in large-scale source-to-sink studies (Paola & Martin, 2012; Michael et al., 2013; Hampson et al., 2014; Lin & Bhattacharya, 2017; Watkins et al., 2018) and could be a pragmatic approach to picking apart supply signals, by understanding volume excess and deficits in the hangingwall basin to footwall erosion.

Here, we analyse footwall degradation and associated hangingwall fill across an individual fault block in the northern Carnarvon Basin, NW Shelf, using a novel volume-balancing approach, to satisfy three aims: 1) assess the interaction between multiple depositional systems with different origins in a fault confined basin and the influence of evolving structure on their development; 2) identify the position of footwall-derived through-going sediment entry points to the basin in the absence of catchment imaging, and, 3) present a quantitatively-informed interpretation of the tectono-sedimentary evolution of the basin. This study can be used to inform other systems where the coeval footwall system is poorly preserved, and emphasises the need to incorporate multiple

sediment sources and detailed interactions between their deposits into tectono-stratigraphic models of rift basin-fills.

6.2. Study area

The northern Carnarvon Basin (535 000 km²; Fig. 6.1) is positioned towards the southern limit of the NW Shelf, Australia, and is bounded by the Roebuck and Canning Basins to the north-east, the southern Carnarvon Basin to the south, and the Argo, Gascoyne and Cuvier Abyssal Plains to the north and west (Hocking, 1988). Internally, the basin comprises a number of NE-trending, Palaeozoic-Cenozoic structural elements that accommodate a <15 km thick sedimentary succession. The Beagle, Dampier, Barrow and Exmouth sub-basins constitute failed rift systems in the inboard region of the basin (Fig. 6.1A). The Exmouth Plateau sits outboard of these sub-basins, separated by the Kangaroo Syncline (Stagg & Colwell, 1994; Gartrell, 2016). The Exmouth Plateau is a relatively undeformed, broad platform (600 km long and 300-400 km wide) that consists of continental crust that was stretched, rifted and subsided to form a series of NNE-trending, domino-style extensional faults (Exon et al., 1992). A number of footwall-crests have been exploited for hydrocarbons, with one of the most distal discoveries being the Thebe Gas Field, approximately 350 km offshore, in the north-central part of the plateau. The fault accommodating the Thebe-2 appraisal well and its associated hangingwall basin is the focus in this study (Figs. 6.1B and 6.1C).

The pre-rift succession that is juxtaposed against syn-rift sediments across the Thebe-2 Fault comprises the Triassic, fluvio-deltaic, interbedded mudstone-sandstone Mungaroo Formation. Erosion of this formation at the fault crest is evident (Fig. 6.2). Fault scarp degradation is characterised by Bilal et al. (2018) in a northern and adjacent fault block. The different erosional styles of the fault crest are attributed to different mechanical properties within the footwall succession. The infill of the degraded scarp at the Thebe-2 Fault and overlying sequence is the Late Jurassic Dingo Claystone and Jansz Sandstone Formations (Ellis et al., 2009). The

hangingwall basin stratigraphy is not drilled, but comprises the Murat and Athol Formations (Marshall & Lang, 2013). These formations thin to a condensed unit on the footwall of the fault. The base and top of the hangingwall syn-rift package are defined by the TR30 transgressive surface and the J40 sequence boundary, respectively (Marshall & Lang, 2013; Fig. 6.2).

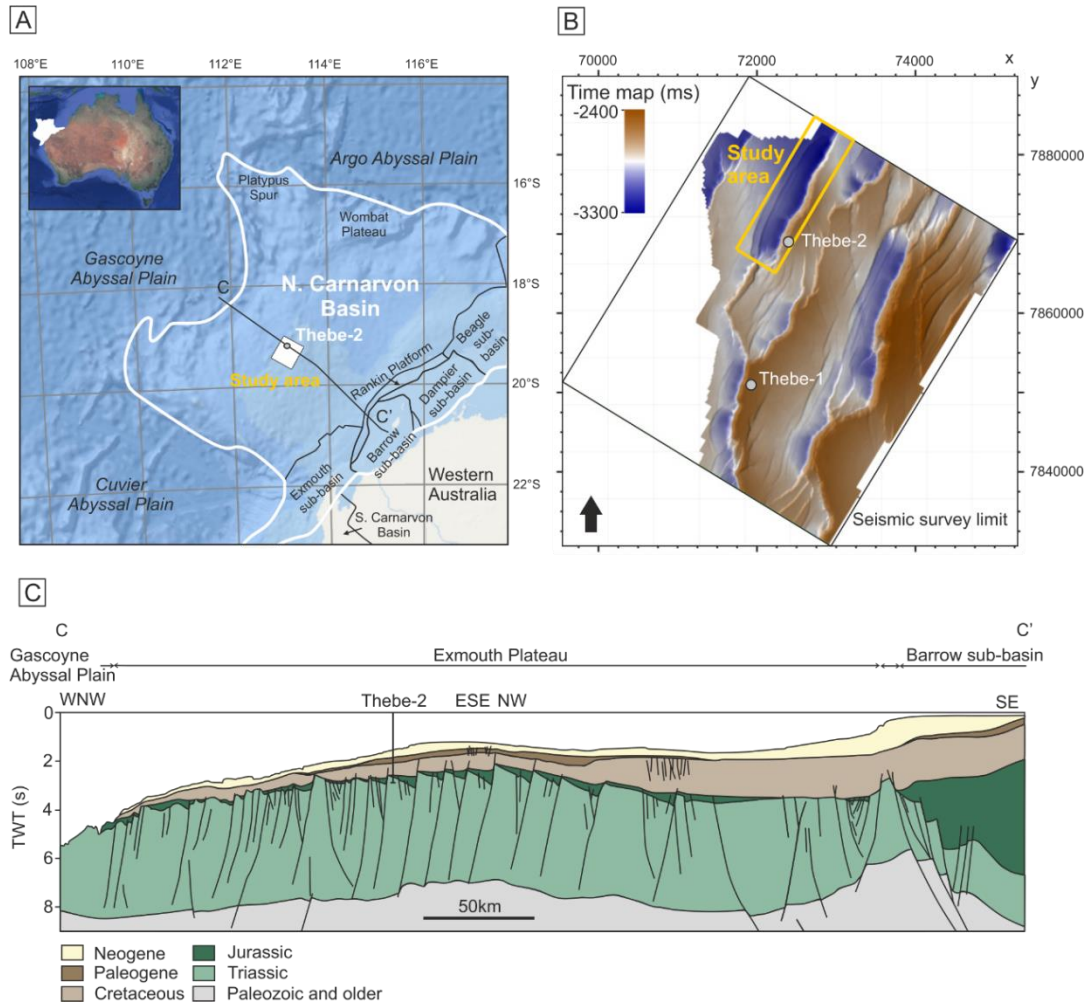


Figure 6.1. Study area location. A) Regional map of the NW Shelf, Australia. White box indicates study area. B) Map to show the limit of the seismic dataset. A time map of the Top Pre-Rift surface is presented to highlight the faults. The specific study area covers the most north-western fault block, where the Thebe-2 well penetrates the footwall of the main border fault. C) Regional interpreted seismic line showing the position of the Thebe-2 well. Line position shown in A (C-C'). Interpreted seismic section modified from Geoscience Australia.

6.3. Geological context

The break-up of Gondwanaland resulted in multiple phases of rifting during the Palaeozoic and Mesozoic that impacted the development of the NW Shelf (Fig. 6.2). The Late Carboniferous to Early Permian was characterised by the break-away of the Sibamasu block, and resulted in the development of the Westralian Superbasin and the dominant NE-SW structural grain of the NW Shelf (Yeates et al., 1987; Bradshaw et al., 1994; Etheridge & O'Brien, 1994). Following extension, a post-rift thermal sag basin developed during the Triassic, which was punctuated by shorter periods of compression (e.g. Fitzroy Movement; Forman & Wales, 1981). During this time, thick marine siliciclastic sediments accumulated (Locker Shale) that subsequently shallowed-upwards into the fluvial-shallow marine Mungaroo Formation during the Carnian-Norian, as a result of significant uplift-related erosion from the onshore Canning Basin (Longley et al., 2002; Marshall & Lang, 2013).

The major Late Triassic-Jurassic rifting phase followed (Fig. 6.2) and is responsible for the disintegration of Argoland and the formation of the northern Carnarvon Basin sub-basins, exploiting older structural fabrics (Longley et al., 2002). The Lhasa micro-plate separated from Gondwana during the Norian (Metcalf, 1999) and the West Burma micro-plate separated over three phases from the Hettangian (earliest Jurassic) to the Kimmeridgian (Late Jurassic) (Longley et al., 2002). The inboard sub-basins received abundant syn-rift sediments through the Jurassic, accumulating a >6 km thick succession. However, the more distal Exmouth Plateau was sediment starved, and a condensed (<400 m) succession was deposited, represented by the Murat and Athol siltstone formations (Marshall & Lang, 2013; Gartrell et al., 2016; Bilal et al., 2018). The Oxfordian J40 SB (Marshall & Lang, 2013) defines the cessation of fault activity.

After a period of quiescence, renewed tectonic activity occurred during the Berriasian (Early Cretaceous) resulting in the separation of Greater India and formation of the Gascoyne and Cuvier oceanic abyssal plains (Veevers, 1988; Longley et al., 2002). Valanginian-Aptian marine shales (Muderong Fm.) comprise the post-rift succession and act as regional seals to Late Triassic-Early

Cretaceous hydrocarbon reservoirs (Bradshaw et al., 1988; Tindale et al., 1998). Carbonate deposition replaced siliciclastic during the Late Cretaceous, blanketing the basin with NW-prograding wedges (Bradshaw et al., 1994). Two later periods of regional tectonic activity acted upon the Exmouth Plateau, resulting in reactivation of older, rift-related structures (Longley et al., 2002). The first occurred during the Campanian (Late Cretaceous) from far field plate motion on the southern Australian margin and resulted in transpressional growth of pre-existing normal faults (Bradshaw et al., 1988; Tindale et al., 1998). The latter occurred during the Neogene, when collision between the Australian plate and the Java-Banda arc (SE Asia) caused inversion and reactivation of faults across the northern Carnarvon Basin (Keep et al., 1998; Hengesh & Whitney, 2016).

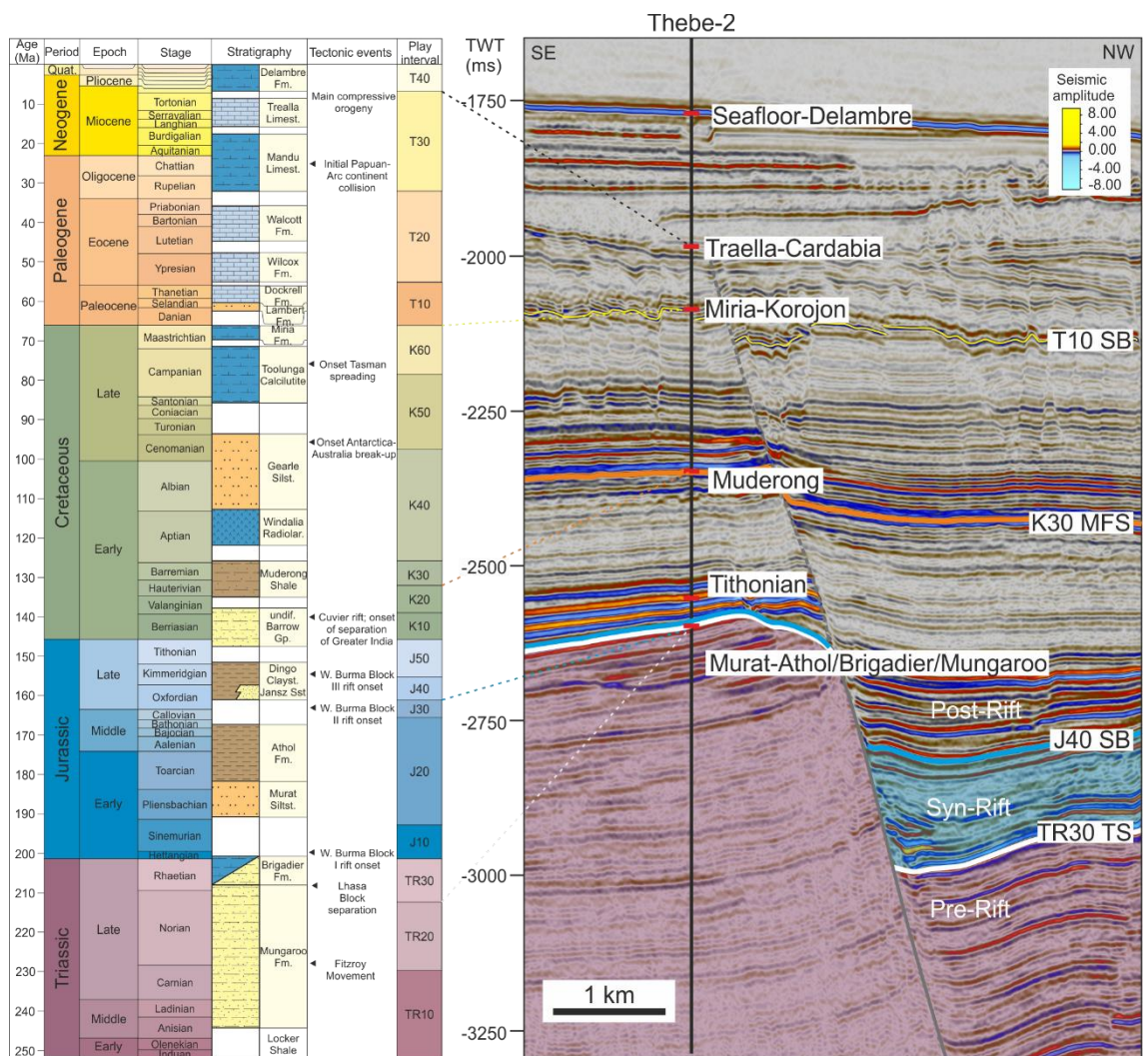


Figure 6.2. Stratigraphy of the northern Carnarvon Basin with formation tops (biostratigraphic data) from the Thebe-2 well presented on a NW-SE seismic section. The syn-rift interval of interest is between the TR30 transgressive surface and J40 sequence boundary, which is expressed as a vertical succession in the hangingwall (blue shading), but a surface in the footwall. Pre-rift stratigraphy is shaded in pink. TS = Transgressive surface; MFS = Maximum flooding surface; SB = sequence boundary. Tectonic events from Longley et al. (2002). Play intervals from Marshall & Lang (2013).

6.4. Dataset

This study uses a full angle PSTM (Pre-Stack Time Migrated) 3D seismic reflection dataset (HEX07B) that covers an 1800 km² area around the Thebe gas field, and wireline log and biostratigraphic data from the Thebe-2 appraisal well (Fig. 6.1). The seismic reflection data were acquired in 2007 with a Bolt airgun array (2000 psi) and 8 x 3600 m streamer cables with 100 m spacing, reaching a maximum penetration of 4609.5 ms TWT. Inlines are orientated NW-SE with an interval of 25 m, and crosslines are orientated NE-SW with 12.5 m intervals. Seismic reflection data are displayed as zero phase and with the European-Australian Normal polarity convention, whereby a downwards increase in acoustic impedance corresponds to a negative reflection; ‘trough-peak-trough’ is presented with ‘red-blue-red’ colours. All seismic reflection sections are presented with 5x vertical exaggeration. Seismic frequency within the interval of interest (~2500 to 3200ms TWT) ranges from 15 to 65 Hz, with an average of ~40 Hz. The average velocity at the Top Pre-Rift surface in Thebe-2 is 1668 m/s. The average wavelength of the data is 42 m, which yields a maximum vertical resolution of 10.5 m ($\lambda/4$) and a limit of detectability of 1.4 m ($\lambda/30$) (Widess, 1973; Kallweit & Wood, 1982). Three normal fault blocks are imaged in the data, and the Thebe-2 well penetrates the footwall of the most north-western fault within the survey area (Fig. 6.1). Key chronostratigraphic surfaces and formation tops were extracted from biostratigraphic well data (Ellis et al., 2009) and formed the basis for regional seismic mapping (Fig. 6.2).

6.5. Methodology

In order to understand the tectono-sedimentary evolution of the basin and to locate the position of fixed drainage systems on the footwall crests that supplied the hangingwall basin, the following steps were taken:

1. Identify seismic facies and map key stratal surfaces
2. Build a stratigraphic framework that sub-divides the hangingwall basin-fill into stratal units and relate those into major unit sets
3. Distinguish depositional styles, origins and variability of the observed sedimentary inputs: footwall-derived, hangingwall-derived and axial-derived fans
4. Mapping of footwall-derived fans for volume calculations
5. Identify areas of footwall crest degradation using seismic cross-sections and maps
6. Measurement of fault throw and footwall degradation (headward and vertical erosion)
7. Measurement of the bulk volume of eroded material from the footwall
8. Volume balancing using the ratio of hangingwall fill (footwall-derived fans) to footwall erosion (V_{HW}/V_{FW})

6.5.1. Stratigraphic analysis (Steps 1-4)

Facies changes, bedding dips and stratal terminations (onlap, downlap, truncation) were used to distinguish 12 seismic units (A-L) in the hangingwall stratigraphy. Units are defined based on observations and sequence stratigraphic significance is not assumed. The top and base of each unit were mapped manually at high resolution (every inline and crossline). Mapped surfaces change character and merge laterally. As such, some seismic units are time equivalent in some places, whilst further along-strike they stack successively. A number of seismic units are restricted to and derived from the main border fault (from the south-east), whilst others are restricted to and derived from the north-western parts of the basin. Seismic units were grouped into four unit sets

according to the presence of three key stratal surfaces (KSS1-3), which are defined by multiple stratal terminations. Each unit set represents one of four phases of basin evolution.

The 3D seismic reflection data and stratigraphic framework permitted geometrical analysis of the hangingwall stratigraphy such that footwall-derived fans could be distinguished from hangingwall dip-slope-derived and axial-derived depositional systems. For example, clinoforms and sloping horizons that dip basinward from the main border fault and show a radial geometry in 3D are interpreted as footwall-derived fans. Based on geometry and seismic facies, the depositional systems in the hangingwall basin were characterised and their variation along-strike and through time was assessed.

6.5.2. Measuring footwall degradation (Steps 5-7)

The Top Pre-Rift (Top Mungeroo Fm.) surface that extends across the seismic survey was mapped to reveal the degraded fault scarp (Figs. 6.3 and 6.4). A pseudo-surface was then extrapolated by projecting the fault plane and the trend of an uneroded footwall top surface (Fig. 6.3). This pseudo-surface is the estimated restored footwall. The difference in vertical height between the highest point on the restored footwall to the highest preserved point on the fault scarp is taken as the amount of vertical erosion. The distance between the highest point on the restored footwall to the most headward uneroded point on the footwall top surface is taken as the amount of headward erosion. The volume between the restored footwall pseudo-surface and the Top Pre-Rift surface represents the total amount of erosion of the fault scarp (shown in cross-section in Fig. 6.3). The projected fault throw was measured every 5 inlines (125 m) along the fault and taken as the distance between the highest point on the restored footwall to the Top-Pre Rift surface in the immediate hangingwall (Fig. 6.3). It was also measured from the highest point on the fault scarp that is uneroded to the lowest point in the hangingwall.

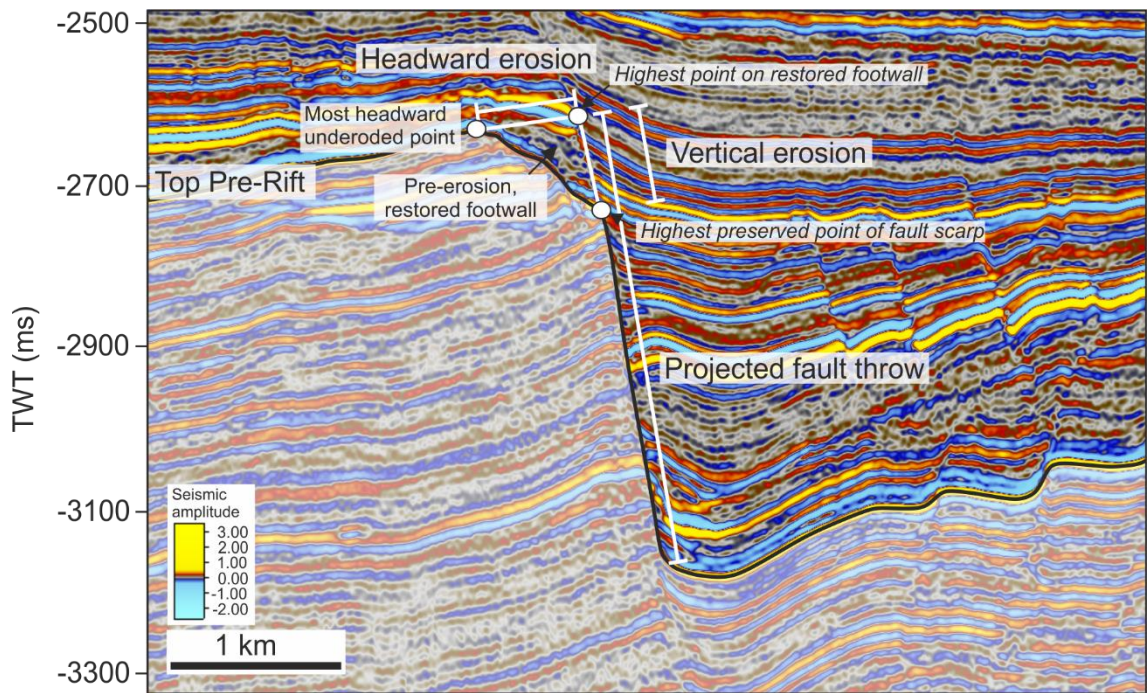


Figure 6.3. Positions on the fault that are used for measuring fault throw, and headward and vertical erosion. Pre-rift stratigraphy is shaded white.

6.5.3. Volume balancing approach (Step 8)

In order to compare the amount of eroded sediment from the footwall (V_{FW}) to the amount of hangingwall fill (V_{HW}), a volume balancing approach was taken. For the footwall erosion, using the structural modelling functions in Petrel software, a grid was constructed between the extrapolated pseudo-surface (restored footwall crest) and the Top Pre-Rift surface. From this, the eroded thickness and eroded bulk volume of sediment was calculated. Figure 6.4B shows a map of the eroded thickness of sediment overlain onto the degraded fault scarp. Figure 6.5 presents the fault scarp degradation in cross-section.

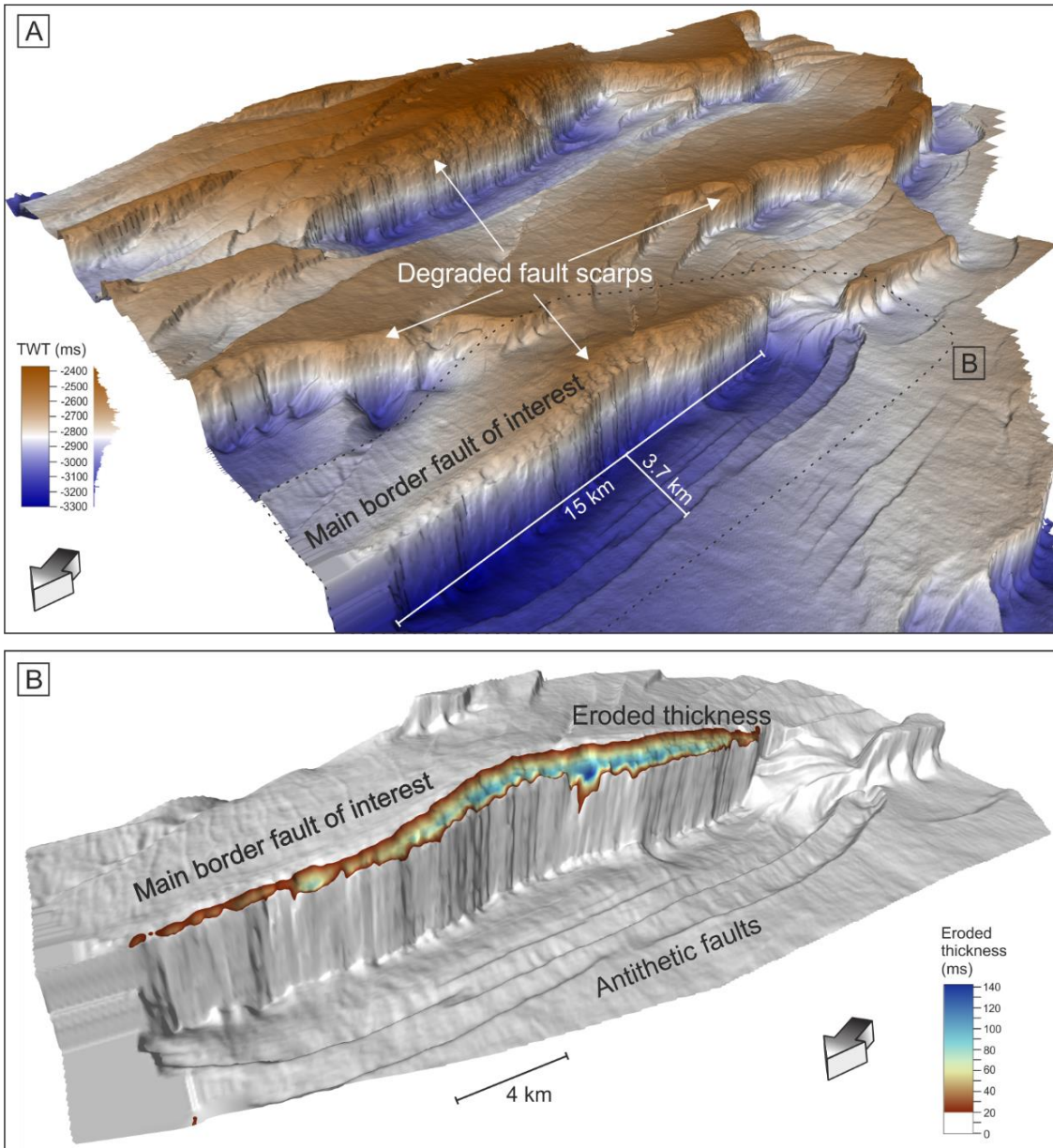


Figure 6.4. A) 3D capture of the Top Pre-Rift surface across the seismic dataset to reveal a series of normal fault blocks with degraded fault scarps. B) 3D image of the fault of interest in the study area (position shown in 'A' with black dashed outline). A map of the eroded thickness of sediment is overlain onto the fault scarp. Eroded thickness colour map from Cramer (2018).

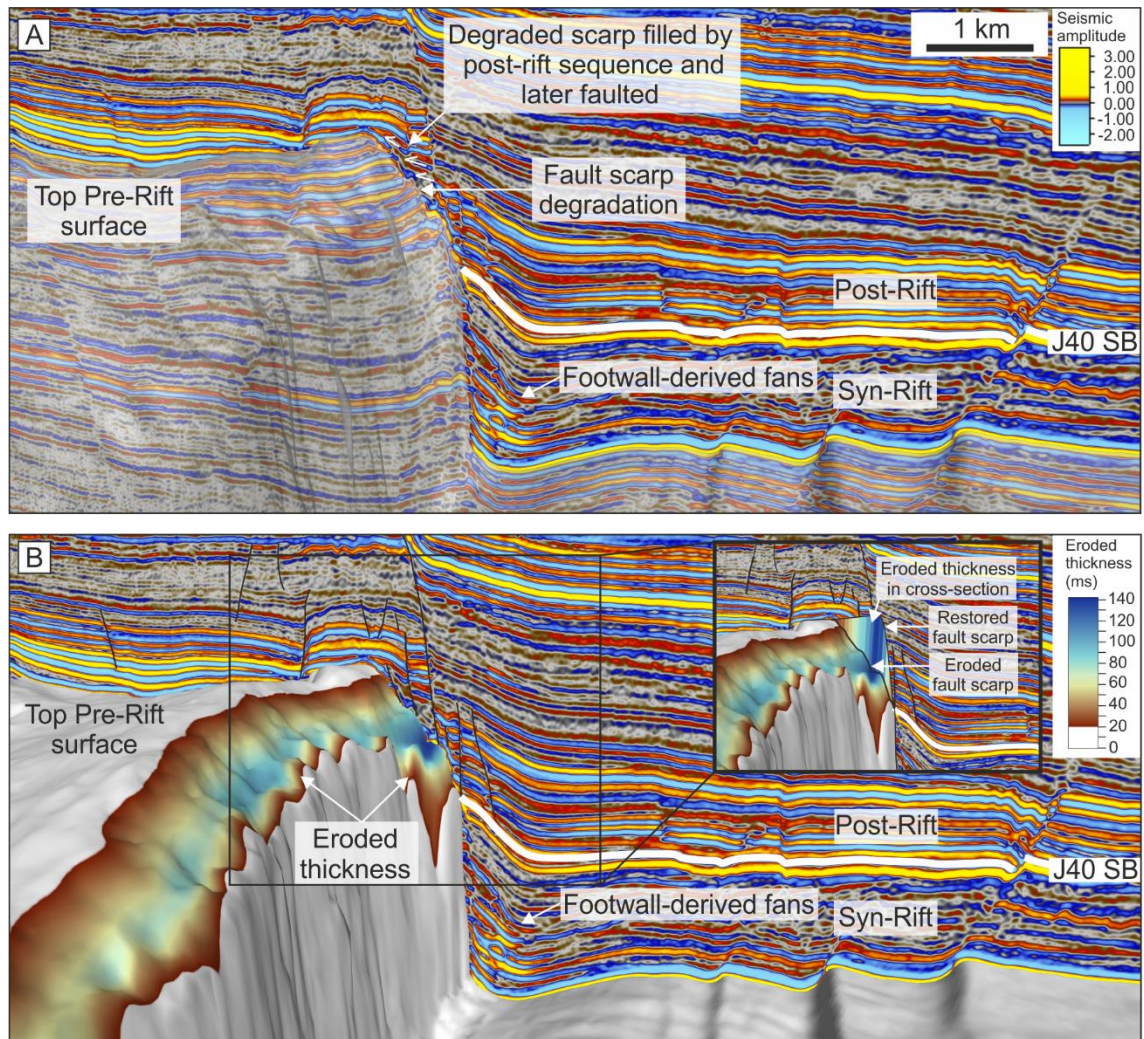


Figure 6.5. Seismic cross-section to highlight the degraded fault scarp. A) Degraded area of the fault scarp is overlapped and filled by the post-rift strata. Transparency is applied to the Top Pre-Rift surface to reveal the footwall seismic character. B) Map of the eroded thickness of sediment is overlain onto the fault scarp. Inset shows the eroded thickness projected onto the seismic cross-section. SB = sequence boundary. Eroded thickness colour map from Crameri (2018).

To calculate the volume of hangingwall fill, the two seismic units comprising radial, basinward-dipping reflectors interpreted to represent footwall-derived fans were identified (Units E and H). The bases and tops of the units were mapped, the areas between were gridded and the bulk volumes were calculated using the same approach as with the footwall degradation (Fig. 6.6).

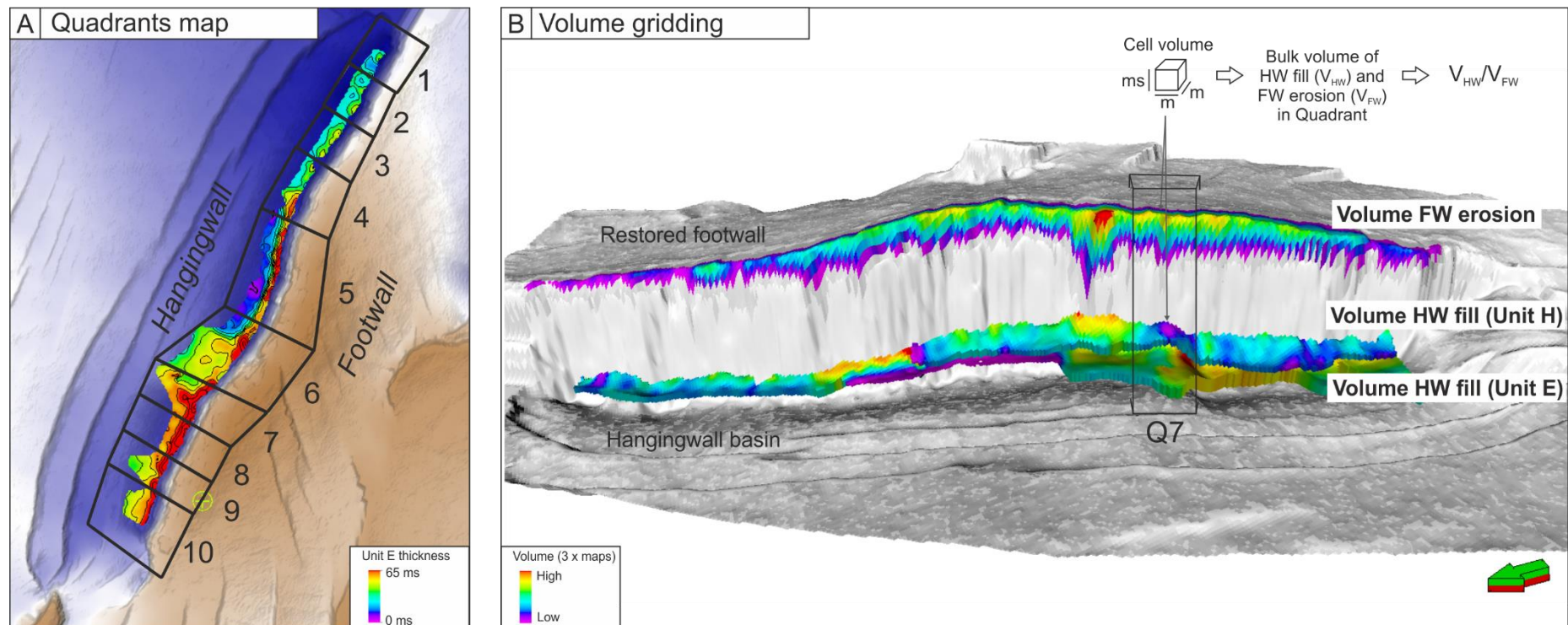


Figure 6.6. Methodology for volume balancing approach (V_{HW}/V_{FW}). A) Layout of quadrants along the fault for analysis. Quadrant boundaries are defined by interfan areas in the hangingwall basin, demonstrated here with an isochron map of Unit E containing footwall-derived fans. Each quadrant encompasses an area of the footwall and hangingwall. B) Volume gridding of the hangingwall units (Units E and H) containing footwall-derived fans, and the volume of eroded material from the footwall scarp. The restored footwall to its pre-erosional state is presented.

The seismic data is presented in time, and the output volumes are not true volumes of eroded and deposited sediment. For simplicity, each millisecond on the vertical axis is assumed to represent one metre in the volume calculation. To help comparison, and remove ambiguous units, a ratio is presented of hangingwall fill to footwall erosion (V_{HW}/V_{FW}). It is assumed that the grid cell volume on the footwall top is equivalent to the grid cell volume in the hangingwall fill, although it is acknowledged that there is some uncertainty due to the lack of depth and therefore thickness conversion from time.

We can reduce some of the uncertainty using a 'back-of-the-envelope' calculation (Fig. 6.7). The Top Pre-Rift surface at the Thebe-2 well lies at 2632 ms, where checkshot data yield an average velocity of 1668 m/s and the total vertical depth is 2217 m. Therefore, one millisecond at that depth represents ~1.67 m. The interval velocity at the Top Pre-Rift surface is greater at 2180m/s and so each millisecond in that interval could represent up to 2.18 m. This is larger than the 1 m assumption used in the volume calculation, and so all bulk volumes are likely to be underestimated and represent minimum values. The tops of the hangingwall fans are at approximately 3000 ms in the hangingwall. Extrapolating the velocity trend in the well beyond its maximum depth to 3000 ms gives a velocity of 1792 m/s. One millisecond at this depth represents ~1.79 m, which is within the range of estimates provided by the interval and average velocities for the footwall cells (Fig. 6.7). The hangingwall sediment succession is different to the footwall succession and likely has different acoustic properties. However, if the hangingwall fans are assumed to be fed from the degraded fault scarp, the interval velocity could be similar, excluding the effects of compaction. Therefore, with similar thickness conversions at the depth of footwall degradation to the depth of fan deposition, the assumption of equivalent cell volumes is deemed acceptable (Figs. 6.6 and 6.7).

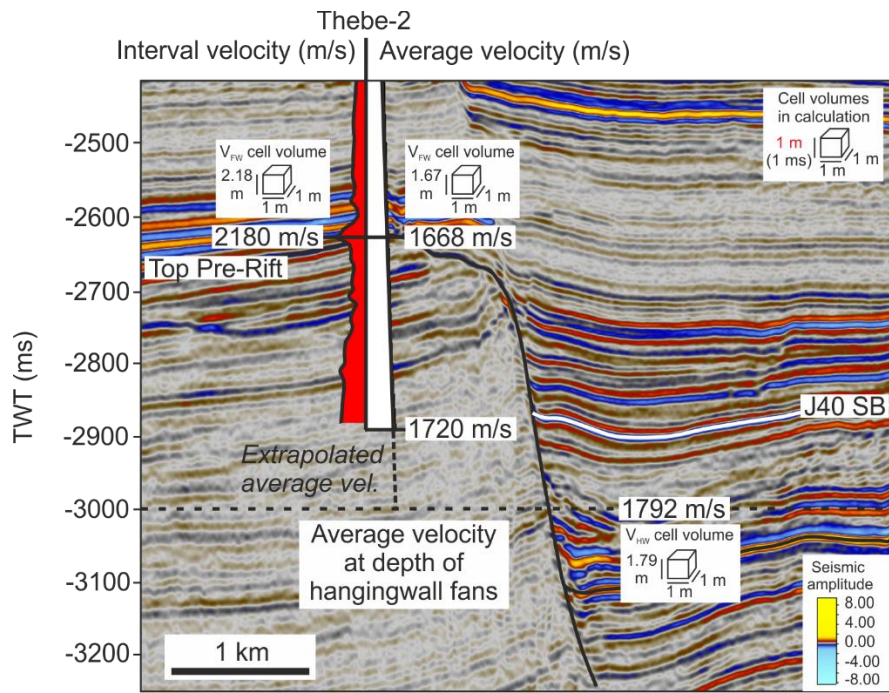


Figure 6.7. Approach for validating cell volume equivalency between the footwall and hangingwall intervals of interest. Data is presented in time and in the volume calculations, 1 ms is assumed to represent 1 m vertical height of a cell. In the footwall, interval (red) and average (white) velocity data from Thebe-2 yield values between 1.67 m and 2.18 m. Average velocity is extrapolated from the maximum depth of the well to the depth of the hangingwall fans and gives a vertical cell height of 1.79 m for the hangingwall fans. Various assumptions are inclusive of this approach (see text). Cell volumes are shown to be approximately equivalent between the footwall and hangingwall positions. Volume calculations are likely to be underestimates and represent minimum values.

6.5.3.1. V_{HW}/V_{FW} quadrant analysis

Only seismic units that are confidently interpreted to contain footwall-derived fans are included in the analysis and so other hangingwall sources are not considered to be contributing to the volumes calculated.

In order to identify where the greatest difference in footwall erosion to hangingwall fill is, 10 quadrants that cover the footwall and hangingwall are assessed (Fig. 6.6A). The volume of footwall erosion, and volume of sediment in Units E and H are calculated for each quadrant. The output volumes, the difference between V_{HW} and V_{FW} , and V_{HW}/V_{FW} ratio are recorded for each quadrant. Any excess volume in the hangingwall (i.e. $V_{HW} > V_{FW}$) is a result of through-going

sediment transport from beyond the footwall crest. Any excess eroded volume in the footwall (i.e. $V_{FW} > V_{HW}$) is a result of sediment bypass or redistribution. Any ratio values close to 1, should be deemed as uncertain.

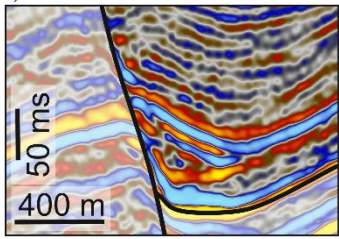
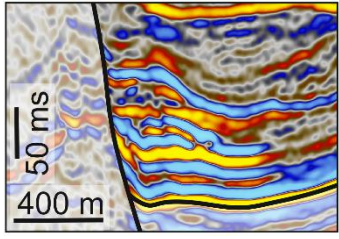
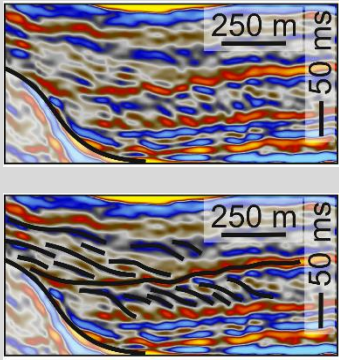
There are three main assumptions and considerations in the quadrant analysis: 1) all footwall-derived material is encompassed within each hangingwall grid, i.e. some fine-grained material may be incorporated into other units or may have left the basin; 2) the degraded footwall area within each quadrant supplies the hangingwall area within the quadrant and there is no along-strike re-distribution; 3) lower and higher units that contain footwall-derived material are not considered in the analysis, yet could increase hangingwall volumes. All assumptions yield conservative estimates for hangingwall fill in each quadrant.

6.6. Results

6.6.1. Stratigraphic framework

For the stratigraphic framework, twelve stratal units (Units A-L) are identified in the hangingwall basin, based on seismic facies (Table 6.1) and geometry (Table 6.2; Fig. 6.8; Fig. 6.9). In some places, units interfinger and in others they stack successively. The twelve stratal units are compiled into four major unit sets (1-4), representing four stages of evolution of the basin, separated by three key stratal surfaces (KSS1-3). Four SE-dipping antithetic faults (AA, AB, AC and AD) trending parallel to the main border fault are identified, which were active at various times during the deposition of the units. For reference, the hangingwall basin is divided into three sub-basins (northern, central and southern; Fig. 6.8A). The southern and central sub-basins are separated by a topographic saddle. The central and northern sub-basins encompass the extents of antithetic faults AA and AB, respectively.

Table 6.1. Seismic facies: example extracts, descriptions and interpretations.

Seismic facies	Example	Description	Interp.	
SF1	a)		<p><i>Character:</i> Mainly high amplitude, low-med. frequency (10-50 Hz), steeply-dipping reflectors. Internal reflections range from continuous to chaotic.</p> <p><i>Geometry:</i></p> <p>a) Planar-slightly concaved slope. 3D prism-apron shape along the fault. No radial geometry.</p> <p>b) Flat-slope cliniform. 3D radial geometry and in some cases interfingering with adjacent fans.</p> <p>Foreset heights ranges from 40 ms-200 ms (70-350 m with 1742 m/s velocity). Internal architectures vary along-strike, but generally exhibit progradational stacking near the base, and aggradational or retrogradational stacking towards the tops of the fans.</p> <p><i>Position:</i> Always positioned in the immediate hangingwall and dipping away from the main border fault.</p> <p>a) Sloping reflectors continue along the fault <4 km and extend <650 m away from the fault.</p> <p>b) Numerous positions – most striking example is ~4.5 km from the southern end of the basin</p>	<p>Footwall-derived subaqueous and submarine fans:</p> <p>a) Slope apron</p> <p>b) Fan delta</p>
	b)			
SF2		<p><i>Character:</i> Low-med. amplitude (peaks brighter than troughs), low-med. frequency (10-50 Hz), discontinuous, dipping reflectors. Separated by high amplitude, flat-lying reflectors that are conformable.</p> <p><i>Geometry:</i> 3D radial geometry. Foreset height 20-40 ms (35-70 m with 1742 m/s velocity). Foresets exhibit a highly progradational stacking pattern.</p> <p><i>Position:</i> Foresets prograde from the northern fault tip in a direction parallel to the fault trend, i.e. the depositional system follows an axial route. Foresets are restricted to a single interval/unit and are confined laterally and at their distal extent by footwall-derived fans. Only occurs in Unit G.</p>	<p>Stacked, prograding fan delta foresets, separated by flooding surfaces.</p>	

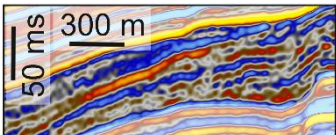
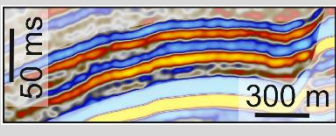
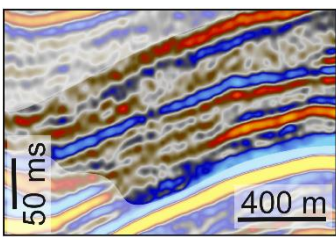
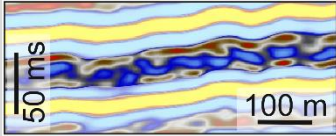
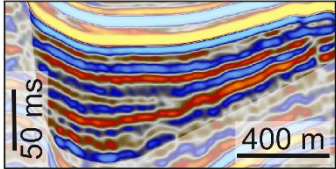
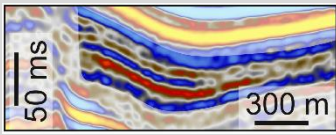












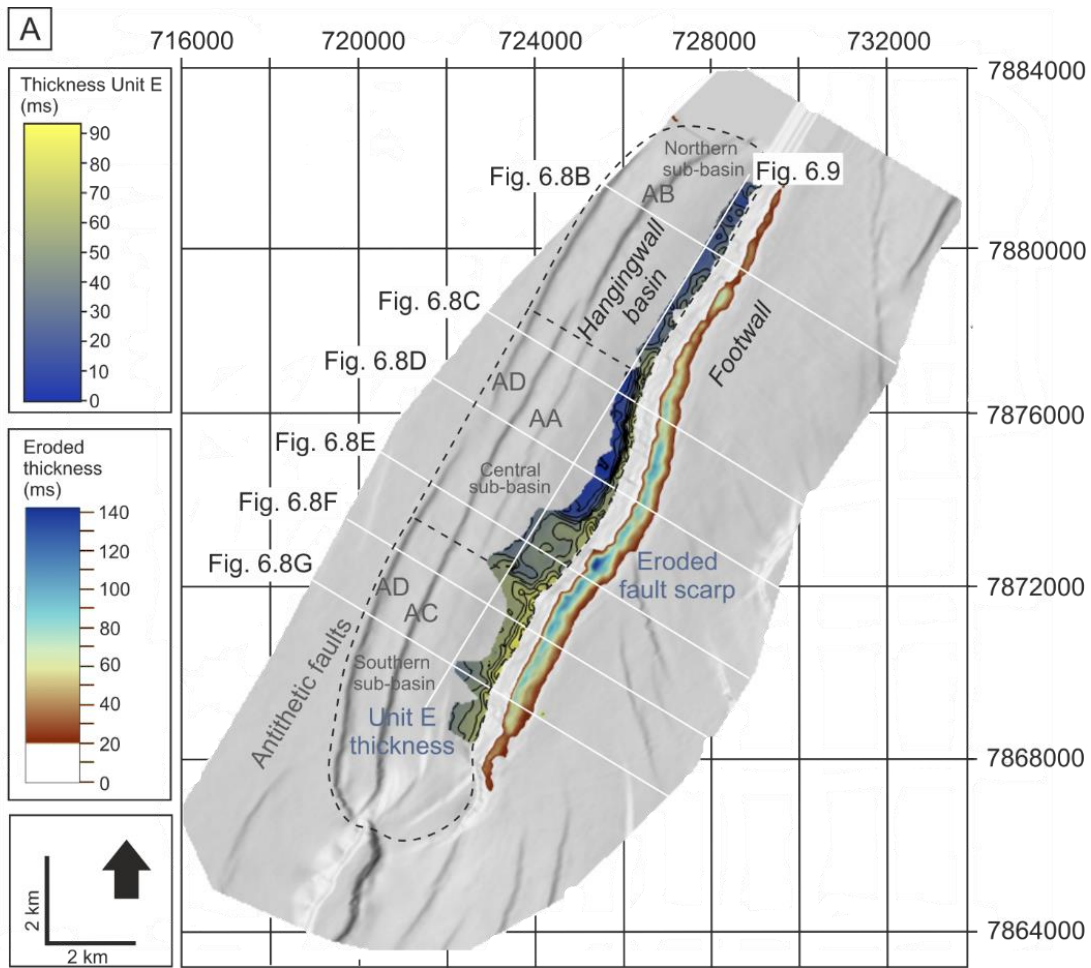
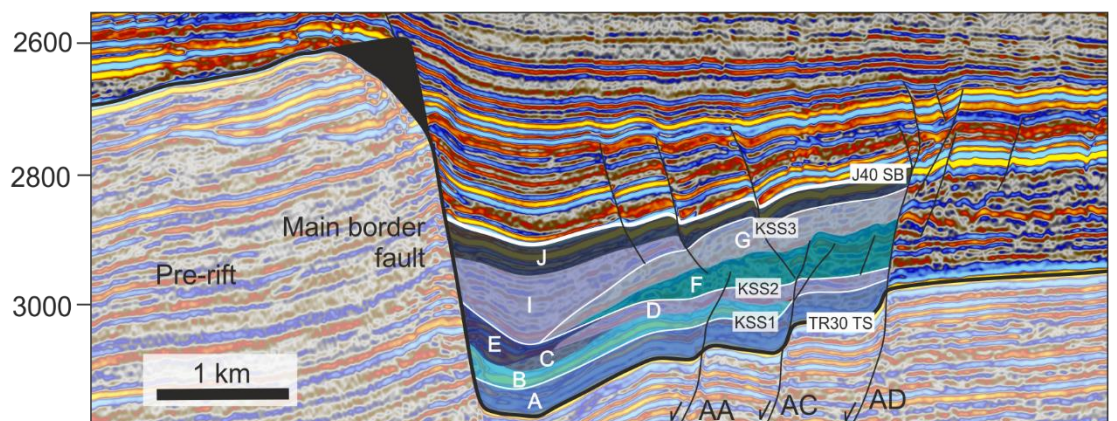
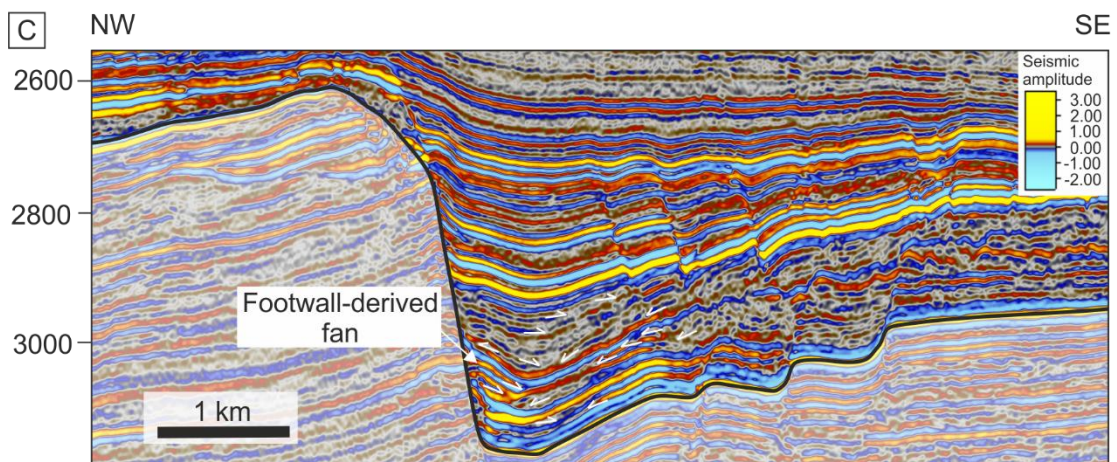
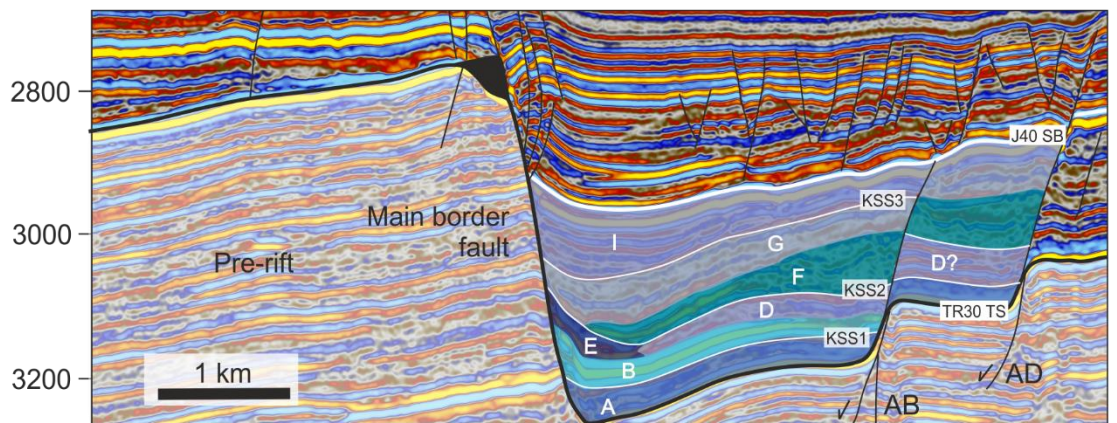
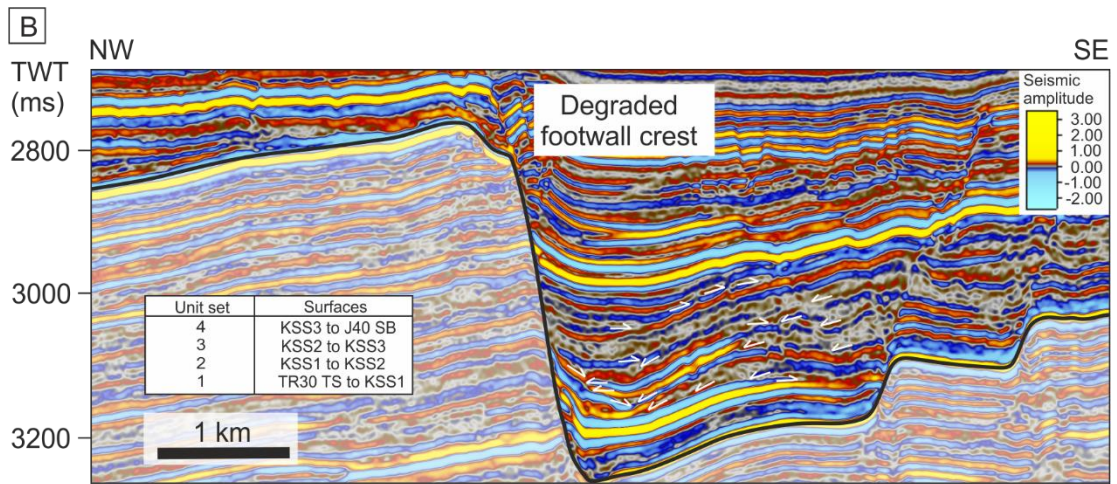
SF3		<p><i>Character:</i> Medium amplitude, med. to high frequency (40-70 Hz) reflectors with moderate continuity.</p> <p><i>Geometry:</i> Shallow, basinward-dipping with clinoformal and radial shape. Foreset height 50-60 ms (90-105 m with 1742 m/s). Topset length <300 m.</p> <p><i>Position:</i> Prograding away from antithetic faults into the southern sub-basin. Occurs only in Unit G.</p>	Deltaic clinoforms prograding basinward from antithetic faults
SF4		<p>Medium to high amplitude, low-med. frequency (20-50Hz), moderate-high continuity, undulating reflectors that are relatively flat-lying to gently-dipping (sometimes following pre-rift topography) and fade/pinch-out down-dip and along-strike. Observed in Units A, B, D, F, K.</p>	Shoreface? Turbidites?
SF5		<p>Low amplitude, low frequency (10-20Hz), chaotic-discontinuous reflections. Apparent at the downdip terminations of higher amplitude, dipping reflectors. Observed in Units B, C, D, E, F, G, H, I, K.</p>	Mass transport deposits in clinoform bottomsets
SF6		<p>Med. amplitude, low-high frequency (10-80Hz), discontinuous reflectors with undulating geometries. Observed in the lowest syn-rift stratigraphy (Unit A).</p>	Unknown – channels?
SF7		<p>Med. amplitude, med.-high frequency (40-70Hz), continuous reflectors, onlapping underlying topography. Some undulations. Observed in the upper part of the syn-rift stratigraphy (Units I, J, K, L).</p>	Turbidites?
SF8		<p>Low to med. amplitude, high frequency (50-80Hz), steeply-dipping reflectors with a planar sloping geometry that appears to be radial in 3D. Observed in Units J, L. Dipping reflectors are <100 ms high.</p>	Submarine fan?

Table 6.2. Stratigraphic framework: seismic unit descriptions. U = Unit; US = Unit set.

U	US	Col.	Key features	Facies	Ext.	Fault thicken.	Top surface character	Max. strat. thick.	Max. foreset height
A	1		Small clinofolds from main border fault	SF6	Whole basin	Main border fault	KSS1. Bright and continuous reflector in N - becomes discontinuous towards S. Change of seismic facies across surface.	63 ms Thins toward S	20 ms
B	2		Fans from main border fault and antithetic faults	SF1a-b; SF4	Whole basin	Main border fault & AB & AC	Change of seismic facies & downlap from reflectors above.	40 ms. Av. 23 ms	30 ms
C	2		East- and west-dipping, interfingering reflectors	SF5	Cent. sub-basin	None	Distinct, flat-lying, high amplitude trough, downlapped by Unit E and F.	53 ms	
D	2		Depos. system from NW, antithetic faults	SF4; SF5	North. and central sub-basins. Restricted to the NW.	AB & AC	KSS2. In the N, downlapped by system from NW (Unit F), and towards S it is downlapped by Unit H. Change in seismic facies. In places eroded by Unit G.	80 ms Av. 43 ms	
E	2		Fans from main border fault	SF1a-b	Whole basin	Main border fault	KSS2. In the N, downlapped by system from NW (Unit F), and towards S it is downlapped by Unit H. Change in seismic facies. In places eroded by Unit G.	93 ms	67 ms
F	3		Depos. systems from the NW, antithetic faults	SF8; SF4; SF5	North. and central sub-basins. Restricted to the NW.	AA, AB, AC & AD	Downlapped by Unit G from the NW. Change in seismic facies.	80 ms	40 ms
G	3		Axial clinofolds between flat-lying reflectors & fans from NW, antithetic faults	SF2; SF3; SF4	Whole basin	AA, AB, AC & AD	KSS3. Onlapped by Units I, J, K, in places onto a high-amplitude approximately flat-lying trough. Change in seismic facies.	86 ms; Av. 41 ms	20-40 ms

H	3		Fans from main border fault	SF1a-b	Cent. and south. sub-basins. Restricted to SE.	Main border fault	KSS3. Onlapped by Units I, J, K, in places onto a high-amplitude approximately flat-lying trough. Change in seismic facies.	98 ms	98 ms
I	4		Possible clinofolds from antithetic fault AB near northern fault tip. Onlapping older reflectors.	SF3; SF7	North. and central sub-basins	Main border fault	In the N sub-basin – J40 SB (high amplitude, continuous reflector). In central sub-basin – downlapped by Unit J. Change in seismic facies.	96 ms Av. 29 ms	34 ms
J	4		Possible fan from main border fault - dipping, low amp. reflectors	SF8	Cent. sub-basin	Main border fault	In the central sub-basin – J40 SB (high amplitude, continuous reflector). At the basinal high, downlapped by Unit K. Change in seismic facies.	100 ms	100 ms
K	4		Shallow clinofolds from main border fault	SF3; SF5	Cent. and south. sub-basins	Main border fault	Relatively flat lying, possibly erosive, high amplitude trough. Change in seismic facies.	79 ms	35 ms
L	4		Flat-lying reflectors	SF4; SF7	South. sub-basin	Main border fault	J40 SB (high amplitude, continuous reflector).	80 ms	31 ms



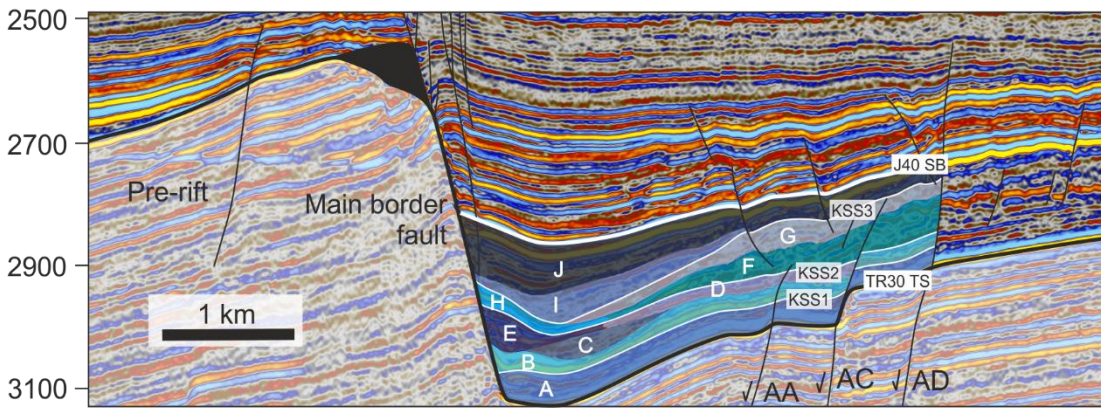
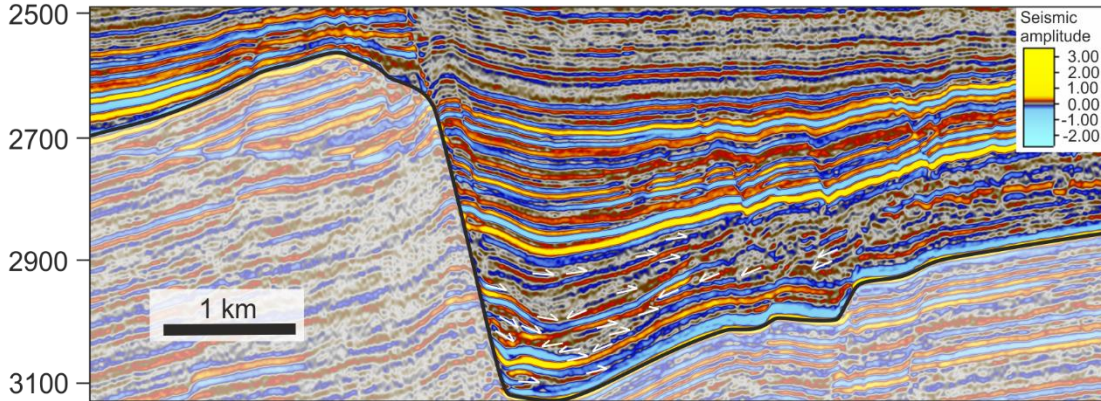


D

TWT
(ms)

NW

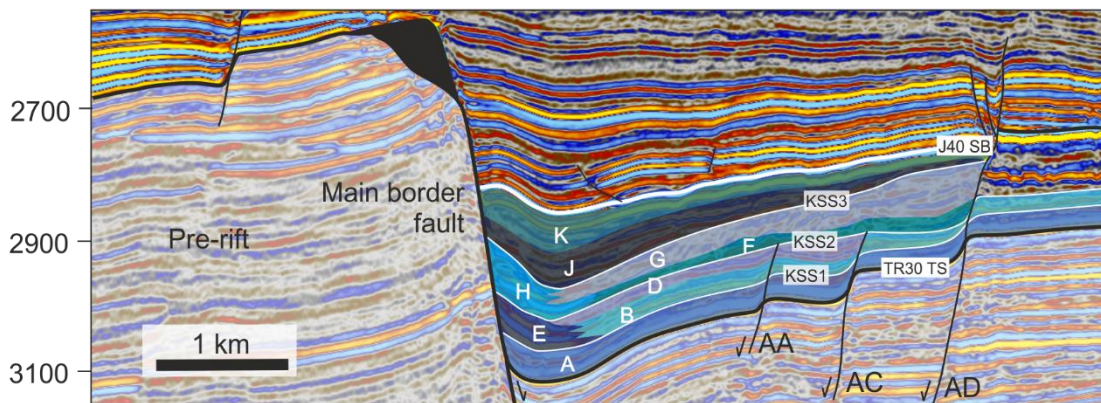
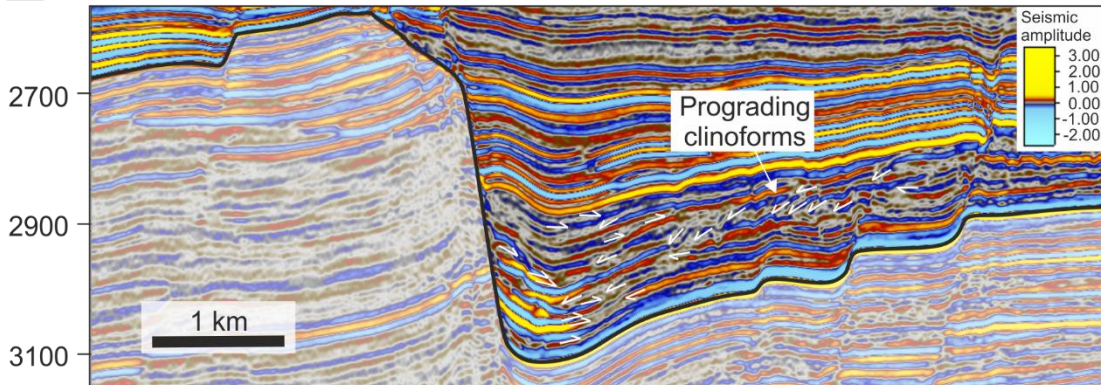
SE



E

NW

SE



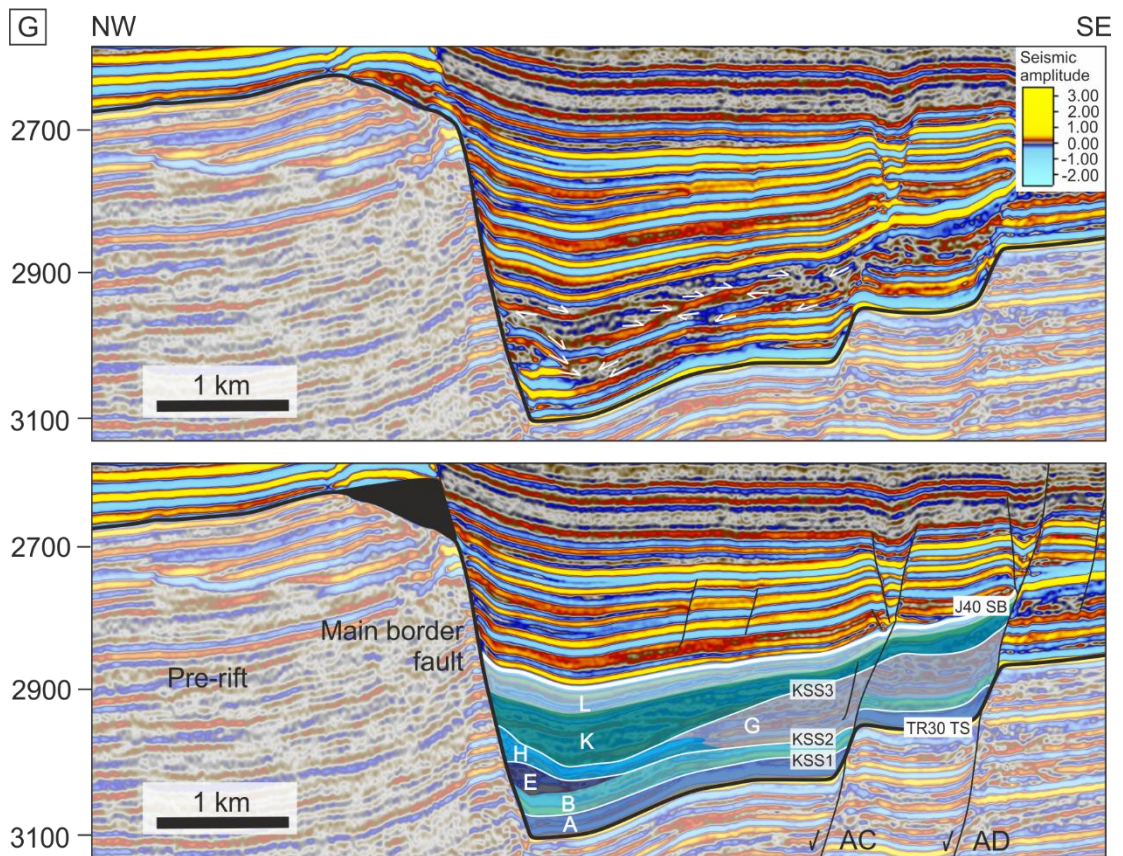
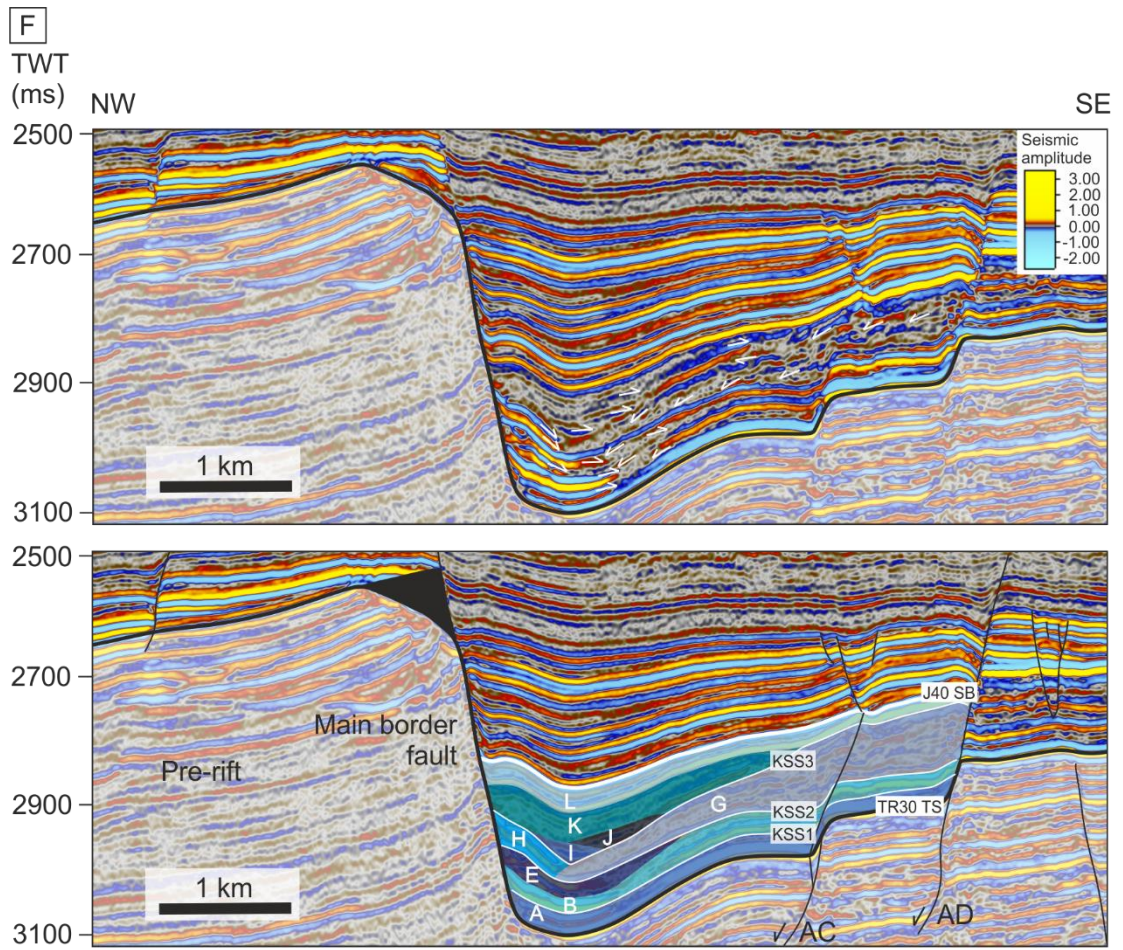


Figure 6.8. Six NW-SE trending representative seismic sections along the fault are presented to show the stratigraphic framework. A) Map of the basin to show positions of seismic sections (B-G). A map of the eroded thickness of the fault scarp is overlain onto the footwall and an isopach map of Unit E is presented in the hangingwall. The basin is divided into three sub-basins for reference (northern, central and southern). Antithetic faults AA-AD are highlighted. Sections B-G: uninterpreted and interpreted seismic sections. Pre-rift stratigraphy is shaded white. Seismic units A-L are shaded in blues. Footwall degradation is shaded in black on interpreted sections. Key stratal surfaces (KSS) are highlighted in white. Eroded thickness colour map from Crameri (2018).

6.6.1.1. Unit set 1

Unit set 1 comprises Unit A, which is bounded by the Top Pre-Rift surface at the base and KSS1 at the top (Fig. 6.8; Fig. 6.9). KSS1 is high amplitude and laterally continuous in the northern sub-basin, but becomes lower amplitude and discontinuous towards the south. A clear change in seismic facies occurs across KSS1. Unit A extends across the entire hangingwall basin. The unit has a maximum stratigraphic thickness of 63 ms, and thins towards the south to ~40 ms. Overall, there is thickening into the main border fault. Thickening (~30 ms) in the immediate hangingwall at the fault centre and towards the northern fault tip occurs where reflectors dip steeply towards the north-west, away from the main border fault (SF1b; Table 6.1). The reflectors exhibit a clinoformal geometry and appear to be fan-shaped in 3D (SF1b). Elsewhere, the unit is dominated by SF6.

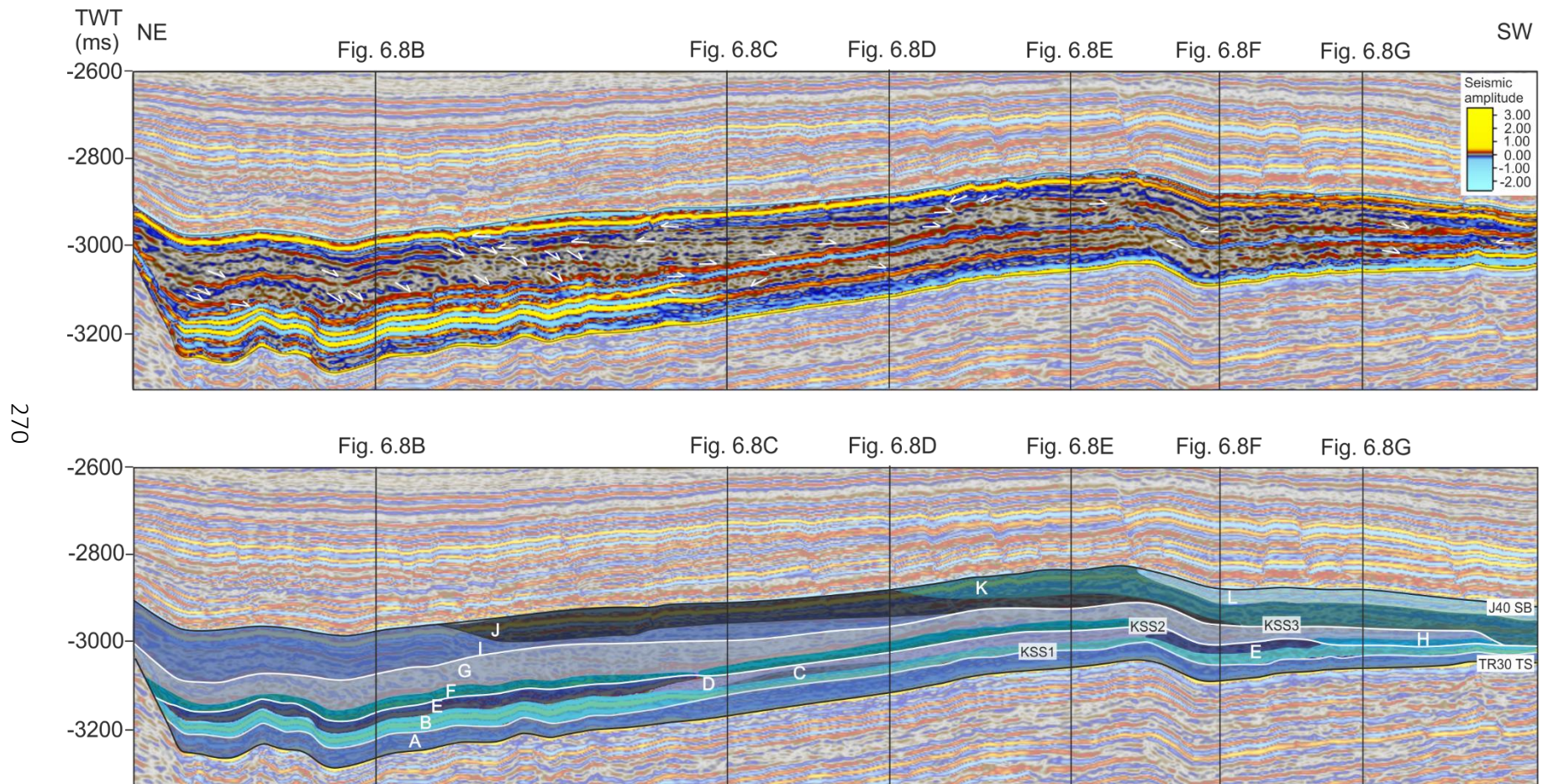
6.6.1.2. Unit set 2

Unit set 2 comprises Units B-E and is bounded at the base by KSS1 and at the top by KSS2 (Fig. 6.8; Fig. 6.9). KSS2 comprises two high amplitude, laterally continuous reflectors that pinch out towards each other down-dip. Both dip towards the basin at the same stratigraphic level, one from the north-west and one from the south-east. The surface is denoted by a change of seismic facies across it and multiple downlaps from reflectors above.

Unit B thickens into the main border fault and also slightly into the antithetic faults, AB and AC that are separated by, a short relay zone (Fig. 6.8A). Unit B is dominated by SF1a and SF4 (Table

6.1). Fan-shaped, dipping reflectors stack against the footwall of the main border fault, with foreset heights of ~30 ms, represented by a single, low frequency, high amplitude wavelet; the internal architecture is below the resolution of the seismic data. SF4 is the dominant facies of the depositional system from the west, and in this case reflectors are gently dipping towards the south-east. Conversely, Unit C is restricted to the basin centre (Figs. 6.8C, 6.8D and 6.9), is dominantly SF5 (Table 6.1), and comprises east- and west-dipping reflectors that offlap and fill the underlying topography. Their down-dip terminations interfinger with, and downlap onto Unit B. The top is a distinct, flat-lying, high amplitude trough that is downlapped by reflectors within Units E and F above. The unit has a bowl shape and is thickest at its centre at 53 ms. Unit D extends across the northern and central sub-basins (Figs. 6.8A-E; Fig. 6.9), but is limited to the west and is not present in the vicinity of the main border fault. The unit thickens into antithetic faults AB and AC. Dominant facies are SF4 and SF5, which dip gently towards the basin, from the north-west (Table 6.1). Unit E extends in the strike direction along the whole hangingwall basin and extends 400-700 m away from the main border fault (Fig. 6.8A; Fig. 6.9). The unit is thickest in the immediate hangingwall of the main border fault (~93 ms). SF1a-b (Table 6.1) are the dominant facies. Overall, reflectors exhibit fan-shaped, dipping geometries that are clinoformal in some cases and footwall-derived. Foresets have a maximum height of 67 ms. In the north and central sub-basins, Unit E interfingers with Unit D (e.g. Figs. 6.8B, 6.8C and 6.8D), but towards the southern sub-basin, where present, it is downlapped by Unit D (Fig. 6.8E; Fig. 6.9). Unit E is used for volume balancing with footwall degradation because it is one of two units that are dominated by footwall-derived fans with substantial volume.

Figure 6.9. Representative strike section (NE-SW) through the hangingwall stratigraphy with clean and interpreted seismic data. The stratigraphic framework is shaded in blues (Units A-L). Key stratal surfaces (KSS1-3) are highlighted with white lines. Pre-rift stratigraphy is shaded white. Position of section is indicated in Figure 6.8A and is proximal to the main border fault.



6.6.1.3. Unit set 3

Unit set 3 comprises Units F-H and is bound by KSS2 at the base and KSS3 at the top (Fig. 6.8; Fig. 6.9). KSS3 is characterised by a change of seismic facies and multiple onlaps from reflectors within Unit set 4 above. Unit F extends across the northern and central sub-basins from the west, and does not reach the main border fault. The unit thickens into antithetic faults AB, AC and AD, and dominant facies include SF4 and SF5 (Table 6.1). Foresets have a maximum height of 40 ms and dip away from antithetic fault AC, towards the south-east. Unit G extends across the whole hangingwall basin, but is absent ~700 m from the main border fault, as it onlaps underlying topography (Unit E). The unit has a distinct character in the northern sub-basin, comprising three clinoform packages with small foresets (~20 ms). Clinoforms prograded southwards from the northern fault tip and each package is separated by a relatively flat-lying, low-medium amplitude reflector (SF2; Table 6.1). In the central sub-basin, the thickness of the clinoform packages decreases, the flat-lying horizons converge and they onlap KSS2. From the basinal high that separates the central and southern sub-basins and into the southern sub-basin, other clinoforms (SF3; ~40-60 ms high) prograde from the north-west, from antithetic fault AC (Table 6.1). The clinoforms interfinger with and onlap the distal margin of fans within Unit H, and decrease in height down-dip, displaying a falling breakpoint trajectory (Fig. 6.8D). Unit H extends along the immediate hangingwall of the main border fault in the central and southern sub-basins and ~850 m into the basin. Similar to Unit E, it comprises large footwall-derived fans from the main border fault, characterised by SF1a-b (Table 6.1), and generally dips towards the north-west. Foresets have a maximum height of 98 ms. Unit H interfingers with the south-east dipping Unit G. Unit H is used for volume balancing with footwall degradation because, like Unit E, it contains a substantial volume of footwall-derived deposits.

6.6.1.4. Unit set 4

Unit set 4 comprises Units I-L. The unit set is bounded by KSS3 at the base and the Top Syn-Rift surface (J40 SB) at the top (Fig. 6.8 and Fig. 6.9). Only Unit I is present in the northern sub-basin. Units J-L progressively become more prevalent towards the south. Unit I is absent from the

southern sub-basin. In the central sub-basin, it is downlapped and overlain by Unit J, and fills the topography formed by Units G and H. Dominant facies within Unit I are SF7. In the most northerly part of the central sub-basin, the top of Unit J is the J40 SB, and in the southern part of the central sub-basin the unit is downlapped by Unit K. Unit J comprises a thickened area (~2.5 km radius) positioned at the centre of the main border fault and onlaps onto underlying topography. Steeply-dipping reflectors extend ~800 m away from the centre of the main border fault in Quadrant 6, where most footwall scarp degradation is observed. The unit is characterised by SF8, which represents low-medium amplitude, high frequency (50-80Hz), steeply-dipping reflectors with a planar slope geometry. Dipping reflectors are up to 100 ms high. Unit K is mostly limited to the southern sub-basin and is characterised by SF4 and SF5. Gently dipping reflectors downlap Unit G, and away from the main border fault towards the north-west. Unit L is only present in the southern sub-basin. The top of Unit L is the J40 SB. The unit has a maximum thickness of 80 ms, where it fills pre-existing lows in topography and is characterised by SF7 and SF8.

6.6.2. Along-strike variability of hangingwall fans

Footwall-, hangingwall- and axial-derived fans are identified in the hangingwall basin based upon bedding dip orientations and 3D geometries. Expressions of hangingwall-derived fans range from aggradational clinofolds with distinct topsets (SF3; Table 6.1) in the southern sub-basin (Unit G; Fig. 6.8F) to progradational foresets with limited topset development (SF2; Table 6.1) in the central sub-basin (Unit F; Fig. 6.8E). Axial-derived fans similarly display the latter, but with lower foreset heights (20-40 ms), and present three foreset stacks, separated by relatively flat-lying horizons. Substantial variability is observed between footwall-derived fans that build along the footwall of the main border fault. Four along-strike variations between fans are observed: 1) overall 3D geometry, 2) the change in 3D geometry through time, 3) internal character, and 4) stacking patterns.

The overall 3D geometry of the fans varies along-strike and is used to distinguish SF1a (planar-slightly concaved slope, interpreted to be slope aprons) from SF1b (clinoformal shape with clear

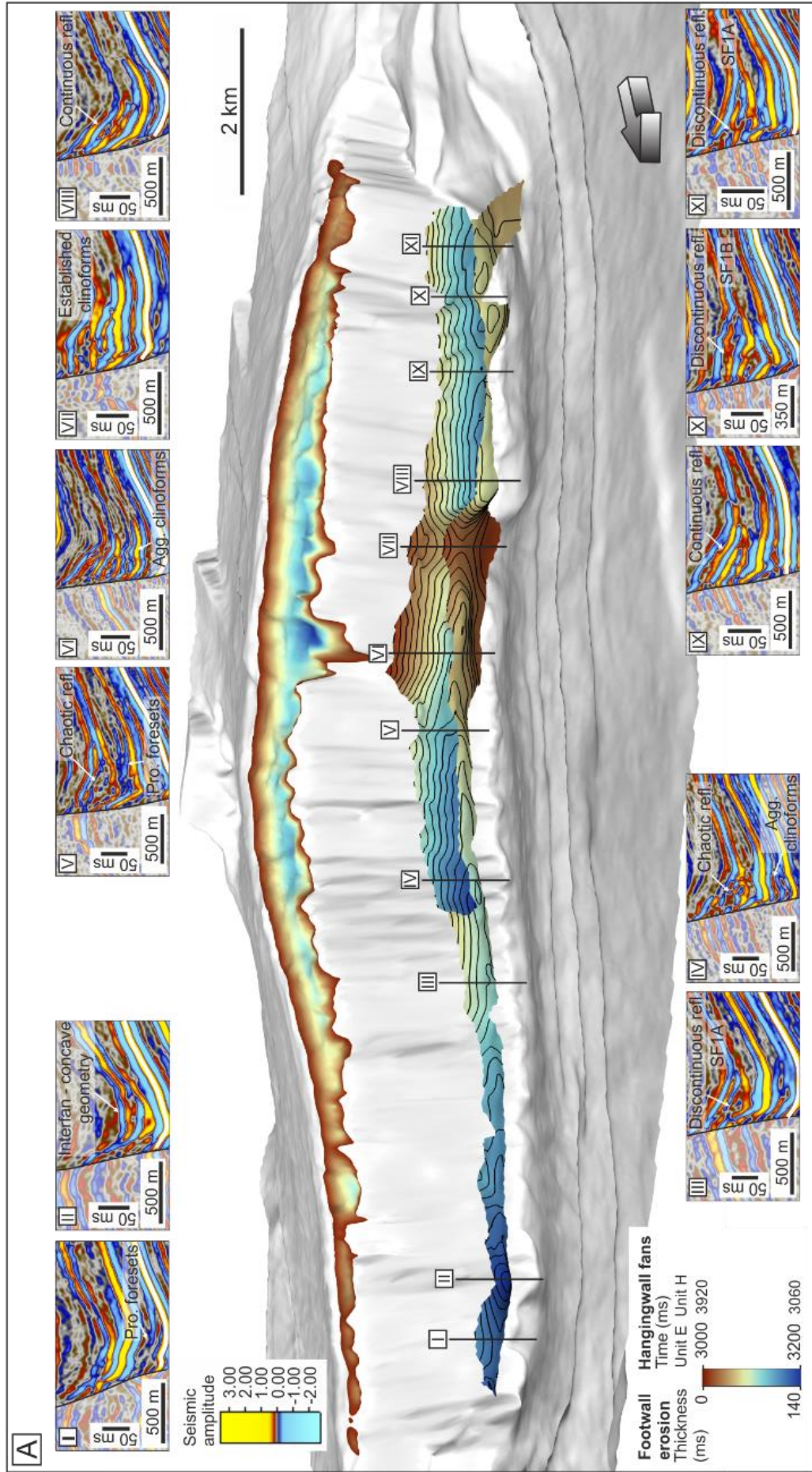
topsets and foresets, interpreted to be fan deltas) (Table 6.1). All three geometries are apparent along the fault during the deposition of Units E and H (Fig. 6.10). Interfan areas (Barrett et al., accepted; e.g. position B, Fig. 6.10A) exhibit concave reflections, as opposed to the sloping or convex to clinoformal shapes of the fans.

The evolution of the fans through time results in a change of 3D geometry in numerous positions along the fault. Small fans (~40 ms foreset height) are observed in Unit set 1, which built against the footwall of the main border fault. Distinct fans are apparent and they do not occupy the whole length of the fault. In Unit sets 2 and 3, fans become more established with greater radius (e.g. ~250 m), higher foresets (e.g. ~100 ms), and extend along ~90% of the main border fault, as slope apron deposits are developed (e.g. positions III, IV, V and VI; Fig. 6.10A). Towards the northern end of the fault, fans remain limited in size through time. Positions III, IV, VI, IX and XI (Figs. 6.10A and 6.10B) show a change from a clinoformal geometry in the lower units to a sloping geometry in Units E and H. The only position that maintains its clinoformal geometry throughout its development is position VII (Figs. 6.10A and B).

Internal seismic character of the fans is also variable along-strike from chaotic (e.g. positions IV and V; Fig. 6.10A), through discontinuous (e.g. positions III, X and XI; Fig. 6.10A), to continuous reflectivity (e.g. positions I, VI, IX and VIII; Fig. 6.10A). The seismic character is also variable through time. For example, at position VII (Fig. 6.10A), reflectivity is continuous towards the base, discontinuous in the middle, chaotic across a short interval thereafter and continuous at the top (Fig. 6.10B).

In the lower units, stacking patterns of clinoforms differ from progradational towards the north-eastern fault tip (Fig. 6.10A, position I) to aggradational towards the fault centre (Fig. 6.10A, position IV). At position VII, where clinoformal geometry is maintained throughout basin evolution, stacking varies between progradational, aggradational and retrogradational trends through time (Fig. 6.10B). However, even with the absence of a topset-foreset breakpoint for stacking analysis, it is clear to see a strong retrogradational trend at position VIII (Fig. 6.10B) (~1

km to the south) and an aggradational trend at position VI (~2 km to the north), relating to the delicate balance between accommodation creation and sediment supply along the fault.



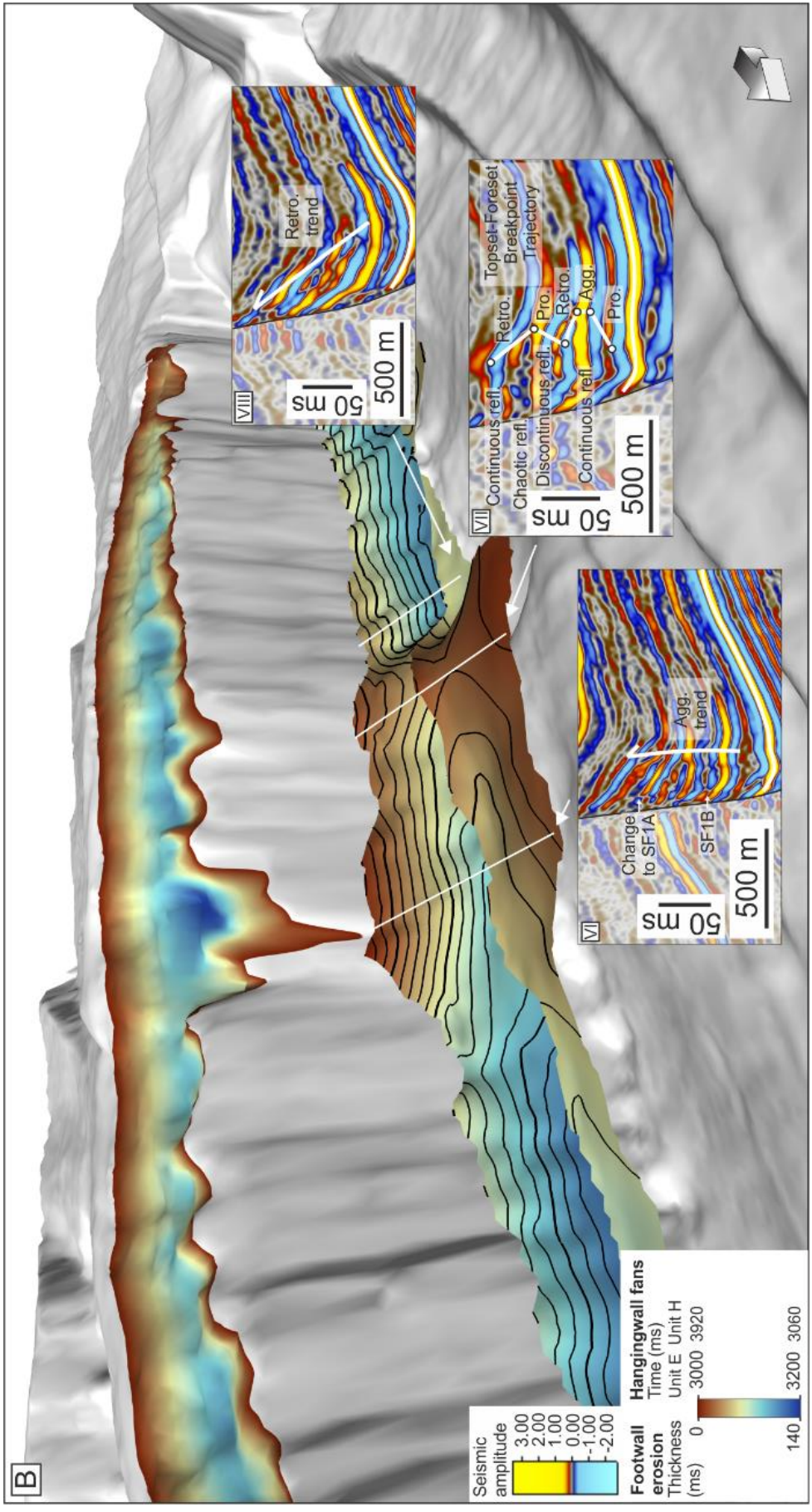


Figure 6.10. Along-strike variability of footwall-derived fans. A) Top surfaces of Units E and H in the hangingwall are presented with the amount of fault scarp erosion overlain onto the footwall. Positions I-XI show the variability in fan character and geometry along the fault. B) Focus upon three positions (VI-VIII) to show internal variability and stacking within the fans through the vertical succession. Eroded thickness colour map from Cramer (2018).

6.6.3. Footwall analysis results

Maximum fault throw is measured towards the fault centre (642 ms) and minima (170 ms) are observed towards the fault tips. Fault throw does not reach zero in the data as the fault tips are not reached. In the south-west, the fault extends into the relay zone with an adjacent fault, and in the north-east, the fault tip is beyond the seismic data limit. A fault throw minimum is observed in Quadrant 7 (IL2300; Figs. 6.6 and 6.11), which coincides with a topographic high in the hangingwall that separates the central and southern sub-basins. The topographic high appears to be inherited from an underlying, perpendicular structure. From the fault throw distribution, it appears that this structure separated two early fault segments, and could have allowed the formation of an early relay zone that was later breached.

The amount of vertical erosion is reflected in the difference between the two plots of fault throw (pre- and post-erosion; Fig. 6.11A). Minimum values are apparent towards the fault tips (23 ms) and it increases towards the fault centre with an approximate parabolic distribution. The maximum vertical erosion (228 ms) is in Quadrant 6 (Figs. 6.6 and 6.11A), which coincides with maximum headward erosion (905 ms). Headward erosion is highly irregular along-strike, with large differences between peaks and troughs over short distances. Notable peaks in headward erosion occur in Quadrants 3, 5, 7. Nonetheless, there is still an overall parabolic trend along the fault, in line with fault throw.

Values of headward erosion are of similar magnitude to the fault throw, suggesting: a) a greatly reduced slope towards the fault scarp during fault development, b) inboard erosional processes modified the slope. However, distinct erosional catchments in the footwall were not imaged, highlighting the requirement for an alternative method to identify fixed, through-going sediment input points.

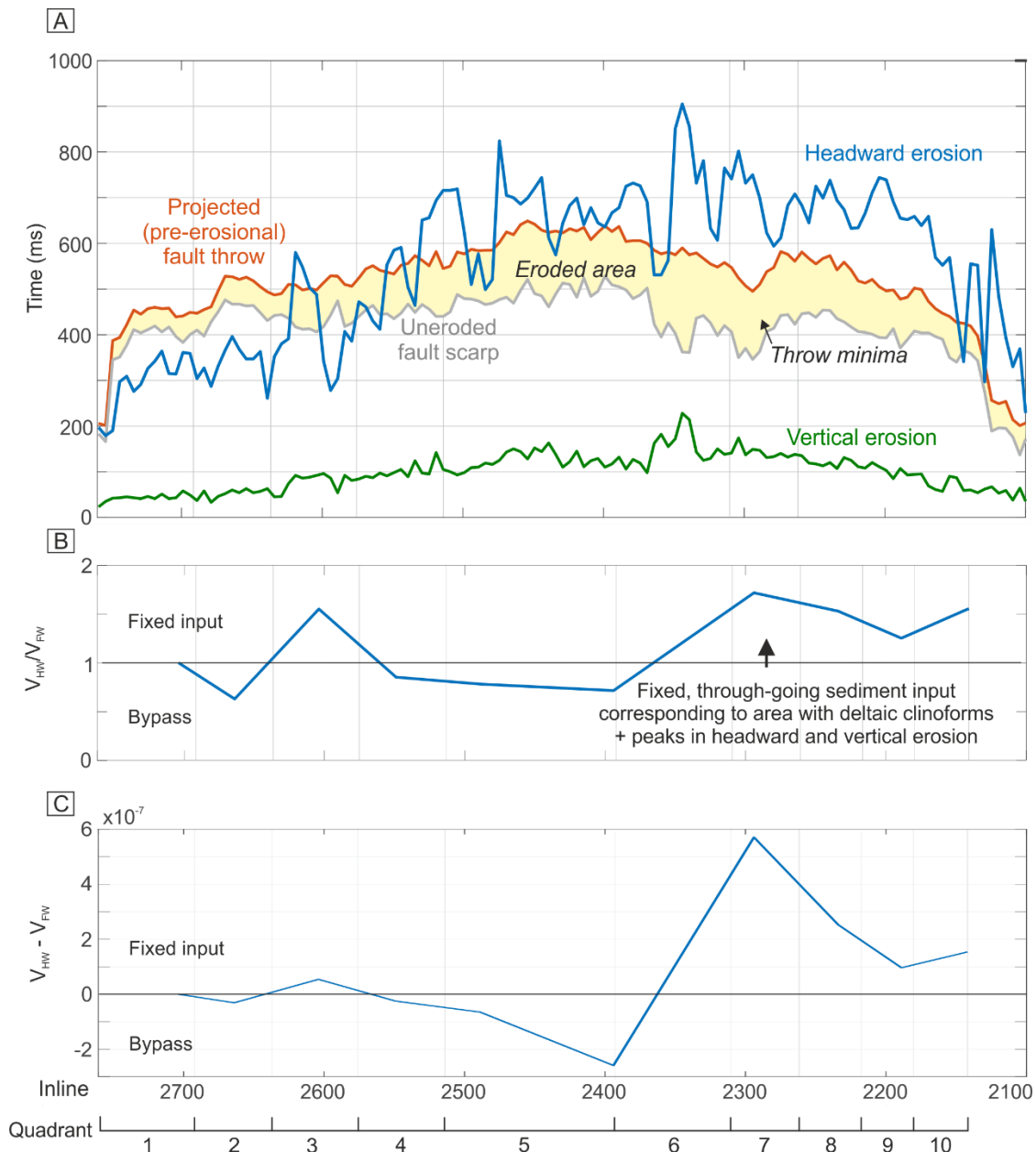


Figure 6.11. Graphs to show results of the footwall analysis. A) Fault throw from the restored footwall (red) and from the preserved state of the fault (grey). Yellow shaded area represents amount of vertical erosion, which is also plotted in green. Vertical and headward erosion (blue) vary along-strike but generally follow the parabolic trend of the fault throw distribution. B) Ratio of footwall erosion to hangingwall fill of footwall-derived fans (V_{HW}/V_{FW}). Values below 1 represent excess footwall erosion, i.e. areas of sediment bypass. Values above 1 represent areas of excess hangingwall fill, i.e. positions of through-going sediment input points. C) Plot to show $V_{HW}-V_{FW}$, which highlights the areas close to a balance. The largest peak is in Quadrant 7 and a minor peak is in Quadrant 3, showing positions of through-going input points, coinciding with clinoformal geometries in the hangingwall stratigraphy. Quadrant 5 shows area of sediment bypass, coinciding with slope apron deposits in the hangingwall.

6.6.4. Volume balancing - V_{HW}/V_{FW}

Volume balancing between the eroded material from the footwall (V_{FW}) and the volume of footwall-derived material in the hangingwall fans (V_{HW} of Units E and H) reveals the position of through-going sediment input points, and areas of sediment bypass and/or redistribution. Quadrants that exhibit excess footwall erosion relative to hangingwall fill represent areas of sediment bypass, and those that exhibit excess hangingwall fill correspond to through-going sediment input points. In the V_{HW}/V_{FW} plot many of the quadrants show values close to ~1 (Fig. 6.11B). The $V_{HW} - V_{FW}$ plot (Fig. 6.11C) highlights those areas that are close to a balance with values ~0. As such, the only area of convincing sediment bypass is in Quadrant 5, which coincides with slope apron deposits in the hangingwall (Fig. 6.10). The highest peak in V_{HW}/V_{FW} and $V_{HW} - V_{FW}$, indicating a through-going input point, corresponds to Quadrant 7. This is coincident with peaks in vertical and headward erosion (Fig. 6.11A), but not their maximum values along the fault. The highest vertical and headward erosion occur in Quadrant 6, which could suggest an oblique transport path to the hangingwall relative to the orientation of the fault. The peak also corresponds to the fault throw minimum and topographic high in the hangingwall basin. The peak occurs exactly where there is convincing clinoform development in the hangingwall, with clear topsets and radial foreset geometries (SF1b; Table 6.1; Fig. 6.10). There is a second, minor peak that is highlighted in the V_{HW}/V_{FW} plot in Quadrant 3. This also coincides with clinoform development in the hangingwall in Unit E (Unit set 2). Unlike the situation in Quadrant 7, where clinoforms are maintained, in Quadrant 3, the clinoforms in Unit set 2 are overlain by planar-sloping reflectors of Unit set 3, interpreted to be a submarine fan.

6.7. Tectono-stratigraphic evolution

6.7.1. Phase 1 – Unit set 1

Thickening of Unit set 1 strata into the main border fault suggests that the fault became active at this time (Fig. 6.12). Small, footwall-derived fan deltas began to build at discrete locations along

the main border fault, as evidenced by the development of clinoforms. Their development, with small foreset heights suggests a shallow marine environment prevailed at this time. The progradational stacking of fans towards the northern fault tip suggests that sediment supply outpaced accommodation creation in the hangingwall. Conversely, aggradational stacking towards the fault centre implies that sediment supply and accommodation creation were approximately equivalent. For a given sediment supply, this stacking distribution is typical of hangingwall basins, where fault-related subsidence presents a parabolic distribution along-strike, with maximum subsidence towards the fault centre and minima at the fault tips (Walsh & Watterson, 1988; Dawers & Anderson, 1995). In Quadrant 7, the fan delta presents a progradational geometry despite being relatively close to the fault centre, either suggesting enhanced sediment supply or reduced accommodation at this position. The fan delta is positioned at the saddle between the central and southern sub-basins on an inherited structural high. The fault throw minimum and breached relay sit at this location and likely focussed sediment transport at the early stages of fault development. The sediment input then became fixed in the landscape and continued to supply sediment.

6.7.2. Phase 2 – Unit set 2

Thickened and dipping Unit set 2 strata towards antithetic faults AB and AC suggest that these faults became active in Phase 2 (Fig. 6.12). Footwall-derived fans continued to aggrade in the immediate hangingwall of the main border fault, but their geometry changed. Locally, earlier fan deltas were overlain by submarine fan/slope aprons (sloping reflectors; SF1a) implying deepening, which is likely a result of increased fault-related subsidence. In the northern sub-basin (Quadrant 3) and at the saddle between the central and southern sub-basins (Quadrant 7), two fan deltas continued to build, suggesting a reduced subsidence or enhanced sediment supply at these specific locations. The stacking within the fan delta in Quadrant 7 changed from progradational to aggradational-retrogradational at this time, suggesting reduced sediment supply or enhanced accommodation creation relative to Phase 1. The deposition of the spatially-restricted Unit C and the anomalously flat-lying top reflector that is overlapped by younger units, suggests a brief

period of relative base level fall during overall relative base level rise in response to subsidence. Hangingwall-derived, submarine fans prograde from antithetic faults AB and AC and interfinger at their distal margin with footwall-derived fans from the main border fault. The fault crest was subaerially exposed at this time, facilitating degradation, which was greatest at the fault centre and least at the fault tips, in line with fault throw distribution.

6.7.3. Phase 3 – Unit set 3

Fault scarp degradation continued and fed the slope apron and submarine fans in the hangingwall basin during Unit set 3 deposition (Phase 3; Fig. 6.12). The through-going, fixed sediment input persisted in Quadrant 7, as the fan delta underwent a period of progradation before retrogradation. Progradation could reflect an increased sediment supply, reduced activity on the fault or a relative base level fall at that time, before returning to the general retrogradational trend that is apparent elsewhere along-strike, as fault-related subsidence increased. Strata thicken into antithetic faults AA and AD at this time, implying onset of their activity. At the saddle between the central and southern sub-basins (Quadrant 7), a hangingwall-derived fan delta prograded from antithetic fault AD, towards the SE. The fan delta downlapped and prograded up the distal margin of the fan delta prograding from the main border fault, towards the NW. A falling topset-foreset breakpoint trajectory at this time is suggestive of a forced regression. During this phase, the footwall-derived fan delta in Quadrant 3 was drowned and became a submarine fan, as evidenced by clinofolds overlain by sloping reflectors. Axial drainage, parallel to the fault, from the northern fault tip then dominated. Strongly progradational clinofolds suggest a deltaic origin with a high sediment supply, which could be related to drainage realignment in Quadrant 3. The foresets are observed to route around the topography derived from the preceding and concurrent footwall-derived deposits. Three stacks of foresets are observed, separated by flat-lying reflectors interpreted to represent flooding surfaces on three minor base level cycles.

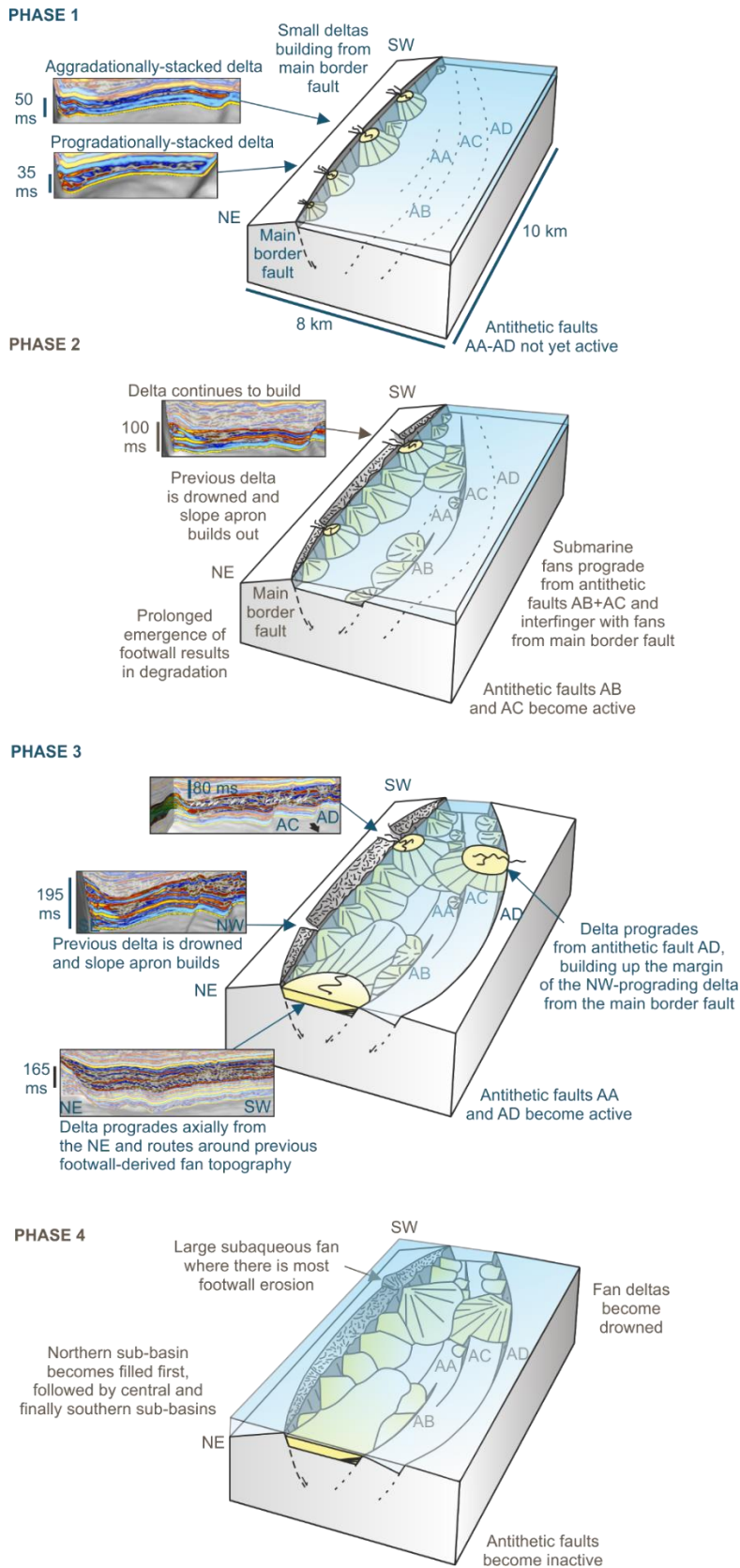


Figure 6.12. Block models to show the tectono-sedimentary evolution of the basin from Phases 1-4. Representative seismic extracts are shown to highlight evidence for interpretations. Antithetic faults AA-AD are indicated.

6.7.4. Phase 4 – Unit set 4

Some slope apron/submarine fan deposits continued to be sourced from the footwall of the main border fault, but are not dominant in Phase 4 (Fig. 6.12). An exception lies at Quadrant 6, where a large submarine fan formed, coinciding with the area of most footwall degradation. Absence of clinofolds suggests that the fan delta in Quadrant 7 switched off. Elsewhere, shallower dips and multiple onlaps in various directions indicate passive infilling of the basin. The depositional environment is unclear, but given the absence of clinoformal geometries indicative of a marginal setting and the presence of a suspected subaqueous fan, it is speculated to be a deeper water basin than in Phases 1-3. There is no longer thickening of units into the antithetic faults, suggesting their activity ceased during this phase. The cessation of intrabasinal faulting suggests that strain rates on the main border fault may have been decreasing during this time, but the depositional environment does not appear to shallow. Hence, the block may have subsided in the hangingwall of the newly active, basinward major fault to the west. The northern sub-basin became filled first, followed by the central and finally the southern sub-basin, where units K and L built until the end of the syn-rift period.

6.8. Discussion

Integrated and quantitative analysis of footwall erosion and hangingwall fill provided insight into the catchment history from the fault footwall, by identification of fixed, through-going sediment input points. Moreover, the relative contribution of sediment sources from other positions in the basin (hangingwall- and axial-derived), and the along-strike variability of their deposits through time has been constrained. Here, we discuss these two outcomes in terms of their value and within the context of the broader literature and study area.

6.8.1. Where are the footwall catchments?

We undertook a novel, volume balancing approach to identify whether sediment was sourced solely from footwall degradation, or from inland catchments. We found excess hangingwall fill, suggesting that fault scarp degradation was not the only sediment source, where $V_{HW} > V_{FW}$. Using the ratio and difference between the two (V_{HW}/V_{FW} and $V_{HW}-V_{FW}$) in various quadrants along the fault, we could more precisely constrain the areas that were dominated by sediment bypass ($V_{HW} < V_{FW}$) and the areas that coincide with fixed, through-going sediment input points ($V_{HW} > V_{FW}$).

Excess hangingwall fill was identified in Quadrants 3 and 7, indicating the positions of through-going sediment input points and thus, catchments beyond the fault crest. Quadrant 7 coincides with the saddle (topographic high) between the central and southern sub-basins, a fault throw minimum, peaks in vertical and headward erosion, and sustained clinof orm development in the immediate hangingwall. It is interpreted that during the earliest stage of fault activity, two fault segments existed with a relay positioned at the location of Quadrant 7. This geometry was inherited from an older, deeper and perpendicular structure, influencing the strain distribution (e.g. Phillips et al., 2018; Henstra et al., 2017) and the position of the topographic high (saddle) in the hangingwall basin. Sediment transport was focussed through the relay between the two fault segments and persisted throughout fault evolution, even when the relay was breached, as the fault established its final length (Jackson et al., 2017). The elevated position of the saddle supported deltaic deposition, during subaqueous fan deposition in adjacent, deeper parts of the basin. In Quadrant 3, there is only a minor peak in V_{HW}/V_{FW} and the clinof orms in the hangingwall (Unit set 2) are overlain by deeper water deposits (Unit set 3). It is speculated that this area had a through-going input point that fed the fan delta in Phase 2, but upon structural adjustment, the transport path was re-routed, potentially to the fault tip. This is supported by the abrupt influx of sediment from the northern fault tip in the form of an axial-fan in the subsequent Phase 3. Landscapes are dynamic in tectonically-active areas and slope changes in response to faulting and

degradation often lead to sediment transport pathway modifications (Cowie et al., 2006; Attal et al., 2008).

Catchment imaging from beyond the fault crest using seismic mapping and attribute analysis was not possible, although it was possible to validate our volumetric approach with stratigraphic mapping in the hangingwall. In areas where poorer data quality restricts the imaging of clinoforms, this quantitative approach could be used to identify the position of through-going sediment input points and thus catchment supply from beyond the footwall in other basins. Similarly, it could be used to identify those areas dominated by sediment bypass (Stevenson et al., 2015); a useful tool in the search for prospective subaqueous fans, and updip stratigraphic traps.

The hangingwall fill volume is less than two times the footwall degradation volume in each quadrant. This limited local input rate suggests that through-going transport lasted for a short time, was eroding a small catchment (e.g. Ravnås & Steel, 1998; McArthur et al., 2016b) or sediment was trapped in upstream depocentres. The sustained clinoform development in Quadrant 7 through Phases 1-3 omits the former scenario. The latter scenarios depend on the relative timing of activity across adjacent fault terraces (Fig. 6.4), which is not constrained due to the absence of wells for correlation across hangingwall basins. The location and size of the eroding catchments are not known, but if local, inboard (SE), faults were active prior to the main border fault studied here, it is likely that their localised structural highs produced the catchments. Moreover, associated structural lows could have trapped sediment and thus limited the overall supply to this outboard basin. The catchment size may have been greater and trapping potential reduced if the inboard faults were younger than the main border fault studied here. This seems less likely, as for a catchment to develop beyond the fault scarp, at least the closest fault terrace must have been exposed, and not only this single fault crest. Later uplift of the footwall outboard of the main border fault (to the NW) may have generated the drainage that crossed the antithetic faults during Phase 3. The absence of degradation of the crests of antithetic faults suggests that they were submerged throughout the duration of deposition or not creating topography due to sediment

filling. If the outboard fault was active earlier, the dominant drainage might be expected to have routed down the dip-slope into the Thebe hangingwall, which appears not to be the case, especially in the early phases. As such, our data infers fault activity propagating from SE to NW (inboard to outboard), or possibly concurrent faulting, but clearly highlights the requirement for further investigation of the relative timing of fault activity and drainage dispersal.

The Thebe sub-basin was relatively outboard in the northern Carnarvon basin and regional work reports a deepening between the TR30 TS and J40 SB (J10-J30), from fluvio-deltaic deposition in the Late Triassic to deep water deposition in the Late Jurassic (J40) (Hocking et al., 1988; Longley et al., 2002; Marshall & Lang, 2013). Although we do not have constraint on the precise timing of the basin fill, our volume balancing approach, and observations of clinoform development in the hangingwall of the fault studied here and degradation of the fault scarp, suggests: 1) a relatively shallow water environment, 2) exposure of the footwall crest and, 3) the presence of palaeo-coastlines against the main border fault during Phases 1-3 and against antithetic fault D during Phase 3. In Phase 4, these became drowned, as the depositional environment deepened. Bilal et al. (2018) argue that adjacent footwall scarps in the northern Carnarvon Basin were degraded in a subaqueous environment, based on the absence of submarine canyon development and subaerial indicators in well data. It is possible that the basin-fill stratigraphy in their studied fault block is younger than that studied here. If not, it is difficult to envisage clinoform development and degradation of this scale, and fixed through-going input points in a fully marine setting without a subaerial source. Our interpretation is consistent with large-scale, palaeogeographic maps from the J30 sequence (Longley et al., 2002) that show deposition in narrow rift valleys and palaeo-coastlines fringing exposed fault blocks. Similar scenarios of uplifted and exposed footwall highs and islands supplying hangingwall basins are interpreted in the Late Jurassic North Sea (Yielding et al., 1992; Berger & Roberts, 1999; Nøttvedt et al., 2000; McArthur et al., 2016b) and also in the Quaternary-modern Aegean Sea (Papadopoulos & Palvides, 1992; Stiros et al., 1994).

6.8.2. Sediment sources in rift basins

The volume of sediment in Units E and H amounts to ~10% of the hangingwall fill. There is footwall-derived material in other units, so this is a minimum estimate of footwall-derived material in the hangingwall basin. However, clearly the hangingwall- and axial-derived systems made a substantial contribution to the basin-fill (~90%), and their relative influence changed through time as the basin evolved. In the early stages of the basin, footwall-derived systems were most prominent, likely because of border fault activity. Later, footwall-derived systems continued to build, but changed in style along-strike according to the local ratio of accommodation creation to sediment supply. Hangingwall-derived systems started to play an important role at initiation of the antithetic faults, which influenced topography and transport route gradients across the basin. Subsequently, the axial system, which prograded from the northern fault tip, established itself. No system prograded axially from the southern fault tip. The growth and interaction of adjacent faults outside of the immediate study area and local antithetic faults are likely to have played a role in determining sediment flux, entry points and migration of depositional systems around the basin, through relief and gradient generation (Gawthorpe & Hurst, 1993; Roberts et al., 1993; Ravnås & Steel, 1998; Whittaker et al., 2010).

Competing sediment inputs are an important aspect of tectono-sedimentary models because they result in complex process and architectural interactions. Here, depositional systems are observed to interfinger, abruptly downlap, to build up the flanks of another, or to route around each other, which represents a spectrum of compensational stacking styles (e.g. Mohrig et al., 2000; Olariu & Bhattacharya, 2006; Prélat et al., 2009; Wang et al., 2011; Straub & Pyles, 2012; Bell et al., 2018). Relative timing of different depositional systems clearly plays an important role in this interaction, but also the depositional gradients of the competing systems (Dodd et al., 2018) and individual stream power and the ability to erode and/or bypass (Stevenson et al., 2015). Styles of interaction are important to understand in a given basin for their connectivity, trapping and pinch-out implications on a reservoir scale, but also for understanding the transfer and routing of sediment across a basin around topography. Yet, conceptual models for tectono-sedimentary

evolution do not capture these detailed relationships and generally focus upon footwall-derived depositional systems (e.g. Gawthorpe & Leeder, 2000). This in part due to the prolificacy of the rift basins that have been studied to generate these models; the Gulf of Corinth has been particularly influential in this regard, as it is characterised by a number of large, antecedent, transverse drainage systems that are excellently exposed (Dart et al., 1994; Gawthorpe et al., 1994; Ford et al., 2007; Rohais et al., 2007; Backert et al., 2010; Gobo et al., 2015; Barrett et al., 2019). Such models should be expanded to incorporate the contribution of other sediment entry points to the basin that this and other recent studies have highlighted (e.g. McArthur et al., 2016a; Henstra et al., 2017; Muravchik et al., 2018) and the spectrum of interactions that can occur between competing systems in confined basins.

6.9. Conclusion

A quantitatively-informed interpretation of the tectono-sedimentary evolution of an individual fault block in the northern Carnarvon Basin, NW Shelf, Australia suggests that the basin evolved through four phases linked to the evolution of the main border fault and a number of parallel, antithetic faults, which became active at different times. Through-going sediment input points were identified in Quadrants 3 and 7, of which the latter persisted throughout the basin evolution. It coincides with the saddle (topographic high) between the central and southern sub-basins, a fault throw minimum, peaks in vertical and headward erosion, and convincing and sustained cliniform development in the immediate hangingwall. It is interpreted that during the earliest stage of fault activity, two fault segments existed with a relay positioned at the location of Quadrant 7. This geometry was inherited from an older, deeper and perpendicular structure. Sediment transport was focussed through the relay between the two fault segments and locked itself into the landscape to continue to supply sediment when the fault established its final length. Exposure of the border fault footwall and inboard/adjacent fault terraces (that may have become active earlier) are interpreted to have produced small catchments that fed the hangingwall basin,

reflecting deposition in narrow rift valleys and palaeo-shorelines that fringed emergent fault blocks in this outboard part of the northern Carnarvon Basin.

Overall there are two main outcomes of this study that represent advances in the fields of geomorphology and tectono-stratigraphy:

1) Complex process and architectural interactions are observed between depositional systems within the same basin, but with different origins (footwall-, hangingwall- and axial-derived) that yield similar contributions to the hangingwall fill. Depositional systems are observed to interfinger, abruptly downlap, build up the flanks of another, or route around each other, which essentially represents a spectrum of compensational stacking styles within a fault-confined basin. This is an important outcome which should be incorporated into existing models for tectono-sedimentary development in rift basins.

2) A quantitative approach is presented that could be used to independently locate through-going input points in other basins, particularly where preservation of erosional landscapes are limited and/or subsurface imaging is challenging. Similarly, it could be useful tool for identifying areas along a fault that are dominated by sediment bypass.

6.10. Acknowledgements

This work forms part of the PhD thesis of Bonita Barrett. The authors thank the project sponsor, Neptune Energy that sponsored the SMRG (Shallow Marine Research Group). Geoscience Australia is also thanked for the provision of publicly accessible subsurface data from the northern Carnarvon Basin, Australia. Catherine Skilliter is acknowledged for the regional maps used in this work.

6.11. References

- Attal, M., Tucker, G.E., Whittaker, A.C., Cowie, P.A. & Roberts, G.P. (2008). Modeling fluvial incision and transient landscape evolution: influence of dynamic channel adjustment. *Journal of Geophysical Research*, 113, F03013, doi: 10.1029/2007JF000893.
- Backert, N., Ford, M. & Malartre, F. (2010). Architecture and sedimentology of the Kerinitis Gilbert-type fan delta, Corinth Rift, Greece. *Sedimentology*, 57, 543-586.
- Barrett, B.J., Gawthorpe, R.L., Collier, R.E.Ll., Hodgson, D.M. & Cullen, T.M. (accepted). Syn-rift deltaic interfan stratigraphy as archives of sedimentation and basin evolution. *The Depositional Record*.
- Barrett, B.J., Collier, R.E.Ll., Hodgson, D.M., Gawthorpe, R.L., Dorrell, R.M. & Cullen, T.M. (2019). Quantifying faulting and base level controls on syn-rift sedimentation using stratigraphic architectures of coeval, adjacent Early-Middle Pleistocene fan deltas in Lake Corinth, Greece. *Basin Research*, doi: 10.1111/bre.12356.
- Barrett, B.J., Hodgson, D.M., Collier, R.E.Ll. & Dorrell, R.M. (2018). Novel 3D sequence stratigraphic numerical model for syn-rift basins: analysing architectural responses to eustasy, sedimentation and tectonics. *Marine and Petroleum Geology*, 92, 270-284.
- Bell, D., Stevenson, C., Kane, I., Hodgson, D.M. & Poyatos-Moré, M. (2018). Topographic controls on the development of contemporaneous but contrasting basin-floor depositional architectures. *Journal of Sedimentary Research*, 88, 1169-1189.
- Berger, M. & Roberts, M. (1999). The Zeta Structure: a footwall degradation complex formed by gravity sliding on the western margin of the Tampen Spur, Northern North Sea. *Geological Society, London, Petroleum Geology Conference series*, 5, 107-116.
- Bilal, A., McClay, K. & Scarselli, N. (2018). Fault-scarp degradation in the central Exmouth Plateau North West Shelf, Australia. In: K.R. McClay & J.A. Hammerstein (Eds.), *Passive margins: tectonics, sedimentation and magmatism*. Geological Society, London, Special Publications, 476, doi: 10.1144/SP476.11.
- Bradshaw, M.T., Bradshaw, J., Murray, A.P., Needham, D.J., Spencer, L., Summons, R.E., Wilmot, J. & Winn, S. (1994). Petroleum systems in west Australian basins. In: P.G. Purcell & R.R. Purcell (Eds.), *The Sedimentary Basins of Western Australia: Proceedings of the Petroleum Exploration Society of Australia Symposium*. PESA, Perth, 93-118.
- Bradshaw, M.T., Yeates, A.N., Beynon, R.M., Brakel, A.T., Langford, R.P., Totterdell, J.M. & Yeung, M. (1988). Palaeogeographic evolution of the North West Shelf region. In: P.G. Purcell & R.R. Purcell (Eds.), *Proceedings of the North West Shelf Symposium*. PESA, Perth, 29-54.
- Collier, R.E.Ll. & Gawthorpe, R.L. (1995). Neotectonics, drainage and sedimentation in central Greece: insights into coastal reservoir geometries in syn-rift sequences. *Geological Society, London, Special Publications*, 80, 165-181.
- Cowie, P.A., Attal, M., Tucker, G.E., Whittaker, A.C., Naylor, M., Ganas, A. & Roberts, G.P. (2006). Investigating the surface process response to fault interaction and linkage using a numerical modelling approach. *Basin Research*, 18, 231-266.
- Crameri, F. (2018). Scientific colour-maps. Zenodo. doi: 10.5281/zenodo.1243862.
- Dart, C.J., Collier, R.E.Ll., Gawthorpe, R.L., Keller, J.V.A. & Nichols, G. (1994) Sequence stratigraphy of (?)Pliocene-quadernary synrift, gilbert-type fan deltas, Northern Peloponnesos, Greece. *Marine and Petroleum Geology*, 11, 545-560.
- Dawers, N. H. & Anderson, M.H. (1995). Displacement-length scaling and fault linkage. *J. Struct. Geol.*, 17, 607-614.
- Dodd, T.J., McCarthy, D.J. & Richards, P.C. (2018). A depositional model for deep-lacustrine, partially-confined, turbidite fans: Early Cretaceous, North Falkland Basin. *Sedimentology*, 66, 53-80.

- Dorsey, R.J. & Umhoefer, P.J. (2000). Tectonic and eustatic controls on sequence stratigraphy of the Pliocene Loreto Basin, Baja California Sur, Mexico. *GSA Bulletin*, 112, 177-199.
- Dorsey, R.J., Umhoefer, P.J. & Renne, P.R. (1995). Rapid subsidence and stacked gilbert-type fan deltas, Pliocene Loreto Basin, Baja California Sur, Mexico. *Sedimentary Geology*, 98, 181-204.
- Elliott, G.M., Wilson, P., Jackson, C.A.-L., Gawthorpe, R.L., Michelsen, L. & Sharp, I. (2012). The linkage between fault throw and footwall scarp erosion patterns: an example from the Bremstein Fault Complex, offshore Mid-Norway. *Basin Research*, 24, 180-197.
- Ellis, C., Woodall, M., Goody, A., Lim, D. & Locke, M. (2009). Thebe-2 and Thebe-2CH well completion report, interpretive volume, WA-346-P. BHP Billiton Petroleum Pty Ltd.
- Etheridge, M.A. & O'Brien, G.W. (1994). Structural and tectonic evolution of the Western Australia margin system. *PESA Journal*, 22, 45-63.
- Evans, A.L. (1990). Miocene sandstone provenance relations in the Gulf of Suez: insights into synrift unroofing and uplift history. *AAPG Bulletin*, 9, 1386-1400.
- Exon, N.F., Haq, B.U. & von Rad, U. (1992). Exmouth Plateau revisited: scientific drilling and geological framework. *Proceedings of the Ocean Drilling Program, Scientific Results*, 122, 3-20.
- Ford, M., Williams, E.A., Malartre, F. & Popescu, S.M. (2007). Stratigraphic architecture, sedimentology and structure of the Vouraikos Gilbert-type fan delta, Gulf of Corinth, Greece. In: G. Nichols, E. Williams & C. Paola (Eds.), *Sedimentary Processes, Environments and Basins. A Tribute to Peter Friend*. Int. Assoc. Sedimentol. Spec. Publ., 38, 49-90.
- Forman, D.J. & Wales, D.W. (1981). Geological evolution of the Canning Basin, Western Australia. *Bureau of Mineral Resources, Geology and Geophysics Bulletin*, 210, 91pp.
- Fraser, S.I., Robinson, A.M. et al. (2002). Upper Jurassic. In: A. Armour, D. Evans & C. Hickey (Eds.), *The Millennium Atlas: Petroleum Geology of the Central and Northern North Sea*. The Geological Society, London, 157-189.
- Gartrell, A., Torres, J., Dixon, M. & Keep, M. (2016). Mesozoic rift onset and its impact on the sequence stratigraphic architecture of the Northern Carnarvon Basin. *The APPEA Journal*, 56, 143-158.
- Gawthorpe, R. L., Fraser, A.J. & Collier, R.E.LI. (1994). Sequence stratigraphy in active extensional basins: implications for the interpretation of ancient basin-fills. *Marine and Petroleum Geology*, 11, 642-658.
- Gawthorpe, R. L., Andrews, J. E., Collier, R. E. LI., Ford, M., Henstra, G.A., Kranis, H., Leeder, M.R., Muravchik, M. & Skourtsos, E. (2017). Building up or out? Disparate sequence architectures along an active rift margin – Corinth rift, Greece. *Geology*, 45, 111-114.
- Gawthorpe, R. L. & Hurst, J.M. (1993). Transfer zones in extensional basins: their structural style and influence on drainage development and stratigraphy. *Journal of the Geological Society, London*, 150, 1137-1152.
- Gawthorpe, R.L. & Leeder, M.R. (2000). Tectono-sedimentary evolution of active extensional basins. *Basin Research*, 12, 195-218.
- Ghinassi, M. (2007). The effects of differential subsidence and coastal topography on high-order transgressive-regressive cycles: Pliocene nearshore deposits of the Val d'Orcia Basin, Northern Apennines, Italy. *Sedimentary Geology*, 202, 677-701.
- Gobo, K., Ghinassi, M. & Nemeč, W. (2015). Gilbert-type deltas recording short-term base-level changes: delta-brink morphodynamics and related foreset facies. *Sedimentology*, 62, 1923-1949.
- Hampson, G.J., Duller, R.A., Petter, A.L., Robinson, R.A.J. & Allen, P.A. (2014). Mass-balance constraints on stratigraphic interpretation of linked alluvial-coastal-shelfal deposits from source to sink: example from Cretaceous Western Interior Basin, Utah and Colorado, USA. *Journal of Sedimentary Research*, 84, 935-960.

- Hengesh, J.V. & Whitney, B.B. (2016). Transcurrent reactivation of Australia's western passive margin: an example of intraplate deformation from the central Indo-Australian plate. *Tectonics*, 35, 1066-1089.
- Henstra, G.A., Grundvåg, S-A., Johannessen, E.P., Kristensen, T.B., Midtkandal, I., Nystuen, J.P., Rotevatn, A., Surlyke, F., Sætherf, T. & Windelstad, J. (2016). Depositional processes and stratigraphic architecture within a coarse-grained rift-margin turbidite system: The Wollaston Forland Group, East Greenland. *Marine and Petroleum Geology*, 76, 187-209.
- Henstra, G.A., Gawthorpe, R.L., Helland-Hansen, W., Ravnås, R. & Rotevatn, A. (2017). Depositional systems in multiphase rifts: seismic case study from the Lofoten margin, Norway. *Basin Research*, 29, 447-469.
- Hocking, R.M. (1988). Regional Geology of the Northern Carnarvon Basin. In: P.G. Purcell and R.R. Purcell (Eds.), *The North West Shelf, Australia. Proceedings of Petroleum Exploration Society of Australia Symposium*. PESA, Perth, 97-114.
- Jackson, C.A.-L., Bell, R.E., Rotevatn, A., Tvedt, A.B.M. (2017). Techniques to determine the kinematics of syn-sedimentary normal faults and implications for fault growth models. In: C. Childs, R.E. Goldsworth, C.A.-L. Jackson, T. Manzocchi, J.J. Walsh & G. Yielding (Eds.), *The Geometry and Growth of Normal Faults*. Geological Society, London, Special Publications, 439, 187-217.
- Jackson, C.A.-L., Larsen, E., Hanslien, S. & Tjemsland, A.-E. (2011). Controls on synrift turbidite deposition on the hanging wall of the South Viking Graben, North Sea rift system, offshore Norway. *AAPG Bulletin*, 95, 1557-1587.
- Jackson, J. A. & Leeder, M.R. (1993). Drainage systems and the evolution of normal faults: an example from Pleasant Valley, Nevada. *Journal of Structural Geology*, 16, 1041-1059.
- Kallweit, R.S. & Wood, L.C. (1982). The limits of resolution of zero-phase wavelets. *Geophysics*, 47, 1035-1046.
- Keep, M., Powell, C.M. & Baillie, P.W. (1998). Neogene deformation of the North West Shelf, Australia. In: P.G. Purcell & R.R. Purcell (Eds.), *The Sedimentary Basins of Western Australia 2: Proceedings of Petroleum Exploration Society Australia Symposium*. PESA, Perth, 81-91.
- Leeder, M.R., Mack, G.H. & Salyards, S.L. (1996). Axial-transverse fluvial interactions in half graben: Plio-Pleistocene Palomas Basin, southern Rio Grande Rift, New Mexico, USA. *Basin Research*, 8, 225-241.
- Leppard, C.W. & Gawthorpe, R.L. (2006). Sedimentology of rift climax deep water systems; Lower Rudeis Formation, Hammam Faraun Fault Block, Suez Rift, Egypt. *Sedimentary Geology*, 191, 67-87.
- Lin, W. & Bhattacharya, J.P. (2017). Estimation of source-to-sink mass balance by a fulcrum approach using channel paleohydrologic parameters of the Cretaceous Dunvegan Formation, Canada. *Journal of Sedimentary Research*, 87, 97-116.
- Longley, I.M., Buessenschuett, C., Clydsdale, L., Cubitt, C.J., Davis, R.C., Johnson, M.K., Marshall, N.G., Murray, A.P., Somerville, R., Spry, T.B. & Thompson, N.B. (2002). The North West Shelf of Australia – a Woodside perspective. In: M. Keep & S.J. Moss (Eds.), *The Sedimentary Basins of Western Australia 3: Proceedings of the Petroleum Society of Australia Symposium*. PESA, Perth, 966pp.
- Marshall, N.G. & Lang, S.C. (2013). A New Sequence Stratigraphic Framework for the North West Shelf, Australia. In: M. Keep & S.J. Moss (Eds.), *The Sedimentary Basins of Western Australia 4: Proceedings of Petroleum Exploration Society of Australia Symposium*. PESA, Perth, 18-21.
- McArthur, A.D., Hartley, A.J., Archer, S.G., Jolley, D.W. & Lawrence, H.M. (2016a). Spatiotemporal relationships of deep-marine, axial, and transverse depositional systems from the synrift Upper Jurassic of the central North Sea. *AAPG Bulletin*, 100, 1469-1500.
- McArthur, A.D., Jolley, D.W., Hartley, A.J., Archer, S.G. & Lawrence, H.M. (2016b). Palaeoecology of syn-rift topography: a Late Jurassic footwall island on the Josephine Ridge, Central Graben, North Sea. *Palaeogeography, Palaeoclimatology, Palaeoecology*, 459, 63-75.

- McLeod, A.E. & Underhill, J.R. (1999). Processes and products of footwall degradation, northern Brent Field, Northern North Sea. Geological Society, London, Petroleum Geology Conference series, 5, 91-106.
- Metcalf, I. (1999). Gondwana dispersion and Asian accretion: An overview. In: I. Metcalfe (Ed.), *Gondwana Dispersion and Asian Accretion – IGCP 321 Final Results Volume*. A.A. Balkema, Rotterdam, 9-28.
- Michael, N.A., Whittaker, A.C. & Allen, P.A. (2013). The functioning of sediment routing systems using a mass balance approach: example from the Eocene of the Southern Pyrenees. *The Journal of Geology*, 121, 581-606.
- Mohrig, D., Heller, P.L., Paola, C. & Lyons, W.J. (2000). Interpreting avulsion process from ancient alluvial sequences: Guadalupe-Matarranya (northern Spain) and Wasatch Formation (western Colorado). *Geological Society of America Bulletin*, 112, 1787-1803.
- Morley, C.K., Ionnikoff, Y., Pinyochon, N. & Seusutthiya, K. (2007). Degradation of a footwall fault block with hanging-wall fault propagation in a continental lacustrine setting: how a new structural model impacted field development plans, the Sirikit field, Thailand. *AAPG Bulletin*, 91, 1637-1661.
- Mortimer, E.J. & Carrapa, B. (2007). Footwall drainage evolution and scarp retreat in response to increasing fault displacement: Loreto fault, Baja California Sur, Mexico. *Geology*, 35, 651-654.
- Muravchik, M., Gawthorpe, R.L., Sharp, I.R., Rarity, F. & Hodgetts, D. (2018). Sedimentary environment evolution in a marine hangingwall dip slope setting. El Qaa Fault Block, Suez Rift, Egypt. *Basin Research*, 30, 452-478.
- Nøttvedt, A., Berge, A.M., Dawers, N.H., Færseth, R.B., Häger, K.O., Mangerud, G. & Puigdefabregas, C. (2000). Syn-rift evolution and resulting play models in the Snorre-H area, northern North Sea. In: A. Nøttvedt (Ed.), *Dynamics of the Norwegian Margin*. Geological Society, London, Special Publications, 167, 179-218.
- Olariu, C. & Bhattacharya, J.P. (2006). Terminal distributary channels and delta front architecture of river-dominated delta systems. *Journal of Sedimentary Research*, 76, 212-233.
- Paola, C. & Martin, J.M. (2012). Mass-balance effects in depositional systems. *Journal of Sedimentary Research*, 82, 435-450.
- Papadopoulos, G. & Pavlides, S. (1992). The large 1956 earthquake in the South Aegean: macroseismic field configuration, faulting and neotectonics of Amorgos Island. *Earth Planet. Sci. Letters*, 113, 383-396.
- Pechlivanidou, S., Cowie, P.A., Hannisdal, B., Whittaker, A.C., Gawthorpe, R.L., Pennos, C. & Riiser, O.S. (2018). Source-to-sink analysis in an active extensional setting: Holocene erosion and deposition in the Sperchios rift, central Greece. *Basin Research*, 30, 522-543.
- Phillips, T.B., Jackson, C. A. L., Bell, R. E. & Duffy, O. B. (2018). Oblique reactivation of lithosphere-scale lineaments controls rift physiography – the upper-crustal expression of the Sorgenfre-Tornquist Zone, offshore southern Norway. *Solid Earth*, 9, 403-429.
- Prélat, A., Hodgson, D.M. & Flint, S.S. (2009). Evolution, architecture and hierarchy of distributary deep-water deposits: a high-resolution outcrop investigation from the Permian Karoo Basin, South Africa. *Sedimentology*, 56, 2132-2154.
- Ravnås, R. & Steel, R.J. (1998). Architecture of Marine Rift-Basin Successions. *AAPG Bulletin*, 82, 110-146.
- Reading, H.G. & Richards, M. (1994). Turbidite systems in deep-water basin margins classified by grain size and feeder system. *AAPG Bulletin*, 78, 792-822.
- Richards, M., Bowman, M. & Reading, H. (1998). Submarine fan systems characterization and stratigraphic prediction. *Marine and Petroleum Geology*, 15, 689-717.

- Roberts, A. M., Yielding, G. & Badley, M.E. (1993). Tectonic and bathymetric controls on stratigraphic sequences within evolving half-graben. In: G. D. Wouliams & A. Dobb (Eds.), *Tectonics and seismic sequence stratigraphy*. Geological Society Special Publication, 71, 87-121.
- Rohais, S., Eschard, R., Ford, M., Guillocheau, F. & Moretti, I. (2007). Stratigraphic architecture of the Plio-Pleistocene infill of the Corinth Rift: implications for its structural evolution. *Tectonophysics*, 440, 5-28.
- Sharp, I.R., Gawthorpe, R.L., Underhill, J.R. & Gupta, S. (2000). Fault-propagation folding in extensional settings: examples of structural style and synrift sedimentary response from the Suez rift, Sinai, Egypt. *Geological Society of America Bulletin*, 112, 1877-1899.
- Stagg, H.M.J. & Colwell, J.B. (1994). The structural foundations of the Northern Carnarvon Basin. In: P.G. Purcell & R.R. Purcell (Eds.), *The North West Shelf, Australia. Proceedings of Petroleum Exploration Society of Australia Symposium*. PESA, Perth, 349-372.
- Stevenson, C.J., Jackson, C.A.-L., Hodgson, D.M., Hubbard, S.M. & Eggenhuisen, J.T. (2015). Deep-water sediment bypass. *Journal of Sedimentary Research*, 85, 1058-1081.
- Stewart, S.A. & Reeds, A. (2003). Geomorphology of kilometre-scale extensional fault scarps: factors that impact seismic interpretation. *AAPG Bulletin*, 87, 251-272.
- Stiros, S.C., Marangou, L. & Arnold, M. (1994). Quaternary uplift and tilting of Amorgos Island (southern Aegean) and the 1956 earthquake. *Earth Planet. Sci. Letters*, 128, 65-76.
- Straub, K.M. & Pyles, D.R. (2012). Quantifying the hierarchical organization of compensation in submarine fans using surface statistics. *Journal of Sedimentary Research*, 82, 889-898.
- Tindale, K., Newell, N., Keall, J. & Smith, N. (1998). Structural evolution and charge history of the Exmouth Sub-basin, northern Carnarvon Basin, western Australia. In: P.G. Purcell & R.R. Purcell (Eds.), *The Sedimentary Basins of Western Australia 2: Proceedings of the Petroleum Exploration Society of Australia*. PESA, Perth, 447-472.
- Turner, C.C. & Cronin, B.T (Eds.). (2018). *Rift-related coarse-grained submarine fan reservoirs; the Brae Play, South Viking Graben, North Sea*. AAPG Memoir, 115, 630pp.
- Veevers, J.J. (1988). Morphotectonics of Australia's northwestern margin – a review. In: P.G. Purcell & R.R. Purcell (Eds.), *The North West Shelf, Australia: Proceedings of Petroleum Exploration Society of Australia Symposium*. PESA, Perth, 651pp.
- Walsh, J.J. & Watterson, J. (1988). Analysis of the relationship between displacements and dimensions of faults. *J. Struct. Geol.*, 10, 239-247.
- Wang, Y., Straub, K.M. & Hajek, E.A. (2011). Scale-dependent compensational stacking: an estimate of autogenic time scales in channelized sedimentary deposits. *Geology*, 39, 811-814.
- Watkins, S.E., Whittaker, A.C. Bell, R.E., McNeill, L.C., Gawthorpe, R.L., Brooke, S.A.S. & Nixon, C.W. (2018). Are landscapes buffered to high-frequency climate change? A comparison of sediment fluxes and depositional volumes in the Corinth Rift, central Greece, over the past 130 k.y. *GSA Bulletin*, 131, 372-388.
- Widess, M.B. (1973). How thin is a thin bed? *Geophysics*, 38, 1176-1180.
- Whittaker, A.C., Attal, M. & Allen, P.A. (2010). Characterising the origin, nature and fate of sediment exported from catchments perturbed by active tectonics. *Basin Research*, 22, 809-828.
- Yeates, A.N., Bradshaw, M.T. & Dickins, J.M. (1987). The Westralian Superbasin: an Australian link with Tethys. In: K.G. McKenzie (Ed.), *Shallow Tethys, vol. 2*. A. A. Balkema, Rotterdam, Netherlands, 199-213.
- Yielding, G., Badley, M.E., Roberts, A.M. (1992). The structural evolution of the Brent Province. *Geological Society, London, Special Publications*, 61, 27-43.

Chapter 7

Discussion

This chapter draws upon the results presented in Chapters 3-6 to answer the research questions posed in Chapter 1:

1. How can the stratigraphic approach be improved to account for architectural complexities arising from along-strike variability in allogenic controls?
2. How can the signal of temporally- and spatially-variable allogenic controls be deconvolved from the depositional record of syn-rift basin-fills?
3. How can quantitative approaches be applied to stratigraphic analysis?
4. How should 'accommodation' be used in interpretations to incorporate the complexity observed in tectonically-active basins, and is the $\delta A/\delta S$ ratio valid?

7.1. Research Question 1

How can the stratigraphic approach be improved to account for architectural complexities arising from along-strike variability in allogenic controls?

Along-strike variability in tectonic displacement and sedimentation is characteristic of all rift basins, and occurs from the whole basin, to fault segment- and depositional system-scales. How this is manifest in terms of stacking patterns and the nature of key surfaces has been addressed to some extent along fault segments (e.g. Dart et al., 1994; Gawthorpe et al., 1994; 2003; Dorsey & Umhoefer, 2000; Hardy & Gawthorpe, 1998; Jackson et al., 2005; Backert et al., 2010), and it ultimately depends on the local ratio of accommodation and sediment supply ($\delta A/\delta S$). However, some gaps persist, including i) a detailed and quantitative assessment of diachroneity of key surfaces, ii) along-strike interaction of multiple, spatially-distributed depositional systems, and iii) quantitative characterisation of along-strike variation in stratigraphic architecture. Addressing these gaps is important in order to improve stratigraphic predictions in rift basins, and have been addressed throughout this thesis through integration of numerical modelling, and field and subsurface investigations. Along-strike variability of allogenic controls in rift basins adds complexity to stratigraphic analysis, because an interpretation made along a single dip-transect is unlikely to be applicable to any other position along-strike. Better 3D constraint of the interactions between controls along-strike in rift basins allows the stratigraphic approach to become better informed, manipulated and applied, which is demonstrated across Chapters 3-6. Figure 7.1 presents a summary diagram of some of the main outcomes of the thesis in this regard.

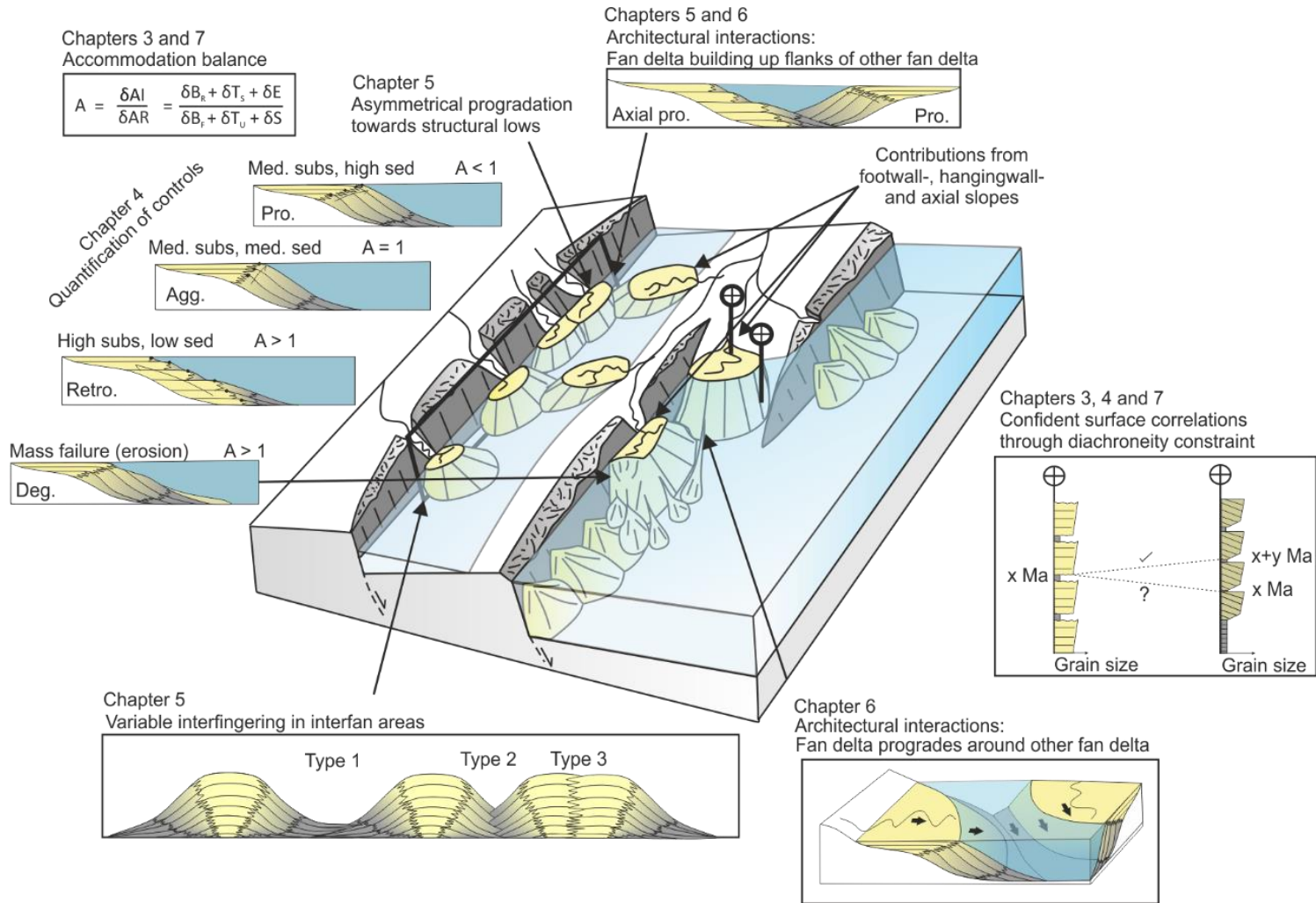


Figure 7.1. Summary block model to present some of the main outcomes of the thesis that represent advances in the field of tectono-stratigraphy.

7.1.1. Diachroneity of key surfaces

A key aspect of stratigraphic analysis is the ability to identify and correlate key surfaces across a basin-fill. Typically, this is applied in the dip direction, and is challenging along-strike because the nature of surfaces can vary, they can be spatially-restricted, and their formation may not be synchronous across a basin (Gawthorpe et al., 2003; Jackson et al., 2005; Catuneanu, 2006, Holbrook & Bhattacharya, 2012; Burgess & Prince, 2015; Hodgson et al., 2016; Madof et al., 2016). However, the diachroneity of surfaces is addressable. If one can constrain the diachroneity, then greater confidence can be given to the correlation of surfaces in rift basin-fills. In Chapter 3, it is shown that the greater the along-strike subsidence distribution, the more diachronous the sequence boundaries, with an absence of subaerial exposure and associated erosion at the fault centre where the highest subsidence rates outpace the maximum rates of base level fall. Similarly, sequence boundaries are shown to become more diachronous with an increasing sedimentation distribution along-strike, and occur earlier at positions of higher sedimentation than at positions with lower sedimentation. Such observations have been made in previous studies (e.g. Gawthorpe et al., 1994; Madof et al., 2016), but the approach of using 3D accommodation curves to present the data is novel. This approach allows the nature of diachroneity to be visualised and quantified, and is readily applicable to any scenario with real input data. For example, in Chapter 4, diachroneity from sedimentation and subsidence variability is quantified by use of Syn-Strat, whereby sequence boundaries are found to occur ca. 6 kyr earlier at the axes of the fan deltas than at the margins. Therefore, along-strike variability in allogenic controls enhances the diachroneity of key surfaces, which increases uncertainty when using these surfaces for correlation. A method is provided here to alleviate that uncertainty by putting some constraint on how the diachroneity may vary along-strike for a given set of controls (Chapter 3), and by what amount (Chapter 4).

Diachroneity is not only a feature of sequence boundaries, but can be characteristic of any position on a relative base level curve. In Chapter 3, the interpretative choice of the flooding surface position and its implication on diachroneity is discussed. It was highlighted that the diachroneity of the initial transgressive surface is expressed differently to the maximum flooding surface

(referring to the 'genetic sequence' scheme of Catuneanu, 2006); the initial transgressive surface occurred earlier at the fault centre than the fault tips, with the converse for the maximum flooding surface. This concept has been revisited here with Syn-Strat, by removing all sequence stratigraphic schema and dividing a given accommodation curve into eight segments. The output is generated using arbitrary values, with high maximum subsidence at the fault centre, high sedimentation input from the fault tips and five base level cycles with an order of magnitude lower amplitude than subsidence and sedimentation. The boundaries between each curve segment represent nodes that are often referred to as key surfaces across the sequence stratigraphic schemes (numbered 1-8 in Fig. 7.2). Each segment is defined by its placement on the accommodation curve relative to the first (f') and second (f'') derivatives of the curve and average amplitude of two consecutive segments (f_{av}). This is demonstrated with a simple sine wave in Figure 7.2A. Plotting the eight segments along the fault, through time highlights the diachroneity of each node/potential stratigraphic surface along the fault (Fig. 7.2B and 7.2C). Figure 7.3 (a 1D plot) shows the accommodation curve at the fault tip and at the fault centre and also demonstrates the offsets of the nodes through time. Results show that each node/surface expresses different diachroneity along-strike, with the highest and lowest nodes of the curve (2 and 6 in Fig. 7.2) exhibiting the most diachroneity. The two nodes at the inflection points of the accommodation curve (f'), which traditionally would be considered the maximum flooding surface and sequence boundary (4 and 8 in Fig. 7.2), are synchronous. For all nodes on the negative side of the curve between the 'sequence boundary' and subsequent 'maximum flooding surface' (lowstand; 5 to 7 in Fig. 7.2), during the onset of accommodation increase, occur earlier at the fault centre than at the fault tips. For all nodes on the positive side of the curve between the 'maximum flooding surface' and subsequent 'sequence boundary' (highstand; 1 to 3 in Fig. 7.2), during the onset of accommodation decrease, they occur later at the fault centre than at the fault tips. The reason that the highest and lowest nodes (2 and 6 in Fig. 7.2) of the accommodation curve are the most diachronous positions is because the gradients of base level and subsidence interact. Accommodation only starts to fall from its maximum point when the rate of base level fall exceeds the rate of subsidence. Because subsidence rate is greater at the fault centre than at the fault tip, it

takes longer for the rate of base level fall to exceed subsidence. Therefore, there is a lag time between the highest accommodation at the fault tip and highest accommodation at the fault centre. This does not occur at the inflection points of the accommodation curve (maximum rate of rise or fall; 4 and 8). Thus, it is shown here that all positions on a relative base level or accommodation curve are diachronous along strike, apart from the points of maximum rate of rise or fall. This suggests that the most correlatable nodes on a relative base level or accommodation curve are in fact the points of maximum rate of rise or fall (4 and 8 in Fig. 7.2), but whether it is these that are truly expressed in the rock record, is unknown. For all prior interpretations of diachronous sequence boundaries or maximum flooding surfaces from the rock record with age constraints, the position of those surfaces on a relative base level curve cannot be points of maximum rate of accommodation rise or fall. In Chapter 4, when surfaces across the Selinous and Kerinitis fan deltas were modelled, the sequence boundary was taken as the onset of base level fall, which explains the diachroneity in the model outputs. This is feasible in shallow water, where there would be early exposure of the delta top following base level fall. It is often not possible to pinpoint the position of the sequence boundary on a relative base level curve, as the duration of the relative base level fall could be represented by a single surface.

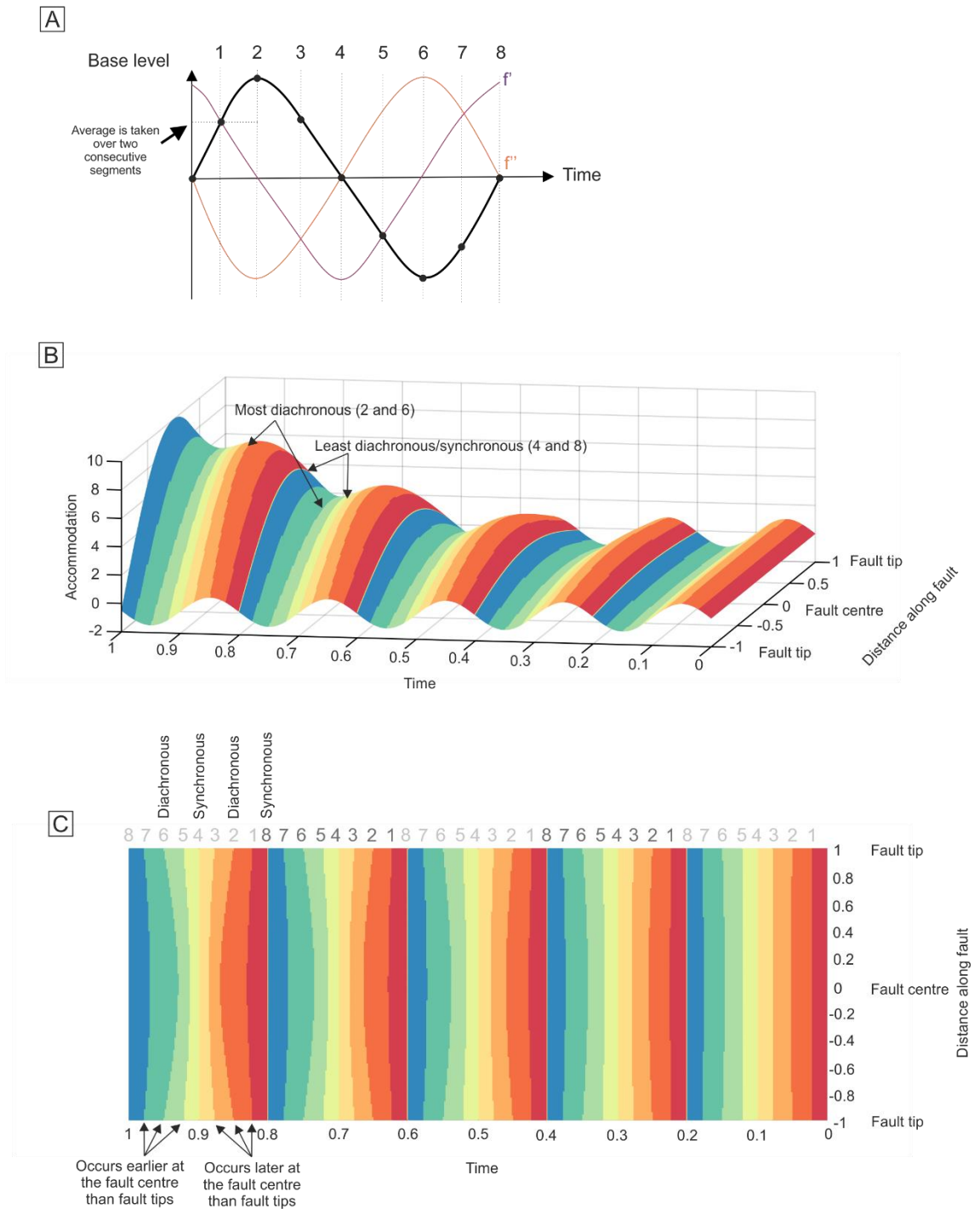


Figure 7.2. Diachroneity at different positions of a relative base level or accommodation curve. A) Method for splitting the curve into 8 segments, defining 8 key inflection points. Segments are defined based on their position relative to the first and second derivatives of the curve (f' and f'') and the average value between two consecutive segments. B) 3D plot from Syn-Strat showing the diachroneity along-strike of the fault. C) Flattened plot to highlight the positions of the curve that are most and least diachronous, and which occur earlier or later at the fault centre relative to the fault tips. Plots show the most diachronous positions to be '2' and '6' (highest and lowest points of the curve) and the least diachronous to be '4' and '8' (points of maximum rate of rise and fall).

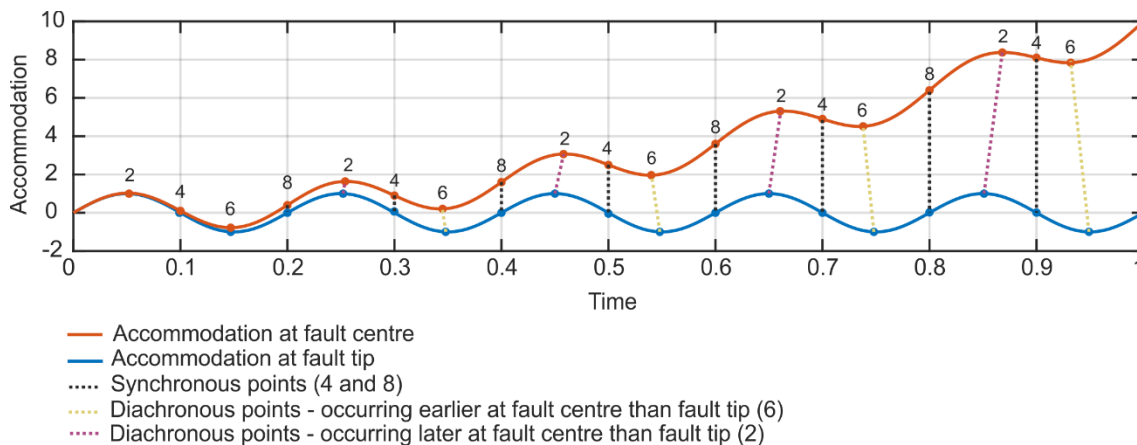


Figure 7.3. Plot to show the offset in time (diachroneity) between points on an accommodation curve at the fault centre (red) versus the fault tip (blue). Most offset occurs at the highest and lowest points on the curve. Zero offset occurs at the points of maximum rate of rise and fall. Numbers refer to positions in Fig. 7.2.

7.1.2. Stacking patterns

Sedimentation varies along-strike with climate, geomorphology, and substrate variability in any given basin. In rift basins, tectonics play a key role in influencing the supply signal. Along-strike variability of tectonic movement influences the topography and gradient of the footwall high of a single fault segment, and across multiple fault terraces. This impacts sediment entrainment and transport, the position of sediment entry points and routing within the basin, and the stacking patterns of depositional systems. As a result, multiple depositional systems can interact within rift basins, which make stratigraphic interpretations challenging. In Chapter 6, depositional systems from the footwall, the hangingwall dip-slope and the fault tip share the Thebe hangingwall sub-basin space. They exhibit a number of architectural interactions, including: interfingering, abrupt downlap, building up the flanks of one another, and re-routing. The relative contribution of various sediment input points to a basin and the spectrum of interactions that can occur must be considered for accurate stratigraphic interpretations. Ultimately, understanding how various systems interact through time is needed to place them in a chronostratigraphic framework.

Analysis of rift basin-fills requires 3D assessment of stratigraphic architecture across different scales. In Chapter 5, it is shown at a depositional system-scale that the stratigraphic record at the

proximal or distal axial position of a fan delta can be different to that at an interfan position. Together, they yield the most complete stratigraphic record through basin evolution. Interfan analysis is encouraged as it provides insight into potential along-strike asymmetry of depositional systems that may not be recorded at the axis of fan deltas. Geometric asymmetry of fan delta tops is attributed to prevailing wind and wave direction, and architectural asymmetry of fan delta stratigraphy is attributed to sediment transport following structural gradients to the lowest points. Fan delta asymmetry in rift basins is seldom discussed in the literature, most likely because the interfans that yield this information are understudied. Yet, if along-strike sediment routing through time is not considered or fully understood, stratigraphic analysis in rift basins will be inaccurate.

Overall, it is clear that sequence stratigraphic analysis is complicated by along-strike variability of allogenic controls in rift basins, but this work demonstrates that improvements can be made to tectono-stratigraphic models (e.g. Gawthorpe & Leeder, 2000) to better inform the approach. Key advances are: 1) better and more precise constraint of the diachroneity of key surfaces, 2) fuller understanding of the relative contribution and interaction of multiple sediment input points within a basin, 3) consideration of along-strike depositional system asymmetry and sediment routing, and 4) a 3D approach. The latter is fundamental. In this study, a 3D sequence stratigraphic numerical model and a high resolution 3D seismic dataset are used. In the field, dip and strike sections of exhumed fan deltas provide 3D constraints. However, in the absence of 3D constraint, stratigraphic analysis in rift basins is highly limited.

7.2. Research Question 2

How can the signal of temporally- and spatially-variable allogenic controls be deconvolved from the depositional record of syn-rift basin-fills?

A relative base level curve is the tuned signal of tectonic movement, base level and sedimentation fluctuations (Schlager, 1993). It underpins stratigraphy in a given position by providing the framework for the style of stacking and key surfaces in the depositional record (Posamentier et al., 1988; Posamentier & Vail, 1988), prior to autogenic modification and it is known to vary across a rift basin due to spatial variation of the allogenic controls (Gawthorpe et al., 1994). A number of control combinations can generate similar relative base level curves and thus, stratigraphic patterns ('non-unique solutions'; Heller et al., 1993; Flemings & Grotzinger, 1996; Burgess & Prince, 2015), which highlights the challenge of distinguishing allogenic control signals in the rock record (Chapter 1). This is problematic, as an understanding of the specific controls acting on a basin are central to making accurate stratigraphic predictions.

Inverting the stratigraphic record to distinguish allogenic controls is addressed in Chapters 3, 5 and 6, and is a focus of Chapter 4. The stratigraphic architecture from different combinations of control parameters are explored using Syn-Strat in Chapter 3. The transition from net subsidence to net uplift regimes is observed in field data from the interfan area between two fan deltas in the Gulf of Corinth in Chapter 5. Accommodation control from the main border fault and various antithetic faults are differentiated through time in the subsurface dataset from the northern Carnarvon Basin, NW Shelf in Chapter 6. In Chapter 4, the problem of distinguishing and quantifying each allogenic control acting on two adjacent exhumed fan deltas in the immediate hangingwall of a single fault segment was addressed; with one fan delta positioned towards the fault tip (Selinous) and one towards the fault centre (Kerinitis). Overall syn-rift thicknesses provided the magnitude of subsidence at each delta. Aggradational stacking patterns at both sites suggested equivalent sedimentation and subsidence rates, and stacked conglomeratic topset units punctuated by fine-grained intervals implied regular cyclicity. The assumption of 41 kyr climate-

driven cyclicality during the Early-Middle Pleistocene and number of cycles identified at each fan delta allowed their duration to be estimated. Forward modelling with Syn-Strat was used to test the magnitude of lake level change through each cycle, by matching the outputs to field observations of sequence boundary presence or absence at each fan delta. Modelling results (10-15 m amplitude of lake level change) were validated by extrapolation of unit thicknesses from their respective positions along the fault towards the fault tip, where subsidence and unit thickness should theoretically be zero.

'Non-unique solutions' implies that in the field example, overall accommodation could have been created from rising lake level rather than fault-related subsidence, or that the cyclic stratigraphic architecture observed could have been caused by sedimentation variation, rather than lake level fluctuations. The former is not valid because the cumulative subsidence is an order of magnitude greater than the space creation possible from lake level rise. Sedimentation variability associated with climatic fluctuations since the Pleistocene was likely. For example, there were enhanced sediment discharge rates in the Alkyonides Basin, Greece during the last glacial lowstand compared to those in the preceding interglacial period, as a result of reduced tree coverage, more seasonality and storms, and enhanced runoff (Collier et al., 2000). That trend is apparent over the last ~500 ka in the Gulf of Corinth (McNeill et al., 2019). However, the analysis in Chapter 4 shows that base level must have fallen on some occasions to form sequence boundaries, and there must have been an additional mechanism to fluctuate accommodation. Moreover, there is regional understanding from core analysis, seismic mapping, and dating of marine terraces and corals that the level of Lake Corinth fluctuated since the Early Pleistocene (Collier, 1990; Doutsos & Piper, 1990; Westaway, 1997; Moretti et al., 2004; Collier et al., 2000; Perissoratis et al., 2000; Kershaw et al., 2005; Portman et al., 2005). Therefore, lake level changes were deemed to be the most likely control for the observed cyclicality.

For a stratigraphic column at a single position in 3D space, it is not possible to constrain whether the recorded stacking is a result of, for example, increasing subsidence and fluctuating base level, or increasing base level and fluctuating sedimentation. Mathematically, the parameters are

interchangeable. However, when numerous 1D positions or 2D segments are considered, stratigraphic trends are observed because many geological processes/controls follow ‘rules’. Geological processes follow rules in time, space and scale and these rules are predictable.

The simplest example of a trend in stratigraphy that follows geological rules in time is the basis of sequence stratigraphy itself. Cyclical patterns in stratigraphy observable in up-dip and down-dip positions within a basin were attributed to a common cyclical forcing; eustatic sea level (Posamentier et al., 1988; Posamentier & Vail, 1988), which was known to force coastal migratory trends and vary according to ice sheet expansion and retreat at the poles (Alley et al., 2005). Furthermore, eustatic sea level cyclicity occurs over different timescales, which are associated to different orbital motions that affect the planet’s insolation (Hays et al., 1976; Emiliani, 1978). Thus, these patterns in the rock record are observed across the world, because the cyclical ‘rules’ on eustatic base level are universal and largely unchanged through time. Another geological rule is the approximately parabolic subsidence distribution along the hangingwall of normal faults. This was used to distinguish the space created by subsidence from the space created from lake level rise in the unit thickness extrapolation approach in Chapter 4. Moreover, it may be challenging to differentiate sedimentation from base level cyclicity, but the long-term strain distribution across a rift means that any cyclicity that includes evidence of relative base level fall cannot be attributed to tectonics, as repeated episodes of subsidence and uplift on the same fault cannot occur over such short timescales. These are just three examples of geological rules that counter the argument of non-unique solutions of stratigraphic architecture (e.g. Burgess and Prince 2015), as they demonstrate that allogenic controls do not behave in the same way in time, space and scale, and thus can be differentiated.

Fundamentally, it was the contrasting architectures of the two fan deltas that provided the ability to deconvolve the control signals acting on their development in Chapter 4. Along-strike variability of stratigraphic architecture makes predictions of rift basin-fills complicated, yet here it is shown that their very variability allows control signals to be picked apart. The ability to deconvolve the allogenic controls from the depositional record is possible from: a) assessment of

multiple systems within a basin (quasi-3D analysis), b) interpretation and modelling based on geological rules, and c) regional understanding. In summary, ‘non-unique solutions’ theory is only arguable in cases with one-dimensional data and limited regional knowledge.

7.3. Research Question 3

How can quantitative approaches be applied to stratigraphic analysis?

In the push for more quantitative analysis of stratigraphy, we should consider four quantitative goals: 1) data, 2) classification, 3) techniques, and 4) modelling. Each of these goals are targeted through Chapters 3-6 and yield opportunity for numeric analyses and better prediction. Quantitative data is utilised in the form of subsurface seismic reflection data (Chapter 6) and UAV photogrammetry-based 3D outcrop models from the field (Chapters 4 and 5). The latter’s ability to extract large quantitative datasets from the field is a valuable advance in field geology and yields the potential to undertake numeric and statistical analyses that would be less possible from classic, sparse field datasets. Quantitative field observations are taken to deconvolve and quantify allogenic controls in Chapter 4. Quantitative classification of scaling and spatial relationships is common in geology and here, a quantitative classification was undertaken of interfan geometries (Chapter 5). Quantitative classification of temporal relationships between strata is more challenging and addressed in Section 7.4. Quantitative techniques in basin analysis can improve interpretations and facilitate predictions. A novel volume balancing approach is taken in Chapter 6 to pick apart supply signals in the Thebe hangingwall basin. Quantitative modelling is invaluable for testing infinite and unbiased control system scenarios in a short time and is the technique that allows the closest predictive capability. A novel 3D sequence stratigraphic model, Syn-Strat was developed and utilised in this work (Chapters 3 and 4), which has a simple construct and delivers a new approach to visualising stratigraphic data.

7.3.1. Quantitative data

The fields of sedimentology and stratigraphy are characterised by qualitative observations. They are necessary, but quantitative observations are required to complement them for more sophisticated overall analyses. Seismic data, in its 3D and numeric form, is a good example of data that provides abundant opportunity to assess and map various geological attributes. This is because the strata are represented by waveforms, characterised by values. The three-dimensionality of the data allows direct measurement of geometries (e.g. Chapter 6), but resolution is limited. Field data is generally higher resolution, but more challenging to quantify in terms of textural, spatial and geometric descriptions, and the potential for restricted exposure or access. However, in Chapter 4, quantitative data from the field were extracted across two fan deltas (overall syn-rift thickness, unit thickness and topset-foreset breakpoint (TFBP) trajectories) and used to deconvolve and quantify the allogenic controls responsible for their formation. Quantitative field data collection (e.g. bedding data, unit thicknesses, foreset heights and TFBP trajectories) was facilitated by the use of UAV photogrammetry-based 3D outcrop models (Chapters 4 and 5). Vertically-stacked units that are several 10s-100s m thick were accurately measured using the outcrop models, which would have been much more challenging in the field. In addition, 167 bedding plane measurements were taken from the models to assist the interfan analysis in Chapter 5. At present, the use of 3D outcrop models in stratigraphic analysis is relatively novel (e.g. Nieminski & Graham, 2017; Nesbit et al., 2018), but as they become more mainstream practice, quantitative field data collection will become more common and bigger datasets may be presented in the literature, improving the potential for statistical analyses.

7.3.2. Quantitative classification

One way to broaden the utility of qualitative data is to classify it quantitatively, or semi-quantitatively. It could be the classification of uncertainty underpinning an observation or interpretation (e.g. Chapter 4) or the use of matrices to categorise data by numeric parameters, for example, carbonate texture (Folk, 1959; 1962; Dunham, 1962) or bedform type (Van den Berg & Van Gelder, 1993; Baas et al., 2009; Stow et al., 2009). In this work, classification of interfan

geometries is addressed in Chapter 5, and it was decided that a quantitative rather than descriptive approach would be most suitable and widely applicable. Interfans were classified as Types 1-3, depending on the separation of two adjacent fan deltas, according to the radius of the fan delta topsets and foresets. This is a spatial classification, is scale-independent, and can be applied to modern and ancient systems alike, where their geometries can be measured.

Scaling relationships are often quantitatively classified, with perhaps the most traditional example being grain size (Udden, 1914; Wentworth, 1922; Krumbein, 1938). A number of statistical analyses (e.g. Folk & Ward, 1957; Krumbein and Pettijohn, 1938; Friedman and Johnson, 1982) are possible from grain size datasets to yield depositional insights (Blott & Pye, 2001; Allen et al., 2017; Cosgrove et al., 2018; 2019a,b). Other sedimentological examples of quantitative scaling classifications include bed thickness (Campbell, 1967), bioturbation (Taylor & Goldring, 1993), and clinoform size (Patruno et al., 2015; Patruno & Helland-Hansen, 2018), and in the wider geological literature, quantitative scaling classifications extend to earthquake magnitude (Richter, 1935; Hanks & Kanamori, 1979) and volcano explosivity (Newhall & Self, 1982).

Spatial relationships are simpler to quantitatively classify than temporal relationships because in the spatial domain, direct measurements can be taken with reference to known coordinates. For example, image classification is a type of spatial classification that has a number of environmental and socioeconomic applications, including land-use mapping (Klein & Press, 1992; Lu & Weng, 2007; Borzov & Potaturkin, 2018). Temporal relationships are more difficult to quantitatively classify, particularly between strata, where relationships are described by stacking patterns and termination geometries (Van Wagoner et al., 1990). The former can be quantified using the ratio of $\delta A/\delta S$ (Sloss, 1962; Curray, 1964; Vail et al., 1977), but there are a number of limitations behind this approach, which are discussed in Chapter 7.4.

7.3.3. Quantitative techniques

In Chapter 6, a volume balancing method was used to locate the through-going sediment input points to a basin in the subsurface. Areas supplied by through-going sediment inputs from beyond the fault crest were differentiated from those areas supplied by fault scarp degradation, by assessing the balance between footwall (fault crest) erosion and footwall-derived, hangingwall fill. This is a novel, quantitative approach to stratigraphic analysis across a fault, which was demonstrated to be particularly useful in scenarios with limited preservation or imaging of erosional catchments.

In general, quantitative balancing approaches have high utility in making or supporting interpretations. Mass or volume balancing is a good example of a quantitative approach that can provide additional insight into basin processes. It has been used in source-to-sink analyses across different scales and basins to assess sediment budgets (Paola & Martin, 2012; Allen et al., 2013; Michael et al., 2013; Hampson et al., 2014; Lin & Bhattacharya, 2017; Pechlivanidou et al., 2017; Watkins et al., 2018). Another useful, quantitative balancing approach that has been proposed for improving sequence stratigraphic interpretations is the analysis of the ratio between parasequence thickness and sandstone fraction ('TSF analysis'), which are quantitative proxies for accommodation creation and sediment supply (Ainsworth et al., 2018). The $\delta A/\delta S$ ratio is a common quantitative balancing approach, but fails to incorporate all potential controls and outcomes, as discussed in Chapter 7.4.

7.3.4. Quantitative modelling

Numerical modelling is undertaken in Chapter 3 to assess along-strike variability in stratigraphic architecture as a result of different control combinations, and in Chapter 4 to quantify particular controls acting on fan deltas in the Gulf of Corinth. Numerous models (e.g. Sedpak, Dionisos, Strata, Sedsim, Cascade, pyBadlands) have been applied in the stratigraphic realm to assist interpretations and predictions (Strobel et al., 1989; Kendall et al., 1991a,b; Granjeon, 1997; Granjeon & Joseph, 1999; Granjeon, 2014; Flemings & Grotzinger, 1996; Burgess & Prince, 2015; Madof et al., 2015; Geurts et al., 2018; Pechlivanidou et al., 2019), as discussed in Chapter

2. However, prior to this study, geometrical modelling of simple control scenarios in 3D space along a fault segment, was missing.

Syn-Strat was developed through this work and introduced in Chapters 3 and 4. It is a novel, 3D, forward sequence stratigraphic model that was used for sensitivity analysis, whereby a number of different scenarios were tested to find the best fit to the data observed (Chapter 4). The model takes a unique approach to presenting the outcomes of stacking and surfaces, whereby they are visualised on a 3D graphical surface. It has the value of being able to test hypothetical (Chapter 3) and real (Chapter 4) scenarios, allowing the user to manipulate the inputs and output presentations as they choose. The 3D accommodation curve can be coloured to highlight specific information. For example, systems tracts in any particular sequence stratigraphic scheme (e.g. Catuneanu, 2006) can be applied. Or, stacking patterns can be applied according to four different schemes: a) with three colours according to the absolute value of $\delta A/\delta S$, e.g. where $\delta A > \delta S$, the surface is coloured to represent retrogradation, where $\delta S = \delta A$ it is coloured to represent aggradation, and where $\delta S > \delta A$, the surface is coloured to represent progradation; b) with five colours based on a normalised accommodation curve stretching from -1 to 1, divided into equally spaced intervals from strongly retrogradational to strongly progradational stacking; c) five colours according to the angle of the accommodation curve, with the highest angles referring to the strongest retrogradation and progradation (e.g. Fig. 7.4); and d) according to the new scheme presented in Chapter 7.4. The accommodation curve can be presented in 3D form, with any two of the three dimensions (distance along the fault, distance away from the fault and time). It can also plot 1D and 2D sections amounting to stratigraphic columns and sections at any position within the basin-fill. Examples of these outputs are presented in Figure 7.4, with a scenario of five point sources along a fault and five base level cycles. The user is thus given the flexibility to choose how to interpret and present the accommodation curve.

Syn-Strat has the benefit of being able to test multiple control system scenarios in a short time, with an unbiased approach. In its geometric form, it is a simple construct and avoids many of the assumptions that process-based models have inflicted. It could provide the underlying framework

to which a process-based model could be applied. The model has two main limitations. Firstly, the tectonic basis of a single fault segment that is presented here does not account for fault segment interaction and linkage through time. If that interaction can be defined graphically as an input to the model, then it might be possible, but this is beyond the scope of this work. In this study, hangingwall basins are modelled, but footwall basins are just as possible. Similarly, the generator of space does not necessarily need to be a normal fault, but any mechanism that can create or reduce accommodation, e.g. salt diapirs. The second limitation is that the sedimentation inputs are defined in graphical form across the space, and therefore do not accurately represent real depositional geometries. For the purpose of accurate representation, it would be more beneficial to run a process-based model to generate the geometry.

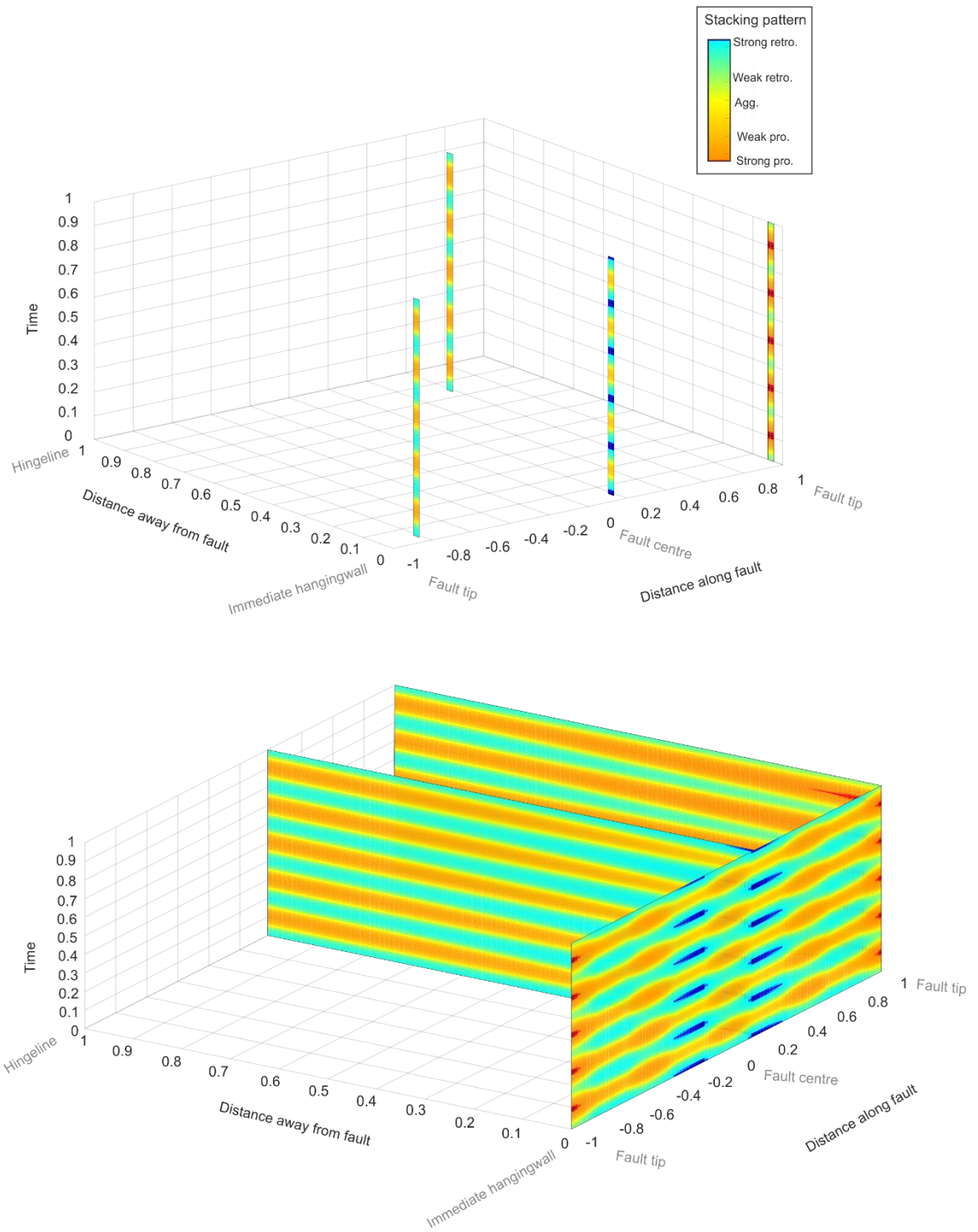


Figure 7.4. Stratigraphic columns and cross-section outputs from Syn-Strat to demonstrate its utility, with stacking patterns presented.

7.4. Research Question 4

How should 'accommodation' be used in interpretations to incorporate the complexity observed in tectonically-active basins, and is the $\delta A/\delta S$ ratio valid?

The accommodation/supply ($\delta A/\delta S$) ratio is a well-established concept for depositional system and shoreline migration, and therefore the nature of stratal unit stacking (Sloss, 1962; Curray, 1964; Vail et al., 1977). Accommodation was originally defined as “the space made available for potential sediment accumulation” and generally equates to depth from the water surface to the depositional surface (Jervey, 1988; Posamentier et al., 1988), with the depositional surface as “the level above which erosion will occur” (Jervey, 1988). This clarification is important because it implies that deposition or erosion will elevate or lower the depositional surface and will therefore decrease or increase accommodation, which defies the notion of accommodation and supply being independent terms, as advocated with the use of $\delta A/\delta S$ (Van Wagoner et al., 1990; Thorne & Swift, 1992; Swift & Thorne, 1992; Neal & Abreu, 2009; Neal et al., 2016). The term ‘accommodation’ in its current use within the $\delta A/\delta S$ implies ‘creation’, which does not account for the decay of accommodation through base level fall, uplift or sedimentation. Similarly, erosion is not accounted for as a control for creating space for deposition, yet the scale of incision can be comparable to other allogenic controls (Backert et al., 2010; Gomis-Cartesio et al., 2017).

Stacking patterns are described as progradational, retrogradational (both lateral migrations of the shoreline), aggradational or degradational (vertical migrations of the shoreline), which depend upon the rate of change of $\delta A/\delta S$ (Van Wagoner et al., 1990; Neal & Abreu, 2009; Neal et al., 2016). An outcome that is not considered in this scheme, yet may be a prominent feature of depositional status through time, is stasis (Tipper, 2015), whereby there is no change in the system because either: the controlling parameters are unchanged, or the balance of the controls over time cancels the effect to a state of equilibrium or continuity (Martinius et al., 2014). The identification of stacking patterns in the stratigraphic record is a useful and pragmatic, observation-based approach to stratigraphic analysis, but the assignment of the stacking patterns to the $\delta A/\delta S$ ratio

for control interpretations and prediction is problematic. With the flaws described, the $\delta A/\delta S$ ratio is not conceptually sound and there is room for improvement.

An alternative solution for making interpretations and predictions with the $\delta A/\delta S$ is proposed that considers all allogenic controls and stratigraphic outcomes. A ratio of the rate of change of ‘accommodation increasers’ to the rate of change of ‘accommodation reducers’ ($\delta AI/\delta AR$) is proposed. This ratio equates to accommodation that changes through time, i.e. the accommodation balance. Accommodation increasers refer to base level rise, tectonic subsidence and erosion. Accommodation reducers refer to base level fall, tectonic uplift and sedimentation.

$$A = \frac{\delta A \text{ increasers}}{\delta A \text{ reducers}} = \frac{\delta B_R + \delta T_S + \delta E}{\delta B_F + \delta T_U + \delta S}$$

where B_R is base level rise, T_S is tectonic subsidence, E is erosion, B_F is base level fall, T_U is tectonic uplift and S is sedimentation, such that:

- A transgressive trend occurs when $\delta AI/\delta AD > 1$ and $\delta AI > \delta AD$
- A regressive trend occurs when $\delta AI/\delta AD < 1$ and $\delta AI < \delta AD$
- Static positioning occurs when $\delta AI/\delta AD = 1$ and $\delta AI = \delta AD$

In our numerical modelling with Syn-Strat, this ratio is translated into an equation, such that:

$$A = \delta B + \delta T + \delta E - \delta S$$




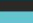



where each term refers to a vector that defines a position relative to a given datum, with B as base level, T as tectonic movement, E as erosion and S as sedimentation.

The transgressive and regressive trends represent a horizontal migration of the depositional system through time in one position in space (1D). Where there is net deposition, in 2D and 3D, these would represent retrogradational and progradational stacking patterns, respectively. The 1D record of horizontal stasis is more cryptic and may instead reveal a vertical migration from a given datum, or no migration at all. In a 2D or 3D record, it could thus reveal aggradation, degradation or stasis. Aggradational stacking occurs when $\delta AI = \delta AD$ ($\delta AI/\delta AD = 1$) and there is net deposition. Where there is a surface in 1D, this may be from degradation or a hiatus in broader

space. Unlike aggradation that occurs as a vertical expansion of the depositional record, degradation occurs with a loss of the depositional record from erosion, and therefore occurs when $\delta AI > \delta AD$ ($\delta AI/\delta AD > 1$), as a result of an increase in ΔE . This is a marked departure from the Neal et al. (2016) model where their ‘aggradation-progradation-degradation’ trend is represented by $\delta A/\delta S$ as a number <1 and decreasing, which is unintuitive as implies an increase in sedimentation and not a loss. Degradation and progradation are fundamentally different outcomes that could occur simultaneously at different parts of the basin (e.g. degradation up-dip and associated progradation down-dip). They represent different migration vectors and therefore must be differentiated in a stratigraphic framework. A period of stasis occurs when the system is neither depositing nor eroding (Tipper, 2015). In this case, there must be nothing happening at that position from basin controls, and both δAI and δAR must be equal to zero. Tipper (2015) argues that stasis is “the norm, and not the exception”. It is necessary for a stratigraphic framework to consider all scenarios that could be recorded. Although the $\delta A/\delta S$ could account for it, stasis is rarely included in stratigraphic models.

Table 7.1 shows the possible outcomes of the accommodation balance in 1D space. It considers all of the parameters within the accommodation balance and whether there is sedimentation or not. It shows whether the depositional record will reveal a surface (brown) or a rock record (blue). The surface can be erosive (degradation) or non-erosive (hiatus). The rock record can be progradational, aggradational or retrogradational. The table also shows the migration vector in each outcome as a result of the accommodation balance, which is either landward (transgressive), basinward (regressive) or stationary. As an example of this approach, Figure 7.5 shows two positions in a basin with different sedimentation models. Both positions have the same accommodation curve controlling their sedimentary evolution. The first position receives no sediment from t_0 to t_2 , receives sediment from t_2 to t_4 and no sediment from t_4 to t_6 . At the second position, the opposite trend occurs. The accommodation balance changes through time at each position and thus the occurrence of stacking and surfaces follows suit. Simple stratigraphic columns are shown to visualise this effect (Fig. 7.5).

Table 7.1. Matrix of outcomes for the accommodation balance.

$A = \frac{\Delta B_R + \Delta T_S + \Delta E}{\Delta B_F + \Delta T_U + \Delta S}$	No sedimentation	Sedimentation
$A > 1$	 Degradation (E) or Hiatus (B_R or T_S) Transgressive surface	 Retrogradation (B_R or T_S)
$A = 1$	 Hiatus	 Aggradation
$A < 1$	 Hiatus Regressive surface	 Progradation
$A = 0$	 Hiatus - Stasis	

Accommodation at a given position can be considered as an absolute value at a given time, i.e. equating to water depth at time, 't', or as a dynamic change over a time period, 't₁ to t₂'. At a given time, any 1D position within a basin can be in one of three states: underfilled (sediment accumulates but does not reach the water level datum), filled (sediment accumulation reaches the water level datum), or overfilled (sediment accumulation exceeds the water level datum) (Ravnås & Steel, 1998). The remaining water depth at that position is the absolute value of accommodation, and this is the available space for deposition at the next time step. In 3D, the remaining volume of water in the basin is the absolute value of accommodation.

When considering accommodation over a time period in 1D, the state of the basin is important, but the magnitude and rate of change over time is the determinant of the stacking pattern that arises. Moreover, it is the magnitude and rate of change of mechanisms that act to create space relative to that of those that reduce space. All parameters can exert an equal influence on accommodation. Considering the parameters purely mathematically, one would assume that the

resultant stacking pattern is non-unique (Heller et al., 1993; Flemings & Grotzinger, 1996; Burgess & Prince, 2015) and that a given stacking pattern could arise as a result of numerous combinations of those parameters. This makes prediction problematic. However, geologically the control parameters do not act in the same way and context is crucial. Each control produces characteristic patterns as a result of their underlying mechanisms and is therefore more interpretable and predictable than the ratio alone suggests, as discussed in Chapter 7.2.

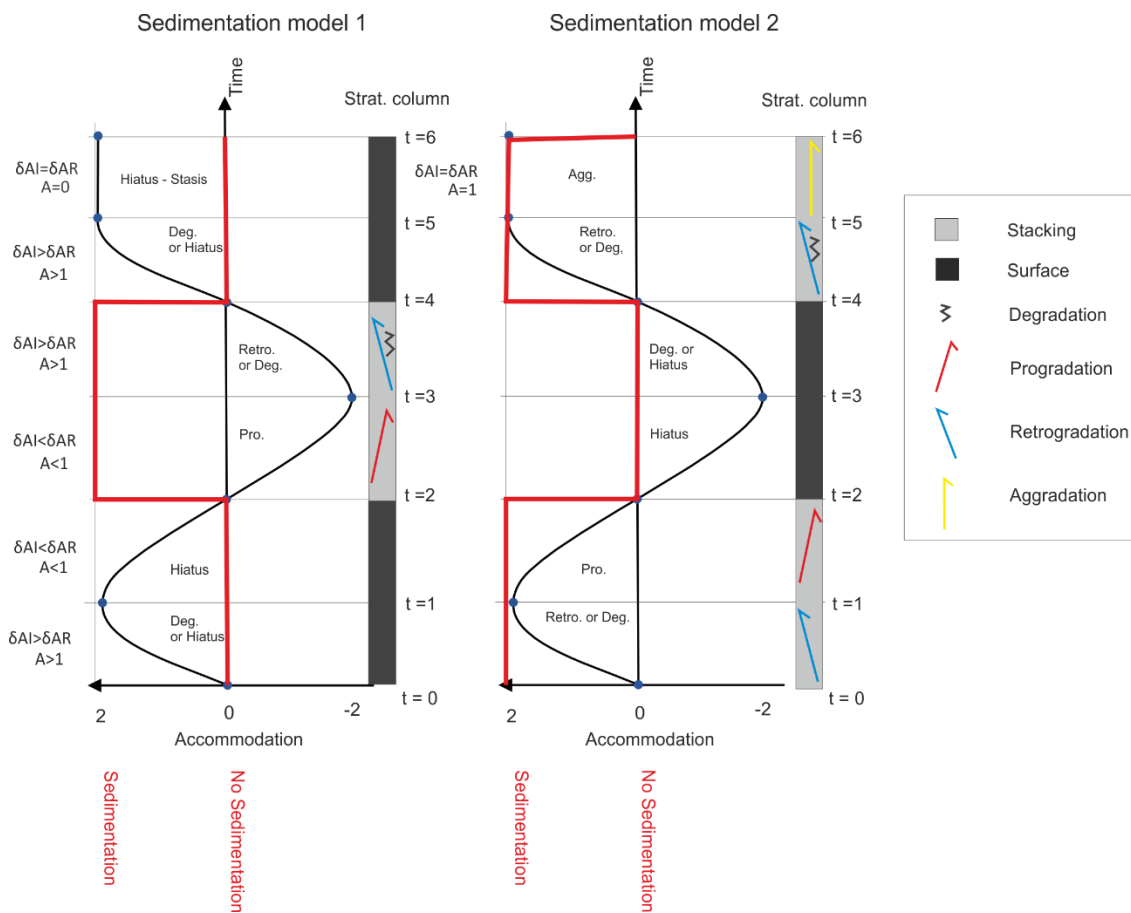
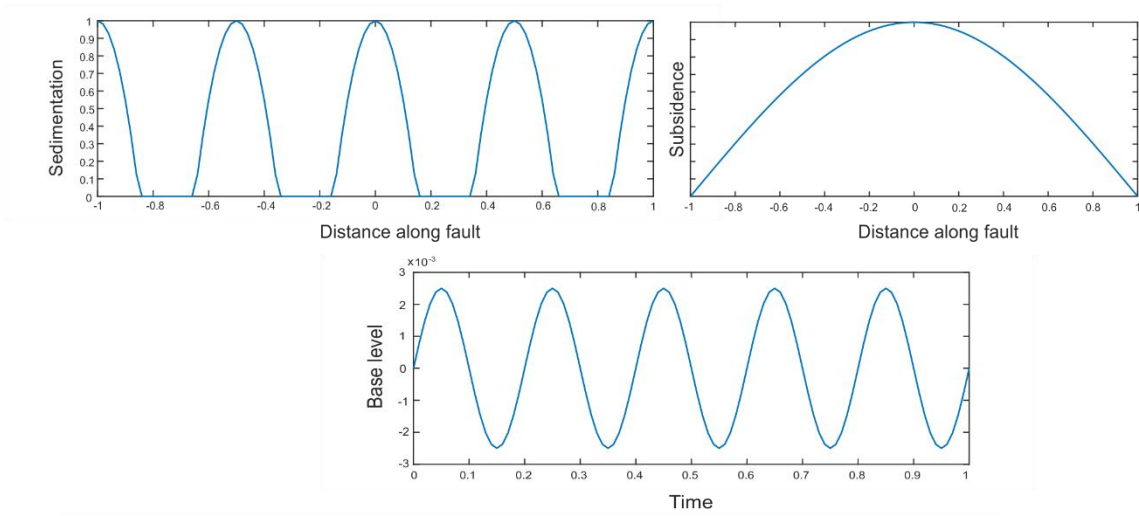


Figure 7.5. Plots to show an example of the accommodation balance approach. Two positions in a basin are chosen with different sedimentation models through time. The same accommodation curve controls both positions. The occurrence of stacking and surfaces through time are presented at both positions, as a result of the accommodation balance ($\delta AI/\delta AR$). Simple stratigraphic columns are presented to visualise the outcomes.

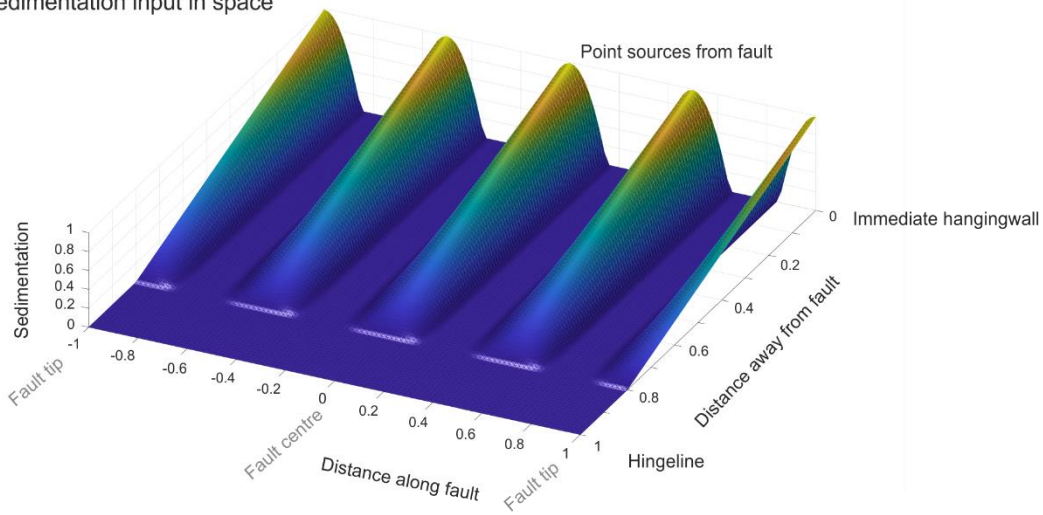
The accommodation balance approach to interpretation is applicable to surfaces output by Syn-Strat. As an example, a scenario with five point sources along a fault with high sedimentation rates, high subsidence and five base level cycles is modelled. Figures 7.6A and 7.6B show the

main model inputs and Figure 7.6C shows the output in time and along the fault, with stacking patterns overlain. Figure 7.6D shows the same output but with the accommodation balance overlain, which shows significant variability in stacking and surfaces along-strike. At point source locations, stacking is apparent, whereby there is progradation during accommodation falls and retrogradation during accommodation rises. Some aggradation occurs at the transitions between the two. Periods of progradation become longer, as sedimentation increases and overcomes the subsidence for longer. Stacking is more aggradational during accommodation falls towards the fault centre, and more progradational towards the fault tips. At positions where sedimentation is zero, transgressive surfaces arise during accommodation rise. During accommodation fall, regressive surfaces form towards the fault tips and hiatus surfaces form towards the fault centre. Figure 7.6E shows two dip- and a strike-section across the area; plots that are equivalent to Wheeler diagrams (Wheeler, 1958; 1959; 1964a,b). This example highlights the benefit of the accommodation balance approach, as it encompasses all allogenic controls acting on the basin and all possible outcomes in terms of stacking and surfaces.

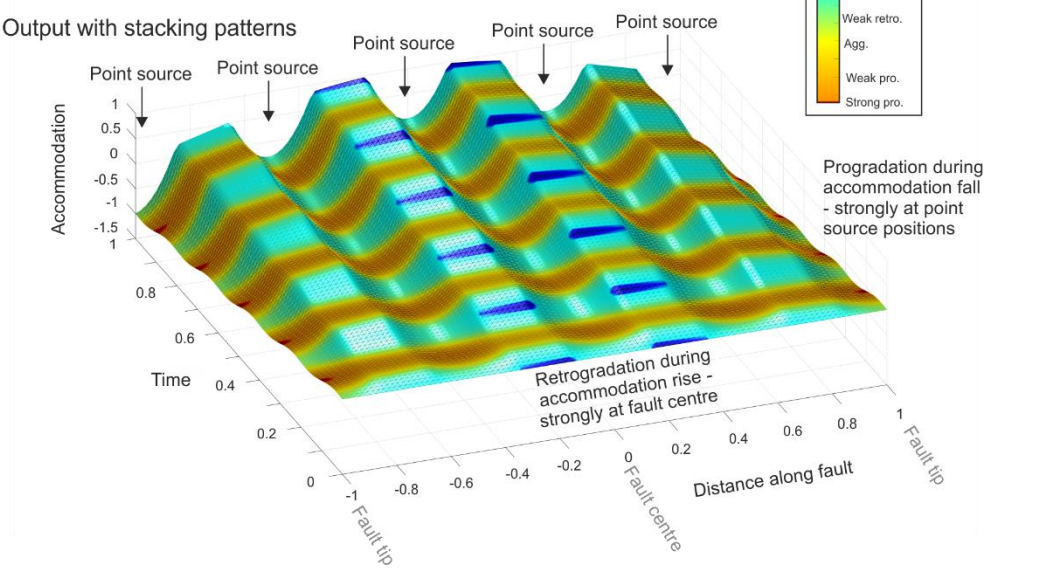
A Inputs



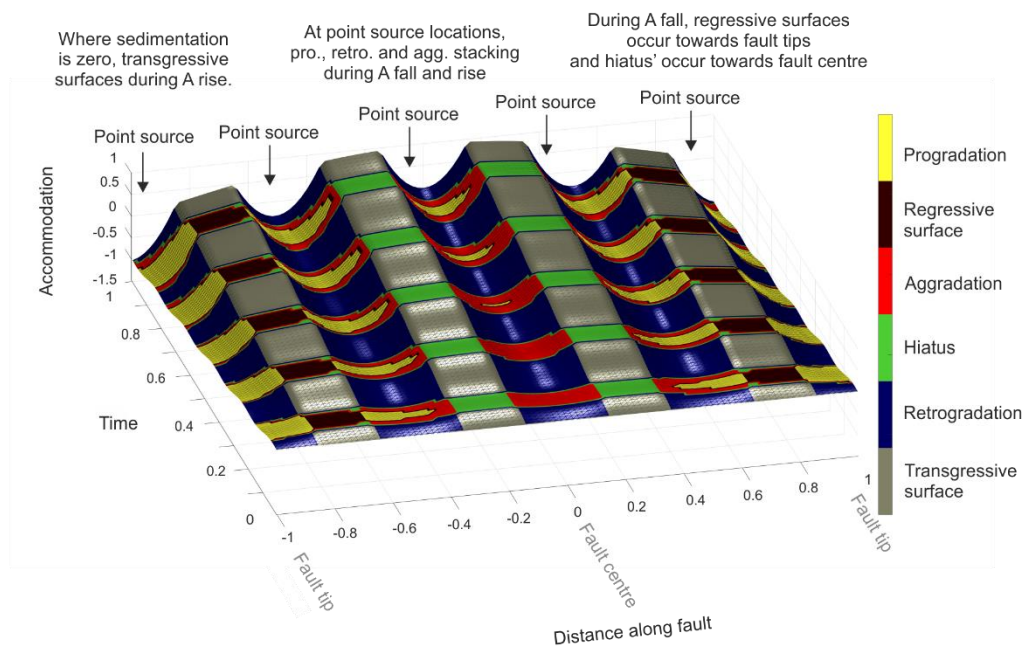
B Sedimentation input in space



C Output with stacking patterns



D Output with accommodation balance - surfaces and stacking



E Cross-sections presenting the accommodation balance - surfaces and stacking

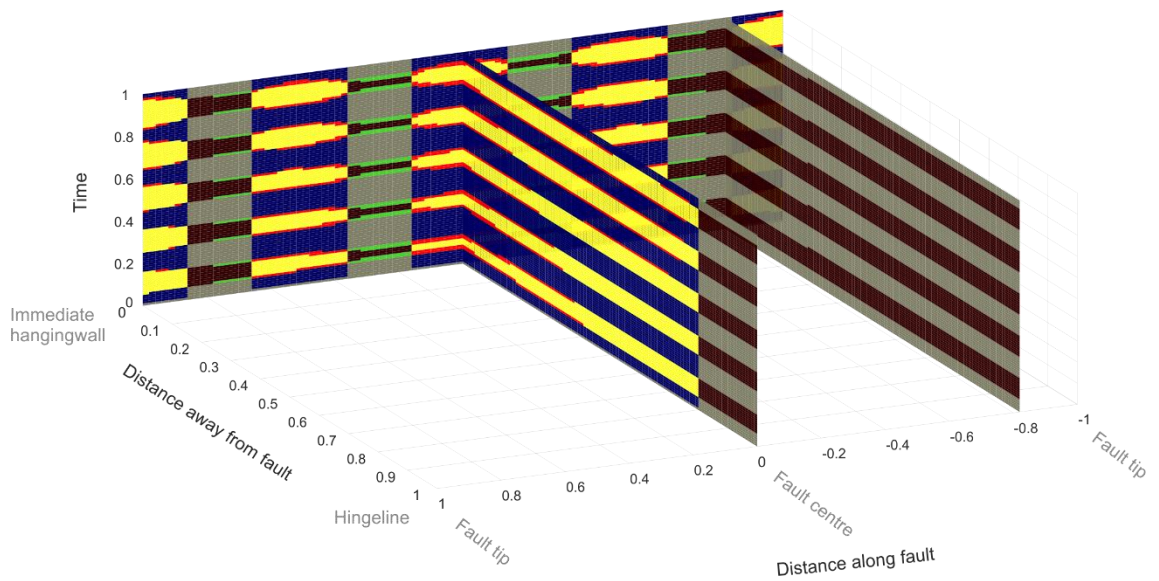


Figure 7.6. Scenario to show the utility of the accommodation balance approach using Syn-Strat. A) some of the main model inputs; B) 3D plot to show sedimentation input in space; C) 3D accommodation plot with stacking patterns overlain – presented in time and along the fault; D) 3D accommodation plot with accommodation balance overlain. E) Dip- and strike-sections across the basin, equivalent to Wheeler diagrams.

In conclusion, there is substantial variability in stratigraphic architecture in tectonically-active basins, as a result of dynamic tectonic and climatic processes, and associated feedbacks in sedimentation. Several flaws in the $\delta A/\delta S$ ratio have been highlighted: 1) accommodation and supply are not independent terms; 2) accommodation is generally considered as being created and not reduced, yet decay of accommodation can occur through base level fall, uplift or sedimentation; 3) erosion is not accounted for as a control for creating space for deposition, yet the scale of incision can be comparable to other allogenic controls; and 4) stasis is not considered as an outcome, yet may be a common status of the depositional system. As such, the $\delta A/\delta S$ does not provide a suitable framework for interpretations of stacking patterns or predictions in tectonically-active basins. A new framework ($\delta AI/\delta AR$) is proposed, which equates to accommodation. In its construct, the accommodation balance ($\delta AI/\delta AR$) is similar to $\delta A/\delta S$, but it negates problems described above by including erosion and removing the 'A' term from the ratio. Instead, all control parameters are clearly described. In doing so, the definition of accommodation is kept true in a dynamic system, as "the space available for deposition" through time. In addition, the framework is not only inclusive of all control parameters, but also of all recorded outcomes. It considers erosive and non-erosive surfaces, and stasis that are important aspects of a depositional system, which are neglected in $\delta A/\delta S$. The accommodation balance better represents time in the depositional record with this inclusion. With this in mind, it is a better communicator of the allocation of time across surfaces and strata.

7.5. References

- Ainsworth, R.B., McArthur, J.B., Lang, S.C. & Vonk, A.J. (2018). Quantitative sequence stratigraphy. *AAPG Bulletin*, 102, 1913-1939.
- Allen, P.A., Armitage, J.J., Carter, A., Duller, R.A., Nikolas, A.M., Sinclair, H.D., Whitchurch, A.L. & Whittaker, A.C. (2013). The Q_s problem: sediment volumetric balance of proximal foreland basin systems. *Sedimentology*, 60, 102-130.
- Allen, P.A., Nikolaos, A.M., D'Arcy, M., ROda-Boluda, D.C., Whittaker, A.C., Duller, R.A. & Armitage, J.J. (2017). Fractionation of grain size in terrestrial sediment routing systems. *Basin Research*, 29, 180-202.
- Alley, R.B., Clark, P.U., Huybrechts, P. & Joughin, I. (2005). Ice-sheet and sea-level changes. *Science*, 310, 456-460.

- Baas, J.H., Best, J.L., Peakall, J. & Wang, M. (2009). A phase diagram for turbulent, transitional and laminar clay suspension flows. *Journal of Sedimentary Research*, 79, 162-183.
- Backert, N., Ford, M. & Malartre, F. (2010). Architecture and sedimentology of the Kerinitis Gilbert-type fan delta, Corinth Rift, Greece. *Sedimentology*, 57, 543-586.
- Blott, S.J. & Pye, K. (2001). GRADISTAT: a grain size distribution and statistics package for the analysis of unconsolidated sediments. *Earth Surface Processes and Landforms*, 26, 1237-1248.
- Borzov, S.M. & Potaturkin, O.I. (2018). Spectral-spatial methods for hyperspectral image classification, review. *Optoelectronics, Instrumentation and Data Processing*, 54, 582-599.
- Burgess, P.M. & Prince, G.D. (2015). Non-unique stratal geometries: Implications for sequence stratigraphic interpretations. *Basin Research*, 27, 351-365.
- Campbell, C.V. (1967). Lamina, laminaset, bed and bedset. *Sedimentology*, 8, 7-26.
- Catuneanu, O. (2006). Principles of sequence stratigraphy. Elsevier, Amsterdam, The Netherlands. 375pp.
- Collier, R.E.L. (1990). Eustatic and tectonic controls upon Quaternary coastal sedimentation in the Corinth Basin, Greece. *Journal of the Geological Society*, 147, 301-314.
- Collier, R.E.L., Leeder, M.R., Trout, M., Ferentinos, G., Lyberis, E. & Papatheodorou, G. (2000). High sediment yields and cool, wet winters: test of last glacial paleoclimates in the northern Mediterranean. *Geology*, 28, 999-1002.
- Cosgrove, G.I.E., Poyatos-Moré, M., Lee, D., Hodgson, D.M., McCaffrey, W.D., Mountney, N.P. (2019a). Intra-clinothem variability in sedimentary texture and process regime recorded down slope profiles. *Sedimentology*, doi: 10.1111/sed.12648.
- Cosgrove, G.I.E., Hodgson, D.M., Mountney, N.P., McCaffrey, W.D. (2019b). High-resolution correlations of strata within a sand-rich clinothem using grain fabric data, offshore New Jersey, USA. *Geosphere*, 15, doi: 10.1130/GES02046.1.
- Cosgrove, G.I.E., Hodgson, D.M., Poyatos-Moré, M., Mountney, N.P., McCaffrey, W.D. (2018). Filter Or Conveyor? Establishing Relationships Between Clinoform Rollover Trajectory, Sedimentary Process Regime, and Grain Character Within Intraself Clinothems, Offshore New Jersey, U.S.A. *Journal of Sedimentary Research*, 88, 917-941.
- Curray, J.R. (1964). Transgressions and regressions. In: R.L. Miller (Ed.), *Papers in Marine Geology*. Macmillan, New York, 175-203.
- Dart, C.J., Collier, R.E.L., Gawthorpe, R.L., Keller, J.V.A. & Nichols, G. (1994). Sequence stratigraphy of (?)Pliocene-quaternary synrift, gilbert-type fan deltas, Northern Peloponnesos, Greece. *Mar. Pet. Geol.*, 11, 545-560.
- Dorsey, R.J. & Umhoefer, P.J. (2000). Tectonic and eustatic controls on sequence stratigraphy of the Pliocene Loreto Basin, Baja California Sur, Mexico. *GSA Bulletin*, 112, 177-199.
- Doutsos, T. & Piper, D.J.W. (1990). Listric faulting, sedimentation, and morphological evolution of the Quaternary eastern Corinth rift, Greece: first stages of continental rifting. *GSA Bulletin*, 102, 812-829.
- Dunham, R. J. (1962). Classification of carbonate rocks according to depositional texture. In: W.E. Ham (Ed.), *Classification of carbonate rocks*. American Association of Petroleum Geologists Memoir, 1, 108-121.

- Emiliani, C. (1978). The cause of the ice ages. *Earth & Planetary Science Letters*, 37, 349-352.
- Flemings, P.B. & Grotzinger, J.P. (1996). STRATA: Freeware for analysing classic stratigraphic problems. *GSA Today*, 6, 1-7.
- Folk, R.L. (1959). Practical petrographic classification of limestones. *American Association of Petroleum Geologists Bulletin*, 43, 1-38.
- Folk, R.L. (1962). Spectral subdivision of limestone types. In W.E. Ham (Ed.), *Classification of carbonate rocks*. American Association of Petroleum Geologists Memoir, 1, 62-84.
- Folk, R.L. & Ward, W.C. (1957). Brazos River bar: a study in the significance of grain size parameters. *Journal of Sedimentary Petrology*, 27, 3-26.
- Friedman, G.M. & Johnson, K.G. (1982). *Exercises in Sedimentology*. Wiley, New York. 208pp.
- Gawthorpe, R.L., Fraser, A. & Collier, R.E.LI. (1994). Sequence stratigraphy in active extensional basins: implications for the interpretation of ancient basin fills. *Marine and Petroleum Geology*, 11, 642-658.
- Gawthorpe, R.L., Hardy, S. & Ritchie, B. (2003). Numerical modelling of depositional sequences in half-graben rift basins. *Sedimentology*, 50, 169-185.
- Gawthorpe, R.L. & Leeder, M.R. (2000). Tectono-sedimentary evolution of active extensional basins. *Basin Research*, 12, 195-218.
- Geurts, A.H., Cowie, P.A., Duclaux, G., Gawthorpe, R.L., Huisman, R.S., Pedersen, V.K. & Wedmore, L.N.J. (2018). Drainage integration and sediment dispersal in active continental rifts: a numerical modelling study of the central Italian Apennines. *Basin Research*, doi: 10.1111/bre.12289.
- Gomis-Cartesio, L.E., Poyatos-Moré, M., Hodgson, D.M. & Flint, S.S. (2017). Shelf-margin clinothem progradation, degradation and readjustment: Tanqua depocentre, Karoo Basin (South Africa). *Sedimentology*, 65, 809-841.
- Granjeon, D. (1997). Modelisation stratigraphique deterministe: conception et applications d'un modele diffusif 3D multilithologique. These Doct. University of Rennes, France.
- Granjeon, D. (2014). 3D forward modelling of the impact of sediment transport and base level cycles on continental margins and incised valleys. In: A.W. Martinius, R. Ravnås, J.A. Howell, R.J. Steel & J.P. Wonham, (Eds.), *From Depositional Systems to Sedimentary Successions on the Norwegian Continental Margin, First Edition*. International Association of Sedimentologists, 46, 453-472.
- Granjeon, D. & Joseph, P. (1999). Concepts and applications of a 3D multiple lithology, diffusive model in stratigraphic modeling. In: J.W. Harbaugh, W.L. Watney, E.C. Rankey, R. Slingerland, R.H. Goldstein & E.K. Franseen (Eds.), *Numerical Experiments in Stratigraphy: Recent Advances in Stratigraphic and Sedimentological Computer Simulations*. SEPM Special Publication, 62, 197-210.
- Hampson, G.J., Duller, R.A., Petter, A.L., Robinson, R.A.J. & Allen, P.A. (2014). Mass-balance constraints on stratigraphic interpretation of linked alluvial-coastal-shelfal deposits from source to sink: example from Cretaceous Western Interior Basin, Utah and Colorado, USA. *Journal of Sedimentary Research*, 84, 935-960.

Hanks, T.C. & Kanamori, H. (1979). A moment magnitude scale. *Journal of Geophysical Research*, 84, 2348-2350.

Hardy, S. & Gawthorpe, R.L. (1998). Effects of variations in fault slip rate on sequence stratigraphy in fan deltas: insights from numerical modeling. *Geology*, 26, 911-914.

Hardy, S. & Waltham, D. (1992). CLASTIC 2.0: a Clastic modelling program for the Macintosh (User Manual). Department of Geology, Royal Holloway & Bedford New College, University of London, London, UK, 17p.

Hays, J.D., Imbrie, J. & Shackleton, N.J. (1976). Variations in the earth's orbit: pacemaker of the ice ages. *Science*, 194, 1121-1132.

Heller, P.L., Burns, B.A. & Marza, M. (1993). Stratigraphic solution sets for determining the roles of sediment supply, subsidence and sea level on transgressions and regressions. *Geology*, 21, 747-750.

Hodgson, D.M., Kane, I.A., Flint, S.S., Brunt, R.L. & Ortiz-Karpf, A. (2016). Time-transgressive confinement on the slope and the progradation of basin-floor fans: implications for the sequence stratigraphy of deep-water deposits. *J. Sediment. Res.*, 86, 73-86.

Holbrook, J.M. & Bhattacharya, J.P. (2012). Reappraisal of the sequence boundary in time and space: case and considerations for an SU (subaerial unconformity) that is not a sediment bypass surface, a time barrier, or an unconformity. *Earth Sci. Rev.*, 113, 271-302.

Jackson, C.A.L., Gawthorpe, R.L., Carr, I.D. & Sharp, I.R. (2005). Normal faulting as a control on the stratigraphic development of shallow marine syn-rift sequences: the Nukhul and Lower Rudeis Formations, Hammam Faraun fault block, Suez Rift, Egypt. *Sedimentology*, 52, 313-338.

Jervey, M. (1988). Quantitative geological modeling of siliciclastic rock sequences and their seismic expression, In: C. Wilgus, B.S. Hastings, C.G.S.C. Kendall, H.W. Posamentier, C.A. Ross & J.C. Van Wagoner (Eds.), *Sea level changes: an integrated approach*. SEPM Spec. Pub., 42, 47-69.

Kendall, C. G. S. C., Moore, P., Strobel, J., Cannon, R., Perlmutter, M., Bezdek, J. & Biswas, G. (1991a). Simulation of the sedimentary fill of basins. In: E.K. Franseen, W.L. Watney, C.G.S.C. Kendall & W. Ross (Eds.), *Sedimentary Modeling: Computer Simulations and Methods for Improved Parameter Definition*. Kansas Geological Survey Bulletin, Lawrence, Kansas, USA, 233, 9-30.

Kendall, C.G.S.C., Strobel J., Cannon, R., Bezdek, J. & Biswas, G. (1991b). The simulation of the sedimentary fill of basins. *Journal of Geophysical Research*, 96, 6911-6929.

Kershaw, S., Guo, L. & Braga, J.C. (2005). A Holocene coral-algal reef at Mavra Litharia, Gulf of Corinth, Greece: structure, history, and applications in relative sea-level change. *Marine Geology*, 215, 171-192.

Klein, R. & Press, S.J. (1992). Adaptive Bayesian Classification of Spatial Data. *Journal of the American Statistical Association*, 87, 844-851.

Krumbein, W.C. (1938). Size frequency distribution of sediments and the normal phi curve. *Journal of Sedimentary Petrology*, 8, 84-90.

Krumbein, W.C. & Pettijohn, F.J. (1938). *Manual of Sedimentary Petrography*. Appleton-Century-Crofts: New York. 549pp.

Lin, W. & Bhattacharya, J.P. (2017). Estimation of source-to-sink mass balance by a fulcrum approach using channel paleohydrologic parameters of the Cretaceous Dunvegan Formation, Canada. *Journal of Sedimentary Research*, 87, 97-116.

Lu, D. & Weng, Q. (2007). A survey of image classification methods and techniques for improving classification performance. *Int. J. Remote Sens.*, 28, 823-870.

Madof, A.S., Harris, A.D. & Connell, S.D. (2016). Nearshore along-strike variability: is the concept of the systems tracts unhinged? *Geology*, 44, 319-322.

Martinius, A.W., Elflein, C. & Keogh, K.J. (2014). Applying accommodation versus sediment supply ratio concepts to stratigraphic analysis and zonation of a fluvial reservoir. In: A.W. Martinius, R. Ravnås, J.A. Howell, R.J. Steel & J.P. Wonham, (Eds.), *From Depositional Systems to Sedimentary Successions on the Norwegian Continental Margin, First Edition*. International Association of Sedimentologists, 46, 101-125.

McNeill, L.C., Shillington, D.J., Carter, G.D.O., Everest, J.D., Gawthorpe, R.L., Miller, C., Phillips, M.P., Collier, R.E.Ll., Cvetkoska, A., De Gelder, G., Diz, P., Doan, M.L., Ford, M., Geraga, M., Gillespie, J., Hemelsdaël, R., Herrero-Bervera, E., Ismaiel, M., Janikian, L., Kouli, K., Le Ber, E., Li, S., Maffione, M., Mahoney, C., Machlus, M.L., Michas, G., Nixon, C.W., Oflaz, S.A., Omale, A.P., Panagiotopoulos, K., Pechlivanidou, S., Sauer, S., Seguin, J., Sergiou, S., Zakharova, N.V. & Green, S. (2019). High-resolution record reveals climate-driven environmental and sedimentary changes in an active rift. *Scientific Reports*, 9, doi: 10.1038/s41598-019-40022-w.

Michael, N.A., Whittaker, A.C. & Allen, P.A. (2013). The functioning of sediment routing systems using a mass balance approach: example from the Eocene of the southern Pyrenees. *The Journal of Geology*, 121, 581-606.

Moretti, I., Lykousis, V., Sakellariou, D., Reynaud, J.-Y., Benziene, B. & Prinzhofer, A. (2004). Sedimentation and subsidence rate in the Gulf of Corinth: what we learn from the Marion Dufresne's long-piston coring. *Comptes Rendus Geoscience*, 336, 291-299.

Neal, J. & Abreu, V. (2009). Sequence stratigraphy hierarchy and the accommodation succession method. *Geology*, 37, 779-782.

Neal, J.E., Abreu, V., Bohacs, K.M., Feldman, H.R. & Pederson, K.H. (2016). Accommodation succession sequence stratigraphy: observational method, utility, and insights into sequence boundary formation. *Journal of the Geological Society, London*, 173, 803-816.

Nesbit, P.R., Durkin, P.R., Hugenholtz, C.H., Hubbard, S.M. & Kucharczyk, M. (2018). 3-D stratigraphic mapping using a digital outcrop model derived from UAV images and structure-from-motion photogrammetry. *Geosphere*, 14, 2469-2486.

Newhall, C. G. & Self, S. (1982). The Volcanic Explosivity Index (VEI): An Estimate of Explosive Magnitude for Historical Volcanism. *Journal of Geophysical Research*, 87, 1231-1238.

Nieminski, N.M. & Graham, S.A. (2017). Modeling stratigraphic architecture using small unmanned aerial vehicles and photogrammetry: Examples from the Miocene East Coast basin, New Zealand. *Journal of Sedimentary Research*, 87, 126-132.

Paola, C. & Martin, J. M. (2012). Mass-balance effects in depositional systems. *J. Sediment. Res.*, 82, 435-450.

Patruno, S., Hampson, G.J. & Jackson, C.A.-L. (2015). Quantitative characterisation of deltaic and subaqueous clinofolds. *Earth Science Reviews*, 142, 79-119.

Patruno, S. & Helland-Hansen, W. (2018). Clinofold systems: Review and dynamic classification scheme for shorelines, subaqueous deltas, shelf edges and continental margins. *Earth Science Reviews*, 185, 202-233.

Pechlivanidou, S., Cowie, P.A., Duclaux, G., Nixon, C.W., Gawthorpe, R.L. & Salles, T. (2019). Tipping the balance: shifts in sediment production in an active rift setting. *Geology*, 47, 259-262.

Pechlivanidou S, Cowie PA, Hannisdal B, Whittaker AC, Gawthorpe RL, Pennos C, Riiser, O.S. (2017). Source-to-sink analysis in an active extensional setting: Holocene erosion and deposition in the Sperchios rift, central Greece. *Basin Research*, 522-543.

- Perissoratis, C., Piper, D.J.W. & Lykousis, V. (2000). Alternating marine and lacustrine sedimentation during the late Quaternary in the Gulf of Corinth rift basin, central Greece. *Marine Geology*, 167, 391-411.
- Portman, C., Andrews, J.E., Rowe, P.J., Leeder, M.R. & Hoogewerff, J. (2005). Submarine-spring controlled calcification and growth of large *Rivularia* bioherms, Late Pleistocene (MIS 5e), Gulf of Corinth, Greece. *Sedimentology*, 52, 441-465.
- Posamentier, H. Jervey, M. & Vail, P. (1988). Eustatic controls on clastic deposition I conceptual framework. In: C. Wilgus, B.S. Hastings, C.G.S.C. Kendall, H.W. Posamentier, C.A. Ross & J.C. Van Wagoner (Eds.), *Sea level changes: an integrated approach*. SEPM Spec. Pub., 42, 109-124.
- Posamentier, H. & Vail, P. (1988). Eustatic controls on clastic deposition II- sequence and systems tract models. In: C. Wilgus, B.S. Hastings, C.G.S.C. Kendall, H.W. Posamentier, C.A. Ross & J.C. Van Wagoner (Eds.), *Sea level changes: an integrated approach*. SEPM Spec. Pub., 42, 125-154.
- Richter, C.F. (1935). An instrumental earthquake magnitude scale. *Bulletin of the Seismological Society of America*, 25, 1-32.
- Ravnås, R. & Steel, R.J. (1998). Architecture of Marine Rift-Basin Successions. *AAPG Bulletin*, 82, 110-146.
- Ritchie, B.D., Hardy, S. & Gawthorpe, R.L. (1999). Three dimensional numerical modeling of coarse-grained clastic deposition in sedimentary basins. *Journal of Geophysical Research*, 104, 17759-17780.
- Schlager, W. (1993). Accommodation and supply - A dual control on stratigraphic sequences. *Sedimentary Geology*, 86, 111-136.
- Sloss, L.L. (1962). Stratigraphic models in exploration. *AAPG Bulletin*, 46, 1050-1057.
- Stow, D.A.V., Hernández-Molina, E.J., Llave, E., Sayago-Gil, M., Díaz del Río, V. & Branson, A. (2009). Bedform-velocity matrix: the estimation of bottom current velocity from bedform observations. *Geology*, 37, 327-330.
- Strobel J., Cannon R., Kendall C.G.S.C., Biswas G. & Bezdek, J. (1989). Interactive (SEDPACK) simulation of clastic and carbonate sediments in shelf to basin settings. *Computers & Geosciences*, 15, 1279-1290.
- Swift, D.J.P. & Thorne, J. A. (1992). Sedimentation on continental margins, I: a general model for shelf sedimentation. In: D.J.P. Swift, G.F. Oertel, R.W. Tillman & J.A. Thorne (Eds.), *Shelf Sand and Sandstone Bodies: Geometry, Facies and Sequence Stratigraphy*. Special Publications of International Association of Sedimentologists, 14, Blackwell Publishing Ltd., Oxford, UK, 3-31.
- Taylor, A.M. & Goldring, R. (1993). Description and analysis of bioturbation and ichnofabric. *Journal of the Geological Society*, 150, 141-148.
- Thorne, J. A. & Swift, D.J.P. (1992). Sedimentation on continental margins, II: application of the regime concept. In: D.J.P. Swift, G.F. Oertel, R.W. Tillman & J.A. Thorne (Eds.), *Shelf Sand and Sandstone Bodies: Geometry, Facies and Sequence Stratigraphy*. Special Publications of International Association of Sedimentologists, 14, Blackwell Publishing Ltd., Oxford, UK, 33-58.
- Tipper, J.C. (2015). The importance of doing nothing: stasis in sedimentation systems and its stratigraphic effect. In: D.G. Smith, R.J. Bailey, P.M. Burgess & Fraser, A.J. (Eds.), *Strata and Time: Probing the Gaps in Our Understanding*. Geological Society, London, Special Publications, 404, 105-122.
- Udden, J.A. (1914). Mechanical composition of clastic sediments. *Bulletin of the Geological Society of America*, 25, 655-744.
- Vail, P., Mitchum, R.M. & Thompson, S. (1977). Seismic stratigraphy and global changes in sea level, In: C. Payton (Ed.), *Seismic stratigraphy: applications to hydrocarbon exploration*. AAPG Memoir, 26, 49-212.

- Watkins, S.E., Whittaker, A.C. Bell, R.E., McNeill, L.C., Gawthorpe, R.L., Brooke, S.A.S. & Nixon, C.W. (2018). Are landscapes buffered to high-frequency climate change? A comparison of sediment fluxes and depositional volumes in the Corinth Rift, central Greece, over the past 130 k.y. *GSA Bulletin*, 131, 372-388.
- Wentworth, C.K. (1922). A scale of grade and class terms for clastic sediments. *Journal of Geology*, 30, 377-392.
- Westaway, R. (1997). Quaternary elevation change of the Gulf of Corinth in central Greece. *Philosophical Transactions of the Royal Society of London. Series A: Mathematical, Physical and Engineering Sciences*, 354, 1125-1164.
- Wheeler, H.E. (1958). Time stratigraphy. *AAPG Bulletin*, 42, 1208-1218.
- Wheeler, H.E. (1959). Stratigraphic units in time and space. *American Journal Science*, 257, 692-706.
- Wheeler, H.E. (1964a). Base level, lithosphere surface and time stratigraphy. *Geological Society America Bulletin*, 75, 599-610.
- Wheeler, H.E. (1964b). Base level transit cycle. In: D.F. Merriam (Ed.), *Symposium on cyclic sedimentation*. Kansas Geological Survey, 169, 623-629.
- Van den Berg, J.H. & Van Gelder, A. (1993). A new bedform stability diagram, with emphasis on the transition of ripples to plane bed in flows over fine sand and silt. *Spec. Pubs. Int. Assc. Sediment.*, 17, 11-21.
- Van Wagoner, J.C., Mitchum, R.M.Jr., Campion, K.M. & Rahmanian, V.D. (1990). Siliciclastic sequence stratigraphy in well logs, core and outcrops: concepts for high-resolution correlation of time and facies. *AAPG Methods in Exploration Series*, 7, 55.

Chapter 8

Conclusion & Future Work

This chapter presents the conclusions of the thesis, by documenting the main findings in each data chapter (Chapter 3-6) and draws upon the Discussion (Chapter 7) to provide an overarching response to the research questions posed in Chapter 1. A summary of suggestions for future work are also presented.

8.1. Conclusions

This work presents novel, quantitative and 3D approaches to rift basin analysis. Integrated field, numerical, and subsurface methodologies have been used to reduce uncertainty, and improve interpretations and predictions, of shallow marine, syn-rift stratigraphy around normal fault blocks. Four original approaches are presented, including: 1) a new 3D sequence stratigraphic numerical model ‘Syn-Strat’; 2) extraction of quantitative data from 3D outcrop models of multiple, along-strike distributed depositional systems; 3) a unit thickness extrapolation for dissociating fault-related subsidence from base level change; and 4) subsurface volume balancing to pinpoint through-going sediment input points to a basin. Ultimately, a new concept (the accommodation balance; $\delta AI/\delta AR$) is proposed as a framework for the interpretation of stacking and key surfaces for analysis in all sedimentary basin-fills.

Sensitivity tests with Syn-Strat (Chapter 3) were used to assess the impact of along-strike, down-dip and temporal (3D) variation of allogenic controls on the nature of stacking and formation of stratal surfaces. Varying the relative magnitude of subsidence to eustasy and different subsidence and sedimentation regimes through time provided the first quantitative insight into stacking variability and how the diachroneity of key stratigraphic surfaces changes around a fault block. Diachroneity of stratigraphic surfaces has been discussed previously, but this is the first study to show how that diachroneity varies along hangingwall basins and to quantify the variation. Along-strike diachroneity varies according to different positions on a relative base level curve (Chapter 7), with the highest and lowest points of the curve (zero gradient) presenting most along-strike diachroneity, and the inflection points (traditionally positions of the sequence boundary and maximum flooding surface; maximum gradients) presenting the least diachroneity.

The first detailed comparison of stratigraphic architectures between along-strike distributed systems in the hangingwall of a single normal fault was undertaken using the Selinous and Kerinitis fan deltas, Gulf of Corinth, Greece (Chapter 4). Quantitative field data, Syn-Strat, and a unit thickness extrapolation approach constrained the first estimate of lake level change in Lake

Corinth for the Early-Middle Pleistocene (10-15 m), which could aid regional palaeoclimate studies and inform broader climate-system models. Two complementary methods were demonstrated to identify and quantify faulting and base level signals in the stratigraphic record, which could be applied to other rift basin fills.

Analysis of the interfan area between the fan deltas (Chapter 5) revealed five evolutionary phases, linked to net subsidence followed by net uplift regimes, as a result of a basinward shift in the locus of fault activity. Using modern fan delta planform geometries, interfan areas were classified into three types according to fan delta separation relative to the radius of their topsets and foresets. Interfans are shown to provide a condensed, and potentially more complete, stratigraphic record than axial areas of fan deltas, and could be exploited as important complementary stratigraphic archives.

A quantitatively-informed interpretation of the Thebe sub-basin (northern Carnarvon Basin, NW Shelf, Australia; Chapter 6) revealed four phases of stratigraphic development linked to the evolution of the main border fault and a number of parallel, antithetic faults. Complex architectural interactions between footwall-, hangingwall- and axially-derived depositional systems were recorded, which should be incorporated into existing models for tectono-sedimentary analysis. Through-going sediment input points from beyond the border fault crest were identified and distinguished from border fault scarp degradation supply using a novel volume balancing approach, which can independently locate catchments in the absence of landscape preservation or adequate subsurface imaging.

Overall, this work presents a number of improvements to tectono-sedimentary models, through: 1) precise constraint of the diachroneity of key surfaces, 2) understanding the relative contribution and interactions of multiple sedimentary systems within a basin, 3) consideration of along-strike depositional system asymmetry and sediment routing, and 4) a 3D approach. It is shown that the along-strike variability that makes rift basin predictions challenging can be utilised to deconvolve and quantify control signals. This multi-system approach, with the use of geological rules and regional knowledge, can be used to invert the stratigraphic record, rendering the 'non-unique

solutions' theory arguable only in cases with one-dimensional data and limited regional knowledge. Quantitative data, classification, techniques and modelling can be used to improve stratigraphic models and allow the closest approach to predictive capability in rift basins. Several flaws in the $\delta A/\delta S$ ratio have come to light through this work and the accommodation balance ($\delta AI/\delta AR$) is presented as an alternative framework (Chapter 7). It is an unbiased concept, inclusive of all control parameters and possible recorded outcomes. This new approach is a better communicator of the allocation of time across surfaces and strata in the depositional record and is applicable to any tectonically-active basin.

8.2. Future work

The findings of this work present a number of opportunities for future work. Future development and research with Syn-Strat could include:

- Extension of the application of Syn-Strat in rift basins to model footwall architectures.
- The interaction of fault segments through time could be incorporated into Syn-Strat.
- Syn-Strat could be used to assess spatial variability in stacking and diachroneity of surfaces in other tectonically-active or salt-influenced basins.
- Application of the propagating fault tip growth model to Syn-Strat to compare stratigraphic architectures from the constant length model that is utilised currently. Sensitivity analysis with Syn-Strat could then be applied to determine which growth model is applicable in a given rift basin.
- Process-based modelling across numerous scales and disciplines could be undertaken using Syn-Strat as the framework for allogenic forcing.

Other research potential includes:

- Assessment of the relative timing of fault activity across the northern Carnarvon Basin, NW Shelf in order to better constrain sediment routing from source to sink.
- Analysis of interfan stratigraphy between adjacent obliquely-prograding fan deltas
- Establish insights from interfan stratigraphy in other basin types

- Assessment of a field analogue of multiple, interacting depositional systems with different origins to yield further insights into process and architectural interactions that are below subsurface imaging resolution in the Thebe sub-basin.
- Analysis of the deep water expression of accommodation and sedimentation changes through tectonic and climate variability across various temporal and spatial scales in the Gulf of Corinth.
- Application of the accommodation balance ($\delta AI/\delta AR$) to real scenarios to test its full applicability in rift basin-fill interpretations and predictions.

Appendices

Appendix I – Table of input variables for Syn-Strat

Appendix II – Table of instructions for Syn-Strat

Appendix III – Syn-Strat script

Appendix IV – Chapter 3 paper in Marine and Petroleum Geology

Appendix V – Chapter 4 paper in Basin Research

Appendix I – Input table for Syn-Strat. num = the reference value in the Syn-Strat script.

Input parameters should be modified with this table in conjunction with Table of instructions in Appendix II. This table should be saved as input_variables.xlsx or modified in the script with a new name. Highlighted rows are the scales of the allogenic controls.

Input Variable	Value	Options	num
Colouring mode	5	(-2 - 5)	1
Sequence stratigraphic scheme	5	(5 - 9)	2
Subsidence curve standard deviation (shape)	1	(0-1)	3
Subsidence curve scale (max. subsidence)	1	Any	4
Subsidence curve kurtosis	1	1	5
Subsidence curve shape over time	1	(1-7)	6
Sediment supply shape over length of fault	3	(1-6)	7
Sediment supply scale (max. sediment supply)	1	Any	8
Sediment supply curve standard deviation (shape)	1	(0-1)	9
Sediment supply curve kurtosis	1	1	10
Sediment supply shape over time	1	(1-5)	11
Sea level scale (amplitude)	0.05	Any	12
Sea level frequency	5	Any	13
Distance away curve (structure contour) mean position	0		14
Distance away curve (structure contour) standard deviation (shape)	1	(0-1)	15
Distance away curve (structure contour) scale (max. distance)	1	Any	16
Distance away curve (structure contour) kurtosis	1	1	17
Subsidence decay curve	2	(1-3)	18
Selected position away from fault (Y1)	0	Any	19
Sediment supply decay curve	1	(1-3)	20
Selected time (T1)	0.99	(0-1)	21
Selected position along fault (X1)	0	Any	22
Chosen model	1	(1-3)	23
Sediment supply from footwall (no (0) or yes (1) or yes with point sources (2))	2	0-2	24
Footwall supply (% of supply)	0	0-1	25
Sea level dependent sediment supply	0	0-1	26
Footwall uplift	0	Any pos.	27
Sediment supply from footwall shape over X (F_sed_shape)	7	(1-7)	28
Selected value of Y for surf plots	1	1-101	29
Selected value of X for surf plots	51	1-101	30
Selected value of T for surf plots	30	1-101	31
Eustatic sea level rate defined: no (0), yes(1)	0	0 or 1	32
Eustatic sea level rate (gradient)	0.5	Any	33
Sedimentation limit	2	1-3	34
Stacking plotting type	4	(1-4)	35

Appendix II – Table of instructions for Syn-Strat. Numbers refer to parameter options. num = the reference value in the Syn-Strat script.

num	Variable	Description	Options
1	Colouring mode	2nd derivative of accommodation space in time	-2
		1st derivative of accommodation space in time	-1
		accommodation space	0
		rising and falling limbs	1
		local maxima and minima with rising and falling limbs	2
		systems tracts	3
		stacking patterns (3 colours)	4
		stacking patterns (5 colours)	5
2	Sequence Stratigraphic Scheme (Catuneanu et al. (2011))	Genetic sequence: Frazier (1974); Galloway (1989)	5
		T-R sequence: Johnson & Murphy (1984); Embry & Johannessen (1992)	6
		Depositional sequence II: Haq et al. (1987); Posamentier et al.(1988)	7
		Depositional sequence III: Van Wagoner et al. (1988;1990); Christie & Blick (1991)	8
		Depositional sequence IV: Hunt & Tucker (1992;1995); Christie & Blick(1991)	9
3	Subsidence curve along fault standard deviation (shape)	Inverse parabola	1
		Spike' normal distribution	0
4	Subsidence curve along fault scale (max. subsidence)	Any value	NA
5	Subsidence curve along fault kurtosis	Leave as 1 = rounded; 0 = square	1

6	Subsidence curve shape over time	Linear increase	1
		Linear decrease	2
		Exponential increase	3
		Exponential decrease	4
		Constant	5
		Increasing and then decreasing rate	6
		Episodic subsidence	7
		Cumulative distribution function	8
7	Sediment supply shape over length of fault	Linear increase (sediment input from the right fault tip)	1
		Linear decrease (sediment input from the left fault tip)	2
		Exponential increase (sediment input from the right fault tip)	3
		Exponential decrease (sediment input from the left fault tip)	4
		Parabola (sediment input from both fault tips)	5
		Normal distribution (sediment input from the centre of the fault) with channels along footwall	6
		Constant	7
8	Sediment supply scale (max. sediment supply)	Any value	NA
9	Sediment supply curve along fault standard deviation (shape)	Inverse parabola	1
		Spike' normal distribution	0
10	Sediment supply along fault curve kurtosis	Leave as 1 = rounded; 0 = square	1

11	Sediment supply shape over time	Linear increase	1
		Linear decrease	2
		Exponential increase	3
		Exponential decrease	4
		Constant	5
		Episodic sediment supply - not related to sea level	6
12	Sea level scale (amplitude)	Any value	0.1
13	Sea level frequency	Any value	4
14	Subsidence distance away curve (structure contour) mean position	0 infers the mean to be in the centre of the fault	0
15	Subsidence distance away curve (structure contour) standard deviation (shape)	Inverse parabola	1
		'Spike' normal distribution	0
16	Subsidence distance away curve (structure contour) scale (max. distance)	Any value	1
17	Subsidence distance away curve (structure contour) kurtosis	Leave as 1 = rounded; 0 = square	1
18	Subsidence decay curve	Linear interpolation	1
		Parabolic interpolation	2
		Exponential interpolation	3

19	Selected position away from fault (Y1)	Any value for distance away from fault	NA
20	Sediment supply decay curve away from fault	Linear interpolation	1
		Parabolic interpolation	2
		Exponential interpolation	3
21	Selected time (T1)	Any value of time	NA
22	Selected position along fault (X1)	Any value for distance along fault	NA
23	Chosen model	Model 1 - accommodation for distance along the fault in time for a given distance away	1
		Model 2 - accommodation for distance away from the fault in time for any given distance along the fault	2
		Model 3 - accommodation in space for any given time	3
24	Sediment supply from footwall	No supply from footwall	0
		Supply from footwall	1
		Supply from footwall from point sources	2
25	Footwall supply (% of supply)	Any value between 0 and 1 as a percentage of supply from fault tips (e.g. 25% of supply from fault tips also comes from the footwall centre)	NA
26	Sea level dependent sediment supply	0 = no; 1 = yes	0-1
27	Footwall uplift	Any value from 0 to 1 - this is subtracted from hangingwall subsidence to give total displacement	Any pos.
28	Footwall sed supply over X	Same options as num(7) with one extra (7 - inverse parabola)	(1-7)

29	Selected value of Y for surf plots	Any value between 1 and 101	
30	Selected value of X for surf plots	Any value between 1 and 101	
31	Selected value of T for surf plots	Any value between 1 and 101	
32	Eustatic sea level rate defined	Eustatic sea level rate defined: no (0), yes(1)	0-1
33	Eustatic sea level rate	Gradient (any)	Any
34	Sedimentation limit in y	Parabola along fault - min at centre of fault, max at fault tips	1
		Constant along x	2
		Dependent on X_sed	3
35	Stacking type	Plot 3 colours based on sedscurve and space	1
		Plot 5 colours based on A (-1 to 1)	2
		Plot 5 colours base on angle of A curve new way - works for real examples	3
		Accommodation balance matrix	4

Appendix III – Syn-Strat script

```
%3D ACCOMMODATION PLOT
%Step 1 - Create grid (matrix of X,Y,T)to fill by setting resolution
and
%vectors for time (T), distance along fault segment (X) and distance
away from (Y)
%Step 2 - Define input parameters
  %Step 2.1 - Define base level curve (sine wave) that varies in time
  %Step 2.2 - Define subsidence curves
    %Step 2.2.1 - Subsidence along fault
    %Step 2.2.2 - Subsidence in time
    %Step 2.2.3 - Subsidence away from fault
  %Step 2.3 - Define sedimentation curves
    %Step 2.3.1 - Sedimentation along fault
    %Step 2.3.2 - Sedimentation in time
    %Step 2.3.3 - Sedimentation away from fault
%Step 3 - Calculate Accommodation in 3D
%Step 4 - Define colour overlay and plot - e.g. systems tracts or
stacking patterns

%-----START-----%
clear all
close all
clc

[num,txt] = xlsread('input_variables.xlsx',1,'B2:B36'); %reads excel
sheet of input variables

%-----STEP 1 -----%
%Create grid for distance along fault (x), distance away (y) and
time(t)

I = 101; %resolution of X
J = 101; %resolution of Y
K = 101; %resolution of T
xs = -1; % fault start position - vary to change ratio of length of
fault/subsidence
xe = 1; % fault end position - vary to change ratio of length of
fault/subsidence
ye = 1; % distance away end position (position of zero subsidence-
hingeline)
te = 1; % end time
x = linspace(-1,1,I); %distance along fault
y = linspace(0,ye,J); %distance away from fault
t = linspace(0,te,K); %t is time from 0 to 1 with resolution of K
[X,Y,T]=meshgrid(x,y,t); %matrix of X, Y and T

T1 = num(21);
X1 = num(22);
Y11 = num(29); % for surf plots - requires value number not distance
e.g. 51 instead of 0.5
X11 = num(30); % for surf plots - requires value number not distance
e.g. 51 instead of 0.5
T11 = num(31); % for surf plots - requires value number not distance
e.g. 51 instead of 0.5
```

```

%-----STEP 2 -----%
%Define input parameters

%-----STEP 2.1 - Define base level curve in time-----%

sc_sl = num(12); %scale of sea level (amplitude) - read from file
f_sl = 2*pi.*(num(13)); %frequency of sea level curve
sl_rate_defined = num(32); %yes (1) or no (0) depending on data;

if sl_rate_defined == 1 %defined gradient
    scf_sl = num(33);
elseif sl_rate_defined == 0 %not defined gradient
    scf_sl = sc_sl.*f_sl; %scale of gradient
end

slcurve = scf_sl./f_sl*sin(T.*f_sl); %sine wave that varies in time
(T)- does not vary in X or Y

%-----STEP 2.2 - Define subsidence-----%

% STEP 2.2.1 - Subsidence along length of fault
% Parabolic shape along fault so we use a distribution curve

mu_sub = (xs+xe)/2; %mean position of distribution (centre)
sg_sub = num(3); %standard deviation (shape of curve) (0-1) (1 is
inverse parabola)

hw_subsidence = num(4); %max subsidence of hangingwall
fw_uplift = num(27); %max uplift of footwall
sc_sub = hw_subsidence-fw_uplift; %total displacement and therefore
accommodation generation

m_sub = num(5); %kurtosis (squareness) (leave as 1 - rounded)

dist_sub = exp(-0.5*((X-mu_sub)/sg_sub).^2*m_sub); % normal
distribution curve
cenp_sub = exp(-0.5*((mu_sub-mu_sub)/sg_sub).^2*m_sub); % centre
point
endp_sub = exp(-0.5*((xe-mu_sub)/sg_sub).^2*m_sub); % end point = 0
X_sub = (dist_sub - endp_sub)/(cenp_sub-endp_sub); % X curve
(subsidence curve over length of fault)
SX = X_sub; %subsidence curve over length of fault

% STEP 2.2.2 - Subsidence shape over time
% Options:
% Linear increase = 1
% Linear decrease = 2
% Exponential increase = 3
% Exponential decrease = 4
% Constant = 5
% Exponential increase then decrease = 6
% Cumulative distribution curve = 7

sub_time_shape = num(6); %subsidence shape over time

if sub_time_shape == 1
    T_sub = T;
elseif sub_time_shape == 2
    T_sub = -T+1;

```

```

elseif sub_time_shape == 3
    T_sub = T.^2;
elseif sub_time_shape == 4
    T_sub = (-T+1).^2;
elseif sub_time_shape == 5
    T_sub = ones(J,I,K);
elseif sub_time_shape == 6
    T_sub = (tanh((T-0.5)*2*pi)-(tanh((0-0.5)*2*pi)))/((tanh((1-
0.5)*2*pi)-(tanh((0-0.5)*2*pi)));
elseif sub_time_shape == 7
    T_sub = T + 0.02.*(sin(T*2*pi*8));
elseif sub_time_shape == 8
    sp = 0; % subsidence start point
    mp = 0.5; % subsidence inflexion point
    ep = 1; % subsidence end point

    if sp>mp && mp>ep
        disp('points out of order');
        stop
    end
    if sp<0 || sp>1 || mp<0 || mp>1 || ep<0 || ep>1
        disp('points less than 0 or greater than 1');
        stop
    end
    %standard deviation - defines shape
    mu1= 1; % ~ rising rate
    mu2= 1; % ~ falling rate - smaller is straighter

    % calculate a normal distribution of some form
    t_dst = zeros(1,K);
    vec = find(t>sp & t<=mp);
    t_dst(vec) = 1;%
    vec = find(t>mp & t<=ep);
    t_dst(vec) = (exp(-0.5*((t(vec)-mp)/mu2).^2)-exp(-0.5*((ep-
mp)/mu2).^2))/(1-exp(-0.5*((ep-mp)/mu2).^2));

    % integrate normal distribution of some form
    t_idst = zeros(1,K);
    for k=2:K
        t_idst(k) = trapz(t(1:k),t_dst(1:k));
    end

    t_idst = t_idst/t_idst(end);

    % produce 3D matrix
    T_sub = ones(J,I,K);
    for k=1:K
        T_sub(:, :, k) = t_idst(k);
    end
end
end

% STEP 2.2.3 - Subsidence with distance away curve
% Use a distribution curve

Y1 = num(19); % position away (between 0 (at fault) and 1)
mu_dist_away = num(14); %mean position of distribution (centre)
sg_dist_away = num(15); %standard deviation (shape of curve) (0-1) (1
is inverse parabola)
sc_dist_away = num(16); %scale (max. subsidence) (any number)

```

```

m_dist_away = num(17); %kurtosis (squareness) (leave as 1)

dist_dist_away = exp(-0.5*((X-
mu_dist_away)/sg_dist_away).^(2*m_dist_away)); %normal distribution
curve
cenp_dist_away = exp(-0.5*((mu_dist_away-
mu_dist_away)/sg_dist_away).^(2*m_dist_away)); %centre point
endp_dist_away = exp(-0.5*((xe-
mu_dist_away)/sg_dist_away).^(2*m_dist_away)); %end point = 0
XC_dist_away = sc_dist_away*(dist_dist_away -
endp_dist_away)/(cenp_dist_away-endp_dist_away); %X curve (subsidence
curve over length of fault)
ZCL = XC_dist_away; %zero contour line

subs_decay_curve = num(18); %choice of linear, parabolic or
exponential decay curve away from fault
if subs_decay_curve == 1 %for linear interpolation
    subs_decay_s = 1-Y./(ZCL);
    subs_decay_l = 1-Y1./(ZCL);
elseif subs_decay_curve == 2 %for parabolic interpolation
    subs_decay_s = 1-(2*Y-Y.^2)./(2*ZCL-ZCL.^2);
    subs_decay_l = 1-(2*Y1-Y1.^2)./(2*ZCL-ZCL.^2);
elseif subs_decay_curve == 3 %for exponential interpolation
    sg = 0.5; %standard deviation - low is steep curve, high is nearly
linear
    subs_decay_s = 1-(exp(-0.5*(Y/sg))-1)./(exp(-0.5*(ZCL/sg))-1) ;
    subs_decay_l = 1-(exp(-0.5*(Y1/sg))-1)./(exp(-0.5*(ZCL/sg))-1) ;
end
subs_decay_s = max(subs_decay_s,0);
subs_decay_l = max(subs_decay_l,0);
subs_sf_s = SX.*subs_decay_s; %interpolated surface
subs_sf_l = SX.*subs_decay_l; %interpolated line
Y_sub = subs_decay_s;

%-----STEP 2.3 - Define sedimentation-----%

% STEP 2.3.1 - Sedimentation along length of fault

% Options:
% Linear increase (sediment input from the right fault tip) = 1
% Linear decrease (sediment input from the left fault tip) = 2
% Exponential increase (sediment input from the right fault tip) = 3
% Exponential decrease (sediment input from the left fault tip) = 4
% Parabola (sediment input from both fault tips) = 5
% Normal distribution (sediment input from the centre of the fault)= 6

sed_shape = num(7); %sediment supply shape over length of fault (1-6)
sc_sed = num(8); %sediment supply scale (max sediment supply) (any
number)

if sed_shape == 1 % linear increase
    XP_sed = (X-xs)./(xe-xs); %'-xs' so that 0 sed. supply is at '-1'
distance along fault
elseif sed_shape == 2 % linear decrease
    XP_sed = (-X+xe)./(-xs+xe); %'+xe' so that 0 sed. supply is at '1'
distance along fault
elseif sed_shape == 3 % parabolic increase
    XP_sed = ((X-xs)./(xe-xs)).^2;
elseif sed_shape == 4 % parabolic decrease

```

```

    XP_sed = ((-X+xe)./(-xs+xe)).^2;
elseif sed_shape == 5 % parabola
    XP_sed = (X.^2);
elseif sed_shape == 6 % normal distribution
    mu_sed = (xs+xe)/2; % mean position of distribution (centre)
    sg_sed = num(9); % sediment supply standard deviation (shape) (0-
1)
    m_sed = num(10); %sediment supply kurtosis (squareness) (leave as
1 - rounded)
    dist_sed = exp(-0.5*((X-mu_sed)/sg_sed).^(2*m_sed)); % normal
distribution
    cenp_sed = exp(-0.5*((mu_sed-mu_sed)/sg_sed).^(2*m_sed)); % centre
point
    endp_sed = exp(-0.5*((xe-mu_sed)/sg_sed).^(2*m_sed)); % end point
= 0
    XP_sed = ((dist_sed - endp_sed)/(cenp_sed-endp_sed)); % X curve
(sediment supply curve over length of fault)
elseif sed_shape == 7
    XP_sed = ones(J,I,K);
end

%For point sources of sediment supply from the footwall
ML = [-1,-0.5,0,0.5,1]; % source location
SL = [0.5,0.5,0.5,0.5,0.5]; % source spread rate (std deviation)
RL = [0.3,0.3,0.3,0.3,0.3]; % range of source
MG = [1, 1, 1, 1, 1]; % magnitude of the source - proportion of max
for scaling
HW = zeros(J,I,K,5);
for n=1:5 %n is number of peaks - change this and also change in line
303-307
    mg = MG(n);
    m1 = ML(n);
    s1 = SL(n);
    r1 = RL(n);
    v = find(x>=m1-r1/2 & x<=m1+r1/2);
    HWE = (exp(-0.5*((r1/2)/s1).^2));
    HWM = (exp(-0.5*((0)/s1).^2));
    HW0(:,v,:,n) = (exp(-0.5*((X(:,v,:)-m1)/s1).^2)); %normal
distribution curve
    HW0(:,v,:,n) = mg*(HW0(:,v,:,n)-HWE)/(HWM-HWE);
end
HW = sum(HW0,4); %weighted source distribution

X_sed = HW; %XP_sed+XF_sed if superimposed on another curve from
footwall or hangingwall
    %X_sed = X_sed.*T_sed; %this gives sediment supply in time and
space along the fault(3D)
end

% STEP 2.3.2 - Sedimentation over time

% Options:
% Linear increase           = 1
% Linear decrease          = 2
% Exponential increase     = 3
% Exponential decrease     = 4
% Constant                 = 5
% Episodic (unrelated to s1) = 6

sed_time_shape = num(11); %sediment supply shape over time (1-6)

```



```

sl_depend_sed = num (26); %sea level dependent sediment supply (yes or
no)
if sed_time_shape == 1 & sl_depend_sed == 0
    T_sed = T;
elseif sed_time_shape == 1 & sl_depend_sed == 1 %for sediment supply
that varies in time with sea level (high sea level = low sed supply)
    T_sed = T + slcurve;
elseif sed_time_shape == 2
    T_sed = -T+1;
elseif sed_time_shape == 3
    T_sed = T.^2;
elseif sed_time_shape == 4
    T_sed = (-T+1).^2;
elseif sed_time_shape == 5
    T_sed = 1; %constant
elseif sed_time_shape == 6
    T_sed = T + 0.01.*(sin(T*-2*pi*8));
end

%STEP 2.3.3 - Sedimentation away from fault

seds_decay_curve = num(20); %decay curve
sedimentation_limit = num(34); %sedimentation limit model along fault

if sedimentation_limit == 1
y1i = 0.8; %position along y of centre point of parabola or limit of
sed
y1 = y1i + 0.5*x.^2; %parabola - model 1 in notes
YL = repmat(y1,J,1,K); %defining a new 3D matrix
elseif sedimentation_limit == 2
y1i = 0.8;
y1 = y1i*ones(1,I); %constant along fault length - model 2 in notes
YL = repmat(y1,J,1,K); %defining a new 3D matrix
elseif sedimentation_limit == 3
    %y1i here is max sed??
YL = X_sed.*T_sed./(max(max(max(X_sed.*T_sed)))); %varying with X_sed
- modified by time, divided by maximum sedimentation value
end

if seds_decay_curve == 1 %for linear interpolation to YL
    seds_decay_s = max(1-Y./YL,0);
elseif seds_decay_curve == 2 %for parabolic interpolation to YL
    seds_decay_s = max(1-(2*Y-Y.^2)./(2*YL-YL.^2),0);
    %elseif seds_decay_curve == 3 %for exponential interpolation
end

seds_decay_s = max(seds_decay_s,0);
Y_sed = seds_decay_s;

%-----STEP 3 - Calculate Accommodation-----%

TS = sc_sub.*(X_sub.*Y_sub.*T_sub); %3D subsidence curve
S = sc_sed.*(X_sed.*Y_sed.*T_sed); %3D sedimentation curve
A = slcurve + TS - S; %Accommodation - works for all models

model = num(23); %configuration of plot (1,2,or 3)

sedscurve = sc_sed.*(X_sed.*Y_sed.*T_sed);
space = slcurve + sc_sub.*(X_sub.*Y_sub.*T_sub);

```

```

%-----STEP 4 - Colour overlays and plotting-----%

% Choice of overlays (or colouring mode (CM))
% 2nd derivative of accommodation space: -2
% 1st derivative of accommodation space: -1
% Accommodation space: 0
% Rising and falling limbs: 1
% Local maxima and minima with rising and falling limbs: 2
% Systems tracts (uses C matrix): 3
% Stacking patterns (3 colours)(uses D matrix): 4
% Stacking patterns (5 colours)(uses D matrix): 5

CM = num(1); %colouring mode

% Calculate derivatives of the data

for i=1:I
    for j=1:J
        clc
        disp(['% complete: ',num2str(((i-1)*J+j)/2/I/J*100)])
        gy1(:,i,j) = gradient(permute(A(:,i,j),[1,2,3]),y);
%1st derivative - gradient in y-direction
        gy2(:,i,j) = gradient(permute(gy1(:,i,j),[1,2,3]),y);
%2nd derivative - gradient in y-direction

        gx1(i,:,j) = gradient(permute(A(i,:,j),[2,1,3]),x);
%1st derivative - gradient in x-direction
        gx2(i,:,j) = gradient(permute(gx1(i,:,j),[2,1,3]),x);
%2nd derivative - gradient in x-direction

        gt1(i,j,:) = gradient(permute(A(i,j,:),[3,1,2]),t);
%1st derivative - gradient in t-direction
        gt2(i,j,:) = gradient(permute(gt1(i,j,:),[3,1,2]),t);
%2nd derivative - gradient in t-direction

        SLG(i,j,:) = gradient(permute(slcurve(i,j,:),[3,1,2]),t);
%1st derivative - gradient in t-direction
        TSG(i,j,:) = gradient(permute(TS(i,j,:),[3,1,2]),t);
%1st derivative - gradient in t-direction
        SG(i,j,:) = gradient(permute(S(i,j,:),[3,1,2]),t);
%1st derivative - gradient in t-direction
    end
end

C = ones(J,I,K)*NaN;%matrix of ones for systems tracts overlay case 3
C1 = ones(J,I,K)*NaN;%matrix of ones for plotting of surfaces case 3
D = ones(J,I,K)*NaN; %matrix of ones for stacking patterns overlay

```

```

%%%%%%%%%%%%%%%%%%%%%%%%%%%%%%%%%%%%%%%%%%%%%%%%%%%%%%%%%%%%%%%%%%%%%%%%
% Case Specific Colour Schemes
% general
% stationary max          0
% stationary min         -1
% stationary rising      -2
% stationary falling     -3

% case 1 rising and falling limbs
% rising                  1
% falling                 2

% case 2 curve split into 4 segments
% maximum rising         1
% maximum falling        2
% minimum falling        3
% minimum rising         4

%case 3 curve split into 8 segments
% convex (max) rising: below mean    1
% convex (max) rising: above mean    2
% convex (max) falling: below mean   3
% convex (max) falling: above mean   4
% concave (min) falling: below mean  5
% concave (min) falling: above mean  6
% concave (min) rising: below mean   7
% concave (min) rising: above mean   8

%%%%%%%%%%%%%%%%%%%%%%%%%%%%%%%%%%%%%%%%%%%%%%%%%%%%%%%%%%%%%%%%%%%%%%%%

%ch = colorbar;
if CM == 3
%Sequence Stratigraphic Scheme (Catuneanu et al. (2011)

%Genetic sequence (Frazier (1974); Galloway (1989))           : 5
%T-R sequence (Johnson & Murphy (1984); Embry & Johannessen (1992) : 6
%Depositional sequence II (Haq et al. (1987); Posamentier et al.(1988)
                                                                : 7
%Depositional sequence III (Van Wagoner et al. (1988;1990); Christie &
Blick (1991))                                                    : 8
%Depositional sequence IV (Hunt & Tucker (1992;1995); Christie &
Blick(1991))                                                       : 9

scheme = num(2); %sequence stratigraphic scheme (5-9)
end

if CM>=1 & CM<=3
    if model == 1
        C(find(gt1==0 & gt2<0)) = 0; % stationary max
        C(find(gt1==0 & gt2>0)) = 0; % stationary min
        C(find(gt1(2:end-1,:)==0 & gt1(1:end-2,:)<0 & gt1(3:end,:)>0)) =
0; % stationary rising
        C(find(gt1(2:end-1,:)==0 & gt1(1:end-2,:)>0 & gt1(3:end,:)<0)) =
0; % stationary falling
        [faces,verts,colors] = isosurface(X,T,A,Y,Y1,C);
        patch('Vertices', verts, 'Faces', faces, 'FaceVertexCData',
colors,'FaceColor','interp','edgecolor', 'interp');
        elseif model == 2
            C(find(gt1==0 & gt2<0)) = 0; % stationary max

```

```

    C(find(gt1==0 & gt2>0)) = 0; % stationary min
    C(find(gt1(2:end-1,:)==0 & gt1(1:end-2,:)<0 & gt1(3:end,:)>0)) =
0; % stationary rising
    C(find(gt1(2:end-1,:)==0 & gt1(1:end-2,:)>0 & gt1(3:end,:)<0)) =
0; % stationary falling
    [faces,verts,colors] = isosurface(Y,T,A,X,X1,C);
    patch('Vertices', verts, 'Faces', faces, 'FaceVertexCData',
colors, 'FaceColor', 'interp', 'edgecolor', 'interp');
elseif model == 3
    C(find(gy1==0 & gy2<0)) = 0; % stationary max
    C(find(gy1==0 & gy2>0)) = 0; % stationary min
    C(find(gy1(2:end-1,:)==0 & gy1(1:end-2,:)<0 & gy1(3:end,:)>0)) =
0; % stationary rising
    C(find(gy1(2:end-1,:)==0 & gy1(1:end-2,:)>0 & gy1(3:end,:)<0)) =
0; % stationary falling
    [faces,verts,colors] = isosurface(X,Y,A,T,T1,C);
    patch('Vertices', verts, 'Faces', faces, 'FaceVertexCData',
colors, 'FaceColor', 'interp', 'edgecolor', 'interp');
end
end

if CM == -2
    if model == 1
        C = gt2;
        [faces,verts,colors] = isosurface(X,T,A,Y,Y1,C);
        patch('Vertices', verts, 'Faces', faces, 'FaceVertexCData',
colors, 'FaceColor', 'interp', 'edgecolor', 'interp');
    elseif model == 2
        C = gt2;
        [faces,verts,colors] = isosurface(Y,T,A,X,X1,C);
        patch('Vertices', verts, 'Faces', faces, 'FaceVertexCData',
colors, 'FaceColor', 'interp', 'edgecolor', 'interp');
    elseif model == 3
        C = gy2;
        [faces,verts,colors] = isosurface(X,Y,A,T,T1,C);
        patch('Vertices', verts, 'Faces', faces, 'FaceVertexCData',
colors, 'FaceColor', 'interp', 'edgecolor', 'interp');
    end
end

if CM == -1
    if model == 1
        C = gt1;

surf(permute(X(Y11, :, :), [3,2,1]), permute(T(Y11, :, :), [3,2,1]), permute(A
(Y11, :, :), [3,2,1]), permute(C(Y11, :, :), [3,2,1])); %model 1
        figure
        [faces,verts,colors] = isosurface(X,T,A,Y,Y1,C);
        patch('Vertices', verts, 'Faces', faces, 'FaceVertexCData',
colors, 'FaceColor', 'interp', 'edgecolor', 'none');
    elseif model == 2
        C = gt1;

surf(permute(Y(:,X11, :), [3,1,2]), permute(T(:,X11, :), [3,1,2]), permute(A
(:,X11, :), [3,1,2]), permute(C(:,X11, :), [3,1,2])); %model 2
        figure
        [faces,verts,colors] = isosurface(Y,T,A,X,X1,C);
        patch('Vertices', verts, 'Faces', faces, 'FaceVertexCData',
colors, 'FaceColor', 'interp', 'edgecolor', 'interp');
    elseif model == 3
        C = gy1;

```

```

surf(permute(X(:,:,T11),[1,2,3]),permute(Y(:,:,T11),[1,2,3]),permute(A
(:, :,T11),[1,2,3]),permute(C(:,:,T11),[1,2,3])); %model 3
    figure
        [faces,verts,colors] = isosurface(X,Y,A,T,T1,C);
        patch('Vertices',verts,'Faces',faces,'FaceVertexCData',
colors,'FaceColor','interp','edgecolor','interp');
    end
end

if CM == 0
    C = A;
    [faces,verts,colors] = isosurface(X,Y,A,T,T1,C);
    patch('Vertices',verts,'Faces',faces,'FaceVertexCData',
colors,'FaceColor','interp','edgecolor','interp');
end

if CM == 1
    if model == 1
        C(find(gt1>=0)) = 1; % rising
        C(find(gt1<0)) = 2; % falling
        [faces,verts,colors] = isosurface(X,T,A,Y,Y1,C);
        patch('Vertices',verts,'Faces',faces,'FaceVertexCData',
colors,'FaceColor','interp','edgecolor','interp');
    elseif model == 2
        C(find(gt1>=0)) = 1; % rising
        C(find(gt1<0)) = 2; % falling
        [faces,verts,colors] = isosurface(Y,T,A,X,X1,C);
        patch('Vertices',verts,'Faces',faces,'FaceVertexCData',
colors,'FaceColor','interp','edgecolor','interp');
    elseif model == 3
        C(find(gy1>=0)) = 1; % rising
        C(find(gy1<0)) = 2; % falling
        [faces,verts,colors] = isosurface(X,Y,A,T,T1,C);
        patch('Vertices',verts,'Faces',faces,'FaceVertexCData',
colors,'FaceColor','interp','edgecolor','interp');
    end
end

if CM == 2
    if model == 1
        C(find(gt1>=0 & gt2<=0)) = 1; % convex (max) rising
        C(find(gt1<0 & gt2<=0)) = 2; % convex (max) falling
        C(find(gt1<=0 & gt2>0)) = 3; % concave (min) falling
        C(find(gt1>0 & gt2>0)) = 4; % concave (min) rising
        [faces,verts,colors] = isosurface(X,T,A,Y,Y1,C);
        patch('Vertices',verts,'Faces',faces,'FaceVertexCData',
colors,'FaceColor','interp','edgecolor','interp');
    elseif model == 2
        C(find(gt1>=0 & gt2<=0)) = 1; % convex (max) rising
        C(find(gt1<0 & gt2<=0)) = 2; % convex (max) falling
        C(find(gt1<=0 & gt2>0)) = 3; % concave (min) falling
        C(find(gt1>0 & gt2>0)) = 4; % concave (min) rising
        [faces,verts,colors] = isosurface(Y,T,A,X,X1,C);
        patch('Vertices',verts,'Faces',faces,'FaceVertexCData',
colors,'FaceColor','interp','edgecolor','interp');
    elseif model == 3
        C(find(gy1>=0 & gy2<=0)) = 1; % convex (max) rising
        C(find(gy1<0 & gy2<=0)) = 2; % convex (max) falling
        C(find(gy1<=0 & gy2>0)) = 3; % concave (min) falling
        C(find(gy1>0 & gy2>0)) = 4; % concave (min) rising
    end
end

```

```

    [faces,verts,colors] = isosurface(X,Y,A,T,T1,C);
    patch('Vertices', verts, 'Faces', faces, 'FaceVertexCData',
colors,'FaceColor','interp','edgecolor', 'interp');
    end
end

if CM == 3 & model == 1 | 2
    for i=1:I
        for j=1:J
            clc
            disp(['% complete: ',num2str(50+((i-1)*J+j)/2/I/J*100)])
            t1 = polyxpoly(t,permute(gt1(i,j,:),[3,1,2]),t,t*0);
% finding zeros (stationary points) in first derivative
            t2 = polyxpoly(t,permute(gt2(i,j,:),[3,1,2]),t,t*0);
% finding zeros of second gradient/derivative (max. gradient of the
1st derivative)
            vk = sort([t(1),t(J),t1',t2']); % this makes a vector of
t1 and t2 and start time and end time which increases (puts them in
correct order)
            for k=1:length(vk)-1; % -1 means you can't go to the end
                vt = find(t>=vk(k) & t<=vk(k+1)); % finding the points
that you want to find the average between
                MA(i,j,vt) = nanmean(A(i,j,vt)); % average
            end
        end
    end
end

C(find(gt1>0 & gt2<=0 & A-MA<=0)) = 1; % convex (max)rising: below
mean
C(find(gt1>0 & gt2<=0 & A-MA>0)) = 2; % convex(max)rising: above
mean
C(find(gt1<=0 & gt2<=0 & A-MA>0)) = 3; % convex(max)falling: below
mean
C(find(gt1<=0 & gt2<=0 & A-MA<=0)) = 4; % convex(max)falling: above
mean
C(find(gt1<=0 & gt2>0 & A-MA>0)) = 5; % concave(min)falling:
below mean
C(find(gt1<=0 & gt2>0 & A-MA<=0)) = 6; % concave(min)falling: above
mean
C(find(gt1>0 & gt2>0 & A-MA<=0)) = 7; % concave(min)rising: below
mean
C(find(gt1>0 & gt2>0 & A-MA>0)) = 8; % concave(min)rising: above
mean
end

if CM == 3
    if scheme == 5 || scheme == 7 || scheme == 8 || scheme == 9
        for i=1:8
            if i==3 || i==4 || i==5 || i==6
                cmap(i,:)=[1,0,0]; %red
            elseif i==7
                cmap(i,:)=[1,1,0]; %yellow
            elseif i==8
                cmap(i,:)=[0,1,0]; %green
            elseif i==1
                cmap(i,:)=[0,1,0]; %green
            elseif i==2
                cmap(i,:)=[0,0,1]; %blue
            end
        end
    end
end
end

```

```

if CM == 3
if scheme == 5 || scheme == 7 || scheme == 8 || scheme == 9
    for i=1:8
        if i==3 || i==4 || i==5 || i==6
            cmap(i,:)= [1,0.5,0.8]; %pink
        elseif i==7
            cmap(i,:)= [0.3,0.7,0.8]; %light blue
        elseif i==8
            cmap(i,:)= [0,1,0.5]; %turquoise
        elseif i==1
            cmap(i,:)= [0,1,0.5]; %turquoise
        elseif i==2
            cmap(i,:)= [0.2,0,0.9]; %blue
        end
    end
end

    for i=1:8
        if i==3 || i==4 || i==5 || i==6
            cmap(i,:)= [0.2081,0.1663,0.5292]; %purple
        elseif i==7
            cmap(i,:)= [0.0060,0.4086,0.8828]; %turquoise
        elseif i==8
            cmap(i,:)= [0.0641,0.5570,0.8240]; %light blue
        elseif i==1
            cmap(i,:)= [0.0641,0.5570,0.8240]; %light blue
        elseif i==2
            cmap(i,:)= [0.0590,0.6838,0.7254]; %blue
        end
    end
end
if CM == 3 & model == 3
    for i=1:I
        y1 = polyxpoly(y,gy1(:,i,j),y,y*0); % finding zeros
        (stationary points) in first derivative
        y2 = polyxpoly(y,gy2(:,i,j),y,y*0); % finding zeros of second
        gradient/derivative (max. gradient of the 1st derivative)
        vk = sort([y(1),y(J),y1',y2']); % this makes a vector of t1
        and t2 and start time and end time which increases (puts them in
        correct order)
        for k=1:length(vk)-1; % -1 means you can't go to the end
            vy = find(y>=vk(k) & y<=vk(k+1)); % finding the points
            that you want to find the average between
            MA(vy,i,j) = nanmean(A(vy,i,j)); % average
        end
    end
end
C(find(gt1>0 & gt2<=0 & A-MA<=0)) = 1; % convex(max) rising: below mean
C(find(gt1>0 & gt2<=0 & A-MA>0)) = 2; % convex(max) rising: above mean
C(find(gt1<=0 & gt2<=0 & A-MA>0)) = 3; % convex(max) falling: below
mean
C(find(gt1<=0 & gt2<=0 & A-MA<=0)) = 4; % convex(max) falling: above
mean
C(find(gt1<=0 & gt2>0 & A-MA>0)) = 5; % concave(min) falling: below
mean
C(find(gt1<=0 & gt2>0 & A-MA<=0)) = 6; % concave(min) falling: above
mean
C(find(gt1>0 & gt2>0 & A-MA<=0)) = 7; % concave(min) rising: below
mean
C(find(gt1>0 & gt2>0 & A-MA>0)) = 8; % concave(min) rising: above
mean

```

```

end
end

stacking = num(35);
if CM == 4 & model == 1 & stacking == 1
    %To overlay stacking patterns (3 colours)
    D(find (sedscurve > space)) = 1; % progradation
    D(find (sedscurve < space)) = 2; % retrogradation
    D(find (sedscurve == space)) = 3; % aggradation

    for i=1:3
        if i==1
            cmap(i,:)= [0.9763,0.9831,0.0538]; %yellow
            P(i,:) = 1;
        elseif i==2
            cmap(i,:)= [0.0060,0.4086,0.8828]; %blue
            P(i,:) = 2;
        elseif i==3
            cmap(i,:)= [0.2081,0.1663,0.5292]; %purple
            P(i,:) = 3;
        end
    end

    [faces,verts,colors] = isosurface(X,T,A,Y,Y1,D);
    patch('Vertices', verts, 'Faces', faces, 'FaceVertexCData',
    colors, 'FaceColor', 'interp', 'edgecolor', 'interp');
    colormap(cmap)
    ch = colorbar;
    set(ch, 'ytick', [1,2,3], 'yticklabel', [' Progradational
    '; 'Retrogradational'; ' Aggradational ']);
    ylabel(ch, 'Stacking pattern')
end

if CM == 5 & stacking == 2
    %To overlay stacking patterns (5 colours)
    D(find(A>0.6)) = 1;
    D(find(A>0.2 & A<=0.6)) = 2;
    D(find(A>-0.2 & A<=0.2)) = 3;
    D(find(A>-0.6 & A<=-0.2)) = 4;
    D(find(A<=-0.6)) = 5;
    [faces,verts,colors] = isosurface(X,T,A,Y,Y1,D);
    patch('Vertices', verts, 'Faces', faces, 'FaceVertexCData',
    colors, 'FaceColor', 'interp', 'edgecolor', 'interp');
    ch = colorbar;
    ylabel(ch, 'Stacking pattern')
    set(ch, 'ytick', [1,2,3,4,5], 'yticklabel', ['Strongly retrogradational'; '
    Weakly retrogradational '; ' Aggradational '; ' Weakly
    progradational '; ' Strongly progradational ']);
    caxis([1 5])
end

if CM == 5 & stacking == 3

% To overlay stacking patterns by angle of the curve (for model 1
only)
% This works well for real examples
% Highest angle (+ve or -ve) refer to strong pro. or retro.
ch=colorbar;

```



```

[faces,verts,colors] = isosurface(X,T,A,Y,Y1,atan(gt1)*180/pi);%plot
angle - model 1
patch('Vertices', verts, 'Faces', faces, 'FaceVertexCData',
colors,'FaceColor','interp','edgecolor', 'interp');
%produce colormap (cmp)
for i=1:1001 %resolution change
    angle(i) = -90+180*(i-1)/1000;
    if angle(i)<=-89 %values between -89 and -90
        ca = [0,0,147]/255;
        cb = [0,0,255]/255;
        cmp(i,:)=ca+(cb-ca)*(angle(i)--90)/1; %-90 is the start point
and 1 is the interval
    elseif angle(i)>-89 & angle(i)<=-88 %values between -89 and -88
        ca = [0,0,255]/255;
        cb = [0,255,255]/255;
        cmp(i,:)=ca+(cb-ca)*(angle(i)--89)/1; %-89 is the start point
and 1 is the interval
    elseif angle(i)>-88 & angle(i)<=0 %values between -88 and 0
        ca = [0,255,255]/255;
        cb = [255,255,0]/255;
        cmp(i,:)=ca+(cb-ca)*(angle(i)--88)/88; %-88 is the start point
and 88 is the interval
    elseif angle(i)>0 & angle(i)<=88 %values between 0 and 88
        ca = [255,255,0]/255;
        cb = [255,147,0]/255;
        cmp(i,:)=ca+(cb-ca)*(angle(i)-0)/88; %0 is the start point and
88 is the interval
    elseif angle(i)>88 & angle(i)<=89 %values between 88 and 89
        ca = [255,147,0]/255;
        cb = [255,0,0]/255;
        cmp(i,:)=ca+(cb-ca)*(angle(i)-88)/1; %88 is the start point
and 1 is the interval
    elseif angle(i)>89 & angle(i)<=90 %values between 89 and 90
        ca = [255,0,0]/255;
        cb = [147,0,0]/255;
        cmp(i,:)=ca+(cb-ca)*(angle(i)-89)/1; %89 is the start point
and 1 is the interval
    end
end
colormap(cmp)
colormap(flipud(colormap));
ch = colorbar;
ylabel(ch,'Stacking pattern')
end

if CM == 3
    if scheme == 5 || scheme == 7 || scheme == 8 || scheme == 9
        for i=1:8
            if i==3 || i==4 || i==5 || i==6
                cmap(i,:)= [0.2081,0.1663,0.5292]; %purple
                P(i,:) = 2;
            elseif i==7
                cmap(i,:)= [0.0060,0.4086,0.8828]; %blue
                P(i,:) = 3;
            elseif i==8
                cmap(i,:)= [0.0590,0.6838,0.7254]; %turquoise
                P(i,:) = 4;
            elseif i==1
                cmap(i,:)= [0.0590,0.6838,0.7254]; %turquoise
                P(i,:) = 4;
            end
        end
    end
end

```

```

        elseif i==2
            cmap(i,:)= [0.9763,0.9831,0.0538]; %yellow
            P(i,:) = 1;
        end
    end
end

if CM ==3
    if model == 1

surf(permute(X(Y11, :, :), [3,2,1]), permute(T(Y11, :, :), [3,2,1]), permute(A
(Y11, :, :), [3,2,1]), permute(C(Y11, :, :), [3,2,1])); %model 1
        elseif model == 2

surf(permute(Y(:, X11, :), [3,1,2]), permute(T(:, X11, :), [3,1,2]), permute(A
(:, X11, :), [3,1,2]), permute(C(:, X11, :), [3,1,2])); %model 2
        elseif model == 3

surf(permute(X(:, :, T11), [1,2,3]), permute(Y(:, :, T11), [1,2,3]), permute(A
(:, :, T11), [1,2,3]), permute(C(:, :, T11), [1,2,3])); %model 3
        end
    end

if scheme == 6
    for i=1:8
        if i==2 || i==3 || i==4 || i==5 || i==6 || i==7
            cmap(i,:)= [0.2081,0.1663,0.5292]; %purple
        elseif i==1 || i==8
            cmap(i,:)= [0.9763,0.9831,0.0538]; %yellow
        end
    end
end
end

if CM == 3
    colormap(cmap)
    caxis([1 9])
    ch = colorbar;
    if scheme == 5
        ylabel(ch, 'Systems tract (Genetic sequence: Frazier (1974);
Galloway (1989)')
        set(ch, 'ytick', [1,2,4.5,7,8], 'yticklabel', [' TST ' ; ' HST
'; 'early LST'; 'late LST'; ' TST ']);
    elseif scheme == 6
        ylabel(ch, 'Systems tract (T-R sequence: (Johnson & Murphy
(1984); Embry & Johannessen (1992)')
        set(ch, 'ytick', [1,4.5,8], 'yticklabel', [' RST ' ; ' TST
'; ' RST ']);
    elseif scheme == 7
        ylabel(ch, 'Systems tract (Depositional sequence II (Haq et al.
(1987); Posamentier et al.(1988)')
        set(ch, 'ytick', [1,2,4.5,7,8], 'yticklabel', [' TST ' ; ' HST
'; 'early LST'; 'late LST'; ' TST ']);
    elseif scheme == 8
        ylabel(ch, 'Systems tract (Depositional sequence IV (Hunt &
Tucker (1992;1995); Christie & Blick(1991)')

```

```

        set(ch, 'ytick', [1,2,4.5,7,8], 'yticklabel', [' TST ' ; ' HST
';' FST ' ;' LST ' ;' TST ']);
    elseif scheme == 9
        ylabel(ch, 'Systems tract (Depositional sequence IV (Hunt &
Tucker (1992;1995); Helland-Hansen & Gjelberg(1994)')
        set(ch, 'ytick', [1,2,4.5,7,8], 'yticklabel', [' TST ' ; ' HST
';' FST ' ;' LST ' ;' TST ']);
    end
end

if model == 1
    ylabel('Time');
    xlabel('Distance along fault');
    zlabel('Accommodation');
elseif model == 2
    ylabel('Time');
    xlabel('Distance away from fault');
    zlabel('Accommodation');
elseif model == 3
    ylabel('Distance away from fault');
    xlabel('Distance along fault');
    zlabel('Accommodation');
end

camlight headlight %puts lighting on from 'head-on'
lighting phong %different type of lighting

% To plot the Accommodation Balance (Chapter 7.4)

if CM == 5 & stacking == 4

CN = ones(size(A))*NaN; % make new color map
BR = SLG; BR(find(BR<0))=NaN; BR = max(0,BR); %find base level rise
gradient (SLG)less than zero - rise
BF = SLG; BF(find(BF>0))=NaN; BF = max(0,-BF); %find base level
gradient (SLG) greater than zero - fall
EG = ones(size(A))*0; %erosion
TUG = ones(size(A))*0; %uplift
ABT = (BR + TSG + EG); %accommodation balance on top of ratio (space
increasers)
ABB = (BF+TUG+S); %accommodation balance on bottom of ratio (space
decreasers)

CN(find(ABT>(1.3.*ABB) & S==0)) = 1;
%where increasers (ABT) > decreasers (ABB) and sedimentation is zero
CN(find(ABT>(1.3.*ABB) & S>0)) = 2;
%where increasers (ABT) > decreasers (ABB) and sedimentation is > zero
CN(find(ABT<(1.3.*ABB) & ABT>(0.7.*ABB) & abs(ABT)>0 & S==0)) = 3;
%where increasers (ABT) = decreasers (ABB) and all are zero and
sedimentation is zero
CN(find(ABT<(1.3.*ABB) & ABT>(0.7.*ABB) & abs(ABT)>0 & S>0)) = 4;
%where increasers (ABT) = decreasers (ABB) and all are zero and
sedimentation is > zero
CN(find(ABT<(0.7.*ABB) & S==0)) = 5;
%where increasers (ABT) < decreasers (ABB) and sedimentation is zero
CN(find(ABT<(0.7.*ABB) & S>0)) = 6;
%where increasers (ABT) < decreasers (ABB) and sedimentation is > zero
%CN(find(ABT==0 && ABB==0)) = 7; %where increasers (ABT) = decreasers
(ABB) and both are zero

```

```

for i=1:6
    if i==1
        cmap(i,:)= [0.5,0.5,0.4]; %grey - Transgressive
surface
    elseif i==2
        cmap(i,:)= [0,0,0.39]; %dark blue - Retrogradation
    elseif i==3
        cmap(i,:)= [0.3,0.8,0.2]; %green - Hiatus
    elseif i==4
        cmap(i,:)= [1,0,0]; %red - Aggradation
    elseif i==5
        cmap(i,:)= [0.2,0,0]; %black - Regressive surface
    elseif i==6
        cmap(i,:)= [1,1,0.2]; %yellow - Progradation
        %elseif i==7
            %cmap(i,:)= [0.2,0.2,0]; %purple - Hiatus - stasis
    end
end

figure
[faces,verts,colors] = isosurface(X,T,A,Y,Y1,CN);
patch('Vertices', verts, 'Faces', faces, 'FaceVertexCData',
colors, 'FaceColor', 'interp', 'edgecolor', 'interp');

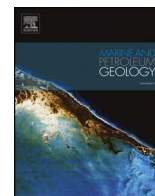
ch = colorbar;
set(ch, 'ytick', [1,2,3,4,5,6], 'yticklabel', ['Transgressive surface';
Retrogradation '; Hiatus '; Aggradation ';
Regressive surface '; Progradation ']);
%set(ch, 'ytick', [1,2,3,4,5,6,7], 'yticklabel', [' Hiatus-stasis
'; Progradation '; Regressive surface '; Aggradation
'; Hiatus '; Retrogradation '; Transgressive
surface']);
caxis([1 6])
colormap(cmap)
end

```

```

% FOR COLOURING 8 segment curve (e.g. Chapter 7.1)
% for i=1:8
%     if i==1
%         cmap(i,:)=(1/255*[213,62,79]); %grey
%     elseif i==2
%         cmap(i,:)=(1/255*[244,109,67]); %dark blue
%     elseif i==3
%         cmap(i,:)=(1/255*[253,174,97]); %green
%     elseif i==4
%         cmap(i,:)=(1/255*[254,224,139]); %red
%     elseif i==5
%         cmap(i,:)=(1/255*[230,245,152]); %black
%     elseif i==6
%         cmap(i,:)=(1/255*[171,221,164]); %yellow
%     elseif i==7
%         cmap(i,:)=(1/255*[102,194,165]); %purple
%     elseif i==8
%         cmap(i,:)=(1/255*[50,136,189]); %purple
%     end
% end
%
% for i=1:I
%     for j=1:J
%         clc
%         disp(['% complete: ',num2str(((i-1)*J+j)/2/I/J*100)])
%
%         sl_gt1(i,j,:) = gradient(permute(slcurve(i,j,:),[3,1,2]),t);
%         sub_gt1(i,j,:) =
gradient(permute(sc_sub.*T_sub(i,j,:),[3,1,2]),t);
%
%     end
% end

```



Research paper

Novel 3D sequence stratigraphic numerical model for syn-rift basins: Analysing architectural responses to eustasy, sedimentation and tectonics



B.J. Barrett*, D.M. Hodgson, R.E. Ll Collier, R.M. Dorrell

School of Earth and Environment, University of Leeds, Leeds, LS2 9JT, UK

ARTICLE INFO

Keywords:

Sequence stratigraphy
Stratigraphic forward modelling
Syn-rift basins
Tectonics and sedimentation

ABSTRACT

Syn-rift clastic sedimentary systems preserve a complicated stratigraphic architecture that records the interplay of tectonics, eustatic sea level change, and storage and routing of sediments. Previous conceptual models describe and explain changes in depositional stacking patterns along a fault segment. However, stacking patterns, and the nature of key stratigraphic surfaces, is challenging to predict accurately with conventional sequence stratigraphic models that do not consider the three-dimensional interplay of subsidence, sedimentation, and eustasy. We present a novel, geometric, 3D sequence stratigraphic model ('Syn-Strat'), which applies temporally- and spatially-variable, fault-scale tectonic constraints to stratigraphic forward modelling, as well as allowing flexibility in the other controls in time and space.

Syn-Strat generates a 3D graphical surface that represents accommodation. Although the model has the capacity to model footwall variation, here we present model results from the hangingwall of a normal fault, with temporal and spatial (dip and strike) predictions made of stacking patterns and systems tracts for a given set of controls. Sensitivity tests are tied to the depositional architecture of field-based examples from the Loreto Basin, Gulf of California and Alkyonides Basin, Gulf of Corinth. Here, the relative influence of major sedimentary controls, different subsidence histories, varying sedimentation distribution, including along-strike variation in stacking patterns, are assessed and demonstrate the potential of Syn-Strat for reducing subsurface uncertainties by resolving multiple scenarios. In addition, the model demonstrates the nature of diachroneity of key stratigraphic surfaces that can arise in syn-rift settings, which could be represented by a bypass surface (sequence boundary) or reservoir seal (which could include the maximum flooding surface) in the rock record. Enabling a quantitative assessment of these surfaces is critical for prospect analysis in hangingwall half-graben-fills, where these surfaces are heavily relied upon for well correlations that are used for hydrocarbon volume and production rate predictions.

1. Introduction

Syn-rift depositional sequences preserve a complicated architecture, due to the spatially- and temporally-variable interplay of major sedimentary controls (eustatic sea level, subsidence and sedimentation). Conventional sequence stratigraphic models (Wheeler, 1958, 1959, 1964; Sloss, 1962, 1991; Mitchum et al., 1977; Vail et al., 1977; Leeder & Gawthorpe, 1987; Jervey, 1988; Posamentier et al., 1988; Posamentier and Vail, 1988; Van Wagoner et al., 1988; Posamentier and Weimer, 1993; Ravnås and Steel, 1998) struggle to predict the depositional architecture of syn-rift successions and the 3D distribution of reservoirs and seals. Various studies have attempted to address this issue by integrating sub-seismic, structural and sedimentological data in order to build tectono-stratigraphic frameworks in various rift settings, including: the Gulf of Suez (e.g. Gawthorpe et al., 1997; Gupta et al.,

1999; Young et al., 2002; Jackson et al., 2005), the Gulf of Corinth (e.g. Poulimmenos et al., 1993; Gawthorpe et al., 1994; Collier and Gawthorpe, 1995; Gawthorpe and Leeder, 2000; Leeder et al., 2002), the Gulf of California (e.g. Dorsey et al., 1995; Dorsey and Umhoefer, 2000; Mortimer et al., 2005), and the Crati Basin (Italy) (e.g. Colella et al., 1987; Colella, 1988a,b,c). Burgess (2016) highlights four key uncertainties in general sequence stratigraphic theory: i) rare quantitative analysis, ii) limited consideration for along-strike variability in sequence architecture (also pointed out by Martinsen and Helland-Hansen, 1995), iii) limited constraint for sediment supply rates, and iv) few studies that demonstrate the interplay of accommodation and supply in three dimensions. These uncertainties are exacerbated in active rift basins, constraining the interaction of allogenic controls in three dimensions remains challenging.

Sequence stratigraphic forward modelling can support

* Corresponding author.

E-mail address: ebbca@leeds.ac.uk (B.J. Barrett).

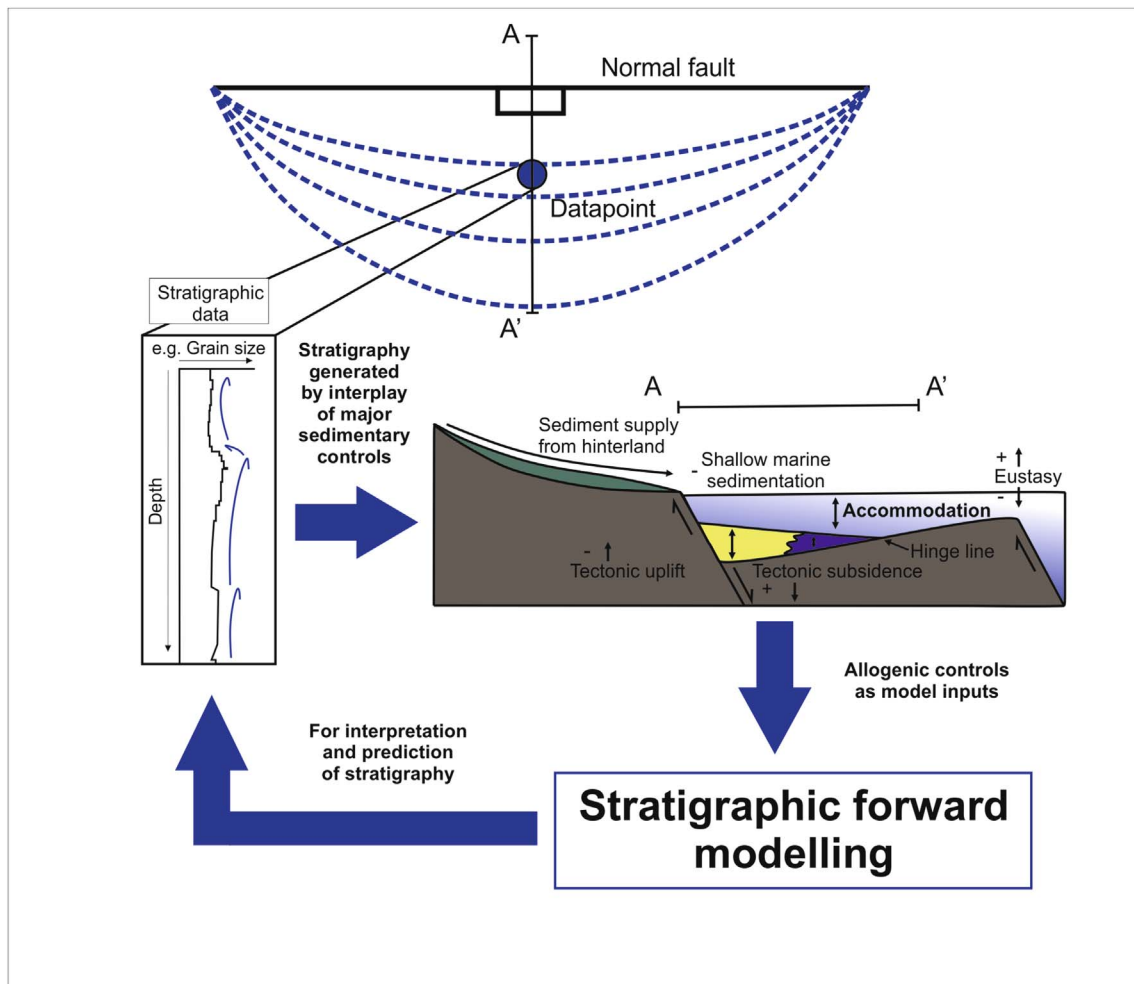


Fig. 1. Process of forward stratigraphic modelling of syn-rift basin-fills. Stratigraphy at a position within the hangingwall of a normal fault is the result of the interplay of the three major sedimentary controls: eustatic sea level, fault-related subsidence and sedimentation. These controls can be modelled to provide insight for interpretation and prediction of syn-rift strata.

interpretation and prediction of depositional sequences and key stratigraphic surfaces (Fig. 1). Early numerical sequence stratigraphic models, which incorporated sinusoidal sea level change and hinged subsidence to simulate accommodation generation and assumed a constant sediment supply, predicted key surfaces in seismic (Jervey, 1988). Burgess and Allen (1996) extended this approach to include temporal variability in sediment supply rate. Subsequently, various stratigraphic forward models have been developed in order to better understand and predict dynamic depositional systems. DIONISOS (Granjeon and Joseph, 1999) and STRATA (Flemings and Grotzinger, 1996) represent significant advances in the power of three-dimensional stratigraphic forward models, and various other geometric, diffusion, fuzzy logic and hydraulic models have emerged, reviewed by Huang et al. (2015). Diffusion-based models are regularly utilised for sediment supply, and have successfully applied hypothesis-testing approaches to some systems (e.g. Burgess and Prince, 2015). However, they are unable to accurately predict mixed process regime systems, gravity-flow dominated systems, and tectonically active systems. Various studies have demonstrated diachronous stratigraphic surfaces due to variable sediment supply and basin margin physiography (Burgess and Prince, 2015; Madof et al., 2016). Hardy et al. (1994), Hardy and Gawthorpe (1998, 2002) and Gawthorpe et al. (2003) (following the methods of Ritchie et al., 1999) introduced simplified tectonic constraints into 2D numerical modelling to assess stratal geometries and suggested that major stratigraphic surfaces may be limited in spatial extent (Gawthorpe et al., 2003). However, there has been little assessment of the full impact of along-strike variations in fault-related subsidence,

and especially, differential tectonic constraints in both time and space and the combined influence of all three variable allogenic controls.

Here, we present a novel, flexible and more comprehensive sequence stratigraphic forward model that applies fault-scale tectonic constraints to 3D sequence stratigraphy. The model demonstrates the sensitivity of sequence architecture (stacking patterns and key stratigraphic surfaces) to the three-dimensional interplay of major sedimentary controls in a hangingwall half-graben by use of experiments, validated by field-based examples from the literature. Within the framework of the model, limitless parameter combinations for testing in any rift setting are permitted. The objectives are: i) to assess the stratigraphic response to various temporal and spatial interactions of eustasy, tectonics and sedimentation patterns, ii) to explore the diachrony of key stratigraphic surfaces, and the conditions under which the nature of those might vary, and iii) to apply temporally- and spatially-variable tectonic constraints to stratigraphic forward modelling for the first time. Syn-Strat demonstrates and illustrates important stratigraphic concepts in a unique manner, which allows syn-rift systems to be explored in 3D and allows scope for testing of all possible outcomes, and assessment of stratigraphic response.

2. Model architecture and assumptions

2.1. Model framework

‘Syn-Strat’ is a geometric model that allows investigation of the interplay of eustasy, sediment supply, and tectonic subsidence in rift

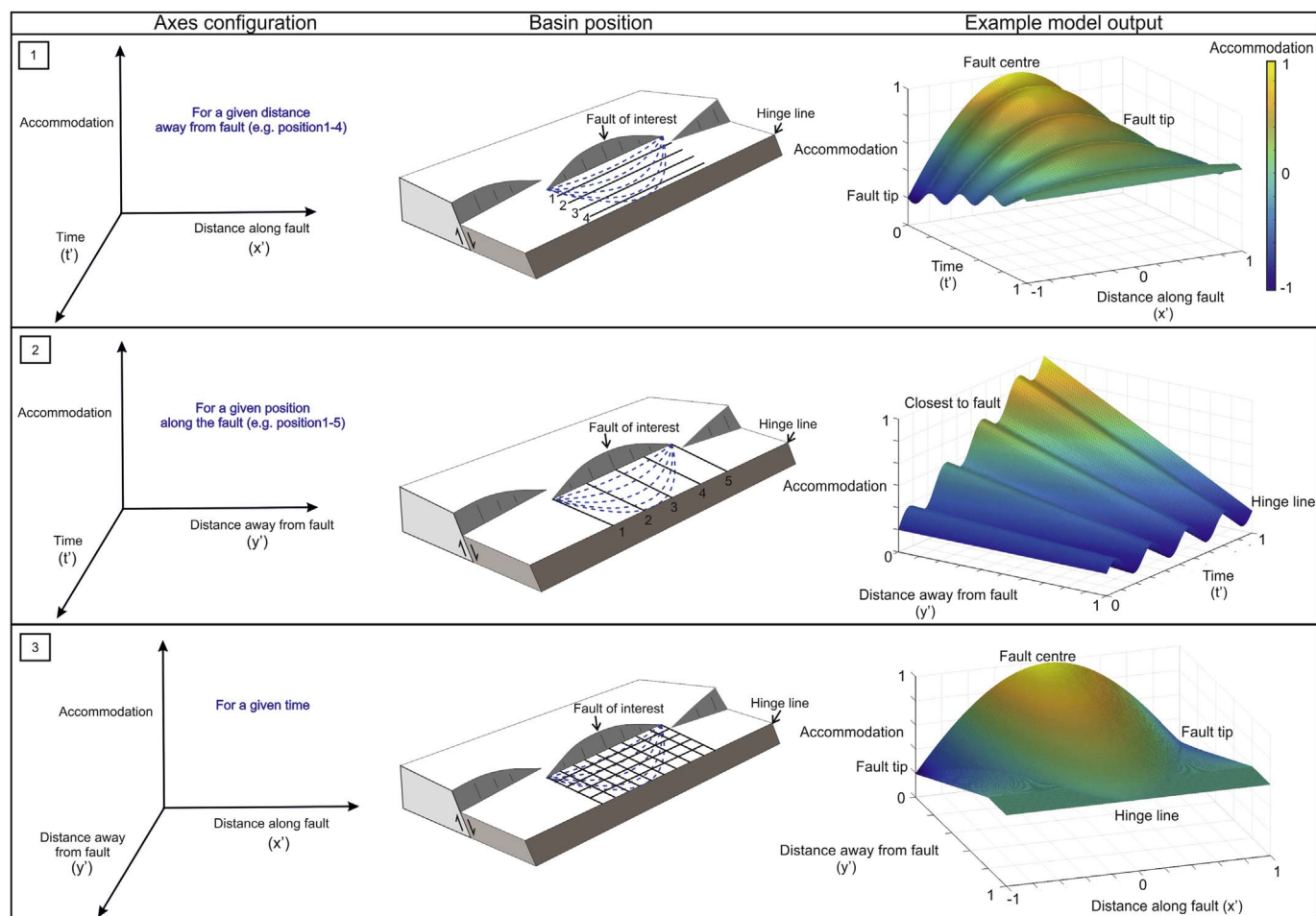


Fig. 2. Model plot axes options, associated geological setting and example model outputs. 1) Plot of accommodation on any line parallel to the fault in the hangingwall in time, for any given distance away from the fault (x',t'). 2) Plot of accommodation on any line orthogonal to the fault in the hangingwall in time, for any given position along the fault (y',t'). 3) Plot of accommodation in space (parallel to and orthogonal to the fault), for any given time (x',y'). Structural contours shown by blue dashed lines. All figures hereafter utilise the axes shown in '1'. (For interpretation of the references to colour in this figure legend, the reader is referred to the web version of this article.)

basins. The model sums changing i) eustatic sea level, ii) fault-related subsidence, and iii) sedimentation curves, to generate a 3D 'accommodation' curve, which is used to predict the stratigraphic infill of a half-graben basin adjacent to an individual normal fault segment. SynStrat also allows the opportunity to explore of a number of other variables that contribute towards these major controls, such as accounting for crustal strength, isostasy and erosion in subsidence. This is because each major control curve can be constructed from composite curves that contribute towards defining that variable and can be varied in time and space. For example, the eustatic sea level variable can be composed of a glacio-eustatic curve and a thermal expansion curve. However, for simplicity, here we use the resultant control curves to show the responses to the sensitivity tests.

We specifically define accommodation as the measurable space (thickness or volume) available at any given time for subsequent deposition that results from the combined influence of the preceding eustatic sea level, tectonic displacement and sedimentation. Eustatic sea level rise, tectonic subsidence and large-scale erosion from mass wasting are mechanisms that increase accommodation at any specific location, and eustatic sea level fall, uplift and sedimentation are mechanisms that reduce (or fill) accommodation. Our definition of accommodation follows original work by Jervey (1988) as the 'space available for deposition', which was also used by Catuneanu et al. (2009), and closely corresponds to definitions by Cross (1988), whereby 'potential accommodation' is the cumulative space created or removed by relative sea level changes and 'realised accommodation' is the

volume of sediment that is actually accumulated. In this terminology, our model plots the sum of 'potential' and 'realised' accommodation, which in a shallow marine setting can be equated to water depth, but need not in other settings. It is 'real-time' accommodation, as opposed to interpreted accommodation from the stratigraphic record that other studies focus upon (Muto and Steel, 2000). To this avail, an assessment can be made of dynamic changes in accommodation as a result of variable controls.

The 3D accommodation function has dynamic along-strike, 'x', down-dip, 'y', and temporal, 't', controls and is visualised as a graphical surface, to which stacking patterns (progradation, aggradation and retrogradation) or systems tracts, following any convention, can be ascribed. This forms a valuable, large-scale stratigraphic framework for a given set of controls, to which a process model could then be applied to predict the nature of a deposit.

The accommodation surface is defined on a three-dimensional mesh and stored in matrix form. At any point of 'x', 'y' and 't', the accommodation surface, $A_S(x,y,t)$, is equal to the sum of eustatic sea level, $E(x,y,t)$, and the total amount of tectonic subsidence until time t , $T(x,y,t)$, minus the total amount of sediment accumulated until time t , $S(x,y,t)$ (after Jervey, 1988; Posamentier and Allen, 1999; Catuneanu, 2002),

$$1) A_S(x,y,t) = -S(x,y,t) + E(x,y,t) + T(x,y,t).$$

A heuristic model is employed to specify the variables that sum to yield A_S . Variables (V) are separated into three normalised functions describing relative spatial and temporal variation, V_x , V_y and V_t that

represent the given control i) along the fault length, ii) away from the fault and iii) in time, respectively. For example, Sedimentation, S is defined in x (V_x), in y (V_y) and in time (V_t). The product of the three functions and the maximum scalar value of the variable, V_{SC} , yields the variable in each case

$$2) V = V_{SC} V_x(x) V_y(y) V_t(t).$$

The dimensionless 3D accommodation surface that ‘Syn-Strat’ outputs, A_S' , is provided to enable comparison between different fault settings. For example, if two fault settings are compared with different subsidence, eustasy and sedimentation histories, the accommodation surface from each is normalised using the maximum amount of cumulative tectonic subsidence for each, to allow comparison between the two, $\max(T)$.

$$3) A_S' = A_S / \max(T).$$

The accommodation surface is plotted in terms of two of the three variables in dimensionless form: distance along fault divided by total fault length, x' , which is any line parallel to the fault segment; distance away from fault divided by distance from fault to the hinge line, y' , which is any line orthogonal to the fault segment; and time divided by the fault evolution timescale, t' . Therefore, three different visualisations are possible from the model (Fig. 2):

- A. Plot of accommodation (A_S') on any line parallel to the fault in the hangingwall in time, for any given distance away from the fault (x' , t')
- B. Plot of accommodation (A_S') on any line orthogonal to the fault in the hangingwall in time, for any given position along the fault (y' , t')
- C. Plot of accommodation (A_S') in space (parallel to and orthogonal to the fault), for any given time (x' , y')

2.2. Eustatic sea level

Eustatic sea level is a major control on accommodation, whereby a rising eustatic sea level increases accommodation and a falling eustatic sea level decreases accommodation (Wheeler and Murray, 1957; Wheeler, 1964; Mitchum et al., 1977; Vail et al., 1977; Jervey, 1988). In Syn-Strat, eustatic sea level is defined in time, and is constant along the length of the fault and away from the fault. Fig. 3 illustrates this information by plotting eustatic sea level along the fault and in time, for a position in the immediate hangingwall of the fault.

2.3. Subsidence

2.3.1. Subsidence along the fault length

Tectonic displacement is defined in three dimensions: in time, and along and away from the fault. In the model, we are interested in tectonic displacement on the hangingwall of a single fault segment, which is subsidence. Cumulatively, hangingwall subsidence is zero at the two fault tips and maximum at the fault centre. When these three data points for subsidence are available, a parabola is calculated that describes the displacement change along the fault length. This distribution of subsidence along-strike of a fault has been extensively documented in the literature (e.g. Stein and Barrientos, 1985; Cowie and Scholz, 1992; Cowie et al., 2000) and is primarily used in our modelling. An observed temporally-variable subsidence distribution along the fault length could be applied instead.

Gawthorpe et al. (1994) and Collier & Gawthorpe (1995) highlight that the curve derived from the sum of the eustatic sea-level and tectonic subsidence curves will be steeper at the centre of a fault in a phase

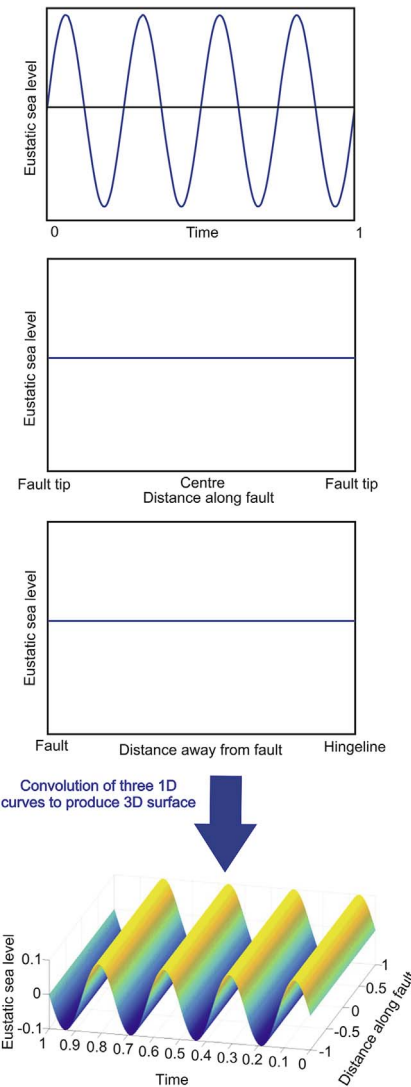


Fig. 3. Derivation of the 3D eustatic sea level curve. Eustasy defined geometrically in time (top), along the fault length (upper middle) and away from the fault (lower middle). The three curves are multiplied to give the 3D plot (bottom) in a given configuration (1 of Fig. 2A). Axes are dimensionless. ‘Time’ varies between 0 and 1. ‘Distance along fault’ varies between -1 and 1 , where these are the fault tips and 0 represents the fault centre. ‘Distance away from fault’ varies between 0 and 1 , where 0 is closest to the fault and 1 is the hinge-line.

of relative sea level rise, where subsidence is greatest (position 1 in Fig. 4), than on either side (position 2 in Fig. 4). At the fault tips subsidence is zero, so accommodation is varying due to eustasy alone (position 3 in Fig. 4).

For the parabolic displacement distribution along the length of the fault, the model utilises a normal distribution curve. This permits alteration of the distribution curve shape depending on the system by varying the standard deviation, skewness and kurtosis. Assigning these variables with a value of one produces a parabola (Fig. 5). The model assumes that during growth, the fault is fixed in length, i.e. it is pinned at the fault tips. This growth model is supported by other studies that document examples of faults demonstrating constant-length growth (Walsh et al., 2002, 2003; Childs et al., 2003; Schlagenhauf et al., 2008; Jackson and Rotevatn, 2013; Nicol et al., 2017; Jackson et al., 2017). In cases where fault tips propagate, stacking will vary from that anticipated by the model, or it can be used to represent the central growth phase of the fault, when it is no longer undergoing linkage (in the terminology of Cowie et al., 2000).

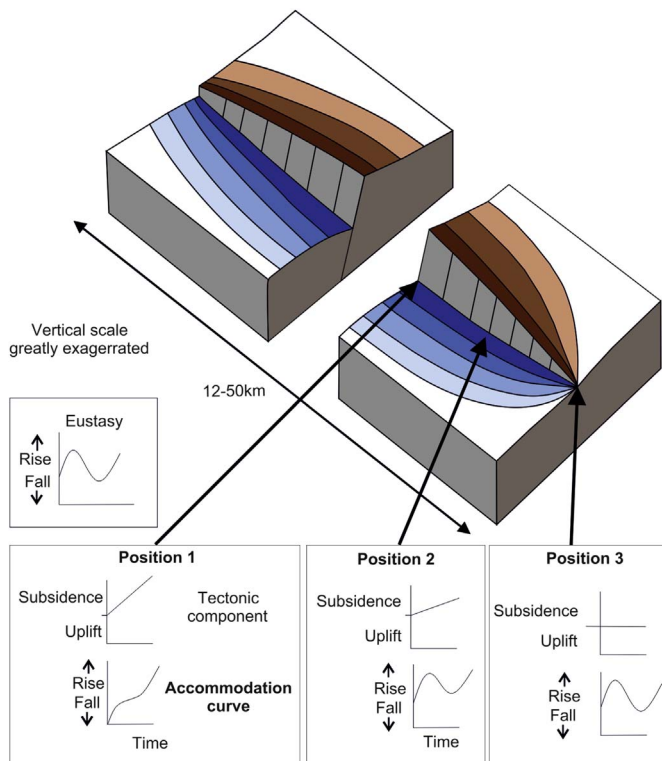


Fig. 4. Diagram to illustrate the various relative sea level/accommodation curves that can be derived from the convolution of eustatic sea level and subsidence at three positions along a hangingwall fault block. The eustatic sea level curve that is used for all three positions is displayed on the left hand side. Modified from Collier & Gawthorpe (1995).

2.3.2. Subsidence away from the fault

In a half graben, rotation is focussed at the hinge line, and beyond this point the net movement is uplift. The model considers subsidence from the immediate hangingwall where it is maximum, up to the hinge line of the block where it is zero. As subsidence is zero at the fault tips and maximum at the fault centre, the displacement from a slip event is distributed radially away from the fault. The structure contours resemble the parabolic shape of the displacement curve along the fault length and a 'zero contour line', the line of zero subsidence, is defined. The model generates the parabolic subsidence curve along the length of the fault, the equivalent zero contour line away from the fault, and the user defines the style of interpolation between them, which can be either linear or parabolic (Fig. 5). The interpolation (decay curve) style is determined by the manner in which the hangingwall deforms. If the hangingwall subsides without changing geometry, i.e. the hangingwall does not deform in dip-section as it rotates, a linear decay curve should be assigned. If the surface of the hangingwall adopts a convex geometry in dip-section during subsidence, a parabolic decay curve can be assigned.

2.3.3. Subsidence in time

During the syn-rift phase of fault growth, cumulative subsidence increases incrementally over time as a result of a series of earthquakes, and the hangingwall will subside in each event. As a result, the hangingwall deepens through time and accommodation is created. The subsidence rate is considered as the subsidence per earthquake over a given recurrence period. For example, the subsidence rate for a fault with a subsidence of 5 m per earthquake event and a recurrence period of 500 years would be 10 mm/yr.

Syn-Strat allows a choice of in-built conceptual subsidence curves with time or the input of an observed subsidence curve. Fig. 5 illustrates three examples of conceptual subsidence curves: a constant, an increasing, and a decreasing subsidence rate. A linear increase in

subsidence through time represents a constant subsidence rate. In this scenario, the hangingwall cut-off deepens by the same increment with each earthquake. For the central growth phase of a fault, it is perhaps most appropriate to choose a linear increase, as the fault is no longer linking with other faults and growth is no longer accelerating (as in Gupta et al., 1998; Cowie et al., 2000). An exponential increase of subsidence in time would represent an increasing strain rate and subsidence rate. In this scenario, each subsequent earthquake must produce a greater amount of subsidence, or there must be an increasing frequency of earthquakes. This could represent the early syn-rift phase of fault evolution, during fault linkage and strain localisation. Conversely, for a decreasing subsidence rate, there must be a reducing amount of subsidence for each subsequent earthquake, or a reduced frequency of earthquakes, which could represent the late syn-rift phase of fault evolution. Composite subsidence curves can be constructed. For example, a curve that represents the evolution of the fault from early-to late-syn rift phases, or a curve that defines the transition from active fault subsidence to either fault inactivity, as strain is partitioned to an adjacent fault, or to a post-rift basinal phase. Similarly, the subsidence rate can be varied through time to show a higher resolution of fault activity, e.g. earthquake clustering on one of a number of faults.

The subsidence curve in each dimension are multiplied to produce a 3D graphical surface. Fig. 5 represents subsidence along the length of the fault, through time in the immediate hangingwall of the fault (configuration 1 of Fig. 2A). It is composed of a parabolic displacement curve along the length of the fault, a linear increase in subsidence over time, and a linear decrease in subsidence away from the fault. Without consideration of eustatic sea level and sediment supply, this represents fault-related, temporal and spatial variations in accommodation.

2.4. Sedimentation

Sedimentation reduces the available space for subsequent deposition. Therefore, sedimentation is subtracted from combined eustatic sea level and subsidence to give the resultant graphical accommodation surface.

Spatial and temporal variations in sediment supply and the number and location of drainage input points arise as a result of climate variability (wind, temperature, rainfall, vegetation and their seasonal fluctuations), size and physiography of each drainage basin (gradient, relief and orientation) and hinterland geology (e.g. Hack, 1957; Leeder & Gawthorpe, 1987; Ravnås and Steel, 1998). Spatial and temporal changes in sediment supply is a complicated variable that is difficult to constrain even in recent systems (Mullenbach and Nittrouer, 2006; Romans et al., 2009, 2016; Allen et al., 2013; Warrick, 2014). Syn-Strat utilises sediment accumulation (or sedimentation), rather than sediment flux. Sedimentation is defined geometrically, in contrast to some other models that utilise a process-based, commonly diffusion-type approach (e.g. Rivaneš, 1992; Flemings and Grotzinger, 1996; Granjeon and Joseph, 1999; Burgess & Prince, 2015). Although the geometric approach has its own inherent assumptions (discussed in Section 3.2), it avoids some of the limitations of process-based models in relation to the interaction of different process-regimes and dispersal mechanisms. The initial and final sedimentation accumulations are assigned, as well as the shape of the input curve in time and in space. A sedimentation rate is not assigned unless a linear curve in time is utilised, as in all other cases, it varies.

2.4.1. Sedimentation along the fault length

Here we model examples of shoreline-attached systems. In some scenarios, these prograde from the relay zones of a fault with, if accommodation allows, maximum deposition occurring at the fault tips and reducing towards the centre of the fault. In a scenario with equal sedimentation from both fault tips, an inverse parabola is used to model the sediment distribution along the length of the fault (Fig. 6). For this distribution, the percentage of total sedimentation that reaches the

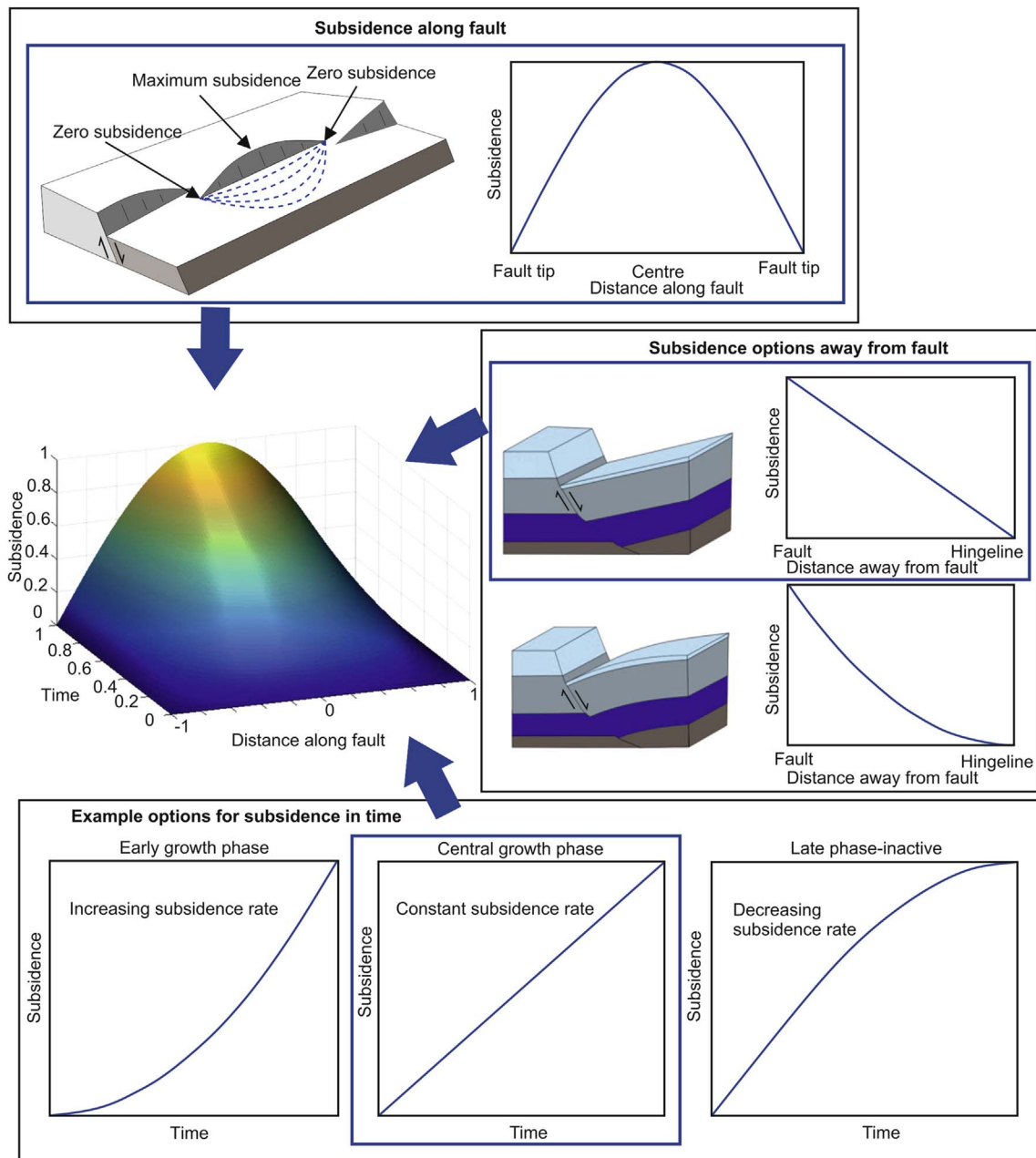


Fig. 5. Derivation of the 3D subsidence curve. Subsidence is defined geometrically in time (lower box), with in-built options of either an increasing, constant, or decreasing subsidence rate. Subsidence is defined along the fault length (upper box), where a parabola describes the distribution of subsidence, and away from the fault (middle-right box), where two configurations are presented as options: either a linear or parabolic regression away from the fault. The highlighted blue boxes denote the chosen input in each case for the example 3D graphical surface. The resultant 3D subsidence plot, in a given configuration (1 of Fig. 2A), is shown to the middle-left. It shows the variation of subsidence with the chosen parameters along the length of the fault, in time, in the immediate hangingwall of the fault. (For interpretation of the references to colour in this figure legend, the reader is referred to the web version of this article.)

centre of the fault is defined. Any geometric curve that describes the distribution of sedimentation along the length of the fault can be utilised. For this study, we utilise curves with maximum deposition at a given location along the fault (the source point), which decreases away from that point radially to represent a prograding, shallow marine system, such as a delta. In a scenario of multiple footwall point sources (Fig. 6), Syn-Strat allows the user to alter the number, location, magnitude, shape and range of sediment input points. For the sediments (and predicted stacking) to be preserved, accommodation values must exceed zero; any ‘negative’ accommodation values generated from the model represent sediments that would be bypassed to deeper water and/or redistributed along strike. However, an exception is with the

presence of pre-existing accommodation, such as antecedent bathymetry, or regional tectonic subsidence that are not included in the model results presented here, and would allow preservation in modelled areas of ‘negative’ accommodation.

2.4.2. Sedimentation away from the fault

Sedimentation with distance away from the fault is not limited to a zero contour line (as with subsidence), and is defined as a linear, parabolic or exponential decrease towards zero at a chosen distance away from the fault. Fig. 6 provides two examples of such options: a linear decrease and a parabolic decrease to zero at the hinge line.

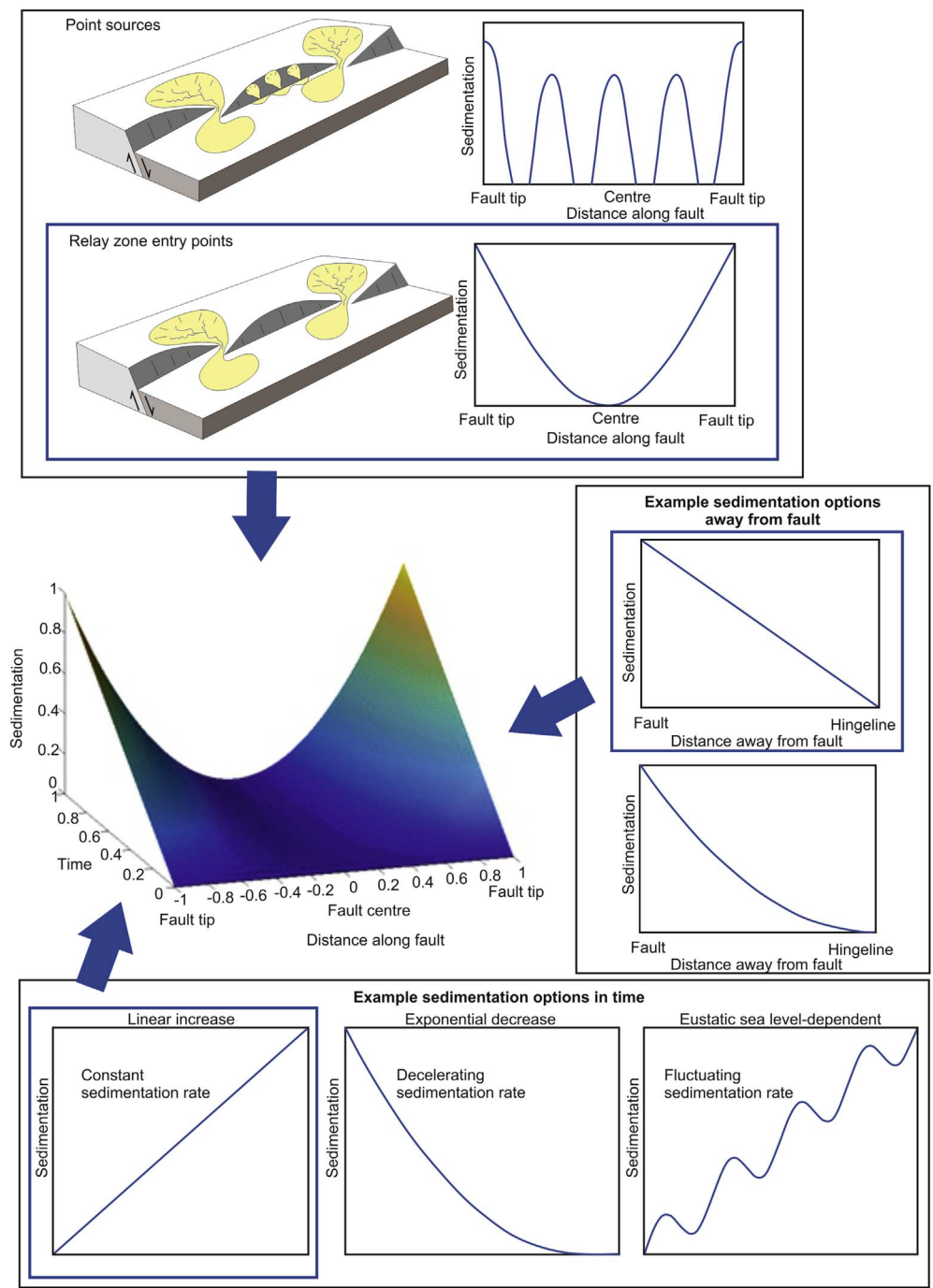


Fig. 6. Derivation of the 3D sedimentation curve. Sedimentation is defined geometrically in time (lower box), where three examples of sedimentation curves that could be chosen are presented: a constant, decreasing, or fluctuating sedimentation rate. Sedimentation is defined along the fault length (upper box), where two examples of sediment distribution curves that could be chosen are presented: relay zone entry points and footwall point sources. Sedimentation is defined away from the fault (middle-right box), where two configurations are presented as options: either a linear or parabolic regression away from the fault up to the hinge line. The highlighted blue boxes denote the chosen input in each case for the 3D graphical surface. The resultant 3D sedimentation plot, in a given configuration (1 of Fig. 2A), is shown to the middle-left. It shows the variation of sedimentation with the chosen parameters along the length of the fault, in time, in the immediate hangingwall of the fault. (For interpretation of the references to colour in this figure legend, the reader is referred to the web version of this article.)

2.4.3. Sedimentation in time

There are a number of controls that cause temporal variations in sedimentation, including changes in climate, source geology and drainage basin physiography on a range of timescales. In Syn-Strat, the user can define sedimentation over time from observed data or from a number of in-built options in the model, e.g. a linear or exponential increase, or decrease, a constant rate or a sinusoidal variation (Fig. 6). The product of sedimentation in each dimension is a 3D graphical surface. For example, Fig. 6 uses an inverse parabola to describe sedimentation along the length of the fault, a linear increase in sedimentation over time and a linear decrease in sedimentation away from the fault to the hinge line. The 3D graphical plot presents sediment accumulation, along the length of the fault, through time in the immediate hangingwall of the fault (configuration 1 of Fig. 2A).

3. Model output results

3.1. 3D accommodation surface

A 3D graphical surface that represents accommodation is produced by summing eustasy and tectonics and subtracting sedimentation. This is presented in Fig. 7, with accommodation along the length of the fault, through time in the immediate hangingwall of the fault (configuration 1 of Fig. 2A). In the example shown, subsidence is maximum and sedimentation is minimum at the centre of the fault. In this case, accommodation generally rises over time and is modified by a lower amplitude sinusoidal sea level. At the fault tip, subsidence is zero and sedimentation is maximum, and accommodation decreases over time into negative values as the basin fills to an overfilled state. This plot

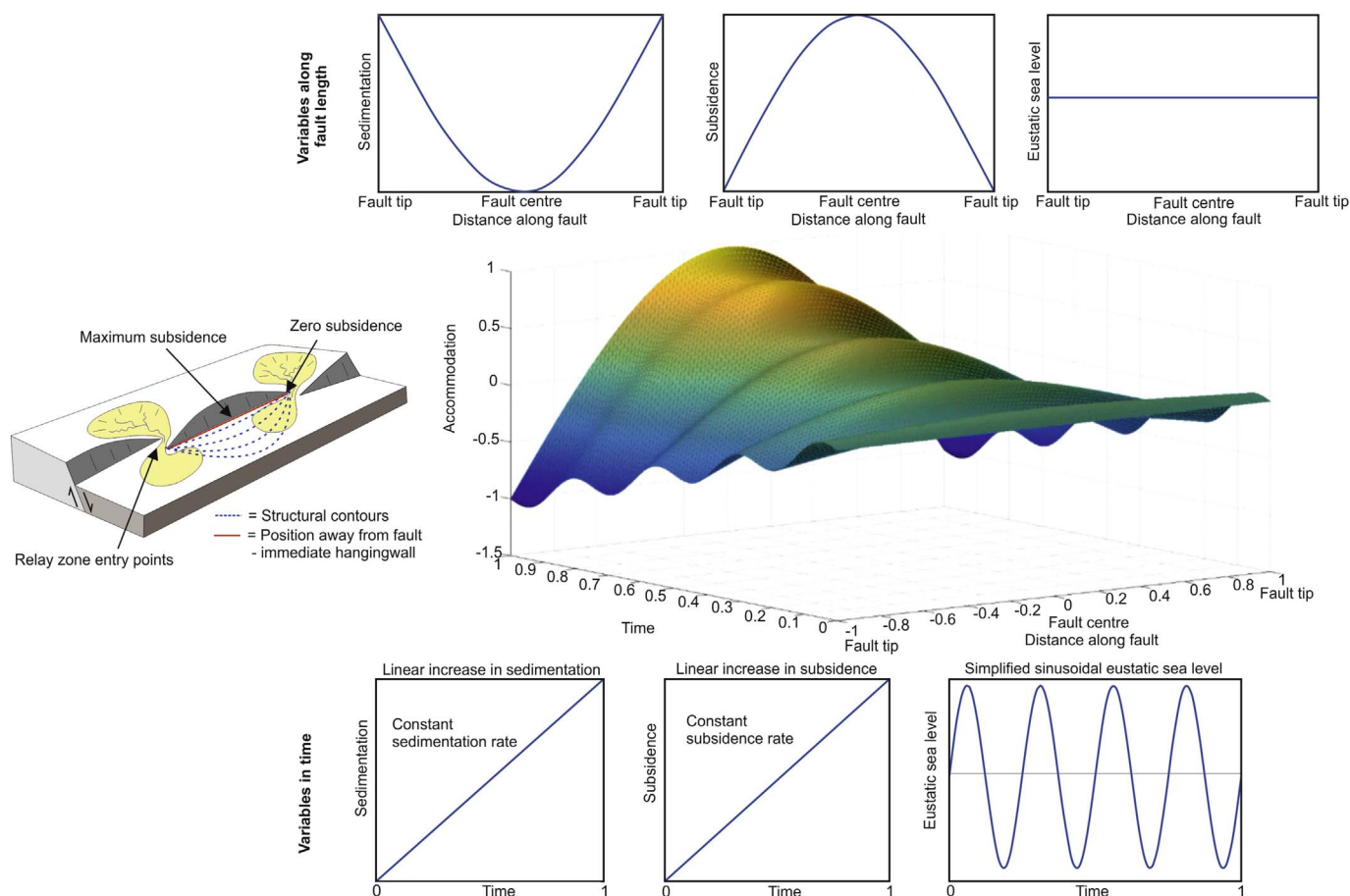


Fig. 7. 3D accommodation plot (configuration 1 of Fig. 2A), generated from the convolution of all three major controls: eustatic sea level, subsidence and sedimentation. The input curves for each control along the fault length and in time are presented above and below the plot, respectively. A block diagram to show the setting of the plot is provided to the left, where the red line shows the position of the plot, in the immediate hangingwall of the fault. (For interpretation of the references to colour in this figure legend, the reader is referred to the web version of this article.)

describes the interaction of the major controls, from which systems tracts can be identified and stacking patterns can be predicted.

3.2. Stacking patterns

For descriptions of stratal stacking patterns, Neal and Abreu (2009) and Neal et al. (2016) propose mainly observation-based, physical stratigraphy that describes the coastal response to accommodation creation and sedimentary fill. The terms progradation, aggradation, retrogradation and degradation are used to describe the way in which a depositional environment moves in space and thus, and how sediments are stacked through time. During progradation, the depositional system advances basinward as deposition exceeds available accommodation. In this case, marginal facies overlie basinal facies, characterised by a coarsening-upwards siliciclastic succession in core and outcrop and a decreasing gamma ray response in well-logs. During retrogradation, the system retreats (landwards) as accommodation exceeds deposition. Here, basinal facies overlie marginal facies and there is a fining-upwards succession in core and outcrop and an increasing gamma ray response in well-logs. During aggradation, deposition is equal to accommodation and the system neither advances nor retreats.

Syn-Strat colours the 3D surface according to these terms and utilises 5 classifications: strong retrogradation, weak retrogradation, aggradation, weak progradation and strong progradation (Fig. 8). The plot shows an overlay of Fig. 7, with progradation (in warm colours) during relative sea level fall and retrogradation (in cold colours) during relative sea level rise. The model output also illustrates enhanced periods of retrogradation near the fault centre, where space is greater than

deposition, and enhanced periods of progradation near the fault tips, where deposition is greater than available space. The plot provides the user with visualisation of how the sediments stack in time and space. Such information is useful to improve prediction of stacking patterns in areas with poor data constraint.

As shown, the model can generate the system response to major sedimentary controls in the form of stacking patterns, but does not predict the nature of the deposit. For this, various autogenic controls and the process regimes (transport mechanisms and directions) responsible for transport and deposition, and remobilisation, need to be considered, which challenge all existing numerical models of stratigraphic architecture. For example, where Syn-Strat anticipates areas of system retrogradation, the deposit may exhibit a fining-upwards profile or there may be a condensed section in the rock record. Similarly, where Syn-Strat shows areas of system progradation, the deposit may exhibit a coarsening-upwards profile or there may be a regressive surface indicating basinward sediment bypass (*sensu* Stevenson et al., 2015). In regard to preservation, areas of the plot with accommodation values less than zero will have low preservation potential. For a more accurate restoration of preservation, the antecedent topography and the broader scale effect of thermal subsidence at the scale of the basin would need to be considered. Therefore, the model is best utilised to provide the stratigraphic framework to which a process-regime(s) can be applied to predict sediment dispersal patterns.

3.3. Systems tracts

Systems tracts are used to subdivide a depositional sequence based

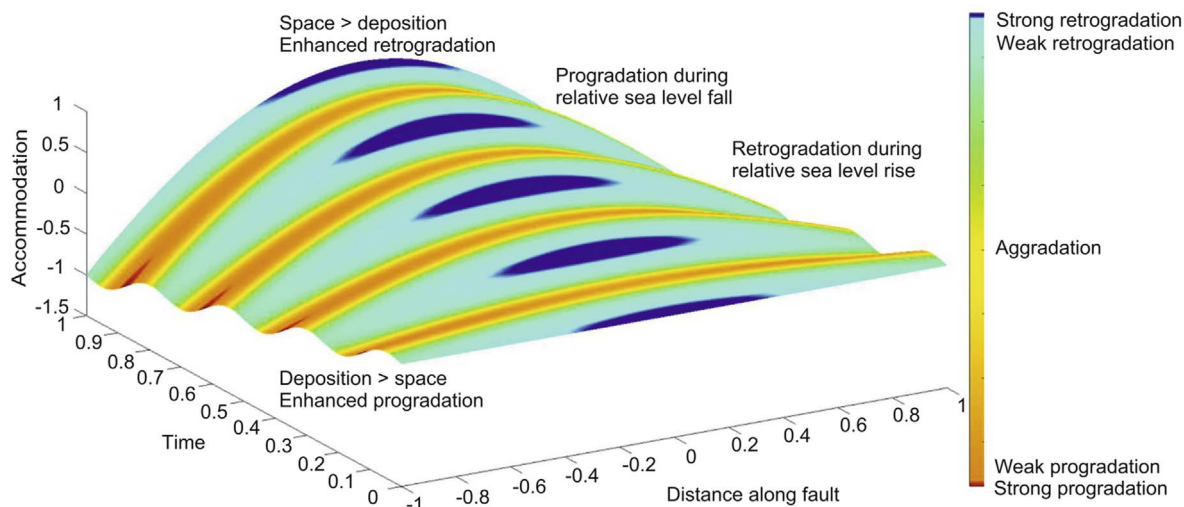


Fig. 8. 3D accommodation plot from Fig. 7 with stacking patterns presented. Plot shows the along-strike variation in stacking patterns as a result of laterally variable allogenic controls. Surface is coloured by 5 classifications: strong retrogradation (dark blue) and weak retrogradation (light blue), occurring during the relative sea level rises; aggradation (yellow); weak progradation (orange) and strong progradation (red), occurring during the relative sea level falls. A block diagram to show the setting of the plot is provided in Fig. 7. (For interpretation of the references to colour in this figure legend, the reader is referred to the web version of this article.)

upon its position on a relative sea level curve (or accommodation curve). As sequence stratigraphy theory has evolved, so complicated and non-universal systems tract schemes have developed (see Catuneanu, 2006, Catuneanu et al., 2009 for summary). For plotting systems tracts, Syn-Strat allows any one of these sequence stratigraphic approaches to be assigned and colours the accommodation surface accordingly (Fig. 9). The example 3D curve presented is an overlay of Fig. 7 and adopts the ‘genetic sequence’ approach (e.g. Frazier, 1974; Galloway, 1989), whereby the Highstand Systems Tracts (HST), the Early Lowstand Systems Tracts (ELST), the Late Lowstand Systems Tracts (LLST) and the Transgressive Systems Tracts (TST) are represented by the yellow, purple, blue and green segments, respectively (Fig. 8). Application of the systems tracts to the 3D surface helps visualisation of the temporal variation in the development of key sequence stratigraphic boundaries along the fault, e.g. maximum flooding surfaces (MFS) and sequence boundaries (SB). The sequence boundary (or ‘correlative conformity’) between the HST in yellow and the ELST in purple is diachronous, and occurs at a later time at the centre of the fault than at the fault tips. In the ‘genetic sequence’ scheme, the MFS is taken to be the position between TST and HST and it also occurs at a later time towards the centre of the fault than at the fault tips (Fig. 8). We later discuss the implications of selecting an alternative MFS position on a relative sea level curve, because this choice will determine the nature of the diachroneity of the MFS along the fault.

4. Discussion

The sensitivity of sequence architecture to major sedimentary controls and the utility of this model is discussed using a number of conceptual tests. In these tests, the major controls in terms of relative magnitude, rates through time and spatial distribution have been varied, with reference to documented examples from exhumed and modern systems.

4.1. Eustatic sea level-vs. subsidence-dominated successions

Two conceptual scenarios that demonstrate the differences between subsidence-dominated and eustatic sea level-dominated systems have been modelled (Fig. 10). In both cases, the rate of change of the dominant control is an order of magnitude higher than the subordinate control. Sedimentation from both fault tips is high and of the same magnitude as the dominant control, resulting in a balanced basin state

in both scenarios. A sinusoidal eustatic sea level and exponential increase in subsidence from zero, through time are applied. Fig. 10 shows the 3D graphical accommodation surface along the length of the fault, in time, in the immediate hangingwall of the fault and is coloured by systems tracts. The sequence boundaries between the HST and ELST are identified in a flattened version. In the subsidence-dominated scenario, the sequence boundaries are diachronous and the expression is lost in the model output at the fault centre towards the end of the time-frame. Here, the rate of subsidence outpaces the maximum rate of eustatic sea level fall with a resultant relative sea level rise. In the rock record, an unconformity that represents the sequence boundary would be expressed in this area as a correlative conformity. In the eustatic sea level-dominated scenario, the sequence boundaries are expressed and are isochronous along the length of the fault.

4.1.1. Field-based example: Loreto Basin

These scenarios strongly resemble the partially-constrained, sediment-rich depositional system of the Piedras Rodadas Formation, Loreto Basin, Gulf of California, which is sub-divided into two sub-basins: the Central sub-basin and the SE sub-basin. Subsidence rates of the Loreto Fault in both sub-basins from 2.6 to 2.4 Ma were derived by Umhoefer et al. (1994) and refined by Dorsey and Umhoefer (2000). The Central sub-basin experienced subsidence rates of 8 mm/yr and the SE sub-basin experienced lower subsidence rates of 1.5 mm/yr over the 200 kyr period. With an estimated eustatic sea level change rate of 4–5 mm/yr (supported by Raymo et al., 1992; Blanchon and Shaw, 1995), Dorsey and Umhoefer (2000) present the contrast between the subsidence-dominated Central sub-basin to the eustatic sea level-dominated SE sub-basin. The authors observe the presence of sequence boundaries in the SE sub-basin and a distinct lack of sequence boundary expression in the central sub-basin, which is consistent with our model results.

A second test (Fig. 11) shows two contrasting model outputs using the same input parameters and configuration (1 of Fig. 2A) as in Fig. 10, except with a low sediment input from the fault tips. Hence, the basin is in a sediment-starved state, as opposed to a balanced state. Here, stacking patterns are presented, rather than systems tracts. In this test, the stacking patterns show more along-strike variation in the subsidence-dominated scenario than the eustatic sea level-dominated scenario due to the influence of subsidence distribution on the accommodation curve. Strong progradation only occurs from the fault tips over short periods during the maximum rate of relative sea level fall.

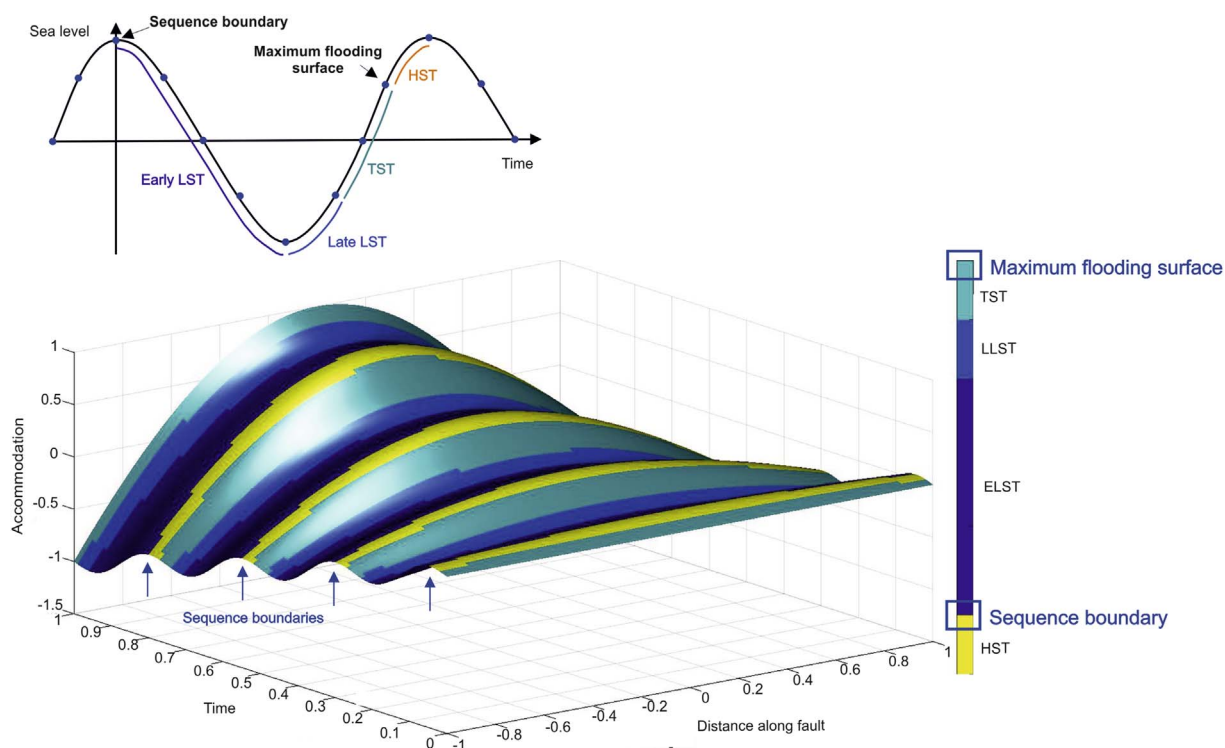


Fig. 9. 3D accommodation plot from Fig. 7 with systems tracts presented. Colours represent systems tracts as per the scheme named ‘Genetic sequence’ in Catuneanu et al. (2009), where: TST = Transgressive Systems Tract, LLST = Late Lowstand Systems Tract, ELST = Early Lowstand Systems Tract and HST = Highstand Systems Tract. Sequence boundaries are indicated by the blue arrows between the HST and ELST and can be seen to be diachronous along the fault, i.e. occurring at a later time towards the centre of the fault than towards the fault tips. The sections of the relative sea level curve that each stage refers to is illustrated on the relative sea level curve at the top-left. A block diagram to show the setting of the plot is provided in Fig. 7. (For interpretation of the references to colour in this figure legend, the reader is referred to the web version of this article.)

The period of each progradational phase shortens towards the centre of the fault, and the period of each retrogradational phase shortens towards the fault tips. Weak retrogradation/aggradation occurs at the fault tips during relative sea level rise. In contrast, the eustatic sea level-dominated plot reveals laterally continuous patterns of alternating strong retrogradation and progradation as eustatic sea level varies through time. In comparison to the previous example (Fig. 10), the accommodation curve shows less along-strike variation due to the lesser influence of sedimentation in this underfilled scenario.

4.1.2. Field-based example: Alkyonides Basin

A modern analogue for this example is the partially-constrained, Holocene-active system surrounding the Psatha-Skinos-Alepori fault system in the Alkyonides Gulf, Greece. Here, sediment inputs have arisen from the relay zones of the fault system. An average sedimentation rate of 1.1 mm/yr (Collier et al., 2000; Bell et al., 2009), an average eustatic sea level rise rate of 5.8 mm/yr (70 m rise in 12 kyr; Collier et al., 2000), and an average hangingwall subsidence rate of 0.5–0.6 mm/yr established near the fault tips (Leeder et al., 2002) over the last 12 kyr have been constrained. This suggests that over the last 12 kyr the system has been eustatic sea level-dominated, and relatively sediment starved, with low subsidence approaching zero towards the fault tips, and as a result, the beach barriers extending from both fault tips are retrograding (Collier & Gawthorpe, 1995). This pattern is anticipated in the model results during the relative sea level rises of the eustatic sea level-dominated model (Fig. 11). With the exception of the possibility of fault tip propagation during this time, it is only this interplay of controls that allow significant retrogradation at the fault tips, in such a eustatically-dominated period such as the Late Quaternary. The sedimentary successions may exhibit greater retrogradation in areas with higher subsidence, such as the centre of the fault. This has been observed in a shallow piston core study from the hangingwall of the West Channel fault, at the western end of the Gulf of Corinth (Bell et al., 2009).

4.2. Sensitivity to varying subsidence rates

Depositional sequences are defined by the relative influence of the major sedimentary controls, and are influenced by the nature of that control through time. Three modelled examples with different subsidence histories demonstrate this (Fig. 12): an increasing subsidence rate (A), an episodic subsidence rate (B), and a decreasing subsidence rate (C). In each example, the same eustatic sea level and sedimentation models are used, hence any variations in the stacking patterns may be attributed solely to variations in subsidence. There is no pre-inherited accommodation. The plot in Fig. 12 is presented in configuration 1 of Fig. 2A.

The scenario with an increasing subsidence rate (Fig. 12A) reveals progressively longer periods of retrogradation and shorter progradational periods, particularly towards the centre of the fault where subsidence is maximal. Because subsidence rate increases through time, the system reveals more along-strike variation in stacking patterns. A scenario with six phases of subsidence (Fig. 12B) reveals a cyclic pattern with periods of progradation separated by periods of strong retrogradation, particularly near the fault centre. Each subsidence event is the same magnitude and duration. The effects of each subsidence event would be more strongly expressed in a scenario with a lower amplitude eustatic sea level signal, as here they are superimposed onto higher amplitude eustatic sea level variations through time. Dorsey and Umhoefer (2000) and Mortimer et al. (2005) attribute episodic, fault-controlled subsidence along the Loreto Fault as the principal control on the accumulation and timing of several fluvio-deltaic progradational units in the Central sub-basin of Loreto, Gulf of California. Each progradational unit is capped by a MFS, expressed as a shell bed. A MFS is predicted during the strong retrogradational periods in the model (Fig. 12B). In the third scenario (Fig. 12C), subsidence rate decreases to zero after 80% of the time has lapsed. This pattern of subsidence may represent a syn-to post-faulting transition, whereby a fault switches off

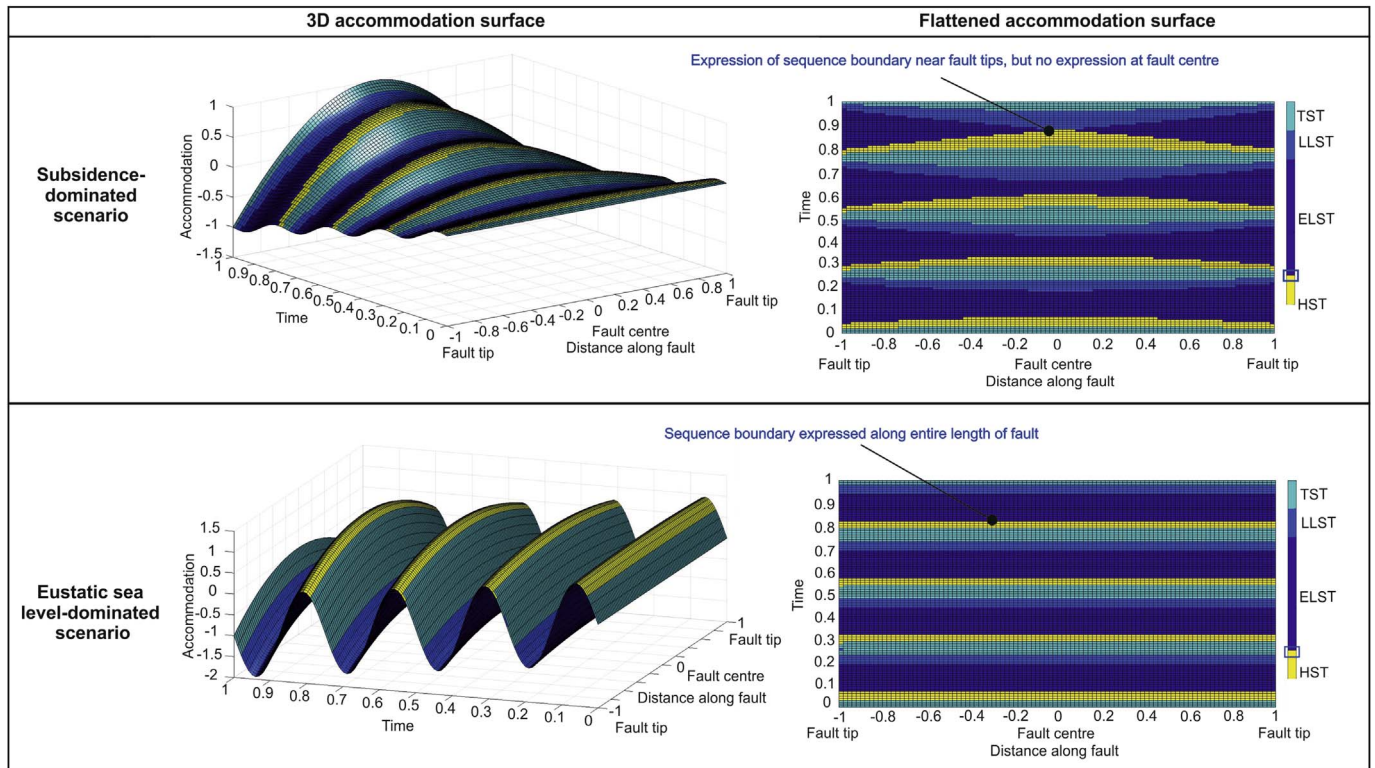


Fig. 10. Diagrams with systems tracts presented to show the difference between two contrasting conceptual scenarios with a high sediment supply: a subsidence-dominated (top) and eustatic sea level-dominated (bottom) system; analogous to the two sub-basins of the Piedras Rodadas Formation, Loreto Basin, Gulf of California. A 3D accommodation surface is shown for both cases with a flattened version adjacent. Both scenarios incorporate high sedimentation from the fault tips, simplified, sinusoidal eustatic sea level and an increasing subsidence rate through time. The rate of change of the dominating control is an order of magnitude higher than that of the subordinate control, in both cases. In the subsidence-dominated scenario, it is clear that each sequence boundary is diachronous and its expression is lost at the fault centre towards the end of the time-frame. In the eustatic sea level-dominated scenario, the sequence boundaries are expressed and are isochronous along the length of the fault.

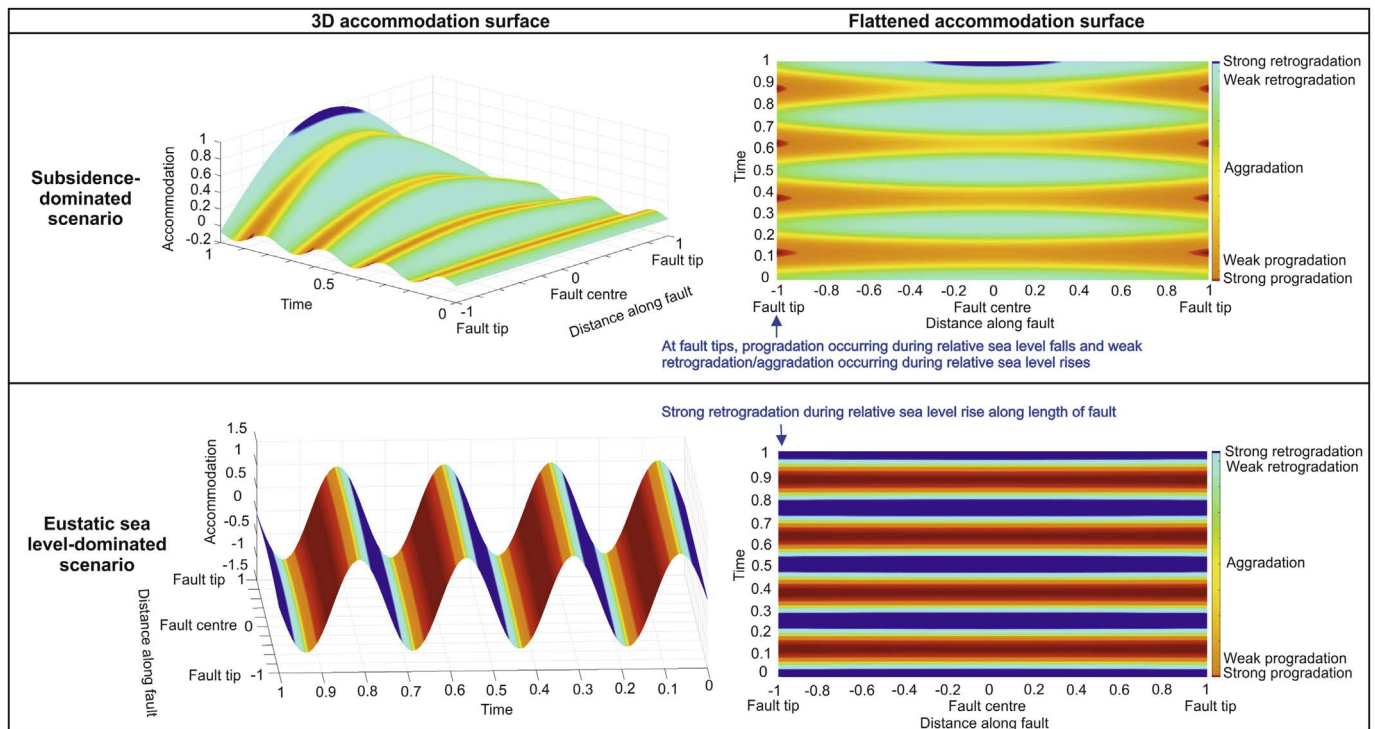


Fig. 11. Diagrams with stacking patterns presented to show the difference between two contrasting conceptual scenarios with a low sediment supply: a subsidence-dominated (top) and eustatic sea level-dominated (bottom) system; analogous to the Holocene-active system surrounding the Psatha-Skinos-Alepochori fault system, Alkyonides Gulf, Greece. A 3D accommodation surface is shown for both cases with a flattened version adjacent. Both scenarios incorporate low sedimentation from the fault tips, simplified, sinusoidal eustatic sea level and an increasing subsidence rate through time. The rate of change of the dominating control is an order of magnitude higher than that of the subordinate control in both cases. There is more along-strike variation in the subsidence-dominated scenario than the eustatic sea level-dominated scenario.

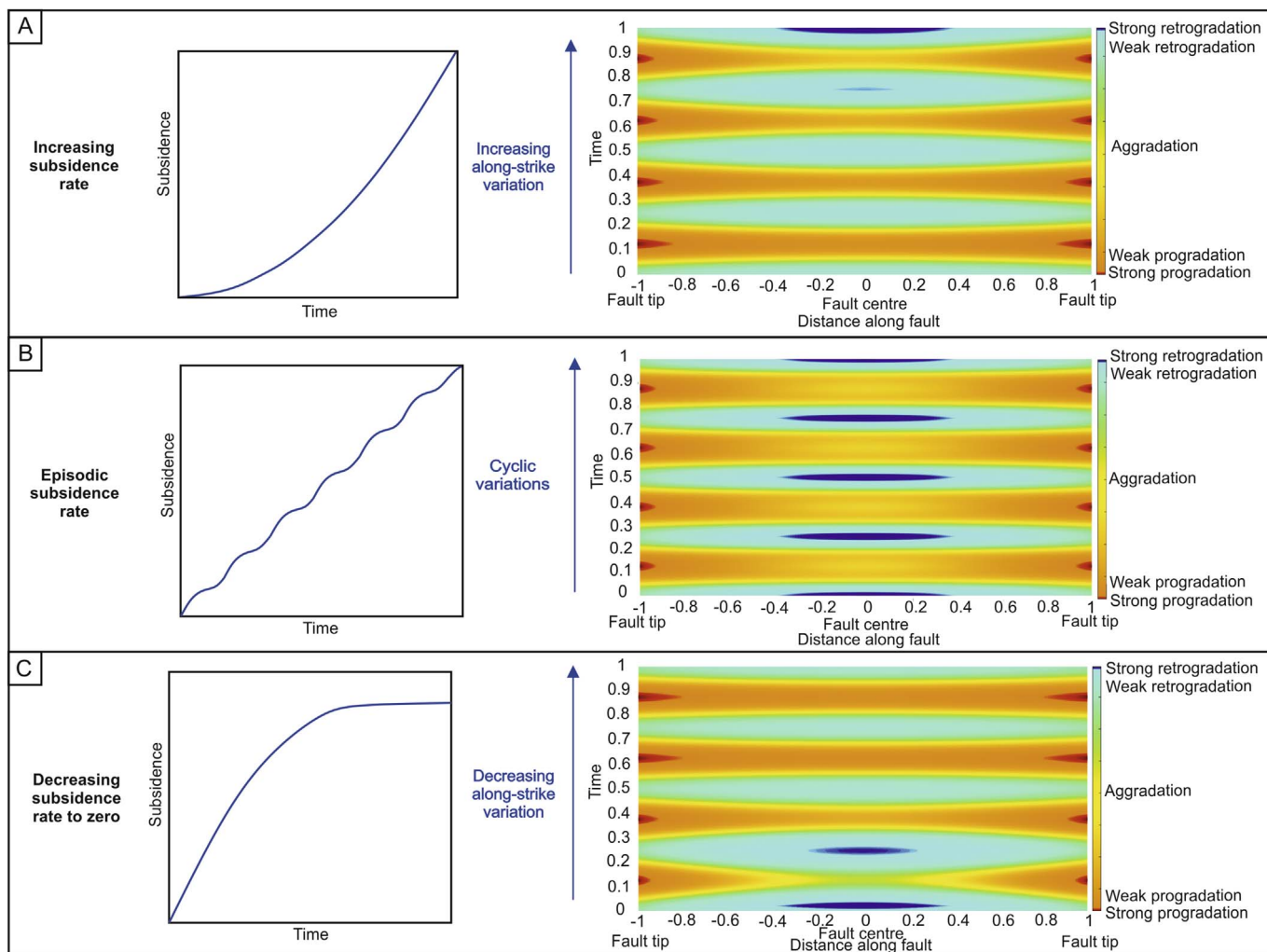


Fig. 12. Diagrams to show the variation in stacking patterns between three conceptual scenarios with different subsidence rate patterns: an increasing (A), episodic (B) and decelerating (C) subsidence rate. Graphs to show the subsidence input through time are presented on the left and flattened accommodation surfaces are presented on the right. The plots exhibit increasing along-strike variation through time, cyclic variations and decreasing along-strike variation through time, respectively.

as strain is taken up on an adjacent fault. The output largely shows the inverse of the first scenario, whereby longer periods of strong retrogradation near the fault centre are expressed initially when subsidence rates are highest, and these are suppressed through time with decreasing subsidence rate. Initially, there are marked along-strike variations in stacking patterns, but as subsidence decreases through time, eustatic sea level becomes increasingly dominant and the stacking patterns become more laterally continuous.

4.3. Sensitivity to varying sedimentation distribution

Spatial and temporal variations in sediment flux from drainage basins to sedimentary basins are hard to quantify, and have been less emphasised in sequence stratigraphic interpretations than accommodation-driven changes (Burgess, 2016). To assess the sensitivity of stacking to sedimentation patterns, three different sedimentation models are superimposed upon the same subsidence and eustatic sea level models in each case (Fig. 13 – in configuration 1 of Fig. 2A), in which subsidence is high and the amplitude of eustatic sea level change is an order of magnitude lower. The distribution of sedimentation along the fault is varied but the magnitude of maximum sedimentation (and rate) is the same in each scenario. With all other controls uniform between the tests, any changes observed in the nature of the SBs and MFSs may only be attributed to the sedimentation model. The three scenarios tested are: a system with equal sediment input from the fault tips (A), a

system with sediment input from one fault tip (B) and a system with sediment input from point sources that could represent fan deltas (C).

Fig. 13A utilises the sedimentation model with equal input from both fault tips. The sequence boundaries are highlighted and it can be seen that they are diachronous due to the combined influence of laterally variable subsidence and sedimentation. As a result of sedimentation being equal from both fault tips, the diachroneity of the sequence boundaries is symmetrical over the centre of the fault. Conversely, where sedimentation occurs from one fault tip (Fig. 13B), the nature of the sequence boundaries is not symmetrical over the centre of the fault. The side that experiences the most sedimentation expresses *more prominent diachroneity* of sequence boundaries than the sediment-starved side, where they are isochronous. At the fault tip with sediment input, the sediment supply counteracts the effects of relative sea level rise because the space that is being created is being filled. It promotes the relative sea level fall and progradation. This effect decreases towards the centre of the fault, away from the sediment source, enhancing the along-strike diachroneity. On the side of the fault where there is no sediment source, the sequence boundaries are influenced only by eustasy and decreasing subsidence towards the fault tip. The 3D accommodation surface illustrates the decreasing accommodation on the sediment-rich side through time, whereas accommodation on the sediment-starved side varies only with eustatic sea level.

In the scenario with sedimentation from five point sources (Fig. 13C), the amount of sedimentation and degree of dispersal is equal

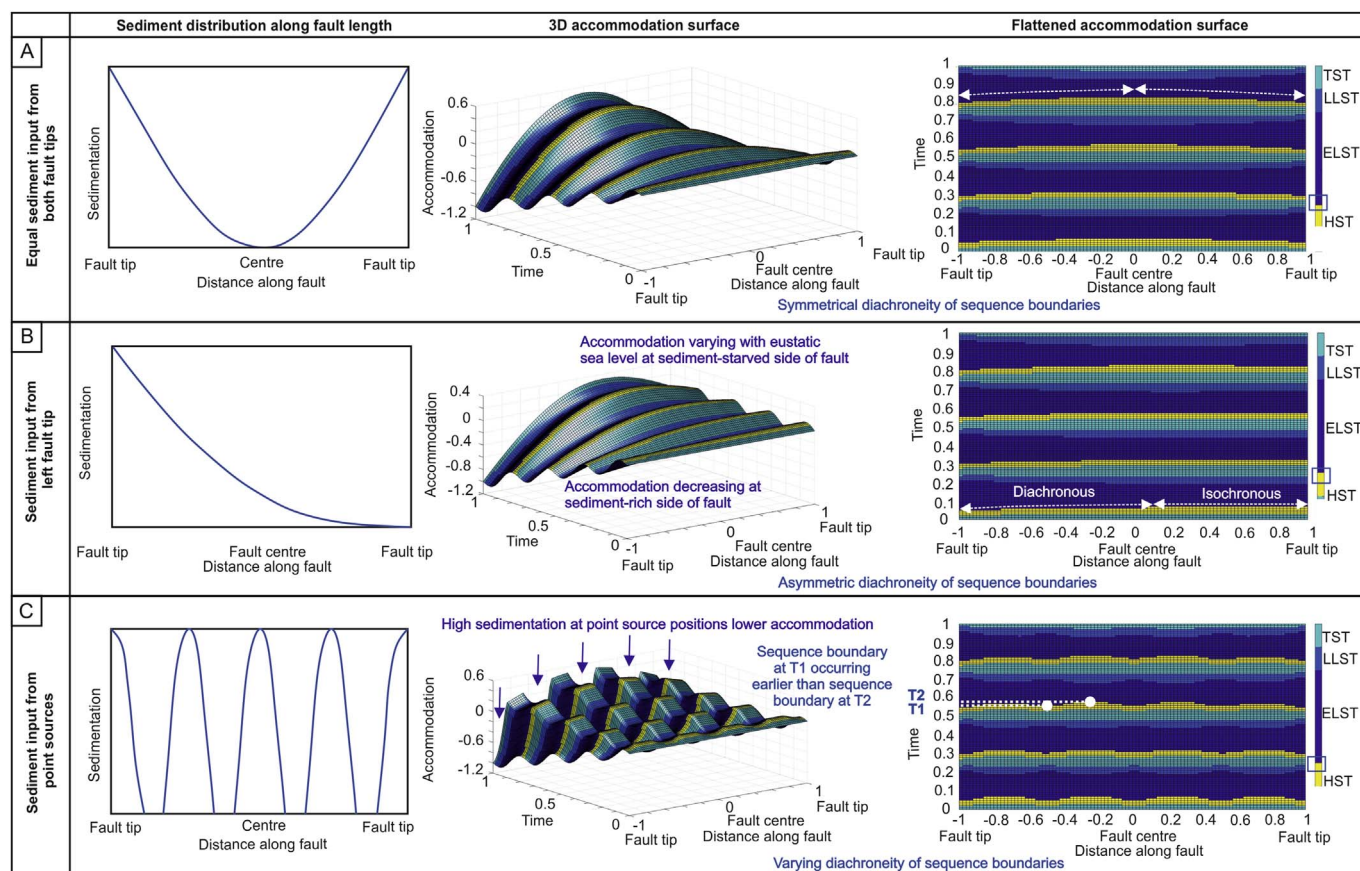


Fig. 13. Diagrams with systems tracts presented to show differences between three conceptual scenarios with different sedimentation distribution patterns along the fault length: equal input from both fault tips (A), input from left fault tip (B) and point sources (C). Graphs to show the sedimentation input along the fault length (left), output 3D accommodation surfaces (middle) and flattened accommodation surfaces (right) are presented. The nature of diachroneity of sequence boundaries varies in each scenario, as labelled in white.

from each source. The plot shows a reduction in accommodation where the point sources are located, hence the irregular shape of the surface. The sequence boundaries are highlighted in the flattened plot and their *degree of diachroneity* varies along the fault length. For example, the sequence boundary occurs earlier where the point sources (T1 in Fig. 13) are located than it does in the areas between them (T2 in Fig. 13). These scenarios support the inference that temporal and spatial changes in sediment supply need to be considered when making sequence stratigraphic interpretations, as well as accommodation changes from eustasy and tectonics that are usually emphasised.

4.4. Implications and applications for subsurface appraisal

During hydrocarbon prospect appraisal and static model generation, key stratigraphic surfaces, such as the MFS and SB, are used to correlate between wells, with the assumption that they are isochronous surfaces. However, recent studies have shown that such surfaces are time transgressive in a range of environments (e.g. Holbrook and Bhattacharya, 2012; Burgess and Prince, 2015; Hodgson et al., 2016; Madof et al., 2016). Here, we not only demonstrate that such surfaces are diachronous along the length of syn-rift faults due to along-strike variation in both sedimentation and subsidence, but also demonstrate the *nature* of that diachroneity. In the case of the MFS, which likely forms part of the seal to a hydrocarbon reservoir, understanding the temporal relationships along-strike of a fault are of critical importance for hydrocarbon volume calculations and production rate predictions. When the MFS is used for correlation, care should be taken when choosing the representative position on the relative sea level curve, or which sequence stratigraphic scheme to adopt because the nature of

diachroneity varies between the different positions. Consider a comparison between two options for MFS position choice: 1) the position between TST and HST, following the ‘genetic sequence’ scheme, 2) the position between LLST and TST (the initial transgressive surface). Both surfaces are diachronous along the fault, but the nature of that diachroneity is different between them, with the former occurring *later* at the centre of the fault than at the fault tips (Fig. 8), and the latter occurring *earlier* towards the centre of the fault than at the fault tips. This difference could be important for trap-seal analysis, where understanding the variability of the shale intervals caused by the MFS in time and space is fundamental. Syn-Strat allows the user to visualise such variations qualitatively and to quantify the variations for a given magnitude of each control. The model also permits flexibility on timing and duration of dominance of one control to the other and thus allows an iterative approach to sequence stratigraphic tests when constraining controlling parameters. Producing a solid foundation to which process-based models can be applied is crucial for prediction of large-scale stacking in complex settings. The Syn-Strat model approach is particularly useful for low-resolution datasets, such as seismic, where small-scale depositional characteristics are not readily apparent. It allows insight into the way a system responds to particular controls and shows the differences by making spatial and temporal adjustments to those controls. An assessment of all the possible outcomes from a particular setting allows the stratigrapher to obtain the best understanding of the controls in play. If a good correspondence is made between the data and the model in one area, the model may then be used to anticipate the potential stacking further along-strike or down-dip, in the absence of good quality data.

5. Conclusion

Syn-Strat, a novel 3D sequence stratigraphic forward model, is presented that introduces both temporally- and spatially-variable tectonic components to sequence stratigraphic modelling. The model provides a framework to which process-based models could be applied and provides the scope to test multiple scenarios where the controlling parameters are poorly constrained. Syn-Strat considers along-strike, down-dip and time variability in sequence architecture on a fault segment-scale and can be used to improve interpretation and prediction of syn-rift depositional architectures, which are the focus of exploration in a number of hydrocarbon basins, by constraining system response to any combination of autogenic controls.

By calculating accommodation in three dimensions, Syn-Strat is able to demonstrate the sensitivity of sequence architecture to laterally variable tectonic constraints and different relative magnitudes of allo-genic controls. A basin largely modified by faulting will exhibit different depositional architecture to one dominated by eustasy, and the model outputs demonstrate *how* this difference is expressed in terms of stacking patterns and stratigraphic surfaces. The model has demonstrated the potential for analysis of along-strike variations in stacking patterns due to different subsidence rate characteristics, and the nature of diachroneity of key stratigraphic surfaces as a result of different sedimentation distribution models. Stratigraphic surfaces are known to be diachronous in these settings. However, understanding *how* the diachroneity of these surfaces changes spatially represents a significant step forward for petroleum system interpretations, where such surfaces may represent bypass zones or stratigraphic traps seals and are heavily relied upon for well correlations, and hence reservoir connectivity and production rate predictions. Additionally, the ability to understand how stacking patterns vary spatially and temporally is highly valuable in areas with little data constraint. Such variation is visualised in the sensitivity tests presented in this paper that are tied to field analogues, but in the future may be constrained with quantitative data from real input parameters.

Acknowledgements

We thank the project sponsor, Engie that support the SMRG (Shallow Marine Research Group). We also thank the two reviewers and the editor, Professor Massimo Zecchin for their contribution; the manuscript has benefited from their insights and comments.

References

- Allen, P.A., Armitage, J.J., Carter, A., Duller, R.A., Michael, N.A., Sinclair, H.D., Whitchurch, A.L., Whittaker, A.C., 2013. The Q_s problem: sediment volumetric balance of proximal foreland basin systems. *Sedimentology* 60, 102–130.
- Bell, R.E., McNeill, L.C., Bull, J.M., Henstock, T.J., Collier, R.E.L.I., Leeder, M.R., 2009. Fault architecture, basin structure and evolution of the Gulf of Corinth Rift, Central Greece. *Basin Res.* 21, 824–855.
- Blanchon, P., Shaw, J., 1995. Reef drowning during the last deglaciation: evidence for catastrophic sea-level rise and ice-sheet collapse. *Geology* 23, 4–8.
- Burgess, P.M., 2016. The future of the sequence stratigraphy paradigm: dealing with a variable third dimension. *Geology* 44, 335–336.
- Burgess, P.M., Allen, P.A., 1996. A forward-modelling analysis of the controls on sequence stratigraphical geometries. *Geol. Soc. Lond. Spec. Publ.* 103, 9–24.
- Burgess, P.M., Prince, G.D., 2015. Non-unique stratal geometries: implications for sequence stratigraphic interpretations. *Basin Res.* 27, 351–365.
- Catuneanu, O., 2002. Sequence stratigraphy of clastic systems: concepts, merits, and pitfalls. *J. Afr. Earth Sci.* 35, 1–43.
- Catuneanu, O., 2006. *Principles of Sequence Stratigraphy*, first ed. Elsevier, Amsterdam.
- Catuneanu, O., Abreu, V., Bhattacharya, J.P., Blum, M.D., Dalrymple, R.W., Eriksson, P.G., Fielding, C.R., Fisher, W.L., Galloway, W.E., Gibling, M.R., Giles, K.A., Holbrook, J.M., Jordan, R., Kendall, C.G.S.T.C., Macurda, B., Martinsen, O.J., Miall, A.D., Neal, J.E., Nummedal, D., Pomar, L., Posamentier, H.W., Pratt, B.R., Sarg, J.F., Shanley, K.W., Steel, R.J., Strasser, A., Tucker, M.E., Winker, C., 2009. Towards the standardization of sequence stratigraphy. *Earth Sci. Rev.* 92, 1–33.
- Childs, C., Nicol, A., Walsh, J.J., Watterson, J., 2003. The growth and propagation of synsedimentary faults. *J. Struct. Geol.* 25, 633–648.
- Colella, A., 1988a. Fault-controlled marine Gilbert-type fan deltas. *Geology* 16, 1031–1034.
- Colella, A., 1988b. Pliocene-Holocene fan deltas and braid deltas in the Crati Basin, southern Italy: a consequence of varying tectonic. In: Nemeç, W., Steel, R.J. (Eds.), *Fan Deltas: Sedimentology and Tectonic Settings*. Blackie and Son, Glasgow and London, pp. 50–74.
- Colella, A., 1988c. Gilbert-type fan deltas in the Crati Basin (Pliocene-Holocene, southern Italy). In: Colella, A. (Ed.), *International Workshop on Fan Deltas*. Calabria, Italy 1988. Excursion Guidebook, Calabria, Italy, pp. 19–77.
- Colella, A., De Boer, P.L., Nio, S.D., 1987. Sedimentology of a marine intermontane Pleistocene Gilbert-type fan delta complex in the Crati Basin, Calabria, Southern Italy. *Sedimentology* 34, 721–736.
- Collier, R.E.L.I., Gawthorpe, R.L.I., 1995. Neotectonics, drainage and sedimentation in central Greece: insights into coastal reservoir geometries in syn-rift sequences. In: Lambiase, J.J. (Ed.), *Hydrocarbon Habitat in Rift Basins*. vol. 80. Geological Society Special Publications, pp. 165–181.
- Collier, R.E.L.I., Leeder, M.R., Trout, M., Ferentinos, G., Lyberis, E., Papatheodorou, G., 2000. High sediment yields and cool, wet winters: test of last glacial palaeoclimates in the Northern Mediterranean. *Geology* 28, 999–1002.
- Cowie, P.A., Scholz, C.H., 1992. Physical explanation for displacement-length relationship for faults using a post-yield fracture mechanics model. *J. Struct. Geol.* 14, 1133–1148.
- Cowie, P.A., Gupta, S., Dawers, N.H., 2000. Implications of fault array evolution for synrift depocentre development: insights from a numerical fault growth model. *Basin Res.* 12, 241–261.
- Cross, T.A., 1988. Controls on coal distribution in transgressive-regressive cycles, upper cretaceous, western interior, U.S.A. In: Wilgus, C.K., Hastings, B.S., Kendall, C.G.S.T.C., Posamentier, H.W., Ross, C.A., Van Wagoner, J.C. (Eds.), *Sea Level Changes: an Integrated Approach*. Soc. Econ. Palaeontol. Mineral, vol. 42. Special Publication, pp. 371–380.
- Dorsey, R.J., Umhoefer, P.J., 2000. Tectonic and eustatic controls on sequence stratigraphy of the Pliocene Loreto Basin, Baja California Sur, Mexico. *GSA Bull.* 112, 177–199.
- Dorsey, R.J., Umhoefer, P.J., Renne, P.R., 1995. Rapid subsidence and stacked gilbert-type fan deltas, Pliocene Loreto Basin, Baja California Sur, Mexico. *Sediment. Geol.* 98, 181–204.
- Flemings, P.B., Grotzinger, J.P., 1996. STRATA: freeware for analysing classic stratigraphic problems. *GSA Today* 6, 1–7.
- Frazier, D., 1974. Depositional Episodes: Their Relationship to the Quaternary Stratigraphic Framework in the Northwestern Portion of the Gulf Basin. Bureau of Economic Geology, University of Texas, pp. 26 Geological Circular 74-1.
- Galloway, W.L., 1989. Genetic stratigraphic sequences in basin analysis I: architecture and genesis of flooding surface bounded depositional units. *AAPG Bull.* 73, 125–142.
- Gawthorpe, R.L., Fraser, A., Collier, R.E.L.I., 1994. Sequence stratigraphy in active extensional basins: implications for the interpretation of ancient basin fills. *Mar. Petrol. Geol.* 11, 642–658.
- Gawthorpe, R.L., Leeder, M.R., 2000. Tectono-sedimentary evolution of active extensional basins. *Basin Res.* 12, 195–218.
- Gawthorpe, R.L., Sharp, I., Underhill, J.R., Gupta, S., 1997. Linked sequence stratigraphic and structural evolution of propagating normal faults. *Geology* 25, 795–798.
- Gawthorpe, R.L., Hardy, S., Ritchie, B., 2003. Numerical modelling of depositional sequences in half-graben rift basins. *Sedimentology* 50, 169–185.
- Granjeon, D., Joseph, P., 1999. Concepts and applications of a 3D multiple lithology, diffusive model in stratigraphic modeling. In: Harbaugh, J.W., Watney, W.L., Rankey, E.C., Slingerland, R., Goldstein, R.H., Franseen, E.K. (Eds.), *Numerical Experiments in Stratigraphy: Recent Advances in Stratigraphic and Sedimentological Computer Simulations*. vol. 62. SEPM Special Publication, pp. 197–210.
- Gupta, S., Cowie, P.A., Dawers, N.H., Underhill, J.R., 1998. A mechanism to explain rift-basin subsidence and stratigraphic patterns through fault-array evolution. *Geology* 26, 595–598.
- Gupta, S., Underhill, J.R., Sharp, I.R., Gawthorpe, R.L., 1999. Role of fault interactions in controlling synrift sediment dispersal patterns: miocene, Abu Alaq group, Suez Rift, Sinai, Egypt. *Basin Res.* 11, 167–189.
- Hack, J.T., 1957. US Geological Survey Prof. Pape.. Studies of Longitudinal Stream Profiles in Virginia and Maryland, vol. 294.
- Hardy, S., Gawthorpe, R.L., 1998. Effects of variations in fault slip rate on sequence stratigraphy in fan deltas: insights from numerical modeling. *Geology* 26, 911–914.
- Hardy, S., Gawthorpe, R.L., 2002. Normal fault control on bedrock channel incision and sediment supply: insights from numerical modeling. *J. Geophys. Res.* 107 2246.
- Hardy, S., Dart, C.J., Waltham, D., 1994. Computer modelling of the influence of tectonics on sequence architecture of coarse-grained fan deltas. *Mar. Petrol. Geol.* 11, 561–574.
- Hodgson, D.M., Kane, I.A., Flint, S.S., Brunt, R.L., Ortiz-Karpp, A., 2016. Time-transgressive confinement on the slope and the progradation of basin-floor fans: implications for the sequence stratigraphy of deep-water deposits. *J. Sediment. Res.* 86, 73–86.
- Holbrook, J.M., Bhattacharya, J.P., 2012. Reappraisal of the sequence boundary in time and space: case and considerations for an SU (subaerial unconformity) that is not a sediment bypass surface, a time barrier, or an unconformity. *Earth Sci. Rev.* 113, 271–302.
- Huang, X., Griffiths, C.M., Liu, J., 2015. Recent development in stratigraphic forward modelling and its application in petroleum exploration. *Aust. J. Earth Sci.* 62, 903–919.
- Jackson, C.A.L., Gawthorpe, R.L., Carr, I.D., Sharp, I.R., 2005. Normal faulting as a control on the stratigraphic development of shallow marine syn-rift sequences: the Nukhul and Lower Rudeis Formations, Hammam Faraun fault block, Suez Rift, Egypt. *Sedimentology* 52, 313–338.
- Jackson, C.A.-L., Rotevatn, A., 2013. 3D seismic analysis of the structure and evolution of a salt-influenced normal fault zone: a test of competing fault growth models. *J. Struct.*

- Geol. 54, 215–234.
- Jackson, C.A.-L., Bell, R.E., Rotevatn, A., Tvedt, A.B.M., 2017. Techniques to determine the kinematics of syn-sedimentary normal faults and implications for fault growth models. In: Childs, C., Holdsworth, R.E., Jackson, C.A.-L., Manzocchi, T., Walsh, J.J., Yielding, G. (Eds.), *The Geometry and Growth of Normal Faults*. Geological Society, London, Special Publications, pp. 187–217 439.
- Jervey, M.T., 1988. Quantitative geological modeling of siliciclastic rock sequences and their seismic expression. In: Wilgus, C.K., Hastings, B.S., Kendall, C.G.St.C., Posamentier, H.W., Ross, C.A., Van Wagoner, J.C. (Eds.), *Sea-level Changes: an Integrated Approach*, vol. 42. SEPM Special Publications, pp. 47–69.
- Leeder, M.R., Gawthorpe, R.L., 1987. Sedimentary models for extensional tilt-block/half-graben basins. In: Coward, M.P., Dewey, J.F., Hancock, P.L. (Eds.), *Continental Extensional Tectonics*, vol. 28. Geological Society, London, Special Publications, pp. 139–152.
- Leeder, M.R., Collier, R.E.L.L., Abdul Aziz, L.H., Trout, M., Ferentinos, G., Papatheodorou, G., Lyberis, E., 2002. Tectono-sedimentary processes along an active marine/lacustrine half-graben margin: Alkyonides Gulf, E. Gulf of Corinth, Greece. *Basin Res.* 14, 25–41.
- Madof, A.S., Harris, A.D., Connell, S.D., 2016. Nearshore along-strike variability: is the concept of the systems tracts unhinged? *Geology* 44, 319–322.
- Martinsen, O.J., Helland-Hansen, W., 1995. Strike variability of clastic depositional systems: does it matter for sequence stratigraphic analysis? *Geology* 23, 439–442.
- Mitchum Jr., R.M., Vail, P.R., Thompson III, S., 1977. Seismic stratigraphy and global changes of sea-level, Part 2: the depositional sequence as a basic unit for stratigraphic analysis. In: In: Payton, C.E. (Ed.), *Seismic Stratigraphy—applications to Hydrocarbon Exploration*, vol. 26. American Association of Petroleum Geologists Memoir, pp. 53–62.
- Mortimer, E., Gupta, S., Cowie, P., 2005. Clinoform nucleation and growth in coarse-grained deltas, Loreto Basin, Baja California Sur, Mexico: a response to episodic accelerations in fault displacement. *Basin Res.* 17, 337–359.
- Mullenbach, B.L., Nittroer, C.A., 2006. Decadal record of sediment export to the deep sea via Eel Canyon. *Cont. Shelf Res.* 26, 2157–2177.
- Muto, T., Steel, R.J., 2000. The accommodation concept in sequence stratigraphy: some dimensional problems and possible redefinition. *Sediment. Geol.* 130, 1–10.
- Neal, J., Abreu, V., 2009. Sequence stratigraphy hierarchy and the accommodation succession method. *Geology* 37, 779–782.
- Neal, J.E., Abreu, V., Bohacs, K.M., Feldman, H.R., Pederson, K.H., 2016. Accommodation succession sequence stratigraphy: observational method, utility, and insights into sequence boundary formation. *J. Geol. Soc. Lond.* 173, 803–816.
- Nicol, A., Childs, C., Walsh, J.J., Manzocchi, T., Schöpfer, M.P.J., 2017. Interactions and growth of faults in an outcrop-scale system. In: Childs, C., Holdsworth, R.E., Jackson, C.A.-L., Manzocchi, T., Walsh, J.J., Yielding, G. (Eds.), *The Geometry and Growth of Normal Faults*. Geological Society, London, Special Publications, pp. 23–29 439.
- Posamentier, H.W., Vail, P.R., 1988. Eustatic controls on clastic deposition II—sequence and systems tracts models. In: Wilgus, C.K., Hastings, B.S., Kendall, C.G.St.C., Posamentier, H.W., Ross, C.A., Van Wagoner, J.C. (Eds.), *Sea-level Changes: an Integrated Approach*, vol. 42. SEPM Special Publications, pp. 125–154.
- Posamentier, H.W., Jervey, M.T., Vail, P.R., 1988. Eustatic controls on clastic deposition I—conceptual framework. In: Wilgus, C.K., Hastings, B.S., Kendall, C.G.St.C., Posamentier, H.W., Ross, C.A., Van Wagoner, J.C. (Eds.), *Sea-level Changes: an Integrated Approach*, vol. 42. SEPM Special Publications, pp. 109–124.
- Posamentier, H.W., Allen, G.P., 1999. Siliciclastic sequence stratigraphy; sequence stratigraphy: concepts and applications. *SEPM Concepts Sedimentol. Paleontol.* 7, 210.
- Posamentier, H.W., Weimer, P., 1993. Siliciclastic sequence stratigraphy and petroleum geology—where to from here? *AAPG Bull.* 77, 731–742.
- Poulimmenos, G., Zelilidis, A., Kontopoulos, N., Doutsos, T., 1993. Geometry of trapezoidal fan deltas and their relationship to extensional faulting along the south-western active margins of the Corinth rift. *Basin Res.* 5, 179–192.
- Ravnås, R., Steel, R.J., 1998. Architecture of marine rift-basin successions. *AAPG Bull.* 82, 110–146.
- Raymo, M.E., Hodell, D., Jansen, E., 1992. Response of deep ocean circulation to initiation of Northern Hemisphere glaciation (3–2 Ma). *Paleoceanography* 7, 645–672.
- Ritchie, B.D., Hardy, S., Gawthorpe, R.L., 1999. Three dimensional numerical modeling of coarse-grained clastic deposition in sedimentary basins. *J. Geophys. Res.* 104, 17759–17780.
- Rivanes, J.C., 1992. Application of a dual-lithology, depth-dependent diffusion equation in stratigraphic simulation. *Basin Res.* 4, 133–146.
- Romans, B.W., Castellort, S., Covault, J.A., Fildani, A., Walsh, J.P., 2016. Environmental signal propagation in sedimentary systems across timescales. *Earth Sci. Rev.* 153, 7–29.
- Romans, B.W., Normark, W.R., McGann, M.M., Covault, J.A., Graham, S.A., 2009. Coarse-grained sediment delivery and distribution in the Holocene Santa Monica Basin, California: implications for evaluating source-to-sink flux at millennial time scales. *Geol. Soc. Am. Bull.* 121, 1394–1408.
- Schlagenhauf, A., Manighetti, I., Malavieille, J., Dominguez, S., 2008. Incremental growth of normal faults: insights from a laser-equipped analog experiment. *Earth Planet. Sci. Lett.* 273, 299–311.
- Sloss, L.L., 1962. Stratigraphic models in exploration. *J. Sediment. Res.* 32, 415–422.
- Sloss, L.L., 1991. The tectonic factor in sea-level change: a countervailing view. *J. Sediment. Res.* 96, 6609–6617.
- Stein, R.S., Barrientos, S.E., 1985. Planar high-angle faulting in the basin and range' geodetic analysis of the 1983 Borah Peak, Idaho, earthquake. *J. Geophys. Res.* 90, 11355–11366.
- Stevenson, C.J., Jackson, C.A.L., Hodgson, D.M., Hubbard, S.M., Eggenhuisen, J.T., 2015. Deep-water sediment bypass. *J. Sediment. Res.* 85, 1058–1081.
- Umhoefer, P.J., Dorsey, R.J., Renne, P., 1994. Tectonics of the Pliocene Loreto Basin, Baja California Sur, Mexico, and evolution of the Gulf of California. *Geology* 22, 649–652.
- Vail, P.R., Mitchum Jr., R.M., Thompson III, S., 1977. Seismic stratigraphy and global changes of sea level, part 3: relative changes of sea level from coastal onlap. In: In: Payton, C.E. (Ed.), *Seismic Stratigraphy-applications to Hydrocarbon Exploration*, vol. 26. AAPG, Memoirs, pp. 63–81.
- Van Wagoner, J.C., Posamentier, H.W., Mitchum, R.M., Vail, P.R., Sarg, J.F., Loutit, T.S., Hardenbol, J., 1988. An overview of the fundamentals of sequence stratigraphy and key definitions. In: Wilgus, C.K., Hastings, B.S., Kendall, C.G.St.C., Posamentier, H.W., Ross, C.A., Van Wagoner, J.C. (Eds.), *Sea-level Changes: an Integrated Approach*, vol. 42. SEPM Special Publications, pp. 39–45.
- Walsh, J.J., Nicol, A., Childs, C., 2002. An alternative model for the growth of faults. *J. Struct. Geol.* 24, 1669–1675.
- Walsh, J.J., Bailey, W.R., Childs, C., Nicol, A., Bonson, C.G., 2003. Formation of segmented normal faults: a 3-D perspective. *J. Struct. Geol.* 25, 1251–1262.
- Warrick, J.A., 2014. Eel River margin source-to-sink sediment budgets: revisited. *Mar. Geol.* 351, 25–37.
- Wheeler, H.E., Murray, H.H., 1957. Base level control patterns in cyclothem sedimentation. *Am. Assoc. Petrol. Geol. Bull.* 41, 1985–2011.
- Wheeler, H.E., 1958. Time stratigraphy. *Am. Assoc. Petrol. Geol. Bull.* 42, 1047–1063.
- Wheeler, H.E., 1959. Unconformity bounded units in stratigraphy. *Am. Assoc. Petrol. Geol. Bull.* 43, 1975–1977.
- Wheeler, H.E., 1964. Base level, lithosphere surface, and time stratigraphy. *Geol. Soc. Am. Bull.* 75, 599–610.
- Young, M.J., Gawthorpe, R.L., Sharp, I.R., 2002. Architecture and evolution of the syn-rift clastic depositional systems towards the tip of major fault segment, Suez Rift, Egypt. *Basin Res.* 14, 1–23.

Quantifying faulting and base level controls on syn-rift sedimentation using stratigraphic architectures of coeval, adjacent Early-Middle Pleistocene fan deltas in Lake Corinth, Greece

Bonita J. Barrett¹  | Richard E. LL. Collier¹  | David M. Hodgson¹  |
Robert L. Gawthorpe²  | Robert M. Dorrell³  | Timothy M. Cullen¹ 

¹School of Earth & Environment, University of Leeds, Leeds, UK

²Department of Earth Science, University of Bergen, Bergen, Norway

³Energy and Environment Institute, University of Hull, Hull, UK

Correspondence

Bonita J. Barrett, School of Earth & Environment, University of Leeds, Leeds, UK.

Email: eebbca@leeds.ac.uk

Abstract

Quantification of allogenic controls in rift basin-fills requires analysis of multiple depositional systems because of marked along-strike changes in depositional architecture. Here, we compare two coeval Early-Middle Pleistocene syn-rift fan deltas that sit 6 km apart in the hangingwall of the Pirgaki-Mamoussia Fault, along the southern margin of the Gulf of Corinth, Greece. The Selinous fan delta is located near the fault tip and the Kerinitis fan delta towards the fault centre. Selinous and Kerinitis have comparable overall aggradational stacking patterns. Selinous comprises 15 cyclic stratal units (ca. 25 m thick), whereas at Kerinitis 11 (ca. 60 m thick) are present. Eight facies associations are identified. Fluvial and shallow water facies dominate the major stratal units in the topset region, with shelfal fine-grained facies constituting ca. 2 m thick intervals between major topset units and thick conglomeratic foresets building down-dip. It is possible to quantify delta build times (Selinous: 615 kyr; Kerinitis: >450 kyr) and average subsidence and equivalent sedimentation rates (Selinous: 0.65 m/kyr; Kerinitis: >1.77 m/kyr). The presence of sequence boundaries at Selinous, but their absence at Kerinitis, enables sensitivity analysis of the most uncertain variables using a numerical model, 'Syn-Strat', supported by an independent unit thickness extrapolation method. Our study has three broad outcomes: (a) the first estimate of lake level change amplitude in Lake Corinth for the Early-Middle Pleistocene (10–15 m), which can aid regional palaeoclimate studies and inform broader climate-system models; (b) demonstration of two complementary methods to quantify faulting and base level signals in the stratigraphic record—forward modelling with Syn-Strat and a unit thickness extrapolation—which can be applied to other rift basin-fills; and (c) a quantitative approach to the analysis of stacking patterns and key surfaces that could be applied to stratigraphic pinch-out assessment and cross-hole correlations in reservoir analysis.

KEYWORDS

forward modelling, Gilbert-type fan deltas, Gulf of Corinth, rift basin, sequence stratigraphy, syn-rift sedimentation, tectonics and sedimentation

1 | INTRODUCTION

Distinguishing faulting, sediment supply and base level signals and quantifying these basin controls in an active rift setting remains problematic, particularly due to along-strike variability in depositional architecture. Characterisation of multiple coeval depositional systems within the same rift basin is required to resolve the record of each control. Syn-rift, Gilbert-type fan deltas (Gilbert, 1885, 1890) provide an ideal record of stratigraphic evolution to achieve this due to their position adjacent to normal growth faults, with high and variable sediment supply rates derived from independent drainage catchments. However, most previous studies focus on single systems, rather than multiple, along-strike spatially distributed deltas (e.g. Backert, Ford, & Malartre, 2010; Dart, Collier, Gawthorpe, Keller, & Nichols, 1994; Dorsey, Umhoefer, & Renne, 1995; Ford, Williams, Malartre, & Popescu, 2007; Garcia-Garcia, Fernandez, Viseras, & Soria, 2006; Garcia-Mondéjar, 1990; Mortimer, Gupta, & Cowie, 2005).

Previous work on the stratigraphic record around normal faults at rifted margins has focussed on the theoretical aspects of sequence development from the interplay of controls in these areas. Leeder and Gawthorpe (1987) assessed the influence of tectonically-induced slopes on facies models. Variation in stacking patterns and sequence stratigraphic surfaces across rift settings (Gawthorpe, Fraser, & Collier, 1994) and as a result of propagating normal faults (Gawthorpe, Sharp, Underhill, & Gupta, 1997) became the later focus. An influential series of conceptual models for tectono-sedimentary evolution in extensional basins was presented by Gawthorpe and Leeder (2000). Eustasy/base level, tectonics and sedimentation influence the nature of sedimentary stacking through the accommodation/supply ratio (Jervey, 1988; Neal & Abreu, 2009) as eustasy and tectonic subsidence act to control space available for deposition (A) and sedimentation fills that space (S). Numerical modelling has supported understanding of rift basin sequence stratigraphy, particularly as simplified tectonic constraints were introduced into forward models (Jervey, 1988; Hardy, Dart, & Waltham, 1994; Hardy & Gawthorpe, 1998, 2002; Ritchie, Hardy, & Gawthorpe, 1999) and stratigraphic surfaces were shown to be limited in spatial extent (Gawthorpe, Hardy, & Ritchie, 2003; Jackson, Gawthorpe, Carr, & Sharp, 2005). Barrett, Hodgson, Collier, and Dorrell (2018) demonstrate and quantify the three-dimensional and along-strike variability in sequence architecture and diachroneity of stratigraphic surfaces in hangingwall fault blocks, using sensitivity tests with a 3D sequence stratigraphic

Highlights

- Integrated field and numerical modelling study of along-fault-strike fan delta stratigraphic architectures
- Two complementary methods to discern and quantify faulting and base level signals in the stratigraphic record
- Quantitative and widely applicable approach to the analysis of stacking and surfaces, constrained by field data
- Application to stratigraphic pinch out assessment and cross-hole correlations in reservoir analysis
- First estimate of lake level change amplitude in Lake Corinth for the Early-Middle Pleistocene (10–15 m)

forward model, 'Syn-Strat'. Complementary field studies have shown that sequence boundary development is best expressed at fault tip regions (Dorsey & Umhoefer, 2000—Loreto Basin) and the observed stratigraphic cyclicity has been attributed to fault-related subsidence events (Dorsey et al., 1995—Loreto Basin) and climatic forcing (Dart et al., 1994; Backert et al., 2010—Gulf of Corinth). Marked differences occur in the sequence stratigraphy of two coeval fan deltas 50 km apart, due to contrasting tectonic controls between footwall (Kryoneri) and hangingwall (Kerinitis) sites (Gawthorpe, Andrews, et al., 2017). However, along-strike and down-dip variation on smaller length-scales (<10 km) within the same hangingwall basin has not yet been attempted. Furthermore, quantification of tectonism, base level and sedimentation signals is also lacking. This is because isolating these controls is difficult, yet is critical to improving our understanding of palaeoenvironmental evolution and for making predictions beyond data limits.

Here, we present an integrated field and numerical modelling investigation of two adjacent and contemporaneous syn-rift fan deltas, 6 km along-strike from one another in the hangingwall of the same normal fault; the Pyrgaki-Mamoussia Fault. The fan deltas are referred to as the Selinous near the fault tip and the Kerinitis near the fault centre (Figure 1). This is the first detailed sedimentological and stratigraphic study of the Selinous fan delta and with comparison to the Kerinitis fan delta, allows a unique insight into the controlling parameters during rift basin evolution. The aim of the study is to resolve and quantify the contribution of tectonics and base level change to sequence

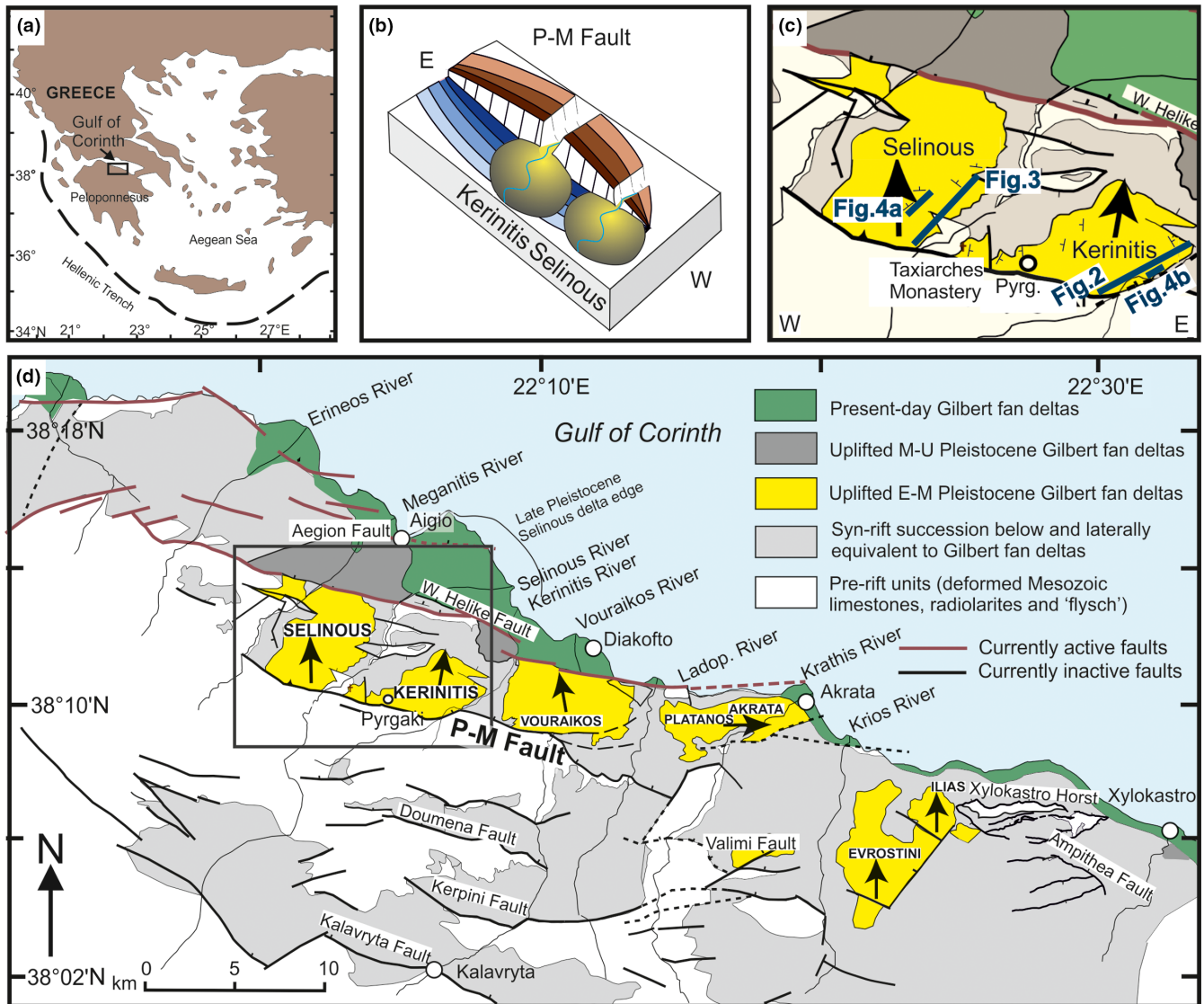


FIGURE 1 Map of the study area on the southern side of the Gulf of Corinth, Greece. (a) Map of Greece. (b) Schematic diagram of the Selinous and Kerinitis syn-rift fan deltas. (c) The highlighted position of the two fan deltas along the P-M Fault with the locations of Figures 2, 3 and 4. Early-Middle Pleistocene fan deltas that are of interest are shaded in yellow and differentiated from present-day fan deltas (green), Middle-Upper Pleistocene fan deltas (dark grey), other contemporaneous syn-rift stratigraphy (light grey) and pre-rift strata (white). The main fan delta progradation directions are indicated by black arrows. Small ticks on faults indicate throw and dip-direction. Currently active faults are in purple and inactive faults are in black. Map is modified from Ford et al. (2007), Ford et al. (2013), Ford et al. (2016) after Ghisetti and Vezzani (2004). Active faults and mapping of eastern area around the Xylokastro Horst and Ampitheia Fault from Gawthorpe, Leeder, et al. (2017)

architecture in Lake Corinth through the Early-Middle Pleistocene. In doing so, methodologies that are applicable to any basin with given data constraints are demonstrated. To satisfy the aim, the objectives are: (a) to derive quantified estimates of the controlling parameters based on comparisons of facies, stacking patterns and the nature of key stratigraphic surfaces between the deltas, (b) to reduce uncertainty of the quantified allogenic control estimates by use of sensitivity tests with the 3D sequence stratigraphic forward model ‘Syn-Strat’ (Barrett et al., 2018) and to elucidate the amplitude of lake level change for Early-Middle Pleistocene Lake Corinth, (c) to validate derivations using an

independent unit thickness extrapolation method; and (d) to make quantitative predictions of unit thickness along-strike variation and diachroneity of key stratigraphic surfaces. This work can be applied to other basin-fills by demonstrating two complementary methodologies for discerning and quantifying faulting and base level signals in the stratigraphic record. We undertake a quantitative analysis of unit thicknesses and surfaces that could be used in stratigraphic pinch-out assessment and cross-hole correlations in syn-rift reservoirs. Finally, the palaeoclimatic data on lake level changes derived from the geological record can be used to inform climate-system models for the Pleistocene.

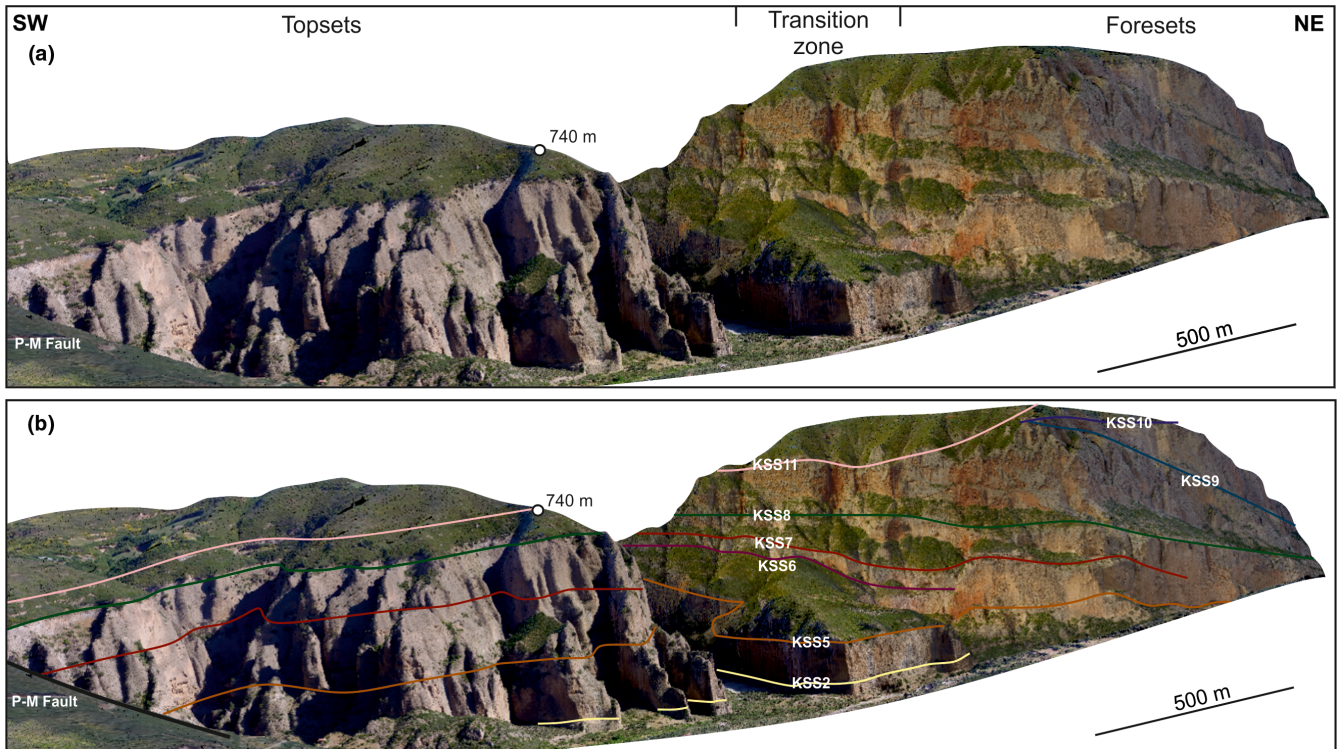


FIGURE 2 The stratigraphic architecture of Kerinitis. (a) UAV photogrammetry-based 3D outcrop model. (b) Key stratigraphic surfaces interpretation by Backert et al. (2010) overlain onto 3D outcrop model. Note overall aggradational stacking trend between units and on the scale of the whole delta, with topsets generally overlying topsets and foresets generally overlying foresets

2 | TECTONO-STRATIGRAPHIC FRAMEWORK

The Gulf of Corinth marks the axis of the ca. 100 km long, 60–80 km wide Corinth Rift that was activated during the Late Miocene/Early Pliocene (ca. 5 Ma; Collier & Dart, 1991; Ford, Hemelsdael, Mancini, & Palyvos, 2016; Gawthorpe, Leeder, et al., 2017; Leeder et al., 2008). Present-day N-S geodetic extension rates are up to 15 mm/year (Avallone et al., 2004; Briole et al., 2000; Clarke et al., 1997; Floyd et al., 2010), which are accommodated on N- and S-dipping normal faults (Bell, McNeill, Bull, & Henstock, 2008; Bernard et al., 2006; McNeill et al., 2005). The oldest part of the rift (Rift 1, ca. 5–3.6 to 2.2–1.8 Ma; Ford et al., 2013; Ford et al., 2016; Gawthorpe, Leeder, et al., 2017; Nixon et al., 2016) lies furthest south in northern Peloponnesos, where faulting was focussed at that time on the Kalavryta, Doumena, Valimi Faults (Figure 1) and other southern border faults. At this time, the Kalavryta alluvial system fed sediment northwards and fluvial and marginal lacustrine environments prevailed (Lower Group; Ford et al., 2016). In the eastern part of the rift (Figure 1), the Kyllini, Mavro, Kefalari and Nemea fan deltas built out into the basin (as described by Gawthorpe, Leeder, et al., 2017). There was an upward deepening through the

‘Rift 1’ sequence at ca. 3.6 Ma (Gawthorpe, Leeder, et al., 2017) from deposition of the fluvial-marginal Korfiotissa and Ano Pitsa Formations, to the deep lacustrine Pellini and Rethi-Dendro Formations, referred to as the ‘Great Deepening’ (Leeder et al., 2012).

Northward migration of faulting (Goldsworthy & Jackson, 2001; Ford et al., 2013, 2016; Nixon et al., 2016) onto the Pyrgaki-Mamoussia (P-M) Fault in the west and faults to the east occurred at ca. 1.8 Ma (Ford et al., 2016; Gawthorpe, Leeder, et al., 2017). In the immediate hangingwall of the faults, thick syn-rift fan deltas built northwards. Four syn-rift fan deltas that sit along-strike from one another in the hangingwall of the P-M Fault developed in the west: the Selinous, Kerinitis, Vouraikos and Platanos fan deltas (from W-to-E, Figure 1). The early development of syn-rift fan deltas along the whole length of the P-M Fault suggests that it grew rapidly in length. The contemporaneous P-M Fault hangingwall fan deltas sit within the Middle Group (Backert et al., 2010; Ford et al., 2007; Rohais, Eschard, Ford, Guillocheau, & Moretti, 2007). Pollen analysis at Vouraikos was used to date the Middle Group, which constrained the development of the P-M fan deltas to the Early-Middle Pleistocene (ca. 1.8–0.7 Ma) but within a period of 500–800 kyr (Ford et al., 2007). Subsequent northward fault migration onto the Helike fault system at ca. 800 ka (Ford et al., 2016) resulted in the uplift of western Plio-Pleistocene syn-rift stratigraphy

in the footwall of the modern, parallel West Helike Fault, exposing a ca. 6 km wide fault block terrace. During uplift, the fan deltas were subject to erosion from their own feeder rivers that now supply the modern fan delta systems on the coast.

Predominant lacustrine conditions with discrete periods of marine incursion lasted until ca. 600 ka, before marine conditions prevailed due to opening at the western end of the gulf to the Ionian Sea (Rion Straits) and/or at the eastern end to the Aegean Sea (Corinth Isthmus; Collier & Thompson, 1991; Ford et al., 2016; Gawthorpe, Leeder, et al., 2017; Nixon et al., 2016).

Here, we focus on the system in the hangingwall of the P-M Fault (Figure 1), which dips 50–55° towards the north and has a maximum throw of >1,200 m. The P-M Fault strikes WNW-ESE and is traced ca. 24 km from SW of Aigio to SW of Akrata. The fault juxtaposes pre-rift Mesozoic limestones in the footwall against Plio-Pleistocene hanging-wall syn-rift fan delta deposits. We study two syn-rift fan deltas, the Selinous that sits towards the western fault tip and the adjacent Kerinitis that sits nearer the fault centre. The fan deltas were influenced by: a) high slip rates on the P-M Fault as a result of rapid extension across the rift; and b) cyclic lake level and sedimentation changes from climatic variations.

3 | THE GILBERT-TYPE FAN DELTAS

3.1 | The Kerinitis fan delta

The Kerinitis Gilbert-type fan delta is presented in Figure 2 in the form of a 3D outcrop model. Kerinitis, studied since the 1990s (Backert et al., 2010; Dart et al., 1994; Gawthorpe et al., 1994; Ori, Roveri, & Nichols, 1991), is exposed on the western side of the modern Kerinitis river valley (ca. 200 m above sea level) along a 3.8 km SW-NE dip section from the P-M Fault towards the West Helike Fault. Topsets are back-tilted by ca. 18° and thicken towards the P-M Fault (Figure 2). The exposed section cuts the fan delta's eastern side, where foresets dip ca. 25° towards N040°. The fan delta extends laterally ca. 6 km along the P-M Fault, west of the Kerinitis River where it interfingers with the Selinous fan delta between the village of Pyrgaki and the Taxiarches Monastery (Figure 1). In total, Kerinitis covers an area of 15 km² and is ca. 800 m thick; the base of the fan delta is not exposed in the Kerinitis valley, but is exposed in the footwall of the West Helike Fault. The point source of the Kerinitis fan delta incised the P-M footwall at a topographic low on an early relay zone (Backert et al., 2010), shown as a hard link on the fault (Figure 1). Its position was locked into the landscape as fault linkage occurred. We interpret the lack of deformation penetrating the Kerinitis delta from the western end of the Mamoussia Fault to indicate early fault linkage with the Pyrgaki Fault with respect to the exposed fan delta strata.

Backert et al. (2010) undertook the most recent and comprehensive study of the Kerinitis fan delta, whereby they characterised its architecture and facies, presented a trajectory analysis and interpreted three stages of fan delta growth linked to initiation, growth and death of the controlling P-M Fault. The fan delta is divided into three zones from south to north, comprising fan delta topsets, a transition zone and fan delta foresets respectively (Figure 2). They identify four facies associations (topset, foreset, bottomset and prodelta) and 11 key surfaces. Trajectory analysis reveals abrupt landward shifts in the topset-foreset breakpoint at each key surface, followed by gradual basinward progradation through each stratal unit. The cyclic stratal units within the fan delta are interpreted to record eustatic variations upon a background subsidence-dominated regime, in which high rates of fault subsidence overcame base level falls, in agreement with earlier studies (Dart et al., 1994; Gawthorpe et al., 1994).

3.2 | The Selinous fan delta

The Selinous Gilbert-type fan delta is presented in Figure 3 using a 3D outcrop model and schematic dip section. It is referred to as Selinous in Ford et al. (2007), Ford et al. (2013) and Backert et al. (2010) and as Palaeo-Meganitis in Ford et al. (2016). The Selinous fan delta has a width of ca. 6 km and its centre sits ca. 4 km from the western tip of the P-M Fault. It is exposed on the western side of the modern Selinous river valley (ca. 150 m above sea level in the valley floor) along a 6 km long SSW-NNE dip section from the P-M Fault towards the West Helike Fault. Topsets thicken and are back-tilted by ca. 12° towards the P-M Fault (Figure 3). The main section is along the west side of the Selinous river valley, where foresets dip ca. 21° towards N310°. On the eastern side of the valley, foresets dip ca. 23° towards 097° (Figure 1). The fan delta's eastern limit interfingers with foresets of Kerinitis. The base of the fan delta is exposed in the valley in the footwall of a secondary normal fault that trends parallel to the P-M Fault. The maximum thickness of Selinous is ca. 400 m. The point source of the Selinous fan delta incises the P-M Fault and continues to feed the Late Pleistocene and modern fan deltas. As with Kerinitis, the Selinous fan delta can also be divided into three broad zones from south to north, with the most southerly ca. 2 km zone comprising delta topsets, a ca. 1 km transition zone in the central part and a ca. 3 km zone of foresets and bottomsets to the north (Figure 3).

4 | METHODOLOGY

In this study we integrate field data with numerical techniques through the five stages of analysis listed below.

1. Facies and stratigraphic architecture are analysed in the field and augmented with Unmanned Aerial Vehicle (UAV) photogrammetry-based 3D outcrop models.
2. Field observations and trajectory analysis of the middle-upper units of the two fan deltas are used to resolve and quantify each allogenic control acting on the delta evolution.
3. Each control parameter (e.g. subsidence rate, sedimentation rate etc.) is assigned a qualitative uncertainty value from 1–5, whereby 1 represents a very low uncertainty estimate and 5 represents a very high uncertainty estimate. This is undertaken in order to ascertain which variable is most uncertain and in need of refinement with numerical model testing.
4. The interpreted control parameters are input into 3D sequence stratigraphic forward model, Syn-Strat (Barrett et al., 2018), to test the least certain parameter(s).
5. Finally, an independent unit thickness extrapolation technique is adopted to validate the outputs of the numerical modelling.

4.1 | Facies analysis

The facies analysis of major stratal units and key stratigraphic surfaces was undertaken by sedimentary logging at cm-scale, documenting lithology, grain size, sedimentary structures and the nature of contacts. For characterising the thicker conglomeratic units, sections were logged at a dm-scale with support of sketches to capture the geometry of larger-scale features. Palaeocurrent data were collected from ripple cross laminations, clast imbrication and cross-bed and foreset plane measurements. Facies associations for both fan deltas are constructed from combinations of identified facies, which are presented in correspondence with those of Backert et al. (2010) for Kerinitis in Supporting Information Appendix S1: Table A. Correlation of key stratigraphic surfaces was carried out by walking out beds and surfaces, by annotations of photopanel in the field and by using UAV photogrammetry-based 3D outcrop models in Agisoft Photoscan software.

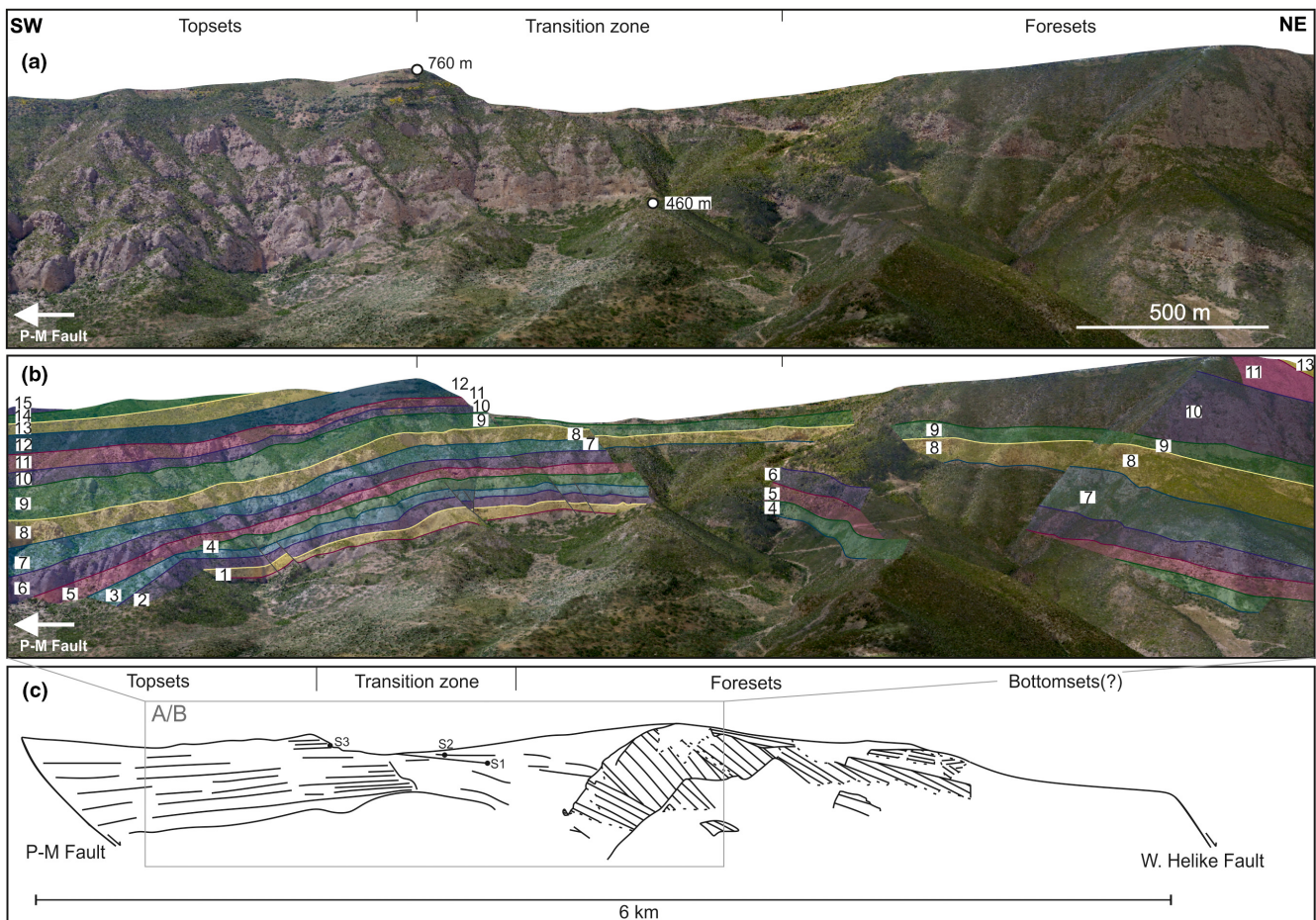


FIGURE 3 The stratigraphic architecture of Selinous. (a) UAV photogrammetry-based 3D outcrop model. (b) Interpretation of major stratigraphic units and surfaces overlain onto 3D outcrop model—colours are arbitrarily assigned to highlight the individual units. (c) Cross-sectional sketch of the Selinous fan delta with grey box to indicate area of outcrop model images in (a) and (b). Note the aggradational stacking trend on the scale of the whole fan delta, with topsets generally overlying topsets and foresets generally overlying foresets

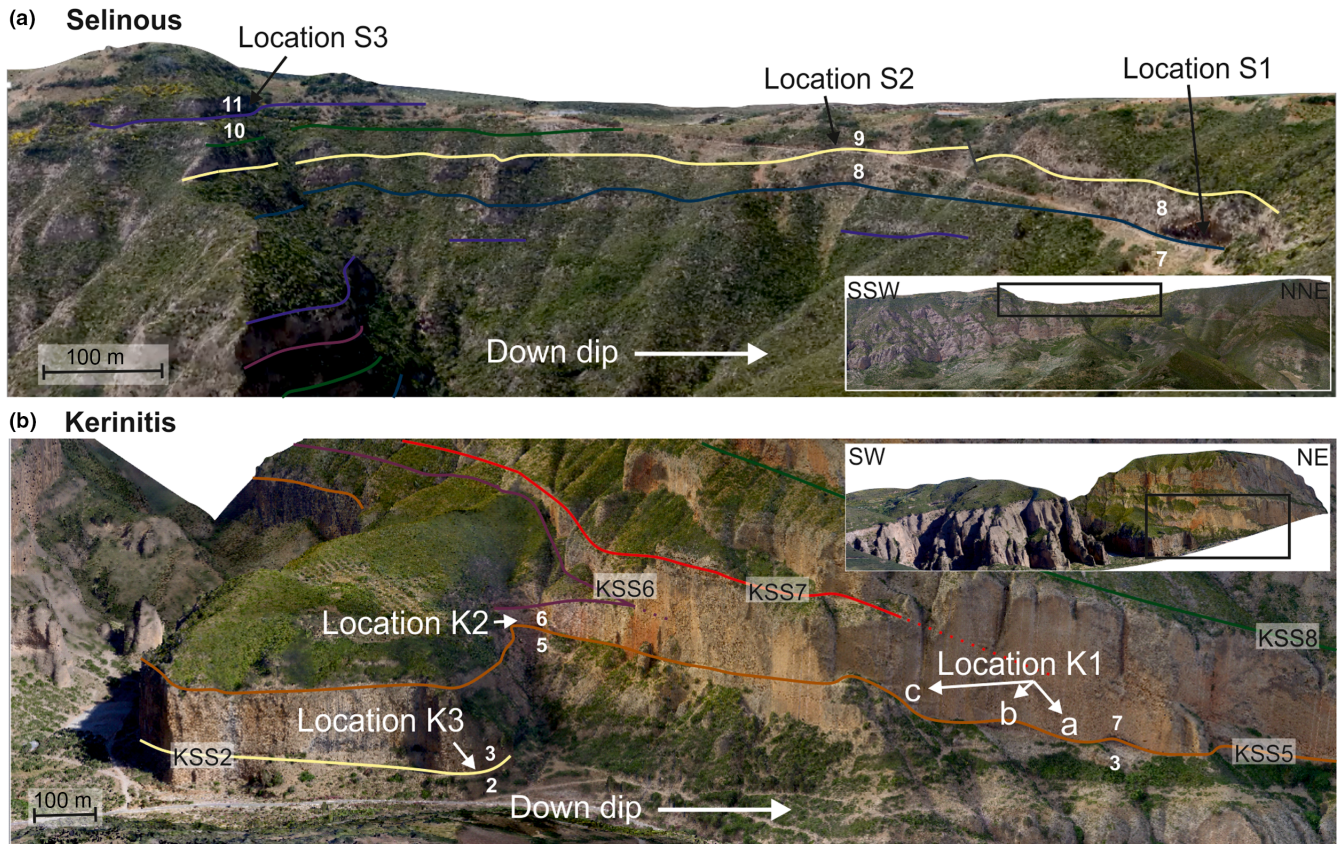


FIGURE 4 Locations of detailed sedimentological studies at fan delta topset-foreset transitions: (a) at Selinous and (b) at Kerinitis. Unit interpretations are overlain onto the 3D outcrop models. Unit numbers are shown in white. Key stratigraphic surfaces (KSS) are differentiated by colour arbitrarily and at Kerinitis, assigned according to the interpretation by Backert et al. (2010). Middle-upper units, Units 7–11 are the focus at Selinous and lower-middle units, Units 2–7 are the focus at Kerinitis. Insets show position (black box) in the context of each fan delta on wider 3D outcrop models (Figures 2 and 3). Locations of sections are shown in Figure 1

4.2 | Trajectory analysis

Trajectory analysis of the topset-foreset breakpoint (TFBP) was undertaken at both fan deltas for the accessible middle units: 4–8 at Kerinitis and 7–11 at Selinous. The position of the TFBP is identified from the transition from flat-lying topsets to steeply dipping foresets. In inaccessible locations, 3D outcrop models are used to identify the TFBP and assess the spatial continuity of stratal surfaces across which the breakpoint moves. If the TFBP is not seen directly, it is inferred from environmental transitions between down-dip outcrops at the same stratigraphic level. It should be noted that the units assessed at Kerinitis are not correlatable to those analysed at Selinous.

4.3 | Numerical modelling with Syn-Strat

In order to refine the quantification of controlling parameters in the basin, we use a 3D sequence stratigraphic forward model, Syn-Strat (Barrett et al., 2018). Syn-Strat produces a 3D graphical surface representing accommodation in the

hangingwall of a normal fault, resulting from spatially- and temporally-variable, tectonic subsidence, sedimentation and base level inputs. Syn-Strat constructs this surface by combining one-dimensional graphical curves that represent each control in time and space. Each parameter is defined along the fault, away from the fault and in time. In this study, we plot accommodation along the fault (x) and in time (y), for a given distance away from the fault. Stacking patterns or systems tracts are then applied to the surface with colours. In this study, we subdivide the relative base level curve with a falling limb and shorter periods of lowstand, transgression and highstand on the rising limb. This resembles the sequence stratigraphic scheme used by Frazier (1974) and Galloway (1989) and termed ‘genetic sequence’ by Catuneanu et al. (2009).

Previously, the model was used to demonstrate the sensitivity of sequence architecture to multiple hypothetical control scenarios, including different relative control magnitudes, subsidence rate regimes and sedimentation distribution models. Key outcomes were the quantitative constraint of along-strike variation in stacking pattern and of the nature of

diachroneity of sequence boundaries and maximum flooding surfaces (Barrett et al., 2018). Here, we input real control parameters derived from field observations and trajectory analyses. We refine the least certain control parameter (amplitude of base level change) with a number of discrete tests, whilst keeping all other control parameters constant, by comparing the modelled output with field observations. The test set-up and results are presented in Section 9.1.

5 | SEDIMENTARY FACIES ANALYSIS

The central parts of the fan deltas are the focus of sedimentological descriptions and interpretations, where the topset-foreset transition records base level change and the relative influence of accommodation and sediment supply. At Selinous, three down-dip locations over ca. 800 m distance, covering the middle-to-upper units of the fan delta were studied: S1—Units 7 and 8, S2—Units 8 and 9 and S3—Units 10 and 11. At Kerinitis, our study also focuses on three down-dip locations over ca. 700 m, covering the lower-middle units of the delta: K1a, b, c—Units 4 and 7, K2—Units 5 and 6 and K3—Units 2 and 3. These are presented on the 3D outcrop models in Figure 4, but are not constrained as time-equivalent units.

Sedimentary facies characteristics are similar between the Selinous and Kerinitis fan deltas. Eighteen sedimentary facies have been identified: six conglomeratic facies (abbreviated as 'Co'), six sandy facies (abbreviated as 'Sa') and six finer facies comprising mudstones and siltstones (abbreviated as 'Fi'). Detailed facies descriptions are provided in Supporting Information Appendix S1: Table A and further facies information on the Kerinitis fan delta can be found in Backert et al. (2010). The facies have been organised into four facies associations (FA) (Figures 5 and 6 and Table 1) that are differentiated based on geometric position (denoted by number) and eight sub-associations that are differentiated based on depositional environment (denoted by letter). The fluvial and shallow water topset FAs (1a–b and 2a–b) and the foreset FA (3) construct the main stratal units of the deltas. The bottomset FAs (4a–c) form the thinner, finer-grained intervals between the units.

5.1 | FA1—Fluvial topsets

We identify two fluvial topset FAs with (1a) channel-fill and (1b) delta plain interpretations (Figure 5). The channel-fill FA constructs the largest proportion of the fan delta topset deposits (ca. 95%). FA 1a is characterised in Unit 7 at Location S1 (Selinous) and in Unit 3 at Location K3 (Kerinitis) as a poorly-sorted, sandy gravel-cobble conglomerate with crude laminations and clast imbrication. The clasts are sub-angular to sub-rounded and the bed bases are highly erosional (facies Co1 and Co2 in Supporting Information Appendix S1: Table A). We interpret this deposit to be the product of bedload transport in a high-energy fluvial flow regime.

The fan delta plain FA (1b) is characterised in Unit 8 at Location S2 (Selinous) (Figures 4 and 5) and at the top of Unit 2 at Location K3 (Kerinitis) as a poorly-sorted, sandy gravel-cobble conglomerate (facies Co1, Sa2, Sa6 and Fi3 in Supporting Information Appendix S1: Table A). The cobbles are <10 cm diameter and sub-angular, implying limited transport time from source to deposition. The gravelly coarse sand beds present normal grading and contain cm-thick, red palaeosols, indicating subaerial exposure.

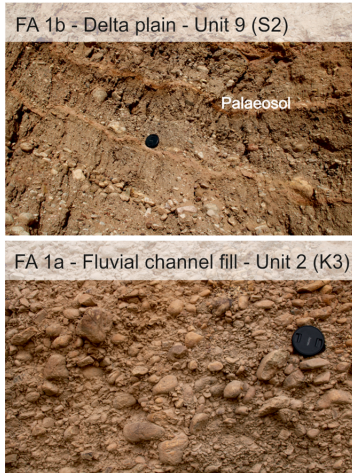
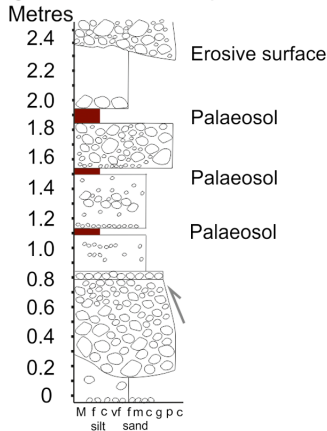
5.2 | FA2—Shallow water topsets

Two shallow water topset FAs have been identified: 2a) beach barrier and 2b) lower shoreface (Figure 5). The beach barrier FA (2a) is characterised at Location S3 (Selinous) by bi-directional metre-scale cross-beds with well-sorted, open-framework, rounded and discoidal pebbles (facies Co4 and Co5 in Supporting Information Appendix S1: Table A). This indicates textural maturity and character typical of beach reworking (Figure 5). FA 2a is present at the top of Unit 10 at Selinous Location S3 and is overlain by a finer-grained interval and subsequently by the 10-m scale foresets of Unit 11 (Figure 4). We have not observed FA 2a at Kerinitis, but Backert et al. (2010) report a foreshore FA at the top of Unit 7. The lower shoreface FA is present in the lower part of Unit 8 at Location S2 (Selinous) and comprises m-scale bi-directional, asymptotic cross-beds resembling hummocky cross-stratification (facies Co5 in Supporting Information Appendix S1: Table A), typical of storm reworking below fair weather wave base.

FIGURE 5 Sedimentological details of Facies Associations 1–3—fluvial topsets, shallow water topsets and foresets. (a) FA 1: log and field photograph of FA 1b (delta plain fluvial topset) highlighting the presence of palaeosol horizons, and field photograph of FA 1a (fluvial channel fill). (b) FA 2: sketch and field photograph of FA 2a (beach barrier) and field photograph of FA 2b (lower shoreface). Note m-scale asymptotic hummocky cross-stratification in FA 2b. Sketch of the outcrop section revealing FA 2a is provided to highlight key features—m-scale, bi-directional cross-beds, texturally mature clasts and normally graded cycles (facies Co5). Facies Co5 is subdivided here to show fining upwards cycles (1–3); 1 = poorly sorted, matrix-supported, rounded gravel-pebble conglomerate; 2 = open-framework rounded pebbles; 3 = poorly sorted gravel. (c) FA 3: field photographs of 10-m scale and 100-m scale foresets at Selinous and Kerinitis and sketch log of foresets at Unit 11, Selinous Location S3

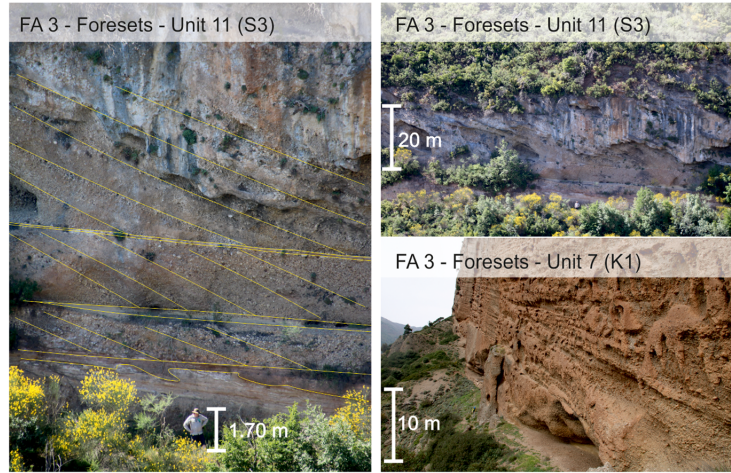
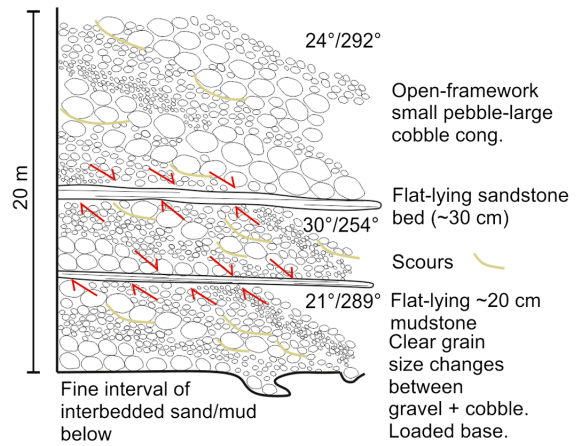
(a) Facies Association: 1 - Fluvial topsets

Log of FA 1b - Delta plain fluvial topset - Unit 9 (S2)



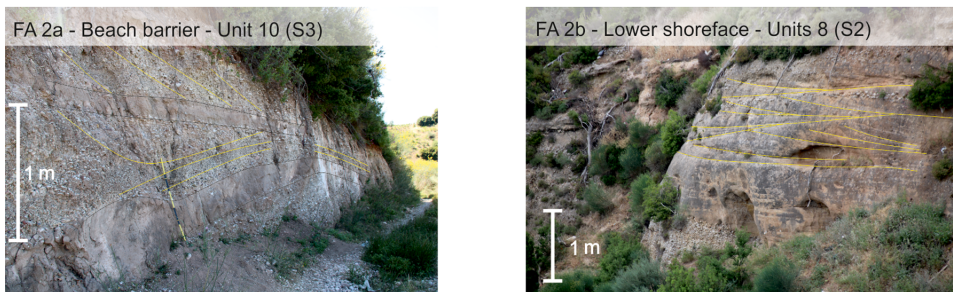
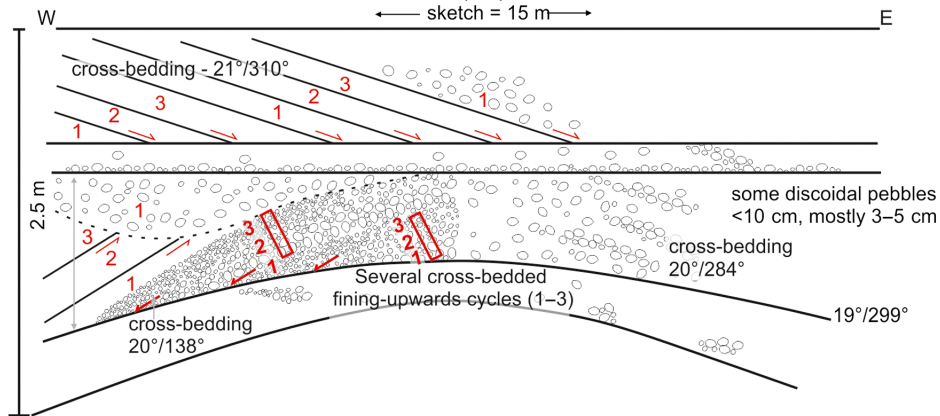
(c) Facies Association: 3 - Foresets

Sketch of FA 3 - Foresets - Unit 11 (S3)



(b) Facies Association: 2 - Shallow water topsets

Sketch of FA 2a - Beach barrier - Unit 10 (S3)



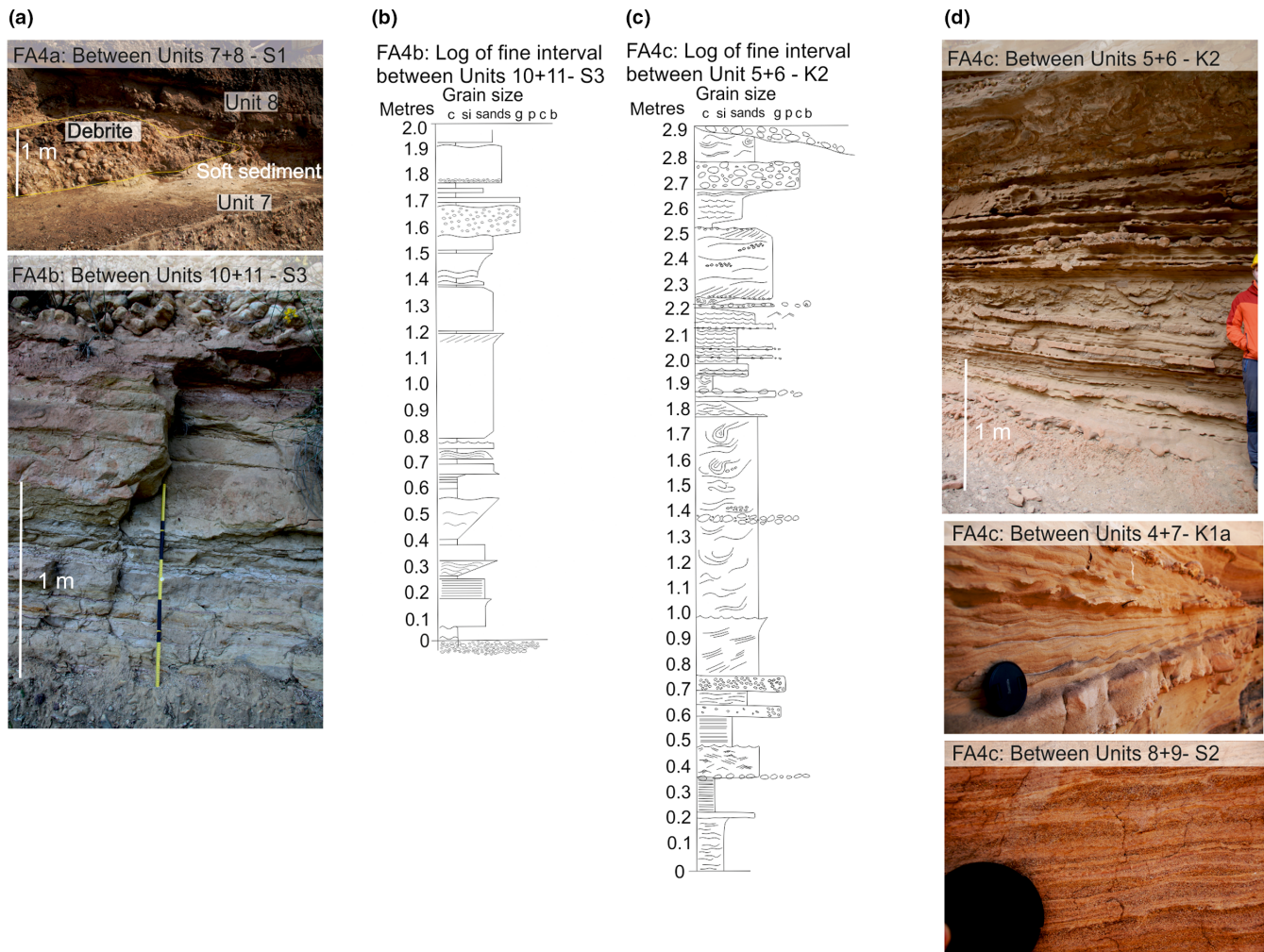


FIGURE 6 (a) Field photographs of FAs 4a and 4b. (b) Log of FA 4b from the fine interval between Units 10 and 11 at Selinous Location S3. (c) Log of FA 4c from the fine interval between Units 5 and 6 at Kerinitis Location K2. (d) Field photographs of FA 4c—note symmetrical ripples, indicating shallow water depth

5.3 | FA3—Foresets

The foreset FA represents most of the down-dip parts of the exposed fan delta successions (Figures 1, 2 and 5). At Selinous, the foreset FA is apparent in Unit 8 at Location S1, Unit 9 at Location S2 and Unit 11 at Location S3 (Figure 4). At the Kerinitis study locations, the foreset FA is apparent in Unit 7 at Location K1a, b and c and Unit 6 at K2. The foreset FA is represented by steep, basinward-dipping (between 22° and 25°), 10–350 m high cross-beds. The cross-beds comprise well-sorted, clast-supported (and sometimes open-framework), sub-rounded cobble conglomerate with some inverse grading and many scours (facies Co3, Co4 and Sa4 in Supporting Information Appendix S1: Table A). In some places, the conglomeratic foreset units are separated by preserved, gently dipping finer-grained intervals (e.g. Figure 5), but in most cases these are eroded. The foreset facies association was emplaced in a high-energy environment occupied by avalanching sediment gravity flows, characteristic of

the upper foreset slope. The height of the foresets indicates the palaeo-water depth and ranges from a few metres when the foresets built over a previous delta topset (e.g. S1–3; Figure 4), to a few hundred metres, when they built beyond the previous fan delta TFBP and into the deep water basin (e.g. Figures 5 and 7).

5.4 | FA4—Bottomsets

Three bottomset FAs have been identified across the fan deltas and are interpreted to represent distal (4a), intermediate (4b) and proximal (4c) positions with respect to the sediment input point (Figure 6 and Table 1). These deposits form the fine-grained intervals between the major stratigraphic units.

The distal bottomset FA (4a) is mainly represented by calcareous mudstone-siltstone (marl) beds and is apparent in the interval between Units 7 and 8 at Location S1 (Selinous; Figures 4 and 6). There is evidence of soft-sediment deformation and cm-wide, 10 cm-length, sand- and mud-filled

TABLE 1 Summary of facies associations with geometric position and depositional environment interpretations

FA code	Constituent facies	FA interpretation	Sub-association
1a	Co1, Co2		Channel fill
1b	Co1, Sa2, Sa6, Fi3	Fluvial topset	Delta plain
2a	Co4, Co5	Shallow water topset	Beach barrier
2b	Co5		Lower shoreface
3	Co3, Co4, Sa4	Foreset	
4a	Sa1, Sa3, Fi1, Fi2, Fi4		Distal
4b	Sa1, Sa2, Sa4, Sa5, Fi1–3, Fi5, Fi6	Bottomset	Intermediate
4c	Co6, Sa1–6, Fi1, Fi2		Proximal

burrows (facies Sa1, Sa3, Fi1, Fi2 and Fi4, in Supporting Information Appendix S1: Table A). A 0.8 m thick, laterally discontinuous, poorly-sorted, clast-supported sandstone-cobble-grade conglomerate (facies Co4 in Supporting Information Appendix S1: Table A) cuts into the finer sediments. We interpret the fine sediments to be deposited from

dilute turbidity currents and suspension fall-out in a low energy environment and the conglomerate as a debrite sourced from the delta front.

The intermediate bottomset FA (4b) is evident between Units 10 and 11 at Location S3 (Figures 4 and 6). It is characterised by interbedded sandstone and mudstone beds with some wavy laminations. The sandstones are inversely graded with slightly erosive bases and gravel lags (facies Sa1, Sa2, Sa4, Sa5, Fi1, Fi2, Fi3, Fi5 and Fi6 in Supporting Information Appendix S1: Table A) and are interpreted as turbidites. Muddy intervals represent periods of quiescence between events or dilute turbidity current deposits. The proximal bottomset FA (4c) is observed between Units 8 and 9 at Location S2, between Units 5 and 6 at Location K2 and between Units 4 and 7 at Location K1a (Figures 4 and 6). It is characterised by coarser, mainly well-sorted sand-gravel-grade sediments (facies Co6, Sa1–6, Fi1 and Fi2 in Supporting Information Appendix S1: Table A), with symmetrical and asymmetrical ripple laminations, gravel dune-scale cross-beds, wavy and planar laminations, soft-sediment deformation (convolute laminations, folds and dewatering structures) and bioturbation. The range of structures is interpreted to be due to a more proximal position with respect to the river outlet, where hyperpycnal flows and wave processes may have operated near the base of small foreset slopes in shallow water.

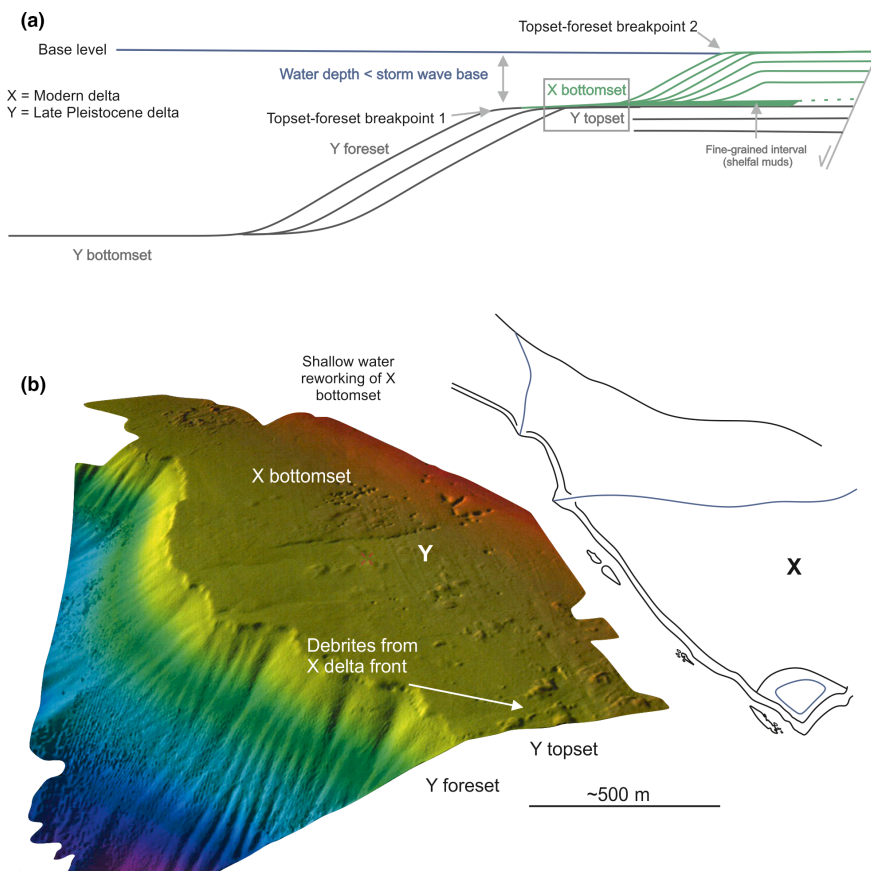


FIGURE 7 Geometric position of shallow water bottomsets (FA 4c). (a) Diagram shows the position of two hypothetical delta units X and Y to show the juxtaposition of underlying topsets of Y and overlying bottomsets of X in shallow water. The bottomsets of X are in a water depth above storm wave base and therefore present shallow water facies even though they are geometric bottomsets. (b) Sketch of the modern Selinus fan delta (X), prograding over the Late Pleistocene Selinus fan delta (Y) as an example of the juxtaposition shown in A (position shown in Figure 1). Bathymetry data from Cotterill (2002) and McNeill et al. (2005)

6 | KEY SURFACES

6.1 | Flooding surfaces

Fan delta successions can be subdivided into major stratal units based on stratal terminations (e.g. downlaps, onlaps and truncations) and major facies changes (Mitchum, Vail, & Thompson, 1977). Fine-grained intervals are present between conglomeratic units in the topset regions and transition zones. Basinward, fine-grained units are poorly preserved, with one exception at Location K1b (Kerinitis). However, their correlative expression can be traced down-dip into the foreset region using onlap and downlap patterns and dip changes between foresets. In both fan deltas, the fine-grained intervals are similar in their position (generally preserved in the topset regions and transition zones) and thickness (ca. 2 m). Locally, the bases of the fine-grained intervals are slightly erosional. The facies of the fine-grained intervals range from laminated mudstones and deformed siltstones (FA 4a), interbedded siltstones-sandstones (FA 4b), to rippled sandstones and gravels (FA 4c).

The bases of the fine-grained intervals are interpreted to represent transgressive surfaces. The maximum flooding surfaces are speculated to be within the fine-grained units in the topset region of the deltas above each transgressive surface. The upper part of the fine-grained intervals may be contemporaneous with the foreset progradation and therefore represents the subsequent regressive trend. In the analogous modern conglomeratic deltas along the southern shore of the Gulf of Corinth, fine-grained deposits are restricted to: (a) inter-distributary bays, (b) lagoons, (c) fluvial overbanks and (d) shelfal, shallow water bottomsets, away from the dynamic, coarse-grained, gravity-driven processes in the foreset region and where dilute turbidity currents and suspension fall-out processes dominate. The two former interpretations are omitted based on the absence of rootlets, palaeosols, intact fauna or overall palaeocurrent changes that would indicate delta lobe avulsion and thus a migration to an inter-distributary bay setting. In addition, the fine-grained intervals are too widespread to represent a single lagoon in this setting. In the more proximal parts of the fan delta, it is not possible to characterise the fine-grained intervals, so it is possible that they could comprise of fluvial overbank deposits (Backert et al., 2010). However, an interpretation of transgressive reworking of the topset region and deposition of shelfal fines is favoured.

We do not infer a great water depth for the deposition of the bottomset facies and interpret the fine-grained deposits to represent shelfal fines as opposed to slope/abyssal plain fines when positioned landward of the large, basinward-dipping foresets. Where small foresets prograde in shallow water in the proximal topset region, widespread bottomset deposition over the previous fan delta topset occurs (Figure 7). If the previous delta topset and thus the subsequent overlying

bottomset, lies at a water depth above storm wave base, upper and lower shoreface environmental facies are possible, even though geometrically they were deposited in the bottomsets (FA 4b and FA 4c). Bathymetry data of the Late Pleistocene and modern Selinous deltas (Cotterill, 2002; McNeill et al., 2005; Figure 7) support the intercalation of bottomset and topset deposits. The topset of the Late Pleistocene delta (Y in Figure 7) is overlain by the fine sediment of the modern system's bottomset (X in Figure 7). Debris from the modern system are identified in the bottomset of X that are placed on the topset of Y.

6.2 | Sequence boundaries

In most cases, there is evidence for minor erosion of the fine-grained intervals by overlying topset units during progradation. However, deeper erosion (at the scale of several metres depth) that is subaerial in nature is only expressed at Selinous. At Selinous Location S2, the progradational foresets of Unit 9 infill a ca. 4 m deep erosional surface that incises into the underlying fine-grained interval. Where the fine-grained interval is missing, foresets are seen to directly overlay Unit 8, which comprises fluvial delta plain facies (FA 1b) with several palaeosols (Figure 8). The large lateral extent of the surface, traceable across the length of the whole fan delta and the basinward shift of depositional environments, supports an interpretation of the erosive surface as a sequence boundary formed by a relative base level fall. Between Units 7 and 8 at S1, another surface with erosion of several metres depth is apparent and could be a sequence boundary. The bottomset deposit at this location is finer and therefore interpreted to be more distal, than those at S2.

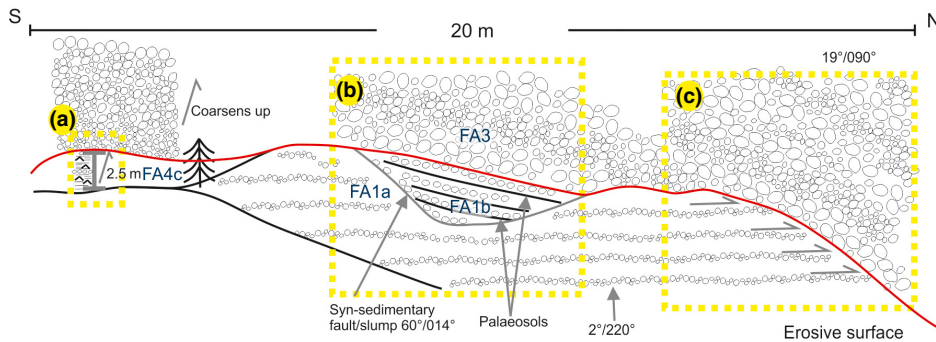
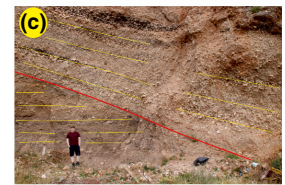
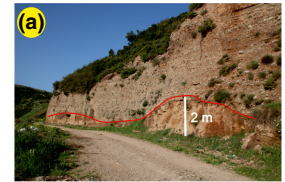
At Kerinitis, there is a ca. 100 m deep erosional cut at Key Stratal Surface 5 (KSS5) between the foresets of Units 3 and 7. Backert et al. (2010) attribute this to a large-scale submarine mass failure unrelated to relative base level change. Otherwise, major surfaces at Kerinitis appear to be either: (a) associated with major facies changes with limited erosion or (b) erosive with a lack of subaerial indicators and occurring at the base of foresets ('cusate erosion surfaces' in Backert et al., 2010). These erosion surfaces are not interpreted to represent sequence boundaries due to the lack of evidence of subaerial exposure. We interpret that the erosion surfaces form by autocyclic processes, in agreement with the interpretation from Backert et al. (2010). Figure 8 shows the difference in the nature of key stratigraphic surfaces between Selinous (erosive sequence boundary) and Kerinitis (non-erosive surface) with examples from S2 and K3.

In summary, sequence boundaries are interpreted near the fault tip at Selinous, but not near the fault centre at Kerinitis. One explanation is that Kerinitis is positioned near the fault centre where greater subsidence could counteract basinwide relative base level falls (cf. Gawthorpe et al., 1994).

Selinous surface character

Location S2

Several m of erosion at surface. Interpreted as a sequence boundary.



Kerinitis surface character

Location K3

Minor erosion at surface. Not a sequence boundary.



FIGURE 8 Sketch and field photographs to present an erosional surface apparent at Selinous Location S2 between Units 8 and 9, interpreted to be a sequence boundary. Photographs shown from KSS2 between Units 1 and 2 of a non-erosive surface at Kerinitis as comparison. Geologist for scale is 1.75 m. Numbers indicated in blue represent Facies Association codes

7 | STRATAL STACKING PATTERNS

7.1 | Description of stratal stacking patterns

At both fan deltas, the major stratal units are dominated by conglomerates, comprising FA 1 and 2 in the topsets and FA 3 in the foresets. The topsets extend for up to 2 km away from the fault to the TFBP, where restored stratigraphic dips increase from sub-horizontal to 20–25°. Average unit thickness is thinner at Selinous (ca. 25 m) compared to Kerinitis (ca. 60 m). At both fan deltas, the units thicken towards the fault by ca. 10 m. The thickness of the units is generally uniform through time at Selinous. At Kerinitis, unit thickness generally increases towards the middle part of the fan delta and thins towards the top (Backert et al., 2010). The units also thicken into the foreset regions down-dip with foreset heights reaching > 350 m, as the fan deltas prograded into deeper water depths towards the basin centre. At Selinous, we observe 15 stratal units. At Kerinitis, we observe 11 stratal units, but the base of the Kerinitis succession is not observed. Previously, Kerinitis has been subdivided into 12 (Dart et al., 1994) or 11 stratigraphic units,

with the uppermost unit designated as the Kolokotronis fan delta of the Upper Group (Backert et al., 2010). A ‘proto-delta’ (Stratal Unit 0 in Backert et al., 2010) recording initiation of subsidence is also identified towards the base of Kerinitis and is differentiated based on the interpretation of a sequence boundary at the top, drainage realignment and basinward shift of the subsequent units (Backert et al., 2010).

Trajectory analysis of the TFBP (Figures 6 and 9) was undertaken at both fan deltas for the middle units: Units 4–8 at Kerinitis and Units 7–11 at Selinous. It should be noted that these units were chosen for analysis based on accessibility alone and there is no evidence for correlation between the units. Trajectory analysis for the whole of the Kerinitis fan delta is presented by Backert et al. (2010). Figure 9 shows schematic dip sections of the two fan deltas juxtaposed along the P-M Fault, with the trajectory analysis of each for comparison. The unit thicknesses are normalised to emphasise the relative patterns in the trajectory styles. From the trajectory analysis, it appears that the stacking patterns are similar at both fan deltas across three scales, from stacking within units (10-m scale), stacking between units (100-m scale), to stacking of the whole fan delta succession (several 100-m scale).

At Selinous, there is a progradational-to-aggradational style within Units 7–10, as shown by the climbing basinward trajectory of the TFBP. Unit 11 has a different trajectory, as small-scale (10 m) foresets are apparent closer to the fault. This is shown by the proximal climbing basinward trajectory of the TFBP (aggrading), followed by the horizontal basinward trajectory (prograding). Between Units 7 and 11 at Selinous there is generally retrogradation, that is, the final TFBP of each unit is landward of that of the previous unit (Figure 9). However, the Selinous fan delta is aggradational given the overall limited horizontal migration of the TFBP. Within Units 4–8 at Kerinitis, there appears to be a progradational-aggradational stacking pattern that resembles the style of Units 7–11 at Selinous. The final TFBP of Unit 5 is landward of that of Unit 4, indicating a phase of retrogradation. The final TFBP of Units 6 and 7 is basinward of their underlying units, indicating a phase of retrogradation. Finally, Unit 8 is landward of that of Unit 7 and indicates retrogradation. Backert et al. (2010) compile the fan delta

units into three packages and interpret the lower package (Units 1–3) as progradational, the middle package as progradation-aggradational (Units 4–9) and the upper package as progradational (Units 10–11). Although there are variations in stacking pattern, the overall position of the TFBP between Units 4 and 8 and indeed of the whole fan delta, migrated a limited distance (ca. 1.5 km; Figure 9). Therefore, Kerinitis also exhibits an overall aggradational stacking pattern. It is not possible to access and characterise the fine-grained intervals across much of the topset part of the fan deltas with some exceptions, so it is not possible to define the landward extent of flooding.

7.2 | Interpretation of stratal stacking patterns

The progradation-aggradation within the units at both fan deltas was a response to building out into space created by base level rise and subsidence, with sedimentation initially

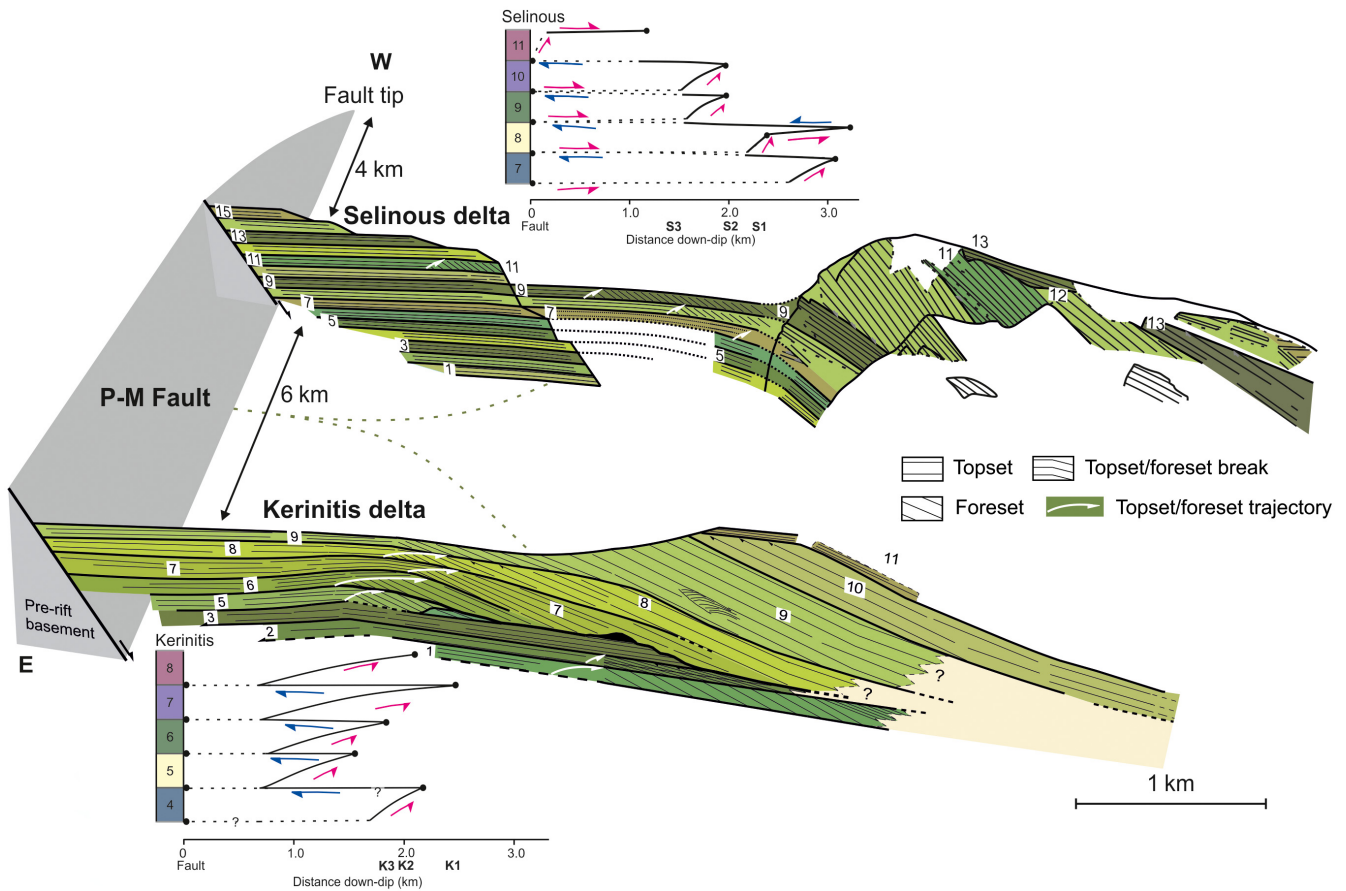


FIGURE 9 Summary diagram of architectural stacking at both fan deltas in their respective positions along the P-M Fault. Trajectory analyses of topset-foreset breakpoint of both fan deltas are shown alongside the cross-sections. Topset-foreset breakpoints are shown by black filled circles and trajectory paths are shown by black lines. Study Locations S1–3 and K1–3 are indicated. Unit thicknesses on trajectory analysis diagrams are normalised to emphasise the relative patterns in the trajectory styles. The trajectory of Unit 4 is less certain (question marks). Solid lines show observable trajectories in the transition zone and dashed lines show our interpretation of retrogradation back to the fault and/or correlative surfaces to down-dip maximum flooding surfaces. Kerinitis cross-section from Gawthorpe, Andrews, et al. (2017) after Backert et al. (2010)

exceeding and then keeping pace with space creation. The retrogradational phase at Selinous, between Units 7–11, represents a time when the relative base level rise outpaced the sedimentation rate. The aggradational phase at Kerinitis between Units 4–8 represents a time when sedimentation was equal to the space available. The overall aggradational trend observed in both fan deltas is a response to overall sedimentation having kept pace with accommodation generation. The greater unit thickness in the topset region at Kerinitis than Selinous may be attributed to the greater space made available from a higher subsidence rate near the fault centre than near the fault tip.

At both fan deltas there is clear cyclicity, with several major conglomeratic stratal units separated by fine-grained intervals, both with relatively constant thickness within each fan delta. Autocyclic switching of channel position is intrinsic to the architecture of fan delta tops. However, based on previous studies and repeated airborne photography of the Gulf of Corinth over the last 75 years, it is apparent that the rivers on the delta tops avulse on decadal-centennial timescales (Soter & Katsonopoulou, 1998; McNeill & Collier, 2004). Here, we are characterising an assumed larger scale cyclical behaviour. Such organised cyclicity is unlikely to develop from clustering of seismic activity (Scholz, 2010) as the long term velocity field over this timescale of 10–100 kyr is constant, due to the viscous flow of the lower crust (Wdowinski, O'Connell, & England, 1989). Given this and the fact that low-mid latitude Pleistocene lakes are characterised by high amplitude base level fluctuations (Benson et al., 1998; Gasse, Lédée, Massault, & Fontes, 1989; Lyons et al., 2015; Marchegiano, Francke, Gliozzi, & Ariztegui, 2017; Marshall et al., 2011), the cyclicity is attributed to periodicity in lake level change associated with climate. Previous authors also advocate this interpretation (Backert et al., 2010; Dart et al., 1994). Sediment supply is also likely to fluctuate with climate (Collier, Leeder, & Maynard, 1990; Collier et al., 2000). Therefore, during the existence of the lake, climatic changes associated with orbital forcing influenced the evolution of the coast through fluctuations in both base level and sediment supply (Collier, 1990; Gawthorpe, Leeder, et al., 2017; Leeder, Harris, & Kirkby, 1998; Moretti et al., 2004). Lake level is interpreted to have risen and fallen multiple times throughout the Early-Middle Pleistocene with close to zero net change over the build times of the fan deltas. Without the addition of fault-related subsidence, there would be no space for the sediments to accumulate on the topsets, as each base level fall would remove the space created by each base level rise. Instead, distinctly progradational stacking pattern would be apparent with a consistent sediment supply, which is not apparent. Sedimentation must therefore have kept pace with the space creation from subsidence.

8 | QUANTIFICATION OF CONTROLS

Here, we attempt to use the field data to discern and quantify the architectural controls on fan delta evolution. Subsidence rates can be estimated using the thickness of the syn-rift successions over the time through which the fan deltas built (fan delta build time), sedimentation rates from the combination of thickness accumulated and stacking pattern over time, and base level change from extrapolation of unit thickness to the fault tip where subsidence is zero. We assign qualitative uncertainty values (1–5) to each control parameter, where 1 represents a very low uncertainty estimate and 5 represents a very high uncertainty estimate. This approach identified which variable is most uncertain and would be a focus for numerical model testing. Table 2 presents each control parameter and uncertainty estimate.

Local climate varied in response to orbital forcing during the Early-Middle Pleistocene with the ca. 41 kyr dominant cyclicity (Capraro et al., 2005; Dodonov, 2005; Suc & Popescu, 2005) that is recorded worldwide (Emiliani, 1978; Head & Gibbard, 2005; Lisiecki & Raymo, 2007). This is assigned a low uncertainty value of 1. The Gulf of Corinth was mainly lacustrine (Lake Corinth) between ca. 3.6 Ma and ca. 600 ka (Collier, 1990; Freyberg, 1973; Gawthorpe, Leeder, et al., 2017; Moretti et al., 2004). It is likely that lake levels fluctuated as a result of the well-constrained cyclical climatic changes, but it is not known how the lake level changed and whether it mimicked global sea level fluctuations. Various studies from the Late Pleistocene show low-mid latitude lakes fluctuating with the same periodicity as global sea level, e.g. Lake Lisan, Dead Sea (Torfstein, Goldstein, Stein, & Enzel, 2013), Lakes Tana and Tanganyika, East Africa (Gasse et al., 1989; Marshall et al., 2011), Mono and Owens Lakes, California (Benson et al., 1998), Lake Trasimeno, Italy (Marchegiano et al., 2017), with low lake levels corresponding to events during glacial periods (low global sea level). However, the climate response (precipitation-evaporation balance) to such events is spatially variable and it is also unknown whether this Late Pleistocene trend is representative of climate changes during the Early-Middle Pleistocene. The cyclical stratigraphy and facies of the deltas indicate that lake level changes did occur, and a frequency of ca. 41 kyr in line with climate during the Early-Middle Pleistocene is consistent with the age of the fan deltas.

Palynological data from the adjacent and contemporaneous Vouraikos delta indicate that the fan deltas started to build at ca. 1.8 Ma (Ford et al., 2007) and stopped developing when they began to be uplifted in the footwall of the West Helike Fault. Using uplift rates on the contiguous East Helike

TABLE 2 Quantitative field observations and control parameter derivations, with assigned uncertainty values (1–5). 1 = low uncertainty; 5 = high uncertainty

	Parameter	Selinous	Kerinitis	Uncertainty value (1–5)	
Observations	Number of units	15	11	1	
	Total thickness of deltas	ca. 400 m	>800 m	1	
	Thickness of units	25 m	60 m	1	
	Distance between the two deltas		6 km	1	
	Unit thickness decay rate along fault		5.8 m/km	1	
Interpretations	Total subsidence	ca. 400 m	>800 m	1	
	Climate change periodicity		ca. 41 kyr	1	
	Lake level change periodicity		ca. 41 kyr	2	
	Delta build time	615 kyr	>451 kyr	2	
	Subsidence rate	0.65 m/kyr	>1.77 m/kyr	2	
	Magnitude of lake level rise through each climatic cycle		<25 m		4
			10–15 m ^a		2 ^a
			12 m ^b		2 ^b
	Average sedimentation rate	0.65 m/kyr	>1.77 m/kyr	2	
Sedimentation model through time		Variable	4		

^aValues refined from numerical modelling exercise with Syn-Strat. ^bValues refined using independent thickness extrapolation method.

Fault of 1–1.5 mm/year (De Martini et al., 2004) and present-day final topset elevation (ca. 800 m) of the fan delta, an age for their demise is estimated as 530–800 ka (Ford et al., 2007). The age constraint from palynology and uplift rates of ca. 1.8 to ca. 700 ka supports the use of ca. 41 kyr as the dominant cyclicity.

Assuming the cyclicity is not autogenic and each fine-grained interval contains a maximum flooding surface on the rising limb of a relative base level curve, the deposition of each unit represents one climatic cycle. At Selinous, there are 15 stratal units, each representing ca. 41 kyr of deposition, from which we infer that the fan delta built over a total of 615 kyr. At Kerinitis, the base is not exposed, but there are at least 11 stratal units and so the minimum delta build time is 450 kyr. If the ‘proto-delta’ at the base were to be included in our framework or the lower units were exposed, this estimated build time would be longer. These approximations are consistent with previous estimates of fan delta build time based on palynological analysis of the concurrent and adjacent Vouraikos fan delta of 500–800 kyr (Ford et al., 2007; Malartre, Ford, & Williams, 2004) and therefore we assign these build time estimates with a low uncertainty value of 2.

There is far greater uncertainty on the amplitude of lake level change. The unit thicknesses at Kerinitis are ca. 60 m and at Selinous are ca. 25 m. As both fan deltas developed only 6 km apart, in the hangingwall of the same fault, the lake level fluctuations affecting both systems were the same and the difference in unit thicknesses is mainly due to variation in local subsidence rate. Subsidence was greater at Kerinitis than at Selinous; at least 35 m of unit thickness accounts

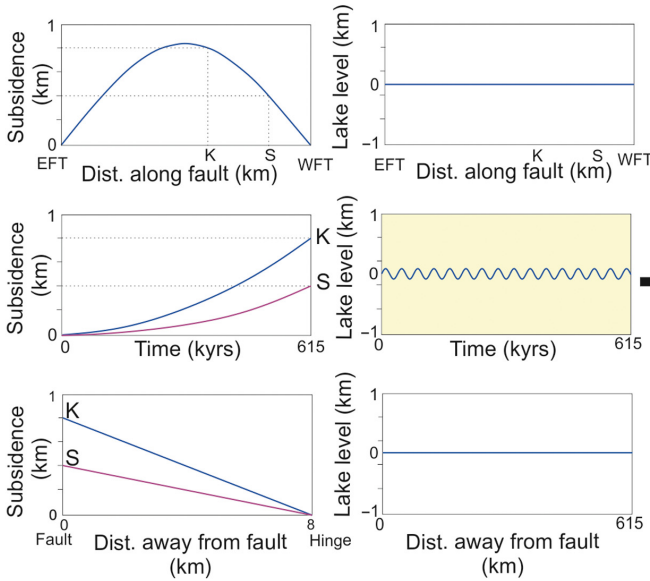
for the contribution from additional subsidence at Kerinitis. Therefore, the maximum base level rise during one cycle is 25 m. As Selinous sits close to the fault tip but still underwent subsidence, lake level change would have been less than 25 m. The amplitude of lake level rise is assigned a high uncertainty value of 4.

Neither succession has undergone significant burial or compaction. The thickness of syn-rift sediments against the fault and therefore maximum total subsidence at Selinous is ca. 400 m. The sediment is inferred to have accumulated over 615 kyr, which gives an average subsidence rate of 0.65 m/kyr. At Kerinitis, there is an estimated thickness and therefore estimated total subsidence of ca. 800 m, which is calculated based on average topset unit thickness of 65 m, average topset thickening into the fault of ca. 10 m and 11 observable units. We infer that the sediment accumulated during 11 cycles over at least 450 kyr, which gives a minimum average subsidence rate of 1.77 m/kyr. The axes of the two fan deltas are positioned 6 km apart along-strike of the fault and therefore using the two estimated average subsidence rates, subsidence decay per kilometre is approximately 0.19 m/kyr towards the fault tip. As Kerinitis is positioned 10 km from the western fault tip and the fault is ca. 24 km in length, it sits ca. 2 km to the east of the fault centre and therefore the average subsidence rate there is slightly lower than the maximum on the fault. The Vouraikos fan delta sits ca. 3–4 km to the west of the fault centre and has a thickness of >800 m (Ford et al., 2007). Extrapolating the subsidence decay rate derived between Selinous and Kerinitis towards the

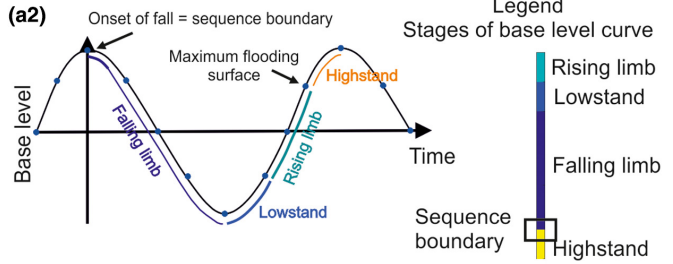
(a) Relative base level curve

(a1)

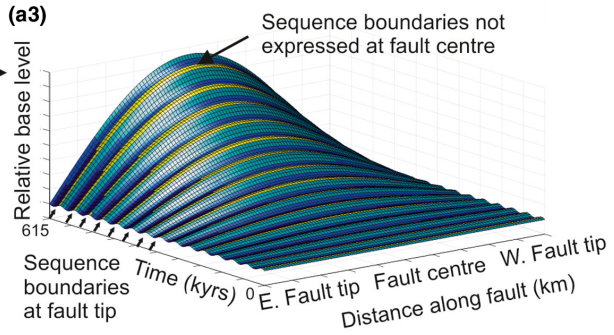
Subsidence + lake level



(a2)



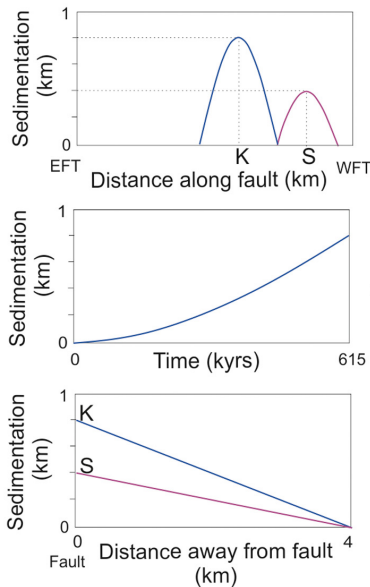
(a3)



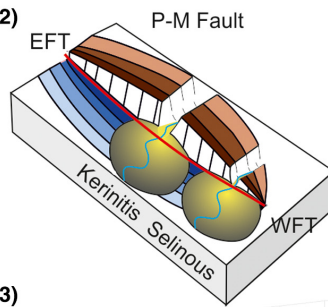
(b) Accommodation curve

(b1)

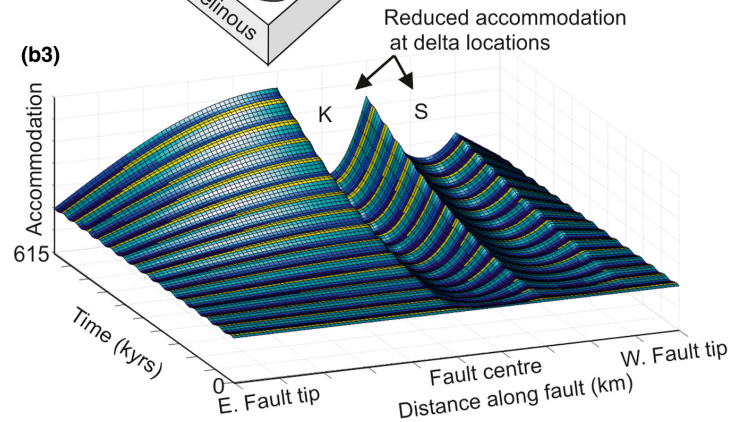
Subsidence +lake level - sedimentation



(b2)



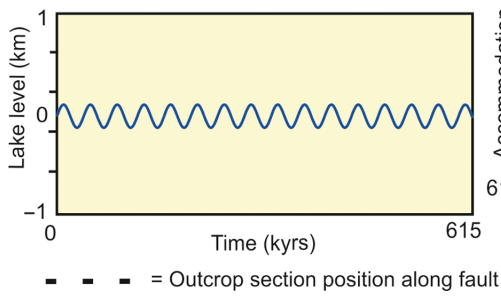
(b3)



Parameter to vary

FIGURE 10 Input parameters for numerical model Syn-Strat, derived from field observations and example outputs. (a) Relative base level curve inputs and output: (a1) 1D input curves representing subsidence and lake level in time and space; (a2) the subdivision of a relative base level curve that is applied to the 3D surface; (a3) resultant surface showing 3D relative base level through time, along the length of the fault. (b) Sedimentation inputs incorporated to produce an accommodation surface: (b1) 1D inputs of sedimentation in time and space; (b2) schematic diagram with red line to indicate position of the plots relative to the fault, i.e. a position in the immediate hangingwall of the fault; (b3) resultant 3D accommodation surface. Positions of Kerinitis and Selinous are shown by K and S labels, respectively. Sequence boundaries are positioned between yellow and purple sections and are apparent at the fault tips, but absent towards the fault centre in both (a3) and (b3). Note reduced accommodation at fan delta locations in (b3) due to sediment-filling. Amplitude of lake level change is varied in the sensitivity tests (pale yellow). EFT = East Fault Tip; WFT = West Fault Tip

(a) Parameter to vary:
Amplitude of lake level change



(b) 3D accommodation surface

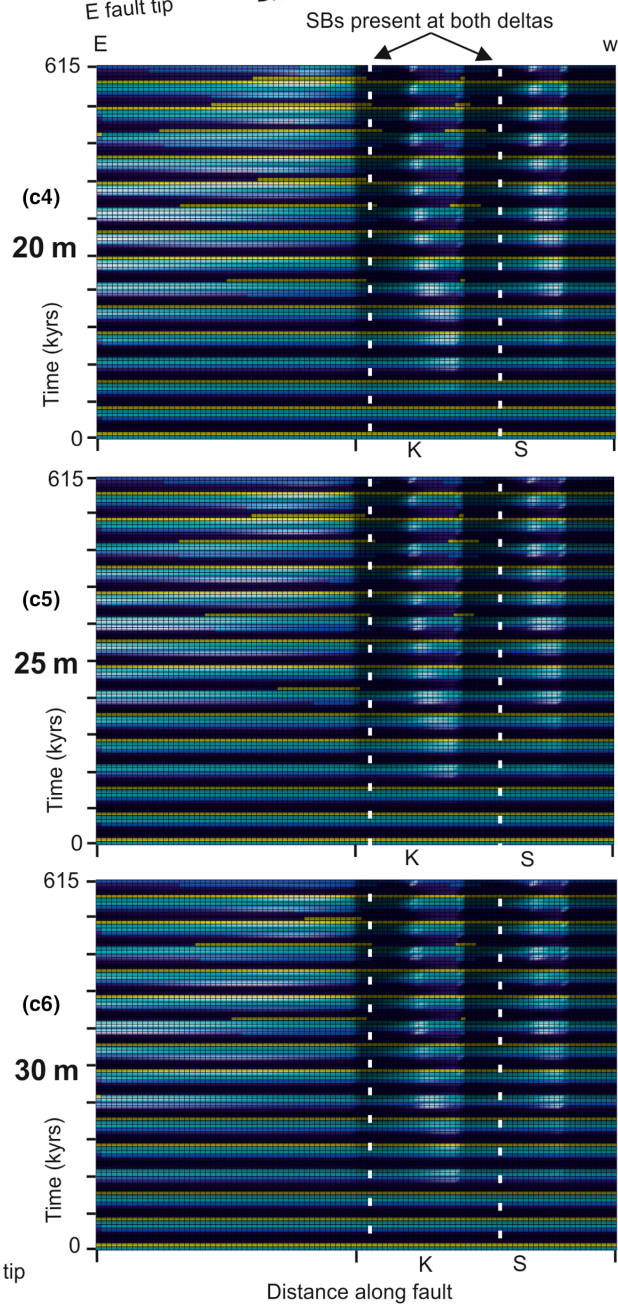
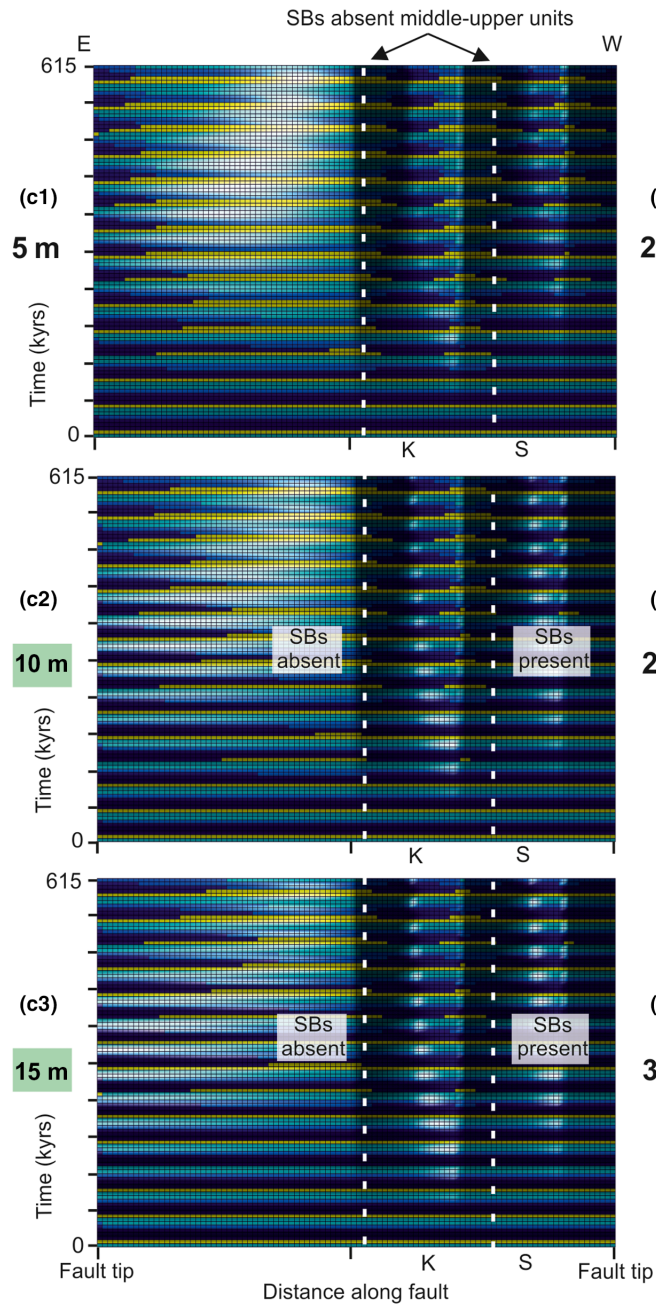
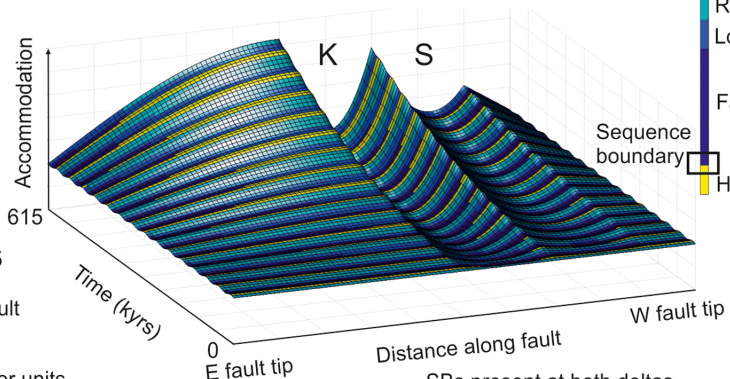


FIGURE 11 Results from numerical modelling sensitivity tests with Syn-Strat. The amplitude of lake level (a) is varied from 5 m to 30 m at 5 m intervals. 3D accommodation surface is shown as example (b). Flattened accommodation surfaces are presented for each test with stages of base level curve presented to allow visualisation of stratigraphic surface extent (c1-c6). Sequence boundaries (SBs) are between yellow and purple sections. Positions of Kerinitis and Selinous are shown by K and S labels, respectively. Approximate outcrop section positions are indicated by dashed lines. The 5 m amplitude test (c1) reveals sequence boundary absence at both outcrop section positions and the 20–30 m (c4-c6) amplitude tests reveal the presence of sequence boundaries at both outcrop section positions—not comparable to field observations. The 10 m and 15 m amplitude tests (c2 and c3, highlighted in green) reveal absence of sequence boundaries at the outcrop section position at Kerinitis and presence of sequence boundaries at the outcrop section position at Selinous—most comparable to field observations—refining the amplitude of lake level fluctuations during the Early-Middle Pleistocene to 10–15 m

fault centre gives an estimated average minimum subsidence rate at the centre of the fault of 2.15 m/kyr. This estimate is highly comparable to Holocene fault-related subsidence rates from the Gulf of Corinth (2.2–3.5 mm/year, McNeill & Collier, 2004), the Gulf of Patras, central Greece (average of 2–5 mm/year and 1–2 mm/year away from the main border faults, Chronis, Piper, & Anagnostou, 1991) and the Wasatch Fault Zone, Basin and Range Province, USA (<2 mm/year, Gawthorpe et al., 1994; Machette, Persounius, & Nelson, 1991; Schwartz & Coppersmith, 1984). The syn-rift sediment thicknesses (total subsidence) are well constrained and we consider that the fan delta build time has relatively low uncertainty; hence the subsidence rates are assigned an equivalent low uncertainty value of 2. If each cycle had a ca. 20 kyr or ca. 100 kyr period, then the calculated subsidence rate would change, but this is neither consistent with the current understanding of climate in Greece in the Early-Middle Pleistocene, nor typical fault displacement rates in the region (Capraro et al., 2005; Dodenov, 2005; McNeill & Collier, 2004; Suc & Popescu, 2005).

The aggradational stacking trend at both fan deltas reveals that overall sedimentation rate kept pace with subsidence rate over the fan delta build times. Accordingly, as aggradation is present at both fan deltas and there is greater subsidence at Kerinitis, the sedimentation rate must be higher at Kerinitis. By dividing the total thickness of syn-rift sediment by the time taken for the sediment to accumulate, the average sedimentation rate at Selinous must be ca. 0.65 m/kyr and at Kerinitis the average sedimentation rate is higher at ca. 1.77 m/kyr. This is similar to estimates for the Vouraikos fan delta that sits along-strike from Kerinitis (Figure 1), where sedimentation rates are estimated to be 1.3–2 mm/year (Ford et al., 2007). We refer to a sedimentation rate and not a sediment supply rate, as some of the sediment may have been bypassed to the deep basin (e.g. Stevenson, Jackson, Hodgson, Hubbard, & Eggenhuisen, 2015) or redistributed along-strike. Although justified as an estimate, an average sedimentation rate does not reflect any probable variation over the fan delta build time, for example from climate or slip rate related changes in erosion rate, we therefore assign these a high uncertainty value of 4.

9 | REDUCING UNCERTAINTY OF CONTROL PARAMETERS

9.1 | Numerical modelling with Syn-Strat

To reduce the uncertainty and more accurately quantify the major controls, we undertake a numerical modelling exercise using Syn-Strat (Barrett et al., 2018). Syn-Strat produces a 3D graphical surface representing accommodation in the hangingwall of a normal fault, resulting from tectonic subsidence, sedimentation and sea- or lake-level inputs. Stacking patterns or systems tracts can be applied to the surface. Control parameters that have been derived from the field data are input into the model (Figure 10). Various sensitivity tests are performed, whereby one of the controls with the least uncertainty is varied to assess the closest match to the field observations. Magnitude of base level change and sedimentation rate has the greatest uncertainty (Table 2). Although the variation in sedimentation rate through time is unknown, we have some constraint on average sedimentation rate from the aggradational stacking patterns at both fan deltas. Lake level change amplitude was tested and is varied at 5 m intervals from 5 m to 30 m (Figure 11). The field observations that we compare are the presence of sequence boundaries at Selinous and absence at Kerinitis and are taken from sections cutting the eastern margins of the fan deltas (positions are indicated on the flattened plots, c1-c6 in Figure 11 by the dashed lines).

Figure 10 explains the set-up of the numerical modelling tests. The size of the basin is defined first in the model and represented by the size of the matrix. In this case, we define the fault block width (6 km) and length (24 km) and the distance between the axis of each fan delta (6 km). The sediment input points are placed at the respective positions of the fan deltas along the fault; 4 km (Selinous) and 10 km (Kerinitis) from the western fault tip. For the timescale, we take the maximum fan delta build time, which is derived from Selinous as 615 kyr. Each parameter is defined with one-dimensional graphical curves plotted along the fault (x), away from the fault (y) and in time (t) (Figure 10a1).

We present the subsidence and lake level controls alone (Figure 10a), in order to show the resultant relative base level curve without sedimentation inputs. All

parameters are kept constant, other than the parameter in question (lake level amplitude). The 3D output shows relative base level change at every point along the length of the fault for a position in the immediate hangingwall of the fault (red line on the schematic diagram in b2 of Figure 10). This position is chosen as it is where the maximum topset unit thickness is observed and has been used to calculate the subsidence and sedimentation rates. Systems tracts (or stages of a base level curve) can be applied to a 3D relative base level (a2 and a3 of Figure 10), just as they can to a traditional 1D relative base level curve. With the given parameters, it is apparent that the key stratigraphic surfaces are diachronous along the fault due to the subsidence variation. The falling limb of the relative base level curve (purple segment on Figure 10a) and therefore sequence boundary is defined as the onset of the fall (between yellow and purple segments). It is not expressed at the fault centre, because subsidence outpaces the maximum rate of lake level fall. Sedimentation fills the space made available through time (Figure 10b), so that at each time step, the space for subsequent deposition is a result of the preceding base level change, subsidence and sedimentation (Barrett et al., 2018). The addition of the sedimentation curves in time and space (Figure 10b1) produces an accommodation curve that is reduced from sediment-filling at the positions of the fan deltas (Figure 10b3).

The suite of sensitivity tests show that the diachroneity of stratigraphic surfaces decreases with increasing amplitude of base level, as the subsidence control becomes less dominant (Figure 11). In the test with the lowest base level change (5 m; c1), the onset of relative base level fall occurs ca. 6–12 kyr earlier at the centre of the fan deltas than at the margins, whereas in the highest amplitude base level change test (30 m; c6), it appears to occur at the same time along the fault and any diachroneity is below the resolution of the model. There is a clear difference in the nature of sequence boundaries diachroneity between the tests. There are also changes within each test through time. It appears that the diachroneity generally increases through time and in doing so, progressively limits the sequence boundaries to positions closer towards the centre of the fan deltas. This is likely to be in response to the subsidence and sedimentation rates increasing through time in the model (Figure 10). Our analysis was undertaken in the middle-to-upper units of the fan deltas and so it is here in the model outputs that we assess the presence or absence of sequence boundaries.

When the amplitude of base level change is >20 m (Figure 11, c4, c5 and c6), sequence boundaries are expressed across both Kerinitis and Selinous. In the field, however, we observe sequence boundaries at Selinous, but not at Kerinitis. In the 5 m amplitude test (Figure 11, c1), sequence boundaries are present at the centre of both fan

deltas as here there is maximum sedimentation; the sediments fill and exceed the available accommodation and this causes the system to prograde basinwards. However, at the margins of the fan deltas, where sedimentation is lower, the sequence boundaries are not expressed. As we observe sequence boundaries at the margin of Selinous, this test is also not comparable to our observations. For base level change amplitudes of 10 m and 15 m (Figure 11, c2 and c3), sequence boundaries are expressed in the model results in the middle-upper units at the margin of Selinous, but not at Kerinitis, which match our field observations. These tests are performed with average sedimentation rate equivalent to subsidence. Sedimentation rate is unlikely to be higher than our estimates, but could be lower. In this case, the effect of a relative base level rise would be amplified, so a lower lake level amplitude would be required to give the same response to match our field observations. The lake level change amplitude estimate is therefore a maximum value. In the 15 m amplitude change test (Figure 11, c3), sequence boundaries are absent at Kerinitis in the upper units, but present in the middle units. In the field, the middle units (Units 4–8) do not reveal sequence boundaries; hence the 10 m amplitude lake level change amplitude is more consistent with field observations than the 15 m. However, we recognise that uncertainties in the inputs do not allow us to constrain the magnitude of lake level amplitude change to less than 5 m, henceforth we utilise a unit thickness extrapolation approach to validate the numerical modelling output.

9.2 | Refinement of lake level change using unit thickness extrapolation method

Lake level changes of 10–15 m amplitude are supported by the extrapolation of unit thicknesses towards the fault tip (Figure 12). Average unit thickness of the Kerinitis topsets is ca. 60 m and at Selinous is ca. 25 m. The thickness contribution from subsidence is at least 35 m at Kerinitis and reduces towards the fault tip (in blue on Figure 12). The unit thickness decay between Kerinitis and Selinous occurs over 6 km, with a decay rate of 5.8 m/km. If the same assumed linear unit decay trend is extrapolated a further 4 km to the fault tip, where fault-controlled subsidence is theoretically zero, the units would hypothetically lose a further 23 m thickness, leaving 12 m of possible unit thickness at the fault tip. There must be a space created for this thickness of sediment to accumulate at the fault tip as subsidence is zero and fluctuation of lake level associated with climate change is the most likely mechanism. There is no actual stratigraphy preserved at the fault tip because there is no net accommodation gain in the immediate hangingwall of the P-M Fault. This analysis assumes that there is no additional space creation from other nearby faults,

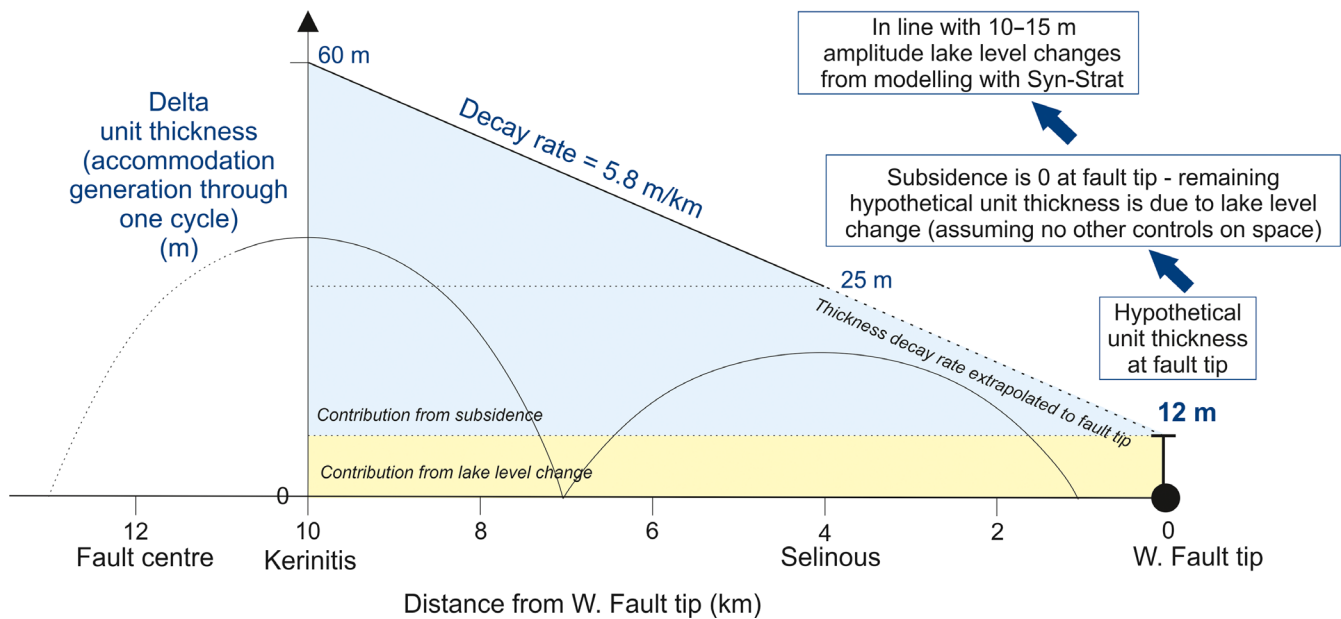


FIGURE 12 Along-strike graphical cross-section to show unit thickness decay extrapolation towards the western fault tip. This is to derive a hypothetical unit thickness at the fault tip, where subsidence is zero and any remaining thickness may have accumulated in space derived from base level change, thus providing an independent derivation of the amplitude of base level change through the Early-Middle Pleistocene in Lake Corinth (12 m), in support of our modelling results (10–15 m). The semi-circular lines are presented to show the extent of the deltas along the fault and to highlight the greater thickness of Kerinitis than Selinous

background subsidence or underlying topography for the sediments to fill. The calculated 12 m base level change is comparable with the model estimate of 10–15 m.

10 | IMPLICATIONS

The implications for this work are three-fold: (a) we demonstrate a method for dissociating base level from faulting, which could be applied to a number of other rift basin-fills; (b) we present a quantitative modelling approach to the analysis of stacking and surfaces, constrained by field data, that could be applied to stratigraphic pinch-out assessment and cross-hole correlations in reservoir analysis; and (c) we derive a lake level change amplitude for the region, which could aid regional palaeoclimate studies and inform broader climate-system models.

10.1 | Applications to other basins

Two independent methods—forward modelling with Syn-Strat and unit thickness extrapolation—provided comparable results for lake level change amplitude in Lake Corinth through the Early to Middle Pleistocene (10–15 m). Other studies have presented the problem of dissociating base level from faulting in rift basins. Dorsey and Umhoefer (2000) attribute the accommodation creation for the Pliocene vertically stacked deltas in the Loreto Basin, Gulf

of California to episodic fault-controlled subsidence near the fault centre and to eustasy near the fault tip, by correlation of parasequences to a marine oxygen isotope curve. It is likely that subsidence rate outpaced eustasy near the fault centre to restrict the development of sequence boundaries to the fault tips. By utilising our methods, it would be possible to affirm whether the stacking cyclicity observed is attributable to faulting or base level change. The numerical modelling approach with Syn-Strat is not limited to rift basins. Any mechanism that creates or reduces accommodation (e.g. salt diapirism or thrust folding) could replace the normal fault in the model and sequence stratigraphic evolution in these settings could be assessed. In areas with good age/eustatic sea level constraints and for given sedimentation rates, different structural styles could be tested to find the best fit to the observed stratigraphy.

10.2 | Subsurface appraisal

By comparing two fan deltas, we have been able to constrain the interplay of allogenic controls responsible for their depositional architectures. The study of a single fan delta would not have been sufficient to do this; hence we highlight the importance of studying multiple systems within a single basin-fill. With subsidence rates of 0.65 m/kyr at Selinous at ca. 4 km from the western fault tip, 1.77 m/kyr at Kerinitis at ca. 10 km from the tip, there should be a maximum subsidence rate of 2.14 m/kyr at the fault centre (ca. 2 km further

along-strike). Unit thickness could, for instance, be extrapolated along-strike to provide a hypothetical estimate of 72 m at the fault centre, assuming predominantly aggradational stacking geometries. We cannot test this in the area as no fan delta is located exactly at the fault centre and there is no point source at the fault tip. However, in other settings the ability to predict the variation of stratigraphic thickness along-strike is important for assessment of stratigraphic pinch-out in hydrocarbon reservoirs. The modelling work also demonstrates the extent and nature of diachroneity of sequence boundaries along-strike. Such spatiotemporal variability in erosion can have implications for reservoir unit correlation and connectivity. Barrett et al. (2018) demonstrate that the surfaces are not only diachronous, but how that diachroneity may change along the fault and through time for given scenarios. Here, we go one step further and quantify that variation. For example, in the 10 m lake level amplitude test, the sequence boundary occurs ca. 6 kyr earlier at the centre of the fan deltas than at the margins (Figure 11). In a subsurface setting, this method could improve confidence in cross-hole correlations of these surfaces.

10.3 | Implications of a lake level change amplitude of 10–15 m

Early-Middle Pleistocene climate for the Mediterranean region has been studied using palynology (e.g. Capraro et al., 2005; Joannin, Quillévéré, Suc, Lécuyer, & Martineau, 2007; Suc & Popescu, 2005) and speleothem analysis as a proxy for local rainfall and air temperature (e.g. Dotsika et al., 2010). Climate fluctuated between cold and dry and warm and wet periods in association with global climatic records during this time (Head & Gibbard, 2005, and references therein). We interpret that these climate changes resulted in changes in the level of Lake Corinth, which have been estimated to have an amplitude of 10–15 m. The geological record of amplitude is a valuable resource and our estimated value could inform hydrological budget calculations in both regional palaeoclimate studies of the Gulf of Corinth or Mediterranean and broader climate-system numerical models that require lake level data as an input. Numerical models used to predict how future climate may impact a region require quantitative palaeoclimatic data from multiple proxies from the land and ocean to understand the forcing mechanisms behind observed climatic patterns and also to validate and improve the models themselves (Abrantes et al., 2012; Luterbacher et al., 2012).

The volume of water that a 10–15 m change in lake level represents is crudely calculated for the Middle Pleistocene Lake Corinth. The lake boundaries are taken from Nixon et al. (2016) and do not include the Alkyonides Basin that may have been disconnected at that time (Nixon et al., 2016). A ca. 240 km perimeter and a volume change of ca. 17–26 km³

are estimated (order of 10¹⁰ m³). How a 10–15 m rise would have impacted the coastline is dependent on the coastal gradient and local sediment supply. With an average gradient of the shelf slope in the Gulf of Corinth of 2.8° (from the Alkyonides Basin, Leeder et al., 2002), a 10–15 m change in lake level would cause the coastline to shift by 250–310 m. However, considering parts of the coastline positioned on a fan delta, with topset gradients of <0.1° and foreset gradients of ca. 22°, this shift would be highly variable, depending on whether there is a lake level rise or fall. Starting at the topset-foreset breakpoint, a fall of 10–15 m, would cause the shoreline to advance only 25–40 m due to the steep foreset slope (not including effects on sediment supply). On the other hand, a rise of 10–15 m from the breakpoint would cause a potential shoreline shift of 5–10 km, due to the near-horizontal (0.1°) topset. In reality, coastal topography and the border faults would prevent such a dramatic shift, but this could explain the ca. 2.5–3 km extent from the P-M Fault of the fine-grained intervals that contain the maximum flooding surfaces between each major unit observed at both Selinous and Kerinitis.

11 | CONCLUSIONS

We have undertaken the first sedimentological and stratigraphic study of the Selinous syn-rift fan delta in the Gulf of Corinth, Greece and made comparisons with the adjacent and contemporaneous Kerinitis syn-rift fan delta. In doing so, we demonstrate that a multi-system-study approach is an effective way of understanding and quantifying allogenic basin controls. This is the first detailed comparison of stratigraphic architectures between along-strike systems in the hanging-wall of a normal fault, positioned near the fault centre and near the fault tip. Eighteen facies and eight facies associations were identified between the deltas and distinguished in terms of their topset to bottomset geometric position and depositional environments. Maximum flooding surfaces are apparent at both fan deltas between the major stratal units, but sequence boundaries are only observed at Selinous, near the fault tip. In spite of this, stacking patterns are similar between the fan deltas, as shown by trajectory analyses of both, with evidence of: (a) progradation within the units (10-m scale), (b) retrogradation at Selinous and aggradation at Kerinitis between middle-upper units (100-m scale), (c) aggradation at the fan delta scale (400–800 m). This implies that overall sedimentation kept pace with accommodation in both cases. As subsidence rate is lower at Selinous near the fault tip, average sedimentation rate must also be lower there than at Kerinitis. The duration for the whole of each fan delta to build was estimated to be 615 kyr for Selinous and at least 450 kyr for Kerinitis. Controlling parameters were quantified from field observations, including subsidence and

average sedimentation rates of 0.65 m/kyr at Selinous and >1.77 m/kyr at Kerinitis, and assigned uncertainty values from 1–5. The amplitude of lake level change through time was deemed the most uncertain parameter. Numerical modelling with Syn-Strat was undertaken using the presence of sequence boundaries at both localities in various scenarios, to reduce the uncertainty and better constrain the amplitude of lake level change. Lake level changes of 10–15 m were estimated from the model and supported by an independent calculation of 12 m from unit thickness extrapolation towards the fault tip. The study has three broad outcomes: (a) demonstration of two complementary methods to identify and quantify faulting and base level signals in the stratigraphic record, which could be applied to other rift basin-fills, (b) a quantitative approach to the analysis of stacking and surfaces, constrained by field data, that can be applied to stratigraphic pinch-out assessment and cross-hole correlations in reservoir analysis; and (c) an estimate of lake level change amplitude in Lake Corinth for the Early-Middle Pleistocene, which could aid regional palaeoclimate studies and inform broader climate-system models.

ACKNOWLEDGMENTS

We thank the project sponsor, Neptune Energy, that supported the SMRG (Shallow Marine Research Group). Barrett was partially sponsored by a VISTA Visiting Scholarship at the University of Bergen. Gawthorpe acknowledges support from the VISTA Professorship.

ORCID

Bonita J. Barrett  <https://orcid.org/0000-0002-3274-822X>

Richard E. LL. Collier  <https://orcid.org/0000-0002-8001-0510>

David M. Hodgson  <https://orcid.org/0000-0003-3711-635X>

Robert L. Gawthorpe  <https://orcid.org/0000-0002-4352-6366>

Robert M. Dorrell  <https://orcid.org/0000-0003-4257-7273>

Timothy M. Cullen  <https://orcid.org/0000-0002-2497-2213>

REFERENCES

- Abrantes, F., Voelker, A. H. L., Sierro, F. J., Naughton, F., Rodrigues, T., Cacho, I., ... Batista, L. (2012). 1 – Paleoclimate variability on the Mediterranean region. *The climate of the Mediterranean region, from the past to the future* (pp. 1–86). London, UK: Elsevier.
- Avallone, A., Briole, P., Agatza-Balodimou, A. M., Billiris, H., Charade, O., Mitsakaki, C., ... Veis, G. (2004). Analysis of eleven years of deformation measured by GPS in the Corinth Rift Laboratory area. *Comptes Rendus Geoscience*, 336, 301–311. <https://doi.org/10.1016/j.crte.2003.12.007>
- Backert, N., Ford, M., & Malartre, F. (2010). Architecture and sedimentology of the Kerinitis Gilbert-type fan delta, Corinth Rift, Greece. *Sedimentology*, 57, 543–586. <https://doi.org/10.1111/j.1365-3091.2009.01105.x>
- Barrett, B. J., Hodgson, D. M., Collier, R. E. L., & Dorrell, R. M. (2018). Novel 3D sequence stratigraphic numerical model for syn-rift basins: Analysing architectural responses to eustasy, sedimentation and tectonics. *Marine and Petroleum Geology*, 92, 270–284. <https://doi.org/10.1016/j.marpetgeo.2017.10.026>
- Bell, R. E., McNeill, L. C., Bull, J. M., & Henstock, T. J. (2008). Evolution of the offshore western Gulf of Corinth. *Geological Society of America Bulletin*, 120, 156–178.
- Benson, L. V., Lund, S. P., Burdett, J. W., Kashgarian, M., Rose, T. P., Smoot, J. P., & Schwartz, M. (1998). Correlation of Late-Pleistocene Lake-Level Oscillations in Mono Lake, California, with North Atlantic Climate Events. *Quaternary Research*, 49, 1–10. <https://doi.org/10.1006/qres.1997.1940>
- Bernard, P., Lyon-Caen, H., Briole, P., Deschamps, A., Boudin, F., Makropoulos, K., ... Linde, A. (2006). Seismicity, deformation and seismic hazard in the western rift of Corinth: New insights from the Corinth Rift Laboratory (CRL). *Tectonophysics*, 426, 7–30. <https://doi.org/10.1016/j.tecto.2006.02.012>
- Briole, P., Rigo, A., Lyon-Caen, H., Ruegg, J. c., Papazissi, K., Mitsakaki, C., ... Deschamps, A. (2000). Active deformation of the Corinth rift, Greece: Results from repeated Global Positioning System surveys between 1990 and 1995. *Journal of Geophysical Research-Solid Earth*, 105, 25605–25625. <https://doi.org/10.1029/2000JB900148>
- Capraro, L., Asioli, A., Backman, J., Bertoldi, R., Channell, J. E. T., Massari, F., & Rio, D. (2005). Climatic patterns revealed by pollen and oxygen isotope records across the Matuyama-Brunhes Boundary in the central Mediterranean (southern Italy). *Geological Society, London, Special Publications*, 247, 159–182. <https://doi.org/10.1144/GSL.SP.2005.247.01.09>
- Catuneanu, O., Abreu, V., Bhattacharya, J. P., Blum, M. D., Dalrymple, R. W., Eriksson, P. G., ... Winker, C. (2009). Towards the standardization of sequence stratigraphy. *Earth-Science Reviews*, 92, 1–33.
- Chronis, G., Piper, D. J. W., & Anagnostou, C. (1991). Late Quaternary evolution of the Gulf of Patras, Greece: Tectonism, deltaic sedimentation and sea-level change. *Marine Geology*, 97, 191–209. [https://doi.org/10.1016/0025-3227\(91\)90026-Z](https://doi.org/10.1016/0025-3227(91)90026-Z)
- Clarke, P. J., Davies, R. R., England, P. C., Parsons, B. E., Billiris, H., Paradissis, D., ... Bingley, R. (1997). Geodetic estimate of seismic hazard in the Gulf of Korinthos. *Geophysical Research Letters*, 24, 1303–1306. <https://doi.org/10.1029/97GL01042>
- Collier, R. E. L., & Dart, C. J. (1991). Neogene to Quaternary rifting, sedimentation and uplift in the Corinth Basin, Greece. *Journal of the Geological Society London*, 148, 1049–1065. <https://doi.org/10.1144/gsjgs.148.6.1049>
- Collier, R. E. L., Leeder, M. R., & Maynard, J. R. (1990). Transgressions and regressions: A model for the influence of tectonic subsidence, deposition and eustasy, with application to Quaternary and Carboniferous examples. *Geological Magazine*, 127, 117–128. <https://doi.org/10.1017/S0016756800013819>
- Collier, R. E. L., Leeder, M. R., Trout, M., Ferentinos, G., Lyberis, E., & Papatheodorou, G. (2000). High sediment yields and cool, wet winters: Test of last glacial paleoclimates in the northern Mediterranean. *Geology*, 28, 999–1002. [https://doi.org/10.1130/0091-7613\(2000\)28<999:HSYACW>2.0.CO;2](https://doi.org/10.1130/0091-7613(2000)28<999:HSYACW>2.0.CO;2)

- Collier, R. E. L., & Thompson, J. (1991). Transverse and linear dunes in an Upper Pleistocene marine sequence, Corinth Basin, Greece. *Sedimentology*, 38, 1021–1040. <https://doi.org/10.1111/j.1365-3091.1991.tb00369.x>
- Collier, R. E. L. (1990). Eustatic and tectonic controls upon Quaternary coastal sedimentation in the Corinth Basin, Greece. *Journal of the Geological Society*, 147, 301–314.
- Cotterill, C. J. (2002). A high resolution Holocene fault activity history of the Aigion shelf, Gulf of Corinth, Greece. PhD Thesis, School of Ocean and Earth Sciences, University of Southampton, UK.
- Dart, C. J., Collier, R. E. L., Gawthorpe, R. L., Keller, J. V. A., & Nichols, G. (1994). Sequence stratigraphy of (?)Pliocene-quaternary synrift, gilbert-type fan deltas, Northern Peloponnesos, Greece. *Marine and Petroleum Geology*, 11, 545–560.
- de Martini, P., Pantosti, D., Palyvos, N., Lemeille, F., McNeill, L., & Collier, R. E. L. (2004). Slip rates of the Aigion and Eliki faults from uplifted marine terraces, Corinth Gulf, Greece. *Comptes Rendus Geoscience*, 336, 325–334.
- Dodenov, A. E. (2005). The stratigraphic transition and suggested boundary between the Early and Middle Pleistocene in the loess record of northern Eurasia. *Geological Society, London, Special Publications*, 247, 209–219. <https://doi.org/10.1144/GSL.SP.2005.247.01.11>
- Dorsey, R. J., & Umhoefer, P. J. (2000). Tectonic and eustatic controls on sequence stratigraphy of the Pliocene Loreto Basin, Baja California Sur, Mexico. *GSA Bulletin*, 112, 177–199.
- Dorsey, R. J., Umhoefer, P. J., & Renne, P. R. (1995). Rapid subsidence and stacked gilbert-type fan deltas, Pliocene Loreto Basin, Baja California Sur, Mexico. *Sedimentary Geology*, 98, 181–204.
- Dotsika, E., Psomiadis, D., Zanchetta, G., Spyropoulos, N., Leone, G., Tzavidopoulos, I., & Poutoukis, D. (2010). Pleistocene palaeoclimatic evolution from Agios Georgios Cave speleothem (Kilkis, N. Greece). *Bulletin of the Geological Society of Greece, Proceedings of the 12th International Congress, Patras, 2*, 886–895.
- Emiliani, C. (1978). The cause of the ice ages. *Earth & Planetary Science Letters*, 37, 349–352. [https://doi.org/10.1016/0012-821X\(78\)90050-X](https://doi.org/10.1016/0012-821X(78)90050-X)
- Floyd, M. A., Billiris, H., Paradissis, D., Veis, G., Avallone, A., Briole, P., ... England, P. C. (2010). A new velocity field for Greece: Implications for the kinematics and dynamics of the Aegean. *Journal of Geophysical Research*, 115, B10403. <https://doi.org/10.1029/2009JB007040>
- Ford, M., Hemelsdael, R., Mancini, M., & Palyvos, N. (2016). Rift migration and lateral propagation: evolution of normal faults and sediment-routing systems of the western Corinth rift (Greece). In C. Childs, R. E. Holdsworth, C.-A.-L. Jackson, T. Manzocchi, J. J. Walsh, & G. Yielding (Eds.), *The geometry of normal faults* (pp. 439). London, UK: Geological Society, London, Special Publications.
- Ford, M., Rohais, S., Williams, E. A., Bourlange, S., Jousselin, D., Backert, N., & Malartre, F. (2013). Tectonosedimentary evolution of the western Corinth rift (Central Greece). *Basin Research*, 25, 3–25. <https://doi.org/10.1111/j.1365-2117.2012.00550.x>
- Ford, M., Williams, E. A., Malartre, F., & Popescu, S. M. (2007). Stratigraphic architecture, sedimentology and structure of the Vouraikos Gilbert-type fan delta, Gulf of Corinth, Greece. In G. Nichols, E. Williams, & C. Paola (Eds.), *Sedimentary processes, environments and basins. A tribute to Peter Friend* (pp. 49–90). London, UK: Geological Society, London, Special Publications.
- Frazier, D. (1974). Depositional Episodes: Their Relationship to the Quaternary Stratigraphic Framework in the Northwestern Portion of the Gulf Basin. Bureau of Economic Geology, University of Texas, Geological Circular 74-1, pp. 26.
- Galloway, W. L. (1989). Genetic stratigraphic sequences in basin analysis I: Architecture and genesis of flooding surface bounded depositional units. *AAPG Bulletin*, 73, 125–142.
- Garcia-Garcia, F., Fernandez, J., Viseras, C., & Soria, J. H. (2006). Architecture and sedimentary facies evolution in a delta stack controlled by fault growth (Betic Cordillera, southern Spain, late Tortonian). *Sedimentary Geology*, 185, 79–92.
- Garcia-Mondéjar, J. (1990). Sequence analysis of a marine Gilbert-type delta, La Miel, Albian Lunada Formation of northern Spain. In A. Colella, & D. B. Prior (Eds.), *Coarse-grained deltas* (pp. 255–269). London, UK: Geological Society, London, Special Publications.
- Gasse, F., Lédée, V., Massault, M., & Fontes, J.-C. (1989). Water-level fluctuations of Lake Tanganyika in phase with oceanic changes during the last glaciation and deglaciation. *Nature*, 342, 57–59. <https://doi.org/10.1038/342057a0>
- Gawthorpe, R. L., Andrews, J. E., Collier, R. E. L., Ford, M., Henstra, G. A., Kranis, H., ... Skourtsos, E. (2017). Building up or out? Disparate sequence architectures along an active rift margin – Corinth rift, Greece. *Geology*, 45, 111–114.
- Gawthorpe, R. L., Fraser, A., & Collier, R. E. L. (1994). Sequence stratigraphy in active extensional basins: Implications for the interpretation of ancient basin fills. *Marine and Petroleum Geology*, 11, 642–658. [https://doi.org/10.1016/0264-8172\(94\)90021-3](https://doi.org/10.1016/0264-8172(94)90021-3)
- Gawthorpe, R. L., Hardy, S., & Ritchie, B. (2003). Numerical modelling of depositional sequences in half-graben rift basins. *Sedimentology*, 50, 169–185. <https://doi.org/10.1046/j.1365-3091.2003.00543.x>
- Gawthorpe, R. L., & Leeder, M. R. (2000). Tectono-sedimentary evolution of active extensional basins. *Basin Research*, 12, 195–218.
- Gawthorpe, R. L., Leeder, M. R., Kranis, H., Skourtsos, E., Andrews, J. E., Henstra, G. A., ... Stamatakis, M. (2017). Tectono-sedimentary evolution of the Plio-Pleistocene Corinth rift, Greece. *Basin Research*, 1–32. <https://doi.org/10.1111/bre.12260>
- Gawthorpe, R. L., Sharp, I., Underhill, J. R., & Gupta, S. (1997). Linked sequence stratigraphic and structural evolution of propagating normal faults. *Geology*, 25, 795–798. [https://doi.org/10.1130/0091-7613\(1997\)025<0795:LSSASE>2.3.CO;2](https://doi.org/10.1130/0091-7613(1997)025<0795:LSSASE>2.3.CO;2)
- Ghisetti, F., & Vezzani, L. (2004). Plio-Pleistocene sedimentation and fault segmentation in the Gulf of Corinth (Greece) controlled by inherited structural fabric. *Comptes Rendus Geosciences*, 336, 243–249. <https://doi.org/10.1016/j.crte.2003.12.008>
- Gilbert, G. K. (1885). The topographic features of lake shores. *United States Geological Survey Annual Report*, 5, 69–123.
- Gilbert, G. K. (1890). Lake Bonneville. *United States Geological Survey Monographs*, 1, 1–438.
- Goldsworthy, M., & Jackson, J. (2001). Migration of activity within normal fault systems: Examples from the Quaternary of mainland Greece. *Journal of Structural Geology*, 23, 489–506. [https://doi.org/10.1016/S0191-8141\(00\)00121-8](https://doi.org/10.1016/S0191-8141(00)00121-8)
- Hardy, S., Dart, C. J., & Waltham, D. (1994). Computer modelling of the influence of tectonics on sequence architecture of coarse-grained fan deltas. *Marine and Petroleum Geology*, 11, 561–574. [https://doi.org/10.1016/0264-8172\(94\)90068-X](https://doi.org/10.1016/0264-8172(94)90068-X)
- Hardy, S., & Gawthorpe, R. L. (1998). Effects of variations in fault slip rate on sequence stratigraphy in fan deltas: Insights from numerical modeling. *Geology*, 26, 911–914. [https://doi.org/10.1130/0091-7613\(1998\)026<0911:EOVIFS>2.3.CO;2](https://doi.org/10.1130/0091-7613(1998)026<0911:EOVIFS>2.3.CO;2)

- Hardy, S., & Gawthorpe, R. L. (2002). Normal fault control on bedrock channel incision and sediment supply: Insights from numerical modeling. *Journal of Geophysical Research*, *107*, 2246. <https://doi.org/10.1029/2001JB000166>
- Head, M. J., & Gibbard, E. L. (2005). Early-middle pleistocene transitions: The land-ocean evidence. *Geological Society, London, Special Publications*, *247*, 1–18.
- Jackson, C. A. L., Gawthorpe, R. L., Carr, I. D., & Sharp, I. R. (2005). Normal faulting as a control on the stratigraphic development of shallow marine syn-rift sequences: The Nukhul and Lower Rudeis Formations, Hammam Faraun fault block, Suez Rift. *Egypt. Sedimentology*, *52*, 313–338. <https://doi.org/10.1111/j.1365-3091.2005.00699.x>
- Jervey, M. T. (1988). Quantitative geological modeling of siliciclastic rock sequences and their seismic expression. In C. K. Wilgus, B. S. Hastings, C. G. S. C. Kendall, H. W. Posamentier, C. A. Ross, & J. C. VanWagoner (Eds.), *Sea-level changes: An integrated approach* (pp. 47–69). Broken Arrow, OK: SEPM Society for Sedimentary Geology.
- Joannin, S., Quillévéré, F., Suc, J.-P., Lécuyer, C., & Martineau, F. (2007). Early Pleistocene climate changes in the central Mediterranean region as inferred from integrated pollen and planktonic foraminiferal stable isotope analyses. *Quaternary Research*, *67*, 264–274. <https://doi.org/10.1016/j.yqres.2006.11.001>
- Leeder, M. R., Collier, R. E. L., Abdul Aziz, L. H., Trout, M., Ferentinos, G., Papatheodorou, G., & Lyberis, E. (2002). Tectono-sedimentary processes along an active marine/lacustrine half-graben margin: Alkyonides Gulf, E. Gulf of Corinth, Greece. *Basin Research*, *14*, 25–41. <https://doi.org/10.1046/j.1365-2117.2002.00164.x>
- Leeder, M. R., Gawthorpe, R. L. (1987). Sedimentary models for extensional tilt block/half-graben basins. In M. P. Coward, J. F. Dewey, & P. L. Hancock (Eds.), *Continental extensional tectonics* (Vol 28, pp. 139–152). London, UK: Geological Society, London, Special Publications.
- Leeder, M. R., Harris, T., & Kirkby, M. J. (1998). Sediment supply and climate change: Implications for basin stratigraphy. *Basin Research*, *10*, 7–18. <https://doi.org/10.1046/j.1365-2117.1998.00054.x>
- Leeder, M. R., Mack, G. H., Brasier, A. T., Parrish, R. R., Mintosh, W. C., Andrews, J. E., & Duremeijer, C. E. (2008). Late-Pliocene timing of Corinth (Greece) rift-margin fault migration. *Earth and Planetary Science Letters*, *274*, 132–141. <https://doi.org/10.1016/j.epsl.2008.07.006>
- Leeder, M. R., Mark, D. F., Gawthorpe, R. L., Kranis, H., Loveless, S., Pedentchouk, N., ... Stamatakis, M. (2012). A “Great Deepening”: Chronology of rift climax, Corinth rift, Greece. *Geology*, *40*, 999–1002. <https://doi.org/10.1130/G33360.1>
- Lisiecki, L. E., & Raymo, M. E. (2007). Plio-Pleistocene climate evolution: Trends and transitions in glacial cycle dynamics. *Quaternary Science Reviews*, *26*, 56–69. <https://doi.org/10.1016/j.quascirev.2006.09.005>
- Luterbacher, J., García-Herrera, R., Akcer-On, S., Allan, R., Alvarez-Castro, M.-C., Benito, G., ... Zorita, E. (2012). 2 – A review of 2000 years of paleoclimatic evidence in the Mediterranean. In P. Lionello (Eds.), *The Climate of the Mediterranean Region, from the past to the future*, (pp. 87–185) Amsterdam: Elsevier Insights, Elsevier.
- Lyons, R. P., Scholtz, C. A., Cohen, A. S., King, J. W., Brown, E. T., Ivory, S. J., ... Blome, M. W. (2015). Continuous 1.3-million-year record of East African hydroclimate, and implications for patterns of evolution and biodiversity. *Proceedings of the National Academy of Sciences of the United States of America*, *112*, 15568–15573. <https://doi.org/10.1073/pnas.1512864112>
- Machette, M. N., Persounius, S. F., & Nelson, A. R. (1991). The Wasatch fault zone, Utah – segmentation and history of Holocene earthquakes. *Journal of Structural Geology*, *13*, 137–149.
- Malarte, F., Ford, M., & Williams, E. A. (2004). Preliminary biostratigraphy and 3D lithostratigraphy of the Vouraikos Gilbert-type fan delta. Implications for the evolution of the Gulf of Corinth, Greece. *Comptes Rendus Geoscience*, *336*, 269–280.
- Marchegiano, M., Francke, A., Gliozzi, E., & Ariztegui, D. (2017). Arid and humid phases in central Italy during the Late Pleistocene revealed by the Lake Trasimeno ostracod record. *Palaeogeography, Palaeoclimatology, Palaeoecology*, *490*, 55–69. <https://doi.org/10.1016/j.palaeo.2017.09.033>
- Marshall, M. H., Lamb, H. F., Huws, D., Davies, S. J., Bates, R., Bloemendal, J., ... Bryant, C. (2011). Late Pleistocene and Holocene drought events at Lake Tana, the source of the Blue Nile. *Global and Planetary Change*, *78*, 147–161. <https://doi.org/10.1016/j.gloplacha.2011.06.004>
- McNeill, L. C., & Collier, R. E. L. (2004). Uplift and slip rates of the eastern Eliki fault segment, Gulf of Corinth, Greece, inferred from Holocene and Pleistocene terraces. *Journal of the Geological Society, London*, *161*, 81–92. <https://doi.org/10.1144/0016-764903-029>
- McNeill, L. C., Cotterill, C. J., Henstock, T. J., Bull, J. M., Stefatos, A., Collier, R., ... Hicks, S. E. (2005). Active faulting within the offshore western Gulf of Corinth, Greece: Implications for models of continental rift deformation. *Geology*, *33*, 241–244. <https://doi.org/10.1130/G21127.1>
- Mitchum, R. M., Vail, P. R., & Thompson, S. (1977). Seismic stratigraphy and global changes of sea level, Part 2: The depositional sequence as a basic unit for stratigraphic analysis. In: *Seismic Stratigraphy – Applications to Hydrocarbon Exploration* (Ed. by C.E. Payton), *AAPG Mem.*, *26*, 53–62.
- Moretti, I., Lykousis, V., Sakellariou, D., Reynaud, J. Y., Benziane, B., & Prinzhofer, A. (2004). Sedimentation and subsidence rate in the Gulf of Corinth: What we learn from the Marion Dufresne’s long-piston coring. *Comptes Rendus Geoscience*, *336*, 291–299. <https://doi.org/10.1016/j.crte.2003.11.011>
- Mortimer, E., Gupta, S., & Cowie, P. (2005). Cliniform nucleation and growth in coarse-grained deltas, Loreto basin, Baja California Sur, Mexico: A response to episodic accelerations in fault displacement. *Basin Research*, *17*, 337–359. <https://doi.org/10.1111/j.1365-2117.2005.00273.x>
- Neal, J., & Abreu, V. (2009). Sequence stratigraphy hierarchy and the accommodation succession method. *Geology*, *37*, 779–782. <https://doi.org/10.1130/G25722A.1>
- Nixon, C. W., McNeill, L. C., Bull, J. M., Bell, R. E., Gawthorpe, R. L., Henstock, T. J., ... Kranis, H. (2016). Rapid spatiotemporal variations in rift structure during development of the Corinth Rift, central Greece. *Tectonics*, *35*, 1225–1248. <https://doi.org/10.1002/2015TC004026>
- Ori, G. G., Roveri, M., & Nichols, G. (1991). Architectural patterns in large-scale Gilbert-type delta complexes, Pleistocene, Gulf of Corinth, Greece. In: *The Three-Dimensional Facies Architecture of Terrigenous Clastic Sediments and Its Implications for Hydrocarbon Discovery and Recovery* Miall, (Ed. by A.D. Miall & N. Tyler), *Concepts in Sedimentology and Paleontology*, *3*. Society for Sedimentary Geology (SEPM), 207–216.

- Ritchie, B. D., Hardy, S., & Gawthorpe, R. L. (1999). Three dimensional numerical modeling of coarse-grained clastic deposition in sedimentary basins. *Journal of Geophysical Research*, *104*, 17759–17780. <https://doi.org/10.1029/1999JB900170>
- Rohais, S., Eschard, R., Ford, M., Guillocheau, F., & Moretti, I. (2007). Stratigraphic architecture of the Plio-Pleistocene infill of the Corinth Rift: Implications for its structural evolution. *Tectonophysics*, *440*, 5–28. <https://doi.org/10.1016/j.tecto.2006.11.006>
- Scholz, C. (2010). Large earthquake triggering, clustering, and the synchronization of faults. *Bulletin of the Seismological Society of America*, *100*, 901–909.
- Schwartz, D. P., & Coppersmith, K. J. (1984). Fault behaviour and characteristic earthquakes - examples from the Wasatch and San Andreas fault zones. *Journal of Geophysical Research*, *89*, 5681–5698.
- Soter, S., & Katsonopoulou, D. (1998). The search for ancient Helike, 1988–1995: geological, sonar and bore hole studies. In D. Katsonopoulou, S. Soter, & D. Scilardi (Eds.), *Ancient Helike and Aigalieia* (pp. 67–116). Aigion, Greece: The Helike Society.
- Stevenson, C. J., Jackson, C. A. L., Hodgson, D. M., Hubbard, S. M., & Eggenhuisen, J. T. (2015). Deep-water sediment bypass. *Journal of Sedimentary Research*, *85*, 1058–1081.
- Suc, J.-P., & Popescu, S.-M. (2005). Pollen records and climatic cycles in the North Mediterranean region since 2.7 Ma. *Geological Society, London, Special Publications*, *247*, 147–158. <https://doi.org/10.1144/GSL.SP.2005.247.01.08>
- Torfstein, A., Goldstein, S. L., Stein, M., & Enzel, Y. (2013). Impacts of abrupt climate changes in the Levant from Last Glacial Dead Sea levels. *Quaternary Science Reviews*, *69*, 1–7. <https://doi.org/10.1016/j.quascirev.2013.02.015>
- Von Freyberg, B. (1973). Geologie des Isthmus von Korinth. *Erlanger Geologische Abhandlungen*, *95*. Junge und Sohn, Universitäts-Buchdruckerei, Erlangen.
- Wdowinski, S., O'Connell, R. J., & England, P. (1989). A continuum model of continental deformation above subduction zones' application to the Andes and the Aegean. *Journal of Geophysical Research*, *94*, 10331–10346. <https://doi.org/10.1029/JB094iB08p10331>

SUPPORTING INFORMATION

Additional supporting information may be found online in the Supporting Information section at the end of the article.

How to cite this article: Barrett BJ, Collier RELL, Hodgson DM, Gawthorpe RL, Dorrell RM, Cullen TM. Quantifying faulting and base level controls on syn-rift sedimentation using stratigraphic architectures of coeval, adjacent Early-Middle Pleistocene fan deltas in Lake Corinth, Greece. *Basin Res.* 2019;00:1–26. <https://doi.org/10.1111/bre.12356>



Syn-rift delta interfan successions: Archives of sedimentation and basin evolution

Bonita J. Barrett^{1,2} | Rob L. Gawthorpe² | Richard E. Ll. Collier¹ |
David M. Hodgson¹ | Timothy M. Cullen¹

¹School of Earth & Environment, University of Leeds, Leeds, UK

²Department of Earth Science, University of Bergen, Bergen, Norway

Correspondence

Bonita J. Barrett, School of Earth & Environment, University of Leeds, Leeds LS2 9JT, UK.
Email: eebbca@leeds.ac.uk

Abstract

Models that aim to capture the interactions between sediment supply, base level and tectonism recorded in fan delta successions in rift basins have not considered the stratigraphic archive preserved in interfan areas; yet interfan stratigraphy can provide a complementary record to the fan delta axes. The exhumed Early–Middle Pleistocene Kerinitis and Selinous fan deltas, in the hangingwall of the Pyrgaki–Mamoussia (P-M) Fault, Corinth Rift, Greece, offer an ideal laboratory for the assessment of interfan architecture. Furthermore, using the geometry of adjacent present-day fan deltas, interfans are classified into three end-members. The classification is based on their lateral separation, which determines the degree of interfingering of topset, foreset and bottomset deposits. Qualitative (facies, stratal geometries, nature of key surfaces) and quantitative (stratigraphic thickness, bedding dip, palaeocurrents, breakpoint trajectories) data were collected in the field and from unmanned aerial vehicle photogrammetry-based 3D outcrop models of the exhumed fan delta successions. The ancient Kerinitis–Selinous interfan architectures record: (a) initial westward progradation of the Kerinitis fan delta into the interfan area (Phase 1), (b) subsequent progradation of the Selinous fan delta into the interfan area and asymmetric growth of both fan deltas eastward (Phase 2), (c) stratal interfingering of foresets from both systems (Phase 3), and (d) relative base-level fall, erosion and reworking of sediments into the interfan area (Phases 4 and 5). The Kerinitis–Selinous interfan evolution is linked to initial net subsidence of the P-M Fault (Phases 1–3) and subsequent net uplift (Phases 4 and 5) resulting from a northward shift in fault activity. The interfan area provides a more complete stratigraphic record than the proximal axial areas of the fan deltas of the early stages of basin uplift, through higher preservation potential and protracted submergence. Therefore, for the most comprehensive insight into basin evolution, interfan analysis should be undertaken in concert with analysis of the fan delta axes.

KEYWORDS

Basin evolution, fan delta, interfan, stratigraphy, syn-rift.

1 | INTRODUCTION

The sedimentary successions preserved between adjacent, contemporaneous fluvial, deltaic or deep water fan systems (Figure 1) preserve an alternative stratigraphic archive to the fan axes (Higgs, 1990; Hook *et al.*, 2003; Bhiry and Occhietti, 2004; Leppard and Gawthorpe, 2006; Assine *et al.*, 2015; Turner and Connell, 2018). The interfan area is defined here as the area between two lines that project from the apices of two fan deltas to their intersection at the most distal point of bottomset interfingering (Figure 1). In this area, the fans coalesce from the proximal to distal parts. Identification of the most distal point of bottomset interfingering in modern and ancient systems is challenging, and as such the definition can be considered a theoretical, rather than a measurable limit.

The interfan areas between fan deltas may record the sedimentary response to relative base-level changes, yet are unstudied and therefore remain a missing piece in the published conceptual models that aim to capture the interactions of sediment supply, base level and tectonism in rift basins (Leeder and Gawthorpe, 1987; Gawthorpe *et al.*, 1994, 1997; Gawthorpe and Leeder, 2000; Leeder *et al.*, 2002; Young *et al.*, 2002). The interfan offers a complementary stratigraphic record to the fan delta axes of relative base-level change and tectono-sedimentary evolution. For example, during a relative base-level fall, the fan delta axis may become exposed and degraded, but the deeper and more sediment-starved interfan will remain submerged and thus preserve a more complete record of sedimentation and

basin evolution. The frontal deepwater setting along the fan delta axis may also record this transition in deepwater sediments, but the interfan area captures the interaction of two adjacent fan deltas through basinal change, as well as offering a more proximal record. The key regressive and transgressive surfaces that mark the pivotal moments in relative base-level change can also be expressed differently (e.g. suppressed erosion or thicker condensed intervals) and may be diachronous (Barrett *et al.*, 2018). Thus, a better grasp of interfan sedimentary facies, architecture and stratal surfaces would allow a more complete understanding of along-strike interactions between adjacent fan deltas during basin evolution.

The southern shore of the Gulf of Corinth (Figure 2) offers an ideal field laboratory for exploring interfan architectures, as there are a series of modern fan deltas along the coast, Late Pleistocene lowstand fan deltas that are submerged and imaged in bathymetry data, and a number of exhumed syn-rift fan deltas that formed along normal faults since ~1.8 Ma (Ford *et al.*, 2016; Gawthorpe *et al.*, 2017a). A number of studies focus upon the stratigraphic architecture of the Early–Middle Pleistocene Gilbert-type fan deltas in the Gulf of Corinth: Evrostini/Ilias (Zelilidis and Kontopoulos, 1996; Zelilidis, 2003; Rohais *et al.*, 2007a, 2008; Gobo *et al.*, 2014, 2015), Kryoneri (Gawthorpe *et al.*, 2017b), Vouraikos (Ford *et al.*, 2007), Kerinitis (Ori *et al.*, 1991; Poulimenos *et al.*, 1993; Dart *et al.*, 1994; Gawthorpe *et al.*, 1994; Backert *et al.*, 2010; Gawthorpe *et al.*, 2017b) and Selinous fan deltas (Poulimenos *et al.*, 1993; Barrett *et al.*, 2019). These studies highlight the

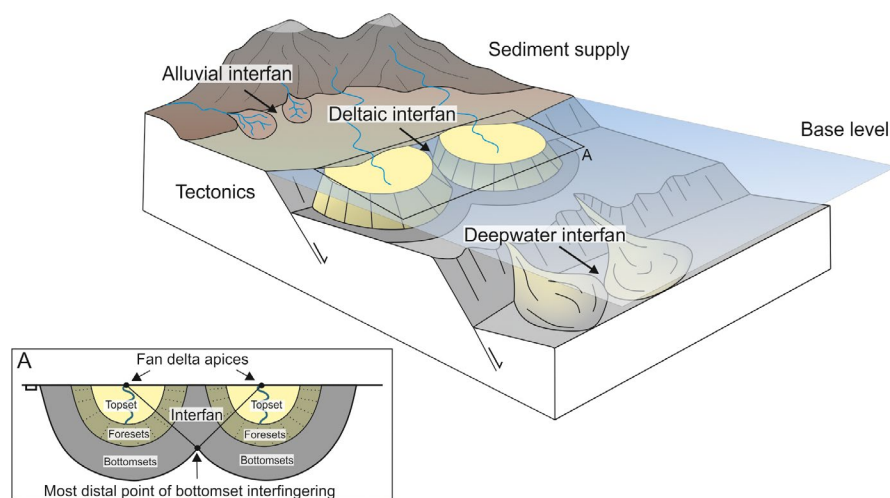
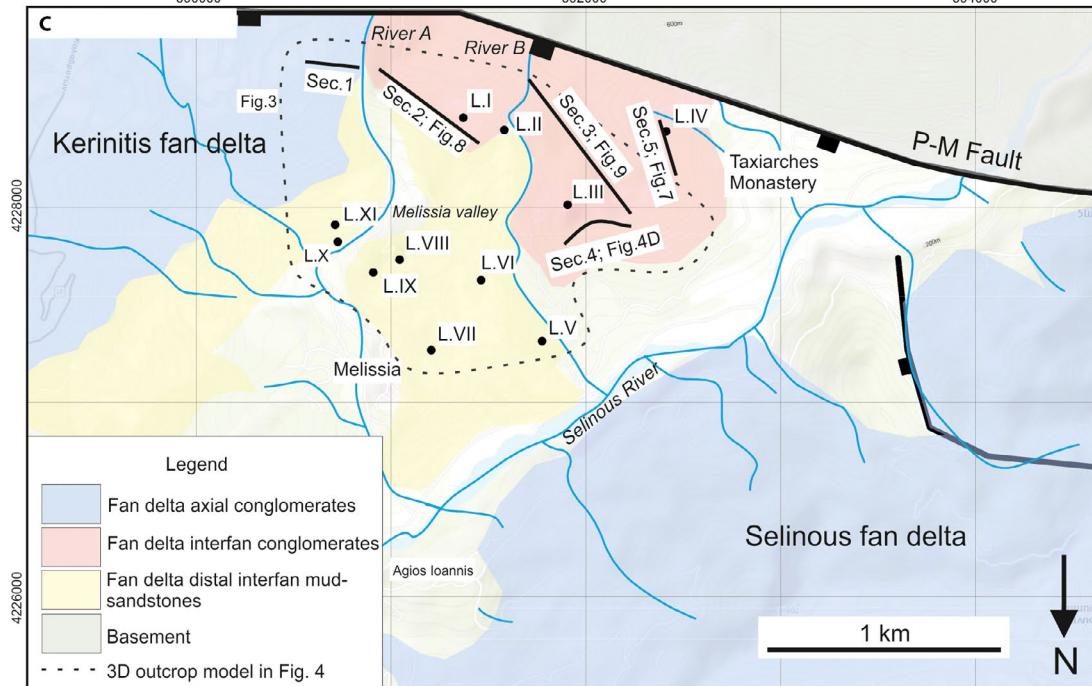
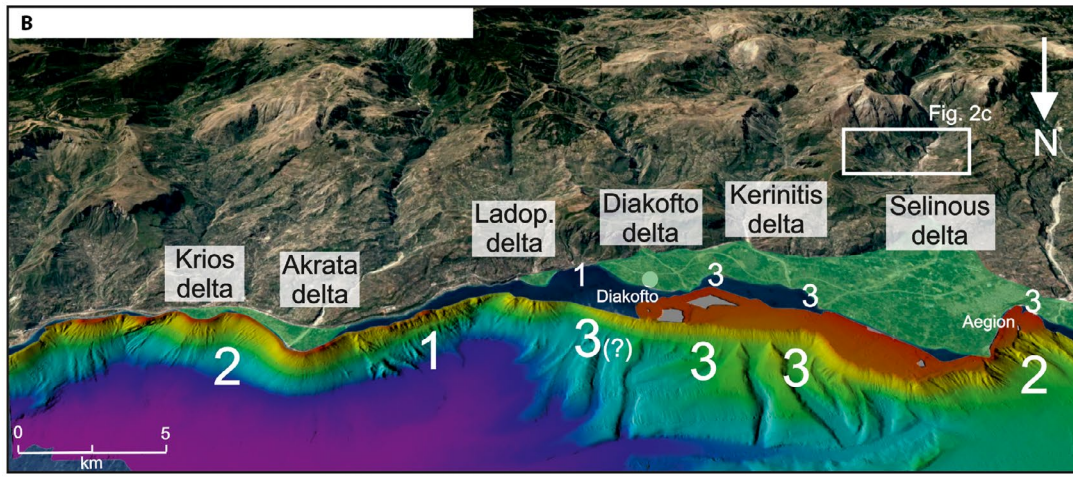
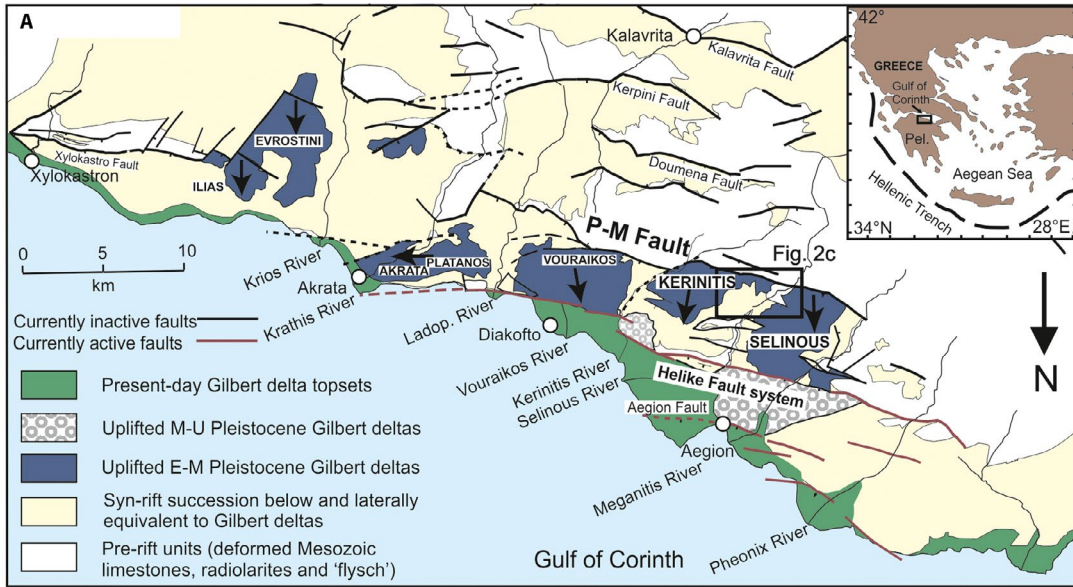


FIGURE 1 Source-to-sink block model with interfan areas highlighted in alluvial, deltaic and deepwater settings. (A) Deltaic interfans more specifically defined as the area between two lines that project from the two fan delta apices to their intersection at the most distal point of bottomset interfingering.

FIGURE 2 (A) Location map of southern shore of the Gulf of Corinth with the Early–Middle Pleistocene Kerinitis and Selinous fan deltas highlighted. Modified from Barrett *et al.* (2018) after Ford *et al.* (2010, 2007, 2013), Ghisetti and Vezzani (2004) and Gawthorpe *et al.* (2017a). (B) Modern fan deltas on topographic map (Google Earth) and Late Pleistocene examples imaged in bathymetry data. Numbers denote interfan classification according to scheme in Figure 11. Bathymetry data from McNeill *et al.* (2005) and Cotterill (2002). (C) Area of focus with key sections and localities indicated. Position of (C) is indicated in (A) and (B). Pel. = Peloponnesus.



sedimentary facies distribution and sequence stratigraphic relationships within these deposits, and the role of tectonics, lake level and sediment supply on fan delta development. However, none of these studies address the interfan areas between the fan deltas.

Here, the focus is placed upon the interfan area between the Early–Middle Pleistocene, Selinous and Kerinitis syn-rift fan deltas located in the immediate hangingwall of the Pyrgaki–Mamoussia (P–M) Fault. Geometric observations from the associated modern and Late Pleistocene submerged fan deltas are used to inform the analysis. The aim of this paper is to advance our understanding of along-strike interactions in syn-rift settings through analysis of interfan stratigraphy. Using field data and UAV photogrammetry-based 3D outcrop models, the objectives of the study are to: (a) describe and interpret the Kerinitis–Selinous (K–S) interfan evolution from the stratigraphic architecture and sedimentology; (b) propose a classification scheme for ancient interfans based on modern delta geometries; (c) discuss the mechanisms for the observed asymmetry in the ancient and modern fan deltas, and the value of including interfan analysis in sedimentary basin analysis.

2 | STUDY AREA

The Corinth Rift was activated at ~5 Ma (Collier and Dart, 1991; Leeder *et al.*, 2008) and currently accommodates extension rates of up to 5–10 mm/year across the Gulf of Corinth (Clarke *et al.*, 1997; Briole *et al.*, 2000; Avallone *et al.*, 2004; Floyd *et al.*, 2010). The locus of faulting on the southern coast of the present gulf has migrated northwards over time (Goldsworthy and Jackson, 2001; Leeder *et al.*, 2008; Ford *et al.*, 2013, 2016; Nixon *et al.*, 2016), recording two major rifting phases (Rohais and Moretti, 2017; Gawthorpe *et al.*, 2017a). Rift 1 occurred from 5–3.6 Ma to 2.2–1.8 Ma, and strain was accommodated on the present-day onshore faults. In the west, activity was focussed upon the Kalavrita Fault in Northern Peloponnesos, before activity migrated basinwards onto the P–M Fault (study area, Figure 2) at ~1.8 Ma (Ford *et al.*, 2016; Gawthorpe *et al.*, 2017a). Rift Phase 2 commenced, and the Kerinitis and Selinous fan deltas formed, before activity migrated from the P–M Fault onto the Helike Fault system around ~0.8 Ma (Ford *et al.*, 2013). Today, strain is primarily accommodated on faults offshore in the Gulf of Corinth (Nixon *et al.*, 2016). Lacustrine conditions prevailed during Rift 1, with a transition from episodic marine incursions to periodically fully marine conditions during Rift 2 (~0.6 Ma). This occurred as the Gulf of Corinth opened during interglacial highstands to the Ionian and Aegean seas and into its modern configuration (Freyberg, 1973; Collier, 1990; Collier and Thompson, 1991; Moretti *et al.*,

2004; Rohais *et al.*, 2007b; Ford *et al.*, 2016; Nixon *et al.*, 2016; Rohais and Moretti, 2017; Gawthorpe *et al.*, 2017a).

Siliciclastic sediments sourced from the Hellenide fold and thrust belt (eroded Mesozoic carbonates, radiolarites and Cenozoic turbidites) were transported northwards and deposited syn-kinematically during Rift phases 1 and 2 (Degnan and Robertson, 1998; Ford *et al.*, 2013; Gawthorpe *et al.*, 2017a). The related stratigraphy is split into three groups in the study area; the Lower, Middle and Upper groups (Ford *et al.*, 2007, 2013, 2016; Rohais *et al.*, 2007a). The Lower Group was deposited during Rift 1, and the Middle and Upper groups during Rift 2. The earliest fluvial and marginal lacustrine deposition occurred from the widespread Kalavrita River system, now preserved in the Lower Group. Subsequently, giant syn-rift fan deltas prograded into the hangingwalls of the major faults: Platanos, Vouraikos, Kerinitis and Selinous (from east to west) in the hangingwall of the P–M Fault, and Evrostini/Ilias to the east of the study area (Figure 2).

The P–M Fault hangingwall deltas constitute the Middle Group, deposited during early Rift 2 (Gawthorpe *et al.*, 2017a). The age of these deltas is constrained to ~1.8 to 0.7 Ma based on pollen analysis at the Vouraikos fan delta (Ford *et al.*, 2007). These syn-rift sediments on the P–M Fault terrace are the target of this study. Previous studies interpret the mudstone–sandstone deposits in Melissia Valley (Figures 2 and 3) as the fluvio-lacustrine Melissia Formation (Backert *et al.*, 2010), constituting part of the older Lower Group (Ford *et al.*, 2007, 2013). These authors describe this succession as being unconformable with overlying fine-grained deposits of the Zoodhochos Formation within the Middle Group, which are interpreted to represent distal turbidites in a bottomset setting (Backert *et al.*, 2010). However, the present study did not observe substantial facies variations between the deposits of the Zoodhochos and Melissia formations, nor was the erosive contact reported by Backert *et al.* (2010) identified. An alternative interpretation is that all of the fine-grained deposits in Melissia Valley represent fan delta bottomsets to the Selinous and Kerinitis foresets updip (Middle Group), and are equivalent to the Zoodhochos Formation of Backert *et al.* (2010). Projection of key surfaces within the Selinous foresets into the bottomsets using 3D outcrop models has allowed their correlative foreset packages to be approximately constrained. In addition, the base of the Selinous fan delta axis directly overlies basement rocks; fine-grained fluvio-lacustrine deposits are absent. The Upper Group consists of younger marine terraces and smaller Gilbert-type fan deltas with erosive bases, primarily deposited in the hangingwall of the Helike Fault system (Ford *et al.*, 2007, 2013, 2016; Rohais *et al.*, 2007a).

The focus of this study is the eastern part of the Selinous fan delta and the western part of the Kerinitis fan delta, in the hangingwall of the P–M Fault (Middle Group) (Figures 2C and 3). The Kerinitis fan delta is positioned slightly to the

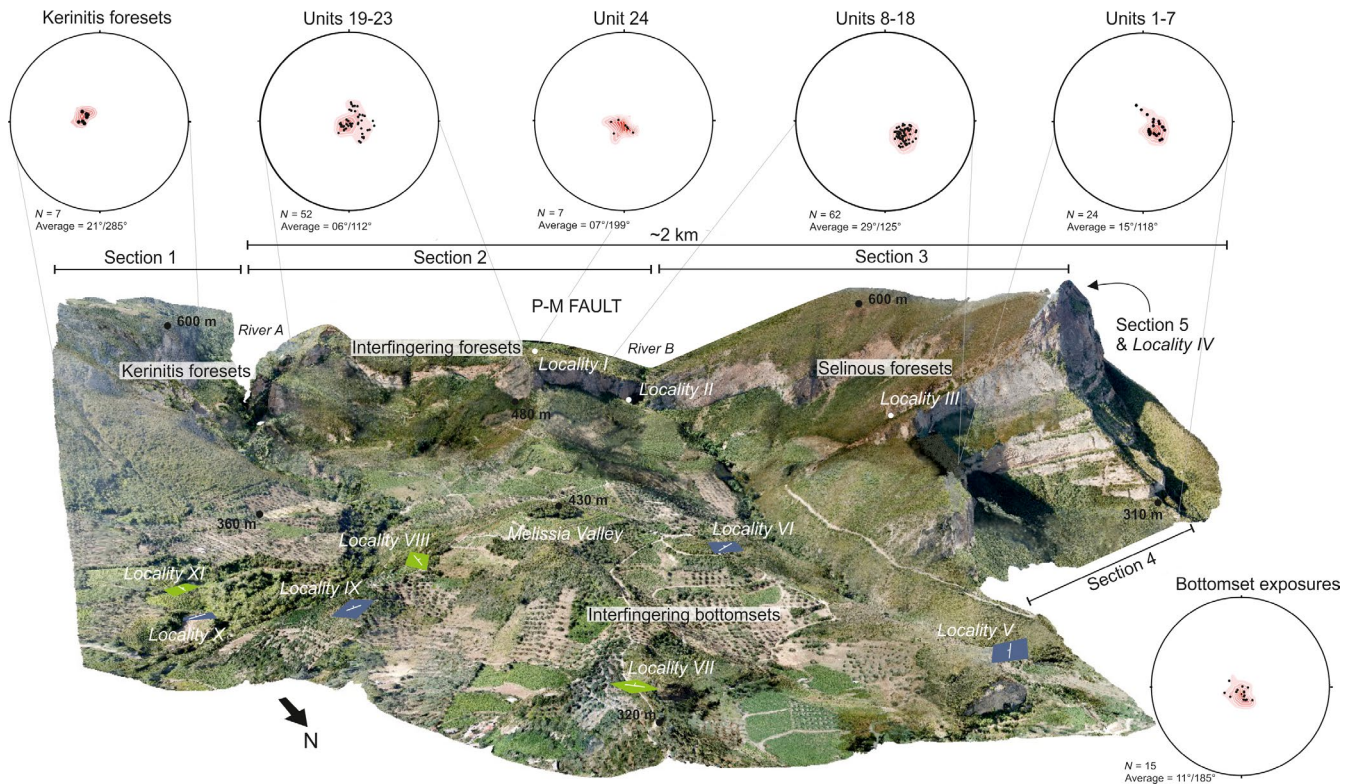


FIGURE 3 Study area and data overview. 3D outcrop model of the interfan study area was created using UAV-photogrammetry data and Agisoft Photoscan software. Stereonets, Sections 1–5, Localities I–XI (bottomset outcrops with coloured planes—created using LIME software) are presented. Green planes represent W-dipping (Kerinitis-derived) outcrops. Blue planes represent E-dipping (Selinous-derived) outcrops. Dip data is taken from the field and from 3D outcrop model structural planes in LIME software and presented with southern hemisphere-projected stereonet plots using Stereonet software. N = number of data points.

west of the P–M fault centre and the Selinous fan delta is positioned ~4 km from the western fault tip. Barrett *et al.* (2019) quantify the minimum period of deposition, average subsidence and sedimentation rates at the Kerinitis and Selinous fan deltas as >451 and 615 kyr, and 0.65 and >1.77 m/kyr, respectively, based upon stratigraphic observations. Numerical modelling was used to quantify the amplitude of climate-induced lake-level changes in Lake Corinth during the Early–Middle Pleistocene at 10–15 m (Barrett *et al.*, 2019). Previous studies focus on the facies and stratigraphic architecture of the axial sections of the Kerinitis and Selinous fan deltas (Dart *et al.*, 1994; Gawthorpe *et al.*, 1994; Backert *et al.*, 2010; Gawthorpe *et al.*, 2017b; Barrett *et al.*, 2019).

The study area consists of a ~300 m high conglomeratic cliff with a ~2 km wide, main north-facing exposure (Sections 1–3; Figures 2C and 3), and additional west (Section 4; Figures 2C and 3) and south-facing (Section 5; Figures 2C and 3) exposures that provide 3D constraints. Section 1 exhibits thick, west-dipping (‘W-dipping’) units from the Kerinitis fan delta. While these are considered in the interpretation, they are not characterised within the stratigraphic framework due to limited access and difficulty in obtaining reliable UAV-photogrammetric data in that region. The units within Section 2 are generally thinner and stratigraphically

higher than the units in Sections 3–5, and both east-dipping (‘E-dipping’) and ‘W-dipping’ units are present with inter-fingering geometries. This is considered to be the centre of the interfan area. Section 3 consists of several thick ‘E-dipping’ foreset units from the Selinous fan delta. Section 4 is a curved, generally west-facing section and Section 5 faces SW. Both Sections 4 and 5 consist of ‘E-dipping’ units. The Old Taxiarches Monastery is built into the Selinous foresets in Section 5. Here, part of the conglomeratic section and a thin, fine-grained interval is accessible (Locality IV; Figures 2C and 3). Otherwise, access to the interfan sections is limited. Associated fine-grained exposures can be found in the valley to the north of the cliff, near Melissa (Localities V–XI; Figures 2C and 3) and represent the fan delta bottomsets.

3 | METHODOLOGY

A DJI Mavic Pro drone was used to collect the photogrammetric data that was augmented by annotated photograph panels and field sketches. Agisoft Photoscan/Metashape and LIME software were used to build and interpret the 3D outcrop models (e.g. Figure 3). Sedimentological and structural data were collected directly in the field where access allowed and

complemented by outcrop model measurements where the exposures were inaccessible. Measured sections of sandstone successions were collected at millimetre to centimetre-scale to document lithology, grain size, sedimentary structures and the nature of bedding contacts. Conglomeratic units were logged at decimetre-scale, with the support of sketches to capture the geometry of large-scale features, such as the continuity of surfaces. Palaeocurrent data were collected from ripple cross laminations, clast imbrication, cross-bed plane measurements and dips of foresets generated from sediment gravity flows. Presented data are unrestored due to the lack of a reliable palaeo-horizontal datum, but the steepest tectonic tilt is $\sim 12^\circ$ (S).

Figure 4 outlines the methodology for extracting data from 3D outcrop models, which are able to represent measurable objects with a lower limit of ~ 10 cm. The stratigraphic framework was established from interpretation of the interfan cliff section using LIME software to map stratal surfaces. The 3D outcrop models allowed qualitative (detailed stratal geometries, nature of major surfaces and accurate correlation of surfaces around topography) and quantitative (dip data from bedding planes, stratigraphic thickness, topset-foreset breakpoint trajectories and height of foresets) data collection (Figure 4). In total, 167 bedding dip measurements were collected in the field and using LIME software-based mapping of the 3D outcrop models (Figure 3). Multiple measurements within each unit were taken for averages to be calculated. The data have not been re-orientated in the absence of a reliable palaeo-horizontal datum. Bedding data collected from the outcrop models were validated against field measurements at the Old Taxiarches Monastery (Figure 2). The east and west components of dip are used to differentiate between beds or units from the Selinous and Kerinitis fan delta systems, respectively.

Bedding measurements often have north or south dip components as well, but as both fan deltas prograde northward and both are back-tilted to the south towards the P–M fault, the east and west components are the most useful diagnostic criteria.

Correlation of surfaces around topography and constraining the stratigraphic position of associated bottomset outcrops in the valley were refined with the use of 3D outcrop models. By projecting planes following the dip of the foresets in Sections 3 and 4 into Melissa Valley, the E-dipping (Selinous) fine-grained, bottomset outcrops could be correlated to their updip foreset counterparts in the interfan area. A typical clinoform profile shallows in dip at the foreset-bottomset transition. Therefore, the constant dip of the projected foreset planes mean that the units assigned to bottomset deposits are approximate, but are more likely to be associated with lower units than higher units. Where the bottomset outcrops are W-dipping, they are derived from the Kerinitis fan delta and cannot be tied updip, but instead their relative position to Selinous units is recorded.

4 | RESULTS

4.1 | K–S facies association characterisation

Eight facies associations (FAs) characterise the Selinous and Kerinitis fan deltas, based on geometric position (topset–bottomset) and depositional environment (Table 1; Figures 5 through 7). The main fan delta units are constructed from conglomeratic, fluvial and shallow water topset and foreset facies associations (FA 1a–b; 2a–b; 3). The facies associations observed in the interfan area are the focus: the foreset facies association

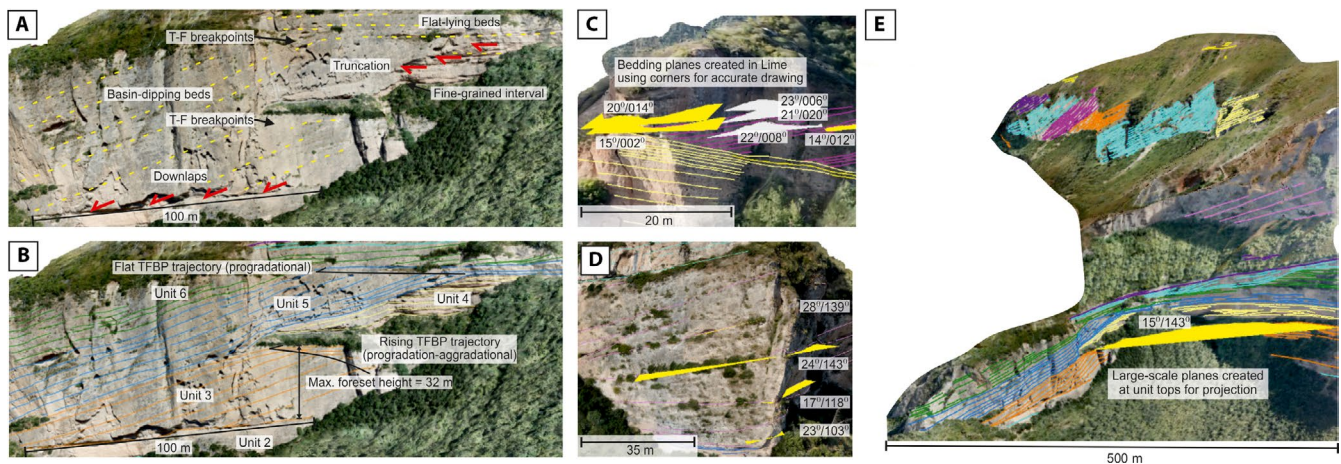


FIGURE 4 Methodology for stratigraphic architecture interpretation and for obtaining quantitative information from UAV photogrammetry-based 3D digital outcrop models. (A) observations from part of Section 4, where remnants of fine-grained intervals, truncation and clear stratal termination geometries allow units to be divided and contacts to be classified. Topset-foreset breakpoints (TFBPs) can be identified. (B) Interpretation of section shown in (A) with TFBP trajectories and foreset heights indicated. (C and D) Demonstrations of obtaining accurate dip data (convention: dip/dip direction) from small-scale bedding planes (assured using field data) in parts of Section 2. (E) Large-scale planes from unit tops are created and used for projecting across valleys to assist correlations and constraining the stratigraphic position of bottomset outcrops (Sections 3 and 4). 3D outcrop models created in Agisoft Photoscan and interpreted in LIME software.

TABLE 1 Facies associations at the Selinous and Kerinitis fan deltas (modified from Barrett *et al.*, 2018). See Supporting information for facies information.

FA code	Constituent facies	FA interpretation	Sub-association
1a	Co1, Co2	Fluvial topset	Channel-fill
1b	Co1, Sa2, Sa6, Fi3		Delta plain
2a	Co4, Co5	Shallow water topset	Beach barrier
2b	Co1, Co4, Co5, Co7, Sa1, Sa2 and Sa4		Upper shoreface
2c	Co5		Lower shoreface
3	Co3, Co4, Sa4	Foreset	
4a	Sa1-6, Fi1-2, Fi4-8	Bottomset	Deep-water
4b	Co6, Sa1-6, Fi1, Fi2		Shallow-water

that occupies the majority of the interfan cliff sections (FA 3), and the bottomset facies associations that are found in Melissia Valley, and in the Unit 8-9 fine-grained interval/flooding surface (FA 4a). An additional facies association to the scheme of Barrett *et al.* (2019) is FA 2c (upper shoreface, which occurs in the shallow water topset; Locality I; Figure 2; Table 1). Four facies (Supporting information) have been added to the bottomset facies association of Barrett *et al.* (2019).

4.1.1 | FA 1: Fluvial topsets

Two fluvial topset facies associations are identified from the fan delta axes: FA 1a) channel-fill, and FA 1b) delta plain depositional environments. Channel-fill (FA 1a) is the most common and comprises poorly-sorted, sub-angular to sub-rounded, sandy gravel-cobble conglomerate with clast imbrication and erosive bed bases. These deposits are interpreted to represent bedload deposits during high energy fluvial flow regime. The delta plain FA 1b comprises poorly-sorted, sub-angular, sandy gravel-cobble conglomerates interbedded with normally graded, gravelly-coarse sand beds. Red palaeosols (centimetre-thick) are found between gravelly coarse sandstone beds (Barrett *et al.*, 2019). A variable, periodic flow regime is envisaged, with periods of subaerial exposure indicative of overbank deposits in a delta plain environment.

4.1.2 | FA 2: Shallow water topsets

The shallow water topset (FA 2) is divided into three sub-associations: 2a) beach barrier, 2b) upper shoreface, and 2c) lower shoreface. Only the upper shoreface (FA 2b) is observed in the interfan area, during the latest stage. The beach barrier (FA 2a) consists of a mounded body and internal bi-directional metre-scale cross-beds, with well-sorted, open-framework and mainly rounded pebbles. This indicates textural maturity and character typical of beach reworking. The lower shoreface FA 2c comprises metre-scale, bi-directional, asymptotic cross-beds resembling hummocky-cross stratification (Barrett *et al.*, 2019). These deposits are characteristic of storm reworking below fair weather wave base.

The upper shoreface (FA 2b) is identified in the interfan area (Locality I, Section 2, Figure 2; logs and photographs in Figure 5). Locality I is situated 650–800 m from the fault and the FA 2b are the highest and youngest rocks encountered. Figure 5 presents representative logs and photographs of two of the exposures; one where cross-beds dip eastward and are part of the Selinous fan delta, and one where cross-beds dip westward and are part of the Kerinitis fan delta. Despite opposing bedding dips between the various outcrops at Locality I, the facies are similar, comprising interbedded fine sand to pebble conglomerate (decimetre-scale) beds, between thicker (metre-scale) and coarser grained conglomerates at the bases and tops. Several pebbly gravel beds pinch out laterally over 1–2 m with slight convex-up geometries. These bedforms generally have erosive bases and are matrix and clast-supported, with sub-angular to rounded clasts. Beds are well-sorted, either normally or inversely graded and sands contain gravel and pebble clasts. The thicker conglomeratic beds generally coarsen upwards (sometimes normally-graded) and are poorly-sorted, mostly clast-supported, pebble-cobble grade with sub-rounded to rounded clasts (<18 cm). Clasts are imbricated following the bedding dip (e.g. log 2; Figure 5).

These deposits are interpreted to represent a variable, but generally high energy regime. The lack of fine-grained sediment, and the observed lenticular geometry of the beds, maturity of the clasts and spatial context within a flat-lying unit, suggests reworking of material in the interfan topset area and bedform migration by wave-related currents. The sediments are interpreted to have been deposited in an upper shoreface environment with longshore transport as the main depositional process. Similar processes are observed at the modern Selinous and Meganitis fan deltas in the Gulf of Corinth, as sediments are reworked with the prevailing westerly wind/wave direction into interfan embayments (Figure 2A).

4.1.3 | FA 3: Foresets

The foreset facies association was described previously by Backert *et al.* (2010) and Barrett *et al.* (2019) and occupies most of the interfan cliff section. It comprises well to

poorly-sorted, clast-supported and open-framework, sub-rounded, mainly pebble-cobble conglomerates. Scours and inverse grading are common. Any matrix is sand-gravel grade, and locally clasts are imbricated. Foresets comprise steep, basinward-dipping (22–25°) beds with heights ranging from ten to a few hundred metres, dependent on palaeo-water depth (and subsequent erosion). The processes responsible are interpreted to be dominated by sediment gravity flows (conglomerate-rich inertial grain flows to non-cohesive debris flows) on the delta foresets (Postma, 1984; Nemeč, 1990; Orton and Reading, 1993; Sohn *et al.*, 1997; Sohn, 2000; Rohais *et al.*, 2008; Gobo *et al.*, 2015). In the interfan, the foresets are accessible and described at Localities II and III on Section 3 and Locality IV on Section 5 (Figures 2C and 3).

4.1.4 | FA 4: Bottomsets

Bottomset deposits occur in relatively shallow water when delta clinothems build out over a previous fan delta topset following a transgression (shallow water bottomsets) and in deeper water, basinward of the foreset slope, when it builds past the topset-foreset breakpoint (deep water bottomsets). The interfan bottomset deposits here are characterised within this scheme and provide further insight into the processes at the toe of the foreset slope in interfan areas.

Within both shallow and deep bottomset facies associations, pebble-cobble horizons are present within fine-grained sections, representing sediment gravity flows or rock falls. In other cases, thicker beds are present that comprise poorly-sorted, matrix-supported (fine-coarse sand), graded, gravel-boulder conglomerates with erosive and/or loaded bases and occasional injectites in the underlying beds (Figure 6). These deposits are interpreted as debrites sourced from the delta foresets.

FA 4a: Deep water bottomsets

Deep water bottomsets (FA 4a) comprise interbedded sandstones and calcareous mudstones (FA 4a and 4b in Barrett *et al.*, 2019). Soft sediment deformation features, such as convolute laminations at the upper contact with overlying conglomerates are common. At the fan delta axes, the sandstones contain wavy laminations, inverse grading, slightly erosive bases and localised gravel lags (Backert *et al.*, 2010; Barrett *et al.*, 2019). In the interfan area, the more extensive and thicker exposures allow this FA to be characterised further. Representative logs and photographs are presented in Figure 6. Locally, thin, current-ripple laminated sandstones are draped by black organic material (e.g. Locality X; Figure 6), or intercalated with decimetre-scale, organic-rich mudstone-siltstone beds (e.g. Locality VIII; Figure 6). Thicker, normally graded sandstone beds (~5 to 10 cm) with planar and wavy-laminations, gravel and mudstone clasts, and broken and whole brachiopod shells (<2 cm diameter) are common.

Much like the fan delta axes, the conglomeratic interfan succession is punctuated by thin (<2 m), fine-grained intervals. The only fine-grained interval that is accessible in the interfan area is exposed in Section 5 (Locality IV), within the Old Taxiarches Monastery (Figure 7). The section comprises a coarsening-upwards succession of mudstone to gravel, overlain by an erosional ~1 m thick, poorly sorted, clast-supported gravel-cobble conglomerate (mainly large pebble) with sub-rounded to sub-angular clasts. The mudstone-siltstones at the base of the section are planar and wavy laminated. There are two thin, normally graded sandstones before a dark, organic-rich silty mudstone. The mudstone is overlain by lower medium sandstone (0.8–0.9 m) containing gravel and broken shell lenses (gravelly-coarse sand matrix) with evidence for soft sediment deformation (Figure 7). The interval is positioned basinward of the topset-foreset breakpoint and between two units of high (>100 m), steeply-dipping foresets, suggesting a relatively deep water position that is below wave base, even allowing for changes in base level.

The sandstones are interpreted to be turbidites, with finer-grained beds representing quiet periods between events, or dilute turbidity currents. Some outcrops have a narrow palaeo-current dispersal pattern (e.g. Locality VIII, Figure 6), which implies the deposits are inherited from a single system. Others have multiple palaeo-current directions between beds (e.g. Locality X, Figure 6) implying both Kerinitis and Selinous fan delta sources (Figure 6). In addition, a number of palaeo-current measurements have a southerly component, opposite to the regional trend, which could indicate flow reflection and deflection from local topography (Potter and Pettijohn, 1977; Kneller *et al.*, 1991; Lomas and Joseph, 2004; Bell *et al.*, 2018).

FA 4b: Shallow water bottomsets

Barrett *et al.* (2019) previously classified the shallow water bottomset (FA 4b) as coarse (sand to gravel-grade) sediments with multiple and diverse sedimentary structures, such as symmetrical and asymmetrical ripple laminations, wavy and planar laminations, dune-scale gravel cross-beds and soft-sediment deformation, indicating sediment gravity flows and wave reworking operating at the base of slope in shallow water. This facies association is identified at the fan delta axis (Barrett *et al.*, 2019), but not in the interfan area. Some bottomset deposits are observed in Section 2 of the interfan area (Figure 8) at the down-dip termination of relatively short foresets that could exhibit FA 4b, but it is not possible to access them to constrain the facies.

4.2 | Stratigraphic architecture

4.2.1 | Key stratal surfaces

Key surfaces were identified in the field and 3D outcrop models, and are used to subdivide the interfan succession into stratal units associated with both the Selinous and Kerinitis fan deltas. Key surfaces are recognised based on the presence

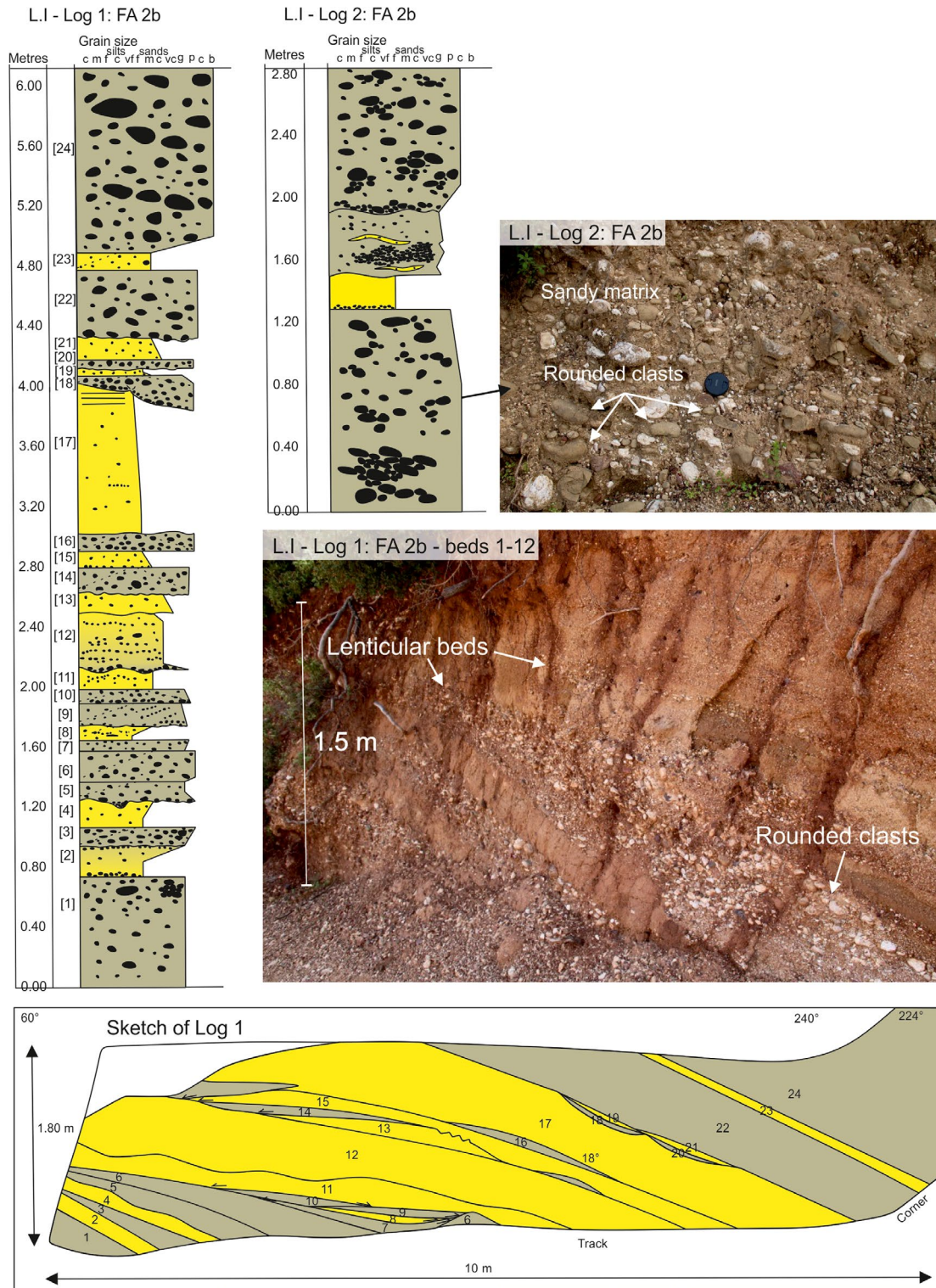


FIGURE 5 Shallow water topset—upper shoreface facies association (FA 2b). Logs 1 and 2 and associated photographs show two representative outcrops from Locality I. The bracketed numbers on Log 1 correspond to the numbered beds on the outcrop sketch. Yellow = sandstone; grey = conglomerate. Log 1 and Log 2 outcrops have an average bed dip/dip direction of 17°/270° (Kerinitis-derived) and 05°/160° (Selinous-derived), respectively.

of fine-grained deposits, deeply erosional surfaces and/or evidence of onlap, downlap, offlap or truncated stratal relationships. Fine-grained intervals (<2 m thick) are apparent between

the delta topsets, with some remnants between foreset units, both in the fan axes and in the interfan area. The interpretation of each surface is described as either confident or uncertain.

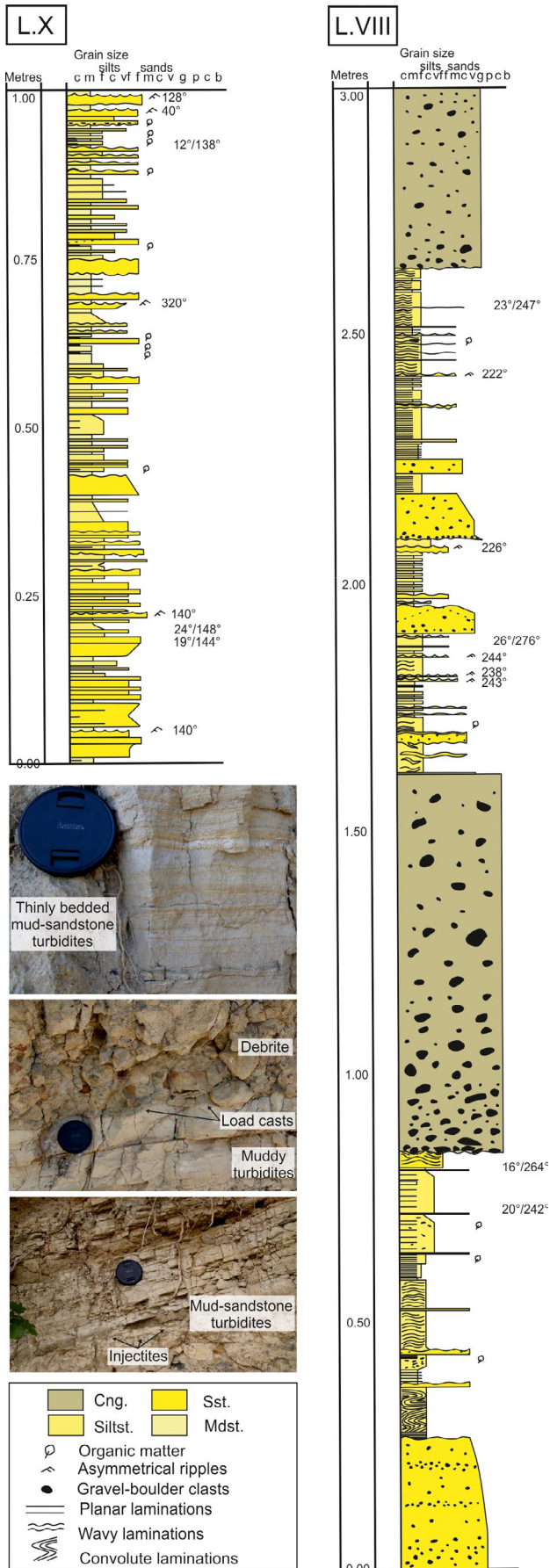


FIGURE 6 Representative bottomset logs from Localities L.X and L.VIII (Figures 2C and 4) in Melissia Valley (FA 4a). Mudstone-sandstone turbiditic successions with occasional debrites are shown. The sandstone-mudstone content is variable between them. Palaeocurrent directions suggest input from both Kerinitis and Selinous systems and in some cases with a southerly component, suggesting redirection from local topography. Photographs illustrate some of the features in the logs. Cng = conglomerate, Sst = sandstone, Siltst. = siltstone, Mdst = mudstone.

The nature of each surface is described in Table 2 and examples from Section 2 are presented in Figure 8. Units 1–9 (Section 4; Figures 2C and 9) and 13–15 (Section 3; Figures 2C and 9) have top contacts that have been identified confidently as key surfaces. The top of Unit 1 is a major downlap surface (Unit 15). Fine-grained intervals are preserved in places at the tops of Units 2, 3, 8 and 13–15, despite their position in the dynamic foreset region where fine-grained material has a low preservation potential. Units 3–5 have topset-foreset breakpoint trajectories exposed, suggesting a transitional position between delta topsets and foresets, but generally the interfan is characterised by steeply-dipping, foreset units. Erosive surfaces that clearly truncate underlying foresets are present at the tops of Units 4, 6 and 7. The interpretation of the top contacts of Units 10–12 and 16 are uncertain. Units 17–22 have confident key surfaces identified at their tops. Surfaces at the tops of Units 17–19 are erosive and fine-grained intervals are preserved. Erosional surfaces are more pervasive towards the top of the section and fine-grained intervals are not present between the upper units (20–22). The tops of Units 23 and 24 are not exposed.

4.2.2 | Key stratal surface interpretation

The base of each fine-grained interval is interpreted to represent a transgressive surface, although the lateral extent of the surfaces is unknown. Fine-grained intervals are present between units in all of the fan deltas in the hangingwall of the P-M Fault, but due to lack of age constraint it is not possible to correlate the surfaces. Between Units 8–9, an organic-rich silty mudstone bed separates graded sandstones in a generally coarsening-upward, mudstone to gravel sequence. This could be interpreted to contain a maximum flooding surface, but the regional continuity of the surface is unknown. The surface is overlain by storm reworked shallow marine deposits (overlying broken shell fragments in gravelly sand lenses) and turbidites, likely associated with the progradation of the subsequent foreset unit.

In the topsets, abrupt shifts in depositional environment are apparent from facies changes and evidence of subaerial exposure. Deep erosion surfaces overlain by palaeosols are interpreted to occur as a result of relative base-level fall,

but cannot be correlated across adjacent fan deltas. In the foreset to bottomset regions, as with the interfan, base-level changes and stratigraphic surfaces can be expressed differently to topset axial regions. Lack of subaerial exposure and significant environmental shift during relative base-level fall mean that major sediment bypass zones (Stevenson *et al.*, 2015) are candidate sequence boundaries. However, erosive events are not only triggered by relative base-level fall, particularly in seismically-active regions. As such, sequence boundaries can either be masked or simply misinterpreted—a common problem in deep water successions (Covault and Graham, 2010; Hodgson *et al.*, 2016). Where foresets overlie fine-grained prodelta deposits, there are often erosive contacts ('cusped' erosion surfaces at the Kerinitis fan delta axis; Backert *et al.*, 2010), which could be slide scars or scour surfaces. Unlike the Selinous fan delta, subaerial unconformities are absent at Kerinitis, because the rate of accommodation increase exceeded the rate of base-level fall at the fault centre (Gawthorpe *et al.*, 1994; Hardy and Gawthorpe, 1998; Backert *et al.*, 2010; Barrett *et al.*, 2019).

The base-level changes are attributed to changes in lake level (~10 to 15 m; Barrett *et al.*, 2019) in response to climate variations that followed 41 kyr orbital cycles. This cyclicity is documented in Greece and the Mediterranean (Capraro *et al.*, 2005; Dodonov, 2005; Suc and Popescu, 2005) and globally during the Early–Middle Pleistocene (Emiliani, 1978; Head and Gibbard, 2005; Lisiecki and Raymo, 2007). There is some evidence of episodic marine flooding, as global sea-level rise opened Lake Corinth to the Ionian Sea and Aegean Sea

during interglacial highstands (Freyberg, 1973; Collier, 1990; Moretti *et al.*, 2004; Rohais *et al.*, 2007b, 2008). Overall, relative base-level changes were superimposed onto a lower frequency, background tectonic regime, initially dominated by high subsidence rates on the P–M Fault, and later by uplift from the West Helike Fault. A variable sedimentation rate is also likely influenced by climate-driven fluctuations in sediment supply (Collier, 1990; Collier *et al.*, 2000).

4.2.3 | Major unit sets

The fan delta stratigraphy is generally made up of topset or foreset conglomerate beds (10s m thick), separated by thinner (<2 m), finer-grained mudstone-sandstone intervals. Twenty-four stratal units are identified in the interfan area, comprising both E-dipping (Selinous-derived) and W-dipping (Kerinitis-derived) beds. These units are separated by the key stratal surfaces described above. Considering only the key surfaces interpreted confidently, there are a minimum of 20 units. At the fan delta axes, 15 units are identified at the Selinous fan delta (Barrett *et al.*, 2019), and 11 are identified at the Kerinitis fan delta, although the base of the Kerinitis fan delta is not exposed (Backert *et al.*, 2010). Successive units that share characteristics are compiled into unit sets. The common characteristics are progradation direction and/or relative geometrical position. Units and unit sets are defined based on observations and may or may not have sequence stratigraphic significance; they do not imply a particular position within a depositional sequence. Observations

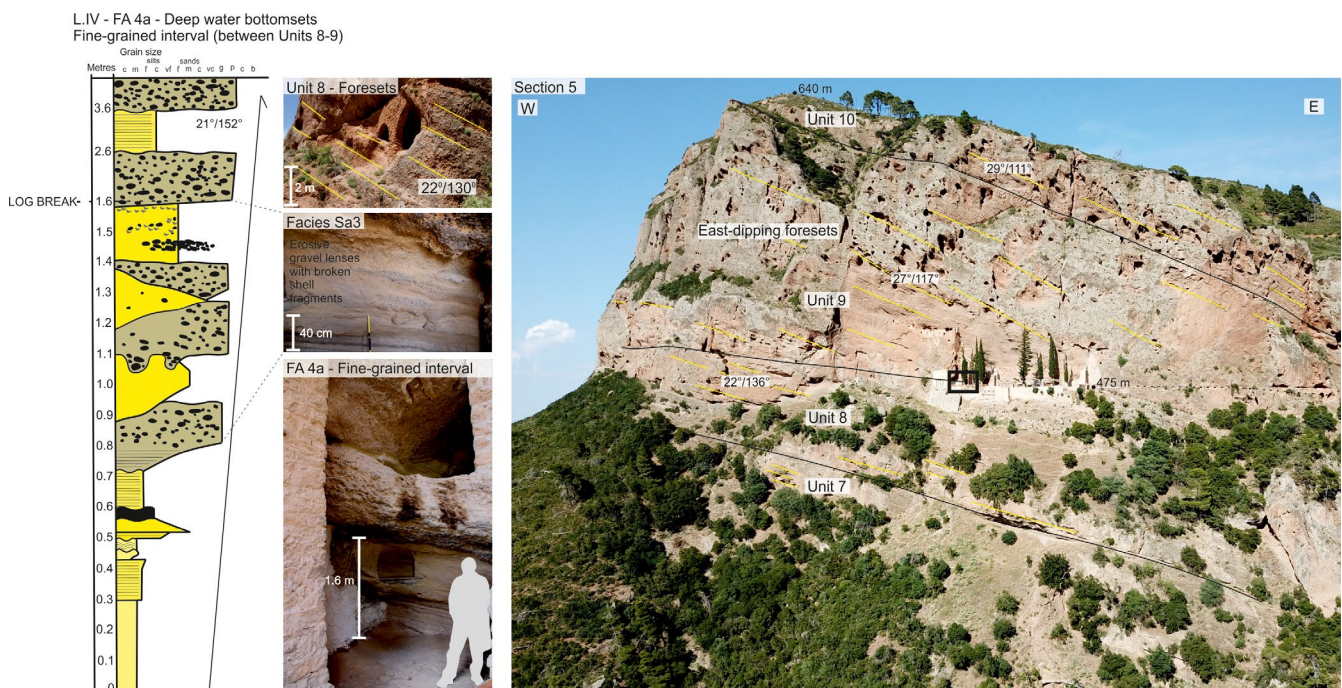


FIGURE 7 Section 5 and Unit 8 and 9 fine-grained interval character at Locality IV. Photographs of foreset facies association (FA 3). Log and photographs of distal bottomset facies association (FA 4a) and facies Sa3 (Supporting information) therein.

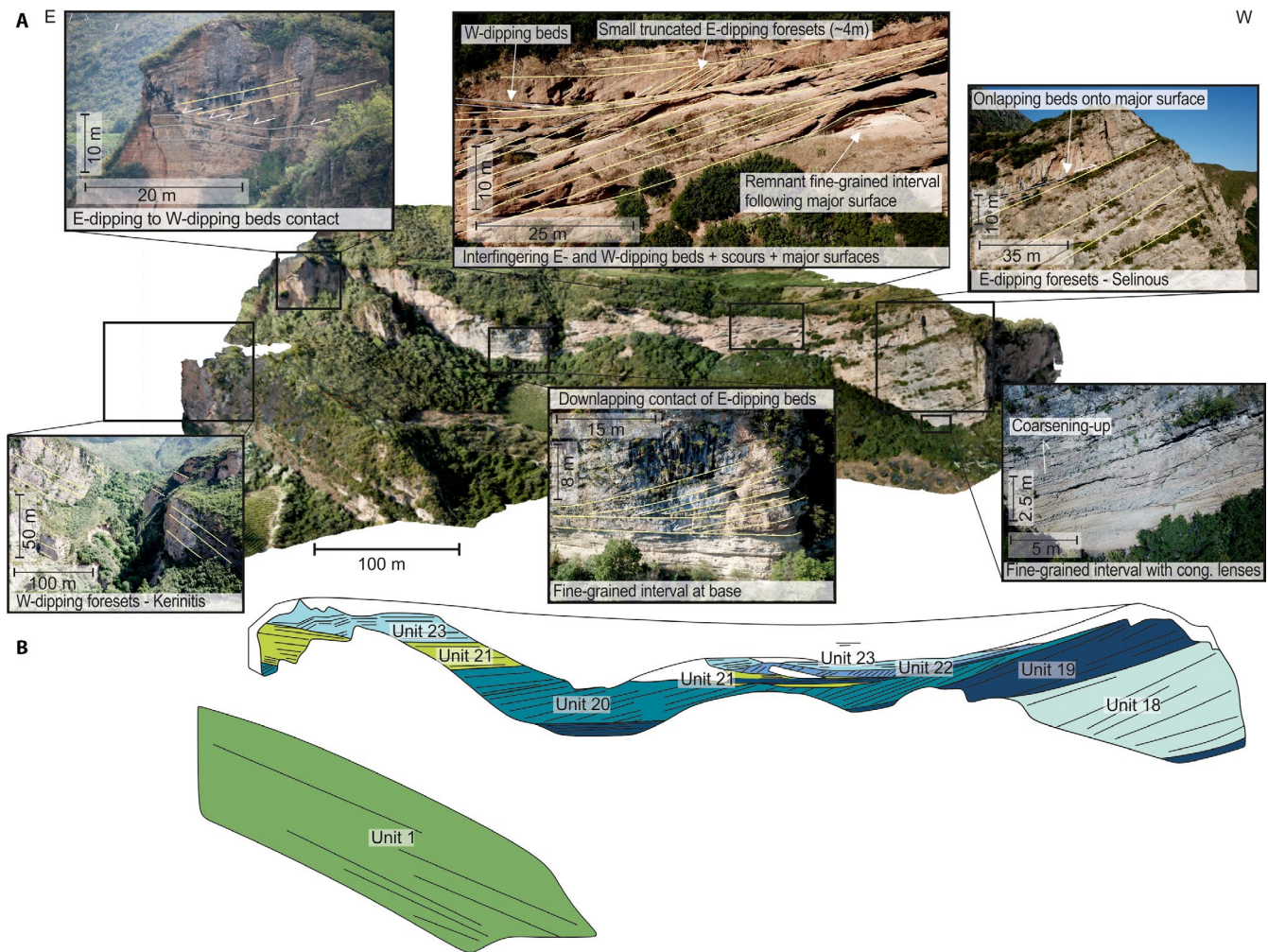


FIGURE 8 (A) Key stratigraphic observations of Section 2. E-dipping beds are Selinous-derived and W-dipping beds are Kerinitis-derived. (B) Stratigraphic framework of the central interfan face—Units 18–23 (Section 2). 3D outcrop model created in Agisoft Photoscan.

and the stratigraphic framework of Section 2 are presented in Figure 8. The stratigraphic framework for the whole interfan (Sections 2–4) is presented in Figure 9. Table 2 summarises data derived from each unit. Bedding data are presented with dip and dip direction (Figure 3).

The surfaces from the interfan cannot be accurately correlated to those at the Selinous and Kerinitis axes due to accessibility, outcrop continuity across river valleys and the absence of chronostratigraphic data. However, it is assumed that all units expressed at the Selinous fan delta axis (15 units) are observed in the interfan area (20 Selinous-derived units). Unit 1 in the interfan is part of the Kerinitis fan delta and can be traced updip to sit within the middle of the Kerinitis axial stratigraphy. The foresets markedly thicken and become higher in Units 9 and 10 at both the axis of Selinous (Barrett *et al.*, 2019) and in the interfan stratigraphy, so the lower stratigraphy in the interfan (Units 2–16) is tentatively correlated to the axial Selinous units (Figure 10). Correlations of the bottomset deposits in Melissa Valley were attempted using the 3D outcrop

models, but these remain uncertain given the limited continuity of the outcrop.

Unit set 1

Unit set 1 only comprises Unit 1, a foreset unit (FA 3) with average foreset dips of 20° towards 345° , which suggests it is part of the Kerinitis fan delta. The unit is at least 60 m thick, although the base is not observed. In Section 3, the top is downlapped by E-dipping beds of Unit 15 (Figure 9). It is not possible to tie this unit directly to the stratigraphic framework of the Kerinitis axis, but it sits somewhere within the middle units of Kerinitis. Bottomsets at Locality VII (FA 4b; Figure 3) also dip westward, supporting a Kerinitis fan delta origin. The outcrop is positioned between planes projected from the top of Unit 2 and top of Unit 3 Selinous foresets. However, these planes have a constant dip and likely overestimate bedding dip. This, combined with the absence of W-dipping foresets associated with Unit set 2, indicates that these bottomsets are likely to be associated with Unit 1.

TABLE 2 Stratigraphic information of the units in the K–S interfing area.

Unit	Observed position of unit	Average dip/dip dir.	Nature of basal contact	Top contact interp.	Fine-grained interval at top? (Y/N)	Nature of top contact	Observation type for contacts	Stratigraphic thickness	Forest height	T-F breakpoint? (Y/N)	T-F trajectory
1	Sections 2 and 3	20°/345°	Not exposed	Confident	N	Downlapped by overlying, E-dipping beds	Multiple 2D	>60 m	>100 m	N	
2	Section 4	12°/140°	Not exposed	Confident	Y	Conformable contact with thin (<2 m) fine-grained interval at top	2D	>18 m; Max. preserved 35 m		N	
3	Section 4	14°/074°; 15°/143°	Slightly erosive contact with down-lapping beds onto the fine-grained interval between Units 2 and 3	Confident	Y	Conformable contact with thin (<2 m) fine-grained interval at top	2D	33 m	32 m	Y	Progradation-aggradation
4	Section 4	15°/075°; 15°/150°	Erosive contact with fine-grained interval	Confident	N	Erosive	2D	16 m	>8 m	Y	Aggradation
5	Section 4	17°/088°; 17°/146°	Erosive contact in NE-dipping region and conformable in SE-dipping region	Confident	N	Conformable contact with Unit 6	2D	8–22 m	>45 m	Y	Progradation
6	Section 4	25°/104°	Conformable	Confident	Y	Erosive	2D	Max. preserved 25 m	>45 m	N	
7	Section 4	26°/133°	Erosive	Confident	N	Slightly erosive		<23 m		N	
8	Sections 4 and 5	22°/136°	Erosive	Confident	Y	Conformable contact with thin (<2 m) fine-grained interval at top	Multiple 2D	~35 m		N	
9	Section 4 and 5	27°/117°	Slightly erosive contact with fine-grained interval	Confident	N	Poorly imaged at top of out-crop model	Multiple 2D	90 m	>50 m	N	
10	Section 3	29°/111°	Appears conformable in western section	Uncertain	N	Poorly exposed	2D	<80 m	>100 m	N	
11	Section 3	34°/140°	Poorly exposed	Uncertain	N	Dip and geomorphological change	2D	~60 m	>100 m	N	
12	Section 3	36°/111°	Dip and geomorphological change	Uncertain	N	Geomorphological surface—cut back into cliff	2D	~65 m	>90 m	N	
13	Section 3	38°/135°	Geomorphological surface—cut back into cliff	Confident	Y	Conformable contact with fine-grained interval	2D	~43 m	>90 m	N	
14	Section 3	37°/125°	Erosive	Confident	Y	Conformable contact with fine-grained interval	2D	~30 m	>80 m	N	

(Continues)

TABLE 2 (Continued)

Unit	Observed position of unit	Average dip/dip dir.	Nature of basal contact	Top contact interp.	Fine-grained interval at top? (Y/N)	Nature of top contact	Observation type for contacts	Stratigraphic thickness	Forest height	T-F break-point appar-ent? (Y/N)	T-F breakpoint trajectory
15	Section 3	31°/111°	Slightly erosive	Confident	Y	Conformable contact with fine-grained interval	2D	~40 m	>50 m	N	
16	Section 2 and 3	27°/123°	Conformable	Uncertain	N	Conformable	Multiple 2D	~30 m	>50 m	N	
17	Section 2	26°/134°	Conformable	Confident	Y	Erosive and fine-grained interval present	2D	~65 m	>50 m	N	
18	Section 2	24°/125°	Erosive in places and coarsens up from underlying fine-grained interval	Confident	Y	Slightly erosive and remnants of fine-grained interval	2D	~58 m	>50 m	N	
19	Section 2	26°/127°	Slightly erosive and remnants of a fine-grained interval	Confident	Y	Erosive and fine-grained interval present	2D	~27 m	>40 m	N	
20	Section 2	16°/073°	Downlaps underlying erosive surface and fine-grained interval	Confident	N	Erosive	2D	16–26 m	>25 m	N	
21	Section 2	12°/247°; 09°/196°; 08°/231°; 14°/133°; 14°/236°	Erosive	Confident	N	Conformable	2D	7–16 m		N	
22	Section 2	28°/148°	Downlapping Unit 21	Confident	N	Erosive	2D	<4–5 m	>4 m	N	
23	Section 2	19°/015°	Truncates Unit 22 in central part and downlaps Unit 21 in eastern part	Uncertain	Not exposed	Not exposed	2D	>18 m		N	
24	Section 3	15°/113°	Not exposed	Not exposed	Not exposed	Not exposed	2D	>20 m		N	

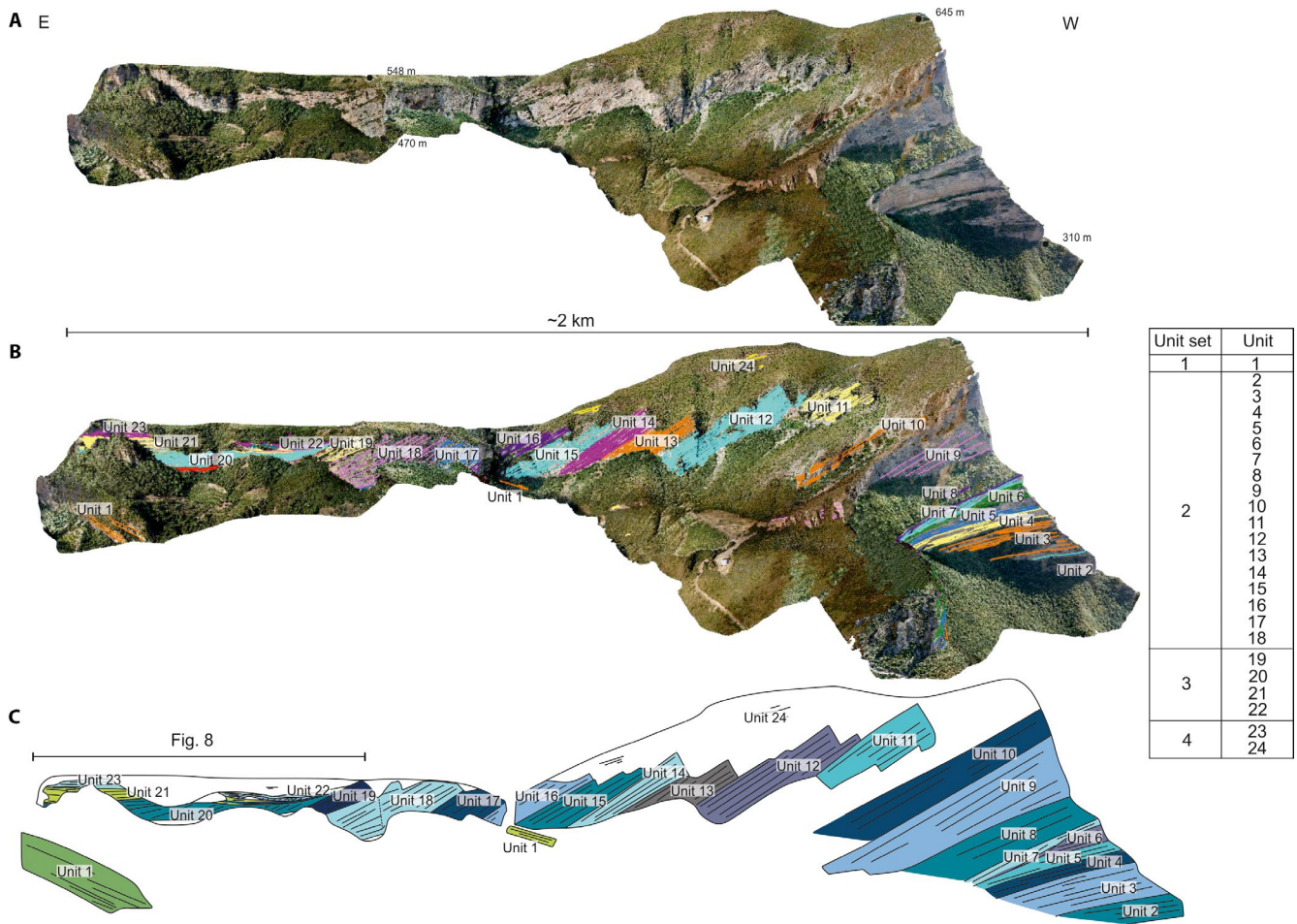


FIGURE 9 Stratigraphic framework of entire north-facing interfan cliff section (Sections 2–4). (A) Clean 3D outcrop model. (B) Interpreted 3D outcrop model with stratigraphic framework—Units 1-24. (C) Schematic cross-section of stratigraphic framework. Blues indicate units from Selinous; green indicates units from Kerinitis. 3D outcrop models are UAV-photogrammetry based, built in Agisoft Photoscan and interpreted with LIME software. Inset table shows the corresponding units within the four unit sets.

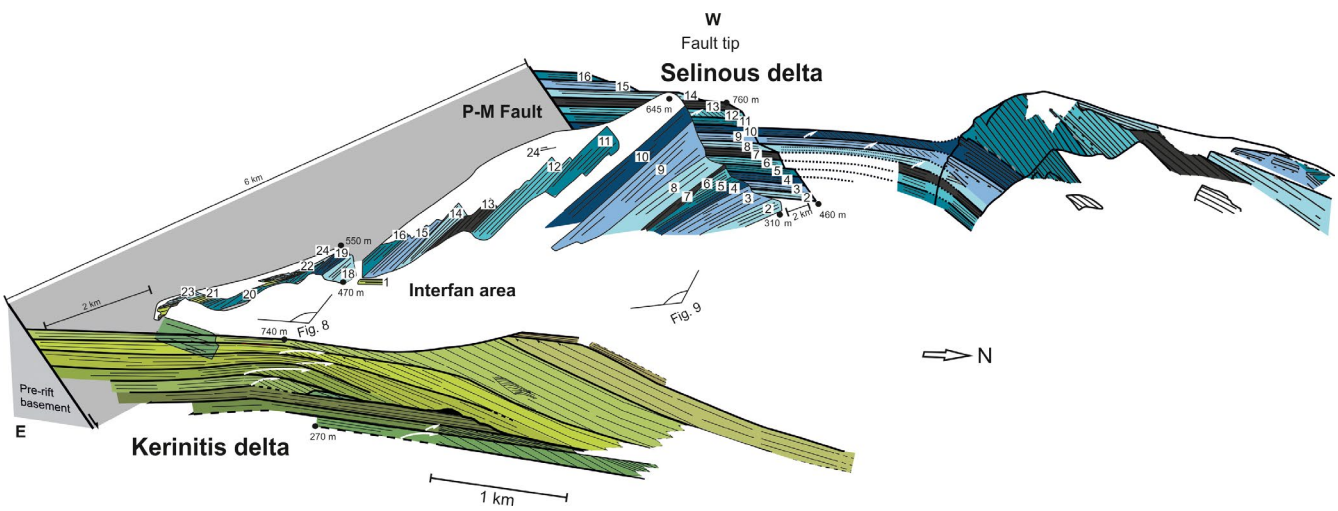


FIGURE 10 Summary diagram of stratigraphic architecture of Kerinitis (green units) and Selinous (blue units) fan deltas. Two dip sections are presented (modified from Barrett et al., 2018). An along-strike section from this study showing interfingering of the two systems in the interfan area is added to show both down-dip and along-strike stratigraphic architecture. White arrows indicate topset-foreset breakpoint trajectories. Numbers correspond to unit numbers from this study. Correlative topset units are numbered at the Selinous fan delta axis, but do not correspond to unit numbers in Barrett et al. (2018).

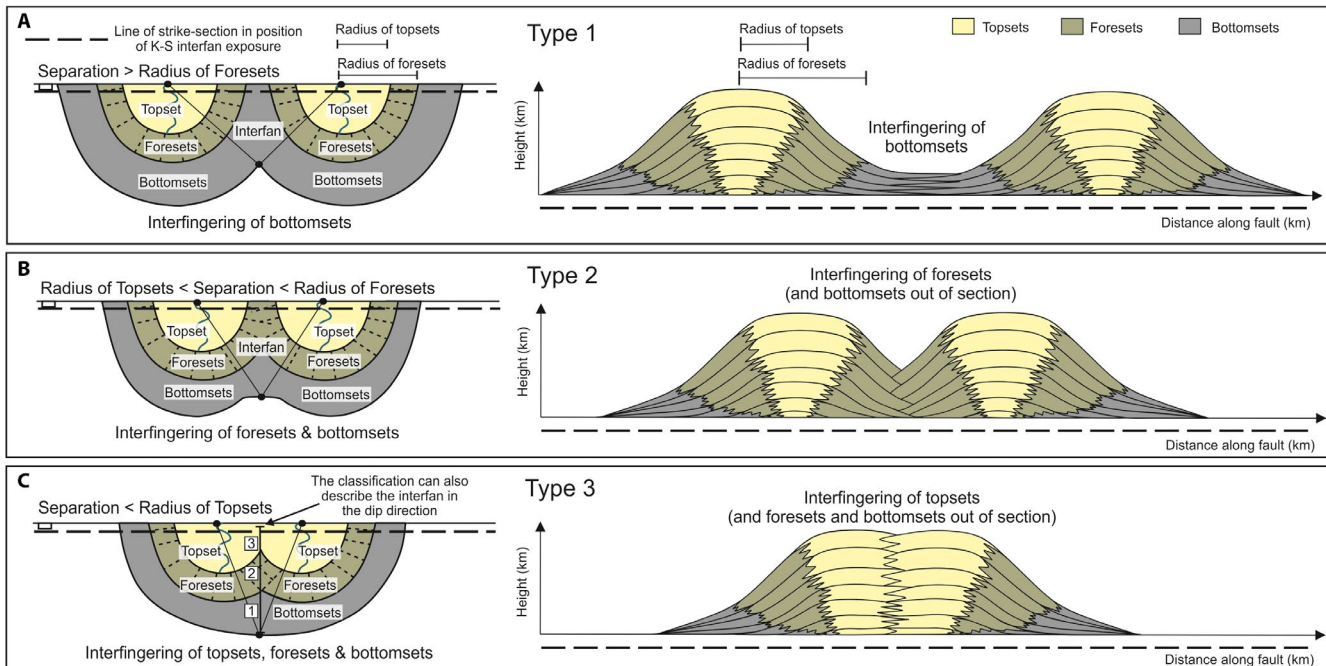


FIGURE 11 Interfan classification scheme, Types 1-3 in plan view and strike cross-section. (A) Type 1—two adjacent fan deltas are separated by a distance $>$ foreset radius and only the bottomsets interfinge in the interfan. (B) Type 2—two adjacent fan deltas are separated by a distance $>$ topset radius and $<$ foreset radius, and foresets and bottomsets interfinge in the interfan. (C) Type 3—two adjacent fan deltas are separated by a distance $<$ topset radius, and topsets, foresets and bottomsets interfinge in the interfan.

Unit set 2

Units 2–18 comprise Unit set 2, and all have eastward bedding dips (average 27° towards 122°) indicating they are part of the Selinous fan delta (Figures 3 and 9). According to projected planes in the 3D outcrop model, the bottomset outcrop at Locality V in Melissia Valley (FA 4b; position in Figure 3) is E-dipping and positioned between the top of Unit 1 and the top of Unit 2, and is therefore assigned to Unit 2.

Topset-foreset breakpoints are apparent in the lower Units 3–5 (Figure 4). Within Unit 3, the topset-foreset breakpoint presents a progradational–aggradational trajectory. Beds are observed that dip to the NE (14° towards 074°) and SE (15° towards 143°) revealing the radial pattern of the fan delta. The NE-dipping beds downlap the fine-grained interval below, and the SE-dipping beds project into the outcrop face. The maximum height of the NE-dipping foresets from topset-foreset breakpoint to the downlap position is 32 m (Figure 4). A thin, fine-grained interval overlies Unit 3, which is eroded by Unit 4. The topset-foreset breakpoint of Unit 4 is observed above that of Unit 3 and has an aggradational (near vertical) trajectory. Beds dip to the NE (15° towards 075°) and SE (15° towards 150°). The height of the youngest foreset before Unit 5 is 8 m. The upper part of Unit 4, with NE-dipping beds, is eroded by Unit 5. The topset-foreset breakpoint of Unit 5 reveals a near-horizontal, that is, progradational, trajectory (Figure 4). The beds dip eastward (15° towards 088°) and SE (17° towards 146°). The thickness in the SE-dipping region is 8 m and thickness in the ENE-dipping region is 22 m. At the top, there is a conformable contact with Unit 6. The

upper part of Unit 6 comprises a fine-grained interval which is widely removed by an ~ 17 m deep erosion surface.

Units 10–18 are thicker (average 52 m), and comprise steeply-dipping (towards SE) foreset packages (Figure 9). Foresets are taller than those in the lower units (>100 m) (Figure 4). Bottomset outcrops at Locality VI (FA 4b; Figure 3) are positioned just above the projected plane from the top of Unit 12, and are therefore assigned to Unit 13. Outcrops at Localities VIII and IX (FA 4b; Figures 3 and 6) are positioned between the top of Unit 12 and the top of Unit 16. The Locality IX outcrop is E-dipping and is associated with Units 13–16. The Locality VIII outcrop is W-dipping (Kerinitis-derived) and stratigraphically higher, so deposited at the same time as Units 13–16, but after that at Locality IX. Outcrops at Localities X and XI (FA 4b; Figure 3) are positioned just below the projected plane for the top of Unit 16. The Locality X outcrop is E-dipping and assigned to Unit 16. The Locality XI outcrop is W-dipping and deposited at a similar time to the Locality X outcrop (Figure 3).

Unit set 3

Unit set 3 comprises Units 19–22 and is differentiated from Unit set 2 by the presence of shallower foreset dips, smaller preserved foreset heights (4–40 m), overall thinner units (average 16 m) and the interfingering of E and W-dipping beds (Figure 8). The dominant facies association is FA 3 (foresets). Unit 19 bedding (26° towards 127° ; i.e. Selinous) shallows eastward, and is ~ 27 m thick. In the western part, it is eroded at the top. A ~ 7 m thick flat-lying fine-grained interval (3°

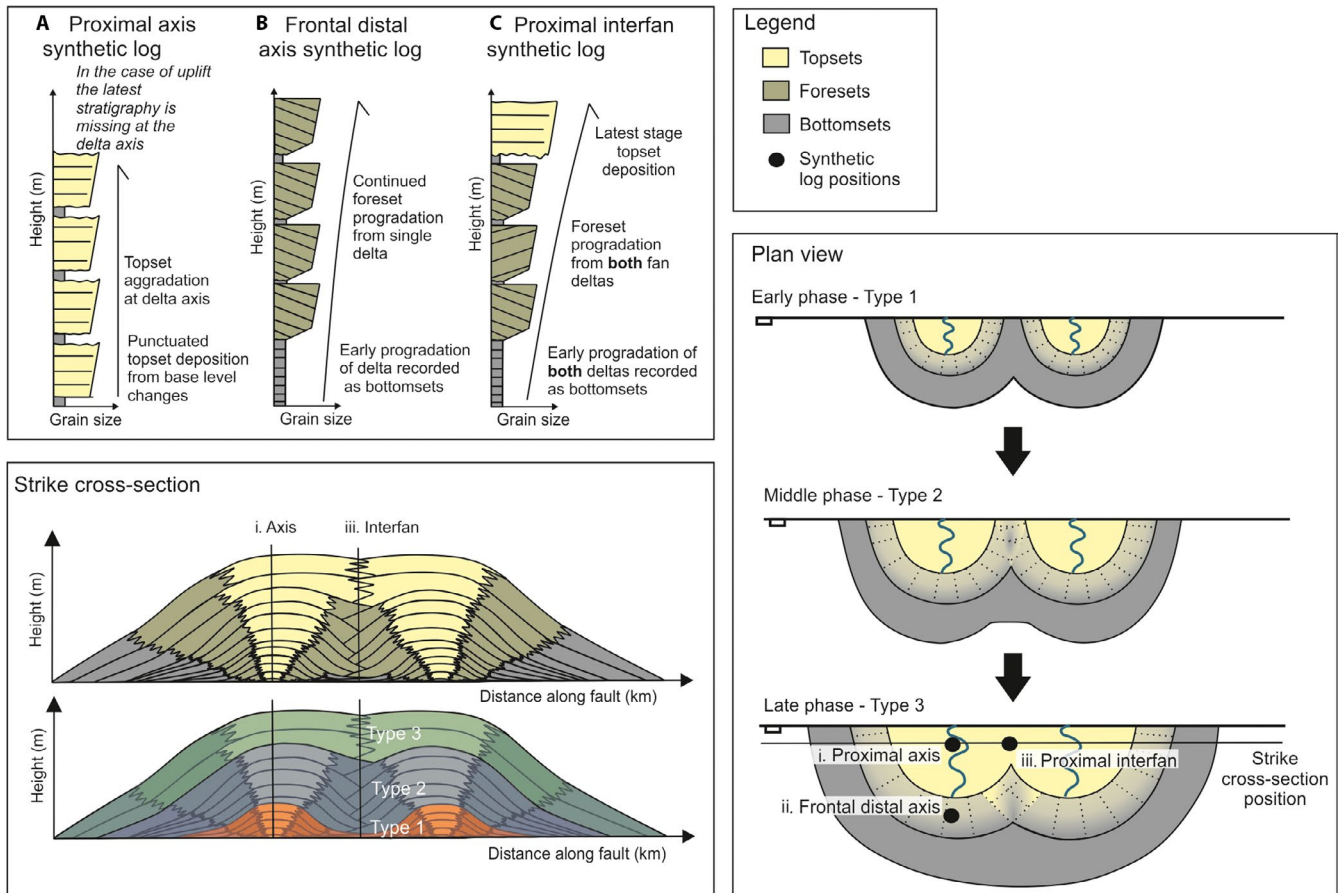


FIGURE 12 Typical evolution of an interfan through Types 1–3 with the progradation of two fan deltas. (A) Synthetic logs to show the differences in stratigraphic evolution between the delta axes and the interfan area. Synthetic logs are shown from the proximal axis (i), frontal distal axis (ii) and the interfan (iii). (B) Plan view evolution of the fan deltas, coalescing further as they grow and transitioning through interfan Types 1–3. (C) Strike cross-section through the proximal part of the deltas (position shown in B).

towards 154°) in the centre of Section 2 is interpreted to represent the correlative bottomsets (Figure 8). Unit 20 is also part of the Selinous fan delta, and its foresets downlap the erosion surface and the fine-grained interval at the centre of the outcrop. Unit 20 comprises thinner-bedded, smaller foresets than those in Unit set 2, although it is truncated at the top by an erosion surface (7° towards 154°). Within the unit, the bedding dip shallows eastward (from 16° towards 073°, to 7° towards 138°), but correlative bottomsets are not identified. Unit 21 is part of the Kerinitis fan delta and thins and shallows westward. In the area that it is thinnest, E-dipping, Selinous-derived beds (14–133°) interfinger and downlap W-dipping beds (10–233°). The E-dipping beds cannot be traced updip as they are eroded by the base Unit 22 surface. Unit 22 downlaps that surface and is distinct with thinly-bedded, small (4–5 m high) foresets dipping eastward (28° toward 148°—from Selinous). It is top truncated by a flat-lying erosion surface (Figure 8).

Unit set 4

Unit set 4 comprises Units 23 and 24, which are distinct from lower units as they have northward dip components (19° towards 015°), and in the west are flat-lying relative to

the underlying Unit set 2. Eastward, there is a sharp, angular lower contact with Unit 21, marked by downlap of Unit set 4 foresets. The top is not exposed, but the unit has a minimum thickness of 18 m. Limited exposures of Unit 24 are apparent in Section 3 (min. 20 m thick) (Figure 9), but outcrops are accessible at Locality I (FA 2c) (Figures 3 and 5).

4.3 | Interfan end-members

To augment the interpretation of the K–S interfan, a classification scheme is proposed for interfans using modern fan delta morphologies (Figure 2B). Interfans can be classified as one of three end-members according to their separation relative to fan delta topset and foreset radius, which determines the degree of interfingering of fan delta topset, foreset and bottomset deposits. The three types are presented in planform view and in strike cross-section in Figure 11, and with modern examples in Figure 2B. In Type 1, fan deltas are separated by a distance greater than the foreset radius and the interfan area is occupied by interfingering bottomset deposits. In Type 2, fan deltas are separated by a distance greater than the topset radius and less

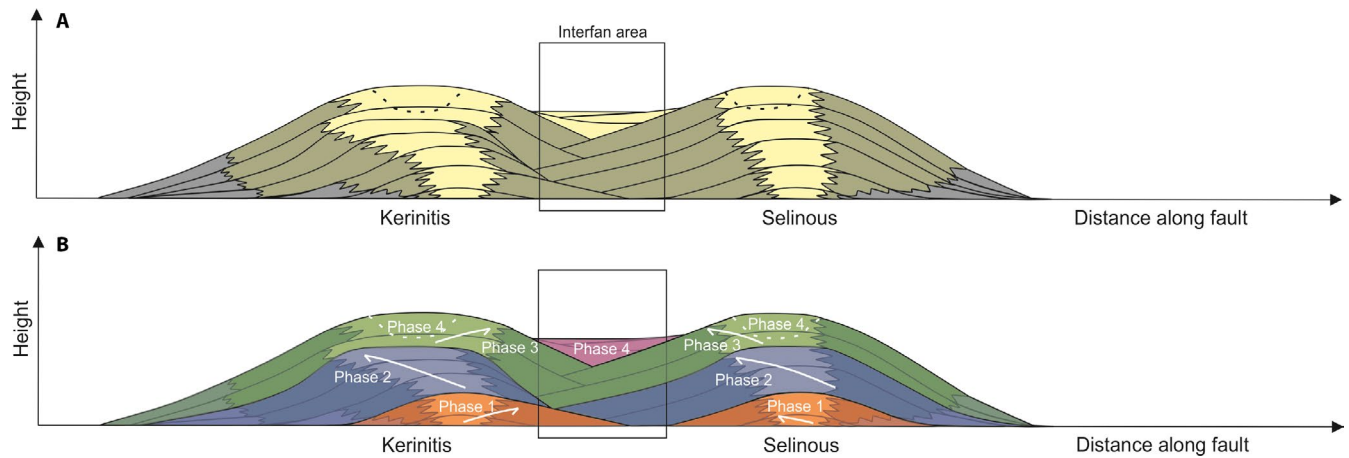


FIGURE 13 (A) Strike cross-section schematic diagram of the Early–Middle Pleistocene Kerinitis–Selinous interfan (grey box) large-scale architecture. (B) Diagram overlain with colours indicating Phases 1–4 of interfan evolution. Dashed lines indicate erosion during Phase 4. White arrows indicate progradation direction of each fan delta during each phase.

than the foreset radius, and both foresets and bottomsets interfinger in the interfan area. In Type 3, topsets, foresets and bottomsets interfinger as the fan delta systems are closely abutted at a distance less than the topset radius. The equivalent of a Type 3 interfan in an alluvial setting is a bajada (Blackwelder, 1931; Hooke, 1972; Bull, 1977; Miliareis, 2001).

In each type, the interacting process regime and deposits will differ. When considering the evolution of an interfan, the geometry may evolve between these types and will depend largely on the allogenic forcing responsible for the building of the fan deltas and the basin evolution. Figure 12 shows a model for the evolution of an interfan area as two fan deltas prograde and coalesce. Three synthetic logs are presented to show the differences in the stratigraphic record through this process at different positions: the proximal axis, the distal axis and the interfan area. In this respect, each type can be considered as a single stage of evolution. This classification also represents the degree of coalescence in the dip direction. For example, an interfan could present Type 3 geometry in the proximal region and Types 2 and 1 with distance away from the sediment source (Figure 11C).

5 | INTERPRETATION OF THE K–S INTERFAN TEMPORAL EVOLUTION

The stratigraphic framework at Selinous and Kerinitis is presented as a fence diagram to illustrate an along-strike section across the interfan (Figure 9) and dip sections through the deltas axes (Figure 10; after Backert *et al.*, 2010; Gawthorpe *et al.*, 2017b; Barrett *et al.*, 2019). The interfan evolved through five distinct phases of progradation:

1. Initial progradation of the fan deltas into the interfan area, starting with Kerinitis.

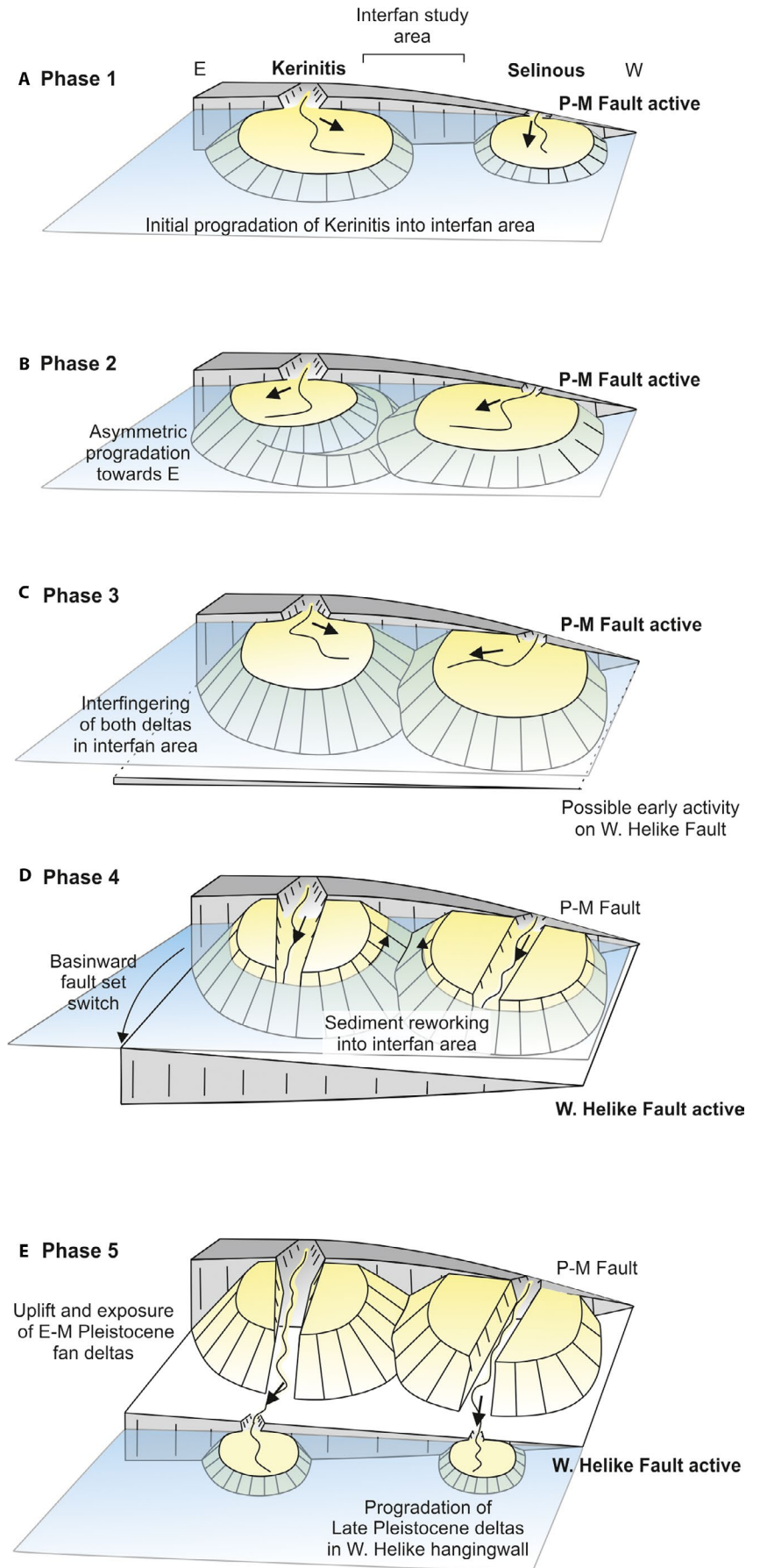
2. Progradation of the Selinous fan delta into the interfan area and asymmetric eastward delta growth.
3. Aggradation and interfingering of the two systems, and shallowing of the interfan area.
4. Relative base-level fall, erosion and reworking of eroded sediments into the interfan area.
5. Continued uplift of the West Helike footwall and exposure of the Early–Middle Pleistocene deltas and growth of Late Pleistocene deltas in the West Helike hangingwall basin.

These phases are further described in the following sections and are presented in Figures 13 and 14.

5.1 | Phase 1 (Unit set 1)

Activity on the P–M Fault began ~1.8 Ma (Ford *et al.*, 2016) and hangingwall subsidence created space for sediments to accumulate. The Kerinitis and Selinous rivers cut through the uplifting footwall and fed sediment to the new hangingwall basin. The development of Gilbert-type fan deltas along the fault suggests that the fault line defined the coastline at this time. Displacement is greatest at fault centres (Walsh and Watterson, 1988; Dawers and Anders, 1995), resulting in the greatest accommodation at this position. The first unit apparent in the interfan area (Unit 1 within Unit set 1) is W-dipping and part of the Kerinitis fan delta, which sits closest to the fault centre. Unit 1 is not tied directly to the Kerinitis axial stratigraphy, but can be traced up-dip approximately to the middle units. This suggests that earlier progradation of Kerinitis did not extend as far as the interfan study area, and that the interfan is younger than early units deposited at the Kerinitis delta axis. It is unclear whether the progradation of the Kerinitis fan delta into the interfan area represents directional westward progradation, or overall expansion of the fan during this phase. There is no evidence that Selinous foresets prograded as far as

FIGURE 14 The Kerinitis–Selinous interfan evolution records: progradation of deltas into the interfan area (Phase 1), asymmetry of growth towards the east (Phase 2), stratal interfingering during net subsidence (Phase 3) and relative base-level fall, erosion and reworking during net uplift, as a result of a basinward fault set switch (Phases 4–5).



the interfan area during deposition of Unit set 1, as downlap at this location is only observed in later units. A plane projection of the top Unit 1 surface using the 3D outcrop model indicates that in the west, it sits below the earliest E-dipping units from Selinous. Hence, Kerinitis prograded into the interfan area before Selinous (Figures 13 and 14).

During Phase 1, the interfan can be classified as Interfan Type 1, separated by a distance greater than the radius of the foresets (Figure 11), as only Kerinitis foresets are evident in the interfan at this stage. It is not Type 2 because Selinous foresets are absent and thus the foresets of the two systems are not interfingering. Bottomset exposures in the interfan area linked to early Selinous progradation are not observed, but it is likely that fine-grained bottomset deposits were interfingering in the interfan area at this time.

5.2 | Phase 2 (Unit set 2)

During Phase 2, the Selinous fan delta began to prograde eastward into the interfan area, as indicated by E-dipping Unit set 2 (Units 2–18). Units 3–5 reveal topset-foreset breakpoint trajectories (Helland-Hansen and Hampson, 2009) at a distance of ~1 km from the fault (Section 4), suggesting the shoreline was proximal to the fault in the interfan area. The progradation–aggradational trajectory of Unit 3, suggests that sedimentation rate was high, and kept pace and exceeded the rate of accommodation creation. The progradational trajectory of Unit 4 suggests sedimentation rate exceeded the rate of accommodation creation, whereas the aggradational trajectory of Unit 5 suggests sedimentation rate kept pace with the rate of accommodation creation. The middle units at the Selinous delta axis present similar progradational–aggradational trajectories (Barrett *et al.*, 2019). Through the development of these three units the breakpoint remains in a similar position, suggesting overall aggradation (i.e. sedimentation kept pace with the rate of accommodation creation). In Unit 3, a full clinoform is preserved with a foreset height of 32 m, suggesting a ~30 m palaeo-water depth in the interfan area at this time. Foreset height increases to <200 m in Units 9–18. Foreset height increases as a result of the greater space available in the deeper water into which the foresets prograded. The fact that the foresets aggraded as well as prograded, suggests relative base-level rise outpaced sediment supply, most likely because of high subsidence rates of the P–M Fault hangingwall.

The E-dipping Unit 15 (Selinous-derived) downlaps onto the W-dipping Unit 1 (Kerinitis-derived; Unit set 1) (Figures 13 and 14). This is the first evidence of foresets interfingering between the two fan deltas. Units 16–19 continue to build up the flanks of these older Kerinitis foresets. They decreased in height as they built out into shallower water. At this stage, there is no evidence of Kerinitis building into the interfan area. Thus, Kerinitis was likely prograding to the north and east at this time. It is clear that there is an asymmetric architecture

in the interfan during Phase 2, with significant progradation from Selinous to the east, and inferred progradation from Kerinitis in the same direction. Presumably, therefore, both Selinous and Kerinitis exhibited asymmetric planform geometries, comparable to that of the modern Meganitis, Selinous, Kerinitis and Ladopotamos fan deltas (Figure 2).

During Phase 2, the interfan evolves from a Type 1 to Type 2 interfan (Figure 11) as foresets from both fan deltas are now apparent and interfingering in the interfan area. However, this interfingering occurred in two discrete phases, firstly from Kerinitis and then from Selinous (Figure 13), as opposed to continuous abutting (Figure 11).

5.3 | Phase 3 (Unit set 3)

Phase 3 is differentiated from Phase 2 by shallower dips, thinner units and continuous interfingering of E (Selinous) and W-dipping (Kerinitis) beds, which suggest a different depositional setting to Phase 2. During Phase 3, Selinous prograded eastward and Kerinitis prograded westward, into the interfan area (Unit set 3; Figures 13 and 14). Bedding dips within Unit 19 decrease laterally and have correlative bottomsets apparent in Section 2 (Figure 8). Unit 20 bed dips shallow upwards, and Units 20–22 are thinner than the preceding units (5–25 m thick), suggesting less available accommodation. Therefore, Selinous built into gradually shallower water as it encroached onto the Kerinitis margin. Sharp contacts formed as progradation from both systems caused foresets to downlap onto each other. Unit 22 comprises thinly-bedded, small (4–5 m high) foresets that are top truncated. Despite the truncation meaning that the true height of the foresets cannot be determined, water depth clearly shallowed significantly. Progradation occurred within the units, but generally the units aggraded, rather than prograded. This is likely to be a result of restricted lateral space as Selinous built up the flanks of Kerinitis, but with sufficient water depth for aggradation. The units thin towards the top of the section as they aggraded, which is likely to be due to decreasing activity on the P–M Fault causing reduced subsidence rates. Units 20 and 22 are truncated by major erosion surfaces. The top erosional contact of Unit 22 reveals a transition from small foresets to flat-lying beds that could be topsets. There is also a lack of fine-grained intervals towards the top of Unit set 3. This may be due to erosion, with the higher energy conditions limiting fine-grained sediment preservation. Alternatively, their formation was restricted by either: slowing subsidence rates reducing the rate of base-level rise such that climate-induced lake-level falls could overcome it, or new activity on the parallel, basinward West Helike Fault causing uplift of the footwall, and the associated overall relative base-level fall exceeding any climate-induced lake-level rises.

During Phase 3, the interfan continues to present the Type 2 interfan geometry, whereby foresets interfinger in the

interfan area. However, the foreset interfingering is expressed differently to that of Phase 2, with consistent abutment, rather than discrete phases of progradation.

5.4 | Phase 4 (Unit set 4)

Unit set 4 (Units 23–24) developed during Phase 4. Unit set 4 is more flat lying than the steeply-dipping underlying units, has a northern component of dip and consists of metre-scale, well-sorted lenses of sand and conglomerate (FA 2b) that dip eastward and westward (Figures 5, 13 and 14). These are interpreted to represent subaqueous migrating bedforms that are made up of reworked material transported into the interfan area by wave-related longshore currents, for example, longshore bars (Orme, 1985; Ashley, 1990; Larson, and Kraus, 1992; Drønen and Deigaard, 2007). Some accommodation (shallow water) therefore existed in the interfan at this time. Activity on the P–M Fault ceased at ~0.7 Ma, at which time the West Helike Fault became active and dominant (Ford *et al.*, 2007). Uplift of the West Helike footwall caused the delta axes to become exposed above base-level (relative base-level fall). The uplift rate of the contiguous East Helike Fault is 1–1.5 mm/year (De Martini *et al.*, 2004), and the Kerinitis and Selinous rivers incised their own topsets. The modern geomorphology of the valleys shows that the main river direction and sediment pathway was, and continues to be, northwards. Unit set 4 deposits are interpreted to mark the erosion and reworking of topset material into the shallow interfan in response to basinward migration of strain and net basin uplift. The shallow water topsets from Selinous and Kerinitis were abutting at this time (Figure 13). The interfan therefore finally evolved to Type 3 during this phase.

5.5 | Phase 5

Phase 5 is not recorded in the interfan stratigraphy, but soil development and surficial erosion has occurred during and since Phase 5. Late Pleistocene fan deltas formed in the hangingwall of the West Helike Fault. By this time, the shoreline had therefore migrated to the West Helike Fault scarp. The Early–Middle Pleistocene fan deltas continued to be eroded by their feeder rivers (Figure 14).

In summary, the Kerinitis and Selinous interfan evolution can be divided into two parts according to the basin evolution (Figure 14). In the first part, growth of the P–M Fault caused net subsidence of the hangingwall basin and resulted in Phases 1–3 of interfan evolution: initial progradation of the fan deltas into the interfan area, starting with Kerinitis (Phase 1), asymmetric Selinous fan delta growth eastward (Phase 2), and interfingering of the two systems and shallowing of the interfan (Phase 3). In the second part, the P–M Fault ceased to be active and strain was accommodated on the West Helike Fault

(basinward fault set switch), causing uplift of the West Helike Fault footwall and thus net uplift of the P–M Fault hangingwall basin through its transition from a marginal fault block to fault terrace. This resulted in relative base-level fall, erosion and reworking of sediments into the interfan area (Phase 4), and continued uplift until base-level fell below the West Helike fault scarp, which cut off the Early–Middle Pleistocene deltas and accommodated growth of Late Pleistocene fan deltas in the West Helike hangingwall basin (Phase 5).

6 | DISCUSSION

Based on observations of modern fan deltas and detailed analysis of the exhumed Early–Middle Pleistocene interfan between the Kerinitis and Selinous fan deltas, there emerges a more complete understanding of the stratal architecture resulting from along-strike interfingering of fan deltas during basin evolution. The following section discusses the classification scheme for interfans in terms of its applicability to other ancient systems, the mechanisms for the observed asymmetry in the ancient and modern systems, and the value of including interfan analysis in basin research.

6.1 | Style and classification of interfans

Proposed here is the first classification scheme for deltaic interfans based on modern fan delta geometries, which has been used to describe the evolution of the ancient system studied. Interfan styles are differentiated based on their separation relative to the radius of the delta topsets and foresets; this determines the interfingering of topsets, foresets and bottomsets in the interfan area (Figure 11). The interfan between the Kerinitis and Selinous fan deltas evolved from Type 1 (Phase 1) to Type 2 (Phases 2 and 3), and finally reached Type 3 (Phase 4). The interfan evolved through all three end-members (Figure 11). Although these types were characterised from, and represent end-members of modern systems (Figure 2B), they also represent an evolutionary continuum of an interfan, assuming a sufficient sediment supply and progradation that eventually occupies the distance between the fan deltas (Figure 12). It is also possible to use the classification scheme to subdivide an interfan in the dip direction (Figure 11C). In the exhumed system studied, it is the geometries proximal to the fault/sediment source that are considered for the classification (strike line presented in Figure 11). However, in a case with topsets adjoined in the proximal area (Type 3), the interfan will also exhibit Type 2 and Type 1 in a proximal to distal trend (Figure 11C).

The scheme is presented with adjacent fan deltas in the hangingwall of a fault, but it is worth noting that the scheme also applies to adjacent systems in the footwall, and also fans that are obliquely prograding. For example, one fan

prograding down a relay ramp may coalesce with one in the immediate hangingwall and the classification scheme is still applicable (Figure 2B).

6.2 | Asymmetry of fan deltas

In previously published models of fan deltas in rift settings (Gawthorpe and Leeder, 2000), and in the interfan models presented here (Figure 11), a symmetrical planform geometry and architecture of fan deltas is assumed. This follows the originally described Gilbert-type fan delta descriptions from the tectonically quiescent Lake Bonneville (e.g. American Fork delta; Gilbert, 1890; Milligan and McDonald, 2016) that were principally controlled by lacustrine base-level change in a glacial climate and which exhibit a symmetrical delta architecture (Gilbert, 1890; Lemons *et al.*, 1996; Godsey *et al.*, 2005). However, it is clear that during Phase 2 the Selinous fan delta, and most likely the Kerinitis fan delta, were asymmetric, and skewed eastward (Figures 13 and 14). Many of the modern fan deltas along the southern shore of the Gulf of Corinth also have an asymmetric delta plain geometry, representing a snap-shot of their tectono-stratigraphic evolution (e.g. the Meganitis, Selinous, Kerinitis and Akrata fan deltas; Figure 2A,2). The definition of the interfan is proposed here as ‘the area between two lines that project from the apices of two fan deltas to their intersection at the most distal point of bottomset interfingering’ is applicable to asymmetric fans, but the limit of distal interfingering is more challenging to pinpoint in these cases.

There are two potential mechanisms for this asymmetry: (a) preferential reworking of sediments from the dominant wind and wave direction and/or, (b) principal sediment supply towards structural lows. In the modern Gulf of Corinth, a westerly wind and wave direction prevails, conditions that are expected to have been similar in the Early–Middle Pleistocene. The carrying energy of the longshore current would have been dependent on the weather conditions, with local storms producing currents with a higher energy that allow greater loads to be transported along-shore (Bagnold, 1966). A number of formulas have been derived to predict longshore sediment transport in swell and storm conditions (Bijker, 1967; Engelund and Hansen, 1967; Ackers and White, 1973; Van de Graaff and Van Overeem, 1979; Bailard and Inman, 1981; Van Rijn, 1984; Watanabe *et al.*, 1991); and these are compared in Bayram *et al.* (2001). As a result, sediments above wave base have been pervasively reworked eastward. This is a likely mechanism for the skewing of planform topset geometry in the modern fan deltas (Figure 2A,2) and may have driven migration of the barforms present in Unit 24 of the K–S interfan (Figure 5). In cases where shallow water foresets have prograded over a previously flooded delta topset there is also the potential for longshore current reworking. For example, the foresets of the modern Selinous delta that overlie the submerged Late Pleistocene Selinous fan delta (Figure 2B).

For the overall fan delta architecture to be asymmetrical, there must be a driver to deflect the rivers. Differential subsidence along the border faults results in structural gradients, where the lowest point typically lies at the fault centre (Walsh and Watterson, 1988; Dawers and Anders, 1995). Over time, the rivers and resultant fan deltas preferentially follow the structural contours. A structural influence on river course has been documented for the modern Selinous and Kerinitis rivers. The modern Kerinitis River has migrated towards the north–west since AD 450–1400 (Schmidt, 1879; Soter and Katsonopoulou, 1998; McNeill and Collier, 2004) as a result of differential displacement in the relay zone between the East and West Heliki Faults (Figure 2). The modern Selinous River has gradually migrated towards the south-east in response to growth of the Aigion Fault (Soter and Katsonopoulou, 1998; McNeill and Collier, 2004; Figure 2). Asymmetry of fan delta architecture should be expected in tectonically-active settings subjected to differential subsidence. Interfans in these settings are therefore likely to exhibit a dominant influence from one fan delta, as can be seen in the K–S interfan, where the Selinous fan delta dominates during Phase 2. The highest rates of hangingwall subsidence are interpreted during Phase 2, which coincides with the most pronounced asymmetry. Ultimately, the degree of asymmetry through time is controlled by the interplay of external controls. In rift basins, this can be complicated by fault segment linkage that influences along-strike subsidence patterns. If the fan deltas prograde towards the area with more subsidence, which may change its position through time, the rivers will respond to change the dominant system in the interfan area.

In summary, the observed asymmetry in the ancient succession is architectural, with large foresets from the Selinous fan delta dominating the interfan succession (Figures 9 and 13), and thus reflecting a response to the structural gradient towards the fault centre. The asymmetry observed in the planform geometry of the modern fan deltas (Figure 2), and in the higher units of the interfan (Figure 8), is more likely to be a result of the prevailing wind and wave direction.

6.3 | Interfans as stratigraphic archives

Interactions of tectonics, base level and sediment supply are spatially and temporally complex. Interfan stratigraphy can record the complexity of the temporal evolution in rift settings, and the transition from net subsidence to net uplift, which is not recorded stratigraphically at the fan delta axes. Here, this regime shift was the result of a 6 km northward (basinward) transfer of fault activity from the P–M Fault to the West Helike Fault, and is recorded by (a) an overall shallowing upwards facies trend from Unit set 2–4, (b) reduced foreset heights, (c) a vertical stacking pattern suggesting a restriction of lateral space, (d) a greater number of units in the interfan than at the delta axes, and (e) subsequent erosion and

progradation of younger fan deltas in the hangingwall of the West Helike Fault. During basin uplift, due to its deeper water position, the K–S interfan retained accommodation for longer than the delta axes, which became exposed first. Although, the axial parts of fan deltas record the earliest phases of delta evolution, prior to progradation into the interfan area, the K–S interfan provides a more complete stratigraphic record of the final stages of delta evolution (Figures 13 and 14). In Figure 12, synthetic logs are presented to show the differences in the stratigraphic record at three positions through the progradation of two fan deltas: the proximal axis, the frontal distal axis and the interfan area. The proximal axis records the aggradation of topset units from the earliest growth phase, but in the case of uplift, is missing the latest stage of evolution. At the frontal distal axis, the earliest progradation of a single fan delta is recorded with bottomset deposits, and becomes overlain by foresets from that fan delta. As it is in a deeper water position, the frontal distal axis continues to preserve stratigraphy during the latest stage, but only from one fan delta. The proximal interfan records the early progradation of both fan deltas as interfingering bottomset deposits. The middle phase is represented by the progradation of foresets from both fan deltas and the latest stage is occupied by topset deposition. Thus, the interfan area not only provides a more complete record through uplift, but also records the history of both fan deltas, their architectural interactions through time, and potentially reveals their asymmetry more readily than in axial dip sections. Both the axial and interfan areas are complementary and together yield the most complete record of basin evolution (Figure 12), which has high utility. For example, if more complete biostratigraphic and palaeomagnetic records were available from fine-grained intervals and with more accurate correlation of stable, cosmogenic and radiogenic isotope curves to the fan delta succession, greater confidence in dating and tying of the eustatic sea-level curve to the stratigraphy could be achieved (Emiliani, 1955; Imbrie *et al.*, 1984; Lisiecki and Raymo, 2005). Interfan areas could therefore represent valuable but underutilised stratigraphic archives, which merit further investigation.

7 | CONCLUSIONS

This is the first detailed study of syn-rift stratigraphic architectures in the interfan area of coeval fan deltas. Field data and UAV photogrammetry-based 3D outcrop models are used to extract qualitative and quantitative data from the Early–Middle K–S interfan. Modern planform geometries of interfan areas allow the classification of interfans into three end-members based on their separation according to delta topset and foreset radius, which can be applied to ancient systems. The Early–Middle Pleistocene K–S interfan evolved from Type 1 to Type 3 through five evolutionary phases from net subsidence to

net uplift, due to a northward migration of fault activity from the P–M Fault to the West Helike Fault. The interfan architectures record: early progradation of the Kerinitis delta into the interfan area (Phase 1), subsequent progradation of the Selinous delta into the interfan area and asymmetry of growth of both fan deltas eastward (Phase 2), stratal interfingering of foresets from both fan deltas during net subsidence (Phase 3), and relative base-level fall, erosion and reworking during net uplift, as a result of a basinward fault set switch (Phases 4 and 5). Planform asymmetry in the modern fan deltas is interpreted to be a result of wind and wave directional reworking. Architectural asymmetry is interpreted to be due to preferential river avulsion towards structural lows driven by subsidence patterns along active faults. Thus, architectural asymmetry may be a common feature in rift basins, and as such interfans in these settings are likely to preserve evidence of a dominant depositional system. Interfan areas provide a condensed, and potentially more complete, stratigraphic record than the axial areas of the fan deltas through high preservation potential and longer submergence during the early stages of basin uplift, and therefore allow further insight into basin evolution. Interfan areas are underrepresented in terms of their importance in the literature, yet could be exploited as important stratigraphic archives that complement fan delta axial records.

ACKNOWLEDGEMENTS

Hannah Kearns is thanked for her assistance on fieldwork. The authors are grateful to Casey Nixon for the loan of a Mavic Pro drone and to Simon Buckley for access and assistance with LIME software. The authors thank the project sponsor, Neptune Energy, who supports the SMRG (Shallow Marine Research Group). Barrett is also grateful for fieldwork support from the BSRG Trevor Elliott fund and an IAS Post-Graduate Research grant. Stereonets were generated using Rick Allmendinger's Stereonet 10 software. Gawthorpe acknowledges support from VISTA and the Syn-Rift Systems Project, the Research Council of Norway (project number 255229). The manuscript has benefited from constructive reviews by Sébastien Rohais and Christopher Jackson.

CONFLICT OF INTEREST

The authors confirm that they have no affiliations with or involvement in any organization or entity with any financial or non-financial interest in the subject matter or materials discussed in this manuscript.

DATA AVAILABILITY STATEMENT

The data that support the findings of this study are available from the corresponding author upon reasonable request.

ORCID

Bonita J. Barrett  <https://orcid.org/0000-0002-3274-822X>
 Rob L. Gawthorpe  <https://orcid.org/0000-0002-4352-6366>
 Richard E. Ll. Collier  <https://orcid.org/0000-0002-8001-0510>
 David M. Hodgson  <https://orcid.org/0000-0003-3711-635X>
 Timothy M. Cullen  <https://orcid.org/0000-0002-2497-2213>

REFERENCES

- Ackers, P. and White, W.R. (1973) Sediment transport: new approach and analysis. *Journals of Hydraulics Division*, 99, 2041–2060.
- Ashley, G.M. (1990) Classification of large-scale subaqueous bedforms: a new look at an old problem. *Journal of Sedimentary Research*, 60, 160–172.
- Assine, M.L., Renato Merino, E., Do Nascimento Pupin F., De Azevedo Macedo, H. and Guerreiro Martinho Dos Santos, M. (2015) The Quaternary alluvial systems tract of the Pantanal Basin, Brazil. *Brazilian Journal of Geology*, 45(3), 475–489.
- Avallone, A., Briole, P., Agatza-Balodimou, A.M., Billiris, H., Charade, O., Mitsakaki, C. *et al.* (2004) Analysis of eleven years of deformation measured by GPS in the Corinth Rift Laboratory area. *Comptes Rendus Geoscience*, 336, 301–311.
- Backert, N., Ford, M. and Malartre, F. (2010) Architecture and sedimentology of the Kerinitis Gilbert-type fan delta, Corinth Rift, Greece. *Sedimentology*, 57, 543–586.
- Bailard, J.A. and Inman, D.L. (1981) An energetics bedload model for plane sloping beach: local transport. *Journal of Geophysical Research*, 86, 2035–2043.
- Barrett, B., Hodgson, D.M., Collier, R.E.LI, Collier, R.E.LI and Dorrell, R.M. (2018) Novel 3D sequence stratigraphic numerical model for syn-rift basins: analysing architectural responses to eustasy, sedimentation and tectonics. *Marine and Petroleum Geology*, 92, 270–284. Available at: doi:<https://doi.org/10.1016/j.marpetgeo.2017.10.026>.
- Barrett, B., Collier, R.E.L.L., Hodgson, D.M., Gawthorpe, R.L., Dorrell, R.M. and Cullen, T.M. (2019) Quantifying faulting and base level controls on syn-rift sedimentation using stratigraphic architectures of coeval fan deltas: constraining Early-Middle Pleistocene base-level amplitude change in Lake Corinth. *Basin Research*. Available at: doi:<https://doi.org/10.1111/bre.12356>.
- Bagnold, R.A. (1966) An approach to the sediment transport problem from general physics. Geological Survey Professional Paper. Washington: United States Government Printing Office, 37pp.
- Bayram, A., Larson, M., Miller, H.C. and Kraus, N.C. (2001) Cross-shore distribution of longshore sediment transport: comparison between predictive formulas and field measurements. *Coastal Engineering*, 44, 79–99.
- Bell, D., Stevenson, C.J., Kane, I.A., Hodgson, D.M. and Poyatos-Moré, M. (2018) Topographic controls on the development of contemporaneous but contrasting basin-floor depositional architectures. *Journal of Sedimentary Research*, 88, 1166–1189.
- Bhiry, N. and Occhietti, S. (2004) Fluvial sedimentation in a semi-arid region: the fan and interfan system of the Middle Souss Valley, Morocco. *Proceedings of the Geologists' Association*, 115, 313–324.
- Bijker, E.W. (1967) Some considerations about scales for coastal models with movable bed. Delft Hydraulics Laboratory, Publication 50, Delft, the Netherlands. *Journal of the Waterways, Harbors and Coastal Engineering Division*, 97, 687.
- Blackwelder, E. (1931) Desert plains. *Journal of Geology*, 39, 133–140.
- Briole, P., Rigo, A., Lyon-Caen, H., Ruegg, J.C., Papazissi, K., Mitsakaki, C. *et al.* (2000) Active deformation of the Corinth rift, Greece: Results from repeated Global Positioning System surveys between 1990 and 1995. *Journal of Geophysical Research-Solid Earth*, 105, 25605–25625.
- Bull, W. (1977) The alluvial fan environment. *Progress in Physical Geography*, 1, 222–270.
- Capraro, L., Asioli, A., Backman, J., Bertoldi, R., Channell, J.E.T., Massari, F. *et al.* (2005) Climatic patterns revealed by pollen and oxygen isotope records across the Matuyama-Brunhes boundary in the central Mediterranean (southern Italy). *Geological Society, London, Special Publications*, 247, 159–182.
- Clarke, P.J., Davies, R.R., England, P.C., Parsons, B.E., Billiris, H., Paradissis, D. *et al.* (1997) Geodetic estimate of seismic hazard in the Gulf of Korinthos. *Geophysical Research Letters*, 24, 1303–1306.
- Collier, R.E.LI. (1990) Eustatic and tectonic controls upon Quaternary coastal sedimentation in the Corinth Basin, Greece. *Journal of the Geological Society*, 147, 301–314.
- Collier, R.E.LI. and Dart, C.J. (1991) Neogene to Quaternary rifting, sedimentation and uplift in the Corinth Basin, Greece. *Journal of the Geological Society, London*, 148, 1049–1065.
- Collier, R.E.LI. and Thompson, J. (1991) Transverse and linear dunes in an Upper Pleistocene marine sequence, Corinth Basin, Greece. *Sedimentology*, 38, 1021–1040.
- Collier, R.E.LI., Leeder, M.R., Trout, M., Ferentinos, G., Lyberis, E. and Papatheodorou, G. (2000) High sediment yields and cool, wet winters: test of last glacial paleoclimates in the northern Mediterranean. *Geology*, 28, 999–1002.
- Cotterill, C.J. (2002) A high resolution Holocene fault activity history of the Aigion shelf, Gulf of Corinth, Greece. PhD Thesis, School of Ocean and Earth Sciences, University of Southampton.
- Covault, J.A. and Graham, S.A. (2010) Submarine fans at all sea-level stands: tectonomorphologic and climatic controls on terrigenous sediment delivery to the deep sea. *Geology*, 38, 939–942.
- Dart, C.J., Collier, R.E.L., Gawthorpe, R.L., Keller, J.V.A. and Nichols, G. (1994) Sequence stratigraphy of (?)Pliocene-quaternary synrift, gilbert-type fan deltas, Northern Peloponnesos, Greece. *Marine and Petroleum Geology*, 11, 545–560.
- Dawers, N.H. and Anders, M.H. (1995) Displacement-length scaling and fault linkage. *Journal of Structural Geology*, 17, 607–614.
- De Martini, P., Pantosti, D., Palyvos, N., Lemeille, F., McNeill, L. and Collier, R.E.LI. (2004) Slip rates of the Aigion and Eliki faults from uplifted marine terraces, Corinth Gulf, Greece. *Comptes Rendus Geoscience*, 336, 325–334.
- Degnan, P.J. and Robertson, A.H.F. (1998) Mesozoic-early Tertiary passive margin of the Pindos ocean (NW Peloponnese, Greece). *Sedimentary Geology*, 117, 33–70.
- Dodenov, A.E. (2005) The stratigraphic transition and suggested boundary between the Early and Middle Pleistocene in the loess record of northern Eurasia. *Geological Society, London, Special Publications*, 247, 209–219.
- Drønen, N. and Deigaard, R. (2007) Quasi-three-dimensional modelling of the morphology of longshore bars. *Coastal Engineering*, 54, 197–221.
- Emiliani, C. (1955) Pleistocene temperatures. *Journal of Geology*, 63, 538–578.
- Emiliani, C. (1978) The cause of the ice ages. *Earth & Planetary Science Letters*, 37, 349–352.

- Engelund, F. and Hansen, E. (1967) *A Monograph On Sediment Transport in Alluvial Streams*. Copenhagen, Denmark: Teknisk Forlag.
- Floyd, M.A., Billiris, H., Paradissis, D., Veis, G., Avallone, A., Briole, P. *et al.* (2010) A new velocity field for Greece: implications for the kinematics and dynamics of the Aegean. *Journal of Geophysical Research*, *115*, B10403.
- Ford, M., Williams, E.A., Malartre, F. and Popescu, S.M. (2007) Stratigraphic architecture, sedimentology and structure of the Vouraikos Gilbert-type fan delta, Gulf of Corinth, Greece. In: Nichols, G., Williams, E. and Paola, C. (Eds.) *Sedimentary Processes, Environments and Basins. A Tribute to Peter Friend*. International Association of Sedimentology Special Publications, *38*, 49–90.
- Ford, M., Rohais, S., Williams, E.A., Bourlange, S., Jousselin, D., Backert, N. *et al.* (2013) Tectonosedimentary evolution of the western Corinth rift (Central Greece). *Basin Research*, *25*, 3–25.
- Ford, M., Hemelsdael, R., Mancini, M. and Palyvos, N. (2016) Rift migration and lateral propagation: evolution of normal faults and sediment-routing systems of the western Corinth rift (Greece). In: Childs, C., Holdsworth, R.E., Jackson, C.A.-L., Manzocchi, T., Walsh, J.J. and Yielding, G. (Eds.) *The Geometry of Normal Faults*. Geological Society, London, Special Publications, *439*, 131–168.
- Gawthorpe, R.L. and Leeder, M.R. (2000) Tectono-sedimentary evolution of active extensional basins. *Basin Research*, *12*, 195–218.
- Gawthorpe, R.L., Fraser, A. and Collier, R.E.L. (1994) Sequence stratigraphy in active extensional basins: implications for the interpretation of ancient basin fills. *Marine and Petroleum Geology*, *11*, 642–658.
- Gawthorpe, R.L., Sharp, I., Underhill, J.R. and Gupta, S. (1997) Linked sequence stratigraphic and structural evolution of propagating normal faults. *Geology*, *25*, 795–798.
- Gawthorpe, R.L., Leeder, M.R., Kranis, H., Skourtsos, E., Andrews, J.E., Henstra, G.A. *et al.* (2017a) Tectono-sedimentary evolution of the Plio-Pleistocene Corinth rift, Greece. *Basin Research*, *30*, 1–32. Available at: doi:<https://doi.org/10.1111/bre.12260>.
- Gawthorpe, R.L., Andrews, J.E., Collier, R.E.L., Ford, M., Henstra, G.A., Kranis, H., *et al.* (2017b) Building up or out? Disparate sequence architectures along an active rift margin – Corinth rift, Greece. *Geology*, *45*, 111–114.
- Ghisetti, F. and Vezzani, L. (2004) Plio-Pleistocene sedimentation and fault segmentation in the Gulf of Corinth (Greece) controlled by inherited structural fabric. *Comptes Rendus Geosciences*, *336*, 243–249.
- Gilbert, G.K. (1890) Lake Bonneville. *U.S. Geological Survey Monograph*, *1*, 438.
- Gobo, K., Ghinassi, M. and Nemeč, W. (2014) Reciprocal changes in foreset to bottomset facies in a gilbert-type delta: Response to short-term changes in base level. *Journal of Sedimentary Research*, *84*, 1079–1095.
- Gobo, K., Ghinassi, M. and Nemeč, W. (2015) Gilbert-type deltas recording short-term base-level changes: Delta-brink morphodynamics and related foreset facies. *Sedimentology*, *62*, 1923–1949.
- Godsey, H.S., Currey, D.R. and Chan, M.A. (2005) New evidence for an extended occupation of the Provo shoreline and implications for regional climate change, Pleistocene Lake Bonneville, Utah, USA. *Quaternary Research*, *63*, 212–223.
- Goldsworthy, M. and Jackson, J. (2001) Migration of activity within normal fault systems: examples from the Quaternary of mainland Greece. *Journal of Structural Geology*, *23*, 489–506.
- Hardy, S. and Gawthorpe, R.L. (1998) Effects of variations in fault slip rate on sequence stratigraphy in fan deltas: insights from numerical modeling. *Geology*, *26*, 911–914.
- Head, M.J. and Gibbard, E.L. (2005) Early-Middle Pleistocene transitions: an overview and recommendation for defining the boundary. In: Head, M.J. and Gibbard, P.L. (Eds.), *Early-Middle Pleistocene Transitions: The Land-Ocean Evidence*. Geological Society, London, Special Publications, *247*, 1–18.
- Helland-Hansen, W. and Hampson, G.J. (2009) Trajectory analysis: concepts and applications. *Basin Research*, *21*, 454–483.
- Higgs, R. (1990) Sedimentology and tectonic implications of Cretaceous fan-delta conglomerates, Queen Charlotte Islands, Canada. *Sedimentology*, *37*, 83–103.
- Hodgson, D.M., Kane, I.A., Flint, S.S., Brunt, R.L. and Ortiz-Karpf, A. (2016) Time-transgressive confinement on the slope and the progradation of basin-floor fans: implications for the sequence stratigraphy of deep-water deposits. *Journal of Sedimentary Research*, *86*, 73–86.
- Hook, J., Abhvani, A., Gluyas, J.G. and Lawlor, M. (2003). The Birch Field, Block 16/12a, UK North Sea. In: Gluyas, J.G. and Hichens, H.M. (Eds.) *United Kingdom Oil and Gas Fields', Commemorative Millennium Volume*. Geological Society, London, *Memoir*, *20*, 167–181.
- Hooke, R. (1972) Geomorphic evidence for late-Wisconsin and Holocene tectonic deformation, Death Valley, California. *Geological Society of America Bulletin*, *83*, 2073–2098.
- Imbrie, J., Hays, J.D., Martinson, D.G., McIntyre, A., Mix, A.C., Morley, J.J. *et al.* (1984) The orbital theory of Pleistocene climate: Support from a revised chronology of the marine delta ¹⁸O record. In: Berger, A. (Ed.) *Milankovitch and Climate*. Dordrecht, The Netherlands: Plenum Reidel, pp. 269–305.
- Kneller, B., Edwards, D., McCaffery, W. and Moore, R. (1991) Oblique reflection of turbidity currents. *Geology*, *19*, 250–252.
- Larson, M. and Kraus, N.C. (1992) Dynamics of longshore bars. In: Edge, B.L. (Ed.), *Proceedings of 23rd Conference on Coastal Engineering*, Venice, Italy, *23*, 2219–2232.
- Leeder, M.R. and Gawthorpe, R.L. (1987) Sedimentary models for extensional tilt block/half-graben basins. In: Coward, M.P., Dewey, J.F. and Hancock, P.L. (Eds.), *Continental Extensional Tectonics*. Geological Society, London, Special Publications, *28*, 139–152.
- Leeder, M.R., Collier, R.E.L., Abdul Aziz, L.H., Trout, M., Ferentinis, G. and Papatheodorou, G. (2002) Tectono-sedimentary processes along an active marine/lacustrine half-graben margin: Alkyonides Gulf, E. Gulf of Corinth, Greece. *Basin Research*, *14*, 25–41.
- Leeder, M.R., Mack, G.H., Brasier, A.T., Parrish, R.R., Mintosh, W.C., Andrews, J.E. *et al.* (2008) Late-Pliocene timing of Corinth (Greece) rift-margin fault migration. *Earth and Planetary Science Letters*, *274*, 132–141.
- Lemons, D.R., Milligan, M.R. and Chan, M.A. (1996) Paleoclimatic implications of late Pleistocene sediment yield rates for the Bonneville Basin, northern Utah. *Palaeogeography, Palaeoclimatology, Palaeoecology*, *123*, 147–159.
- Leppard, C.W. and Gawthorpe, R.L. (2006) Sedimentology of rift climax deep water systems; Lower Rudeis Formation, Hammam Faraun Fault Block, Suez Rift, Egypt. *Sedimentary Geology*, *191*, 67–87.
- Lisiecki, L.E. and Raymo, M.E. (2005) A Pliocene-Pleistocene stack of 57 globally distributed benthic delta 18O records. *Paleoceanography*, *20*, PA1003. Available at: doi:<https://doi.org/10.1029/2004PA001071>.

- Lisiecki, L.E. and Raymo, M.E. (2007) Plio-Pleistocene climate evolution: trends and transitions in glacial cycle dynamics. *Quaternary Science Reviews*, 26, 56–69.
- Lomas, S.A. and Joseph, P. (2004) Confined turbidite systems. In: Lomas, S.A. and Joseph, P. (Eds.) *Confined Turbidite Systems*. Geological Society, London, *Special Publications*, 222, 1–7.
- McNeill, L.C. and Collier, R. (2004) Uplift and slip rates of the eastern Eliki fault segment, Gulf of Corinth, Greece, inferred from Holocene and Pleistocene terraces. *Journal of the Geological Society*, 161, 81–92.
- McNeill, L.C., Collier, R.E.L.L., De Martini, P.M., Pantosti, D. and D'Addezio, G. (2005) Recent history of the Eastern Eliki Fault, Gulf of Corinth: geomorphology, palaeoseismology and impact on palaeoenvironments. *Geophysical Journal International*, 16, 154–166.
- Miliareisis, G.Ch. (2001) Extraction of bajadas from digital elevation models and satellite imagery. *Computers & Geosciences*, 27, 1157–1167.
- Milligan, M. and McDonald, G. (2016) Shorelines and vertebrate fauna of Pleistocene Lake Bonneville, Utah, Idaho and Nevada. *Geology of the Intermountain West*, 4. A Field Guide Prepared for Society of Vertebrate Paleontology Annual Meeting, October 26–29, 2016 Grand America Hotel Salt Lake City, Utah, USA.
- Moretti, I., Lykousis, V., Sakellariou, D., Reynaud, J.Y., Benziane, B. and Prinzhofer, A. (2004) Sedimentation and subsidence rate in the Gulf of Corinth: what we learn from the Marion Dufresne's long-piston coring. *Comptes Rendus Geoscience*, 336, 291–299.
- Nemec, W. (1990) Aspects of sediment movement on steep delta slopes. In: Collela, A. and Prior, D.B. (Eds.) *Coarse-Grained Deltas*. *Special Publications of International Association of Sedimentology*, 10, 29–73.
- Nixon, C.W., McNeill, L.C., Bull, J.M., Bell, R.E., Gawthorpe, R.L., Henstock, T.J. et al. (2016) Rapid spatiotemporal variations in rift structure during development of the Corinth Rift, central Greece. *Tectonics*, 35, 1225–1248.
- Ori, G.G., Roveri, M. and Nichols, G. (1991) Architectural patterns in large-scale Gilbert-type delta complexes, Pleistocene, Gulf of Corinth, Greece. In: Miall, A.D. and Tyler, N. (Eds.) *The Three Dimensional Facies Architecture of Terrigenous Clastic Sediments and its Implications for Hydrocarbon Discovery and Recovery*. *SEPM, Concept in Sedimentology and Paleontology*, pp. 207–216.
- Orme, A.R. (1985) The behaviour and migration of longshore bars. *Physical Geography*, 6, 142–164.
- Orton, G.J. and Reading, H.G. (1993) Variability of deltaic processes in terms of sediment supply, with particular emphasis on grain size. *Sedimentology*, 40, 475–512.
- Postma, G. (1984) Slumps and their deposits in fan delta front and slope. *Geology*, 12, 27–30.
- Potter, P.E. and Pettijohn, F.J. (1977) *Paleocurrents and Basin Analysis*, 2nd edn. New York, NY: Springer-Verlag, 425 p.
- Poulimenos, G., Zelilidis, A., Kontopoulos, N. and Doutsos, T. (1993) Geometry of trapezoidal fan deltas and their relationship to extensional faulting along the south-western active margins of the Corinth rift, Greece. *Basins Research*, 5, 179–192.
- van Rijn, L.C. (1984) Sediment transport: part I: bed load transport; Part II: suspended load transport; Part III: bed forms and alluvial roughness. *Journal of Hydraulic Division*, 110, 1431–1754.
- Rohais, S. and Moretti, I. (2017) Structural and stratigraphic architecture of the Corinth rift (Greece): an integrated onshore to offshore basin-scale synthesis. In: Roure, F., Amin, A.A., Khomsi, S. and Al Garni, M.A.M. (Eds.) *Lithosphere Dynamics and Sedimentary Basins of the Arabian Plate and Surrounding Areas*. *Frontiers in Earth Sciences*, 89–120. Available at: doi:https://doi.org/10.1007/978-3-319-44726-1_5.
- Rohais, S., Eschard, R., Ford, M., Guillocheau, F. and Moretti, I. (2007a) Stratigraphic architecture of the Plio-Pleistocene infill of the Corinth Rift: implications for its structural evolution. *Tectonophysics*, 440(1), 5–28.
- Rohais, S., Joannin, S., Colin, J.P., Suc, J.P., Guillocheau, F. and Eschard, R. (2007b) Age and environmental evolution of the syn-rift fill of the southern coast of the gulf of Corinth (Akrata-Derveni region, Greece). *Bulletin de la Societe Geologique de France*, 178, 231–243.
- Rohais, S., Eschard, R. and Guillocheau, F. (2008) Depositional model and stratigraphic architecture of rift climax Gilbert-type fan deltas (Gulf of Corinth, Greece). *Sedimentary Geology*, 210, 132–145. Available at: doi:<https://doi.org/10.1016/j.sedgeo.2008.08.001>.
- Schmidt, J. (1879) *Studien uber Erdbeben*. Leipzig: Alwin Georgi, pp. 68–83.
- Sohn, Y.K. (2000) Coarse-grained debris-flow deposits in the Miocene fan deltas, SE Korea: a scaling analysis. *Sedimentary Geology*, 130, 45–64.
- Sohn, Y.K., Kim, S.B., Hwang, I.G., Bahk, J.J., Choe, M.Y. and Chough, S.K. (1997) Characteristics and depositional processes of large-scale gravelly Gilbert-type foresets in the Miocene Doumsan fan delta, Pohang Basin, SE Korea. *Journal of Sedimentary Research*, 67, 130–141.
- Soter, S. and Katsonopoulou, D. (1998) The search for ancient Helike, 1988–1995: geological, sonar and bore hole studies. In: Katsonopoulou, D., Soter, S. and Scilardi, D. (Eds.) *Ancient Helike and Aigalioia*. Aigion, Greece: The Helike Society, pp. 67–116.
- Stevenson, C.J., Jackson, C.A.-L., Hodgson, D.M., Hubbard, S.M. and Eggenhuisen, J.T. (2015) Deep-water sediment bypass. *Journal of Sedimentary Research*, 85, 1058–1081.
- Suc, J.-P. and Popescu, S.-M. (2005) Pollen records and climatic cycles in the North Mediterranean region since 2.7 Ma. In: Head, M.J. and Gibbard, P.L. (Eds.) *Early-Middle Pleistocene Transitions: The Land-Ocean Evidence*. Geological Society, London, *Special Publications*, 247, 147–158.
- Turner, C.C. and Connell, E.R. (2018) Mid to Late Jurassic graben margin development and evolution of shallow marine to submarine fan systems in the Brae area of the South Viking Graben, U.K. North Sea. In: Turner, C.C. and Cronin, B.T. (Eds.) *Rift-related Coarse-Grained Submarine Fan Reservoirs: The Brae Play, South Viking Graben, North Sea*. *AAPG Memoir*, 115, 163–212.
- Van De Graaff J. and Van Overeem, J. (1979) Evaluation of sediment transport formulae in coastal engineering practice. *Coastal Engineering*, 3, 1–32.
- Von Freyberg, B. (1973) Geologie des Isthmus von Korinth. Erlanger Geologische Abhandlungen, 95. Junge und Sohn, Universitäts-Buchdruckerei, Erlangen.
- Walsh, J.J. and Watterson, J. (1988) Analysis of the relationship between displacements and dimensions of faults. *Journal of Structural Geology*, 10, 239–247.
- Watanabe, A., Shimizu, T. and Kondo, K. (1991) Field application of a numerical model for beach topography change. *Proceedings of Coastal Sediments*, 91, 1814–1829.
- Young, M.J., Gawthorpe, R.L. and Sharp, I.R. (2002) Architecture and evolution of the syn-rift clastic depositional systems towards the tip of major fault segment, Suez Rift, Egypt. *Basin Research*, 14, 1–23.

- Zelilidis, A. (2003) The geometry of fan-deltas and related turbidites in narrow linear basin. *Geological Journal*, 37, 1–16.
- Zelilidis, A. and Kontopoulos, N. (1996) Significance of fan deltas without toe-sets within rift and piggyback basins: examples from the Corinth graben and the Meso-hellenic trough, Central Greece. *Sedimentology*, 43, 253–262.

How to cite this article: Barrett BJ, Gawthorpe RL, Collier REL, Hodgson DM, Cullen TM. Syn-rift delta interfan successions: Archives of sedimentation and basin evolution. *Depositional Rec.* 2019;00:1–27. <https://doi.org/10.1002/dep2.95>

SUPPORTING INFORMATION

Additional supporting information may be found online in the Supporting Information section.